

IGS

1 9 9 6 A N A L Y S I S

C E N T E R W O R K S H O P

P R O C E E D I N G S

M A R C H 1 9 - 2 1 , 1 9 9 6

IGS Central Bureau
Jet Propulsion Laboratory
California Institute of Technology
Pasadena, California U.S.A.

Edited by
R. E. Neilan
P. A. Van Scoy
J. F. Zumberge



International GPS Service for Geodynamics



Association Internationale de Geodesie
Union Geodesique et Geophysique
Internationale

International Association of Geodesy
International Union of Geodesy and
Geophysics

IGS

1996 ANALYSIS

CENTER WORKSHOP

PROCEEDINGS

MARCH 19-21, 1996



International GPS Service for Geodynamics



Association Internationale de Géodésie
Union Géodésique et Géophysique
Internationale

International Association of Geodesy
International Union of Geodesy and
Geophysics

IGS Central Bureau

Jet Propulsion Laboratory
California Institute of Technology
Pasadena, California U.S.A.

Edited by

R. E. Neilan

P. A. Van Scoy

J. F. Zumberge

ABSTRACT

Components of the IGS — International GPS (Global Positioning System) Service for Geodynamics — have operated a GPS tracking system for several years. The network now contains more than 100 stations and has produced a combined GPS ephemeris that has become the standard for geodesists and geophysicists worldwide. IGS data and products are freely available to all, thanks to the cooperation and participation of all the IGS members. The IGS has initiated development of several new products, and technical issues permitting greater accuracy of IGS products have been identified. The IGS convened a workshop in March 1996 in Silver Spring, Maryland, USA, to coordinate these developments and to examine technical problems and solutions. The following topics were addressed: orbit/clock combination; Earth orientation; antenna calibration; SINEX and densification of the International Terrestrial Reference Frame (ITRF) using the GPS; receiver standards and performance; and atmospheric topics.

ACKNOWLEDGEMENT

This publication was prepared by the Jet Propulsion Laboratory, California Institute of Technology, under a contract with the National Aeronautics and Space Administration. It contains material from contributors in United States Government agencies, agencies of other governments, and universities.

Reference herein to any specific commercial product, process, or service by trade name, trademark, manufacturer, or otherwise, does not constitute or imply its endorsement by the United States Government, the National Aeronautics and Space Administration, or the Jet Propulsion Laboratory, California Institute of Technology.

FOREWORD

Gerald L. Mader

Silver Spring, MD, June 1996

For the past several years, the IGS has operated a global GPS tracking network, now numbering over 100 stations, and has produced a combined GPS ephemeris that has become the standard for geodesists and geophysicists around the world. IGS data and products are easily and freely available to all thanks to the cooperation and participation of all the IGS members.

As a consequence of this success and its acceptance by the scientific community, the IGS has initiated the development of several new products. In addition, technical issues permitting even greater accuracy of IGS products have been identified.

In order to more effectively define and coordinate these developments and to examine in detail technical problems and solutions, the Analysis Centers of the IGS convened a workshop which was held March 19-21, 1996 in Silver Spring, Maryland, USA. The Workshop was hosted by the National Oceanic and Atmospheric Administration (NOAA) and was jointly organized by NOAA and the Geodetic Survey Division, Geomatics Canada.

As these Proceedings demonstrate, there were significant contributions made by the presenters on the primary themes of this workshop. The discussions, which were central to the plan of the workshop, led to numerous specific recommendations which are also documented in these Proceedings.

The workshop's success followed primarily from this balance between presentations and discussions. In most of the sessions, about half the scheduled time was devoted to discussions focused on the specific issues of that session. The physical arrangement of the workshop was designed to encourage these discussions. The participants from the analysis centers and the invited speakers were seated facing each other around a "U-shaped" arrangement of tables. The remaining participants and interested observers, of which there were many, were seated in an audience section of the conference room. This design, which drew an overwhelmingly favorable reaction, contributed to the informal atmosphere and close interaction necessary to productive discussions while allowing a large number of persons to feel involved.

I would like to thank all the session chairpersons for the time and effort that went into organizing their sessions and for preparing their session position papers and summaries. Ruth Neilan and Gerhard Beutler deserve special mention for ensuring that our discussions stayed on track and led to the numerous productive recommendations contained herein. I also want to thank my co-convenor, Jan Kouba, who, while he was unable to attend, was certainly present in spirit and whose energetic contributions to the IGS are an inspiration to us all.

INTRODUCTION

Ruth E. Neilan

IGS Central Bureau,

Jet Propulsion Laboratory, California Institute of Technology

Pasadena, California, September 1996

We hope that you find these proceedings from the Silver Spring Analysis Center Workshop a valuable resource within the family of IGS documentation. The meeting hosted by NOAA proved to be very stimulating, and ensuring that these technical developments and directions of the IGS are documented is a key responsibility of the Central Bureau. Certainly the level of editing is less formal than the IGS Annual Report Series, especially this year when the Central Bureau was involved with both documents simultaneously. However, the papers included in these workshop proceedings will be of great benefit to many colleagues, students, and institutions, and so the effort of each contributing author is greatly appreciated.

I would like to especially recognize the efforts of Priscilla Van Scoy at the Central Bureau who assisted in organizing the document and routing it through its various stages to completion. I also want to thank the co-chairs of each session for reviewing and commenting on the document, and with special thanks as well to Gerhard Beutler, Jan Kouba, Gerry Mader, Jim Ray and Tim Springer.

C O N T E N T S

Introduction

Foreword	iii
G. Mader	
Introduction	v
R. Neilan	
Executive Summary	xi
G. Beutler	
Agenda	xvii
List of Participants	xxi
Summary Recommendations	xxiii

Orbit/Clock Combination

GPS Orbit/Clock Combinations and Modeling	3
J. Kouba/G. Beutler/Y. Mireault	
Evaluation of IGS GPS Orbits with Satellite Laser Ranging	9
M. Watkins/Y. Bar-Sever/D. Yuan	
Using the Extended CODE Orbit Model: First Experiences	13
T. Springer/M. Rothacher/G. Beutler	

GPS Earth Orientation

GPS Earth Orientation Combinations and Results: Session Summaries and Recommendations	25
J. Ray/D. McCarthy	
IGS Combination of GPS Earth Orientation Parameters (EOP)	33
J. Kouba	
GPS Measurements of Length-of-Day: Comparisons with VLBI and Consequences for UT1	43
J. Ray	
Multi-technique EOP Combinations	61
D. Gambis	
Daily & Semi-daily Earth Orientation Parameter Variations and Time Scales	71
D. McCarthy	
International Earth Rotation Service Conventions (1996)	73
D. McCarthy	

GPS Antenna Calibration

Calibration of GPS Antennas	81
G. Mader/J. MacKay	
Field and Anechoic Chamber Tests of GPS Antennas	107
C. Meertens/C. Alber/J. Braun/C. Rocken/ B. Stephens/R. Ware/M. Exner/P. Kolesnikoff	

SINEX and Pilot Project

Compact RINEX Format and Tools	121
Y. Hatanaka	
Polyhedron Assembly at Newcastle Method and Initial Results	131
P. Davies	

Atmospheric Trends

Troposphere

IGS Tropospheric Estimations—Summary	147
G. Gendt	
Comparison of IGS Troposphere Estimations	151
G. Gendt	
Strategies for Near Real Time Estimation of Precipitable Water Vapor	165
Y. Bar-Sever	

Ionosphere

Ionosphere Maps—A New Product of IGS?—Summary	177
J. Feltens	
Daily Global Ionosphere Maps Based on GPS Carrier Phase Data Routinely Produced by the CODE Analysis Center	181
S. Schaer/G. Beutler/ M. Rothacher/T. Springer	
The Effect of Shell Height on High Precision Ionospheric Modelling Using GPS	193
A. Komjathy/R. Langley	
Verification of ESOC Ionosphere Modelling and Status of IGS Intercomparison Activity	205
J. Feltens/J. Dow/T. Martín-Mur/ C. García Martínez/M. Bayona-Pérez	
Comparison of GPS/IGS-Derived TEC Data with Parameters Measured by Independent Ionospheric Probing Techniques	221
N. Jakowski/E. Sardón	

Appendix 1

SINEX	233
-------------	-----

Appendix 2

Orbit/Clock Combination

Towards a New IGS Orbit Model	279
T. Springer/G. Beutler/M. Rothacher	

GPS Earth Orientation

Multi-technique EOP Combination 299
D. Gambis

Special GPS Solutions Based on ITRF94 307
Z. Altamimi

GPS Antenna Calibrations

Ashtech Radome Tests on Dorne-Margolin Choke Ring Antennas 309
(R. King/A. E. Niell/McClusky/T. Herring)

Antenna Phase Center Offsets and Variations Estimated from GPS Data 321
M. Rothacher/S. Schär

What Are Phase-Center Variations and Why Should I Worry? 347
T. A. Clark/B. R. Schupler

SINEX and Pilot Project

MIT T2 Analysis Report 369
T. Herring

Atmospheric Trends

Ionospheric Profiling Using GPS/MET Data 379
G. Hajj/L. Romans

Global Ionospheric Mapping Using GPS: Validation and Future Prospects 397
B. Wilson/A. Mannucci/D.-N. Yuan/C. Ho/X. Pi/T. Runge/U. Lindqwister

The Potential Use of GPS/MET in Operational Numerical Weather Prediction 421
R. McPherson/E. Kalnay/S. Lord

DLR-Neustrelitz Comments over Ionospheric IGS Products 437
E. Sardon

Other Contributions

GPS Orbit Determination Including Various Adjustments (GODIVA) 441
C. Goad/A. Mueller

CORS Project 457
N. Weston

NOAA GPS Antenna-Calibration Website 473
G. L. Mader

Average Median Data Delivery/Retrieval Delay at CDDIS for 1996 (All Sites) 475
C. Noll

EXECUTIVE SUMMARY †

G. Beutler

Chair, IGS Governing Board

Dear Colleagues,

The 1996 IGS Analysis Center Workshop took place March 19-21, in Silver Spring, MD. Gerry Mader and Jan Kouba, who organized this meeting, arranged it as a real workshop. The setup was perfect to focus the discussion, and I believe that everybody enjoyed a very fruitful three days at the NOAA facilities.

On Friday, 22 March, a business meeting of the IGS Governing Board with the session chairs as guests was organized with the goal to come up with the appropriate action items.

It was a shock for the participants to learn immediately before the start of the workshop that Jan Kouba, IGS Analysis Coordinator, could not attend the workshop due to a very sudden health problem, which virtually immobilized our Coordinator for a week. I am convinced that everybody is relieved to hear now that Jan — according to his own diagnosis — is in perfect shape again, and that he continues his coordinating task for the IGS with the same energy as before.

Let us now try to summarize the sessions and some events of the workshop.

The following topics were addressed, where each topic was introduced by a position paper prepared by the session chairpersons:

- | | |
|--|--------------------------------|
| • Orbit/Clock Combination | <i>Chair: Kouba/Beutler</i> |
| • Earth Orientation | <i>Chair: Ray/McCarthy</i> |
| • Antenna Calibration | <i>Chair: Mader/Rothacher</i> |
| • SINEX, Densification of the ITRF using the GPS | <i>Chair: Blewitt</i> |
| • Receiver Standards and Performance | <i>Chair: Zumberge/Gurtner</i> |
| • Atmospheric Topics | <i>Chair: Feltens/Gendt</i> |

The position papers were available before the beginning of the workshop. They will serve as a first draft for the session summary, including all recommendations and decisions, which will be included into the workshop proceedings. Let me go through the individual sessions now.

Orbit/Clock Combination *Chair: Kouba/Beutler*

Currently the best AC's and the combined IGS solutions are approaching the 5cm(orbits)/0.5ns(clocks) precision level. Combinations, comparisons, evaluations and free exchange of information within the IGS and amongst the IGS AC's are essential to the health and growth of the IGS.

The development of the IGS orbit quality showed that orbit parameterization became an important issue even if the arc length is only one day. The weekly analyses of the IGS coordinator made it also clear that different orbit modeling techniques led to different estimates (or realizations) of the ITRF origin. This is why it was recommended that "all AC's make every effort to align their orbit, station and EOP solution to conform to the ITRF origin. It was shown that this could be effectively achieved by means of stochastic orbit modeling or radiation pressure modeling."

Recently the ITRF94 was made available by the ITRF section of the IERS (Boucher and Altamimi). It was recommended that the ITRF94 should replace the ITRF93 within the IGS, provided the tests performed by the

† Distributed as IGS Mail Message #1266, dated March 29, 1996.

IGS AC's in collaboration with the IERS clearly indicate the superiority of the ITRF94. The IGS AC Coordinator will coordinate these activities with the IERS.

Today all IGS AC's take part in yet another IGS combination, called the "IGS Preliminary orbit/clock combination" which is now approaching a precision of about 10cm/1ns and is made available with a delay of 38 h only. In order "to economize and to minimize the IGS combination effort and to speed up the delivery of the IGS Final orbits/clocks it is recommended that starting on 30 June, 1996 (day 182, start of GPS week 860) the IGS Final combination be discontinued, the current Rapid IGS combination becomes the IGS Final and the IGS Preliminary (IGP) becomes the IGS Rapid (IGR) combination. This way the most precise Final orbits/clocks will become available within 11 days and the IGS Rapid orbits/clocks will be available within about 1 day." It was moreover decided that the 38h deadline for the (now really) rapid orbit will be replaced by a 23h deadline, allowing it to make available the official IGS Rapid Orbit with a delay of 24h. This is of course only possible if the data are available at the AC's about 6 hours after midnight UT (!). Again these changes shall be implemented on 30 June, 1996.

It became clear at the workshop that there is considerable interest in 1-2 day predicted orbits. This is why IGS Analysis Centers will start producing 1- and 2- day predicted orbits. The interest in predictions became even more apparent at the business meeting, which is why the IGS AC-coordinator will be asked to study options leading to the production of an official IGS predicted orbit.

Mike Watkins from JPL presented a very encouraging agreement of few centimeters of SLR measurements to GPS satellites (PRNs 5 and 6 are equipped with a Laser reflector) with distances derived from individual and the combined IGS orbits. He addressed in particular the importance of modeling the actual attitude of the GPS satellites during eclipse phases. It was also agreed that SLR data at present would have little impact on IGS orbits, but that more SLR data would be most desirable for calibration purposes. There were indications that a concentrated and coordinated SLR observation campaign of PRNs 5 and 6 might take place in fall 1996.

Clyde Goad from OSU presented a very elegant and most efficient triple difference algorithm which was successfully used for orbit determination and estimation of erp-series. It was pointed out that the approach is equivalent to a correct double difference scheme (without ambiguity resolution) because mathematical correlations of the triple differences are modeled correctly.

Tim Springer from CODE presented first experiences using the "new" orbit model developed in Bern. There are indications that the model is particularly well suited for orbit predictions.

Earth Orientation *Chair: Ray/McCarthy*

The session was opened with a review of the method developed and applied by the IGS Analysis Coordinator to produce the combined IGS EOP series. The review was presented by Pierre Tetreault. In the next presentation by Marshall Eubanks we were reminded that the IGS combined EOP series agree very well with the VLBI derived values. Periodic variations seen in the differences "IGS - IERS EOP series" could be attributed to smoothing effects in the IERS series which disappeared after a review of the IERS algorithms to produce the combined series.

Only the x- and y- components of IGS polar motion series have been extensively used by the IERS. The GPS-based length of day (LOD) or UT1-UTC drift values have not been given much weight by the IERS so far. The presentations by Jim Ray and Daniel Gambis revealed that much more attention is given to that topic now. It became clear that GPS-derived LOD values are biased (because of correlations with the dynamical orbit parameters); it became also clear on the other hand that much very valuable information is contained in the IGS-derived LOD series. We will undoubtedly observe in the future that these IGS products will play a more important role in the determination (and the prediction) of the IERS UT1-UTC series. This might become true in particular if the correlation between these drift parameters and the (empirical) radiation pressure parameters becomes more clearly understood.

Dennis McCarthy and Tom Herring pointed out that sub-diurnal EOP variations play a crucial role for the EOP series derived by the IGS Analysis Centers. It is true on the one hand that the effects are minimized if constant EOP values are derived for time intervals covering one or several of these periods. But in view of the fact that the amplitudes may reach the 1 mas level, biases of the order of 0.1 - 0.3 mas still may remain in such series. Tom Herring also pointed out that such effects are difficult for IGS analysts to see because they may be absorbed by the estimated radiation pressure parameters. It was argued that the well established diurnal and semi-diurnal terms should be applied by all IGS Analysis Centers.

The oral presentations were concluded by a review of the existing and a preview of the new IERS standards. It was argued that IGS Analysis Centers should follow more closely the IERS standards. If departures from these standards cannot be avoided this fact should emerge from the AC's processing specifications (AC questionnaire).

The recommendations of this session really emerged from the oral presentations: All Analysis Centers are asked to follow the IERS conventions (standards) to the extent possible (something which is facilitated by making available software source code), all AC's are urged to update their AC questionnaire (available at the IGS Central Bureau Information System) at least once per year and the AC coordinator is asked to review these schemes in the IGS annual report. It was further recommended that the general users use the IGS rapid and preliminary polar motion series (in future rapid and final) together with the corresponding final and rapid, resp. IGS orbits. The IERS further asks the IGS Analysis Coordinator to develop a method to combine submitted LOD/UT1 results with the goal to form an official IGS series of such values. The series of recommendations was concluded by the requests to take into account 12h- and 24h- terms in EOP series using the latest tidal model of Richard Ray (to be made available by the IERS) and to document the actual procedures of the AC's (which is of particular importance in this case). Of course such terms have to be taken into account in all transformations between the terrestrial and the celestial frames.

Antenna Calibration *Chair: Mader/Rothacher*

The "state of the art" in anechoic chamber measurements was introduced by two papers, namely Chuck Meertens from UNAVCO and Bruce Schupler from NASA/GSFC. This underlines the broad interest in absolute precise phase center information. These presentations were complemented by discussions of the "in situ" techniques focusing on the differential antenna behavior (relative to one antenna or one antenna type) by Gerry Mader from NOAA and by Markus Rothacher from CODE.

It became apparent that "in situ" calibrations from different groups are in good agreement and are well suited to correct relative antenna biases. Some inconsistencies still exist, however, between these in situ and the chamber test results. Using the (absolute) chamber test models to correct the phase center of the Dorne-Margolin antennas leads to an unexplained and significant scale bias of about 0.015 ppm in global GPS analyses.

It was therefore recommended to make available to all parties interested the relative antenna phase center models for (if possible) all commercially available geodetic antenna types stemming from in situ measurements. Provided that the final tests performed with this set are successful the IGS Analysis Centers will start using these relative models on 30 June, 1996, at the latest. This will remove obvious discrepancies, e.g., for sites equipped with Trimble antennas, in solutions which did not yet account for such relative models. The amount of work invested by all involved parties is amazing, and it was acknowledged that all efforts are necessary to come to a satisfactory model, eventually.

It was acknowledged that the scale effect resulting from the use of absolute chamber tests needs to be directly addressed in the future.

SINEX, Densification of the ITRF *Chair: Blewitt*

We are now in the middle of the IGS pilot project "densification of the ITRF through regional GPS networks."

In September 1995 the IGS AC's started submitting to the global data centers so-called free network solutions in a still experimental version of the SINEX format (Software Independent EXchange format). Today such series are available from all seven AC's. Three institutions (JPL, MIT, University of Newcastle) are analyzing and combining these weekly products. The procedures of each of the centers were presented and discussed in the session. It became obvious that the philosophy and the actual procedures were quite different. The "final" products, on the other hand, agree amazingly well. Is this possibly a consequence of the Central Limit Theorem formulated by C.F. Gauss? The consequence of these weekly analyses is remarkable: a consistent set of coordinates (referring to the ITRF) for all the sites analyzed by at least one AC are openly available! It is generally expected that these activities will make the updating of the ITRF (GPS part) much easier.

In any case one could draw the conclusion that this first phase of the pilot project was quite successful. The second phase, where the products of regional Associate Analysis Centers will be included into these weekly comparisons, too, is scheduled to start on 30 June, 1996. It was initiated by the call for participation in January 1996. The proposals are now evaluated; the "new players" will be introduced by IGS mail soon.

It also became clear that there was too much flexibility in the SINEX format in the past. A working group is now revising the SINEX format with the goal to have the weekly AC and AAC contributions transmitted in the SINEX Version 1.0, starting 30 June, 1996. The AC coordinator is responsible for finalizing this version, of course in close contact with the AC's and the new associates!

All recommendations of this session were related to the SINEX format; most of them were very technical in nature. There was, however, the recommendation to include the EOP information into the SINEX file which will require some additional thought. In view of the variety of methods used by the AC's to implement a priori information and to parameterize the EOP series, the implementation seems to be non-trivial at first sight. There is little doubt, on the other hand, that the AC coordinator in collaboration with the AC's will come up with a solution that makes sense. It was the general understanding that the inclusion of this information shall NOT serve the generation of a "new" IGS polar motion series, but allow it to remove reference frame inconsistencies between solutions in a more rigorous way.

Receiver Standards and Performance *Chair: Zumberge/Gurtner*

The network performance and in particular data latency were reviewed by Werner Gurtner and Jim Zumberge. These analyses were based on statistics routinely made at the global data centers and at some of the AC's. The result was encouraging in the sense that with a "minor" organizational effort, it actually should be possible to make the observations (at least of a sub-net) available to the AC's early in the morning (UT) which actually would allow them to turn out rapid products within 24h.

Data quality was not well monitored so far within the network. The goal, to my understanding, is to have a short information concerning quality available together with the RINEX data files coming in. Such tools are prepared right now.

A very interesting and (at least for me) surprising presentation was given by Dr. Hatanaka from the Geographical Survey Institute (GSI) of Japan. He presented an algorithm (based on forming differences of the observables) allowing it to compress the data before transmission by about a factor of 2.4 (in addition to the compression that is already used today). First experience with the algorithm made by some of the IGS components is positive.

The following recommendations concluded the session:

A set of stations will be identified by the Central Bureau together with the AC Coordinator and the AC's for which data have to be available at the AC's at 6 a.m. UT. This implies that the data must be available at all Global Data Centers before 5 a.m. UT. Obviously such stations have to be operated in a fully automatic way. Data of sites which are used for the final products must be made available to the AC's within 48 hours.

Should this step be successful, we would undoubtedly see the (currently rapid, but future) final IGS orbits and EOPs with a delay of much less than the 11 days guaranteed so far.

The Central Bureau prepares procedures for the "Hatanaka compression" to be made available for extensive tests.

The need for improved mechanisms for problem detection and reporting was clearly seen by the network specialists. A routine monitoring of the entire network must be put in place by the CB. It was also requested that not only negative, but also positive feedback should flow back to operating agencies.

Atmospheric Topics *Chair: Gendt/Feltens*

The issue of using the IGS network for modeling the troposphere and the ionosphere was first addressed within the IGS at the 1995 Potsdam Workshop. Meanwhile a broad discussion of this topic inside and outside the IGS was taking place. It becomes clear by now that the IGS actually must play an active role in these fields.

Troposphere aspects were first looked at from the user's point of view: Eugenia Kalnay from the USA National Centers for Environmental Prediction was particularly interested in data stemming from satellites of the type GPS-MET. It seems clear that temperature profiles with a high spatial density are of greatest use in meteorology.

The IGS is not actively involved in the GPS-MET experiment, at present. It may make available total tropospheric delays which, if accompanied by high accuracy barometer and temperature measurements, may be transformed into the "total precipitable water content." The IGS network and the IGS Analysis Centers have the potential to make available such information with a high temporal and spatial resolution (of its tracking network) on a routine basis to the atmospheric physicists. Many are convinced that such time series are relevant for climatological purposes, and, if indeed rapid orbits of the "new kind" (see above) become routinely available, for weather prediction.

That the IGS is "in principle" ready for such a development was one conclusion from Neil Weston's presentation about the CORS network. MET data are transmitted in near real time for selected sites within this US-wide GPS network; the MET data are processed together with the receivers' code and phase observations to generate the information required by the meteorologists. A presentation prepared by Rocken (and presented by Meertens) demonstrated how well GPS-derived water contents agree with WVR results; Gerd Gendt's analysis showed that the tropospheric delays as derived by different IGS AC's are consistent on the level of a few millimeters now. That the issue of weather prediction is taken seriously by IGS AC's was underlined by presentations from JPL (Bar Sever discussing methods to use predicted orbits for meteorological studies) and SIO (Fang presenting methods for near real time meteorology and crustal deformation using GPS).

It was recommended that MET stations of a defined high quality should be deployed — at least in a part of the IGS network. MET information already available at the stations or becoming available in the near future shall be sent routinely in MET RINEX files to the IGS data centers, where they will be available for scientific purpose. Steps leading to the deployment of the appropriate MET equipment will be taken before the end of 1996.

It was also recommended that IGS tropospheric delay estimates should be studied and combined by special Associate Analysis Centers. GFZ is ready to build up such a center (hopefully) by the end of 1996. Other parties will be invited through a call for participation.

Ionosphere models using data from the IGS network were developed by Schaer et al. from CODE, by Wilson et al. from JPL, by Feltens et al. from ESA, by Komjathi et al. from University of New Brunswick, and by Jakowski et al. from DLR Neustrelitz. A data set of five weeks of the year 1995 was used (and is still used) by the "ionosphere groups." It became clear that different groups have different goals in mind: pure GPS-internal use (to correct, e.g., single frequency data or to help ambiguity resolution) is one goal, calibration of altimetry data another, pure ionosphere research a third goal. Methods and models are very different, too. It seems, however, that we are now reaching a state where the models of different groups may be effectively compared.

Such comparisons were presented by the ESA- and the Neustrelitz- groups using a two-dimensional grid in the single layer electron shell. I personally believe that the level of agreement (few TECUs) and not (yet) unexplained biases are amazing. It is fair on the other hand to state that we are still far from the consistency level we have reached, e.g., in modeling the troposphere. Consequently the recommendations are more modest for the near future: In a first step the analyses of the 5-week event and the comparisons emerging from it will be concluded. In a next step a common format for the exchange of ionosphere models is created. A first draft for this format, with the tentative name IONEX, will be available soon. Only in the more distant future (one year from now?) a pre-operational production of IGS ionosphere products is envisaged.

Final Remarks

Although the above summary is rather long it can only give an incomplete picture of the workshop. It was a meeting deserving the name (label) workshop and I have no doubt that important decisions and new directions were the direct result of the considerable amount of work invested in the preparation of this workshop. Let me therefore thank all the contributors to this workshop, and let me congratulate Gerry Mader and Jan Kouba for the organization of this fine IGS event.

AGENDA

IGS Analysis Center Workshop

A Workshop

Sponsored by

National Oceanic and Atmospheric Administration

19-21 March 1996

Silver Spring, Maryland USA

Tuesday Morning, 19 March

08:00-08:30 Opening Activities/Welcome

Orbit/Clock Combination, Modeling & Discussion

Session Chairs: G. Beutler & J. Kouba

- 08:30 M. Watkins GPS/SLR Orbit Comparisons: Two GPS SVs (PRN 5 & 7) are equipped with SLR reflectors and have been observed by several SLR stations for several years. Comparisons done routinely at JPL, apart from JPL orbits also include the IGS and other AC orbit solutions. These comparisons provide another, truly independent check and quality testing for the GPS orbits. They also indicate and confirm peculiarities of some AC solutions in regard to the origin and orientation, in particular.
- 08:50 Discussion
- 08:55 C. Goad A Triple Difference Approach to Global GPS Analysis: Triple differencing when used properly, i.e. with the corresponding var-cov. matrix (due to the triple differencing), produces identical results to the corresponding undifferenced and double differenced traditional approaches. The triple differencing has significant advantages in data editing and intuitive understanding of the significance of ambiguity fixing in global GPS analysis.
- 09:15 Discussion
- 09:20 T. Springer
E. Brockmann
M. Rothacher
G. Beutler Towards a New Orbit Model: From 1992 until 1995 the orbit models as used by individual IGS AC's evolved considerably. Today a number of "different" models are actually in use, ranging from purely deterministic to stochastic models in the Kalman filter sense; they include empirical force models as they underlie, e.g., the "long-arc analysis" performed weekly by the IGS analysis coordinator. The models are critically reviewed; the impact on non-orbit parameters (e.g. LOD) is studied. The contribution is meant to stimulate the discussion which eventually might lead to new "standards" for the modelling of individual AC and IGS orbits.
- 09:40 Discussion
- 09:45 J. Kouba
G. Beutler
Y. Mireault Position Paper Summary and Discussion Points: Many important issues need to be raised, discussed and approaches agreed on: for example the usefulness and necessity of the IGS Final combination (when IGS preliminary (24-36h) and IGS Rapid (11 day delay)) are operational and in place. A complete review of reference frame realization for IGS, the small incompatibilities (e.g., in origin and orientation), solutions reporting, formats, harmonizing SINEX and IGS orbits/EOP, etc.
- 10:05 BREAK

10:30		General Discussion of Orbit/Clock Modeling & IGS Combination Issues, Recommendations, Resolutions, etc.
12:00		End of Session

Tuesday Afternoon, 19 March

GPS Earth Orientation, Combinations & Discussion

Session Chairs: J. Ray & D. McCarthy

13:00	J. Kouba	IGS Combination of GPS EOP Results
13:20		Discussion
13:30	M. Eubanks	Comparison of GPS and VLBI Polar Motion with AAM
13:50		Discussion
14:00	J. Ray	Comparison of GPS and VLBI LOD Results
14:20		Discussion
14:30	D. Gambis	Multi-technique EOP Combinations by the IERS
14:50		Discussion
15:00		BREAK
15:30	D. McCarthy	Daily/Semi-daily EOP Variations and Time Scales
15:50		Discussion
16:00	T. Herring	Consequences of Sub-daily EOPs for GPS Orbits
16:20		Discussion
16:30	D. McCarthy	New IERS Standards & Conventions
16:50		Discussion
17:00		General Discussion of EOP Issues, Recommendations, Resolutions, etc.
17:30		End of Session
17:30		Open Discussion on Extended, Continuous VLBI Campaign
19:00–21:00		Analysis Center Poster Presentations & Reception Holiday Inn

Wednesday Morning, 20 March

GPS Antenna Calibration & Discussion

Session Chairs: G. Mader & M. Rothacher

08:30	C. Meertens C. Rocken	Anechoic Chamber Measurements by UNAVCO
08:50	T. Clark B. Schupler	Anechoic Chamber Measurements by NASA/GSFC
09:10	M. Rothacher	In Situ Antenna Measurements by AIUB
09:30	G. Mader	In Situ Antenna Measurements by NOAA

09:50	J. Johannson	IAG Special Study Group on GPS Antennas
10:00		BREAK
10:30		Discussion: Anechoic Chamber Measurements Field Measurements Phase Centers Standard Antenna Tables for IGS

Wednesday Afternoon, 20 March

SINEX & Discussion

Session Chairs: G. Blewitt & Y. Bock

13:00	G. Blewitt	Pilot Project, Densification, SINEX Documentation
14:00	G. Blewitt M. Watkins T. Herring	Global Network Associate Analysis Center – Discussion
	R. Ferland	SINEX Document
15:00	V. Hatanaka	RINEX Compression Algorithm
15:30		Discussion

Receiver Standards and Performance

Session Chairs: J. Zumberge & W. Gurtner

16:00	J. Zumberge	Review of Data Latency and Quality
16:10		Other Speakers and Discussion
16:40	W. Gurtner	Review of Documented (IGS Mail) Receiver Problems
16:50		AC Concerns (1 Overhead per AC)
17:10–17:30		Other Speakers and Discussion
19:00		Workshop Dinner – Holiday Inn

Thursday Morning, 21 March

Atmospheric Topics

Session Chairs: G. Gendt & J. Feltens

Part 1 – Troposphere

08:30	S. Lord	The USA National Centers for Environmental Prediction Operational Atmospheric Data Assimilation System and Prospects for Usage of GPS Data
08:45	N. Weston	The NGS Continuously Operating Reference Station (CORS) Network
08:55	C. Rocken T. VanHove F. Solheim C. Alber R. Ware C. Meertens	Near-Real-Time Estimation of Atmospheric Water Vapor from GPS

09:05	P. Fang Y. Bock	Rapid GPS Meteorology for Weather Forecasting and Crustal Deformation
09:15	Y. Bar-Sever	Strategies for Near Real Time Estimation of PWV
09:25	G. Gendt	Comparison of IGS Troposphere Estimations
09:35		Discussion
10:00		BREAK

Part II → Ionosphere

10:30	S. Schaer G. Beutler M. Rothacher (presented by M. Rothacher)	Daily Global Ionosphere Maps Based on GPS Carrier Phase Data Routinely Produced by the CODE Analysis Center
10:45	A. Komjathy R. Langley (presented by A. Komjathy)	An Improved Algorithm for High Precision Ionospheric Modelling
11:00	B. Wilson A. Mannucci D. Yuan M. Reyes (presented by B. Wilson)	Global Ionospheric Mapping: Validation and Preliminary Comparisons
11:15	G. Hajj et al. (invited paper) (presented on behalf of G. Hajj by B. Wilson)	Ionospheric Profiling Using GPS/MET Data
11:30	J. Feltens J. Dow T. Martin-Mur C. Garcia-Martinez (presented by J. Feltens)	Verification of ESOC Ionosphere Modeling and Status of IGS Intercomparison Activity
11:45		Discussions

[N. Jakowski and E. Sardon: "Comparison of GPS-Derived TEC Values from Several Groups with Other Ionospheric Probing Techniques." No oral presentation—paper will be delivered for the proceedings only.]

Thursday Afternoon, 21 March

13:00–15:30	J. Dow P. Fang	Contributed Papers Issues Not Covered in Workshop Prospective Topics for Next Workshop
16:00–17:00	G. Mader J. Kouba	Wrap Up: Session Summaries Action Items Recommendations

LIST OF PARTICIPANTS

Name	Institution	E-mail
Zuheir Altamimi	Institut Geographique National	altamimi@ign.fr
Brent Archinal	USNO	baa@CasA.usno.navy.mil
Yoaz Bar-Sever	Jet Propulsion Laboratory	yeb@cobra.jpl.nasa.gov
Gerhard Beutler	AIUB/CODE	beutler@aiub.unibe.ch
Geoff Blewitt	Newcastle University	geoffrey.blewitt@ncl.ac.uk
Miranda Chin	NOAA/NGS	miranda@gracse.grdl.noaa.gov
Thomas Clark	Goddard Space Flight Center	clark@tomcat.gsfc.nasa.gov
Galina Dick	GFZ-Potsdam	dick@gfz-potsdam.de
William Dillinger	NOAA/NGS	billd@dino.grdl.noaa.gov
John M. Dow	ESA/ESOC	jdow@esoc.esa.de
Everett Dutton	NOAA/NGS	everett@geo.grdl.noaa.gov
Etienne Eisop	Paris Observatory	eisop@obspm.fr
Marshall Eubanks	USNO	tme@usno01.usno.navy.mil
Peng Fang	IGPP, SIO, UCSD	pfang@ucsd.edu
Joachim Feltens	EDS at ESOC/OAD	jtellens@esoc.esa.de
Remi Ferland	Geodetic Surveys of Canada	ferland@geod.nrcan.gc.ca
Steve Fisher	JPL/UNAVCO	sfisher@ncar.ucar.edu
Richard Foote	NOAA/NGS	rickf@juccan.ngs.noaa.gov
Daniel Gambis	IERS/CB-Paris	gambis@obspm.fr
Gerd Gendt	GFZ-Potsdam	gend@gfz-potsdam.de
Clyde Goad	Ohio State University	cgoad@magnus.acs.ohio-state.edu
Ramesh Govind	AUSLIG/Geodesy	rameshgovind@auslig.gov.au
Werner Gurtner	AIUB/CODE	gurtner@aiub.unibe.ch
Yuki Hatanaka	GSI, Geographical Survey Institute, Japan	hta@geos.gsi-mc.go.jp
Thomas Herring	MIT	tah@chandler.mit.edu
Stephen Hilla	NOAA/NGS	stevah@linus.ngs.noaa.gov
Jan Johansson	Onsala Space Observatory Chalmers University of Technology	jmj@oso.chalmers.se
Eugenia Kalnay	NCEP	
Peter Kammeyer	USNO	kammeyer@bos.usno.navy.mil
William Kass	NOAA/NGS	billk@ngs.noaa.gov
Attila Komjathy	University of New Brunswick	w43y@unb.ca
Eric Krantz	Trimble Navigation	eric_krantz@trimble.com
Brian Luzum	USNO	bjl@maia.usno.navy.mil

LIST OF PARTICIPANTS (cont.)

Dan MacMillan	GSFC	dsm@leo.gsfc.nasa.gov
Dennis McCarthy	USNO	dmc@maia.usno.navy.mil
Gerald Mader	NOAA/Geosciences Lab	gerry@mozart.grdl.noaa.gov
Charles Meerteus	UNAVCO	chuckm@unavco.ucar.edu
Bill Melbourne	Jet Propulsion Laboratory	bill_melbourne@jpl.nasa.gov
Dennis Milbert	NOAA/NGS	dennis@ngs.noaa.gov
Yves Mireault	Geodetic Survey of Canada	mireault@geod.emr.ca
Ruth Neilan	Jet Propulsion Laboratory	ren@logos.jpl.nasa.gov
Arthur Niell	Haystack Observatory	aen@wells.haystack.edu
Carey Noll	NASA/GSFC	noll@cddis.gsfc.nasa.gov
Jim Ray	NOAA/Geosciences Lab	jimr@ray.grdl.noaa.gov
Chris Reigber	GFZ	reigber@gfz-potsdam.de
Markus Rothacher	AIUB/CODE	rothacher@aiub.uuibe.ch
Mark Schenewerk	NOAA	mark@tony.grdl.noaa.gov
Bruce Schupter	Allied Signal Technical Services	schuplb@thorin.atasc.allied.com
Tomas Soler	NOAA/NGS	tom@ngs.noaa.gov
Paul Spofford	NOAA, National Geodetic Survey	PAULS@ngs.noaa.gov
Tim Springer	AIUB/CODE	springer@aiub.uuibe.ch
Pierre Tetreault	EMR/Natural Resources Canada	pierre@geod.emr.ca
Tonie van Dam	NOAA/CIRES	tonie@roberson.colorado.edu
Michael Watkins	Jet Propulsion Laboratory	mmw@cobra.jpl.nasa.gov
Neil Weston	NOAA/NGS	nweston@ngs.noaa.gov
Brian Wilson	Jet Propulsion Laboratory	bdw@quimby.jpl.nasa.gov
Jim Yoe	NOAA/NESDIS/ORA	jyoe@nesdis.noaa.gov
James Zumberge	Jet Propulsion Laboratory	jfz@cobra.jpl.nasa.gov

SUMMARY RECOMMENDATIONS

*Silver Spring Workshop
March 1996*

A) Orbits

1. All AC's make every effort to align their orbit, station and EOP solution to conform to the ITRF origin. It was shown to be effectively achieved by means of stochastic orbit or R_p modeling.
2. The ITRF94 (P01) coordinates of the 13 ITRF stations are used for the IGS realization of ITRF starting on June 30, 1996 (Wk 0860).
3. To economize and to minimize the IGS combination effort and to speed up the delivery of the IGS Final orbits/clocks, it is recommended that starting on June 30, 1996 (Wk 0860), the IGS Final combination be discontinued, the current Rapid IGS combination become the IGS Final and the IGS Preliminary (IGP) become the IGS Rapid (IGR) combination. This way the most precise Final orbits/clocks will become available within 11 days, and the IGS Rapid orbits/clocks will be available within about 1 day.
4. Timely data delivery is crucial for rapid and precise IGS products, so it is requested that IGS data delivery deadlines be more effectively observed, in particular for a number of selected global stations. For these stations an 8 hour (maximum) delay could be acceptable, providing that IGS global data center equalization does not add more than 2 hours. (See recommendation E.I.)
5. It is recommended that the current submission deadline of 36h for IGP be shortened to 23h (after the last observation), starting on June 30, 1996 (Wk 0860). If all the participating AC solutions have arrived prior to this deadline, the IGS combination is to be completed within an hour after the last submission. (Dependent on A.4 & E.I.)

B) Earth Orientation Parameters

1. IERS Conventions Adopted for General Use
To ensure the highest degree of compatibility of results from the individual Analysis Centers and with other techniques, it is recommended that all IGS Analysis Centers incorporate the IERS Conventions (Standards) into their data analysis procedures to the greatest extent possible.
Whenever departures from the IERS Conventions are deemed necessary, Analysis Centers are encouraged to document the alternative procedures in their reports to the IGS, IERS, and in updated AC Questionnaires. The new version of the IERS Conventions will be available in printed form by late spring 1996. Some parts will be available sooner as source code.
2. Reporting IGS Analysis Center Models and Methods
To ensure the highest quality of results from the IGS combinations and to avoid misunderstandings, it is essential that the models and methods used by the Analysis Centers be fully understood by the users. It is particularly important that departures from the IGS and IERS Standards and Conventions be noted. Therefore, it is recommended that all IGS Analysis Centers provide updated versions of their AC Questionnaire at least once per year and every time that significant changes are made.
The Analysis Center Coordinator will review the scope of the current Questionnaire, making suitable revisions, and will provide a standard format at the IGS Central Bureau. New responses should be filed by all Analysis Centers by July 1, 1996.
3. IGS Combination of GPS Polar Motion Results
Based on the demonstrated high quality of the weighting methods used by the IGS for its polar motion combination, it is recommended that outside users of GPS polar motion results use the IGS Rapid combination polar motion values.

For those applications requiring more rapid turnaround, it is recommended that the IGS Preliminary combination values be used.

Given the high quality of current polar motion estimates from GPS and considering the potential value for excitation studies, Analysis Centers are encouraged to include and report polar motion rate parameters in their data analyses, in addition to polar motion offset parameters.

4. IGS Combination of GPS LOD/UT1 Results

For near real time applications, where the only UT1 information available is from predictions, it is recommended that the IGS Analysis Center Coordinator devise a method to combine submitted LOD/UT1 results from the GPS Analysis Centers to form a preliminary UT1-UTC estimate.

This new UT1 combination will be used to align the IGS Preliminary orbits rather than IERS Bulletin A predictions. Because the GPS LOD/UT1 errors do not seem to be related to the satellite orbit errors in a simple way, a new method is needed for the combination, different from that used for polar motion. The Analysis Center Coordinator will fully document the UT1 combination procedure adopted.

5. Modelling Sub-daily EOP Variations

To account for variations in Earth orientation at nearly 24-h and 12-h periods, it is recommended that the IGS Analysis Centers follow the IERS Conventions and account for these effects in modelling GPS observables using the tidal model of Richard Ray.

This model should be used in the transformation between inertial and Earth-fixed coordinates (and vice versa) for all transformations used in GPS processing. Specifically, the diurnal and semi-diurnal terms need to be included in the transformation of the inertial GPS orbits into the Earth-fixed frame for submission to the IGS.

About 50% of the errors in this adopted model will "project" into the inertial orbits, and of course the total error will be in the transformation from inertial into Earth-fixed coordinates. The one issue still to be addressed is: do these contributions tend to cancel each other or do they add constructively?

6. Reporting EOP Values

With respect to diurnal and semi-diurnal variations, it is recommended that when Earth orientation parameters are estimated, the procedures for reporting EOP values adhere to the IERS Conventions and guidelines, which are still to be determined. In particular, users must know how to relate the reported EOP values to the corresponding total values (including all tidal contributions) at the associated UTC epoch.

The relationship between reported EOP values and the corresponding total EOP values should be explained in the Analysis Center Questionnaire.

C) Antenna Sessions

1. Two sets of phase calibration corrections (PCC) Tables are put together by a small group (Mader, Meertens, Rothacher) to be used by the IGS and by IGS users:
 - a) A set of "mean" phase center offsets for 15 and/or 20 degrees cut-off.
 - b) A set of elevation-dependent PCC and offsets relative to the Dorne Margolin T Antenna.
2. After checks (e.g., UNAVCO, MIT,...) the correction tables are made available at the CBIS together with an official SINEX name.
3. IGS AC's and Regional AC's start using the official PCC tables on July 1, 1996.
4. Different antenna types have to be uniquely identified (model & serial numbers).

D) Pilot Densification Project & SINEX

1. AC's strive to correct SINEX discrepancies, as reported by AAC's as soon as possible.
2. SINEX version 1.00 to be adopted as the first official release version with format description to be made available at IGSCB.
3. AC's and AAC's adopt SINEX v.1.00 (see Appendix 1) by June 30, 1996.
4. IGS request SSG1.156 to study the use of IGS products and to report back with recommended usage for high precision regional analysis. Blewitt (President of SSG1.156) will provide initial instructions on use immediately.
5. AC's strive for a wide global distribution of stations: New stations which improve coverage should be given preference to existing stations in dense regions.
6. AC's should include Earth rotation parameters in their weekly SINEX files. The AC Coordinator will work with the AC's to ensure that each AC produces compatible sets of parameters. Combine station & EOP parameters in consistent fashion.
7. AC's should strive to ensure that information in the SINEX file and information used in the analysis come from the same source.

E) Network

1. Data of sites for rapid orbits available at all AC's at 06:00 UT.
Available at all Global Data Centers (GDC) before 05:00 UT.
2. Data of sites for final products available at all AC's within 48 hours.
3. CB (+ ACs) prepares:
 - a) List of "6^h-sites," data available within 6 hours.
 - b) List of "48^h-sites."
4. OC's and DC's improve data flow to meet deadlines.
5. CB prepares procedures for the "Hatanaka" - compression to be made available for extensive tests.
6. Need improved mechanisms for problem detection and reporting.
7. Routine network monitoring by CB.
 - a) Feedback to stations.

F) Atmospheric

1. The IGS-sites are asked to install MET-Stations with the below given characteristics until the end of 1996. The meteorological data (reduced to the GPS-antenna location, RINEX format) should be sent simultaneously with the RINEX observations to the Global Data Centers. In a pilot phase, a time delay of a few days is acceptable for the Met RINEX files.

Proposed characteristics of the MET-Stations:

Pressure:	≤ 0.5 mbar, very stable ≤ 0.5 mbar throughout 2 years
Temperature:	≤ 0.5 K
Humidity:	$\leq 10\%$
Sampling rate:	<10 minutes

2. Climate Research

Starting by the end of 1996, the Analysis Centers compute series of total zenith path delay (ZPD) with a default sampling rate of minimum 2 hours. (Data intervals starting at 00:00 GPS-time.)

An associate IGS processing center combines the individual time series of delay to an IGS Mean series of ZPD and converts the delays to estimates of precipitable water vapor (PWV). By the end of 1996 GFZ will be ready to act as an associate processing center. Other agencies will be invited through a call of participation.

Formats for exchange and distribution of results should be defined. For the exchange between the AC's and the associate processing center, the SINEX format, and for distribution of results the RINEX format, should be used. Necessary extensions or modification of both formats must be discussed.

3. Weather Forecasting

The contribution of IGS to the weather forecast will be restricted by orbit computation, rapid orbits with 23-hour delay and predicted orbits.

If data from the IGS network are needed, the analysis centers engaged in weather forecast should make bilateral agreements for nearly real-time data transfer with tracking sites of interest.

G) Ionospheric

1. Complete the 5 weeks comparison in process.
2. Agree on common standards, e.g., on format (IONEX). Working group established.
3. Continue e-mail discussion of results and agree on future work.
4. Prepare a pilot phase in which ionosphere products should be computed, compared and checked under pre-operational conditions.

H) Other

The IGS Stations that use external frequency standards (especially MASERs) need information on frequency standard performance and Epoch timing derived by IGS. AC's are requested to transmit such data obtained from routine analysis to the stations and groups responsible for the operation of the frequency standards.

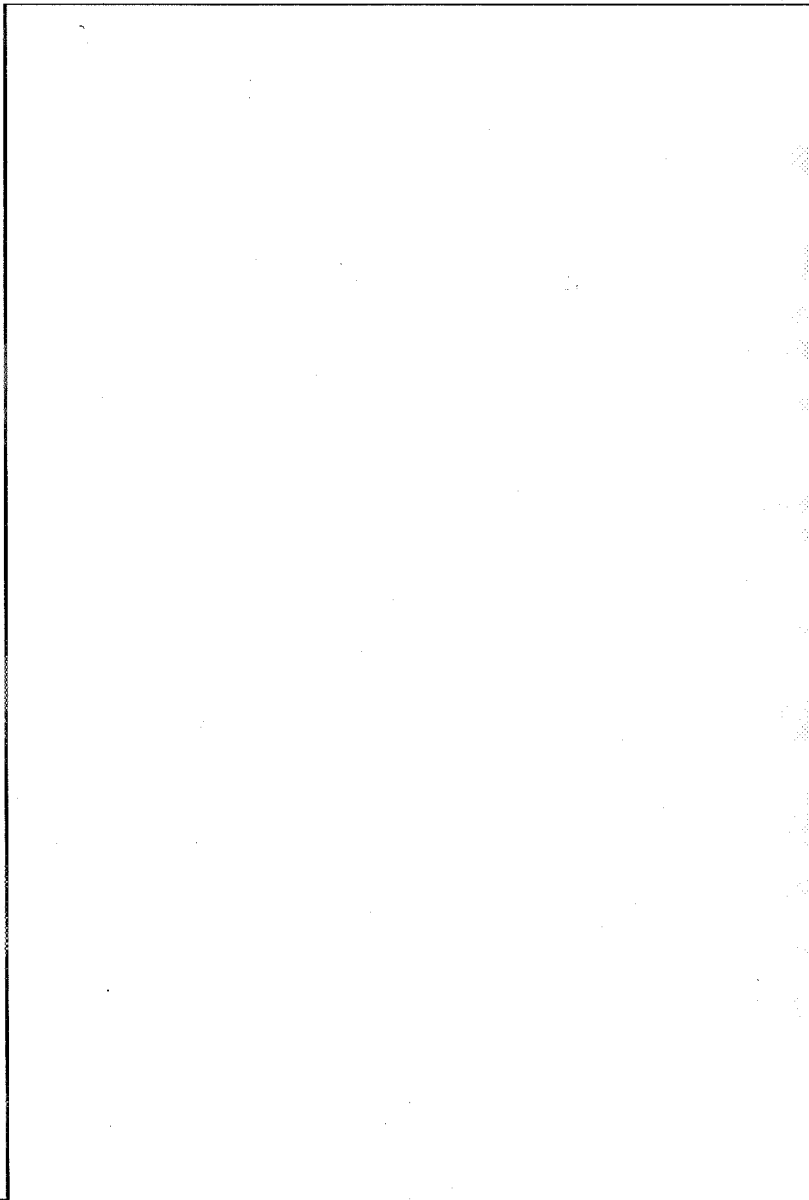
The IGSCB begin to develop a database for monumentation details and local surveys (geophysical and geodetic) at IGS sites, in order to (i) allow AC's and AAC's to make a more informed choice of sites, and (ii) provide geophysicists/geodesists with data to enhance interpretation of results.

I) Recommended Topics for the Next Workshop

Calibration of IGS orbits using SLR (Denser Tracking, Different Software...)	Longer Term Global SINEX Analysis
New Analysis Methods	Regional SINEX Analysis
Parameterizations of Orbit Model	Near Real Time Orbits and Supporting Data Flow
LOD/UT1 from GPS	Monuments/Stability
Experience with Sub-Daily Tidal Model of EOP's	Possible Role of GLONASS in IGS
New IERS 1996 Standards	Troposphere
Phase Centre Correction Models (+GPS Spacecraft ??)	Ionosphere
	Spaceborne Arrays

IGS

ORBIT/CLOCK COMBINATION



Page intentionally left blank

GPS ORBIT/CLOCK COMBINATIONS AND MODELING

J. Kouba⁽¹⁾, G. Beutler⁽²⁾ and Y. Mireault⁽¹⁾

(1) Geodetic Survey Division, Natural Resources Canada, Ottawa, Canada; e-mail: kouba@geod.emr.ca, mireault@geod.emr.ca

(2) Astronomical Institute of University of Bern, Bern, Switzerland, CH-3012; e-mail: beutler@aiub.unibe.ch

INTRODUCTION

Since October 1993 a close and productive cooperation between the seven IGS Analysis Centers (ACs) resulted in an unprecedented increase of precision, reliability and the delivery speed of individual AC and combined IGS orbit/clock solutions. Currently the AC and IGS solutions approaching the 5cm(orbital)/0.5ns(clocks) precision are available within hours or days after observations rather than weeks or months. Combinations, comparisons, evaluations and exchange of information within the IGS are essential to continuous improvements of the service. The recent precision advances are mainly due to (a) modeling and analysis innovations and (b) better global deployment of receivers rather than instrumentation improvements as was the case during the initial stages of IGS. The modeling advances and innovations have been brought about by the AC cooperation and competition. With increasing solution precision and processing speed more emphasis should be put on analysis of possible solution biases to increase accuracy. The focus should be on multi-technique comparisons and analyses as individual, single technique solutions for station positions, velocities and EOP are susceptible to systematic effects.

The main focus of this position paper is to suggest ways how to increase precision, accuracy and efficiency of the IGS data processing and products. Antenna, tropospheric and ionospheric (error) modeling are not dealt with here as they are addressed in other sessions of this workshop.

ORBIT AND ERROR MODELING

Global GPS analyses effectively "absorb" some systematic effects. In particular solution parameters pertaining to solar radiation pressure and initial phase ambiguities can effectively either absorb or produce systematic biases. For example, a small constant change of a few cm in all satellite or receiver antenna offsets is effectively absorbed, with no effect on the solution scale or height.

The IGS combination/evaluation detects small orientation and origin differences for individual AC solutions. For example, a y-coordinate shift of about 5cm, noticed for JPL solutions at the end of 1994 (GPS Week 770), was later confirmed to be real and in

fact aligned the JPL solutions closer to the real (ITRF) geocenter (Figure 1). This alignment also resulted in a better statistics in the IGS long-arc analyses and GPS-SLR comparisons (Watkins, 1996).

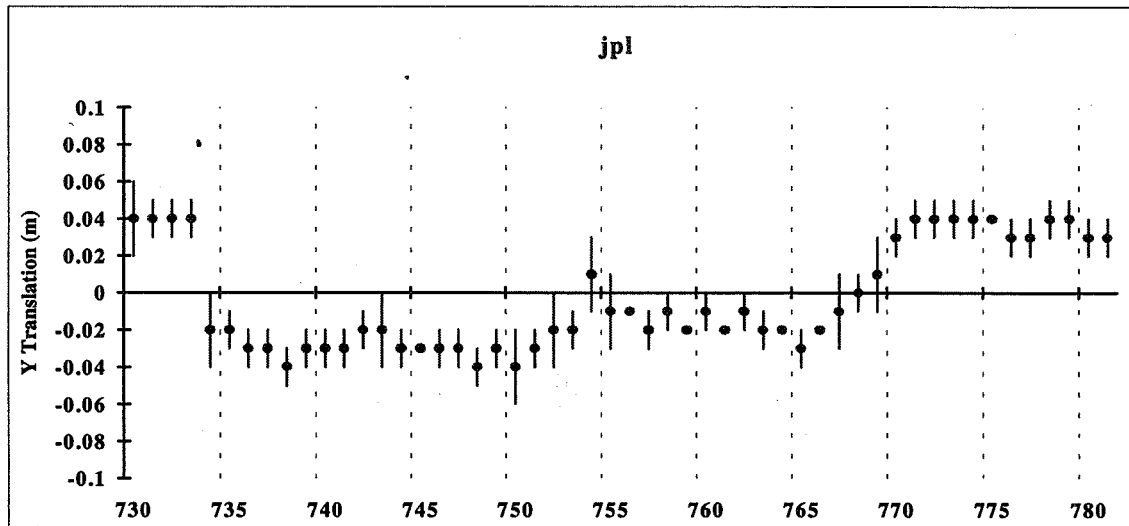


Figure 1. JPL 1994 Weekly Mean Y translations (meters) from IGS Final Orbits. For more details see the 1994 IGS Annual Report (Zumberge et al., 1995).

Subsequently, two additional ACs followed JPL and aligned their solutions with the geocenter, namely CODE in June 1995 by introducing small stochastic velocity changes once per revolution and SIO in November 1995 by introducing independent Rp scales for each revolution. Although the stochastic orbit/Rp modeling can effectively remove the coordinate origin bias, the cause may be different, e.g. a regionally biased tropospheric modeling and/or an unsuitable station distribution. The effect on unconstrained station solutions is even more pronounced: (a) y-coordinate shifts of up to 15cm have been detected in the weekly GNAAC (Global Network Associate AC) SINEX analyses, (b) a y-pole misalignment of about 0.5 mas has been also detected. Considering that these effects are almost an order of magnitude larger than the respective formal errors, and could bias combination solutions, it is strongly recommended that:

RECOMMENDATION # 1:

"All ACs make every effort to align their orbit, station and EOP solution to conform with the ITRF origin. It has been shown to be effectively achieved by means of stochastic orbit or Rp modeling."

Furthermore, the most significant precision/accuracy improvements are likely to be achieved by processing longer arcs than the current 1 to 3 days. This will only be possible with either improved or stochastic models, for radiation pressure in particular. Increased research effort in this direction is strongly recommended.

It must be pointed out that each change in the "dynamical modeling" has implications on

the estimation of the parameters defining the "change" of the reference frame during the time interval of the arc. Such parameters are UT1-UTC drifts (or length of day), drifts in the nutation in obliquity and ecliptical longitude. These aspects have to be carefully studied before any changes of the dynamical orbit models. For more information we refer to Rothacher et al. (1996) and Springer et al. (1996).

ITRF REALIZATION

Ideally an unbiased IGS combination solution for station coordinates, properly aligned with ITRF and spanning at least one year should be used as the day to day ITRF reference for the IGS data processing. In the past two years all IGS ACs have been fixing or tightly constraining the same 13 station ITRF92 or ITRF93 coordinates. This has the advantage of clear ties to ITRF which incorporates contributions by other space techniques, but it introduced discontinuities and may have caused distortions due to small GPS/ITRF inconsistencies and errors. An alternative, consistent but potentially biased realization might be achieved by selecting a combined GPS/IGS solution properly oriented and positioned with respect to the official ITRF.

Both approaches should converge with decreasing GPS biases and increasing ITRF accuracy. For the time being a compromise approach is to constrain rather than fix ITRF coordinates according to their estimated ITRF sigmas. For example, constraining the ITRF93 to 20 mm (1 sigma) produces virtually no relative position inconsistencies with respect to the corresponding free GPS solutions (note that unconstrained GPS solutions are not necessarily unbiased!). Considering that ITRF94 coordinates for the 13 stations have significantly improved while showing more realistic, larger formal errors, both approaches to ITRF realizations are expected to produce similar results. Figure 2 and Table 1 compare the ITRF94 solutions (P01 in Figure 1 and P01, P02, P03 in Table 2) to a 16 week average of the MIT SINEX weekly station combinations (MIT95P01(SNX)):

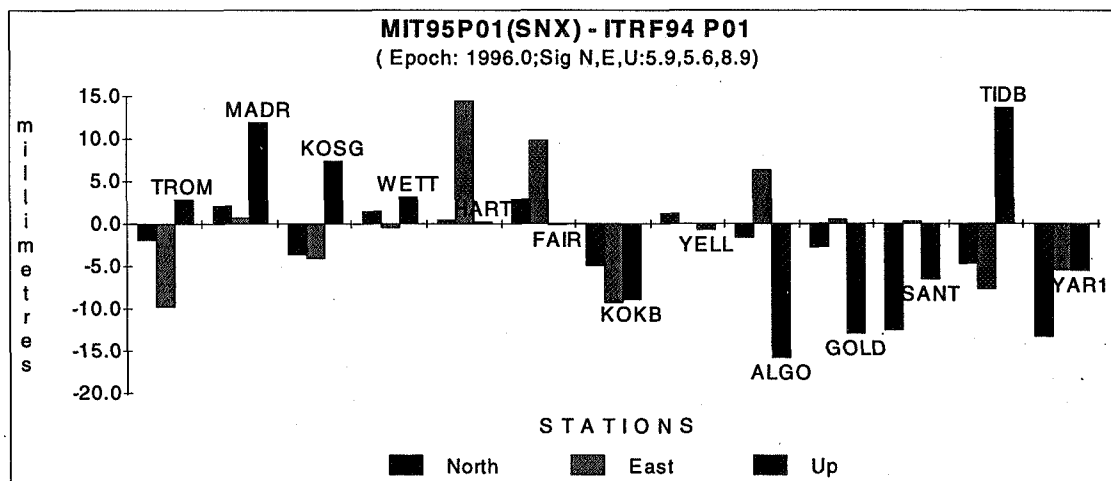


Figure 2. POSITION DIFFERENCES FOR THE 13 ITRF STATIONS USED BY IGS FOR ITRF REALIZATION

Table 1. ITRF94 P01,P02,P03 coordinate differences (after a 7 parameter transformation) for the 13 ITRF stations used by IGS for ITRF realization. (Epoch 1996.0; P01 - ALL techniques + GPS(COD,EMR,JPL); P02 - GPS(COD,EMR,JPL); P03 - ALL techniques except GPS(COD,EMR,JPL))

	DX	DY	DZ	N	E	Up	
Mean (mm)	2.7	4.0	-3.4	-3.0	0.4	-1.2	MIT95P01-ITRF94 P01
Sigma (mm)	5.0	7.4	6.8	5.1	6.7	8.9	
Mean (mm)	0.4	5.1	-1.4	-1.6	-2.4	-0.1	MIT95P01-ITRF94 P02
Sigma (mm)	7.0	7.1	6.2	4.9	9.0	7.1	
Mean (mm)	7.2	-2.6	-11.9	-7.5	-4.9	0.5	MIT95P01-ITRF94 P03
Sigma (mm)	10.9	8.6	14.9	15.1	7.5	15.6	
Mean (mm)	3.5	0.8	1.2	2.2	1.0	-0.1	MIT95P01-ITRF93 C02
Sigma (mm)	5.9	9.5	8.8	8.8	4.7	10.6	
Mean (mm)	-1.4	1.9	-4.3	-5.0	-1.1	-0.7	ITRF93C02-ITRF94 P01
Sigma (mm)	8.4	10.4	8.6	9.0	7.1	11.1	

More than 13 stations and a better distribution are needed for an improved ITRF realization. A close examination of the ITRF94 solution, similar to the examination of the previous ITRF solutions in the past, has not reveal any suitable additional stations due to weak station velocity solutions. Therefore, it is suggested that:

RECOMMENDATION # 2:

"The ITRF94 (P01) coordinates of the 13 ITRF stations are used for the IGS realization of ITRF starting on June 30, 1996 (Wk 0860)."

To mitigate the small discontinuities on June 30, 1996 (ITRF94/ITRF93) and January 1, 1995 (ITRF93/ITRF92) it is also recommended that IGS provides appropriate parameters for transformation of the IGS products.

IGS ORBIT/CLOCK COMBINATIONS

The IGS orbit/clock combinations were originally implemented in two phases: the first, so called Rapid orbit/clock combination, was initially produced within 15 days and based on the IERS(Bull. A) EOP; it is now completed within 11 days and averaged directly in the ITRF (without external EOP alignment). The second and final phase, known as the Final combination is based on the IERS(Bull. B) EOP and is available with a delay of about two months. The main reason for the Final combination was to benefit from the final IERS EOP combination and its stability, and to allow the ACs to revise and resubmit their solutions.

Since January 1, 1996, six ACs have provided input for generating an IGS Preliminary

orbit/clock combination which is now approaching precision of about 10cm/1ns with a delay of only 38 h .

During 1995 systematic differences were noticed between both IERS EOP (i.e. Bull. A and B) and the IGS pole combination series. It has been shown that the above differences are mainly due to smoothing procedures employed in the production of the IERS series. Furthermore, GPS/VLBI comparisons show 0.1mas precision for the IGS pole coordinates (see IGSMAIL#1072). The smoothed out signal of the IERS series was as high as 1mas which may affect significantly the Final Orbit precision. The ACs rarely resubmit their solutions since the preliminary processing has been initiated and the IGS Rapid Orbits are now as precise and stable as the IGS Final ones, we therefore propose:

RECOMMENDATION # 3 :

"To economize and optimize the IGS combination efforts and to reduce delays in the IGS Final orbits/clock production it is recommended that starting on June 30, 1996 (Wk 0860) the current IGS Rapid combinations become the IGS Final product and the IGS Preliminary (IGP) product replaces the IGS Rapid (IGR) combination. In this way the precise IGS Final products will become available within 11 days and the IGS Rapid orbits/clocks will be available in about 1 day."

PRELIMINARY/RAPID ORBIT/CLOCK COMBINATIONS

Since January 1, 1996 up to six ACs (COD, EMR, ESA, GFZ, JPL, SIO) have been providing input for the IGS Preliminary orbit/clock computations. Despite the initial difficulties, like data delivery delays and INTERNET problems, this IGP project has exceeded expectations. Delays in data availability are driving the ACs solution precision rather than the number of stations, since often the remote stations providing required station geometry, are most prone to data delays. Table 2 gives a summary of IGP statistics and solution delays. The standard deviations (std) for orbit rms and delivery delays indicate variations in precision and processing delays. Also shown in Table 2 are number of days when AC's input has not been available or had to be excluded .

Table 2: IGS Preliminary orbit/clock combination statistics for days between January 14 to February 29, 1996. (Delays are in hours since the last observation)

CENTER	DELIVERY(h)		ORB RMS(cm)		MISSED/EXCL days
	mean	std	mean	std	
COD	14	4	23	16	1
SIO	18	4	19	8	10
EMR	21	5	15	10	2
JPL	21	4	12	3	2
ESA	26	7	25	8	12
GFZ	30	4	13	10	7

Prompt and reliable station tracking data availability and AC solution input also during weekends and holidays are very important to this project; it is therefore proposed:

RECOMMENDATION # 4:

"Timely data delivery is crucial for rapid and precise IGS product generation and it is therefore essential to meet IGS data delivery deadlines particularly for the selected global stations. For these stations a 6 hour maximum delay should not be exceeded and the data equalization of the IGS Global centers should not require more than 2 hours."

From the above table it is apparent that the current 36h submission delay deadline can be reduced substantially, thus:

RECOMMENDATION # 5:

"It is recommended that the current submission delay deadline of 36h for IGP be reduced to 23h after the last observation as of June 30, 1996 (Wk 0860). If all participating AC solutions arrive prior to this deadline the IGS combination is to be completed within an hour after the last submission. "

There is also considerable interest in IGS orbit predictions to be available in real time, or with delays much shorter than 1 day. There are at least two alternatives to such IGS predictions, one is completely analogous to the current IGS combination, i.e. a weighted average of AC predictions. The second, potentially more reliable and precise, is to use an advanced orbit model to fit several preceding days of IGS orbits and to generate IGS orbit predictions. Benefits and feasibility of different orbit prediction approaches will have to be first discussed and evaluated by all AC.

More research is required in order to make the satellite clock solutions more robust and precise. Additionally, precise external time comparisons at stations equipped with very stable HM clocks are needed to assure continuity and compatibility with the international time standards. For more details and results of IGS orbit/clock combinations see the poster at this workshop.

REFERENCES

Rothacher, M., Beutler, G., Springer, T. (1996). "The Impact of the Extended CODE Orbit Model on the Estimation of Earth Rotation Parameters." IGS Analysis Center Workshop, Silver Spring, March 19-21, 1996.

Springer, T., Rothacher, M., G. Beutler (1996). "Using the New CODE Orbit Model for the Production of Rapid (12h) Orbits: First Experiences." IGS Analysis Center Workshop, Silver Spring, Md., March 19-21, 1996.

Watkins, M.M.. "GPS/SLR orbit comparisons", IGS Analysis Center Workshop, Silver Spring, Md., March, 19-21, 1996.

Zumberge, J.F., R. Liu and R.E. Neilan (edited by) . " 1994 IGS Annual Report, IGS Central Bureau, Jet Propulsion Laboratory, Pasadena, Cal., USA, 1995.

Evaluation of IGS GPS Orbits with Satellite Laser Ranging

M. M. Watkins, Y. E. Bar-Sever, and D. N. Yuan

Jet Propulsion Laboratory, California Institute of Technology, Pasadena, California

Abstract

The accuracy with which orbits for the Global Positioning System (GPS) spacecraft can be computed directly affects the accuracy of the resulting site coordinates and polar motion. Several groups routinely analyze GPS ground tracking data to compute precise orbits and terrestrial reference frame solutions. In this paper, we infer the accuracy of the orbits of two of the GPS satellites by comparing to independent laser ranges of subcentimeter accuracy obtained by a small but reasonably well distributed network of tracking sites. We find that all seven International GPS Service for Geodynamics (IGS) analysis centers achieve range residual root mean square (rms) errors at or below the 100 mm level. The best orbit solutions, from JPL, CODE, and the IGS combined product, yield a residual rms of about 50 mm. These residuals are consistent with three dimensional orbit errors of less than 150 mm. Estimating yaw rates for the spacecraft during shadow events, and using these estimates to compute the laser residual, significantly improves the fit. A small mean residual value of -15 to -30 mm seems to exist for most centers and laser sites which is not fully explained at present, but may be due to uncertainties in the corrections to the laser data, such as the reflector to spacecraft center of mass vector or small reference frame differences between the SLR sites and the GPS orbits.

Introduction

Until the launch of GPS35 (PRN 5) in August, 1993, no other tracking type was available for the GPS spacecraft. GPS35 used a laser retroreflector array (LRA) derived from that used on the Russian GLONASS system navigation satellites which are routinely tracked in Russia with SLR. The LRA is on the nadir (earth pointing) side of the GPS spacecraft, with offsets from the center of mass of 0.8626, -0.5245 , and 0.6584 meters in the spacecraft x , y , and z axes, respectively [Degnan and Pavlis, 1994]. An identical system was used for GPS36 (PRN36) which was launched in March, 1994. We have used this SLR data to evaluate the accuracy of the GPS orbital ephemerides from the 7 IGS Analysis Centers and the IGS combined orbit. The discussion is a summary of the detailed discussion in [Watkins et al., 1996].

Each SLR observation is actually a five minute normal (average) point of higher rate data to reduce the random noise component in the measurements. Each range normal point should be accurate to about 10 millimeters, with the limiting error sources being tropospheric refraction and uncalibrated range biases in the laser system. For the period studied in detail in this paper, 1 Jan 1995 – 30 November 1995, a total of 469 passes (4464 points) for GPS35 and 36 were obtained from 11 sites, presented in Table 1 with both geographic location and Crustal Dynamics Project ID. Note that although the first few sites dominate the observations, they are thankfully well distributed. Because of the sparseness of the SLR tracking of GPS35 and 36, we have elected not to actually fit spacecraft orbits to this data. Instead, we will use the data as an external check on ephemerides computed using only GPS data. This will give a unique and independent assessment of the orbit error derived from the routine analysis of GPS data, and hence present in the solution for site positions and Earth orientation. Because of the high altitude of the GPS spacecraft, observations from the ground, even down to low elevation, are still nearly radial from the spacecraft point of view. In fact, the largest departure from the truly radial direction is about 13

degrees, and so the range residual is a measure primarily of the radial component of orbit error. Thus, a scale factor may be computed to calibrate the radial overlap that may be applied to the cross-track (orbit normal) and alongtrack (transverse) components to approximate the true three dimensional orbit accuracy.

Results

We have taken the orbits from each of the seven analysis centers and from the IGS combined orbit for the period 1/1/95 - 11/30/95 and computed SLR residuals for each using the GIPSY-OASIS II software developed at JPL [Webb and Zumberge, 1995]. The models used for the SLR processing generally adhere to the IERS Standards of McCarthy [1992]. These include solid tides, ocean tidal loading, and we have additionally modelled the subdaily Earth orientation variations due to ocean tides. Since the sp3 files are expressed in the Earth fixed frame, no daily Earth orientation values are required to evaluate the laser residuals. We have fixed the coordinates of the laser sites to the ITRF93 values and used the marker eccentricities of the CSR94L01 solution [Eanes and Watkins, 1994]. Note that no parameters are adjusted from the laser data during the evaluations. The orbits were interpolated to the times of the SLR data using a tenth order polynomial, which has millimeter accuracy compared to a numerical reintegration of the orbit. Finally, since only JPL adjusted the GPS spacecraft yaw rates, we have chosen to feed the JPL estimates back for all centers. These corrections are only applicable during eclipsing periods, which during our data span are 15 June - 31 July for GPS35 and 5 March - 26 April and September - October for GPS36. The fits are summarized during three orbit regimes. The first, denoted in Table 2 as SUN, are those observations obtained when the GPS spacecraft is not in eclipse season. Those denoted ECL are in eclipse season, but not in eclipse during the particular observation. Finally, those denoted SHA are either actually in shadow or within 30 minutes of shadow exit at the time of the SLR observation, and may be maneuvering according to the model described in Bar-Sever [1995a,b]. The resulting fits over all data for each center and each regime are presented in Table 2. We have edited outlier laser residuals which exceeded 300 mm.

Discussion

Several conclusions can be drawn from Table 2. The first is that the radial orbit error for the GPS spacecraft is as low as 50 mm. We say radial here because, as mentioned above, the geometry of the GPS orbit makes the laser data typically within 10 degrees of the radial direction as seen from the spacecraft. Interestingly, this figure is actually slightly lower than the average radial overlap for the GPS spacecraft, and indicates that the overlaps are pessimistic indicators of orbit accuracy. Scaling the radial overlap fit to radial orbit error and applying that scale factor to the other components yields implied orbit errors of 50, 70, and 100 mm in the HCL components. We conclude then that the three dimensional orbit error typically does not exceed 150 mm.

Another conclusion that can be drawn is that the fit rms is indeed degraded during eclipse season, and more so during a shadow event. The JPL orbit, which is the only one estimated simultaneously with GPS s/c yaw rates during eclipse, suffers by far the least degradation. Note that two separate effects cause the range error reflected in the SLR evaluation in the ECL and SHA regimes; a kinematic effect stemming from errors in the applied yaw rates which cause the computed LRA position to be in error, and a dynamic error in the GPS ephemerides due to radiation pressure mismodelling from attitude errors on shadow exit.

References

- Bar-Sever, Y. E., et al., Fixing the GPS Bad Attitude: Modeling GPS Satellite Yaw During Eclipse, *Navigation*, in press, 1995a.
- Bar-Sever, Y. E., A New Model for the GPS Yaw Attitude, *Manuscripta Geodaetica*, in press, 1995b.
- Boucher, C., Z. Altamimi, and L. Duhem, *IERS Tech. Note 18*, Results and Analysis of the ITRF93, Obs. de Paris, Oct., 1994.
- Eanes, R. J., and M. M. Watkins, Earth Orientation and Site Coordinates from the Center for Space Research Solution CSR94L01, *IERS Tech. Note 15*, Earth Orientation, reference frames, and atmospheric excitation functions submitted for the 1993 IERS Annual Report, P. Charlot (ed.), Obs. de Paris, Sep. 1994.

- Kouba, J. Analysis Coordinator Report, *IGS Annual Report for 1994*, JPL Publication 95-18, Jet Propulsion Laboratory, Pasadena, CA, Sept. 1995.
- McCarthy, D. (ed.), *IERS Standards (1992)*, IERS Tech. Note 13, Observatoire de Paris, July, 1992.
- Degnan, J. and E.C. Pavlis, Satellite Ranging to the GPS spacecraft, *GPS World*, pp. 95-113, New York, 1993.
- Remondi, B.W., NGS Second Generation ASCII and Binary Orbit Formats and Associated Interpolation Studies, Proceedings of the XXth General Assembly, International Union of Geodesy and Geophysics, Vienna, Austria, Aug. 11-24, 1991, 28 pp.
- Watkins, M. M., Y. E. Bar-Sever, and D. N. Yuan, Evaluation of GPS Orbital Ephemerides with Satellite Laser Ranging, *Jour. of Geodesy*, in review, 1996.
- Webb, F. H., and J. F. Zumberge (eds.), An Introduction to GIPSY/OASIS II, JPL Course Notes, Jet Propulsion Laboratory, California Inst. of Tech., Pasadena, CA (JPL Internal Document, Contact JPL IGS Central Bureau), July 1993.

Table 1. SLR Data for GPS35 and GPS36

Site	ID	Passes	
		GPS35	GPS36
Haleakala, USA	7210	56	56
Monument Peak, USA	7110	61	32
Yaragadee, Aust.	7090	32	42
Wettzell, Germany,	8834	35	28
Royal Greenwich Obs, U.K.	7840	22	14
Graz, Austria,	7839	16	10
McDonald Obs., USA	7080	15	6
Greenbelt, USA	7105	9	9
Orroral, Aust.,	7843	3	6
Greenbelt, USA	7918	4	0
Quincy, USA	7109	4	0

Table 2. SLR Data Fit to GPS Ephemerides

Center	SUN 3685 pts.		ECL 729 pts.		SHA 50 pts.	
	mean	rms	mean	rms	mean	rms
JPL	-24	51	-9	45	-34	57
CODE	-20	52	-17	70	-16	103
IGS	-11	55	15	72	-3	96
SIO	6	66	58	116	0	125
GFZ	13	77	13	95	-16	88
EMR	-14	82	19	96	-29	130
NGS	-14	92	21	122	0	150
ESA	-1	91	-56	191	-10	250

All units are millimeters

Using the Extended CODE Orbit Model

First Experiences

T.A. Springer, M. Rothacher, G. Beutler
Astronomical Institute, University of Bern
Sidlerstrasse 5, CH-3012 Bern, Switzerland

Abstract

The Extended CODE Orbit Model, an empirical orbit model proposed by *Beutler et al.* [1994], was used for the first time in the actual parameter estimation procedures (using the Bernese GPS Software), to model the orbits of the GPS satellites at the CODE Analysis Center of the IGS. Apart from six Keplerian elements this orbit model consists of nine instead of the usual two parameters to take into account the deterministic part of the force field acting on the satellites.

In this article we focus on the optimum use of this Extended CODE Orbit Model for the CODE IGS activities. Of particular interest are the generation of *rapid orbits*, with only 12 hour delay after the last observation, and (IGS) orbit prediction.

Introduction

The Center for Orbit Determination in Europe (CODE), is one of at present seven Analysis Centers (AC's) of the International GPS Service for Geodynamics (IGS). CODE has been formed as a joint venture of the Astronomical Institute of the University of Bern (AIUB), the Swiss Federal Office of Topography (L+T), the German Institute for Applied Geodesy (IfAG), and the French National Geographical Institute (IGN). CODE is located at the AIUB in Bern.

Since the start of the IGS in June 21, 1992, CODE has produced ephemerides for all active GPS satellites and daily values for the earth rotation parameters. Starting January 2, 1994, all the individual AC orbit (and clock) solutions have been evaluated and combined into official IGS orbit/clock solutions by the Analysis Center Coordinator, [*Beutler et al.*, 1995; *Kouba*, 1995]. The IGS combinations/evaluations, summarized in weekly IGS reports, clearly demonstrate the steady improvements in both, precision and reliability, for all AC's.

The CODE orbit position RMS, compared to the combined IGS orbit, reached the 10 cm level by the end of 1994. By the end of 1995 the RMS had decreased to a level of 6 cm.

Thanks to this improvement of the orbit quality it has become clear that the classical orbit model, using eight parameters, is not accurate enough to guarantee an orbit quality below the 10 cm level. Different AC's solved this problem in different ways by either using deterministic or stochastic orbit models. At CODE the estimation of small velocity changes (pseudo-stochastic pulses) for all satellites at noon and midnight was implemented, starting June 4, 1995, to deal with the model deficiencies of the classical orbit model. However, by mid 1995 it also became clear that the Extended CODE Orbit Model as proposed by *Beutler et al.* [1994] and used in the IGS orbit comparisons for the long-arc analysis [*Beutler et al.*, 1995] should also be capable of producing orbits better than the 10 cm level RMS. Therefore, in early 1996, the model was finally fully implemented into the Bernese GPS Software Version 4.0 and first experiences were gathered.

We will first show some results of the initial tests performed to get a better understanding of the model. We will then discuss two interesting applications of the Extended CODE Orbit Model. Apart from using the new model for our normal processing method (overlapping 3-day arcs) we also apply the new model for the production of our rapid orbits (12 hour delay) and for orbit predictions.

The Extended CODE Orbit Model

In *Beutler et al.* [1994] and *Rothacher et al.* [1996] the new orbit model is discussed in detail, therefore here only the basic characteristics are summarized.

For the Extended CODE Orbit Model the acceleration \vec{a}_{rpr} due to the deterministic part of the solar radiation pressure model is written as:

$$\vec{a}_{rpr} = \vec{a}_{ROCK} + \vec{a}_D + \vec{a}_Y + \vec{a}_X \quad (1)$$

where \vec{a}_{ROCK} is the acceleration due to the Rock-model, and

$$\begin{aligned} \vec{a}_D &= [a_{D0} + a_{DC} \cdot \cos u + a_{DS} \cdot \sin u] \cdot \vec{e}_D = D(u) \cdot \vec{e}_D \\ \vec{a}_Y &= [a_{Y0} + a_{YC} \cdot \cos u + a_{YS} \cdot \sin u] \cdot \vec{e}_Y = Y(u) \cdot \vec{e}_Y \\ \vec{a}_X &= [a_{X0} + a_{XC} \cdot \cos u + a_{XS} \cdot \sin u] \cdot \vec{e}_X = X(u) \cdot \vec{e}_X \end{aligned} \quad (2)$$

where a_{D0} , a_{DC} , a_{DS} , a_{Y0} , a_{YC} , a_{YS} , a_{X0} , a_{XC} , and a_{XS} are the nine parameters of the Extended model, and

- \vec{e}_D is the unit vector sun-satellite,
- \vec{e}_Y is the unit vector along the spacecraft's solar-panel axis,
- $\vec{e}_X = \vec{e}_Y \times \vec{e}_D$,
- u is the argument of latitude

The Extended CODE Orbit Model clearly is a generalization of the standard orbit model

which is, at this time, still used for the official CODE solutions.

To gain experience with the model a test data set of 4 weeks was selected (GPS weeks 0836–0839). Several different 3-day solutions and a couple of 5-day solutions were performed. Furthermore, a test solution, based on the complete (15 parameter) model, was added to the variety of solutions in our reprocessing experiment of the 1995 IGS data.

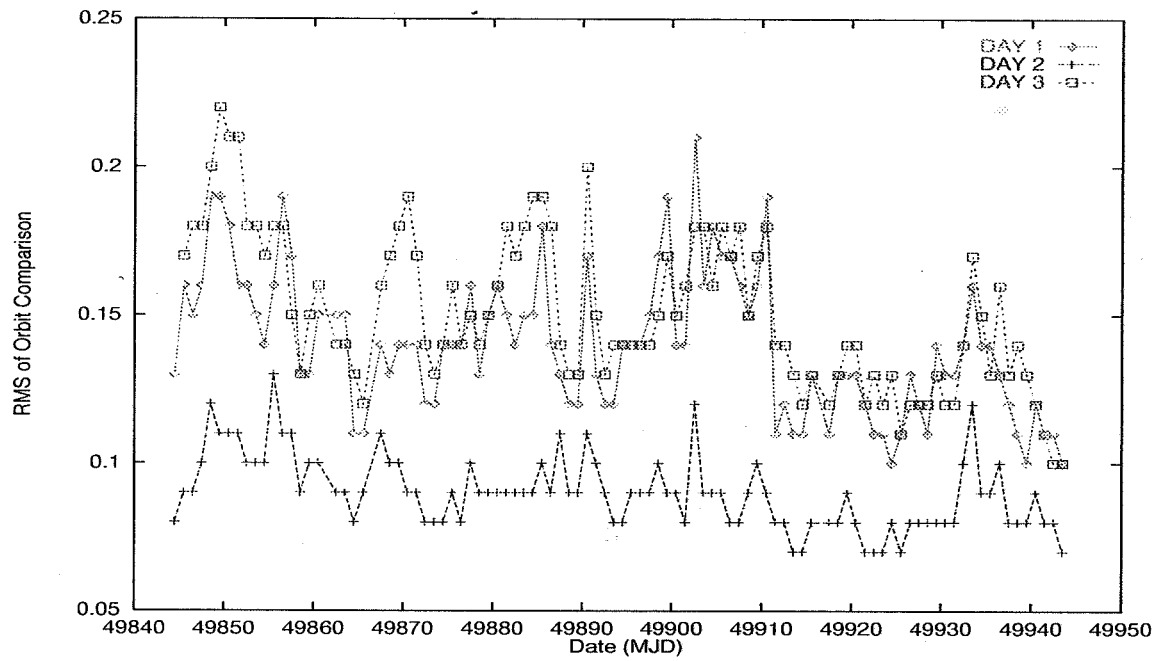
First Results

The most striking result stems from our 1995 reprocessing experiment where we created two different types of solutions. One was based on our current IGS routine strategy estimating the conventional (8 parameter) orbit model and 2 pseudo-stochastic pulses per day for all satellites in the along-track and radial directions. This means that for each satellite five of these pulses are estimated over a 3-day arc, all in all ten additional parameters per satellite. So, for each satellite 18 parameters are estimated: 6 Keplerian elements, 2 radiation pressure coefficients and 10 velocity changes. The second type of solutions used the Extended CODE Orbit Model where pseudo-stochastic pulses were estimated only for the eclipsing satellites and satellite PRN23, which has a solar panel defect. This means that 25 parameters were estimated for the eclipsing satellites and satellite PRN23, but only 15 parameters for all other satellites.

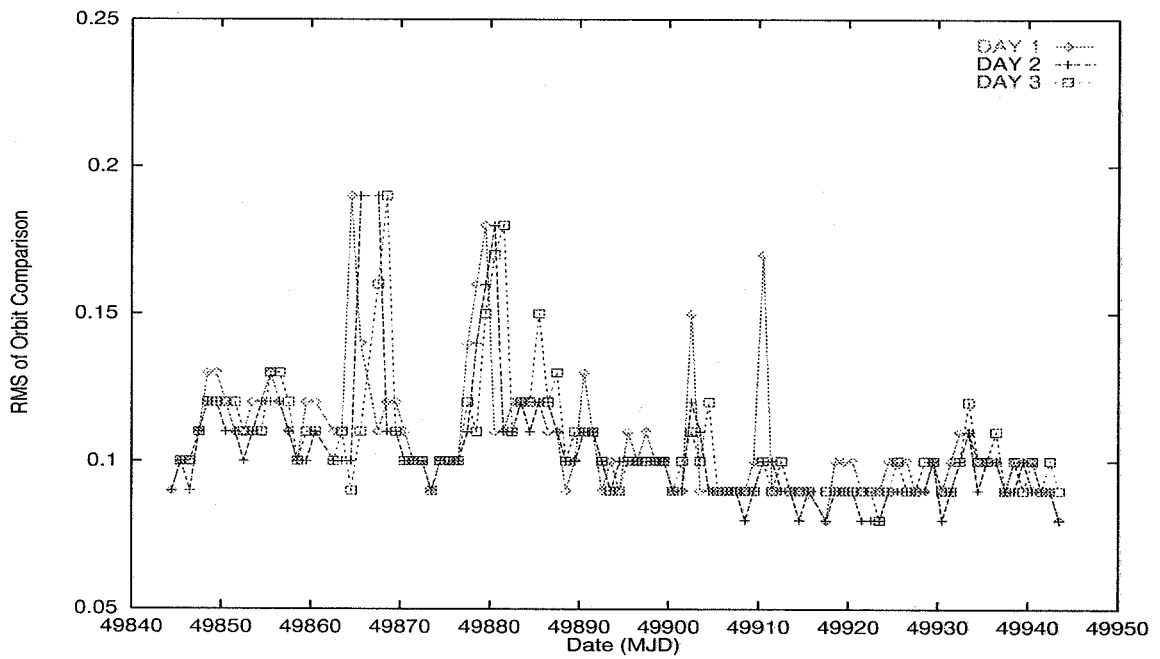
For both types of 3-day solutions individual precise orbit files were created for each day of the 3-day arcs. These (daily) precise files were then compared to the IGS final orbits. The RMS errors of the comparisons, using 7 parameter Helmert transformations (w.r.t. the IGS final orbits), are shown in Figure 1 for the 1995 reprocessing. Clearly the first and third day show a significant decrease of precision when using the conventional orbit model whereas with the Extended CODE Orbit Model all days are of the same high quality.

That the middle day of the conventional orbit model shows a smaller RMS than the middle day of the Extended model is most likely explained by the fact that this solution is very similar to the CODE solution which was taking part in generating the IGS final orbit. However, a detailed analysis using fully independent Satellite Laser Ranging (SLR) data, seems to indicate that using the complete model for the 3-day solutions actually leads to a slightly less accurate orbit solution for the middle day. Different tests using the 4-week data set indicated that for 3-day arcs the Extended model provides too many degrees of freedom. Not all nine parameters should be estimated using an arc length of “only” three days. Correlations between the orbit parameters but also with other parameters, like UT1-UTC, are significant. With 5-day arcs the correlations seem to decrease to an acceptable level. We should note that no tests were performed using a priori constraints on the orbit parameters. If a certain orbit parameter was set up it was estimated without any constraints.

One of the aims of the tests with the 4-week data set was to determine how to make optimum use of the Extended Model for 3-day arcs which we are using for our official IGS



(a) Conventional Orbit Model



(b) Extended CODE Orbit Model

Figure 1. Unweighted RMS values of the orbit comparisons of the 3 individual days of a 3-day arc with the final IGS orbits.

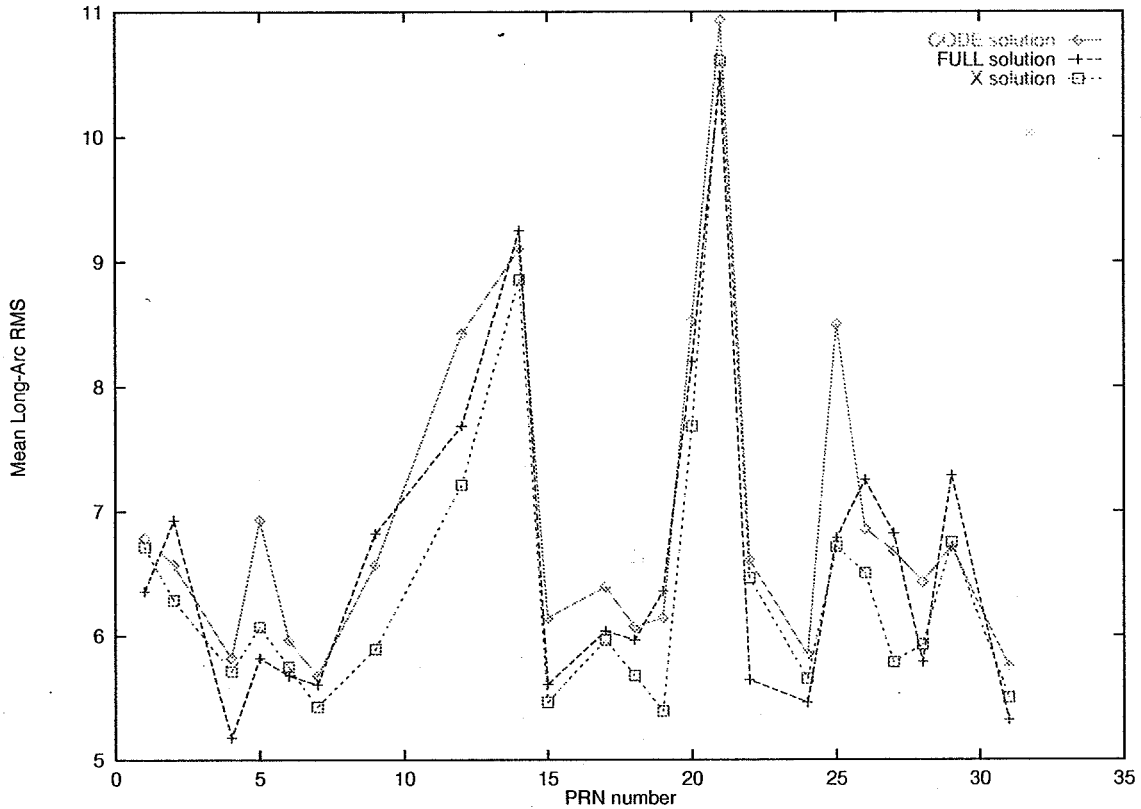


Figure 2. Mean long-arc RMS values over the 4-week test period.

contributions since 1992. The best strategy we have found so far is to not estimate any “X” terms (a_{X0} , a_{XC} , a_{XS} in (2)) of the Extended model and still use five pseudo-stochastic pulses over three days for each satellite. Figure 2 shows the quality, per satellite, of the official CODE solution, a solution using the full Extended model (labelled “FULL”) and a solution using the Extended model without estimating any X-terms (labeled “X”). The RMS is the mean of all the long-arc (7-day) orbit checks performed for the 4-week test data set. Clearly the X-solutions perform better than both other solutions for most satellites. Only for a few satellites the “FULL” solution performs better than the “X” solution.

The stochastic pulses seem to absorb certain (orbit) model deficiencies more efficiently than the parameters of the Extended model, in particular for eclipsing satellites. The directions of the stochastic pulses are based on an orbit specific coordinate system (along-track, radial and out of plane components), whereas the components of the Extended model are defined as described in (2). Furthermore these pulses are estimated every 12 hours which makes them almost exactly “once per revolution” terms. They should therefore have a similar effect as the perturbation model proposed by Colombo [1989] which is well suited to absorb (gravity related) periodic unmodeled forces. In 1994 it was clearly shown [Beutler et al., 1994] that the Extended model performs much better than the Colombo model.

However, at that time the orbit accuracy, based on a 7-day arc fit, was of the order of 15 cm whereas today we are reaching the 5 cm level. With these orbit accuracies it is possible that the errors in the earth gravity field model (GEM-T3 model truncated to degree and order eight) are becoming significant.

It is clear that the modeling of the orbits of eclipsing satellites should be further improved. Implementing the "attitude" model [Bar-Sever, 1995] would improve the model for the eclipsing satellites, but other methods might be useful, too. An alternative method, to solve the modeling problems of the eclipsing satellites, might be a kind of "kinematic" solution for the motion of the satellite antenna phase center during the eclipse phase and for a time period of 30 minutes afterwards.

Applications of the Extended CODE Orbit Model

Rapid Orbits

Since January 1, 1996, the IGS is making available rapid combined orbits with a 36 hour delay. CODE participates in this new IGS activity with orbits which are available within 12 hours. The limiting factor for the accuracy of the rapid orbits is the availability of station data with a good geographical distribution. Especially with our 8 hours deadline, and the bad internet performance between Europe and America during office hours, the available data tend to have a bad geographical distribution. A good way to solve this problem is to use longer arcs. We have to keep in mind however, that we will have to use the last day of an n-day arc as rapid orbit product. With the conventional model the last day would be significantly less accurate than the middle day of the same arc, see Figure 1 The fact that with the Extended model all days of an n-day arc (n=1,2..5) are of the same quality makes it possible to use longer arcs for the rapid orbit computations thereby making the rapid orbit product much less sensitive to the geometry of the available data.

Figure 3 shows the quality of our rapid orbits since January 1, 1996. Around MJD 50130 (February 17) we started to use the Extended Orbit Model to produce 5-day arcs, the last day of this 5-day arc being our official IGS rapid orbit contribution. One clearly sees that, after some initial problems, the 5-day solution (the last day of a 5-day arc) is performing much better than the 1-day solution. In reality the performance is even better because here the unweighted RMS is given which is dominated by satellites with modeling problems, which are of course more pronounced in the 5-day arcs than in the 1-day arcs. The peaks, which show up in the 1-day solutions due to a bad station geometry, are hardly visible in the 5-day solution, although the 5-day arcs are based on exactly the same observations (apart from using more days, of course).

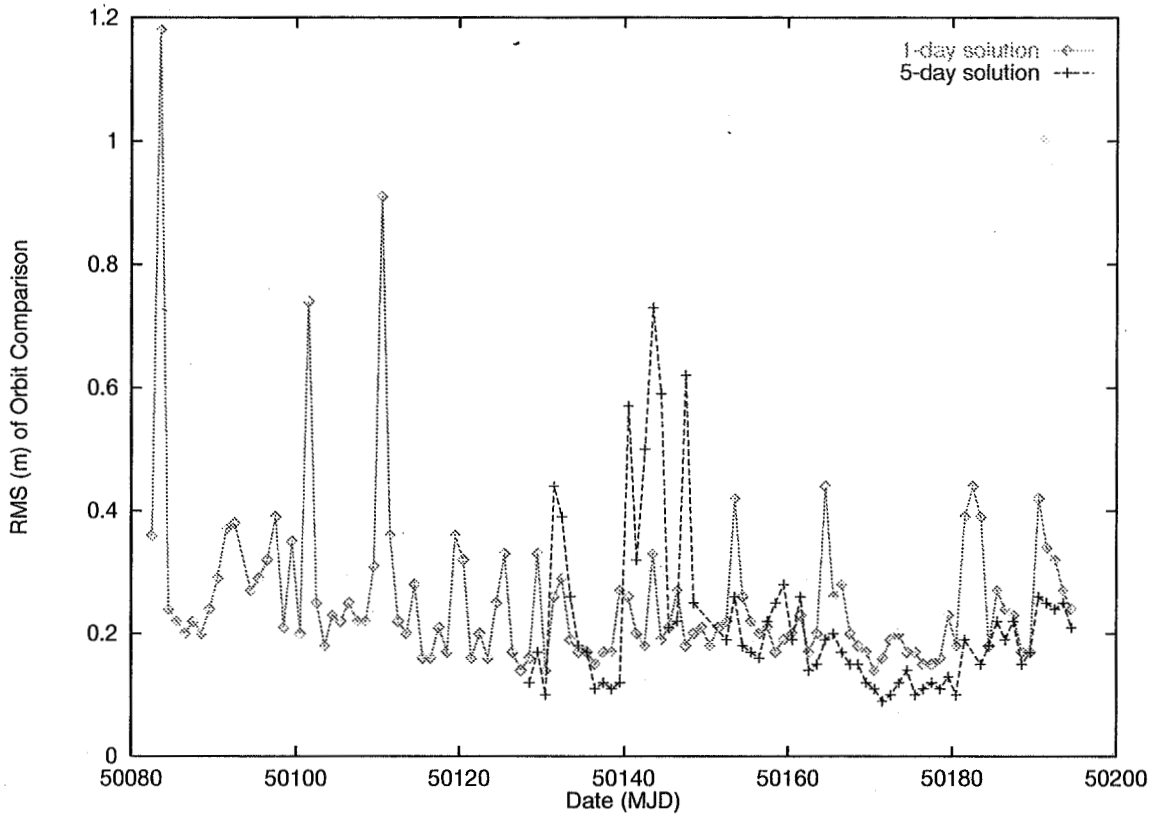


Figure 3. Unweighted RMS values of orbit comparisons showing the quality of the 1-day and 5-day rapid orbits. CODE orbits were used as reference.

Orbit Predictions

Everyone familiar with the weekly summaries of the IGS orbit combination is aware of the fact that the Extended CODE Orbit Model (used for the long-arc analysis of the IGS orbit combination) is capable of modeling the orbits of the GPS satellites over seven days at the few centimeter level. This indicates that the model should also be well suited to generate accurate orbit predictions.

At CODE we create 24- and 48-hour predictions based on our 1-day routine solutions for internal use. The 24-hour predictions are used as a priori orbits in the IGS routine processing rather than the broadcast ephemerides since the predictions have a better accuracy. After the implementation of the Extended model into our software we noticed a significant improvement of our predictions. Figure 4 shows the quality difference of the orbit predictions using the conventional and the Extended model. With the conventional (8 parameter) orbit model our 24-hour predictions had a quality around the 75 cm level and the 48-hour predictions around the 130 cm level. With the Extended (15 parameter) model the quality of the predicted orbits is now around the 25 and 60 cm level for the 24- and 48-hour

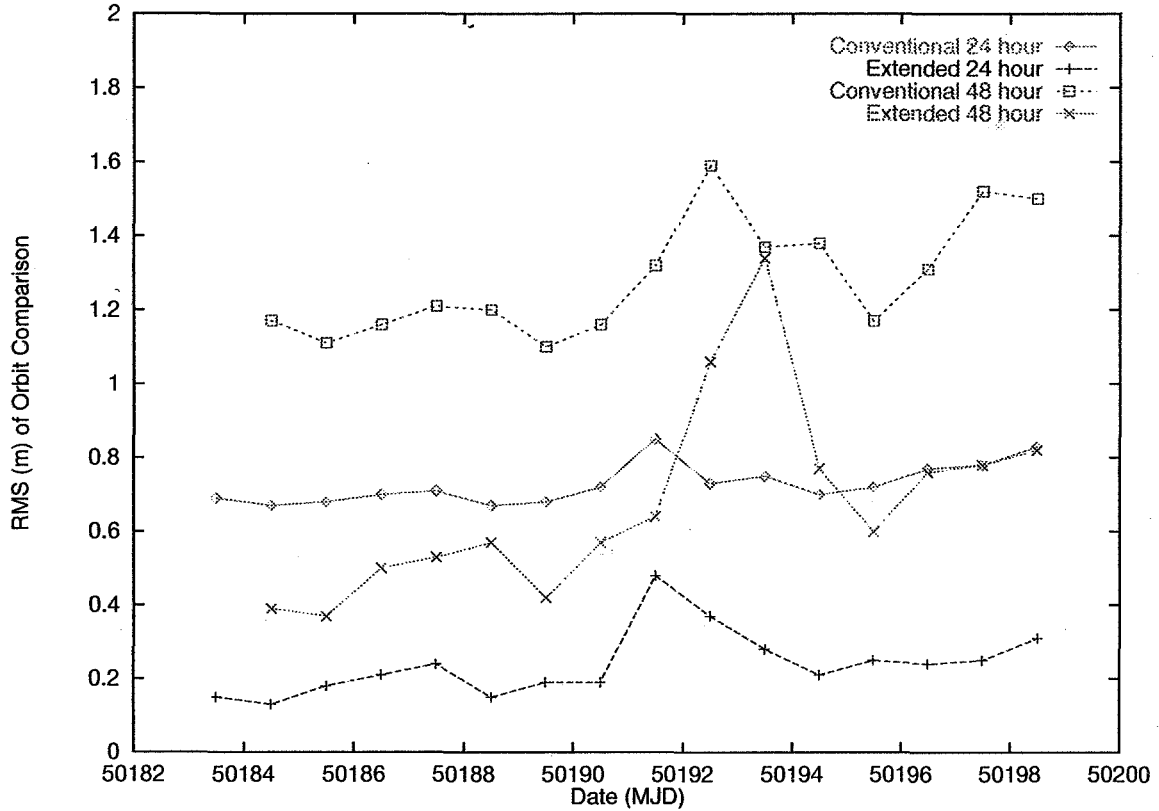


Figure 4. Unweighted RMS values of orbit comparisons showing the quality of 24- and 48-hour orbit predictions using the conventional and Extended orbit model. CODE orbits were used as reference.

predictions respectively. As expected the Extended model is better suited for predictions than the conventional model. The 48-hour predictions of the Extended model are even better, in most cases, than the 24-hour predictions of the conventional model!

At these accuracy levels, and for real-time purposes, the extrapolation of the Earth Orientation parameters starts to play an important role. For predictions to be used in real-time data analysis, based e.g. on the IGS 36-hour orbits, it will be mandatory to predict the Earth Orientation parameters with an accuracy of about 1 milli arc second.

Summary and Outlook

Our first tests revealed that the Extended CODE Orbit Model is very well suited the CODE IGS activities but also for long-arc analyses (arcs longer than 3 days). Furthermore, we have shown that the model gives an important contribution to the generation of high precision rapid orbits and orbit predictions. Our rapid orbits, based on the Extended model, have an

accuracy of approximately 10 cm. Prediction quality is at the 20 and 60 cm level for 24- and 48-hour orbit extrapolations, respectively.

For short arcs, 1- to 3-days, one has to be aware of correlations between some of the parameters of the Extended model. It may not be necessary, and possibly even harmful, to solve for all nine parameters of the Extended model. The best 3-day arc solutions were obtained by not estimating any "X" terms of the Extended model but still estimating five pseudo-stochastic pulses for each satellite in the along-track and radial directions. These pseudo-stochastic pulses, as implemented for the CODE IGS orbit products since June 4, 1995, seem to be capable of absorbing certain (orbit) model deficiencies more efficiently than the parameters of the Extended model. This aspect will be studied in more detail in the near future.

Long arcs are interesting from a scientific point of view but they are *not* practical for the routine IGS analysis as preformed at CODE. Currently we are therefore focusing on how to best implement the Extended model for 3-day arcs as we are using them in our IGS analysis. However, in the more distant future we might consider generating weekly 7-day arcs as our official IGS products.

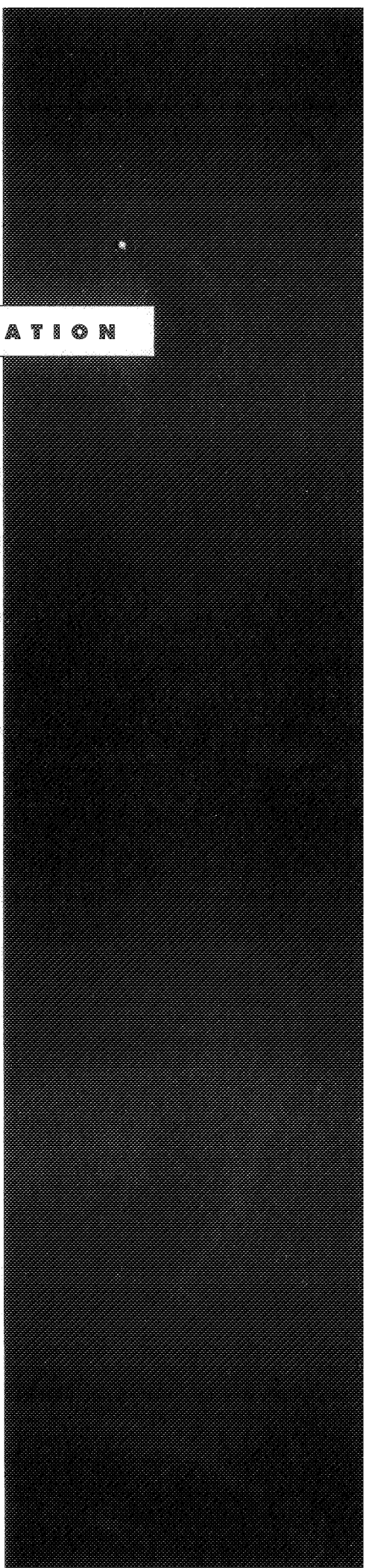
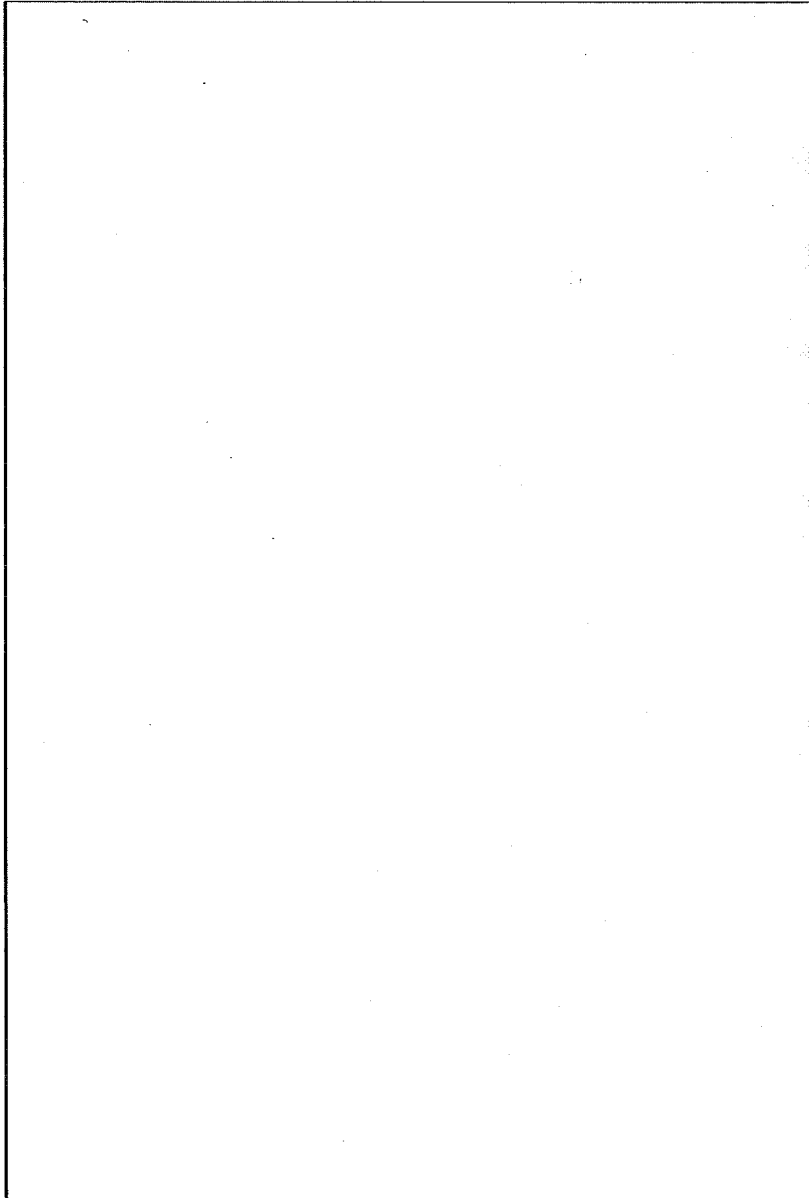
References

- Bar-Sever, Yoaz E. (1995), A new Model for GPS Yaw Attitude, in *Special Topics and New Directions*, edited by G Gendt and G. Dick, GeoForschungsZentrum, Potsdam, Germany, May 15–18 1995.
- Beutler, G., E. Brockmann, W. Gurtner, U. Hugentobler, L. Mervart, and M. Rothacher (1994), Extended Orbit Modeling Techniques at the CODE Processing Center of the International GPS Service for Geodynamics (IGS): Theory and Initial Results, *Manuscripta Geodetica*, 19, 367–386, April 1994.
- Beutler, G., J. Kouba, and T. A. Springer (1995), Combining the orbits of the IGS Processing Centers, *Bulletin Geodesique*, 69(4), 200–222.
- Colombo, O.L. (1989), The Dynamics of Global Positioning Orbits and the Determination of Precise Ephemerides, *Journal of Geophysical Research*, 94(B7), 9167–9182.
- Kouba, J. (1995), Analysis Coordinator Report, in *IGS 1994 Annual Report*, edited by R. Liu J.F. Zumberge and R.E. Neilan, pp. 59–94, IGS Central Bureau, Jet Propulsion Laboratory, Pasadena, California U.S.A., September 1 1995.
- Rothacher, M., G. Beutler, and T. A. Springer (1996), The Impact of the Extended CODE Orbit Model on the Estimation of Earth Rotation Parameters, IGS Analysis Center Workshop, NOAA, Silver Spring, USA, March 19–21 1996.

Page intentionally left blank



GPS EARTH ORIENTATION



Page intentionally left blank

GPS EARTH ORIENTATION COMBINATIONS AND RESULTS: SESSION SUMMARIES AND RECOMMENDATIONS

J.R. Ray
Geosciences Laboratory, National Oceanic and Atmospheric Administration
Silver Spring, MD 20910 USA

D.D. McCarthy
U.S. Naval Observatory
Washington, DC 20392 USA

INTRODUCTION

This session consisted of seven presentations to review the status of current GPS determinations of Earth orientation and to consider further refinements. Brief summaries of each are given in the following sections. The first, by J. Kouba, reported the results of the Analysis Coordinator for the combined IGS time series of daily polar motion (PM) values, a by-product of the regular orbit combinations. The IGS results were compared with similar GPS-only series compiled by the IERS Central Bureau and by the U.S. Naval Observatory (USNO) and with the multi-technique combinations in IERS Bulletins A and B. The accuracy of the IGS PM series, recently estimated to be about 0.1 mas (McCarthy and Luzum, 1995), is now sufficient to reveal the effects of over-smoothing applied in the IERS combined series. While this is roughly comparable to the accuracy of weekly VLBI PM determinations, T.M. Eubanks showed in the following presentation the power of continuous GPS observations to monitor a previously predicted, but undetected, mode of atmospheric excitation. He encouraged the estimation of PM rate parameters, as some Analysis Centers (ACs) already do, to improve excitation studies further.

J. Ray and D. Gambis *et al.* gave largely contrasting views of the information content of GPS determinations of Universal Time (UT1) and length-of-day (LOD). Using direct comparisons with VLBI, Ray characterized the LOD measurements of the seven IGS ACs, noting the significance of pervasive biases, and assessed the potential value for monitoring UT1 variations. Gambis *et al.* synthesized combined UT1 time series using VLBI for the low frequency behavior and GPS for high frequency. Both studies agreed that GPS estimates of UT1 should be valuable when VLBI data are unavailable, such as for near real time applications. Rotational alignment of the very rapid IGS Preliminary orbits, produced daily with only 1.5-day delay, are such an application.

The effects of sub-daily Earth orientation variations were discussed by D. McCarthy and T. Herring. McCarthy examined the consequences for estimated PM values, showing that neglect of the effect leads to aliased errors at longer periods which can approach the 0.1 mas level when data arc lengths are not even multiples of 24 hours. He stressed the importance of understanding the data analysis procedures implemented by the ACs and the precise Earth orientation quantities reported to the IGS. Herring showed that diurnal and semidiurnal errors are effectively absorbed into the orbit and orientation parameters. Both speakers agreed that current models for sub-daily Earth orientation variations are sufficiently accurate that the effects should be fully incorporated into GPS data analyses.

In the closing presentation, McCarthy reviewed new standards soon to be adopted by the IERS. These include a tidal model for sub-daily Earth orientation variations which

IGS ACs are strongly encouraged to use. Adoption of a general convention for reporting EOP values, whether to include tidal contributions or not, was discussed but was not resolved. The results of this session have been distilled by the participants into a set of six recommendations, which are listed in the final section below. These incorporate revisions made based on discussions at the Workshop.

IGS COMBINATION OF GPS EARTH ORIENTATION PARAMETERS

-- J. Kouba

During the IGS Rapid orbit/clock combination, daily GPS-based PM values (IERS series designation: EOP(IGS)95 P 01) are produced weekly since January 1, 1995 with an 11-day delay. They are computed as weighted means from solutions submitted by the seven IGS ACs. Most ACs and the IGS Rapid (IGR) PM solutions have better than 0.5 mas precision, and, in direct comparisons, clearly show the effects of smoothing applied to both IERS series (Bulletins A and B) for periods less than 10 days. Similarly, since January 1, 1996, another daily PM series (EOP(IGS)96 P 01) based on the IGS preliminary (IGP) orbit/clock combination is produced daily with only a 1.5-day delay. Currently, six IGS ACs are contributing to this IGP combination. The IGP PM precision is approaching the IGS Rapid PM precision level. These two PM series imply R_x , R_y orientations of the respective IGS orbit combinations. The R_x , R_y orbit rotations can be effectively used to evaluate orbit reference frame and PM consistency of the IGS and individual AC solutions. The orbit/PM consistency has improved slightly during 1995 and it is at or below 0.1 mas for IGS combined and most AC solutions. The IGR PM combinations (EOP(IGS)95 P 01) was compared to the IERS and USNO GPS-based PM combinations. All three combined GPS PM series were found to be consistent at the 0.1 mas rms precision level, subject only to small offsets not exceeding 0.4 mas.

COMPARISON OF GPS AND VLBI POLAR MOTION WITH AAM

-- T.M. Eubanks

In a paper by Eubanks *et al.* (1988), circularly polarized quasi-periodic polar motions with "periods of ~10 days and inferred polar motion amplitudes <1.0 mas" were predicted based on the existence of an atmospheric normal mode. These retrograde oscillations have now been observed in highly accurate PM results from GPS and VLBI data, with (peak to peak) amplitudes of 0.5 to 1.0 mas. These data are now in fact sufficiently accurate to provide continuous monitoring of this phenomenon. Excellent agreement is found between the geodetic data and Atmospheric Angular Momentum (AAM) estimates from numerical weather forecast assimilation models, with the observed polar wobble being almost entirely driven by atmospheric pressure forcing. The agreement between geodetic and AAM estimates of the PM excitation is better if the "inverted barometer" oceanic effect is ignored, implying that the ocean surface does not compensate pressure loads at these high frequencies.

The normal modes of a linearized barotropic atmosphere model can be separated into two classes, the linearly polarized sub-diurnal gravity modes, and the Rossby-Haurwitz modes, which are always westward propagating, or retrograde circularly polarized. The observed 10-day polar wobble is due to a Rossby-Haurwitz mode, one of only 3 normal modes expected to cause polar motions. The other two such modes, a 1.2-day period Rossby-Haurwitz mode and a 0.6-day period gravity mode, are much smaller, with predicted PM amplitudes of order 50 μ s or less, and are not currently geodetically

observable. Atmospheric normal mode periods depend on the thermal structure of the atmosphere, and continued geodetic monitoring of the 10-day mode will thus provide a resource for long term studies of climate change.

There is a general need for a clearer description of the smoothing/filtering and *a priori* ties applied in the GPS data analysis, both to the EOP, and, in addition, to the orbit analysis. As the estimated orbits provide the framework with respect to which the EOP is measured, a clear understanding of the orbital constraints (including any *a priori* ties to, e.g., Earth rotation predictions) is needed to better interpret the GPS EOP estimates, especially at high frequencies.

GPS MEASUREMENTS OF LENGTH-OF-DAY: COMPARISONS WITH VLBI AND CONSEQUENCES FOR UT1 -- J.R. Ray

Length-of-day (LOD) estimates from the seven GPS ACs of the IGS have been compared to values derived from VLBI for a recent 16-month period. All GPS time series show significant LOD biases which vary widely among the Centers. Within individual series, the LOD errors show time-dependent correlations which are sometimes large and periodic. Clear correlations between ostensibly independent analyses are also evident. In the best case, the GPS LOD errors, after bias removal, approach Gaussian with an intrinsic scatter estimated to be as small as $\sim 21 \mu\text{s/d}$ and a correlation time constant of perhaps 0.75 d. Integration of such data to determine variations in UT1 will have approximately random walk errors which grow as the square-root of the integration time. For the current best GPS performance, UT1 errors exceed those of daily 1-hour VLBI observations after integration for ~ 3 d. Assuming the stability of LOD biases can be reliably controlled, GPS-derived UT1 can be useful for near real time applications where otherwise extrapolations for several days from the most current VLBI data can be inaccurate by up to $\sim 1000 \mu\text{s}$.

DENSIFICATION AND EXTENSION OF VLBI UT1 SERIES WITH SATELLITE TECHNIQUES -- D. Gambis, M. Feissel, and E. Eisop

The GPS technique has recently shown its capability of monitoring PM. Due to the difficulty of determining with accuracy the long-term behavior of the non-rotating system realized through the orbit orientation, Universal Time UT1 cannot be accurately derived from GPS technique since it is affected by long-term errors. Still, on time scales limited to a couple of months the high-frequency signal contained in the GPS UT determination can be used for densifying the series obtained by the VLBI technique and also for UT predictions in non-availability of the operational VLBI solution on a quasi real-time basis. In that case accuracies of about $200 \mu\text{s}$ on 10 days and $300 \mu\text{s}$ on 20 days are currently obtained. These analyses have recently led to the development of operational procedures for both densification of Universal Time and use of GPS UT determinations in non-availability of VLBI solution.

DAILY & SEMI-DAILY EOP VARIATIONS AND TIME SCALES; NEW IERS STANDARDS & CONVENTIONS -- D.D. McCarthy

Accuracy of Earth orientation information derived from the analysis of GPS orbits is limited currently by systematic errors. If ACs could agree on standard models and

practices this situation could be improved. For example, it is now evident that high-frequency variations in Universal time and polar motion can be observed. However, a consensus on the application of existing models in the analysis of observational data has not yet been reached. Another example is the use of *a priori* information on the motion of the celestial ephemeris pole in an inertial reference frame (precession/nutation).

Questions remain on the model to be used as well as the procedure to be used in treating daily and sub-daily variations. Resolution of these problems is important now, both in the analysis of the observations and in reporting the derived Earth orientation. The IERS is in the process of adopting the theoretical sub-daily model of Richard Ray for the forthcoming IERS Conventions. This model will be available in the form of source code.

In comparing Earth orientation values from different analyses for a specified set of epochs, a clearer understanding of the EOP contributions included is also required. Should these values be reported as an estimate of the total instantaneous Earth orientation at that epoch (including all tidal components) or should they report only the estimated non-tidal contributions presumably averaged over the data span?

CONSEQUENCES OF SUB-DAILY EOP VARIATIONS FOR GPS ORBITS

-- T. A. Herring

Sub-daily Earth rotation variations, in principle, have two effects in the analysis of GPS data: (1) the rotation of the gravity field will perturb the orbits of the GPS satellites; and (2) the effect the transformation from inertial to Earth-fixed coordinates.

The former of these is an extremely small effect and can be neglected. (As a rough order of magnitude estimate, we take the total C20 perturbation on a GPS satellite which is approximately 10^{-5} m/sec². The diurnal and semidiurnal changes in the direction of the C20 harmonic is oriented in inertial space would change this perturbation by $5 \cdot 10^{-9}$ resulting in accelerations of less than 10^{-13} m/sec². The resultant orbit perturbation is <0.2 mm.)

The latter effect on the transformation between the inertial and Earth-fixed coordinate systems is the most important effect. The neglect of the diurnal and semidiurnal rotations has itself two impacts: (1) Because of error in the mathematical model, the estimators will be affected (i.e., parts of the semidiurnal and diurnal rotations will be aliased in station coordinate estimates, atmospheric parameter estimates, the orbital parameter estimates, and the post-fit residuals), and (2) The direct transformation effects.

Analyses which we have done for (1) suggest that the diurnal and semidiurnal terms alias into the orientation and rate of change of orientation terms (about 50% of the total terms) and into the inertial orbit parameters (also about 50%). There appears to be only small decreases in the post-fit residuals and changes in station position (of order a few millimeters).

The effects of the direct transformation can be easily accounted and for 1 mas amplitude diurnal or semidiurnal term would result in ~10 cm changes in the satellite positions in the Earth-fixed frame. (The aliasing contribution from the estimator appears to be about 5 cm for this magnitude term.) The aliasing contribution is smaller when pole position and UT1 are not estimated (provided the *a priori* values are accurate).

When the diurnal and semidiurnal terms are not included in the mathematical model, Earth-fixed GPS orbits will have diurnal and semidiurnal rotations in them (because the motion of the Earth in the inertial frame of the orbit is not accounted for). The amplitude of these errors is of order 10 cm and will vary with the beat frequencies between the major terms in the semidiurnal and diurnal model. The major beat frequency is 13.7 days.

It should also be noted that the effects of phase center models appear to be about 3 times larger than the effects of the diurnal and semidiurnal models used in the analysis; i.e., changes in semimajor axis when the diurnal and semidiurnal models are used are ~8 cm when PM/UT1 estimated, ~4cm when PM/UT1 are not estimated. The phase center models change the semimajor axis by ~20 cm.

RECOMMENDATIONS

[1] *IERS Conventions adopted for general use*

To ensure the highest degree of compatibility of results from the individual Centers and with other techniques, it is recommended that

all IGS Analysis Centers incorporate the IERS Conventions (Standards) into their data analysis procedures to the greatest extent possible.

Whenever departures from the IERS Conventions are deemed necessary, Analysis Centers are encouraged to document the alternative procedures in their reports to the IGS, IERS, and in updated AC Questionnaires. The new version of the IERS Conventions will be available in printed form by late spring 1996. Some parts will be available sooner as source code.

[2] *Reporting IGS Analysis Center models & methods*

To ensure the highest quality of results from the IGS combinations and to avoid misunderstandings, it is essential that the models and methods used by the Analysis Centers be fully understood by the users. It is particularly important that departures from the IGS and IERS Standards and Conventions be noted. Therefore, it is recommended that

all IGS Analysis Centers provide updated versions of their AC Questionnaire at least once per year and every time that significant changes are made.

The Analysis Center Coordinator will review the scope of the current Questionnaire, making suitable revisions, and will provide a standard format at the IGS Central Bureau. New responses should be filed by all Analysis Centers by 01 July 1996.

[3] *IGS combination of GPS polar motion results*

Based on the demonstrated high quality of the weighting method used by the IGS for its polar motion combination, it is recommended that

outside users of GPS polar motion results use the IGS Rapid combination polar motion values.

For those applications requiring more rapid turnaround, it is recommended that the IGS Preliminary combination values be used.

Given the high quality of current polar motion estimates from GPS and considering the potential value for excitation studies, Analysis Centers are encouraged to

include and report polar motion rate parameters in their data analyses, in addition to polar motion offset parameters.

[4] *IGS combination of GPS LOD/UT1 results*

For near real time applications, where the only UT1 information available is from predictions, it is recommended that

the IGS Analysis Center Coordinator devise a method to combine submitted LOD/UT1 results from the GPS Analysis Centers to form a preliminary UT1-UTC estimate.

This new UT1 combination will be used to align the IGS Preliminary orbits rather than IERS Bulletin A predictions. Because the GPS LOD/UT1 errors do not seem to be related to the satellite orbit errors in a simple way, a new method is needed for the combination, different from that used for polar motion. The Analysis Center Coordinator will fully document the UT1 combination procedure adopted.

[5] *Modelling sub-daily EOP variations*

To account for variations in Earth orientation at nearly 24-h and 12-h periods, it is recommended that

the IGS Analysis Centers follow the IERS Conventions and account for these effects in modelling GPS observables using the tidal model of Richard Ray.

This model should be used in the transformation between inertial and Earth-fixed coordinates (and visa versa) for all transformations used in GPS processing. Specifically,

the diurnal and semidiurnal terms need to be included in the transformation of inertial GPS orbits into the Earth-fixed frame for submission to the IGS.

About 50% of the errors in this adopted model will "project" into the inertial orbits and of course the total error will be in the transformation from inertial into Earth-fixed coordinates. The one issue still to be addressed is do these contributions tend to cancel each other or do they add constructively.

[6] *Reporting EOP values*

With respect to diurnal and semidiurnal variations, it is recommended that

when Earth orientation parameters are estimated, the procedures for reporting EOP values adhere to the IERS Conventions and guidelines, which are still to be determined. In particular, users must know how to relate the reported EOP values to the corresponding total values (including all tidal contributions) at the

associated UTC epoch.

The relationship between reported EOP values and the corresponding total EOP values should be explained in the Analysis Center Questionnaire.

REFERENCES

Eubanks, T.M., J.A. Steppe, J.O. Dickey, R.D. Rosen, and D.A. Salstein, Causes of rapid motions of the Earth's pole, *Nature*, 334, 115-119, 1988.

McCarthy, D., and B. Luzum, Changes in USNO GPS-only combination procedure, IGS Electronic Mail #1072, <http://igscb.jpl.nasa.gov/igscb/mail/igsmail/igsmess.1072>, 28 Sept. 1995.

Page intentionally left blank

IGS COMBINATION OF GPS EARTH ORIENTATION PARAMETERS(EOP)

J. Kouba

Geodetic Survey Division, Natural Resources Canada, Ottawa, Canada;
e-mail: kouba@geod.emr.ca

ABSTRACT

During the IGS Rapid orbit/clock combination, daily GPS based polar motion (PM) values (IERS designation: **EOP(IGS)95 P 01**) are produced weekly since January 1, 1995 with an 11 day delay. They are computed as weighted means from solutions submitted by the seven IGS Analysis Centers (ACs). Most ACs and the IGS Rapid (IGR) PM solutions have better than 0.5 mas precision, and clearly show smoothing effects in both IERS series (Bulletin A and B) for periods less than 10 days. Similarly, since January 1, 1996, another daily PM series (**EOP(IGS)96 P 01**) based on the IGS preliminary (IGP) orbit/clock combination is produced daily with only a 1.5 day delay. Currently, six IGS ACs are contributing to this IGP combination. The IGP PM precision is approaching the IGS Rapid PM precision level. These two PM series imply R_x , R_y orientations of the respective IGS orbit combinations. The R_x , R_y orbit rotations can be effectively used to evaluate orbit reference frame and PM consistency of the IGS and individual AC solutions. The orbit/PM consistency has improved slightly during 1995 and it is at, or below 0.1 mas for IGS combined and most AC solutions. The IGR PM combination (**EOP(IGS)95 P 01**) was compared to the IERS and USNO GPS based PM combinations. All three combined GPS PM series were found to be consistent at the 0.1 mas rms precision level, subject only to small offsets not exceeding 0.4 mas.

INTRODUCTION

Since January 2, 1994 orbit/clock solutions submitted by seven IGS Analysis Centers (ACs) have been combined into two classes of IGS orbit/clock solutions: the IGS Rapid and the IGS Final combinations. The IGS Rapid (IGR) combination is produced typically within 11 days since the last observation and was initially based on the IERS Bull.A, while the IGS Final combination is based on the IERS Bulletin B and is typically available within one to two month delay. For more details on both IGS combinations see the 1994 IGS Annual Report (Kouba et al., 1995).

Since January 1, 1996 a third IGS preliminary orbit/clock (IGP) combination was initiated with the participation of six ACs and with a much faster production cycle of less than a 38h delay. Since the IGP combination has proven to be successful and to economize the IGS combination efforts, as well as to speed up the delivery of IGS products, it has been recommended that as of June 30, 1996 (Wk 860) the IGP will replace the IGS Rapid combination and the current IGS Rapid will become the IGS Final orbit/clock combination. Both combinations will be carried out directly in the ITRF (Kouba et al., 1996).

EOP/ORBIT CONSISTENCY

The IGS orbit combinations were designed to mitigate small EOP errors and reference frame inconsistencies of individual Analysis Center (AC) solutions. Each AC orbit solution is first rotated to a common reference pole direction by applying appropriate PM differences. An unweighted mean orbit is then computed and AC solutions are further aligned by 7 parameter transformations before the final weighted orbit is generated (Beutler et al., 1995; Kouba et al., 1995). The IERS Bull. B PM, corrected for the IERS-ITRF misalignment, is used as the reference direction of the IGS Final orbit combinations. A high degree of reference frame consistency is ensured by all ACs using the same set of 13 ITRF station positions and velocities. The combination procedure also facilitates checking of orbit/EOP consistencies for all the submitted AC solutions by comparing AC orbit R_y and R_x rotations with the corresponding PM x and y differences. In other words, the AC PM solutions are compared with the IERS Bulletin B directly and by means of orbit alignments. Both comparisons should agree, provided that the AC PM and orbit solutions are consistent. Similarly the consistency of station coordinates and PM solutions could be analyzed; recently IGS and AC station solutions have become available.

The AC orbit orientation and PM solution differences with respect to Bull. B during 1994 and 1995 are summarized in Table 1 and 2, respectively. One can observe a good orbit/PM consistency and especially for 1995, most likely due to a more consistent reference frame (ITRF93), additional stations and AC processing improvements. The average PM and orbit orientation differences are similar and the corresponding sigmas are also consistent for most ACs. There are some y -coordinate differences between PM and orbit orientation in particular in 1994. These may be due to differences in ITRF station constraints, i.e. the sigmas and the number of constrained stations (ACs are free to constrain/fix more than the 13 ITRF stations), as well as in modeling, observation weighting, station distribution (geometry), etc.

Table 1: IGS Final Orbit orientation and IERS (Bull. B) PM differences during 1994.
(corrected for the IERS-ITRF92 misalignment; units: mas)

Center	IGS Final Orbits				IERS (Bull. B)				Difference (IGS-IERS)			
	x	sig	y	sig	x	sig	y	sig	x	sig	y	sig
COD	-.17	.37	-.32	.37	-.18	.31	-.50	.36	.01			.18
EMR	.08	.40	-.28	.47	.04	.39	-.41	.48	.04			.13
ESA	-.18	.46	-.06	.43	-.14	.42	-.08	.44	-.04			.04
GFZ	.39	.45	-.69	.52	.28	.30	-.40	.30	.11			-.29
JPL	-.26	.36	-.28	.38	-.21	.35	-.31	.36	-.05			.03
NGS	.23	.87	-.63	.68	.13	.80	-.84	.76	.10			.21
SIO	.49	1.04	-.41	1.13	.53	.52	-.16	.65	-.04			-.25
MEAN	.08	.11	-.38	.08	.06	.10	-.38	.09	.02	.02	.01	.08

Initially, the IGS Rapid (IGR) and Final orbit/clock combinations were generated in the same way using the IERS Bull. A or B respectively for the combined orbit orientation. Since May 28, 1995 (GPS Week 0803), the IGR orbit combinations are no longer aligned to the Bull. A, but are directly combined in the ITRF93. This was made possible by the

better orbit consistency between ACs in 1995 as discussed above. EOP series, consistent with the new IGR orbits have been produced as a weighted average of AC PM solutions by applying the orbit weights while preserving the Bull. A UT1-UTC values. For completeness, the new IGS (IGR) EOP series (IERS designation: EOP(IGS)95 P 01), together with the new IGS Rapid orbit/clock combinations, were subsequently reprocessed back to Jan. 1, 1995. The differences of the new IGR EOP series (with respect to Bull. B) are summarized in Table 2. One can also see a high degree of consistency between the Final Orbit and the IERS(Bull. B) differences. The IGR EOP combination (EOP(IGS)95 P 01) was used for AC pole comparisons in the next section.

Table 2: IGS Final Orbits and IERS (Bull. B) PM differences during 1995.
(corrected for the IERS-ITRF93 misalignment; units: mas)

Center	IGS Final Orbits				IERS (Bull. B)				Difference(IGS-IERS)			
	x	sig	y	sig	x	sig	y	sig	x	sig	y	sig
CODE	-.05	.29	-.39	.24	-.04	.31	-.35	.29	-.01		-.04	
EMR	-.06	.31	-.03	.38	-.04	.37	.04	.40	-.02		-.07	
ESA	.14	.41	.29	.42	.20	.43	.37	.42	-.06		-.08	
GFZ	.11	.25	-.21	.20	.18	.32	-.14	.26	-.07		-.07	
JPL	.04	.28	-.49	.25	.05	.31	-.34	.26	-.01		-.15	
NGS	.28	.41	-.31	.38	.25	.46	-.20	.43	.03		-.11	
SIO	-.15	.65	.04	.61	-.17	.70	.03	.63	.02		.01	

MEAN	.04	.05	-.16	.10	.06	.06	-.08	.10	-.02	.01	-.07	.02
IGR (EOP(IGS)95 P 01)					.05	.29	-.14	.22				

The last two lines of Table 2 also demonstrate the level of consistency between the IGS Final and Rapid orbit combinations during 1995. The largest differences in PM orientation are smaller than 0.2 mas which is well within the expected stability of both the IGS and IERS PM series.

INDIVIDUAL AC POLE SOLUTIONS

While performing routine evaluation of the IGR PM, significant and sometimes periodic differences approaching 1 mas with periods between 5-10 days (see e.g. Fig.1), with respect to both IERS combinations (Bull. A, B) have been observed. After examining and eliminating a number of potential systematic effects (e.g. the sub-daily PM, interpolation, etc.) it was concluded that the differences between the GPS and the IERS PM series are due to smoothing applied to both IERS PM series. The GPS PM variations correspond to atmospheric PM effects as predicted almost a decade ago by Eubanks et al. (1988), (Eubanks, 1996). It has been detected for the first time thanks to the IGS. Subsequently both USNO and the IERS Central Bureau have adopted much weaker smoothing schemes for the IERS Bulletin A and B.

The differences with respect to the Bull. B (i.e. EOP(IERS)C04) for the IGR PM combination and the individual AC pole solutions (with respect to IGR) are shown in Figures 1-2. The smoothed out atmospheric signal is clearly visible for the IGR PM as

the EOP(IERS)C04 in 1995 did not yet employ the new smoothing scheme. The IGR standard deviations in Table 2 (0.2-0.3 mas) are mainly due to the atmospheric signal smoothed out in the Bull. B, as pointed out above.

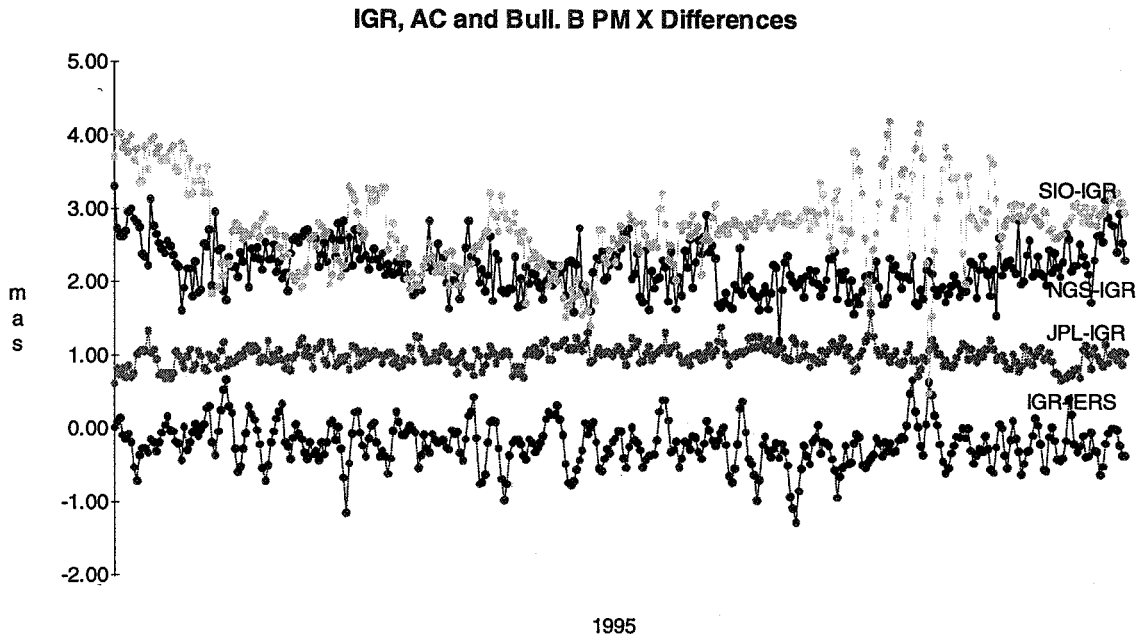


Fig. 1a. Polar Motion (PM) X Coordinate Differences for IGR (EOP(IGS) 95 P 01) with respect to the IERS (Bull. B), and JPL, NGS, SIO (offset by 1, 2, 3 mas, resp.) with respect to IGR

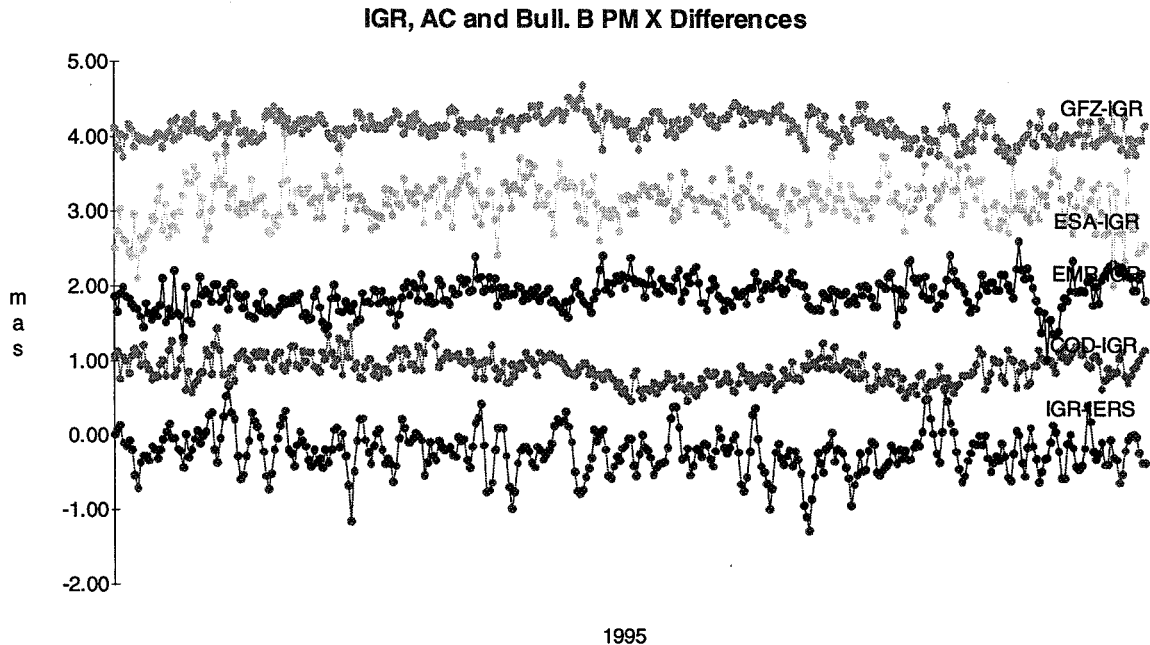


Fig. 1b. Polar Motion (PM) X Coordinate Differences for IGR (EOP(IGS) 95 P 01) with respect to the IERS (Bull. B), and COD, EMR, ESA, GFZ (offset by 1, 2, 3, 4 mas, resp.) with respect to IGR.

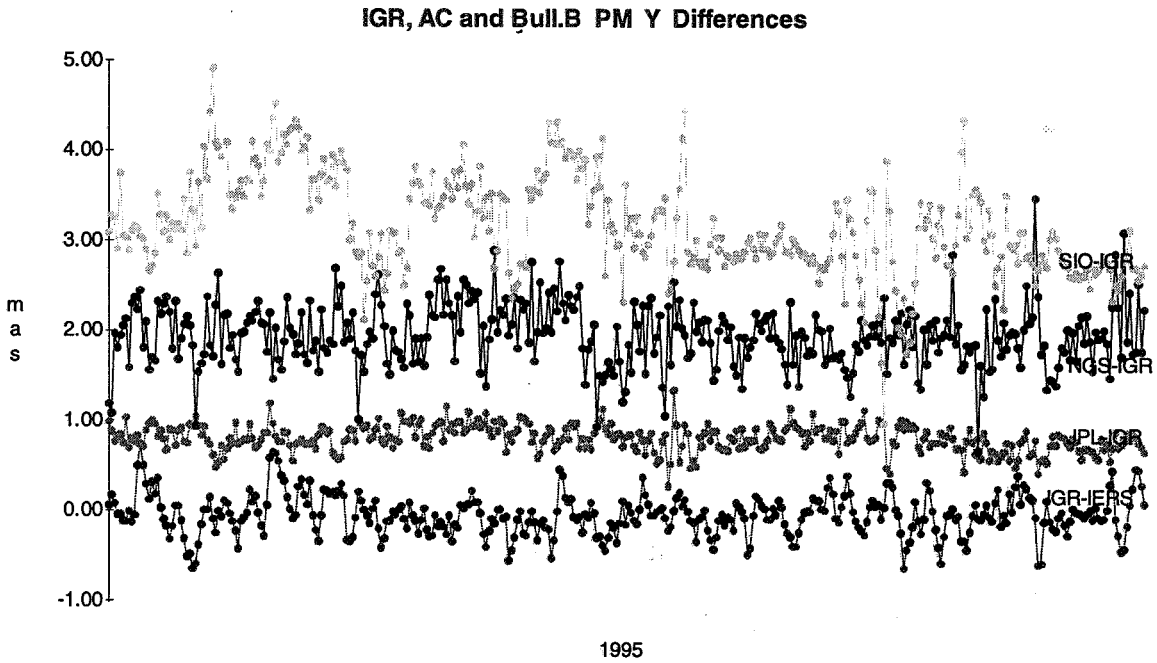


Fig. 2a. Polar Motion (PM) Y Coordinate Differences for IGR (EOP(IGS) 95 P 01) with respect to the IERS (Bull. B), and JPL, NGS, SIO (offset by 1, 2, 3 mas, resp.) with respect to IGR

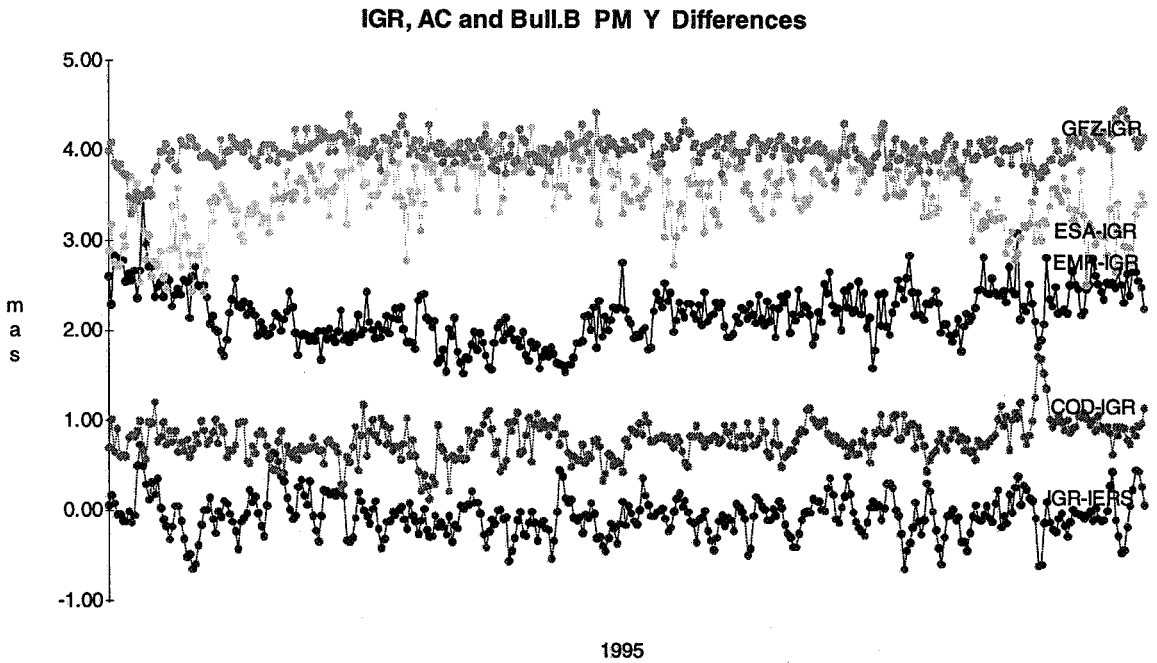


Fig. 2b. Polar Motion (PM) Y Coordinate Differences for IGR (EOP(IGS) 95 P 01) with respect to the IERS (Bull. B), and COD, EMR, ESA, GFZ (offset by 1, 2, 3, 4 mas, resp.) with respect to IGR.

COMPARISON OF GPS PM COMBINATION SERIES FOR 1995

Currently there are three GPS PM combination series: IGR, USNO and IERS. The IGR (EOP(IGS)95 P 01) and IERS combinations utilize identical input series (i.e. the 7 IGS AC EOP solutions), whereas USNO adds its own GPS PM solution. The three PM combinations use different editing, bias removal and smoothing. In the case of the IGR PM combination, it employs the IGR orbit weights and editing, but no biases or smoothing are applied (Kouba, 1995). It is oriented to ITRF93 as realized by the 13 ITRF93 station positions of date. The differences between the three GPS PM combinations and the IERS Bull. A and Bull. B (EOP(IERS)C04) are shown in Table 3. This comparison does not introduce any data filtering, weighting, biases removal, nor the IERS-ITRF93 alignment.

Table 3: Differences for IERS, USNO and IGS GPS PM combination series for 1995 (mas):

Difference	Mean X	sig	Mean Y	sig
IGS GPS -EOP(IERS)C04	-.20	.29	-.04	.22
IERS GPS-EOP(IERS)C04	.08	.29	.02	.24
USNO GPS-EOP(IERS)C04	.17	.29	-.20	.23
BULL A -EOP(IERS)C04	.17	.24	-.22	.27
IGS GPS -BULL A	-.38	.15	.17	.18
IERS GPS-BULL A	-.10	.18	.22	.19
USNO GPS-BULL A	.00	.13	.02	.16
IERS GPS-IGS GPS	.28	.10	.06	.10
USNO GPS-IGS GPS	.37	.08	-.15	.09
IERS GPS-USNO GPS	-.10	.12	.21	.10

Assuming no correlation between the three GPS combined series, the following rms estimates are obtained for the three PM combinations (Table 4):

Table 4: Estimated rms for the GPS PM combination series for 1995 (mas).

Series	Pole X	Pole Y
IERS	.097 mas	.080 mas
USNO	.076	.065
IGS	.038	.061

The differences for the three combined PM series are also plotted in Figure 8. Small differences in smoothing, stability as well as biases can be observed. The biases between IERS and IGS PM, to a large extent, can be explained by the misalignment between the IERS EOP and ITRF93 as published in the 1993 IERS Annual Report (Table II-3, p.11-19).

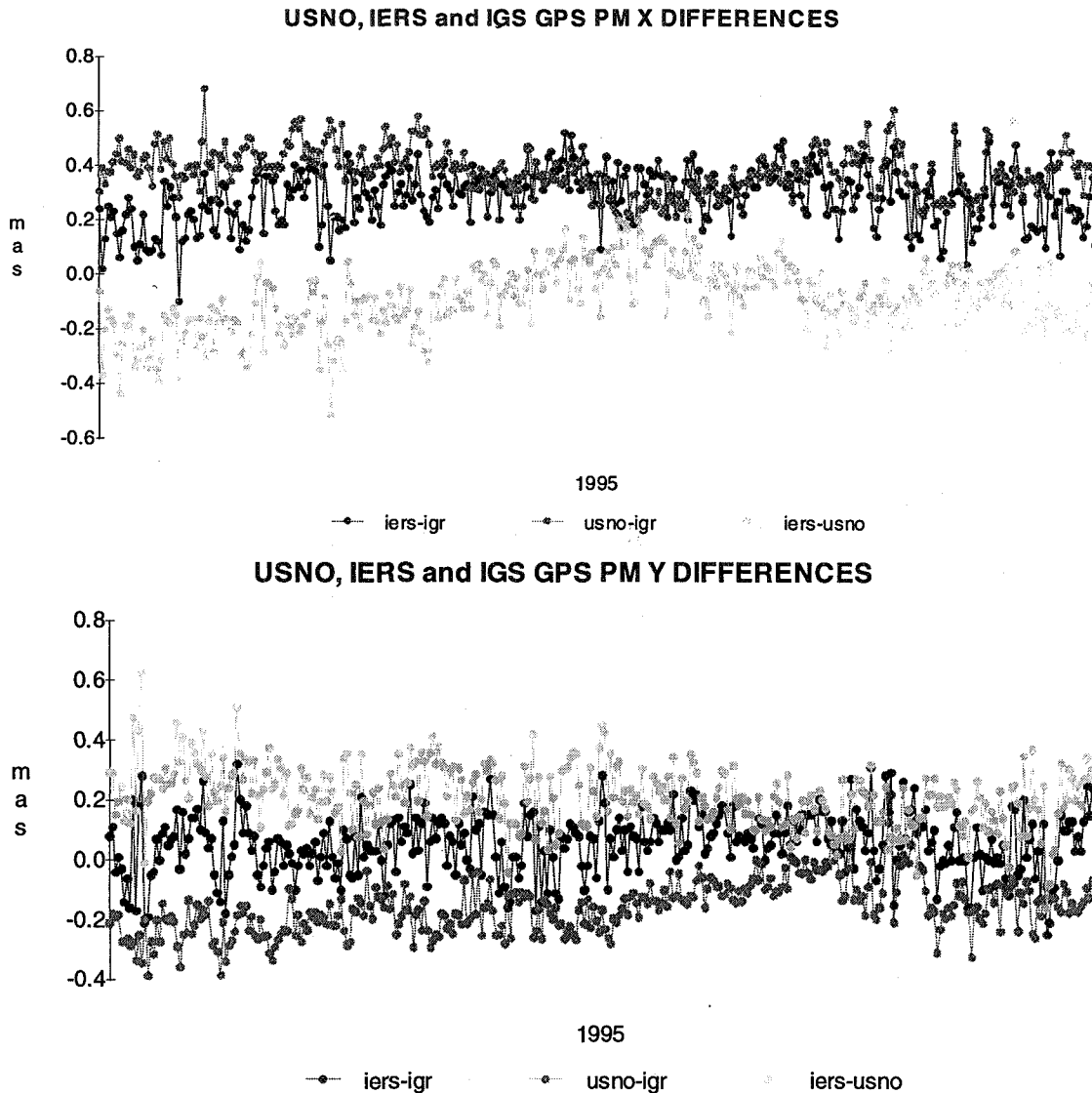


Fig. 3. IERS , USNO and IGR (EOP(IGS)95 P 01) GPS PM combination differences.

IGS PRELIMINARY COMBINATION

The IGS Preliminary (IGP) combination, initiated in January 1996, employs the same strategy as the IGS Rapid (IGR) combination, but it is produced within 38h after the last observation and uses six AC preliminary solutions. The precision of preliminary AC solutions might be affected by an absence of some geometrically important stations which are not available at the time of processing (Kouba et al., 1996). Figure 4 compares the IGP PM (EOP(IGS)96 P 01) to the current Bull. A for the first two months of 1996 and shows rms below 0.5 mas.

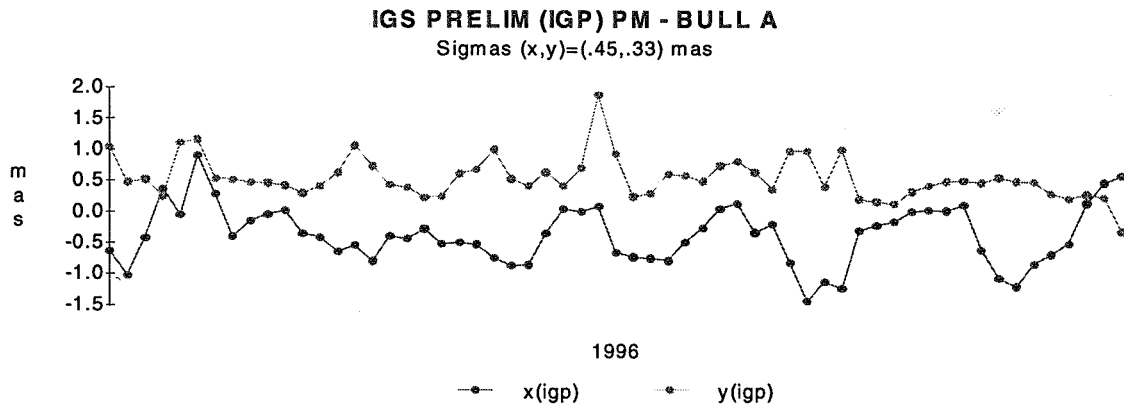


Fig. 4. IGS Preliminary (IGP) PM combination (EOP(IGS)96 P 01) differences with respect to the IERS Bulletin A for January - February, 1996.

Similarly as for the IGR series, UT1-UTC is obtained from the IERS Bull. A, available at the time of combination which are usually predictions of more than one week. This is clearly visible in Figure 5 where IGP UT1-UTC is compared to the IERS Bull. A which already include results from daily VLBI observations. The systematic trend with increasing prediction periods and regular weekly resets produce the saw tooth effect. Also shown in Figure 5 is a simple arithmetic average of the six AC solutions ($UT1(IGS)$) and the same average corrected for a drift averaged over the two months ($UT1c(IGS)$), to show the feasibility and desirability of IGS UT1-UTC combinations. Ray (1996) examines GPS UT1-UTC solutions and possible combinations in more details.

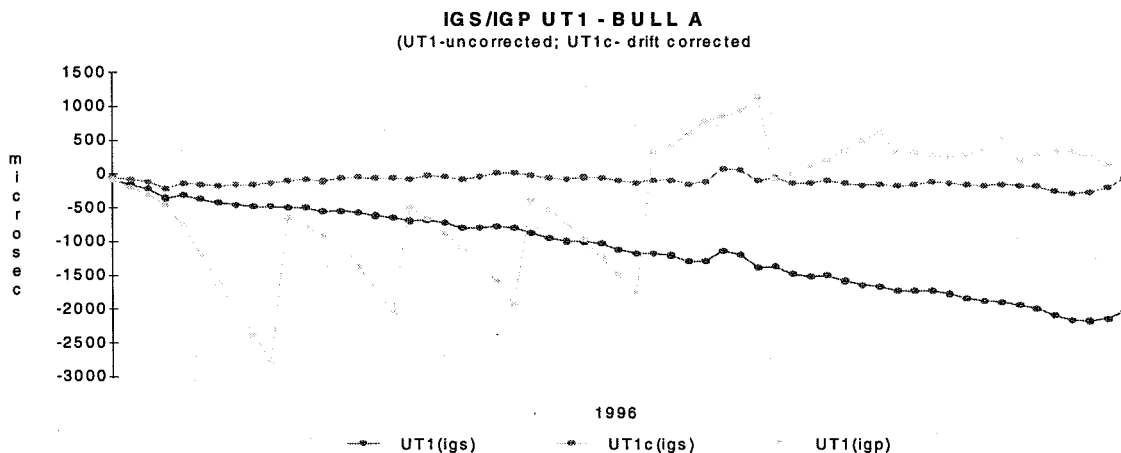


Fig. 5. IGS Preliminary UT1-UTC combination differences with respect to the IERS Bulletin A for January - February, 1996. $UT1(igs)$ - a simple average of 6 AC UT1 solutions; $UT1c(igs)$ - drift corrected $UT1(igs)$; $UT1(igp)$ - the Bull. A prediction used in EOP(IGS)96 P 01.

CONCLUSIONS

The IGS combined and most individual AC PM solutions showed steady improvement in precision and consistency approaching the 0.1 mas level during 1994 and 1995. The IGS Final and Rapid orbit orientations were consistent within 0.1 mas in 1995 and thus no significant orientation discontinuities are expected when the current IGR orbit combination will become the IGS Final products on June 30, 1996.

The IGR PM solutions show real PM variations with 2-10 day periods which have been related to atmospheric effects. The current daily GPS PM solutions produced by AC are typically 24h averages, largely independent from day to day. Any signals with periods less than 24h, such as sub-daily tidal effects are effectively averaged out. As a simple average of sub-daily PM model values over a 24h (UTC) period is typically less than .002 mas, 24h average PM solutions are reported regardless of whether the sub-daily PM is applied or not. This should clarify the matter for most IGS users.

The IGS Preliminary (IGP) combinations, which are soon to replace the IGS Rapid combinations, are producing useful and timely PM and UT1-UTC. The need for improved IERS (Bull. A) predictions, or an IGS UT1-UTC combination is also apparent.

REFERENCES

Beutler, G., J. Kouba, and T. Springer, Combining the orbits of the IGS Analysis Centers, Bull. Geod. (1995) 69: 200-222, 1995.

IERS 1993 Annual Report, International Earth Rotation Service (IERS), Observatoire de Paris, 1994.

Eubanks, T.M., J.A. Steppe and J.D. Dickey, The Atmospheric Excitation of Rapid Polar Motions, The Earth's Rotation and Reference Frames for Geodesy and Geodynamics, (edited by A.K. Babcock and G.A. Wilkins), IAU, 365-371, 1988.

Eubanks, T.M., Comparisons of GPS and VLBI polar motion with AAM, presented at the IGS Analysis Center Workshop, Silver Spring, Md., March 19-21, 1996 (in prep).

Kouba, J., Analysis Coordinator Report, IGS 1994 Annual Report, (edited by J.F. Zumberge, R. Liu and R.E. Neilan), IGS CB, JPL, 59-69, September, 1995.

Kouba, J., Y. Mireault and F. Lahaye, IGS Orbit/Clock Combination and Evaluation, Appendix I, Analysis Coordinator Report, in IGS 1994 Annual Report, (edited by J.F. Zumberge, R. Liu and R.E. Neilan), IGS CB, JPL, 70-94, September, 1995.

Kouba, J., G. Beutler and Y. Mireault, GPS Orbit/Clock Combination and Modeling, Proceedings of the IGS Analysis Center Workshop, Silver Spring, Md., March 19-21, 1996 (in prep.)

Ray, J.R. GPS Measurements of LOD: Comparisons with VLBI and Consequences for UT1, Proceedings of the IGS Analysis Center Workshop, held in Silver Spring, Md., March 19-21, 1996 (in prep.)

GPS MEASUREMENTS OF LENGTH-OF-DAY: COMPARISONS WITH VLBI AND CONSEQUENCES FOR UT1

J.R. Ray

Geosciences Laboratory, National Oceanic and Atmospheric Administration
Silver Spring, MD 20910 USA

ABSTRACT

Length-of-day (LOD) estimates from the seven GPS Analysis Centers of the IGS have been compared to values derived from VLBI for a recent 16-month period. All GPS time series show significant LOD biases which vary widely among the Centers. Within individual series, the LOD errors show time-dependent correlations which are sometimes large and periodic. Clear correlations between ostensibly independent analyses are also evident. In the best case, the GPS LOD errors, after bias removal, approach Gaussian with an intrinsic scatter estimated to be as small as $\sim 21 \mu\text{s/d}$ and a correlation time constant of perhaps 0.75 d. Integration of such data to determine variations in UT1 will have approximately random walk errors which grow as the square-root of the integration time. For the current best GPS performance, UT1 errors exceed those of daily 1-hour VLBI observations after integration for ~ 3 d. Assuming the stability of LOD biases can be reliably controlled, GPS-derived UT1 can be useful for near real time applications where otherwise extrapolations for several days from the most current VLBI data can be inaccurate by up to ~ 1 ms.

INTRODUCTION

The rate of spin of the Earth about its polar axis varies on all observable timescales by up to a few milliseconds (ms) per day. Currently, the average day length exceeds 86400 s (as measured by atomic time or TAI) by roughly 2 ms, with variations over the previous year of more than 1 ms. The related quantity Universal Time (UT1) is the conventional measure of the instantaneous angle of rotation of the Earth, relative to the "fixed" stars, and is expressed in time units. Excess length-of-day is then defined as

$$\text{LOD} = - d(\text{UT1-TAI})/dt$$

(For reference, 1 m of rotation of the Earth at its equator corresponds to a change in UT1 of 2.15 ms.) Tidal distortions of the Earth's moment of inertia induced by the gravitational attractions of the Sun and Moon cause UT1 variations at the 2 ms level which are accurately predictable (Yoder *et al.*, 1981). However, unpredictable UT1 variations of comparable or larger magnitude are produced by a variety of geophysical processes (Hide and Dickey, 1991). To maintain accurate knowledge of the current orientation of the Earth in inertial space therefore requires periodic measurements of the positions of reference celestial objects from known points on the Earth's surface. Historically, this function was performed by timing the meridional transits of stars. In addition to their practical value, accurate UT1 measurements are used to evaluate the bulk geophysical properties of the Earth independently of viscoelastic models (*e.g.*, Robertson *et al.*, 1994) and to study the Earth's excitation mechanisms for angular momentum exchange (*e.g.*, Dickey *et al.*, 1992).

With the development of space geodetic techniques beginning in the late 1970s, the

accuracy of UT1 measurements was improved by about two orders of magnitude (Carter *et al.*, 1985). Very long baseline interferometry (VLBI) has demonstrated highly accurate and stable determinations of UT1, in large part because its very precise observations of extragalactic radio sources provide access to a nearly inertial celestial reference frame. Lunar laser ranging (LLR) is also capable of determining Earth rotation but its measurement history has been sparse and significantly less accurate. It has long been expected that radio observations of satellites in the Global Positioning System (GPS) could be used to determine daily UT1 or LOD values to supplement and eventually to replace, partially, those from VLBI. Indeed, the satellite laser ranging (SLR) technique has already shown that a satellite-based method can provide rapid and frequent estimates of UT1 although the results have not been sufficiently accurate or stable enough to reduce the need for VLBI. GPS offers the potential of improved UT1 or LOD results with higher time resolution and reduced operations costs owing to the more robust constellation of 24 satellites and a dedicated global ground tracking network (Beutler *et al.*, 1994). Improved measurements of high-frequency LOD variations could help resolve remaining discrepancies in the Earth's angular momentum budget in the subseasonal range (Dickey *et al.*, 1992).

All satellite-based techniques are handicapped in their ability to observe UT1 by the fact that the rotation of the Earth is indistinguishable from a uniform rotation of the satellite orbit nodes. Hence, if the satellite orbits are not already accurately known and must be estimated from the same data used to monitor Earth rotation, the problem is singular without applying additional constraints. LOD, on the other hand, can be determined together with the satellite orbit elements. A time series of continuous LOD values can then be integrated to yield UT1 variations as a function of atomic time. However, any unmodeled forces acting on the satellites which affect the rate of change of the satellite nodes will contaminate the LOD estimates. If the systematic errors are constant, the resulting LOD bias can be determined empirically by comparison with VLBI results and corrected. If the unmodeled satellite forces are random, producing LOD estimates with a white noise error distribution, then integration will give UT1 estimates with a random walk error distribution. In reality, a combination of the two cases is expected. Current SLR analyses, for example, have shown UT1 variations can be tracked at 3-day intervals with root-mean-squared (rms) residuals $<100 \mu\text{s}$ while applying constraints to VLBI-based UT1 for periods longer than ~ 60 days (Eanes and Watkins, 1994).

This report examines the quality of LOD results from the seven operational Analysis Centers of the International GPS Service for Geodynamics (IGS) (Beutler *et al.*, 1994) for a recent 16-month period, compared with VLBI determinations. The statistical properties of each GPS time series are characterized and the prospects for their use in multi-technique programs to monitor Earth rotation are evaluated. Following common practice, all UT1 and LOD time series used here have been adjusted to remove zonal tide contributions (for periods up to 35 d) (Yoder *et al.*, 1981; McCarthy, 1992) leaving the purely non-tidal UT1R and LODR components for analysis.

REFERENCE LODR TIME SERIES FROM VLBI

To best characterize GPS-based LOD estimates, we seek an independent time series of clearly superior stability and accuracy sampled at least as frequently as the daily GPS values. VLBI is the only technique both fully independent and sufficiently accurate to qualify for such a reference series; see, for example, IERS (1995). Unlike GPS, however,

VLBI does not operate continuously. A single large VLBI network, organized by the National Earth Orientation Service (NEOS), runs for 24 hours once per week specifically to monitor all components of Earth orientation (Eubanks *et al.*, 1994). Estimates of UT1 and LOD from each weekly session have formal uncertainties of $\sim 5 \mu\text{s}$ and $\sim 10 \mu\text{s/d}$, respectively. To monitor subweekly UT1 variations, a separate series of 1-hour VLBI sessions runs nearly daily using a single east-west baseline between the eastern U.S. and Germany (Ray *et al.*, 1995). These abbreviated VLBI sessions cannot determine LOD but do give UT1 estimates with formal uncertainties of roughly $20 \mu\text{s}$. In addition to the sessions to monitor Earth orientation, a variety of other VLBI networks operate for 24-hour periods at irregular intervals, mostly organized by NASA for such purposes as crustal motions studies. While some of these determine UT1 and LOD as well or better than the NEOS network, others are geometrically weak.

We have considered all available VLBI sessions during a recent 16-month study period (489 days from 03 Jul. 1994 to 03 Nov. 1995; see following section) and used the homogenous analysis performed operationally by the U.S. Naval Observatory (USNO) referred to as series "n9504". This series was submitted to the International Earth Rotation Service for its 1994 annual compilation (IERS, 1995). During the study period, 196 estimates of UT1 and LOD are available from 24-hour VLBI sessions with average formal uncertainties of $8 \mu\text{s}$ and $17 \mu\text{s/d}$, respectively. An additional 310 UT1 determinations, with an average formal uncertainty of $21 \mu\text{s}$, are contributed by the quasi-daily 1-hour sessions. Following tidal correction, these data have then been fit to cubic splines to interpolate LODR values for each daily noon epoch in the study period. Individual spline segments are fit to the UT1R values available between successive 24-hour sessions with the slopes at each end constrained to equal $-\text{LODR}$ from the 24-hour sessions. LODR at each noon epoch is simply the negative derivative of the UT1R spline fit. To avoid sometimes erratic behavior, it is necessary to edit the input data to cull poorly determined sessions and to eliminate data points spaced close together in time. The editing criteria were to omit UT1R and LODR values with formal uncertainties greater than $100 \mu\text{s}$ and $50 \mu\text{s/d}$, respectively, and to delete data points closer together than 0.8 d based on larger formal uncertainty. Figure 1 (top) shows the resulting LODR time series, which is dominated by a large annual variation caused predominantly by the seasonal exchange of angular momentum between the atmosphere and the solid Earth (*e.g.*, Hide and Dickey, 1991).

Errors have also been interpolated in an attempt to estimate the accuracy of the resulting daily time series of LODR values. First, the formal UT1R and LODR uncertainties from the VLBI analysis were rescaled by a factor of 1.35 to account for likely underestimation of the true errors and an error floor of $15 \mu\text{s}$ was applied to the UT1R estimates from the 1-hour sessions; see Ray *et al.* (1995) for a discussion of these issues. Interpolation of the adjusted VLBI errors to the daily noon epochs of the LODR time series generally follows the development of Morabito *et al.* (1988). They have shown that LODR variations can be represented by an integrated white noise process (*i.e.*, a random walk) driven by changes in atmospheric angular momentum; thus UT1R varies as an integrated random walk. Using their formulation, errors will grow as

$$\begin{aligned}\sigma_{\text{LODR}} &= Q^{1/2} t^{1/2} = (60 \mu\text{s/d}) t^{1/2} \\ \sigma_{\text{UT1R}} &= (Q/3)^{1/2} t^{3/2} = (34.6 \mu\text{s}) t^{3/2}\end{aligned}$$

where t is the time (in days) since the last known values of UT1R and LODR, respectively. Q is the power spectral density of the underlying white noise process, equal to $3600 \mu\text{s}^2/\text{d}^3$ according to Morabito *et al.* Since our case involves interpolation between two observed values of UT1R and/or LODR, the above error propagations have been

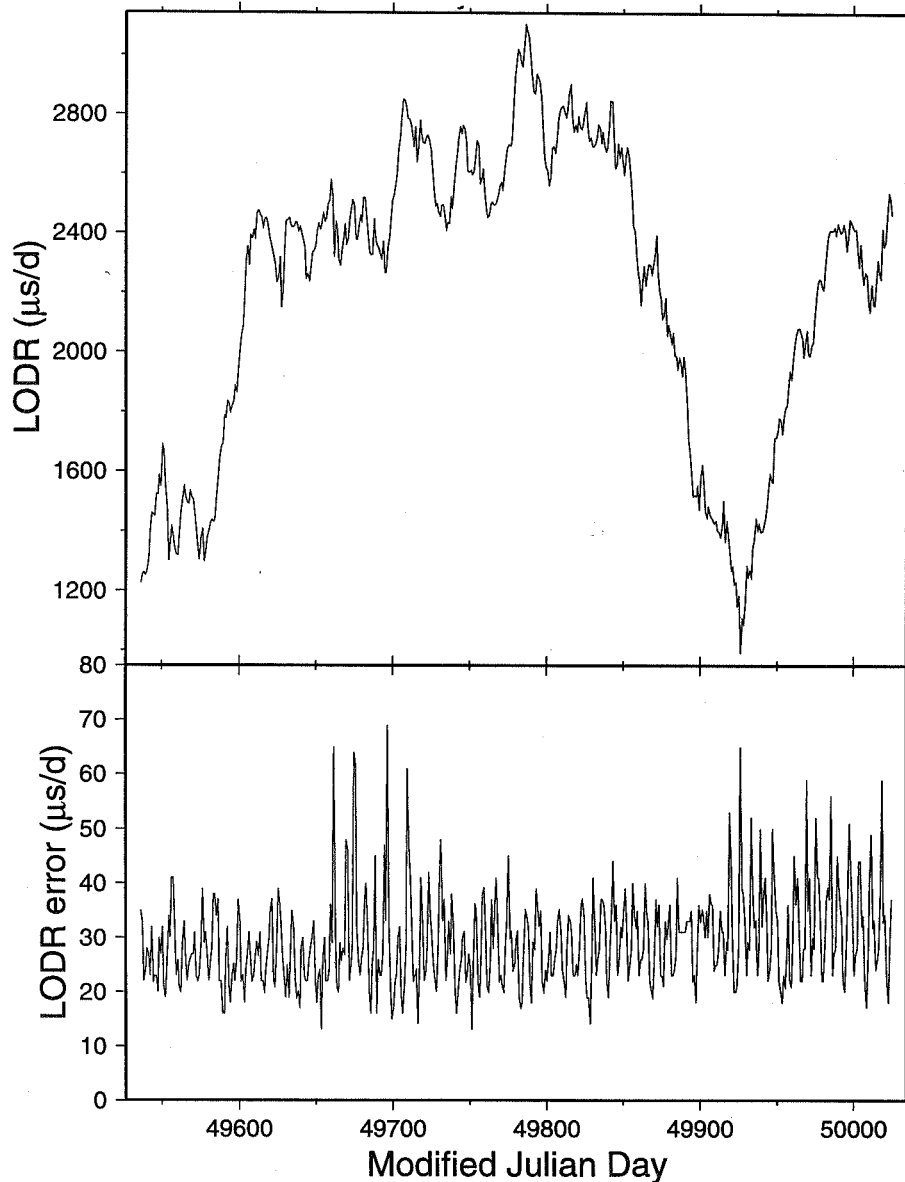


Fig. 1 LODR values (top) determined by a spline fit to UT1 and LOD estimates from VLBI data analysis by USNO. The corresponding LODR errors (bottom) are derived using the AAM excitation model of Morabito *et al.* (1988).

reduced by a factor of $\sqrt{2}$. Finally, the adopted error of each interpolated LODR value has been taken to be the minimum of: the interpolated LODR errors from each of the nearest LODR measurements; the errors in the time rate of change of UT1R interpolated from each of the nearest UT1R measurements. The resulting time series of LODR errors is plotted in Figure 1 (bottom). The average LODR error over this 16-month period is $26.2 \mu\text{s/d}$. The 7-day modulation of the LODR errors evident in Figure 1 is due to the weekly interval between the robust, 24-hour VLBI sessions.

The methodology above may over-estimate interpolated LODR errors somewhat. The power spectral density value of Morabito *et al.* was derived from fits to daily atmospheric

angular momentum estimates and may not apply for periods less than ~2 d. Eubanks and Archinal (1996) offer evidence of an *upper limit* for Q which is about one-fourth the Morabito *et al.* estimate for periods under a day.

LODR TIME SERIES FROM GPS

The GPS data processing functions of the IGS (Beutler *et al.*, 1994) are performed independently by seven Analysis Centers (ACs), each of which receives raw observational data from a set of globally distributed, continuously operating receivers and produces daily estimates of the GPS satellite ephemerides, Earth orientation parameters (EOPs), station coordinates, and other products. The individual orbit results are then combined by the Analysis Center Coordinator to form a single IGS ephemeris for each GPS satellite. All products from the ACs and the IGS combinations are available from the IGS Data Centers. Table 1 lists the IGS ACs together with their three-letter code signifiers. Each AC uses its own data analysis software except that JPL and EMR both use the JPL-developed GIPSY package. Four ACs (COD, ESA, NGS, and SIO) analyze the GPS carrier phase data as double-differences while the other three Centers (EMR, GFZ, and JPL) use undifferenced data. Descriptive reports from each AC, together with additional information about IGS operations, are contained in the *IGS 1994 Annual Report* (IGS, 1995).

Table 1. IGS Analysis Centers

Code	Institution
COD	Center for Orbit Determination in Europe (CODE), Astronomical Institute, University of Bern, Bern, Switzerland
EMR	Natural Resources Canada (NRCan), Ottawa, Canada
ESA	European Space Agency, European Space Operations Center, Darmstadt, Germany
GFZ	GeoForschungsZentrum, Potsdam, Germany
JPL	Jet Propulsion Laboratory, Pasadena, California, USA
NGS	National Oceanic and Atmospheric Administration (NOAA), Silver Spring, Maryland, USA
SIO	Scripps Institution of Oceanography, La Jolla, California, USA

For this study we assume that the LODR (and UT1R where available) estimates of the IGS ACs are strictly independent of the LODR and UT1R values determined by USNO from VLBI observations. Conceivably, this assumption could be violated if constraints were applied in any of the GPS data analyses relative to a priori UT1 information from, for example, an IERS combination UT1 time series or prediction series, dominated by the VLBI contribution. We have no evidence that such constraints are significant.

Earth orientation product files for each AC have been retrieved from the IGS Global Data Centers for the 16-month time period from 03 Jul. 1994 (MJD 49536.5) through 03 Nov. 1995 (MJD 50024.5), a span of 489 days. The starting date corresponds to the implementation of a standard IGS format for reporting Earth orientation results. EOP results are nominally reported for each 24-hour span at UTC noon epochs. Two ACs did not report LODR results for the full period: SIO omitted two weeks (MJD 49921.5-49927.5 and 49956.5-49962.5); NGS began reporting LOD on 06 Aug. 1995 so that only

90 days are available. Where necessary, tidal corrections were applied to reported LOD values.

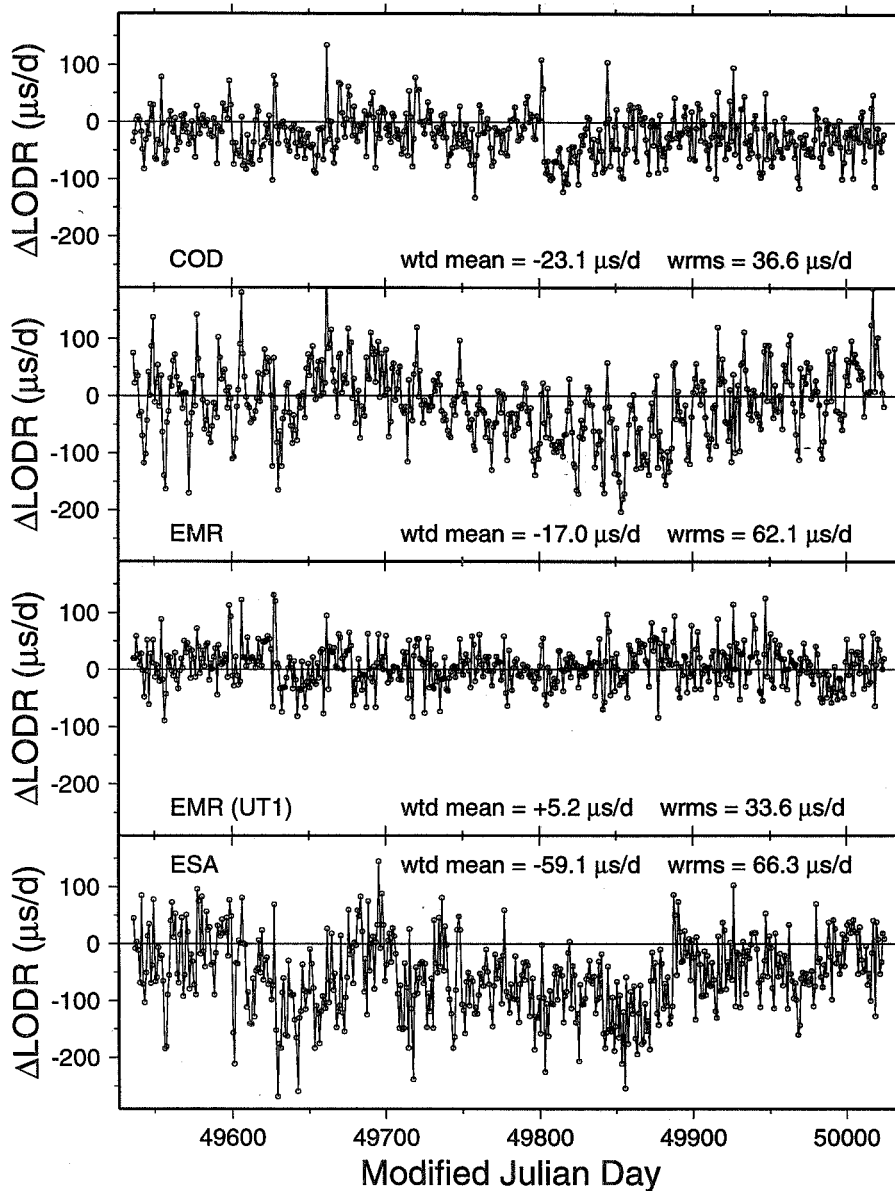


Fig. 2a LODR differences of each GPS time series relative to the VLBI-derived values shown in Figure 1. For each GPS series, weighted mean LODR differences and weighted rms scatters are listed using the VLBI-derived errors only.

EMR is a special case in reporting independent LOD and UT1 time series. (COD and JPL also report UT1 values but theirs are integrals of the estimated LOD values.) Stochastic modeling of the orbit parameters coupled with *a priori* constraints on the initial satellite states (based on the previous day's orbits) permits EMR to determine UT1 and the satellite nodes simultaneously (T treault *et al.*, 1995). In order to include the EMR UT1 series in this study the data were converted to LODR by first removing the tidal variations, then fitting with a cubic spline, and evaluating the spline derivatives at each

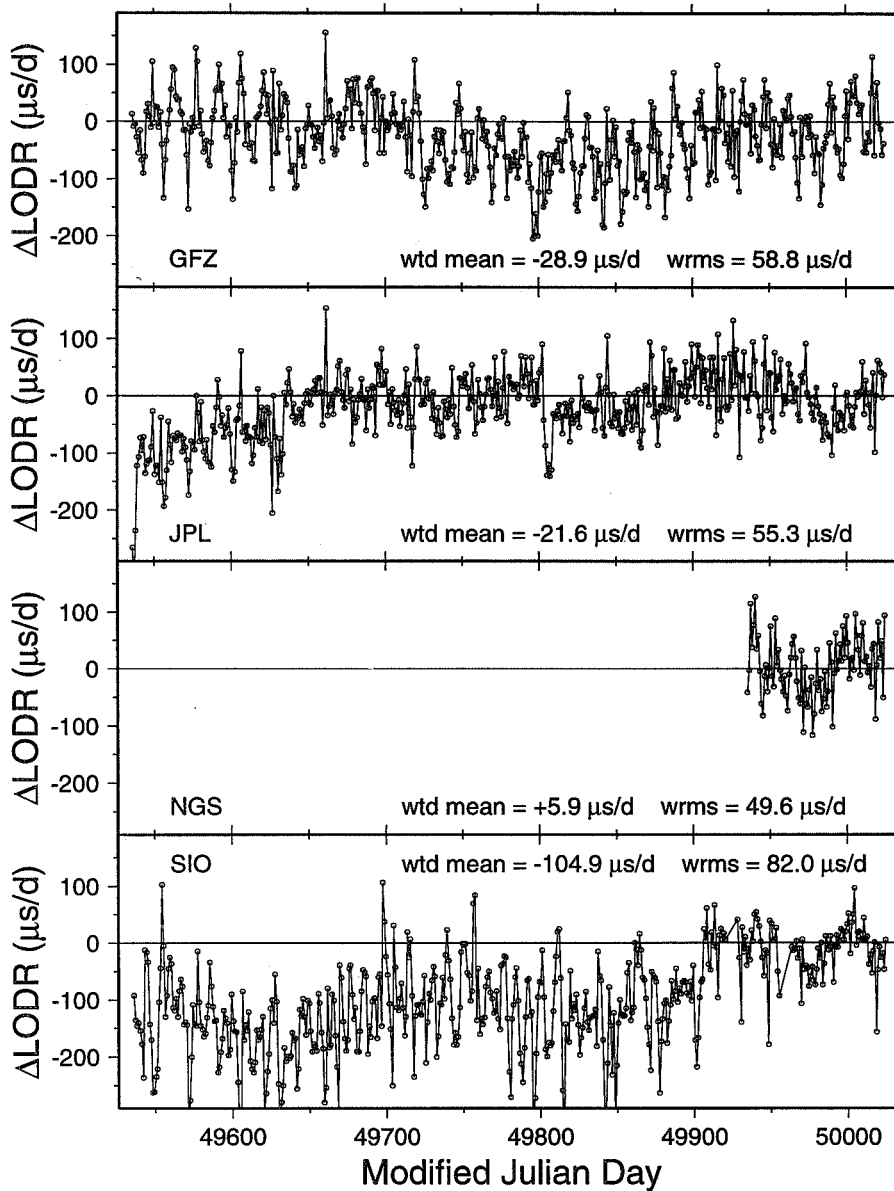


Fig. 2b Continuation of Figure 2a.

UT1 epoch. In the following sections, this derived LODR series is distinguished from EMR's directly estimated LODR series by being labelled "EMR (UT1)".

Figures 2a and 2b plot the differences of each GPS-based LODR time series with respect to the reference LODR series derived from VLBI data (shown in Figure 1). The weighted means of the differences and the weighted rms (wrms) scatters about the means are also shown. In computing these statistics, the LODR differences have been weighted using the estimated LODR errors of the VLBI-derived series only. The formal LODR uncertainties reported by the IGS ACs are very uniform in time and unrealistically small, ranging from an average value of 1.4 $\mu\text{s/d}$ for COD to 17.9 $\mu\text{s/d}$ for ESA. For this reason, the GPS formal uncertainties have been ignored.

IERS TIME SERIES C04

The IERS generates a continuously updated time series of daily EOP values referred to as C04, which is a combination of independent results from a variety of techniques and analyses. It is described as "slightly low-pass filtered" and suited for "all applications where an accurate model of the Earth orientation irregularities is needed" (IERS, 1995). Because this series is often used as a reference for comparison, its differences have also been computed relative to the VLBI-derived LODR series and the results shown in Figure 2c. Note, however, that C04 is not independent of the other series, having incorporated the n9504, COD, and EMR (UT1) series, among others.

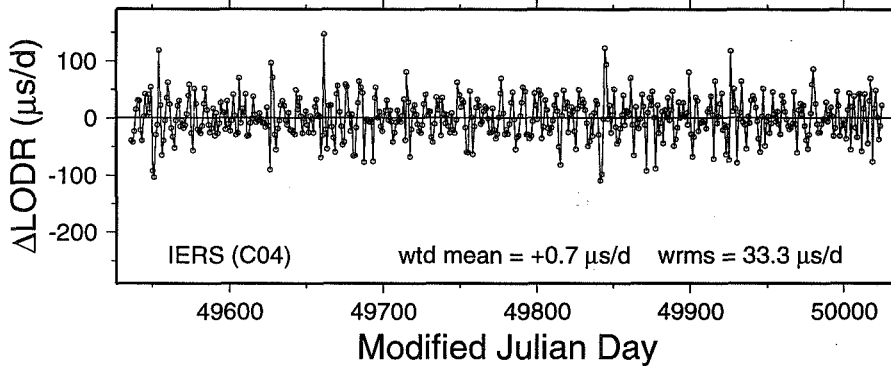


Fig. 2c LODR differences of IERS multi-technique combination series C04 relative to the VLBI-derived values shown in Figure 1. The weighted mean and rms scatter values shown use weights from the VLBI-derived errors only.

DISCUSSION OF LODR DIFFERENCES

A number of interesting observations can be drawn from inspection of the LODR differences plotted in Figures 2a and 2b. Most important is the fact that all GPS series show significant LODR biases relative to VLBI and usually the biases drift considerably with time. A constant LODR bias is equivalent to a linear time-dependent (UT1R - TAI) error (see further discussion below). Among the ACs, EMR (UT1) has the smallest and most stable bias with an overall wrms of 33.6 $\mu\text{s/d}$. COD shows the next best scatter with a wrms of 36.6 $\mu\text{s/d}$ but with a larger bias and an abrupt bias shift around MJD ~49803 (27 Mar. 1995). The remaining series are more variable although most show indications of improvement in the more recent data, particularly JPL and SIO.

Another important feature is the occurrence of correlated differences between series. Because a common VLBI-derived LODR reference has been used for all the differences, correlations are to be expected at some level. However, some correlations appear more likely to reflect errors common to one or more of the GPS series. Figure 3 illustrates such a case. In the top part of the figure are plotted expanded views of the LODR differences for the COD, EMR (UT1), and JPL series relative to VLBI. From MJD 49802.5 to 49803.5 (26-27 Mar. 1995) all three series show large changes in ΔLODR : -127, -99, and -132 $\mu\text{s/d}$, respectively. It is entirely possible that part of these abrupt shifts is caused by inaccuracies in the reference series. The bottom part of Figure 3 shows an expanded view of the daily VLBI-derived LODR series from Figure 1 while the middle part of the figure shows the distribution of available VLBI data (after editing) and their associated errors (after the adjustments discussed previously). It can be seen that

the Δ LODR shifts fall near the middle of a 3.7-d gap in the VLBI data during which an extremum of the LODR variation occurs. Thus the VLBI-derived LODR values around MJD 49803 are sensitive to the spline fit and may be suspect. On the other hand, the COD and JPL series show persistent LODR bias changes following the abrupt shift, whereas EMR (UT1) does not. More than 20 days pass before the COD series returns to its previous bias level; the independent JPL series is similar although the detail behavior appears more complex. It is perhaps noteworthy that the Analysis Center Coordinator reported orbit modelling problems by all ACs for eight GPS satellites during the week 26 Mar. - 01 Apr. 1995 (Kouba *et al.*, 1995).

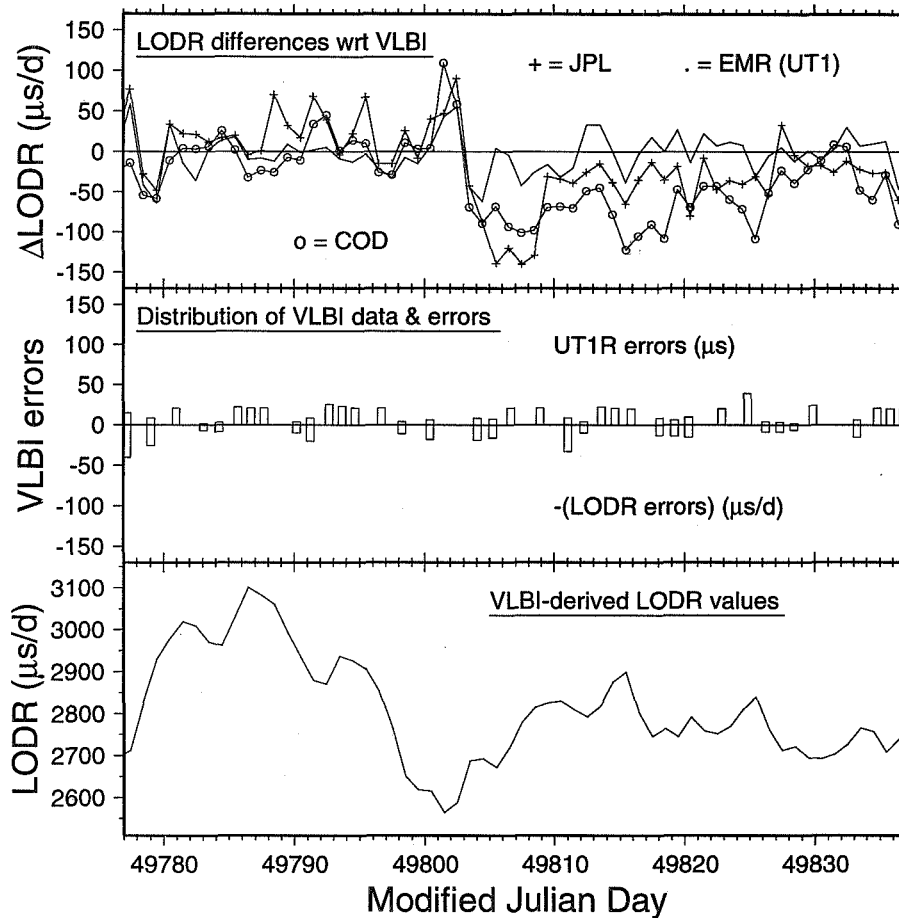


Fig. 3 Expanded view of LODR differences for COD, EMR (UT1), and JPL during March-April 1995 (top). Corresponding VLBI-derived LODR values shown in the bottom with the distribution of VLBI data and errors shown in the middle.

An even more striking example of correlated errors between ostensibly independent GPS time series is shown in Figure 4, which is an expanded view of the last 125 days of Δ LODR time series for EMR (see Figure 2a) and GFZ (see Figure 2b). Both display large, systematic LODR variations that appear quasi-periodic and are highly correlated. This behavior characterizes the full study period, not just the range expanded for Figure 4. In contrast, the EMR series derived from their directly estimated UT1 series, EMR (UT1), has a very different behavior (see Figure 2a). Presumably, some aspect of the satellite orbit modelling by EMR and GFZ allows similar error leakage into their LODR estimates even though their analysis systems are independent.

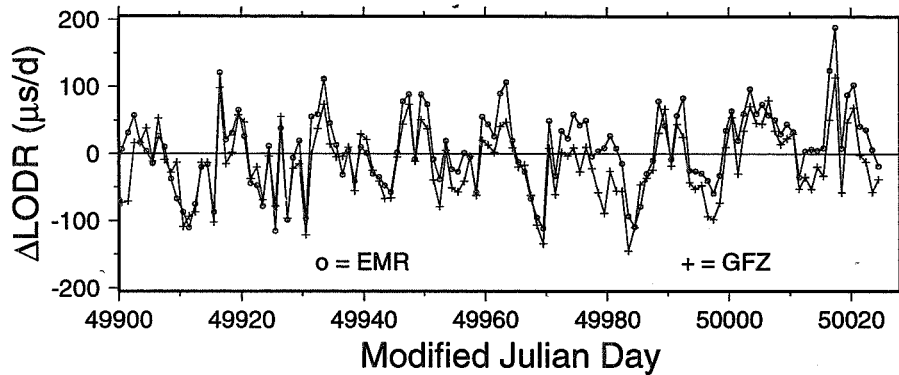


Fig. 4 Expanded view of LODR differences from Figures 2a and 2b for EMR and GFZ showing highly correlated variations.

These ΔLODR time series are direct evidence that: non-zero LODR biases are a natural consequence of the GPS data analysis; LODR bias values and stability range widely depending on the analysis procedures used; LODR bias values are correlated in time for individual analyses and vary over a wide range of timescales; and large LODR errors may be correlated between nominally independent analysis systems. These characteristics must be taken into account if GPS LODR results are to be combined successfully with those from other techniques.

Finally, Figure 5 shows an expanded view of the LODR differences between IERS combined series C04 and VLBI (from Figure 2c). It is evident that the differences are not random and that there appear to be distinct periodicities. Since the n9504 VLBI data are common to both time series the differences should reflect the different styles for interpolating the observational results to an even time grid and the effects of other contributors to the C04 combination. According to IERS (1995), the UT1R and LODR values in series C04 have been smoothed over periods <20 d; the filter response is $\sim 50\%$ at 9-d periods. Thus, it seems reasonable to attribute much, if not most, of the systematic differences between C04 and VLBI to the smoothing applied in the C04 combination. This is important to note when characterizing LODR variations at the few-day level, as

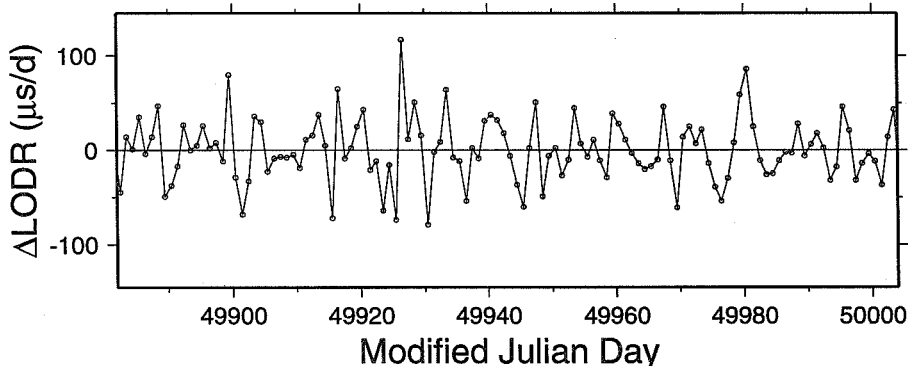


Fig. 5 Expanded view of LODR differences from Figure 2c for IERS combination series C04 showing systematic, quasi-periodic variations probably due to smoothing applied in the combination.

we are here. The C04 series is, however, unbiased relative to VLBI LODR over few-

week periods.

ANALYSIS OF SCATTER OF GPS-DERIVED LODR ESTIMATES

Because the bias levels of GPS-derived LODR time series vary with time, a single wrms statistic for the entire 16-month study period does not adequately convey the performance over shorter intervals. To address this, wrms values for each Δ LODR time series have been recomputed using variable intervals over which to remove mean LODR biases. Figure 6 is a plot of the results for each AC and the IERS combination series C04. (The NGS data have been omitted here and in subsequent discussions due to their limited span.) At the longest interval, the wrms values are those shown in Figures 2a, 2b, and 2c. For a time series with stable LODR bias and random Δ LODR differences, the trend in Figure 6 would be flat with no dependence on bias interval. Only the IERS combination series C04 has an approximately flat trend, down to about 1-month intervals. EMR (UT1) and COD show the least influence of bias shifts among the GPS series. JPL, GFZ, EMR, ESA, and SIO all display steady declines in wrms Δ LODR scatter for shorter bias intervals, revealing the significance of LODR bias drifts.

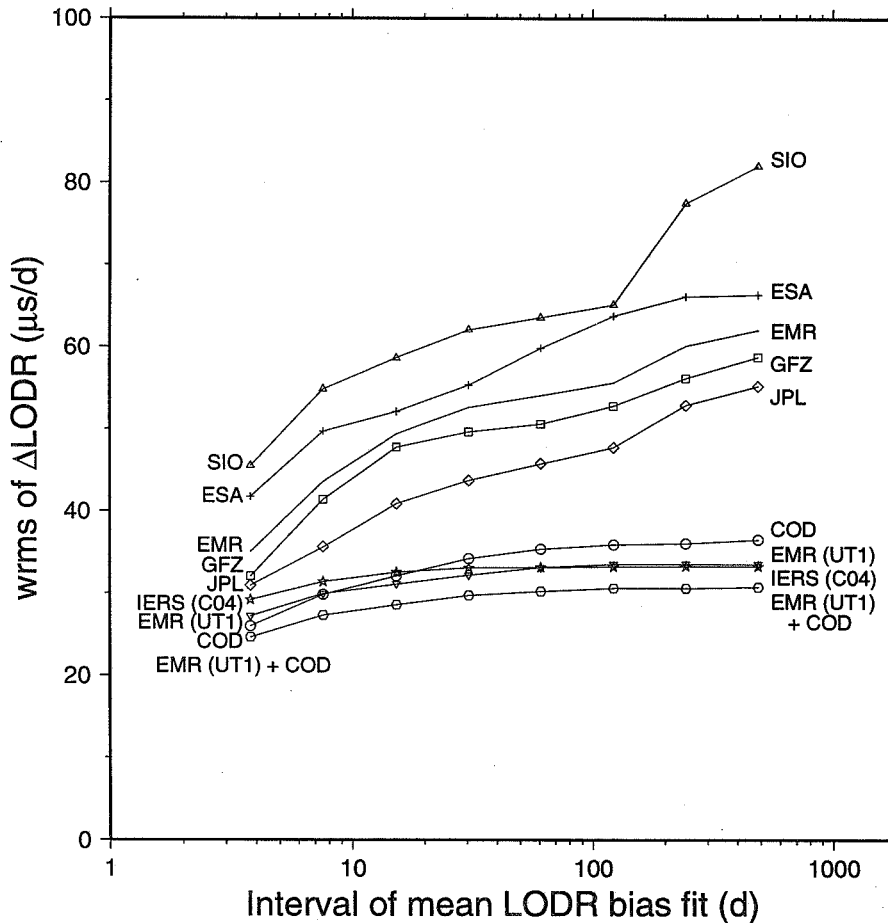


Fig. 6 Scatter of LODR differences for variable intervals used to fit mean LODR biases. Shown in addition to each IGS time series is the IERS combination C04 and an average GPS series formed by EMR (UT1) and COD.

Interestingly, while the wrms of the EMR (UT1) series is only very slightly greater than IERS C04 over the longest spans, it is less over intervals of ~60 d and shorter. At ~1-week periods EMR (UT1) agrees significantly better with VLBI than does IERS, wrms differences being 29.9 $\mu\text{s/d}$ versus 31.4 $\mu\text{s/d}$. This is evident by comparing Figure 2c with Figure 2a where it can be seen that EMR (UT1) tracks VLBI LODR variations very closely for extended periods, a pattern which is less apparent in the IERS LODR differences. Similarly, the COD series also agrees better with VLBI than does IERS over intervals shorter than ~20 d. Again, we attribute the poorer short-term agreement for IERS to smoothing applied in forming the C04 combination series.

Motivated by the encouraging performances of EMR (UT1) and COD, it is worth evaluating an LODR series formed from the combination of those two. If their errors are largely independent, then such a combination should have improved performance. Such a series has been formed by simple averaging and its stability is included in Figure 6 labelled as "EMR (UT1) + COD". This GPS combination LODR series has a weighted mean LODR difference relative to VLBI of -8.8 $\mu\text{s/d}$ and a wrms of 30.8 $\mu\text{s/d}$. It has a smaller wrms ΔLODR scatter than IERS C04 over all intervals, by 2.5 $\mu\text{s/d}$ over the longest spans increasing to 4.6 $\mu\text{s/d}$ at ~4 d. This is a clear indication that the information content of the various contributors (including VLBI, EMR (UT1), and COD) has not been optimally utilized in forming the IERS combination, probably due mostly to smoothing.

Tests with forming GPS-only LODR combinations using additional series have been less successful. While the results will depend to some extent on the scheme used to weight the ACs, only the addition of JPL to the EMR (UT1) + COD combination gives a scatter smaller than the EMR (UT1) series alone, and only very slightly. (See further discussion on GPS combinations below.)

If we accept the validity of the VLBI-based LODR error distribution shown in Figure 1 (where the average error is 26.2 $\mu\text{s/d}$) and assume that all other errors are independent (which is clearly not true for IERS C04) and Gaussian (also not true over short spans, at least) then we can infer the noise-like "error" of each of the other series, after bias correction, averaged over the 16-month span: COD 25.5 $\mu\text{s/d}$, EMR (UT1) 21.0 $\mu\text{s/d}$, EMR 56.3 $\mu\text{s/d}$, ESA 60.9 $\mu\text{s/d}$, GFZ 52.6 $\mu\text{s/d}$, JPL 48.6 $\mu\text{s/d}$, SIO 77.7 $\mu\text{s/d}$, and IERS C04 20.6 $\mu\text{s/d}$. These results imply a noise-like error of 16.5 $\mu\text{s/d}$ for the EMR (UT1) + COD combination. Since the VLBI errors are likely to be pessimistic, the inferred error estimates for the other series are actually lower limits.

IMPLICATIONS FOR MONITORING UT1

Despite the striking statistical agreement presented above between VLBI and some GPS determinations of LODR, the implications for monitoring UT1 remain unclear at this stage. Consider an ideal GPS-derived LODR time series which is unbiased and which has a small, random noise error, σ_{LODR} . Then integration will provide estimates of (UT1R - TAI) variation as a function of time t following some initializing epoch. If the LODR errors are white noise distributed, the error in the derived (UT1 - TAI) will grow as a random walk, that is, as $t^{1/2}$. If there is an uncorrected LODR bias, then the UT1 error will have an additional linear drift contribution proportional to time. Rather than having a single well defined bias, if occasional bias shifts occur, then the resulting UT1 will tend to follow a series of roughly linear segments connected by sharp changes in drift overlaying a random walk pattern.

Compare this expectation with actual results of integrating the differential LODR time series for COD, EMR (UT1), IERS (C04); and EMR (UT1) + COD, shown in Figure 7. (The other GPS series give much larger and more erratic $\Delta UT1R$ variations.) In each case the overall LODR bias has been removed before integration, producing the inferred variation of (UT1-TAI) relative to the VLBI n9504 time series. For clarity, the curves have been offset from one another by 500 μs . Because the mean LODR difference has been removed from each series (equivalent to removing an overall UT1R drift), $\Delta UT1R$ values are equal to zero at the beginning and end of each. Integration of IERS (C04) yields a $\Delta UT1R$ trend which is flat with relatively small scatter. It does not follow a random walk because the IERS LODR series was presumably derived by differentiating the C04 UT1R series. Integration merely restores the original UT1R variation and shows that differencing of the IERS LODR series with VLBI has not introduced any unexpected artifacts.

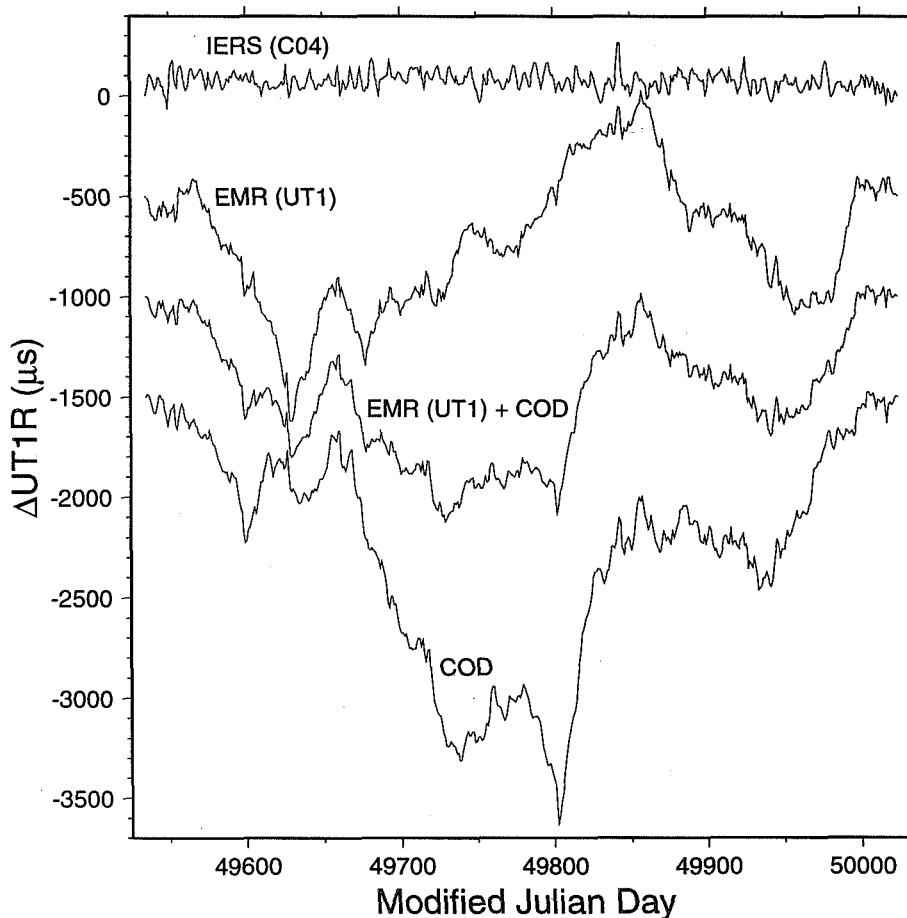


Fig. 7 UT1R variations, relative to VLBI, from integrating LODR differences for the COD and EMR (UT1) series, their average, and the IERS combination C04. Trends have been offset from one another by 500 μs .

The trends of the GPS-derived $\Delta UT1R$ series more closely resemble random walks. The excursions for COD, more than 2100 μs , are distinctly larger than for EMR (UT1), $\sim 1100 \mu s$ despite similar inferred LODR “noise” estimates of 25.5 and 21.0 $\mu s/d$. This difference in behavior is not likely to be related simply to the random walk effect of integrating white noise. Inspection of Figure 2a shows that the COD LODR differences

are not random, even apart from the bias shift at MJD ~49803. There are clear trends in the LODR bias level with time. Computing LODR bias fits at 1-month intervals, gives values ranging from $-2.8 \mu\text{s/d}$ to $-53.3 \mu\text{s/d}$, compared with the overall bias of $-23.1 \mu\text{s/d}$. Over 1-month periods, such biases will accumulate to UT1 excursions of $-600 \mu\text{s}$ to $+900 \mu\text{s}$ relative to the overall trend, as observed in Figure 7. The range of month-long LODR bias drifts is smaller for EMR (UT1), from $-13.0 \mu\text{s/d}$ to $+23.8 \mu\text{s/d}$ about the overall mean of $+5.2 \mu\text{s/d}$, and better distributed about the overall mean bias, as evident in Figure 2a. The derived ΔUT1R for EMR (UT1) could be considered roughly consistent with the random walk model although the effects of small LODR bias shifts are still apparent. However, considering this series was originally estimated directly as UT1, then differentiated for this study before being integrated back to UT1, the behavior should resemble IERS C04. That it does not, but is closer to a random walk, indicates that the EMR analysis procedure actually models this parameter more as an integrated LODR than a true UT1, as expected for a satellite-based technique.

Based on these results, a Gauss-Markov process is probably a better model for the LODR errors of the GPS estimates (after bias correction) than is pure white noise. For this case, the autocorrelation function for a time lag t is $\sigma_{\text{LODR}}^2 \exp(-|t|/\tau)$ where τ is a characteristic correlation time constant. For comparison, the autocorrelation function for white noise is a Dirac delta function. Upon integration, the variance of the resulting

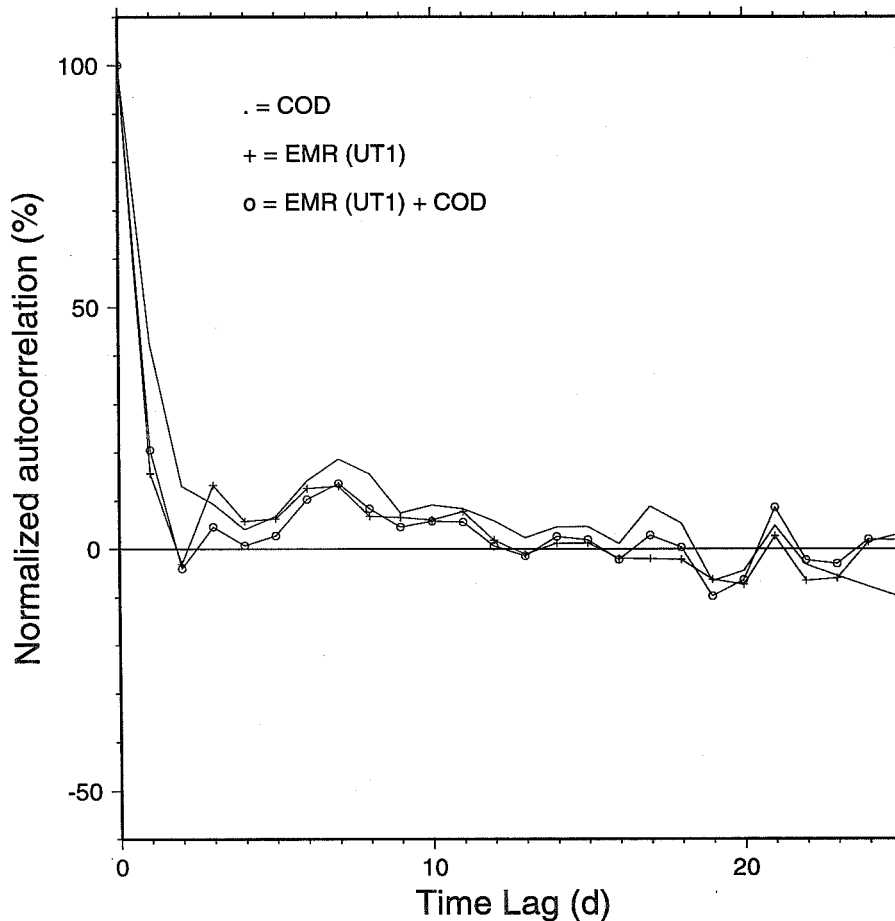


Fig. 8 Autocorrelation functions, normalized by σ_{LODR}^2 , for the LODR differences of the COD and EMR (UT1) series, and the average of those two.

UT1R will then be

$$\begin{aligned}\sigma_{\text{INT-LODR}}^2 &= \int_0^t \int_0^t \sigma_{\text{LODR}}^2 \exp(-|u-v|/\tau) du dv \\ &= 2 \tau \sigma_{\text{LODR}}^2 [t - \tau + \tau \exp(-t/\tau)]\end{aligned}$$

as a function of the length of integration t . (Refer to Brown and Hwang (1992) for background.) Now, to evaluate correlation time constants τ for the best GPS series, Figure 8 shows autocorrelation functions (normalized by σ_{LODR}^2) for COD, EMR (UT1), and the combination EMR (UT1) + COD. It can be seen that τ is slightly greater than 1 d for COD and about 0.75 d for the other two series. Autocorrelation functions for the remaining series (not shown) are not well represented as Gauss-Markov processes, sometimes having large periodicities and with e^{-1} time constants of several days.

To put these results into context, Figure 9 shows the expected UT1R errors due to integration of an unbiased LODR series with Gauss-Markov errors (plotted as the solid lines) compared with the estimated errors of the current operational VLBI program (plotted as '+'). A full 24-hour VLBI session occurs weekly with daily 1-hour sessions in between (see prior discussion). The VLBI errors plotted are the average values for the data used in this study, rescaled as described previously. For the hypothetical GPS-derived UT1R error, we assume a time series of LODR measurements which have been bias-corrected (presumably based on some prior history of measurements) and have a long-term scatter of $\sigma_{\text{LODR}} = 16.5 \mu\text{s/d}$, the estimated value for the EMR (UT1) + COD combined LODR series. The GPS-determined LODR series is then integrated and the initial UT1R value set to the result of one of the weekly 24-hour VLBI sessions. Three different values are considered for the LODR correlation time constant τ , 0.1, 1, and 10 d. For the best observed GPS performance, where $\tau \approx 1$, the UT1R error exceeds that of the 1-hour daily VLBI sessions after 2-3 d of integration and it exceeds 100 μs after 20 d. If τ were improved to ~ 0.1 d, the resulting UT1R error would exceed that of the daily VLBI sessions after ~ 2 weeks of integration. It must be stressed that these results assume

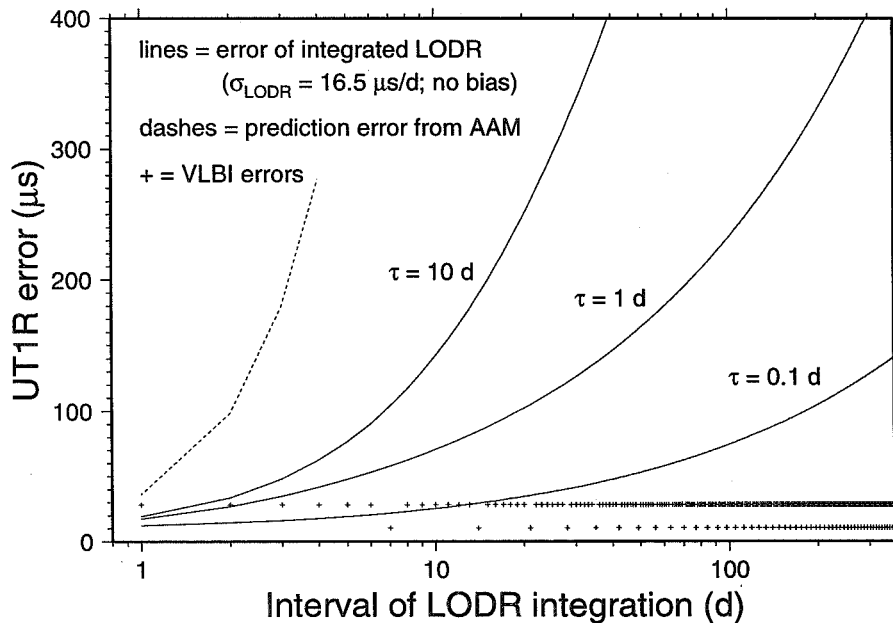


Fig. 9 Growth of inferred UT1R error from integration of hypothetical GPS-derived LODR time series (three cases), compared with current VLBI and prediction.

that the LODR bias has been well determined and removed, and that no changes in bias occur during the integration period.

A STRATEGY FOR IGS LOD/UT1 COMBINATION

The current IGS strategy for combining polar motion results, which weights the individual AC contributions using their weights from the orbit combination, is less likely to be appropriate for combining LOD or UT1 results because of the indistinguishability of UT1 changes from a net node shift. A better strategy would probably rely on the statistical performance of each LOD series, relative to the combination, as determined over a recent time span. For example, consider forming a combined LOD series from the LOD estimates of all the ACs for the most recent N days. Based on the results seen above, particularly in Figures 2a and 2b where LOD biases are shown to sometimes vary systematically over few-week periods, N should probably be chosen to be at least 30 d. For EMR, the differentiated UT1 series should be used instead of the directly estimated LOD series. The LOD combination would be done iteratively, first forming an unweighted mean series for all epochs with data from all ACs. The LOD bias and rms for each AC can then be computed and used to next form a weighted mean LOD series. Iterating, weighted LOD biases and weighted rms values can then be computed and used to recompute the combination series.

The IGS weighted mean LOD series can then be compared to the most recent IERS Bulletin A series to determine and remove the LOD bias and to initialize the UT1 value. (Clearly, the series length N must be sufficiently long to provide adequate overlap with Bulletin A.) This could most simply be done by identifying two recent adjoining days in Bulletin A having accurate UT1 values, then interpolate UT1 to the midpoint noon epoch and use $\text{LOD} = -\Delta\text{UT1}$ to evaluate the LOD bias of the IGS series.

Test LOD combinations have been made using the 16-month data sets described above, with $N = 30, 60,$ and 120 d. In addition, the relative AC weighting was tested using $(1/\text{wrms})^2$ and $(1/\text{wrms})^4$ weights. Compared with the VLBI-derived LOD series, the mean IGS combination is not sensitive to either the weighting factor or the data span, with wrms LOD differences between 30.7 and 31.7 $\mu\text{s/d}$. This compares with a wrms value of 30.8 $\mu\text{s/d}$ for the simple average series of EMR (UT1) + COD.

CONCLUSIONS

First and foremost, it can fairly be said that GPS does not measure LOD (or UT1) proper, but rather “pseudo-LOD” in analogy with “pseudo-range”. All of the GPS-derived LOD time series examined here possess significant biases relative to VLBI determinations and the biases vary widely among the different IGS Analysis Centers. Within individual series, there are time-dependent variations in the LOD bias levels which are in some cases large and periodic and in other cases abrupt. In addition, there are clear correlations between the results of ostensibly independent GPS analyses suggesting the effects of similar choices in data modelling. Taken together, these results demonstrate the critical importance of analysis procedures in influencing LOD bias and stability. Until such time as the sources of LOD bias are understood and corrected, GPS determinations must be regarded as biased estimates and adjustments applied accordingly. In practical terms this can only be done by comparing overlapping LOD time series from VLBI and GPS and computing empirical corrections for GPS. For a retrospective analysis, such a procedure

is straightforward. In an operational environment, such as near real time EOP monitoring and UT1 prediction, accurate VLBI values may not be readily available thus allowing the possibility of undetected LODR bias shifts and substantial UT1 errors.

In the best cases, GPS LOD time series have wrms differences of $\sim 34 \mu\text{s/d}$ compared with VLBI. If the VLBI errors have been estimated accurately here and all errors were Gaussian and uncorrelated, then the intrinsic error of the GPS estimates, after bias correction, approaches $\sim 21 \mu\text{s/d}$. By combining LOD results from the two best GPS series (EMR's UT1-derived and COD's) an even smaller scatter of perhaps $\sim 16.5 \mu\text{s/d}$ can be achieved. However, if such a series is integrated to give UT1, its errors will grow at least as fast as $t^{1/2}$ from the epoch when UT1 is initially fixed. The resulting UT1 error coefficient depends on the LODR error correlation time constant, which is $\sim 0.75 \text{ d}$ in the best case. Given the current VLBI operational mode, the expected UT1 error from integration of GPS LOD, even in the best case, will exceed that of the daily 1-hour VLBI sessions after $\sim 3 \text{ d}$. This observation makes it highly questionable whether GPS can currently contribute much, if any, useful information to the current sequence of UT1 measurements made by VLBI. Indeed, this conclusion is compounded if allowance is made for even small shifts in LOD bias, which give rise to changes in UT1 drift rate and which appear pervasive. The evidence thus indicates that combining GPS results with VLBI-derived UT1 would most likely degrade the quality of a VLBI-only solution. A contrary conclusion has been reached by IERS (1995), which has included the EMR (UT1) and COD GPS series in their combination C04, and by Boucher and Feissel (1995) who present filtered GPS comparisons to C04. However, we have shown above that the smoothing applied in forming the C04 combination renders it unsuitable for assessing UT1 variations for periods under $\sim 20 \text{ d}$, precisely the regime where GPS is expected to be most useful. Resolution of this issue would be aided by a comparison campaign using multibaseline VLBI sessions to observe both UT1 and LOD continuously for an extended period, say 6 months or longer.

Where GPS LOD measurements may stand to be most valuable is for near real time applications and UT1 prediction. Processing delays for global GPS data sets are now only a few days, already usually shorter than for operational VLBI data, and are expected to approach real time in the near future. Near real time LOD estimates from GPS can certainly be more accurate than extrapolation of prior UT1 time series considering that gaps of 5 d and 10 d from the most recent data lead to a UT1 errors of $\sim 387 \mu\text{s}$ and $\sim 1094 \mu\text{s}$ (Morabito *et al.*, 1988), respectively; see Figure 9. However, as stressed before, the reliability of such a service will depend critically on maintaining a high level of stability for LODR biases.

REFERENCES

- Beutler, G., I.I. Mueller, and R.E. Neilan, The International GPS Service for Geodynamics (IGS): Development and start of official service on January 1, 1994, *Bull. Geod.*, 68(1), 39-70, 1994.
- Boucher, C., and M. Feissel, IERS references, contributions of the Central Bureau of IERS, in IGS 1994 Annual Report, pp. 47-57, Jet Propulsion Laboratory, 1995.
- Brown, R.G., and P.Y.C. Hwang, *Introduction to Random Signals and Applied Kalman Filtering*, John Wiley & Sons, New York, 1992.

- Carter, W.E., D.S. Robertson, and J.R. MacKay, Geodetic radio interferometric surveying: Applications and results, *J. Geophys. Res.*, *90*, 4577-4587, 1985.
- Dickey, J.O., S.L. Marcus, J.A. Steppe, and R. Hide, The Earth's angular momentum budget on subseasonal time scales, *Science*, *255*, 321-324, 1992.
- Eanes, R.J., and M.M. Watkins, Earth orientation and site coordinates from the Center for Space Research solution, *IERS Tech. Note 17*, pp. L-7 - L-11, Obs. de Paris, 1994.
- Eubanks, T.M., and B.A. Archinal, Earth rotation changes at extremely high frequencies: Observation equations and empirical bounds, submitted to *Geophys. J. Int.*, 1996.
- Eubanks, T.M., B.A. Archinal, M.S. Carter, F.J. Josties, D.N. Matsakis, and D.D. McCarthy, Earth orientation results from U.S. Naval Observatory VLBI program, *IERS Tech. Note 17*, pp. R-65 - R-79, Obs. de Paris, 1994.
- Hide, R. and J.O. Dickey, Earth's variable rotation, *Science*, *253*, 629-637, 1991.
- International Earth Rotation Service (IERS), 1994 IERS Annual Report, Obs. de Paris, 1995.
- International GPS Service for Geodynamics (IGS), 1994 Annual Report, Jet Propulsion Laboratory, 1995.
- Kouba, J., Y. Mireault, and F. Lahaye, Wk 0794 IGS Rapid Orbits, IGS Electronic Report #1681, WWW document, <http://igs.cb.jpl.nasa.gov/igs.cb/mail/igsreport/igsreport.1681>, 1995.
- McCarthy, D.D. (Ed.), IERS Standards 1992, *IERS Tech. Note 13*, Obs. de Paris, 1992.
- Morabito, D.D., T.M. Eubanks, and J.A. Steppe, Kalman filtering of Earth orientation changes, in *The Earth's Rotation and Reference Frames for Geodesy and Geodynamics*, edited by A.K. Babcock and G.A. Wilkins, pp. 257-267, Kluwer, Dordrecht, 1988.
- Ray, J.R., W.E. Carter, and D.S. Robertson, Assessment of the accuracy of daily UT1 determinations by very long baseline interferometry, *J. Geophys. Res.*, *100*(B5), 8193-8200, 1995.
- Robertson, D.S., J.R. Ray, and W.E. Carter, Tidal variations in UT1 observed with very long baseline interferometry, *J. Geophys. Res.*, *99*, 621-636, 1994.
- Tétreault, P., J. Kouba, R. Ferland, and J. Popelar, NRCan (EMR) analysis report, in IGS 1994 Annual Report, pp. 213-231, Jet Propulsion Laboratory, 1995.
- Yoder, C.F., J.G. Williams, and M.E. Parke, Tidal variations of Earth rotation, *J. Geophys. Res.*, *86*(B2), 881-891, 1981.

MULTI-TECHNIQUE EOP COMBINATIONS

Daniel Gambis
IERS/CB Paris Observatory
61 avenue de l'Observatoire, Paris, France

ABSTRACT

The IERS Central Bureau regularly combines independent estimates of EOP values, mainly based on SLR, VLBI and GPS, to derive its operational series and also for long-term analysis. The contribution of these 3 techniques to geodynamics is important for their complementarity but also for some aspects linked to redundancy in order to eliminate systematic effects. For polar motion these 3 techniques give approximately the same accuracy (about 0.30 mas).

The determination of Universal Time is based on the VLBI technique. Still, satellite techniques (SLR, GPS) give information on the high-frequency UT1 behaviour on time scales limited to a couple of months; this signal can be used for densification of the UT1 series as well as for UT1 extensions on a quasi-real-time basis from the current VLBI available value. In that case errors are limited to about 200 microseconds over one week and 500 over 2 weeks. This represents an improvement of an order of magnitude with respect to the current prediction of UT1.

INTRODUCTION

Until 1972, Astrometry based on a network of optical instruments was the only technique able to monitor the Earth orientation. Since, various techniques have shown their capability for this purpose, doppler observations of navigation satellites, laser ranging to the moon and to dedicated satellites, VLBI and more recently GPS and DORIS. Various phenomena are perturbing the Earth Rotation on time scales ranging from a few hours to centuries and their understandings require extended and continuous series. The different EOP solutions are unequal in time length, quality, time resolution, which supports the concept of combined solutions benefitting of the various contributions. The realization of such series must take advantage of the qualities of the independent series at the various time scales. For practical reasons also linked to statistical applications, these series are given at equidistant intervals (1 day). They should contain no jump and negligible systematic errors; at least 3 independant techniques are thus highly desirable for that purpose. Table 1 shows the evolution of the uncertainty of one single value since 1962.

Table 1 . Uncertainty of one daily value of EOP (IERS) C 04.

Period	1962-1967	1968-1971	1972-1979	1980-1983	1984-1995	1996 --
X (mas)	30	20	15	2	0.5	0.3
Y (mas)	30	20	15	2	0.5	0.3
UT1(0.1 ms)	30	20	15	2	0.5	0.3
dPsi (mas)	12	9	5	3	0.5	0.3
dEps (mas)	2	2	2	2	0.5	0.3

Table 2 . Characteristics of the smoothings adopted for EOP(IERS) C 04. Variations with periods smaller than the values are smoothed out.

Period	1962-1967	1968-1971	1972-1979	1980-1983	1984-1995	1996 --
X	40d	40d	30d	15d	8d	3d
Y	40d	40d	30d	15d	8d	3d
UT1	17d	17d	15d	10d	8d	3d
dPsi					8d	3d
deps					8d	3d

In order to eliminate the white noise, the series are smoothed. The filtering characteristics have evolved (Table 2) according to the improvement of the series accuracies and to the temporal resolution. The present cutoff period corresponds to 2.5 days.

Another main aspect is the maintenance of the IERS reference systems. The transformation between the terrestrial and the celestial reference frame is performed via a product of matrices connected to EOP parameters. The inconsistency of the IERS EOP of Bulletin A and B with the IERS reference frames is given by the values printed on Table 3.

Table 3 . The value to add to the EOP time series in order to make them consistent with 1994 realization of the IERS terrestrial reference systems (ITRF94) is $A+A'$ ($t-1993.0$), t in Besselian years.

	x	y	UT1
	0.001"	0.001"	0.0001s
A	+0.05 (0.28)	+0.76 (0.29)	0.42 (0.16)
A'	+0.12 (0.07)	+0.11 (0.07)	0.04 (0.05)

MULTI-TECHNIQUE EOP COMBINED SOLUTION

The first step in the general procedure for deriving the IERS/CB multi-technique combined solution is the evaluation for each solution of the correction of systematic errors, bias and drift in order to translate it into the IERS system. The formal uncertainties estimated by the analysis centers being an internal consistency value, an external calibration has to be made in order to reflect the real uncertainty of the estimates. This is done using a pair variance analysis. Consequently a scaling factor is given to the series. Weights of the series entering the combined solution are thus estimated.

Figure 1 gives the rough percentage of the contribution of the various techniques for the different EOP parameters. Note that the 3 main techniques (VLBI, SLR and GPS) have about the same contribution in the polar motion series whereas for UT and celestial pole offsets the quasi unique contributor is VLBI. Figure 2 shows for the y-pole component the differences of the main series entering the solution with C04. Table 4 represents the RMS agreement of these series with C04 for both components.

Table 4- RMS agreement with EOP (IERS) C04

	x pole (mas)	y pole (mas)
EOP(IERS) 95 P 01	.17	.12
EOP (USNO) 96 R 04	.17	.13
EOP (IAA) 95 R 01	.18	.16
EOP (CSR) 95 L 01	.18	.18
EOP (USNO) 96 C 01	.17	.14

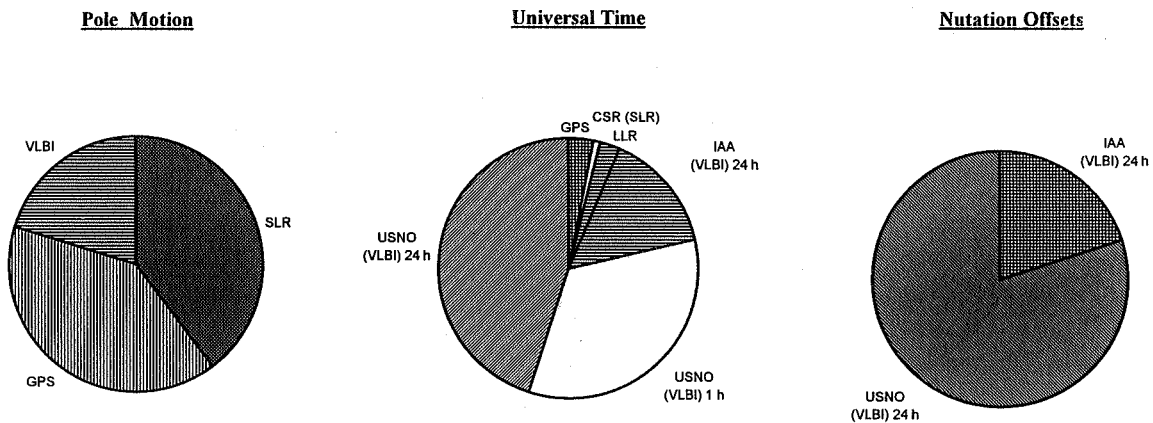


Figure 1 . Percentage of the contribution of techniques in the combined EOP.

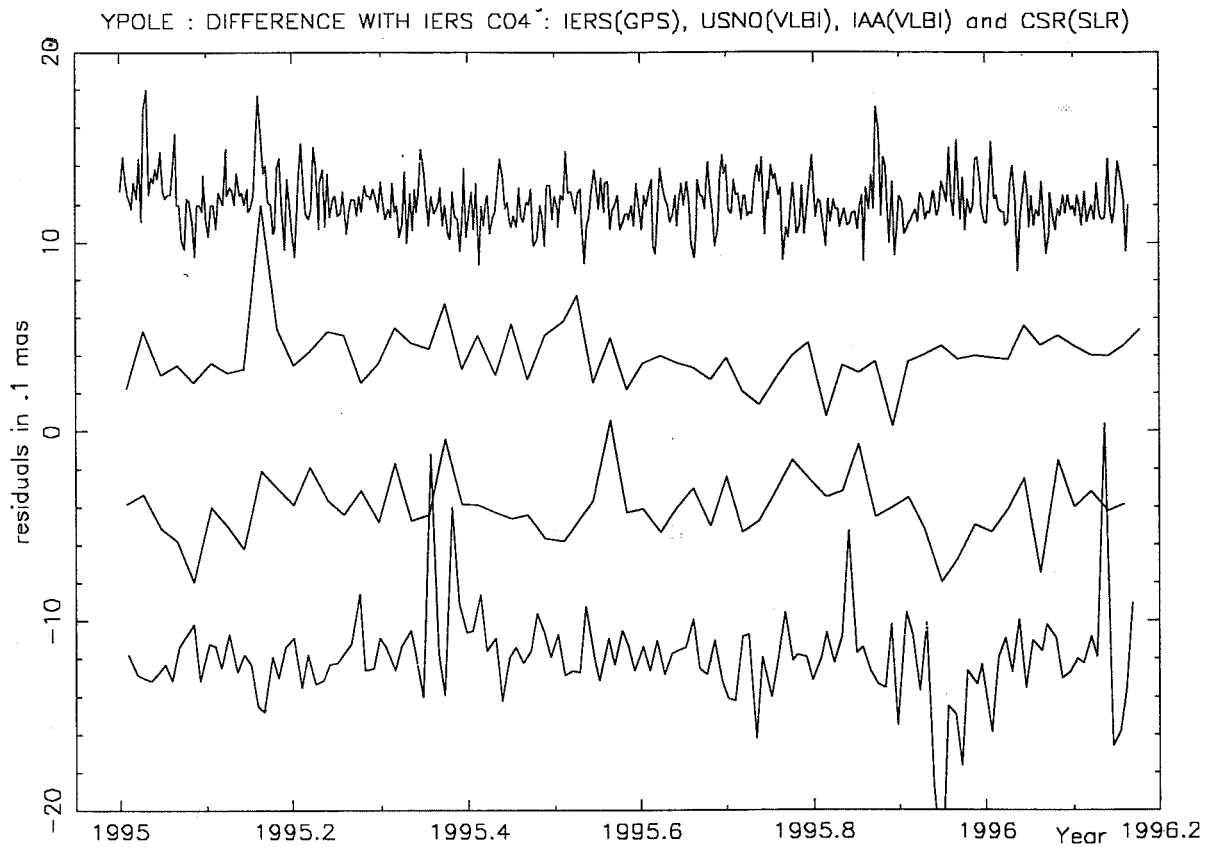


Figure 2 . Differences (in 0.1 mas) of the main series entering the solution with IERS C04 for y pole. The biases are arbitrary.

UNIVERSAL TIME BASED ON BOTH VLBI AND GPS TECHNIQUES

So far, the operational Universal Time solution C04 was based on VLBI series (USNO 24h, USNO 1h and IAA 24h) with a small high-frequency contribution from the SLR technique. Due to the difficulty of determining the long-term behaviour of the non rotating system realized through the orbit orientation, Universal Time UT1 cannot be accurately derived from GPS technique. Still, on time scales limited to a couple of months the high-frequency signal contained in the GPS UT determination can be used for densifying the series obtained by the VLBI technique and also for UT extension from the last available current VLBI estimate.

Data

The UT1 series used in the present analyses are currently collected within IERS; they range from beginning 1995 to the present.

VLBI

EOP(USNO) 96R 04:	24h sessions based on a regional network
EOP(USNO) 96 R 05:	1h sessions on an E-W baseline
EOP(IAA) 95R 01:	24h sessions based on a regional network

GPS

EOP(CODE) 95 P 01: continuous daily
EOP(EMR) 95 P 01: continuous daily
EOP(JPL) 95 P 01: continuous daily

SLR

EOP(CSR) 95 L 01: continuous, approx 3-d intervals calibrated on VLBI, except for the last month

Combined IERS

EOP(IERS) C 04: continuous 1-d solution principally based on VLBI .

Figure 3 shows the differences of these series to the reference series (here C04); note the long-term behaviour of the residuals series except for CSR which is tied to VLBI. Figure 4 shows the amplitude spectrum of the differences of the series to EOP(USNO) R05. A bimodal structure appears for GPS series with spectral power appearing for low frequencies. Based on these results, low and high-frequency signals have been separated using a Vondrak smoothing (cutoff period : 1 month). Figure 5 represents the high-frequency content (< 1 month) of GPS, USNO (1h) and CSR series showing very similar behaviour. The correlation between these series are given on table 5.

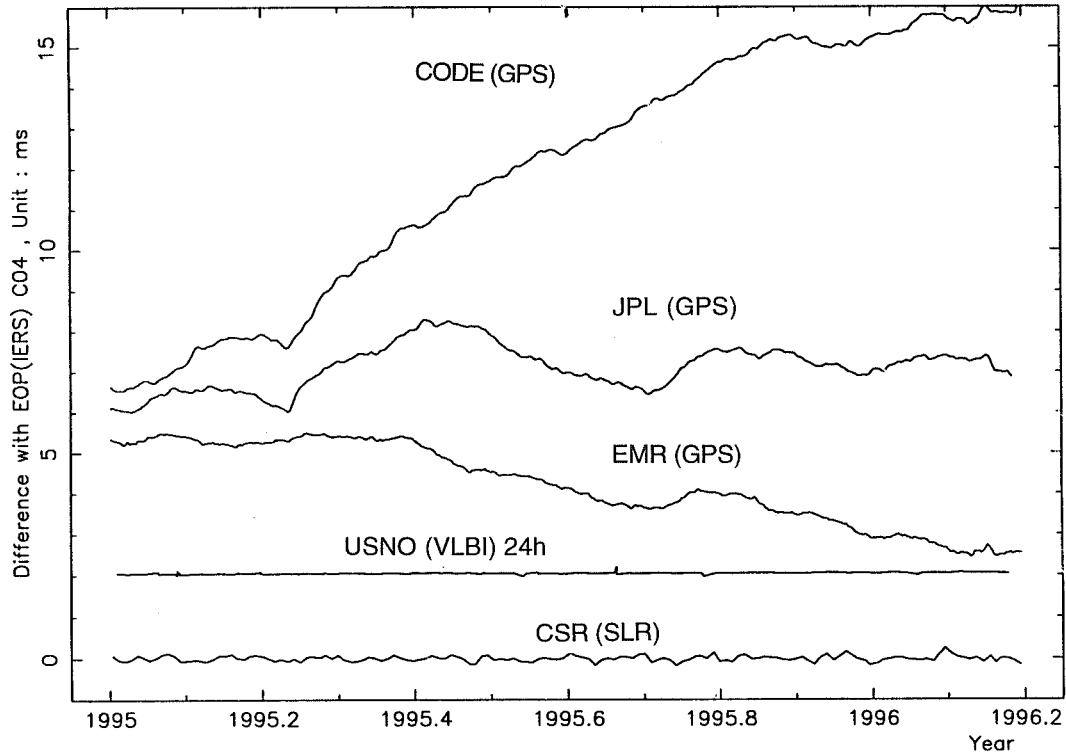


Figure 3 - Raw "UT1" derived from GPS analysis present large systematic low-frequency errors relatively to an external series (here IERS combined solution C04) which prevents their direct use in current analyses.

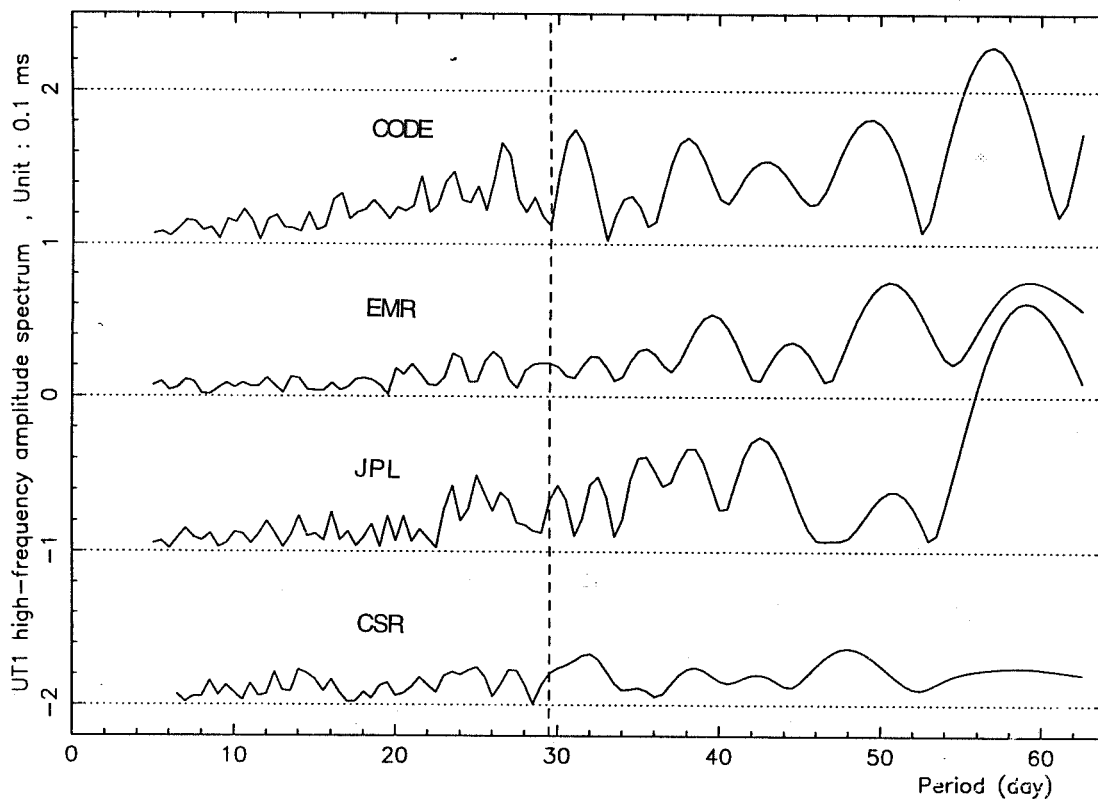


Figure 4 - Amplitude spectrum of the differences of UT1 GPS series with EOP(USNO) 96R 05. This analysis gives the threshold for smoothing characteristics determination.

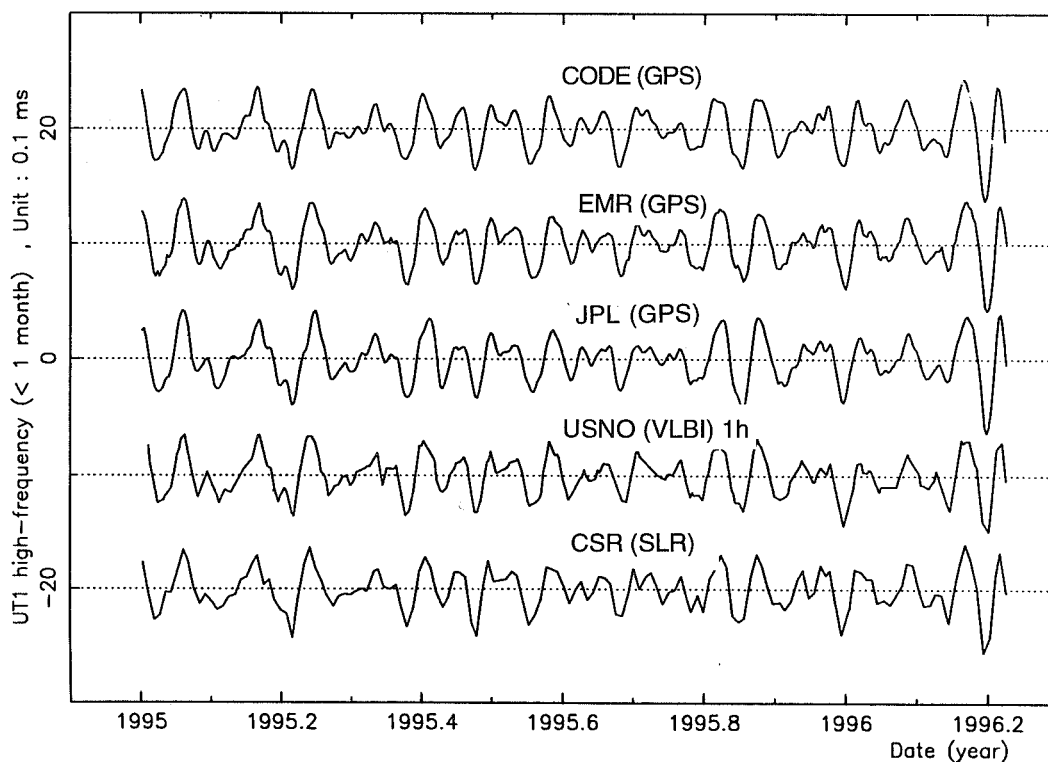


Figure 5 - High-frequency content of the various series. Variations with periods larger than 100 days have been smoothed out.

Table 5. Correlation of VLBI, GPS and SLR UT1 data for periods under one month

	VLBI(1h)	CODE	EMR	JPL
GPS (CODE)	0.89			
GPS (EMR)	0.91	0.96		
GPS (JPL)	0.89	0.94	0.97	
SLR (CSR)	0.89	0.86	0.89	0.87

Combination

Long-term variations of the reference series are merged with the high-frequency signal of the GPS series. For a practical reason, C04 is here used for reference since it is given at one-day intervals. 3 independant series based on CODE, EMR and JPL have been derived and mixed to give a "UT1 GPS combined solution". In the processing, a variance analysis performed on the whole interval leads to the weighting of these 3 series in the combination. The weights take into account the formal uncertainties of the series scaled by an external factor.

The rms agreements between this series and the various series entering or not in the solution are given on Table 6. The uncertainty of the combined solution is about 0.03 ms for a single value which is a slight improvement compared to those of the independant series (about 0.04 ms). A signifiant correlation (about 0.6/0.7) appears between these 3 residuals series.

Table 6. RMS agreement of various solutions with respect to EOP(IERS) 95 P01.

Series	RMS agreement (0.0001 s)
USNO 24h	0.22
USNO 1h	0.28
IAA 24h	0.21
GPS(CODE)	0.23
GPS(EMR)	0.17
GPS(JPL)	0.24
SLR	0.61
C04	0.23
NEOS	0.23
SPACE	0.21

Use of UT1 GPS estimates for near real time applications

Another application of LOD (or UT1 integrated series) derived by GPS is the estimation of Universal Time from the last VLBI estimation. We have tried in this analysis to answer the 2 following questions:

- 1) What is the error of the UT extrapolation based on GPS estimates from the last current VLBI data compared to the usual prediction performed using VLBI data?
- 2) What is the evolution of the errors with respect to the horizon (1, 2 and 3 weeks in advance)?

Based on the structure of the trends of GPS UT1 shown in Figure 3, we estimate as prediction model a linear term, corrected locally by the re-adjustment of a bias. This estimation is performed over some time span ranging from 50 to 200 days preceding the last VLBI solution. A series of simulations have been performed over the interval 1995 - 1996.3. Prediction errors are given on Table 7 for the 3 GPS solutions CODE, EMR and JPL. Comparison is also given in the last column with the performance reached when no adjustment of this model is made. (GPS UT1 estimates are in this case only put at the end of the VLBI UT1 solution).

We can notice that there is only a significant improvement in the case of CODE. A better knowledge is needed concerning the sources of long-term errors of the various GPS UT1 series.

Table 7 - RMS error out to 1, 2 and 3 weeks, with drift and bias estimated on time spans ranging from 50 to 200 days. Unit : 0.0001 s. Last column gives the RMS error with no long-term prediction estimated.

Horizon; 1 week					
Series	50	100	150	200	no model estimated
CODE	2.3	2.1	2.1	1.9	2.5
EMR	1.5	1.5	1.5	1.4	1.2
JPL	1.5	1.4	1.2	1.3	1.3

Horizon : 2 weeks					
Series	50	100	150	200	no model estimated
CODE	3.4	2.9	2.9	2.8	2.5
EMR	2.2	2.2	2.2	2.0	1.7
JPL	3.6	2.8	2.5	2.7	2.6

Horizon: 3 weeks					
Series	50	100	150	200	no model estimated

CODE	4.6	3.4	3.6	3.5	4.7
EMR	2.9	2.6	3.1	2.7	2.4
JPL	4.0	2.5	2.0	2.5	2.2

Note that the uncertainty average is about 0.2 ms over one week for GPS solution. The degradation of the performance is small over time spans of 2 and 3 weeks (respectively 0.3 and 0.4 ms). These results can be compared to the UT1 predicted values based on VLBI data on the same analysis interval. Inaccuracies are 1.2 ms over one week and respectively by 4 and 7 ms for 2 and 3 week predictions (Table 8).

Table 8. RMS errors (in ms) of the Universal Time solution based on GPS and compared to prediction.

UNIT : 1 ms	1 week	2 weeks	3 weeks

Pure Prediction	1.15	4.05	7.20
GPS estimates	.15	.25	.30

CONCLUSIONS

Independent techniques are highly desirable to monitor the Earth rotation for their complementarity aspects but also partly for their redundancy allowing to separate true geophysical signals from systematic fluctuations. This can be for instance illustrated by the 40-50 day oscillation which was only detected when other techniques than astrometry (Doppler tracking and Lunar laser ranging) began to contribute.

Although the internal UT1 series derived from GPS determinations are not directly usable for Earth Orientation monitoring, its high-frequency information can be used together with an external long-term calibration (VLBI or C04) to derive a mixed solution which may be used both for scientific (densification). The combination of independent UT1(GPS) solutions improves the final solution by elimination of white noise. Integration of the operational USNO 1h solution to this series is under investigation.

GPS-derived UT1 can be also useful for near real time applications from the last currently available VLBI estimate. In that case the improvement of the solution is a factor 8 for 1 week and respectively 16 and 24 for 2 and 3 weeks compared to a predicted series.

GPS UT1 results are still in their infancy, and further improvements may be expected both in the short term accuracy and in the long term stability of GPS UT1 determinations; their comparison with VLBI intensive series should bring better understanding of errors on both sides. Nevertheless they already contribute to analysis and operational solutions in the frame of IERS/BC. VLBI will remain the ultimate reference for the motion of the satellite orbit node. When the error budget in the GPS determination is better known, lower acquisition rates may become acceptable for operational work. However, due to the non-dynamical character of its reference direction for UT1, VLBI is also in principle the most accurate technique for high frequency determinations of UT1. The potential high frequency systematic errors in satellite-based UT1 are independent from those that may arise in single baseline VLBI. Scientific investigations of the high frequency structure of the Earth's rotation should benefit from the continuity of the satellite results added to the accuracy of VLBI results.

References

Gambis D., Essaifi N., Eisop E. and M. Feissel, 1993, Universal time derived from VLBI, SLR and GPS, IERS technical note 16, Dickey and Feissel (eds), ppIV15-20.

Gambis D., 1995, Universal time derived from VLBI and GPS techniques, AGU meeting, Baltimore, 29-may -2 june 1995.

DAILY & SEMI-DAILY EARTH ORIENTATION PARAMETER VARIATIONS AND TIME SCALES

Dennis D. McCarthy
U.S. Naval Observatory
Washington, DC, USA 20392

ABSTRACT

Theoretical models of daily and semi-daily variations in Earth orientation due to tides are now in close agreement. Observations indicate that these variations do exist. It is important that the IGS and IERS agree on a convention for the publication of observations in order to avoid confusion among users of these data. The current practice of the IERS is to provide daily smoothed estimates at 0^h UTC. These contain no daily/semi-daily information. IGS Analysis Centers provide daily estimates of polar motion which do not currently take into account the daily/semi-daily variations in their analyses. Therefore, the observations reported by the IGS Centers may, in fact, contain small systematic errors depending on the length of the arcs used in the orbit determinations. It is recommended that all organizations reporting Earth orientation data provide to the user the information required to transform between a celestial and terrestrial reference frame including the daily/semi-daily variations. The details regarding this problem will be the subject of a forthcoming paper

Page intentionally left blank

INTERNATIONAL EARTH ROTATION SERVICE CONVENTIONS (1996)

Dennis D. McCarthy
U.S. Naval Observatory
Washington, DC, USA 20392

ABSTRACT

The accuracy with which reference systems and Earth orientation data can be defined are limited by the systematic errors which arise in the treatment of astronomical and geodetic observations. Constants and models must be re-evaluated and improved, if possible, as measurement precision improves. Both the astronomical and geodetic communities will maintain sets of conventional standards which change slowly with time as well as "current best estimates" for high-precision users of reference systems. These will be available electronically and updated as required. The International Earth Rotation Service (IERS) Conventions are discussed from the theoretical and applied points of view. Specific constants and models are described.

INTRODUCTION

The IERS Conventions is a document intended to define the standard reference system used by the International Earth Rotation Service (IERS). It is based on the Project MERIT Standards (Melbourne *et al.*, 1983) and the IERS Standards (McCarthy, 1989; McCarthy, 1992) with revisions being made to reflect improvements in models or constants since the previous IERS Standards were published.

The recommended system of astronomical constants corresponds closely to those of the previous IERS Standards with the exception of the changes outlined below. The units of length, mass, and time are in the International System of Units (SI) as expressed by the meter (m), kilogram (kg) and second (s). The astronomical unit of time is the day containing 86400 SI seconds. The Julian century contains 36525 days.

SYSTEMATIC ERRORS IN CURRENT OBSERVATIONS

Modern observational methods are able to achieve precision on the order of ± 0.1 millisecond of arc in the determination of Earth orientation parameters. Physical phenomena that are modeled in the analyses of these observations affect the data with magnitudes many times larger than the precision. Errors in these models or use of inconsistent models may produce systematic errors in the Earth orientation parameters derived from modern methods. These systematic errors do, in fact, limit the accuracy of the modern observations. It follows that a concerted effort should be made to use the most representative constants and models to achieve the highest possible accuracy.

CONTENTS OF THE IERS CONVENTIONS

To provide the highest accuracy in its data, the IERS periodically publishes a compendium of the best models and constants to be used in the analyses of its data and in the application of the data to meet user requirements. The contents of the new IERS Conventions document, the final draft of which is being completed, are listed below. It is intended that the models and constants of the IERS Conventions be consistent with the International Astronomical Union (IAU) "current best estimates." All of the IERS Conventions document will be available electronically and on the World Wide Web.

CONVENTIONAL CELESTIAL REFERENCE SYSTEM

Both the equator and origin of right ascension are described in the first chapter of the new IERS Conventions. The accuracy of the definition of the celestial reference system is shown, and procedures are given to obtain the most recent realization of the frame.

CONVENTIONAL DYNAMICAL REFERENCE FRAME

The dynamical frame of the IERS Conventions is defined by the DE 403 ephemeris of the Jet Propulsion Laboratory (Standish *et al.*, 1995). The constants consistent with this frame are listed and procedures are given to obtain the ephemeris electronically.

CONVENTIONAL TERRESTRIAL REFERENCE SYSTEM

Definitions of the Conventional Terrestrial Reference System are shown, and the process to follow in obtaining the most recent realization of the terrestrial frame are given. The chapter lists the transformation parameters to be used to relate this frame to other world coordinate systems and datums. Should observational estimates of station motions not be available, the NUVEL no-net-rotation plate motion model (De Mets *et al.* 1994) is recommended for use and is described.

NUMERICAL STANDARDS

Consistent numerical constants to be used with IERS data are listed. These are current best estimates, and will be updated electronically as required.

TRANSFORMATION BETWEEN THE CELESTIAL AND TERRESTRIAL SYSTEMS

A chapter is devoted to the proper procedures to be followed in transforming between terrestrial and celestial reference systems. It provides two methods, the first being the traditional system making use of the concept of the equinox. The second method involves the "non-rotating-origin" approach. The International Astronomical Union (IAU) 1980 Theory of Nutation (Seidelmann *et al.*, 1982), which is the current standard of the IAU, is provided along with new definitions of the astronomical arguments (Simon *et al.*, 1994)

to be used in implementing the theory. Also presented here, for the first time, is a new model of nutation consistent with the most modern astronomical observations. It is based on an analysis of Very Long Baseline Interferometry (VLBI) observations (Herring, 1995). The IAU model remains the standard and the new IERS model is to be used only for those applications requiring high-precision *a priori* estimates of the nutation angles. A consistent convention to be used to standardize the description of prograde and retrograde motions is presented. A formulation for geodesic nutation is also provided.

GEOPOTENTIAL

In addition to the procedures to be used to obtain the adopted geopotential field electronically, models describing the effect of solid Earth tides are given. A standardized method to account for the permanent tide is provided, and the effect of the ocean tides on the geopotential is described.

LOCAL SITE DISPLACEMENT

Corrections to the positions of observing sites participating in the IERS are required to achieve the highest possible precision. These corrections take into account the effects of ocean loading, solid Earth tides, rotational deformation due to polar motion, antenna deformation, atmospheric loading, and postglacial rebound. Frequency-dependent Love Numbers are given.

TIDAL VARIATIONS IN THE EARTH'S ROTATION

Current observations indicate that high-frequency variations in the Earth's rotation and polar motion occur. These appear to be due to the action of tides on the Earth. A standardized theoretical model of tidal effects on the Earth's orientation is presented for use in the analyses of observational data.

TROPOSPHERIC MODEL

A chapter of the IERS Conventions is devoted to models of the effects of the troposphere on observations made using satellite laser ranging, very long baseline interferometry, and the global positioning system.

RADIATION PRESSURE REFLECTANCE MODEL

One source of systematic error in the analysis of observations of the satellites in the Global Positioning System (GPS) is modeling the effect of radiation pressure on the satellite orbits. A standardized model consistent with current observations is presented.

GENERAL RELATIVISTIC MODELS FOR TIME, COORDINATES AND EQUATIONS OF MOTION

Relativistic equations of motion for an artificial Earth satellite are shown as are equations of motion in the barycentric frame. The effect of relativity on time scales is discussed.

GENERAL RELATIVISTIC MODELS FOR PROPAGATION

A rigorous "consensus model," taking into account relativity, is available to model time delays in VLBI observations. This includes the effects of gravitational delay, geometric delay, and observations close to the Sun. Relativistic propagation corrections are also given for satellite laser ranging.

DIFFERENCES BETWEEN THE IERS CONVENTIONS OF 1995 AND PREVIOUS IERS STANDARDS

Most chapters of IERS Technical Note 13 have been revised, and known typographical errors contained in that work have been corrected in the new edition. There are some major differences between the current version of the IERS Conventions and the past IERS Standards. The following is a brief list of the major modifications.

IERS DYNAMICAL REFERENCE FRAME

In Chapter 2, the JPL DE 403 ephemeris (Standish, 1995) replaces the DE 200 model of IERS Technical Note 13.

IERS TERRESTRIAL REFERENCE SYSTEM

The NUVEL NNR-1A Model (DeMets *et al.*, 1994) for plate motion has replaced the NUVEL NNR-1 Model of IERS Technical Note 13.

NUMERICAL STANDARDS

Numerical values are now given only for the most fundamental constants along with their uncertainties and references. Constants which have been changed include the astronomical unit in seconds and meters, precession, obliquity, equatorial radius, flattening factor and dynamical form factor of the Earth, constant of gravitation, geocentric and heliocentric gravitational constant.

TRANSFORMATION BETWEEN CELESTIAL AND TERRESTRIAL REFERENCE SYSTEMS

An empirical model to be used to predict the difference in the celestial pole coordinates between those published by the IERS and those given by the IAU model is added. The model (Herring 1995) is based on the analysis of fourteen years of VLBI data by the Goddard Space Flight Center and the Souchay and Kinoshita Rigid Earth nutation series (Souchay and Kinoshita, 1995) re-scaled to account for the change in the dynamical ellipticity of the Earth implied by the correction to the precession constant. Terms with

duplicate arguments in the Souchay and Kinoshita series have been combined into single terms. The model includes the effects of the annual modulation of geodetic precession and the effects of planetary perturbations of the lunar orbit from Williams (1994). Since it appears that the free core nutation (FCN) varies in time, the Central Bureau will publish in the IERS Annual Report its current best estimate of the FCN representation. The precession constant will change (from the IAU-1976 value) to be consistent with the IERS nutation model, as will the rate of change of the obliquity. FORTRAN code to generate this series will be available by anonymous ftp.

GEOPOTENTIAL

The JGM3 model replaces the GEM-T3.

LOCAL SITE DISPLACEMENTS

The printed table of the components of site displacement due to ocean loading is no longer included. References to machine-readable files are given. Love Numbers are revised, and atmospheric loading and postglacial rebound are included.

TIDAL VARIATIONS IN EARTH ORIENTATION

The subdaily and daily tidal variations in Earth orientation due to the effect of ocean tides have been added. The model of R. Ray (1995) is recommended.

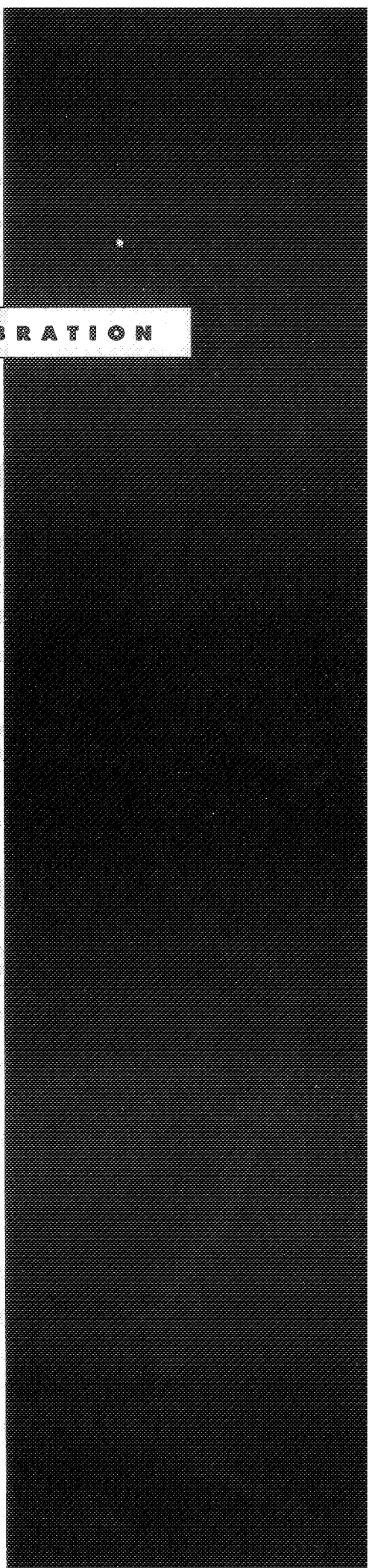
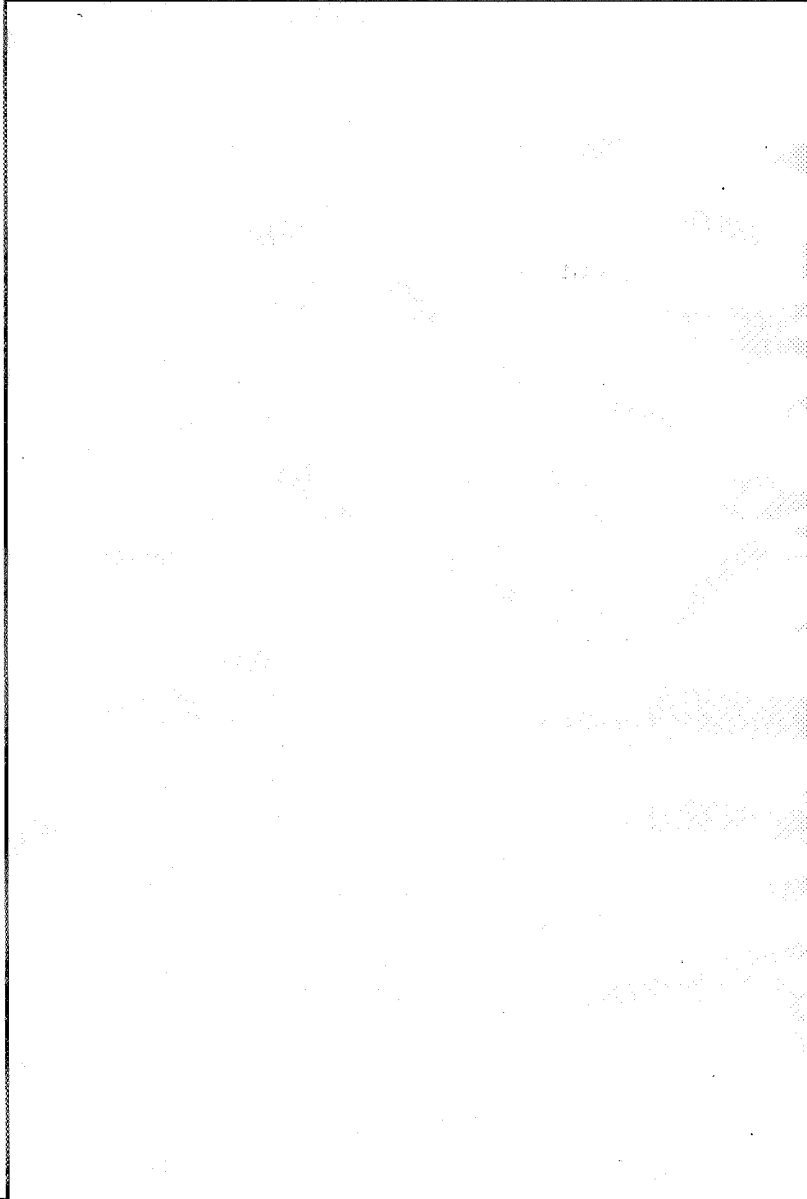
REFERENCES

- DeMets, C., Gordon, R. G., Argus, D. F., and Stein, S., 1994, "Effect of Recent Revisions to the Geomagnetic Reversal Time Scale on Estimates of Current Plate Motions," *Geophys. Res. Lett.*, **21**, pp. 2191-2194.
- Herring, T. 1995, personal communication.
- Melbourne, W., Anderle, R., Feissel, M., King, R., McCarthy, D., Smith, D., Tapley, B., Vicente, R., 1983, *Project MERIT Standards*, U.S. Naval Observatory Circular No. 167.
- McCarthy, D. D., 1989, *IERS Standards*, IERS Technical Note 3, Observatoire de Paris, Paris.
- McCarthy, D. D., 1992, *IERS Standards*, IERS Technical Note 13, Observatoire de Paris, Paris.
- Ray, R., 1995, personal communication.
- Seidelmann, P. K., 1982, "1980 IAU Nutation: The Final Report of the IAU Working Group on Nutation," *Celest. Mech.*, **27**, pp. 79-106.
- Simon, J. L., Bretagnon, P., Chapront, J., Chapront-Touzé, M., Francou, G., Laskar, J., 1994, "Numerical Expressions for Precession Formulae and Mean Elements for the Moon and Planets," *Astron. Astrophys.*, **282**, pp. 663-683.

- Souchay, J. and Kinoshita, H., 1995, "Corrections and New Developments in Rigid Earth Nutation Theory: I. Lunisolar Influence Including Indirect Planetary Effects," submitted to *Astron. Astrophys.*
- Standish, E. M., Newhall, X X, Williams, J. G., and Folkner, W. F., 1995, "JPL Planetary and Lunar Ephemerides, DE403/LE403," JPL IOM 314.10-127, to be submitted to *Astron. Astrophys.*
- Williams, J. G., 1994, "Contributions to the Earth's Obliquity Rate, Precession, and Nutation," *Astron. J.*, **108**, pp. 711-724.



GPS ANTENNA CALIBRATION



Page intentionally left blank

Calibration of GPS Antennas

Gerald L. Mader and J. Ross MacKay
Geosciences Laboratory
Office of Ocean and Earth Sciences, NOS, NOAA
Silver Spring, Maryland

Introduction

As geodetic techniques using the Global Positioning System (GPS) continue to improve, the calibration of the antennas used to track GPS data becomes increasingly important. The establishment of the International GPS Service and by several agencies of continuously operating reference stations (CORS) provides a convenient means to incorporate reference network data into a user's solution for either local or regional geodetic baselines. However, the antennas used by these reference networks will very often not be the same as those employed by the user at his end of the baseline. Moreover, different CORS networks may use different antennas and different antennas may also be found within the same network.

Two antenna characteristics which are frequently not noticed when identical antennas are used, may now become a significant source of error when the antennas at either end of a base line are different. A GPS geodetic solution fundamentally provides the vector between the phase centers of the two antennas. To relate this vector to permanent monuments on the ground, the location of the phase center with respect to an external feature of the antenna structure must be combined with the location of this reference feature with respect to the monument. Since the baseline vector is a relative measurement, errors in phase center location cancel out when identical antennas are used. However, different antennas generally have different phase center locations. Mixed antennas at a minimum require knowledge of the relative positions of the antenna's phase centers and ideally the absolute location of each antenna's phase center.

The antenna phase centers defining a baseline vector are actually average phase center locations for the data used to produce that baseline vector. A real antenna does not have a single well-defined phase center. Instead the phase center is a function of the direction from which it receives a signal. For GPS antennas, the dominant variation occurs with elevation. Since baseline measurements usually

include GPS observations distributed over all elevations above some cutoff value, this effect may not always be noticeable, even when using mixed antennas. However, these phase center variations with elevation, if large enough, can be noticeable on mixed antenna baselines as an apparent change in height with elevation cutoff.

In addition, high precision on longer baselines requires an estimation of the tropospheric scale height along with the baseline components. The estimation of this parameter, which is highly correlated with height, depends on the variation of phase residuals with elevation. If this variation includes an effect that arises from the antennas in addition to that from the troposphere, the scale height parameter, and the height, can be significantly in error. The complete calibration of GPS antennas includes determining this phase center variation as well as the average phase center location.

Calibration Procedure

Previous calibrations of GPS antennas have been in an anechoic chamber. When properly done, these measurements should provide precise descriptions of the phase center and variations with elevation and azimuth. Such measurements have been reported by Schupler et al. (1994) and Meertens et al. (1996) for a number of antenna types. However, scheduling and funding constraints for these test facilities and the ever increasing number of GPS antenna types suggests that an alternate means of antenna calibration would be useful. Furthermore, the signal characteristics and other idiosyncracies of the anechoic chamber suggest that a means of measuring antenna characteristics in situ would be a valuable comparison.

The calibration procedure used here will determine in the field the relative phase center position and phase variations of a series of test antennas with respect to a reference antenna. The phase characteristics of the reference antenna are assumed known from chamber measurements and will allow the phase characteristics of the test antennas to be separately determined.

To perform these antenna calibrations, a test range has been established at the National Geodetic Survey's Corbin facility. This test range consists of two stable 6 in. diameter concrete piers rising about 1.7m above ground. On the tops of these piers, antenna mounting plates are permanently attached. The piers are separated by 5m and are located in a flat grassy field about 21m from the nearest building, a 1-story block structure with asphalt roof. Identical length antenna cables connect these piers to the building. These piers lie along a north-south line and are designated the north and south piers. Leveling data show that the south pier is 3.4mm taller than the north pier. The north pier will be used as the reference pier and the south pier used as the test pier.

The average phase center location can be found by using a standard reference antenna on the reference pier and determining the relative position of a test antenna. Because the baseline length is so short,

tropospheric and ionospheric effects may be ignored and separate L1 and L2 solutions estimated. These solutions provide the vector for the L1 and L2 phase centers from the reference antenna to the test antenna and allow the L1 and L2 offsets for the test antennas to be determined.

The variation of the phase center is found by constraining the test antenna to its L1 or L2 position and using single difference phase residuals over a 24 hr period to estimate the relative clock at each epoch, the satellite phase biases and a polynomial for the phase residuals as a function of elevation. Separate polynomials are estimated for L1 and L2 and azimuth variation is ignored. The polynomials go to fourth order in elevation. A constant term for the polynomial is not estimated since it is not readily separated from the clock values. This inability to determine a constant phase offset does not inhibit the determination of the more important phase variations and may be completely ignored when differencing observations.

The reference antenna used for all these calibration measurements is a Dorne/Margolin choke ring antenna, type T. This is the antenna used with the Trubo Rogue receivers and in standard use throughout the network of the International GPS Service. It's characteristics have been measured in the anechoic chamber by Schupler et al., and Meertens et al., making it a good candidate for the reference antenna.

All test antennas had a north azimuth marker which was oriented toward the north. Several days of data were collected for each antenna pair at a 30 s sample rate using Trimble 4000 SSE receivers for the first series of tests and Ashtech Z12 receivers for the second series of tests. Both receivers used a common external rubidium frequency standard. The test antennas calibrated so far are listed in Table 1.

The first step in processing the calibration data was to estimate the L1 and L2 baselines from the reference antenna to the test antenna. These solutions were done using double differences, a 10 degree elevation cutoff, and no tropospheric scale height adjustment. These initial phase center estimates did not use any phase variation data for either antenna.

These phase center positions were then used to estimate the variation of phase center with elevation. This was done with the NOAA program ANTCAL. ANTCAL uses single frequency, single differences to estimate a polynomial describing the phase residuals as a function of elevation along with phase biases, and clock offsets. The test antenna position is constrained to the previously determined value. ANTCAL accepts as input a file containing antenna phase variation values. This file contained the elevation dependent phase corrections derived by Rocken et al., but rescaled to the standard L1/L2 offsets of 0.110m and 0.128m for the Dorne/Margolin Choke Ring antenna. These phase corrections were applied to the reference antenna data only. No phase corrections were applied to the data from the test antenna. This procedure allowed the phase corrections found for the test antenna, though fundamentally a relative measurement, to be expressed as an absolute correction.

Table 1. Test Antennas

Ashtech 700829
 Ashtech 700718
 Ashtech 700228 w/ notches
 Ashtech 700228 w/ holes
 Ashtech 700936
 Dorne/Margolin Choke Ring Type T
 Leica SR299
 Leica SR399
 Macrometer 4647942
 Topcon 72110
 Trimble 14532
 Trimble 22020 w/ ground plane
 Trimble 22020 w/o ground plane
 Wild AT202

The initial step of estimating the L1 and L2 phase center offsets was repeated but this time using the phase corrections for the reference antenna and those for the test antenna just determined. This iteration made only a slight change to the original offsets but these values will be used to give the final antenna offsets.

Results

The position of the north reference pier was determined from a solution to the IGS station GODE at Goddard Space Flight Center in Greenbelt, MD, approximately 100km from Corbin. This reference position is given in Table 2.

Table 2. Pier Positions

	X (m)	Y (m)	Z (m)	Lat (d,m,s)	Lon (d,m,s)	Height (m)
North	1097042.0569	-4897241.6777	3923122.3574	38 12 7.6906	-77 22 24.5840	36.1406
South	1097042.6579	-4897244.6983	3923118.4514	38 12 7.5293	-77 22 24.5871	36.1445

The Dorne/Margolin test antenna data was used to establish the position of the south pier with respect to the north pier. These solutions yield a height difference between the two piers of 3.9mm which agrees favorably with the leveled height difference of 3.4mm. The south pier and north pier positions, given in Table 2, define the vector between the two Dorne/Margolin L1 and L2 phase centers. This south pier position was then used as the a priori value for all subsequent data processing to yield test antenna phase center positions relative to the Dorne/Margolin antenna. These relative differences were then combined with the L1 and L2 Dorne/Margolin Choke Ring offsets of 0.110m and 0.128m to find the vertical offsets of the test antennas. The horizontal offsets of the Dorne/Margolin Choke Ring antennas was assumed to be zero. The horizontal offsets of the test antennas were also estimated.

The L1 and L2, horizontal and vertical offsets for each test antenna are summarized in Table 3. Wherever more than one measurement was made for a particular antenna model, the separate results have been averaged together in this Table. The vertical offset is always with respect to the bottom-most surface of the antenna structure - i.e. the surface that would contact the tribrach mount.

The polynomials describing the phase variation with elevation have been used to generate the phase corrections in 5 degree elevation increments for both L1 and L2. These L1 and L2 phase corrections are also listed in Table 3. These corrections extend from the zenith down to 10 degrees elevation, below which there was too little data to use reliably.

In practice, these phase correction tables are used within the GPS adjustment software to provide interpolated phase corrections at each epoch for the particular antenna types in use. From Table 3, the corrections would be subtracted from the observed phase to remove the elevation dependence introduced by the antenna.

The phase variation can easily be seen by plotting the single difference phase residuals, after the clock variations have been removed, as a function of elevation. These variations may be seen for L1 and L2 for each of the test antennas in Figures 1-7. The polynomial fit is also shown as a solid line.

These figures also show quite clearly sinusoidal variations with elevation. These variations are due to multipath from ground reflections and are proportional to $2h\sin(\text{elv})$ where h is the height, in wavelengths, of the phase center above the ground. All the mixed antenna pairs show essentially the same multipath pattern, particularly at the lower elevations. Even though the figures show single difference residuals, the multipath is satisfactorily modeled from the height of the test antenna alone. This is because the multipath amplitude is different for the antenna pairs. If the multipath amplitude at the two antennas was the same, the resultant single difference should practically cancel out the multipath. The only remaining multipath would be proportional to the few centimeter height difference between the two phase centers and would be negligible.

Table 3. GPS Antenna Offsets and Phase Variations

Format Description											
VENDOR	MODEL #			DESCRIPTION							YR/MO/DY
[north]	[east]	[up]								L1 Offset (mm)	
[90]	[85]	[80]	[75]	[70]	[65]	[60]	[55]	[50]	[45]	L1 Phase at	
[40]	[35]	[30]	[25]	[20]	[15]	[10]	[5]	[0]		Elevation (mm)	
[north]	[east]	[up]								L2 Offset (mm)	
[90]	[85]	[80]	[75]	[70]	[65]	[60]	[55]	[50]	[45]	L2 Phase at	
[40]	[35]	[30]	[25]	[20]	[15]	[10]	[5]	[0]		Elevation (mm)	
Calibration Results											
ROGUE	SNR-8000										96/03/18
	0.0	0.0	110.0								
	10.0	10.0	9.0	7.0	5.0	3.0	1.0	-2.0	-3.0	-5.0	
	-5.0	-6.0	-7.0	-7.0	-5.0	-4.0	-3.0	0.0	3.0		
	0.0	0.0	256.0								
	3.0	3.0	2.0	2.0	1.0	1.0	0.0	-1.0	-2.0	-2.0	
	-3.0	-4.0	-4.0	-3.0	-2.0	-1.0	0.0	3.0	6.0		
Ashtech	700829										96/03/18
	-0.8	0.4	89.4								
	0.0	1.0	1.7	1.9	1.8	1.4	0.5	-0.6	-2.0	-3.6	
	-5.4	-7.1	-8.9	-10.4	-11.5	-12.2	-12.2	0.0	0.0		
	-0.1	-1.0	61.7								
	0.0	-2.2	-4.0	-5.5	-6.9	-8.2	-9.4	-10.5	-11.5	-12.3	
	-12.9	-13.1	-12.8	-11.8	-9.8	-6.8	-2.4	0.0	0.0		
Ashtech	700718										96/03/18
	1.0	0.6	83.7								
	0.0	0.4	0.6	0.6	0.2	-0.4	-1.2	-2.4	-3.8	-5.3	
	-6.9	-8.6	-10.2	-11.6	-12.6	-13.2	-13.2	0.0	0.0		
	-0.1	-1.9	63.8								
	0.0	-2.5	-4.5	-6.1	-7.5	-8.7	-9.8	-10.9	-11.8	-12.6	
	-13.2	-13.4	-13.2	-12.2	-10.4	-7.6	-3.3	0.0	0.0		
Ashtech	700228N (notches)										96/03/18
	-0.2	-1.0	79.5								
	.0	.2	-.5	-1.7	-3.4	-5.2	-7.0	-8.8	-10.4	-11.7	
	-12.8	-13.5	-14.0	-14.2	-14.2	-14.1	-14.0	0.0	0.0		
	-1.9	3.7	77.4								
	.0	-1.3	-2.2	-2.8	-3.2	-3.7	-4.1	-4.7	-5.4	-6.1	
	-6.8	-7.5	-7.9	-7.9	-7.3	-5.9	-3.3	0.0	0.0		
Ashtech	700228R (rings)										96/03/18
	-1.9	0.0	85.3								
	.0	1.1	1.2	.5	-.8	-2.4	-4.1	-5.9	-7.6	-9.2	
	-10.4	-11.4	-12.1	-12.4	-12.6	-12.6	-12.5	0.0	0.0		
	-3.8	3.4	77.9								
	.0	-1.6	-2.6	-3.1	-3.4	-3.7	-4.0	-4.5	-5.1	-5.8	
	-6.6	-7.4	-7.9	-8.1	-7.6	-6.2	-3.6	0.0	0.0		

Ashtech	700936																		96/03/18
	0.8	-0.7	112.9																
	0.0	0.5	-0.3	-1.9	-4.0	-6.5	-8.9	-11.3	-13.2	-14.8									
	-15.8	-16.2	-16.1	-15.4	-14.2	-12.6	-10.8	0.0	0.0										
	0.2	1.7	135.1																
	0.0	0.7	1.0	0.9	0.6	0.0	-0.8	-1.6	-2.6	-3.5									
	-4.2	-4.7	-4.8	-4.5	-3.6	-2.0	0.5	0.0	0.0										
Trimble	22020-00																		96/03/18
	0.6	-1.9	77.2																
	.0	1.4	3.4	5.3	6.6	7.2	6.8	5.6	3.6	1.2									
	-1.4	-3.9	-6.0	-7.5	-8.3	-8.1	-7.1	0.0	0.0										
	-1.1	1.2	70.5																
	.0	-.1	.1	.5	.8	1.0	1.0	.6	.0	-.9									
	-1.9	-2.9	-3.8	-4.4	-4.4	-3.5	-1.4	0.0	0.0										
Trimble	22020-00	w/o GP																	96/03/18
	2.9	-0.5	88.5																
	.0	.8	1.8	2.9	4.0	5.0	5.9	6.6	7.0	7.1									
	6.9	6.4	5.5	4.2	2.6	.7	-1.4	0.0	0.0										
	0.7	2.2	86.8																
	.0	-.6	-.6	-.2	.3	1.0	1.7	2.3	2.8	3.0									
	3.0	2.7	2.0	1.0	-.2	-1.8	-3.6	0.0	0.0										
Trimble	14532-00																		96/03/18
	0.8	-2.2	84.0																
	0.0	3.5	6.5	8.8	10.2	10.6	10.1	8.8	6.8	4.5									
	2.0	-0.4	-2.4	-3.9	-4.7	-4.7	-3.8	0.0	0.0										
	-2.0	-0.1	79.1																
	0.0	0.6	1.1	1.6	1.8	1.8	1.6	1.1	0.3	-0.6									
	-1.4	-2.4	-3.1	-3.4	-3.1	-2.1	0.1	0.0	0.0										
Macrometer	4647942																		96/03/18
	1.4	0.1	133.9																
	.0	0.6	2.2	4.4	6.3	8.1	9.8	12.4	14.5	13.6									
	10.3	4.9	-0.4	-6.5	-9.9	-12.7	-15.0	0.0	0.0										
	2.2	1.2	100.2																
	.0	-0.2	-0.6	-1.0	0.9	3.7	5.9	7.3	6.8	4.7									
	1.4	-1.8	-4.4	-5.3	-6.1	-4.8	-2.7	0.0	0.0										
Topcon	72110																		96/03/18
	1.3	4.7	139.9																
	.0	-.9	-1.5	-2.0	-2.4	-2.7	-3.1	-3.6	-4.3	-5.2									
	-6.3	-7.7	-9.5	-11.6	-14.2	-17.2	-20.6	0.0	0.0										
	2.1	2.4	121.5																
	.0	.9	1.3	1.4	1.3	1.0	.6	.1	-.4	-.9									
	-1.4	-1.8	-2.2	-2.5	-2.7	-2.9	-3.0	0.0	0.0										

The clarity with which the multipath is visible in these figures using data from satellites at all azimuths is also good evidence for the azimuthal symmetry of these antennas, validating the modeling of antenna corrections by elevation only. Any azimuthal asymmetry in antenna response or multipath reflections would tend to wash out these sinusoidal patterns.

These results include several measurements of identical antenna model numbers. Where repeated measurements are available, the separate results are shown in Figures 8-12. These figures show that the phase variations repeated within a few millimeters for several different antennas within the same model type. The horizontal and vertical offsets also generally repeated within a few millimeters.

These results are also compared with those from Meetens et al. and Rothacher 1996 where possible. These comparisons are shown in Figures 13-16. Though Rothacher used double differences, a spherical harmonic representation for both elevation and azimuth variation, and entirely different data sets, the two in situ measurement type agree fairly well. The results from anechoic chamber tests, designated "Rocken", appear to agree well with the two in situ measurements at L1 but less well at L2. Thus far there is no explanation for this difference.

Summary

The determination of antenna phase centers and phase variations with elevation using very short baseline measurements in the field appears feasible. The success of this technique depends on accurate phase characterization of a standard reference antenna which may be done independently in an anechoic chamber.

Identical model antennas were tested and yielded vertical phase center offsets that repeated within a few millimeters at L1 and L2. These differences are greater than the measurement errors but constitute too small a sample to confidently indicate the variation that might be expected within a particular antenna type.

Horizontal offsets up to 3mm were measured for some of these antennas. However, these offsets may be unique to the particular antennas being tested. The measurement of horizontal offsets is particularly important but will require additional antennas of the same type to get a better indication of the repeatability of this offset.

The phase variation with elevation has been determined and has been shown to repeat within a few millimeters for several antenna types tested. These phase variations have been used to effectively remove the effects of mixed antenna differences on the determination of tropospheric scale height and antenna height.

References

Schupler, B.R., Allshouse, R.L., Clark, T.A., Journal of the Institute of Navigation, Vol. 41, Number 3, p. 277, Fall 1994.

Meertens, C., Rocken, C., Braun, J., Exner, M., Stephens, B., Ware, R., IGS Analysis Centers Workshop Proceedings, Silver Spring, MD, 1996.

Rothacher, M., IGS Analysis Centers Workshop, Silver Spring, MD, 1996.

Figure 1

Ashtech:700718

95_296

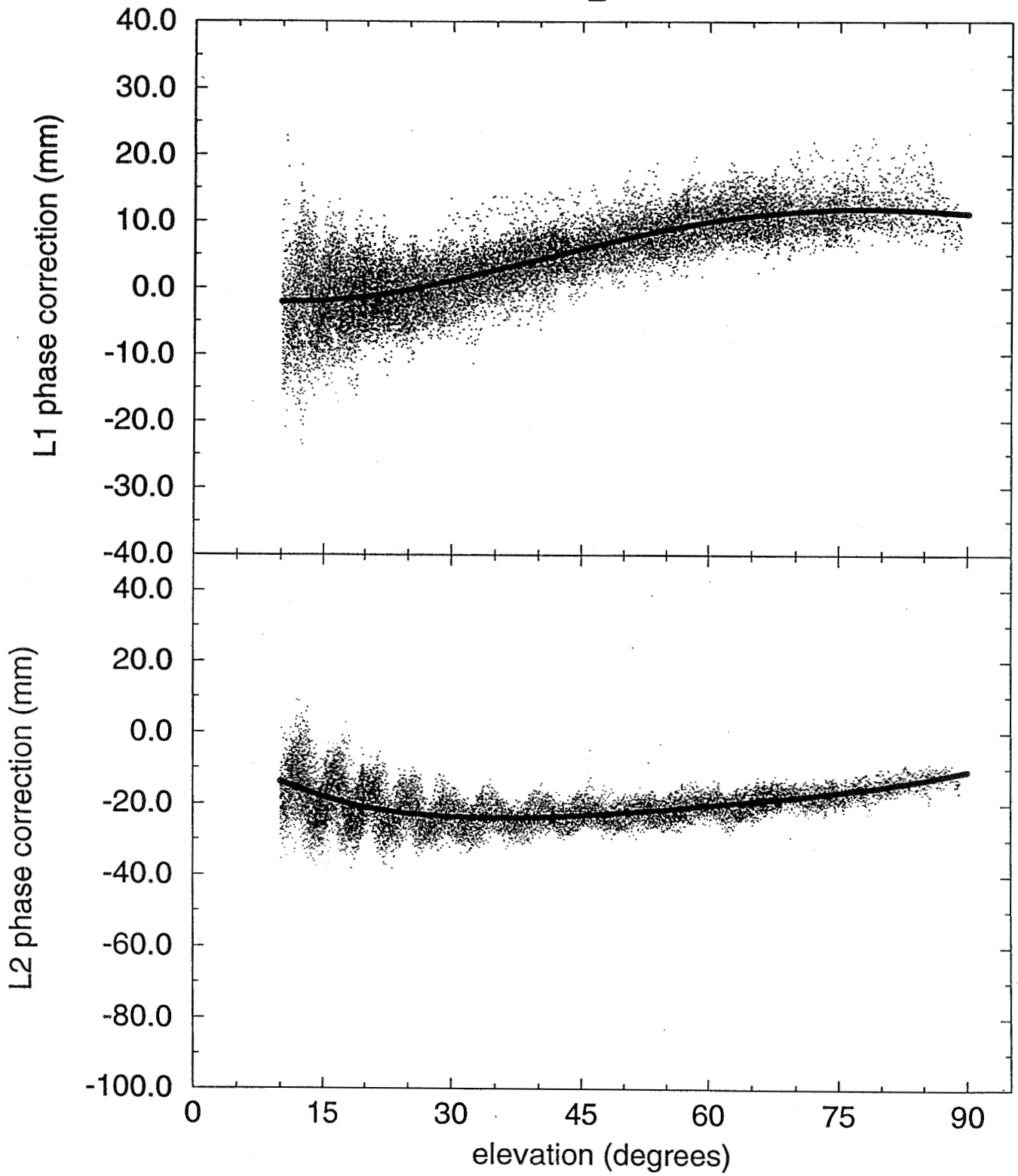


Figure 2

Ashtech:700228-notches

95_340

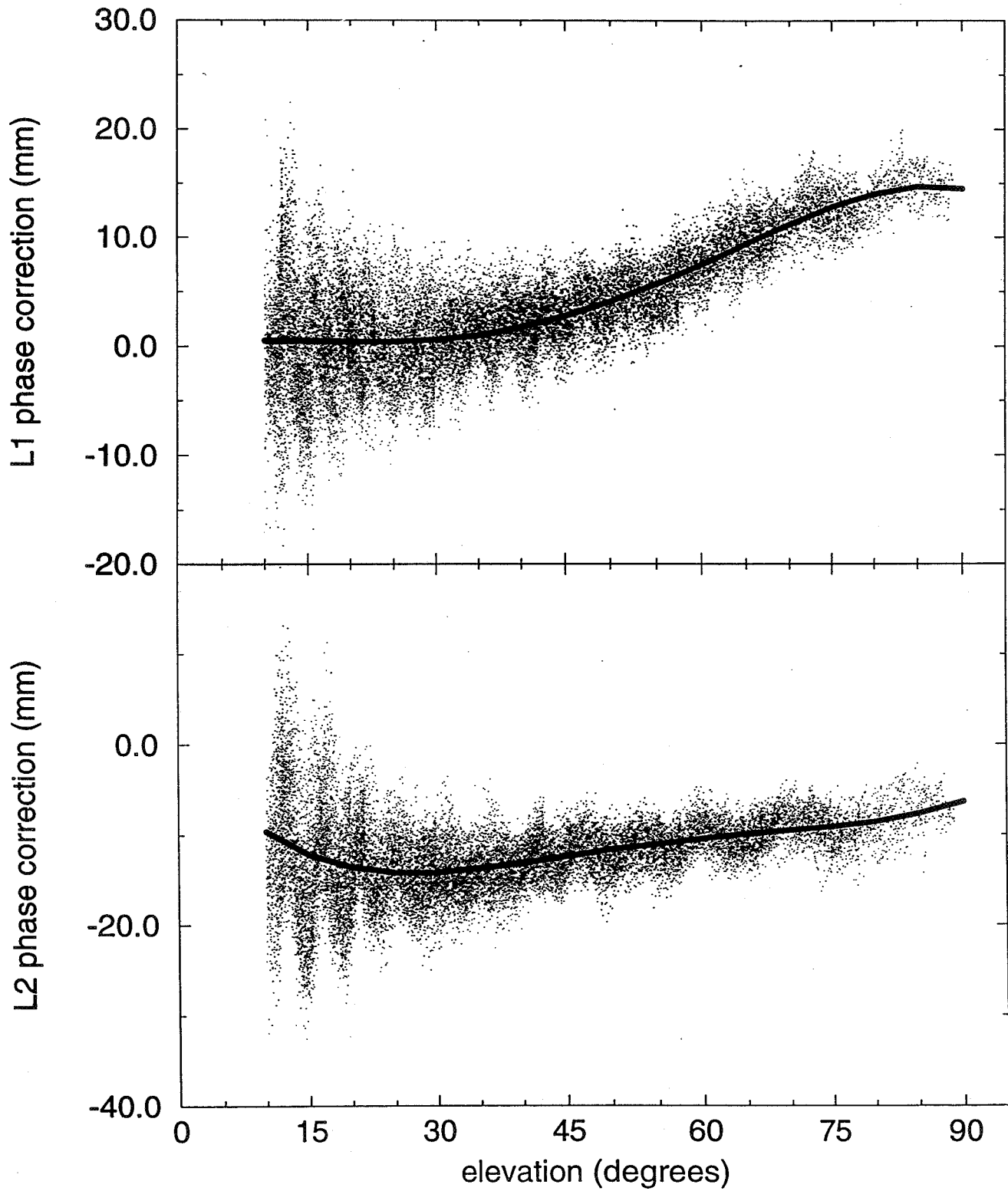


Figure 3

Ashtech:700829

95_091

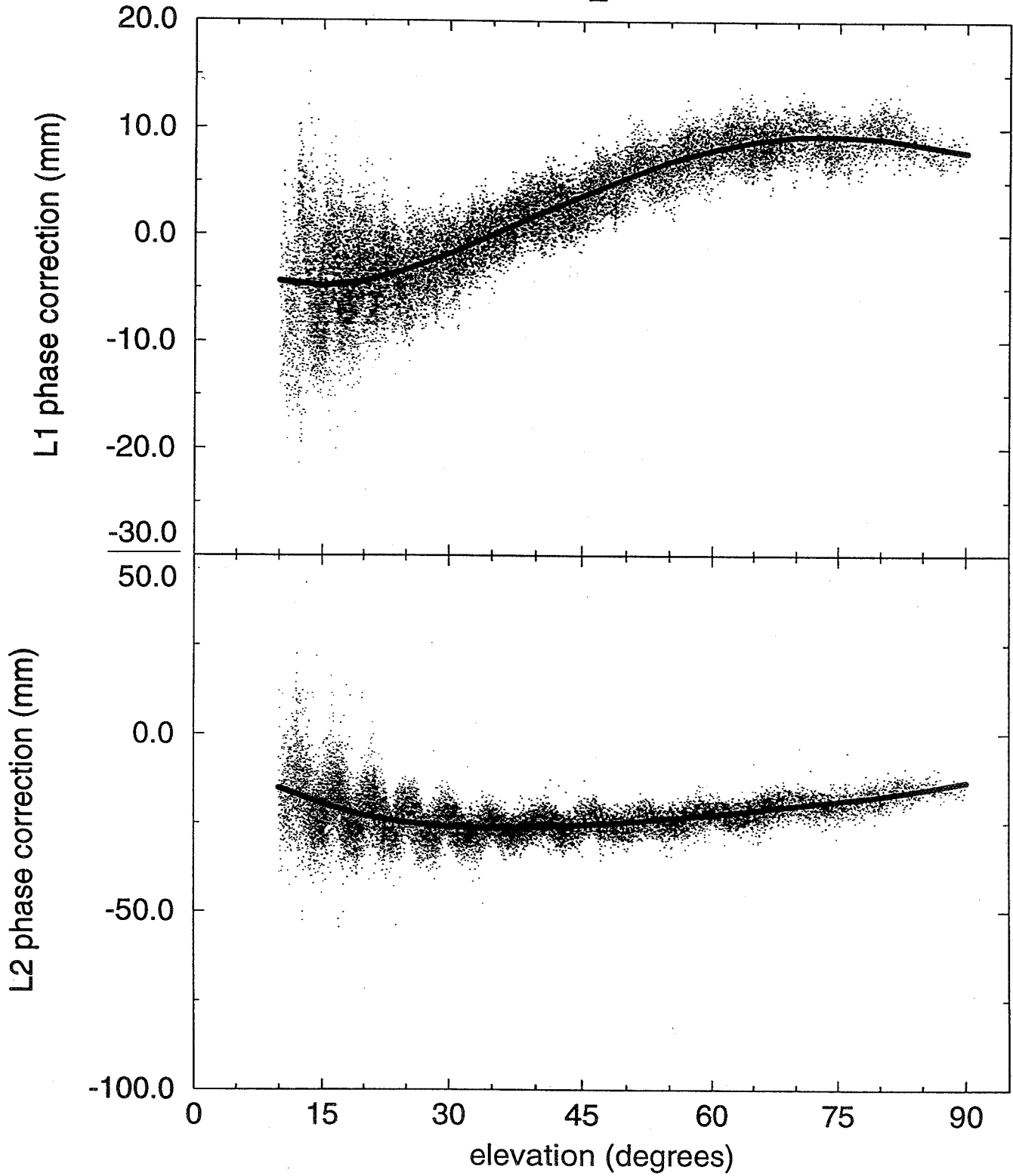


Figure 4

Trimble:22020-00

95_095

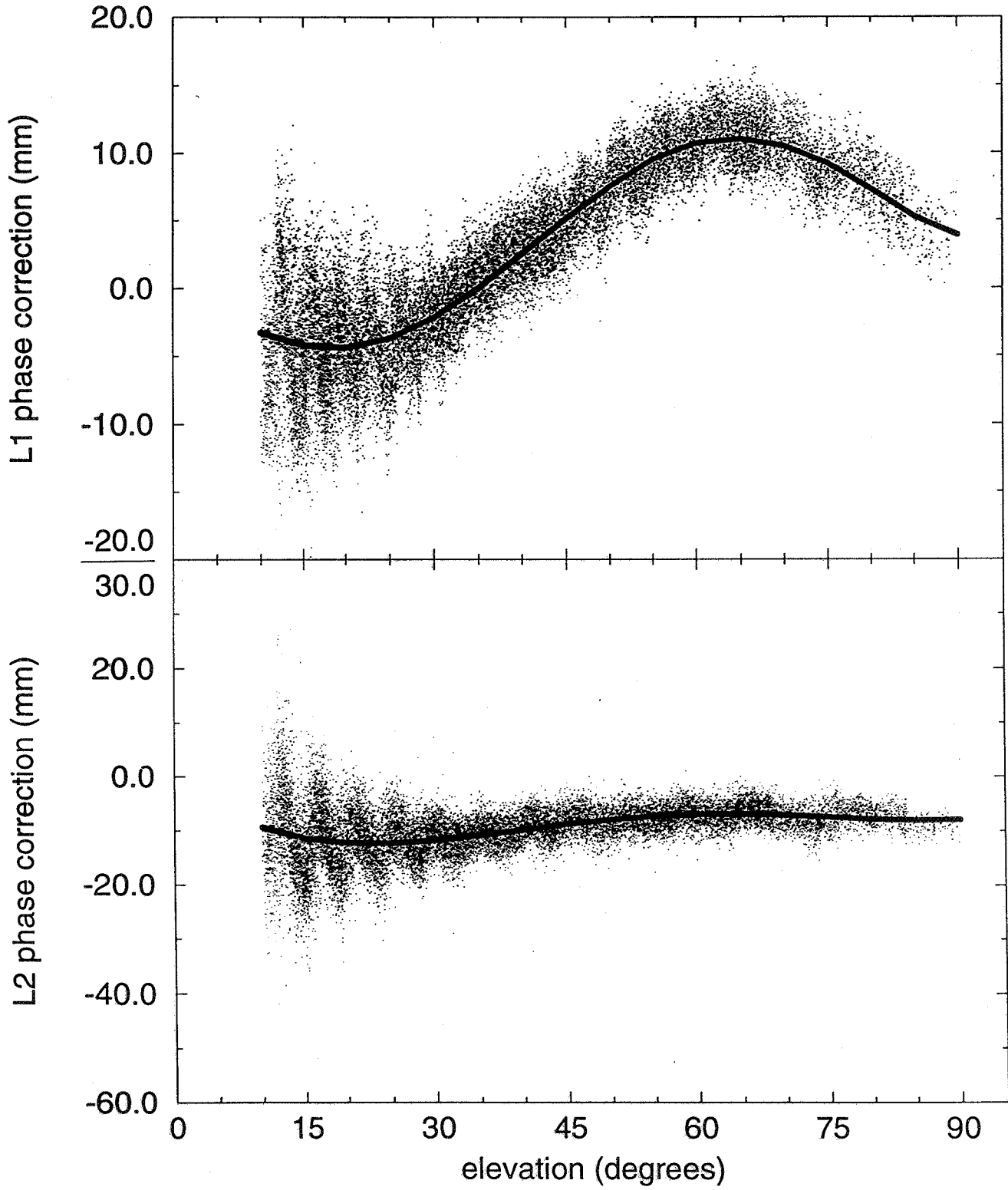


Figure 5

Trimble:22020,no_groundplane

96_067

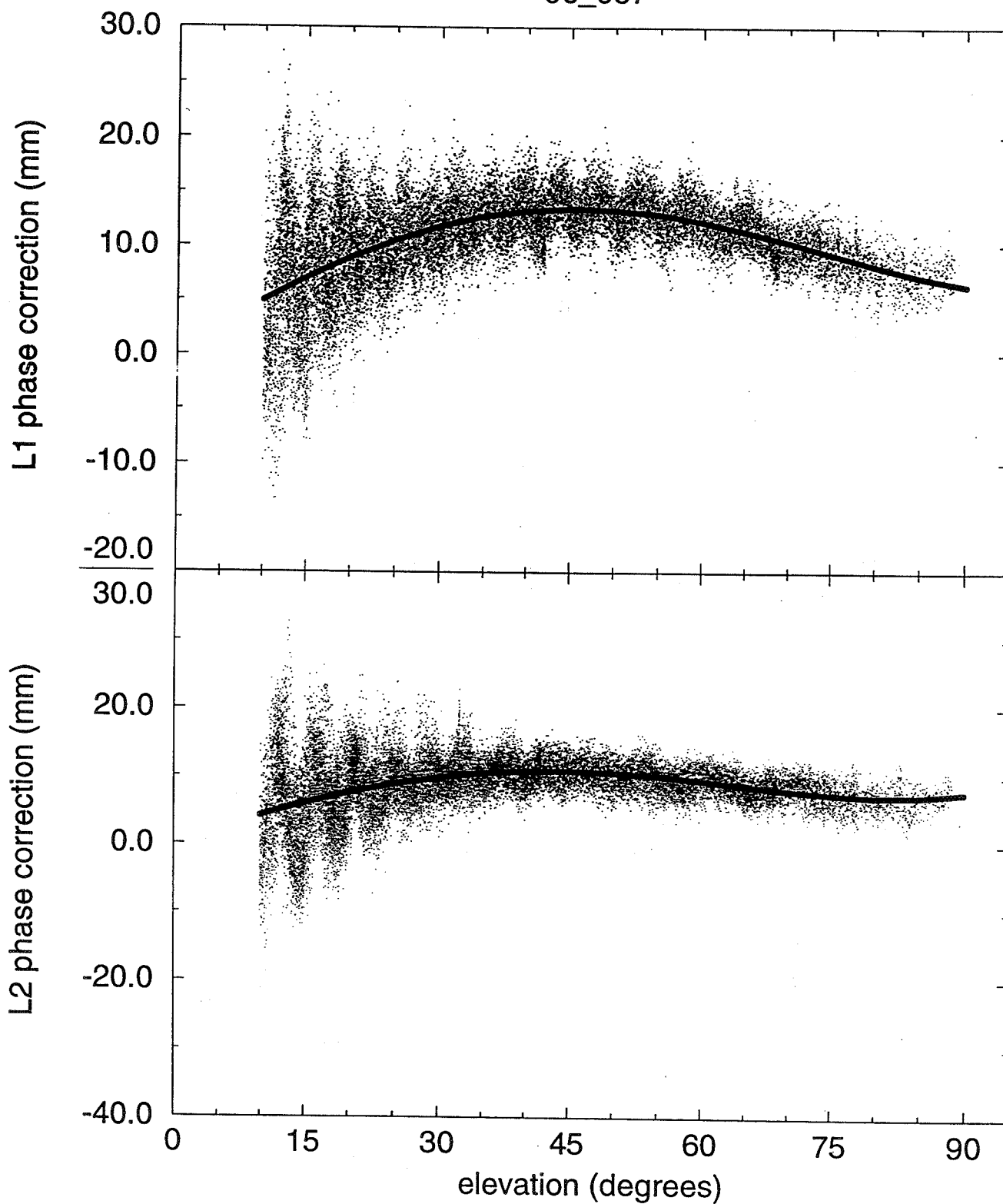


Figure 6

Trimble:14532-00

95_100

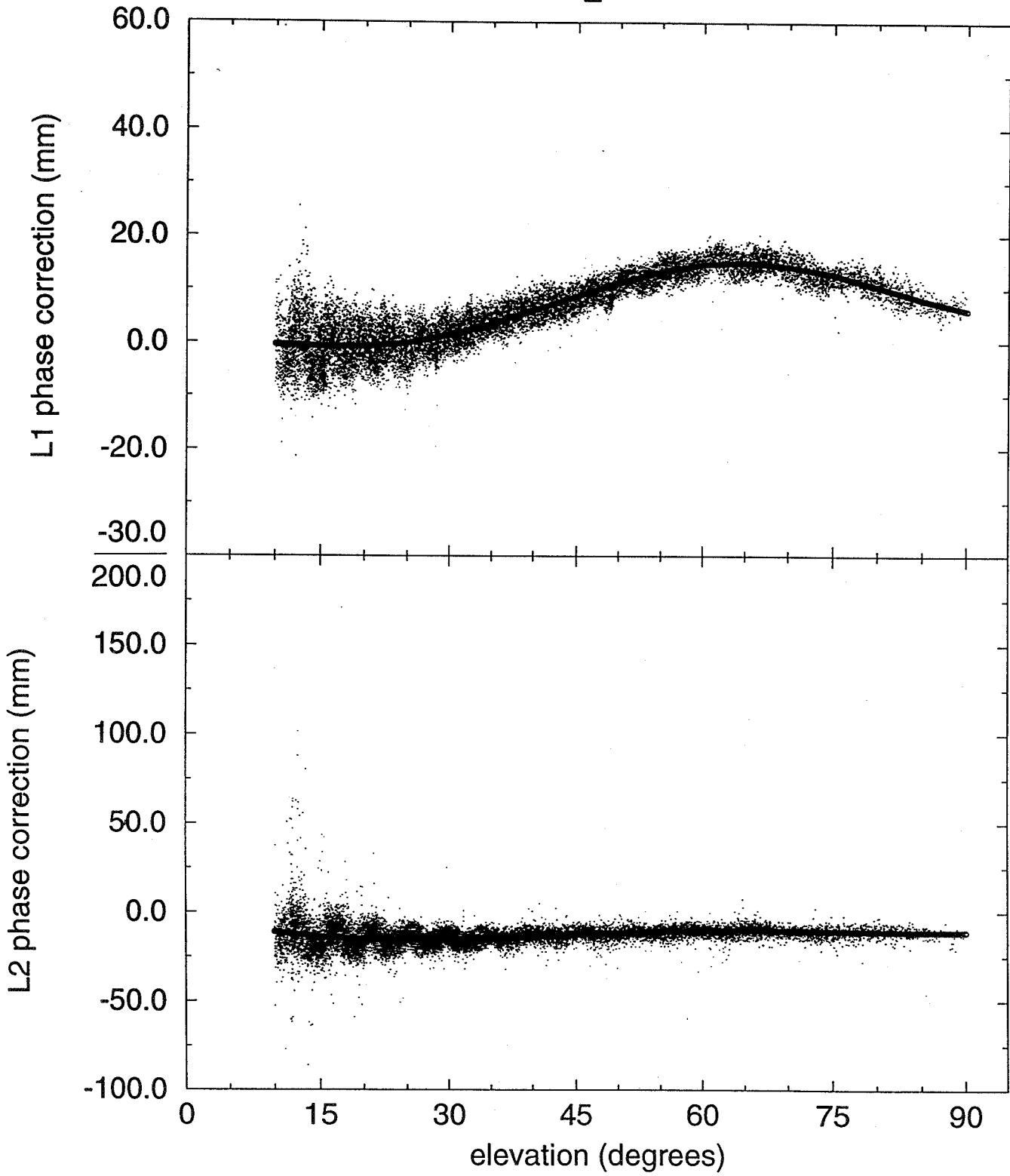


Figure 7

Macrometer:4647942

96_025

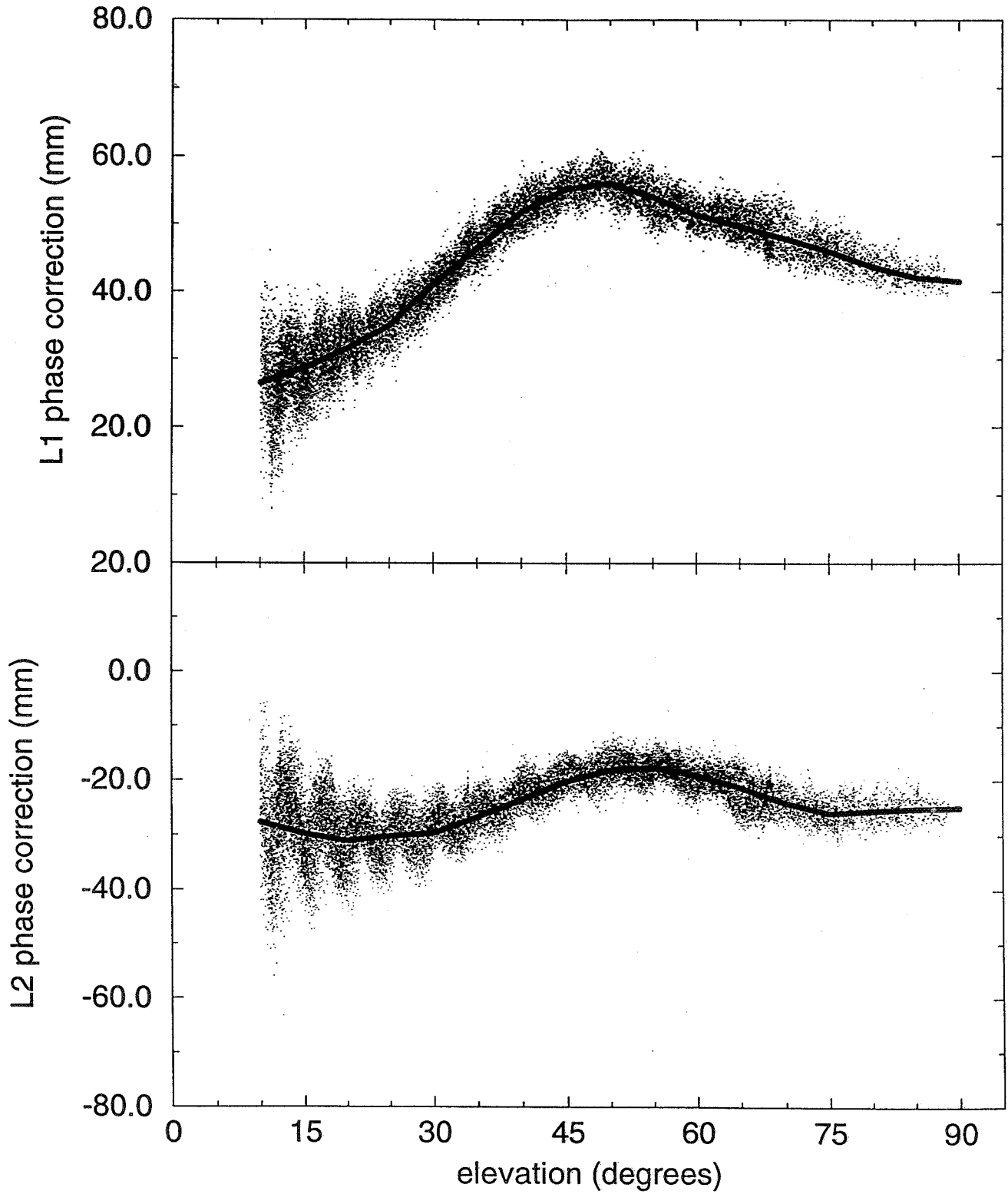


Figure 8

Phase Correction Repeatability

Ashtech:700829

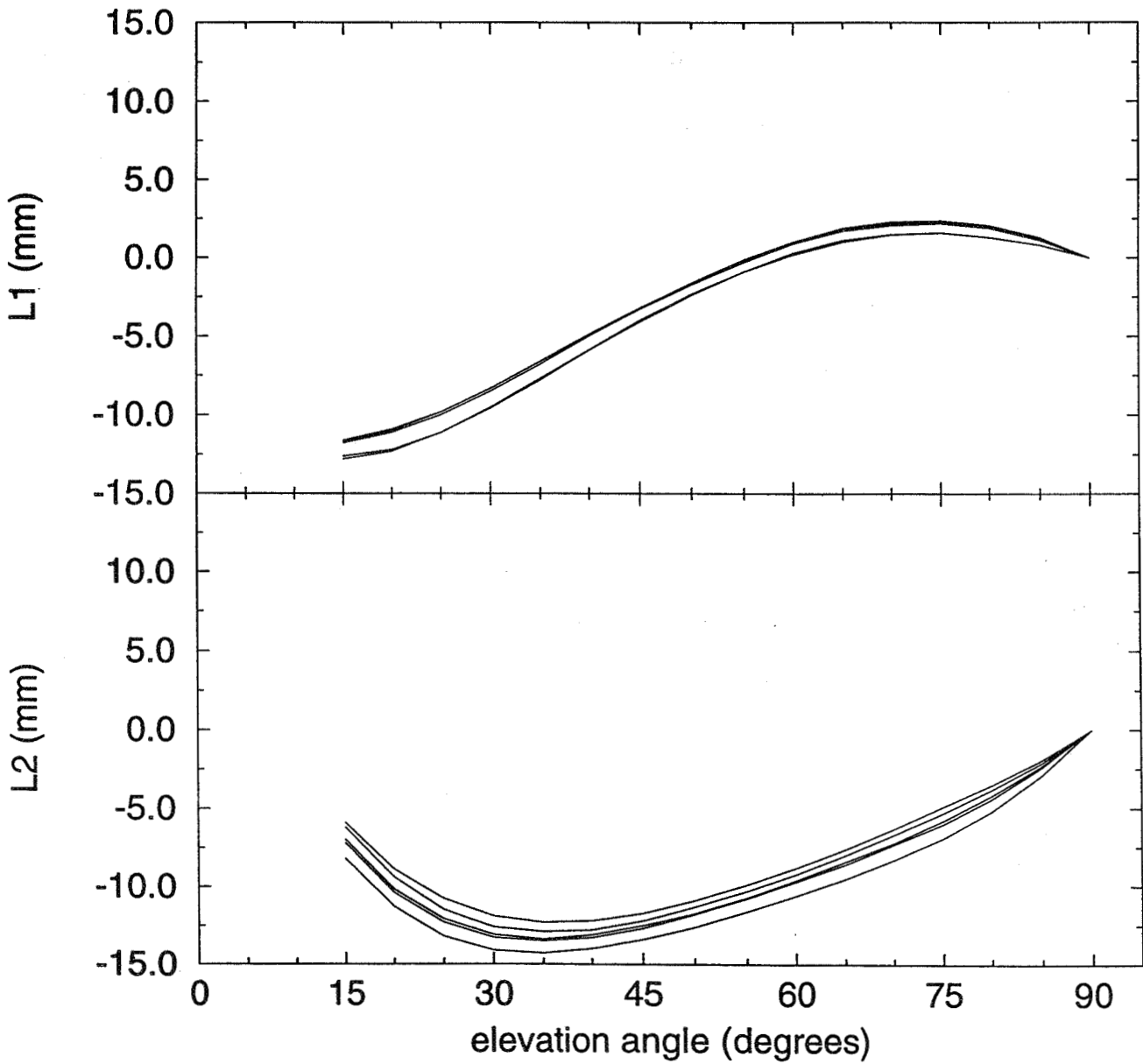


Figure 9

Phase Correction Repeatability

Ashtech:700228

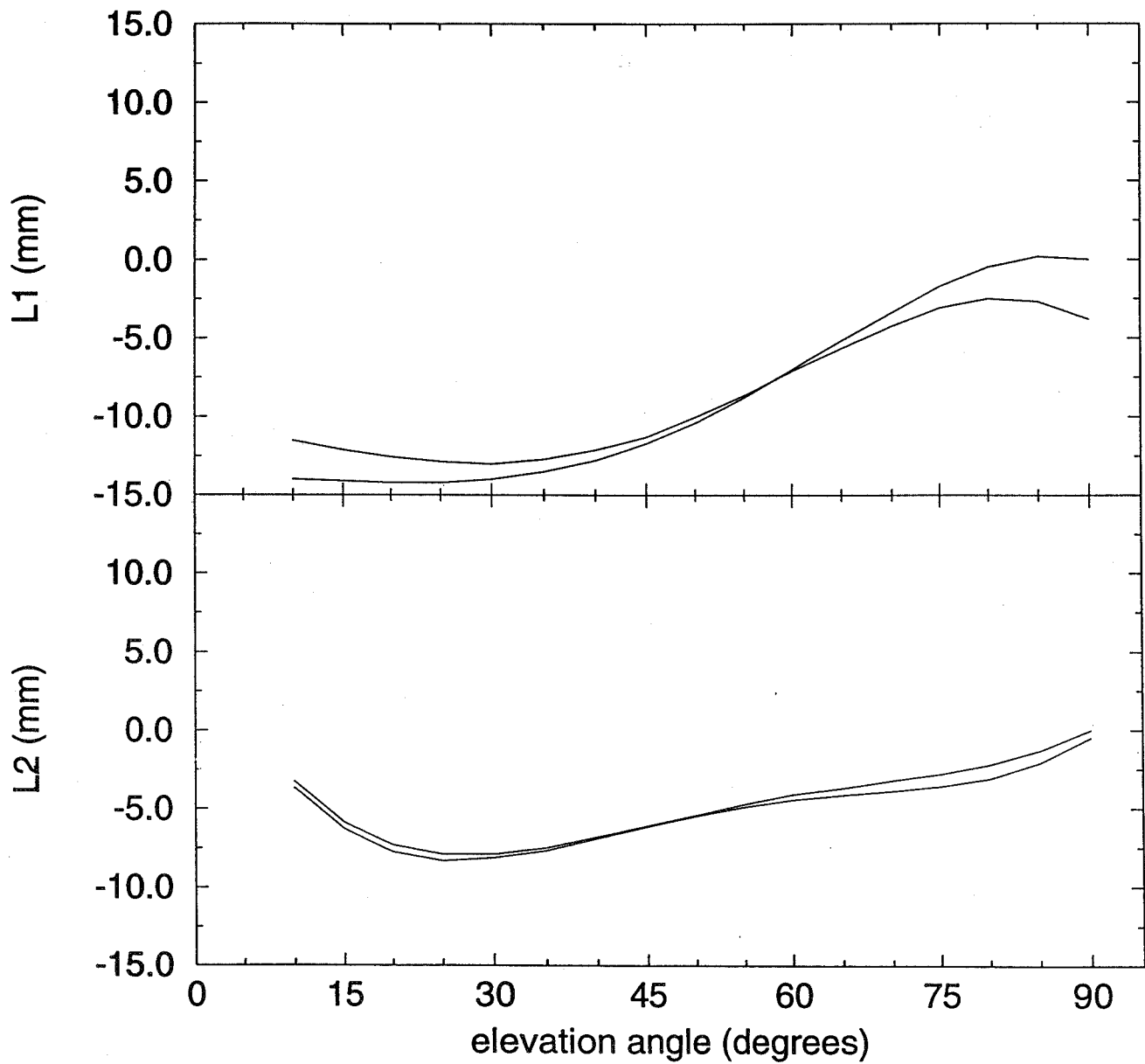


Figure 10

Phase Correction Repeatability

Ashtech:700718

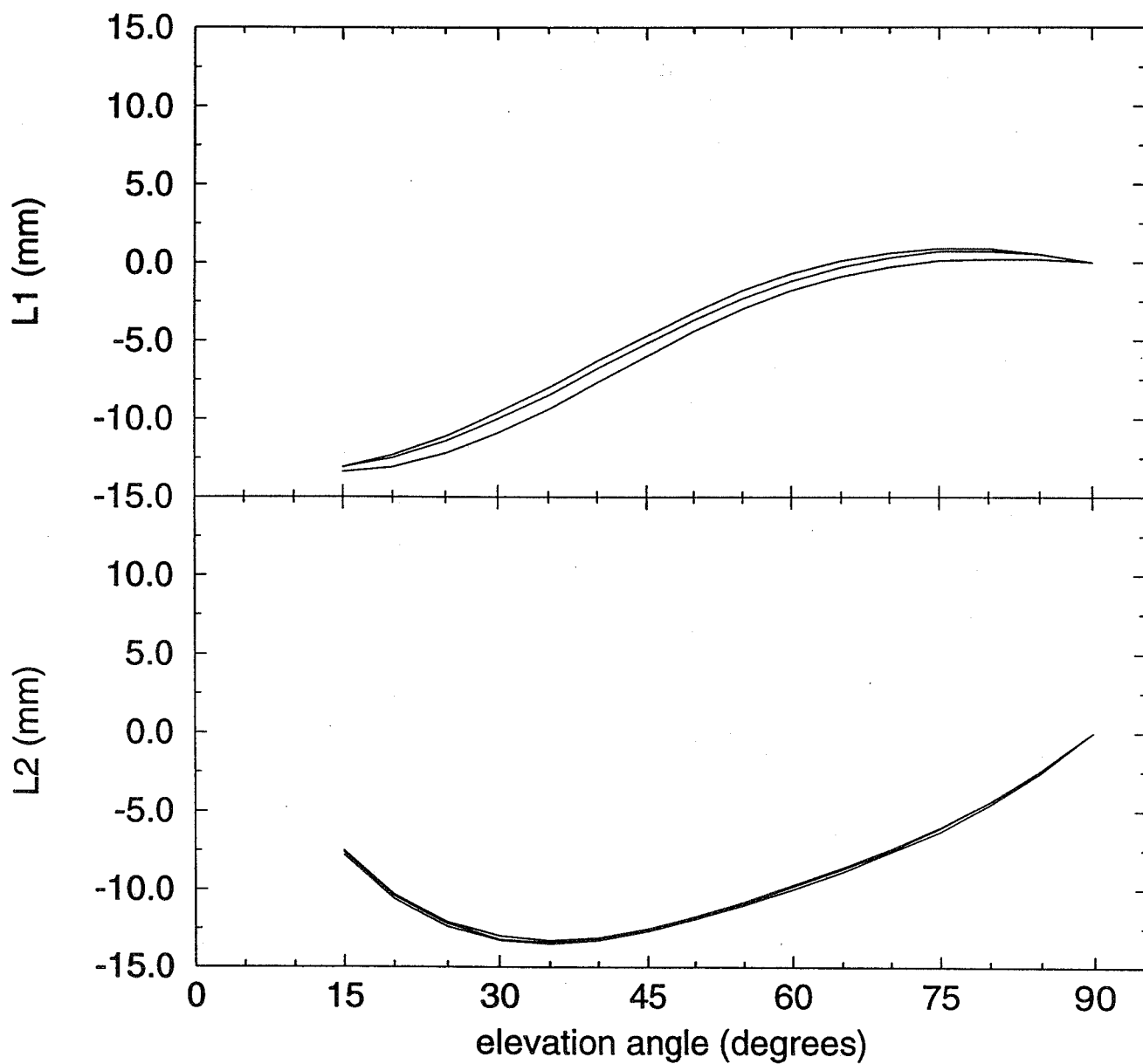


Figure 11

Phase Correction Repeatability

Ashtech:700936

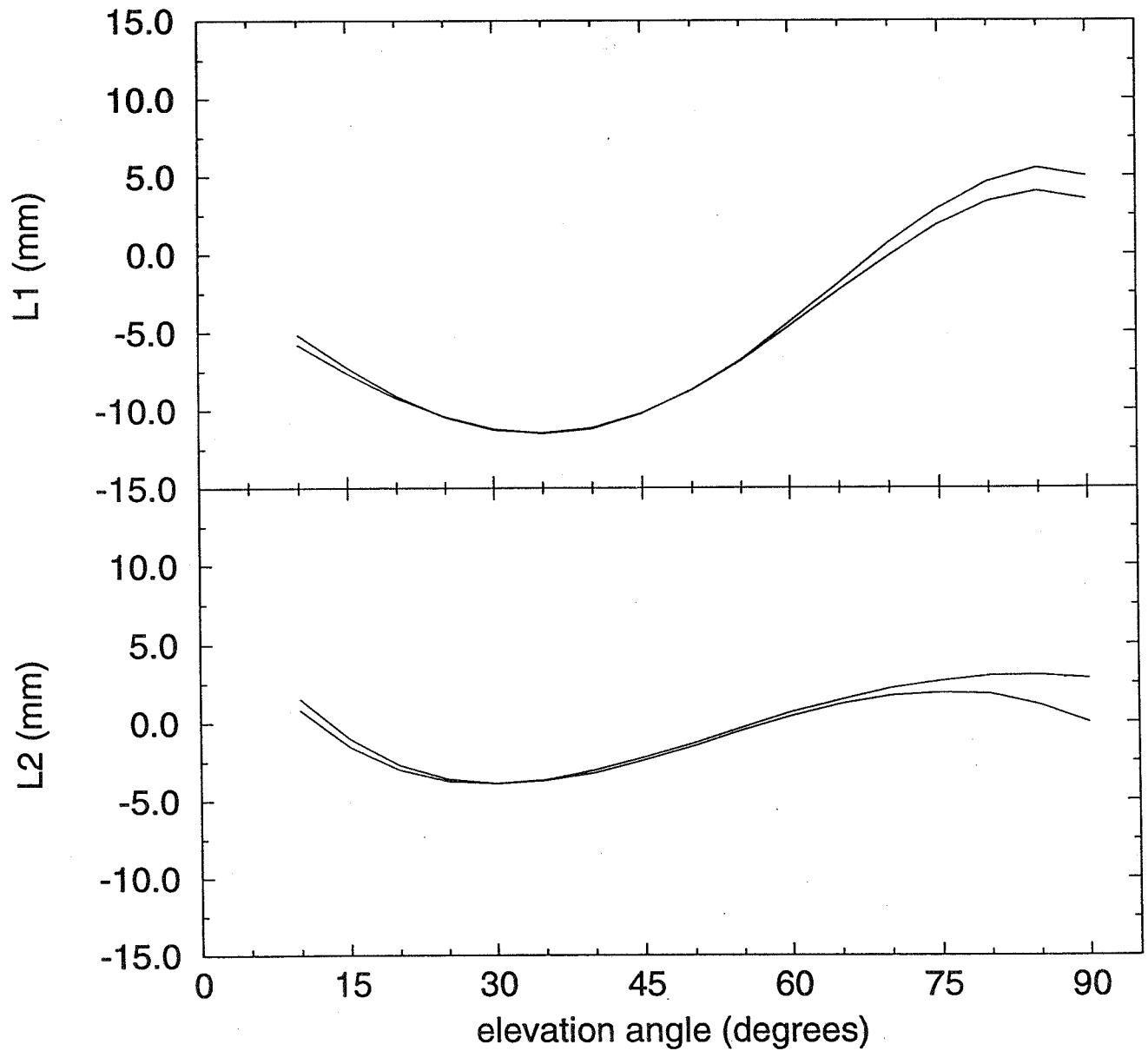


Figure 12

Phase Correction Repeatability

Trimble:14532

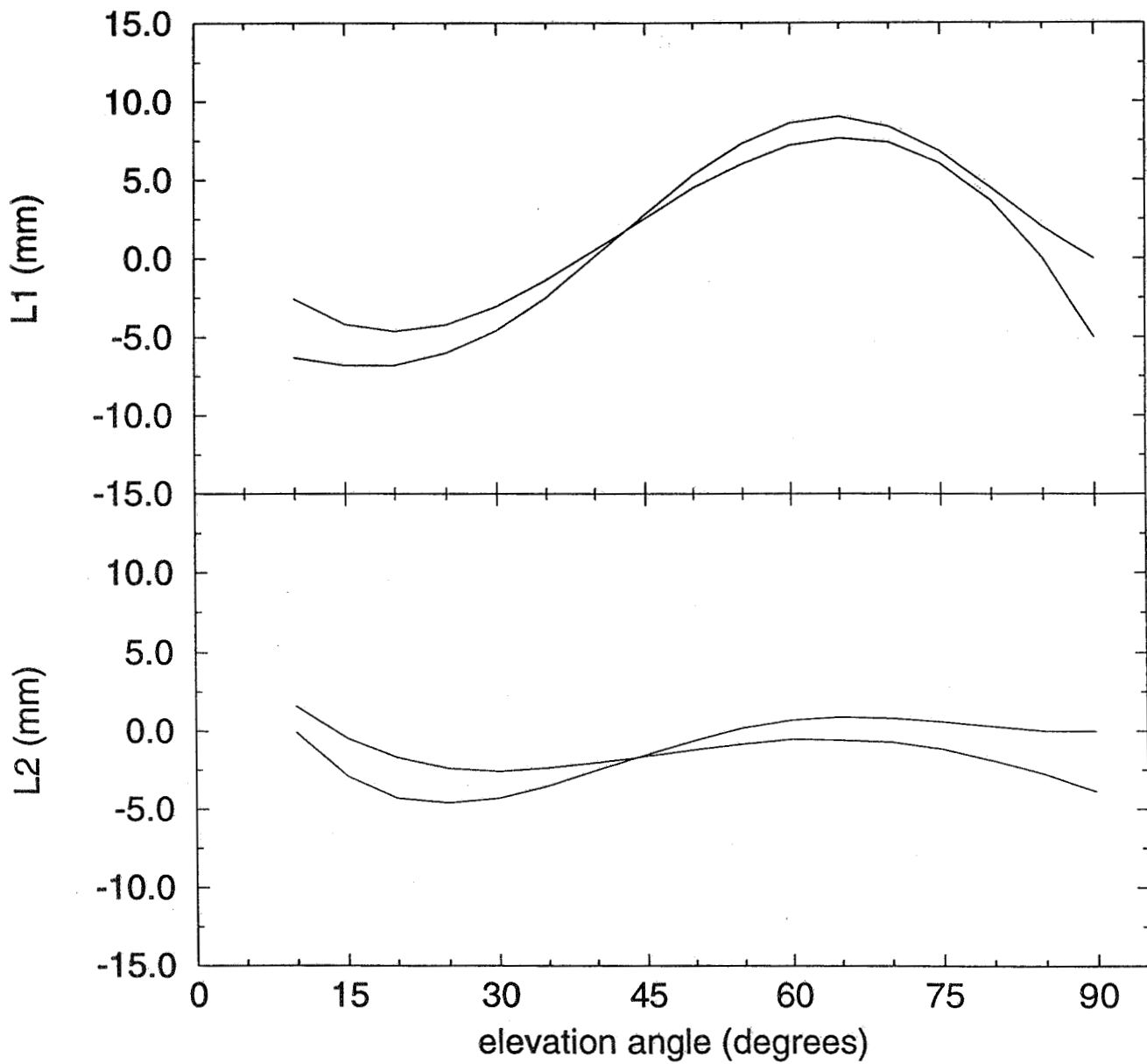


Figure 13

Phase Correction Comparison

Ashtech:700936

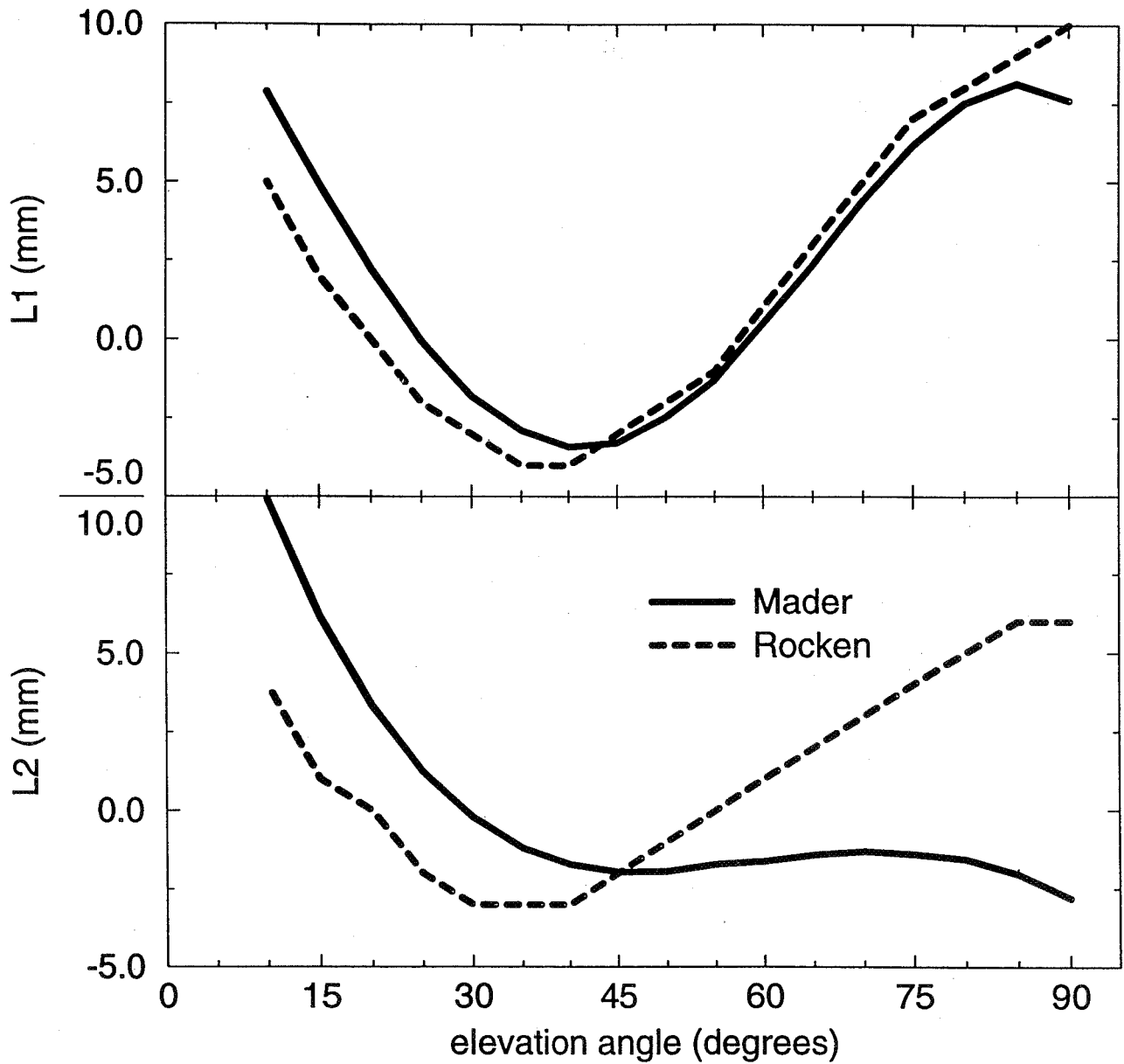


Figure 14

Phase Correction Comparison

Ashtech:700228

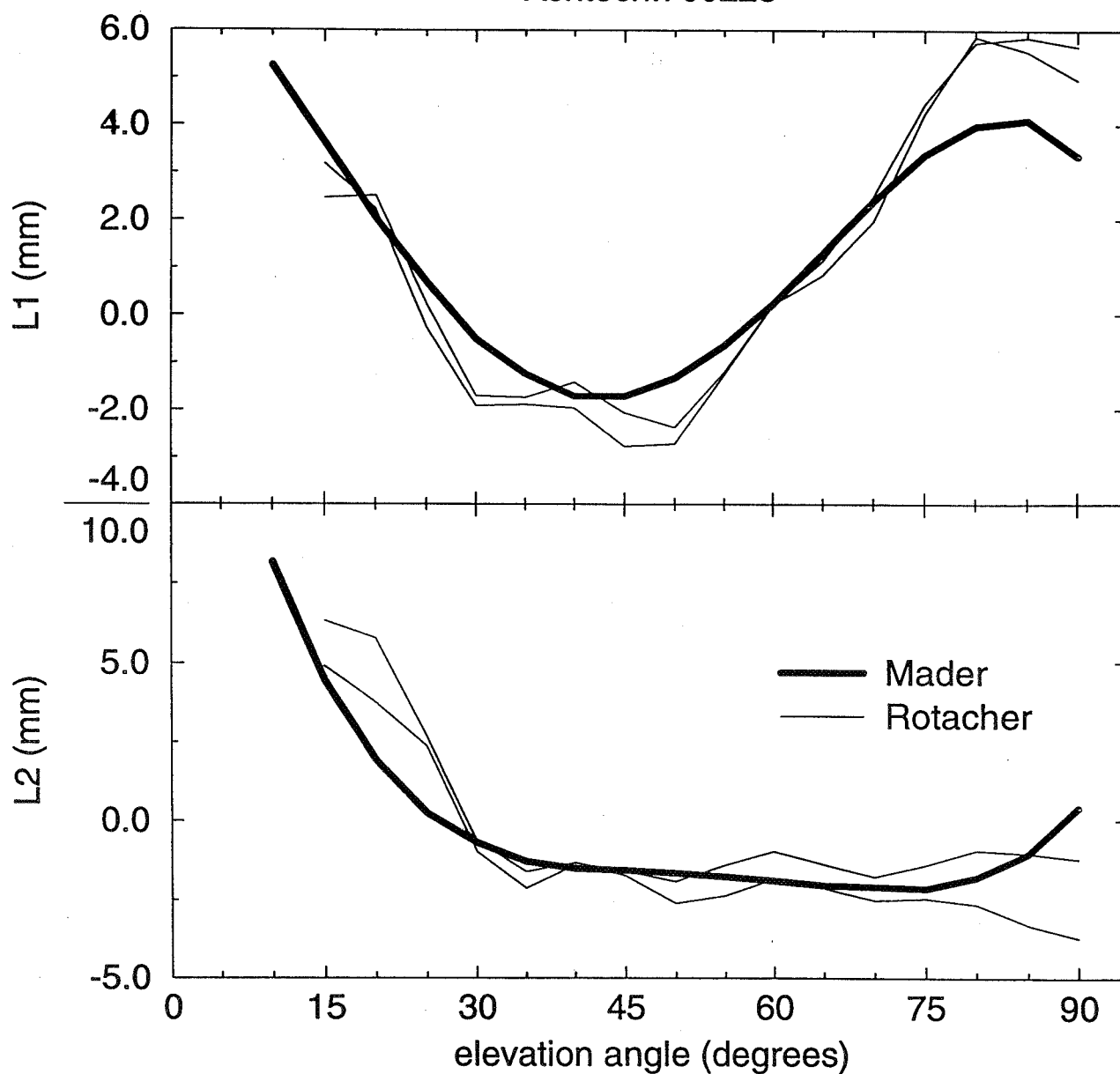


Figure 15

Phase Correction Comparison

Trimble:14532

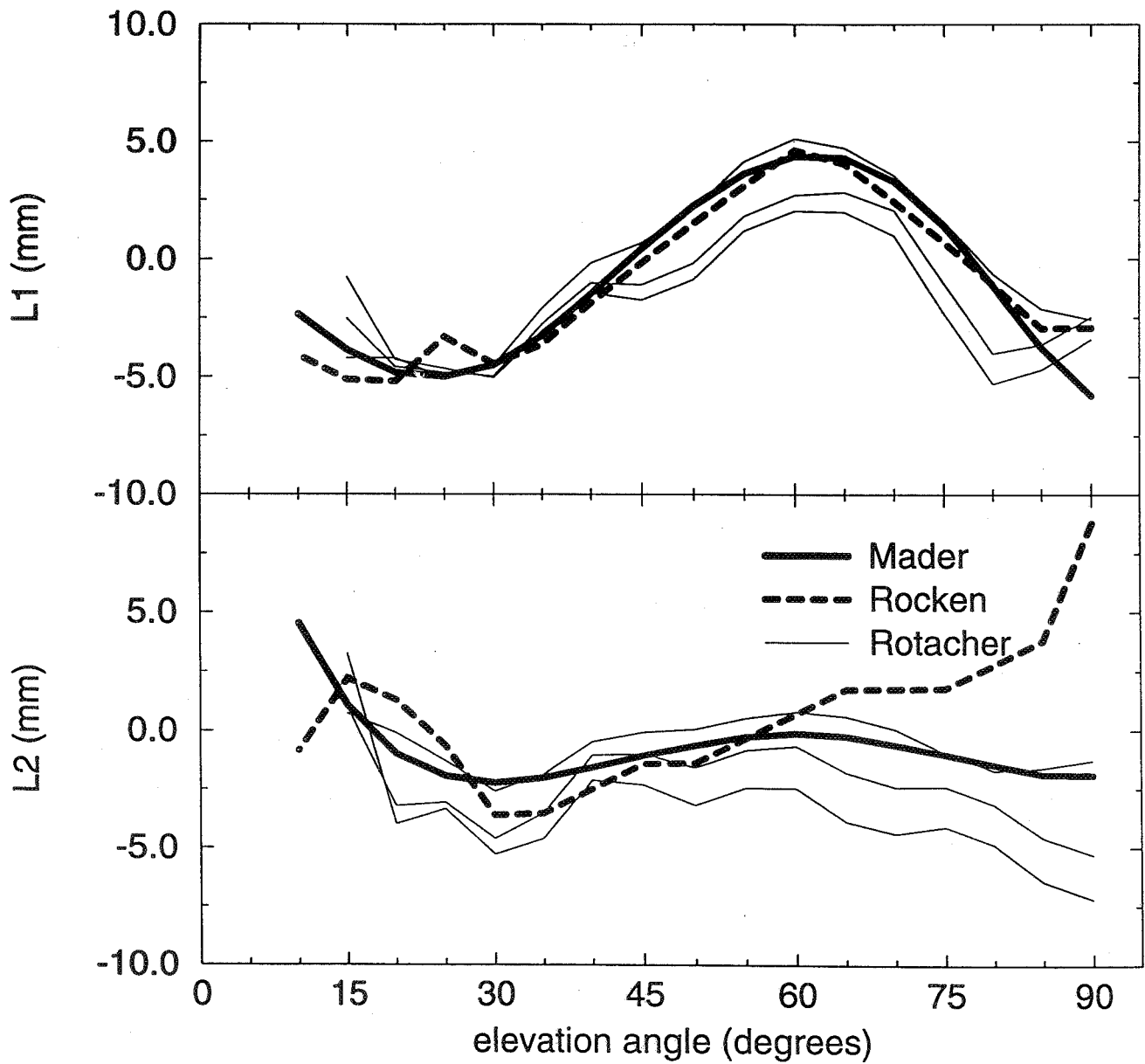
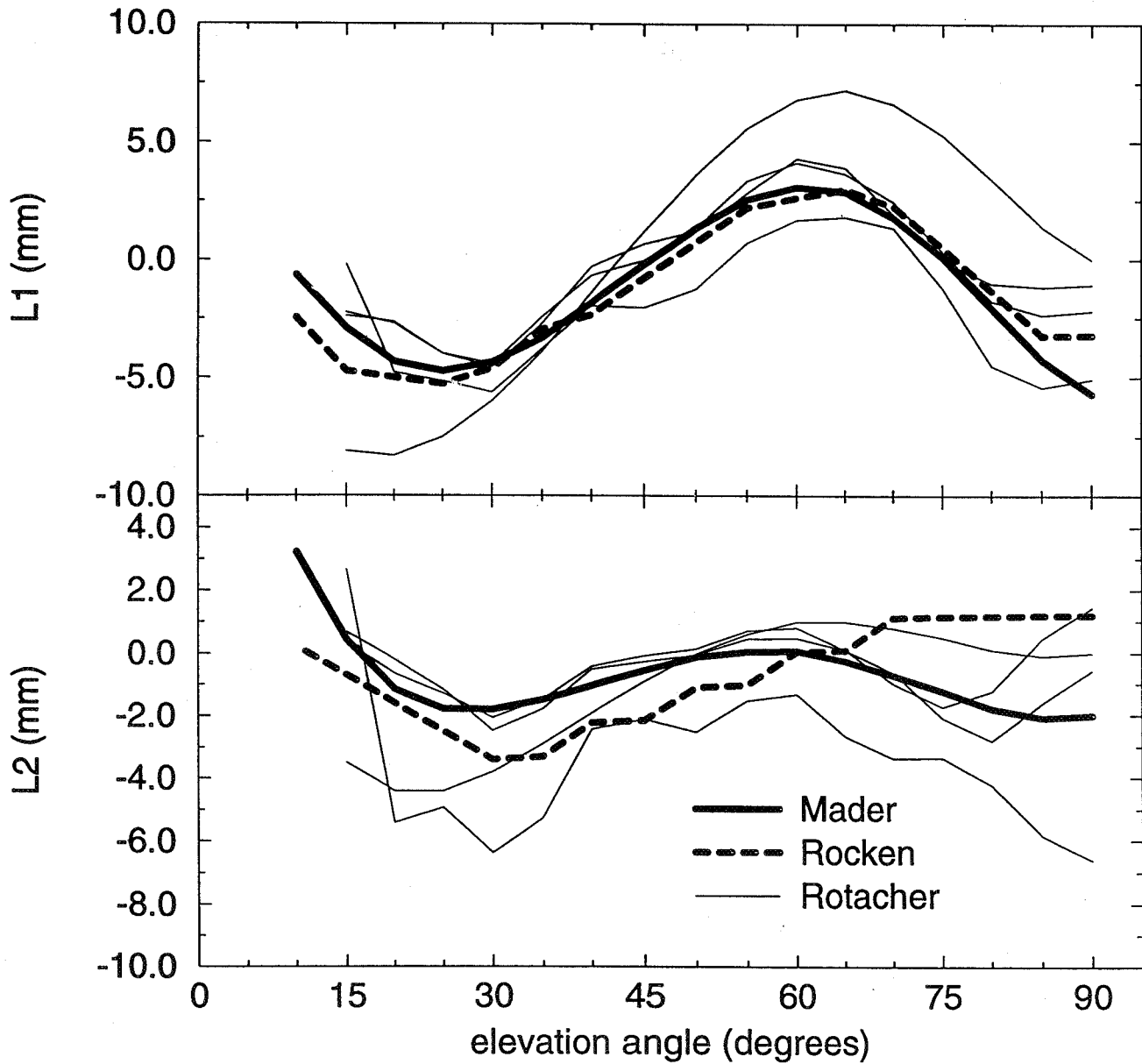


Figure 16

Phase Correction Comparison

Trimble:22020



Page intentionally left blank

Field and Anechoic Chamber Tests of GPS Antennas

C. Meertens, C. Alber, J. Braun, C. Rocken, B. Stephens, R. Ware
University Navstar Consortium (UNAVCO)

M. Exner, University Corporation for Atmospheric Research (UCAR)

P. Kolesnikoff, Ball Aerospace

IGS Meeting, Silver Spring, MD, 20 March 1996

The accuracy of GPS surveys between different GPS antenna types and mounts can be improved using antenna calibration corrections. These corrections range from the 1 mm level to the 100 mm level for commonly used geodetic quality antennas and mounts. In order to calibrate a variety of geodetic antennas and mounts, tests were conducted on short baselines in the field and in a state-of-the-art anechoic antenna chamber. Antennas included in the testing, with available IGS names in parentheses, were the Allen Osborne Associates choke ring T (DORNE MARGOLIN T) and AOA Rascal, Ashtech choke ring (DORNE MARGOLIN ASH) with cover installed, Leica SR399 external (EXTERNAL), and Trimble 4000 SST(4000ST L1/L2 GEOD) and Trimble Geod L1/L2 GP (TR GEOD L1/L2 GP) called in this report the SSE or SSI antenna¹. The results summarized here are described in detail in the **UNAVCO Academic Research Infrastructure (ARI) Receiver and Antenna Test Report²** (<http://www.unavco.ucar.edu/community/ari/report>). Also examined here are the effects of high and low antenna height, snow at the site and protective antenna covers.

Anechoic Chamber Measurements

Antennas can be characterized by phase center offsets and by phase and amplitude patterns for L1, L2 and L3 (ionosphere free) tracking as a function of azimuth and angle. We define the *offsets* as the average phase center locations relative to a physical reference point (typically used in RINEX files) on the antennas, and the *patterns* as the azimuth and elevation dependence of the phase centers and amplitudes. We measured these antenna properties in the Ball Aerospace anechoic test range chamber located in Broomfield, Colorado.

We ran the chamber tests using the antenna and low-noise-amplifier (LNA) combinations provided by the manufacturers. The chamber source transmitted at 9 frequencies near L1 and L2 to simulate GPS spread spectrum modulation. We observed at 5 degree intervals over all azimuths and over ± 120 degrees of elevation. Thus, more than 60,000 digital phase measurements were recorded for each antenna. The centers of rotation of the antennas with respect to the chamber mount were determined using a laser. The detail and high precision of the testing done in this state-of-the-art chamber may account for any disagreement between the results presented here and previous results (Schupler and Clark, 1991, 1994). The L1 phase patterns for various antenna-LNA combinations are shown in Figure 1.

-
1. The SSE and SSI antennas are identical.
 2. SST antennas were tested but the results were not included in the ARI test report because SST antennas were not offered as an ARI purchase option.

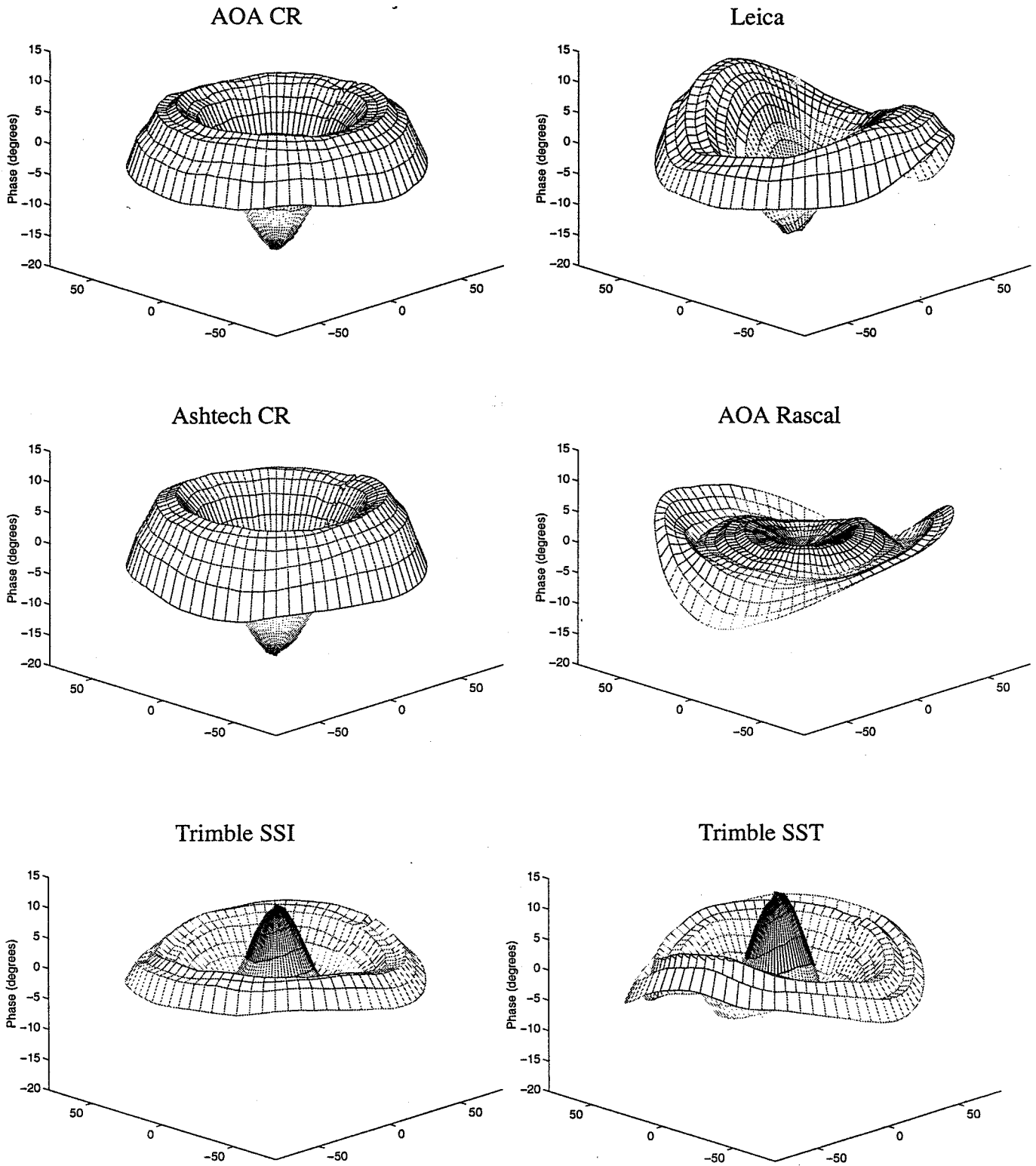


Figure 1: L1 phase center patterns are shown for several antennas (10 degrees of L1 phase is approximately 5 mm). Each of the *sombrero plots* shows zenith values in the center and 5 degree steps outward ending at 10 degrees above the horizon.

Antenna Field Tests

We conducted two types of field tests on Table Mountain near Boulder, Colorado, to validate antenna calibration parameters determined by the chamber tests. First, antenna rotation tests were conducted using antennas of the same type aligned to north on one mount and to the south on another mount, and then each antenna was rotated by 180 degrees. The observed difference in baseline length is equal to four times the average horizontal phase center offset from the rotation axis of the antenna. UNAVCO has conducted antenna rotation tests since 1989 on available antennas including the Trimble SD, SDT, SST and SSI, the Ashtech XIIM, TI-4100, FRPA, and the AOA Dorne-Margolin T with choke ring. The results are available in a series of UNAVCO technical reports (*ftp: unavco/pub/rec_test*). In the second field test, calibration corrections determined by the chamber tests were used in surveys between mixed antenna types on known baselines.

Antenna Rotations

The Ball chamber-measured horizontal phase center offsets are as large as 3 mm (L1) and 4 mm (L2) with an uncertainty of 0.5 mm, yielding as large as 8 mm horizontal offsets for L3 (Figure 2). These offsets agree within 1 mm for L1 and L2 with offsets determined by field rotation tests for the AOA choke ring and Trimble SSI antennas (Figure 3) as well as for the Trimble SST (not shown). The UNAVCO/Ball results offer for the first time a confirmation with chamber measurements of the horizontal offsets observed in the field antenna rotation tests.

The antenna rotation tests results shown here address only the phase center offset. It is possible to estimate phase patterns from field GPS data on short baselines (Mader and MacKay, 1995; Rothacher and others, 1995). This technique has the advantage that possible local site multipath and scattering effects can be accounted for. The results are, however, relative to a reference antenna for which a precise absolute calibration must exist (and the reference antenna must be setup to minimize multipath effects). We do not elaborate on these tests here since we have not compared them to chamber tests.

Field Antenna Mixing with Chamber-Derived Offset and Pattern Corrections

We found that L3 mixed-antenna, offset-corrected measurements with no tropospheric estimations were in error by 20 mm or less in the vertical (Figure 4, plus symbols on left panel) and by 1 mm or less in the horizontal. If hourly tropospheric estimations are included in the L3 solutions, the vertical error increases to as much as 87 mm for the Trimble SSI to Ashtech choke ring (Figure 4, plus symbols on right-hand panel).

Application of offset and pattern corrections reduces the vertical error for troposphere corrected Trimble SSI to AOA and Ashtech choke ring antenna mixes to 13 mm or less. The least successful application of the offset and phase center pattern corrections has been with the Trimble SST antenna where the residual error is as large as 50 mm. SST mixing results can be found in UNAVCO reports available via ftp (*unavco/pub/rec_test*).

UNAVCO/BALL Anechoic chamber

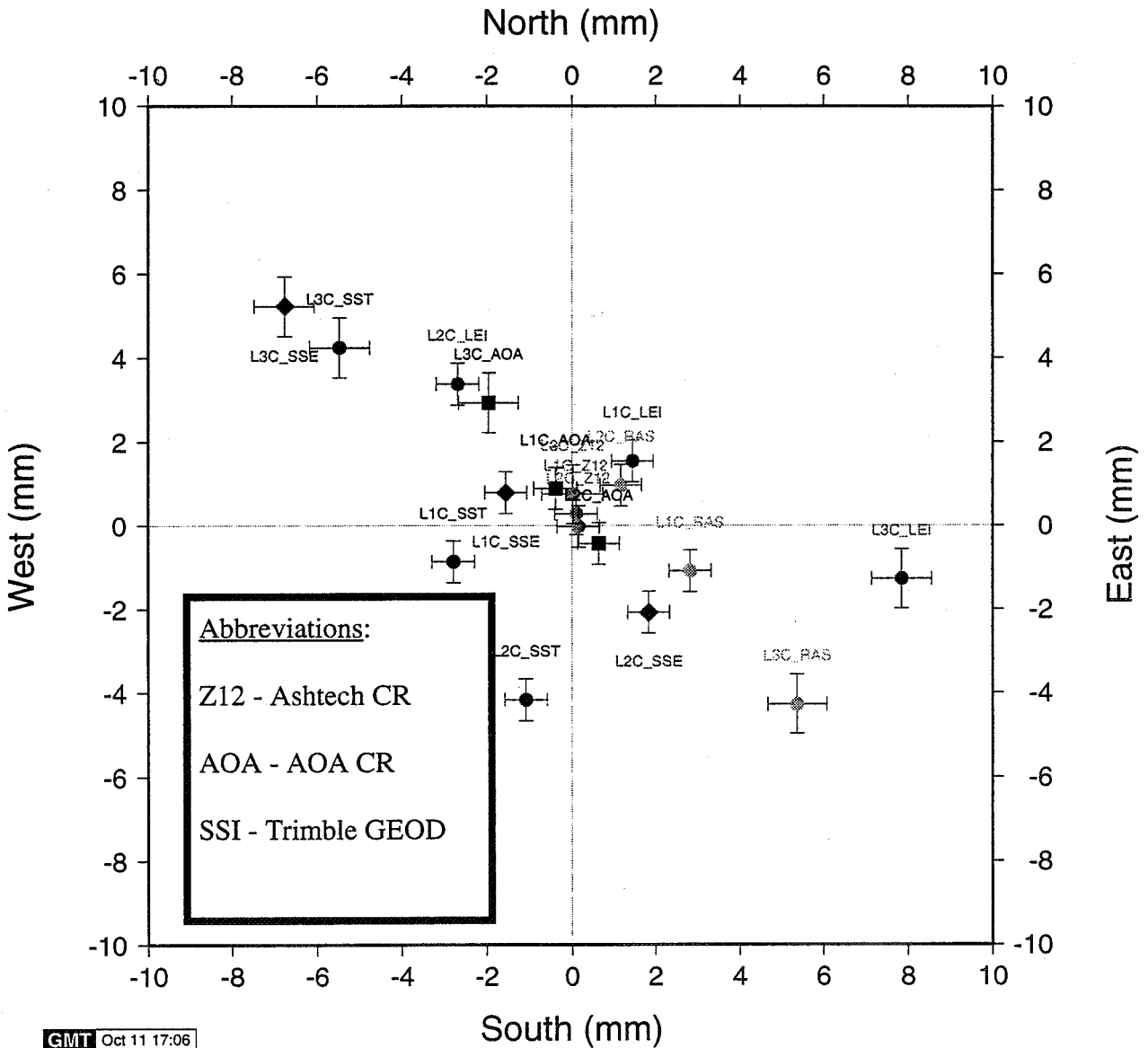


Figure 2: Horizontal phase center offsets (labeled L1C, L2C, and L3C) determined from chamber tests. The antenna axis of rotation is the zero point. Error estimates are ± 0.5 mm for the measured L1 and L2 offsets.

ANTENNA PHASE CENTERS

UNAVCO Antenna rotation ■ L1F/L2F/L3F
 UNAVCO/BALL Anechoic chamber ◆ L1C/L2C/L3C
 GSFC Anechoic chamber ● GL1/GL2/GL3

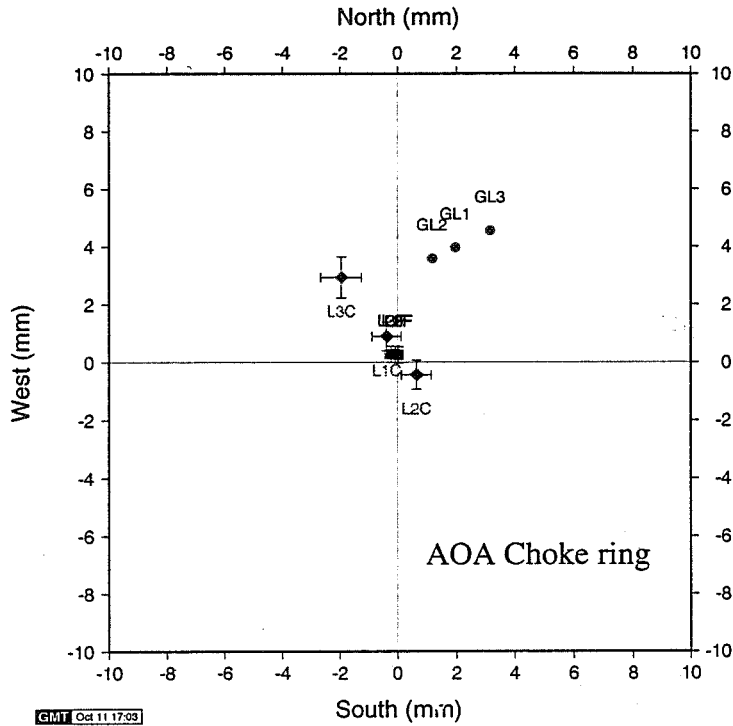
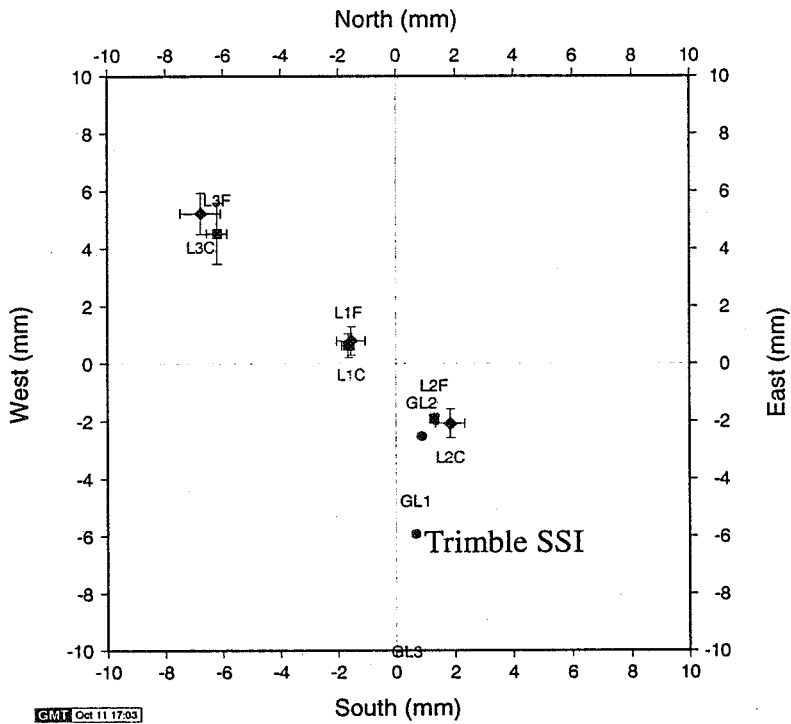


Figure 3: Horizontal phase center offsets derived from UNAVCO field antenna rotation tests (L1F, L2F, L3F), UNAVCO/Ball anechoic chamber tests (L1C,...), and Goddard/Bendix anechoic chamber tests (GL1,...).



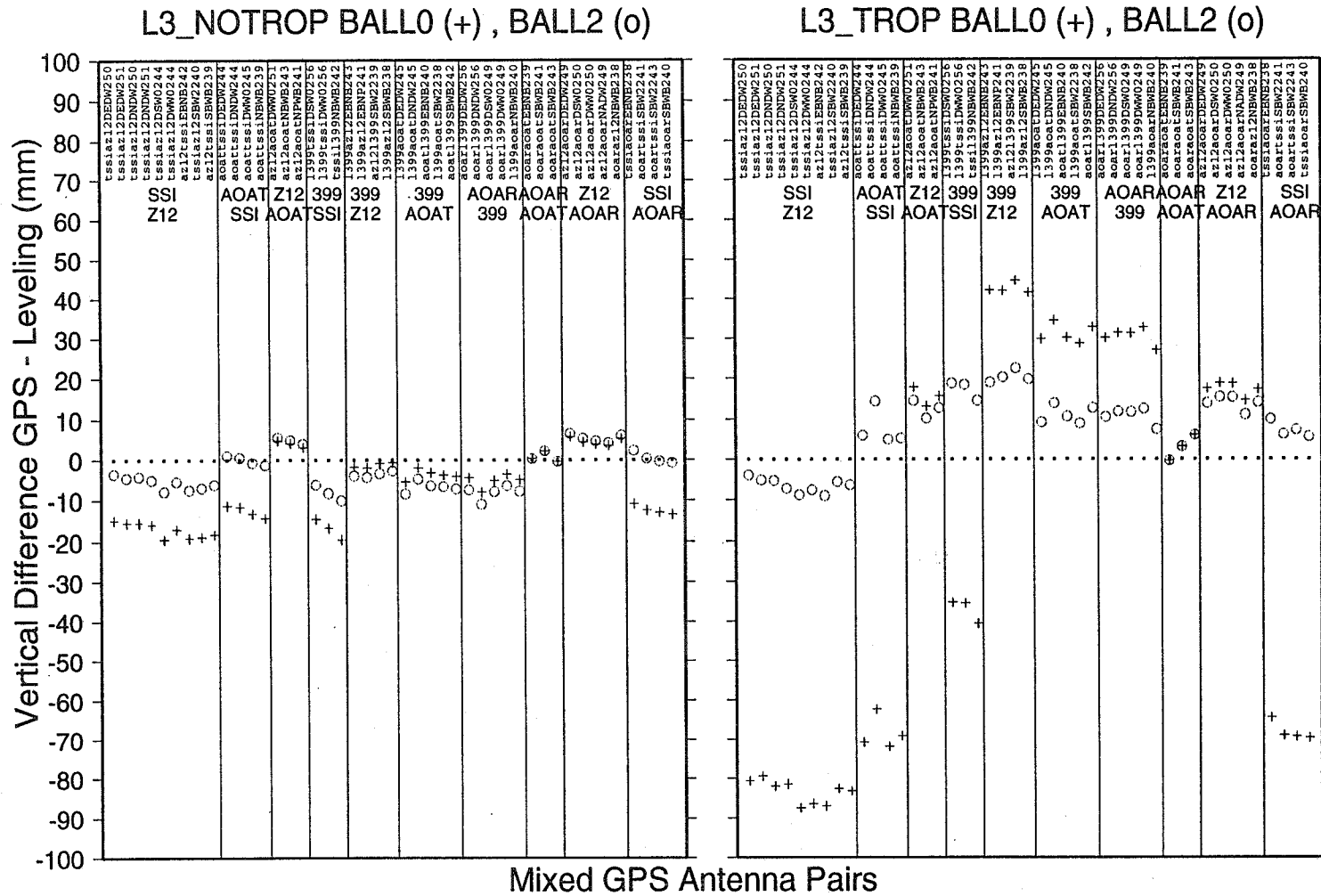


Figure 4: Summary of mixed-antenna vertical solutions with offset corrections (+ symbols) and offset plus phase center pattern corrections (o symbols). L3 solutions are shown with tropospheric estimation (right panel) and without tropospheric estimation (left panel). The columns, separated by vertical lines, show 10 different antenna mixes. Ground truth is indicated by the dotted line.

In general, mixed antenna baseline solutions show vertical errors of 12 mm or less without tropospheric estimation, and up to 50 mm with tropospheric estimation. This compares with 1 mm errors achieved with unmixed antennas on short baselines with no tropospheric estimations. The antenna mixing error has several possible sources. First, an anechoic chamber provides an *ideal* low multipath environment whereas observations in the field are influenced by local site conditions including multipath and monument effects¹. Second, differences in phase patterns between mixed antennas can be easily confused with tropospheric delay, particularly at low elevation angles. These effects are described in the following section.

Effects of High and Low Antenna Height Mounts

In order to investigate the effect of antennas heights on baseline accuracy, we conducted tests at Table Mountain where antennas could be easily mounted near to the ground over rod monuments set in concrete. Monuments were occupied with high (1.5 m) and low (less than 0.5 m) antenna tripod mounts with various GPS receivers and antennas. Baseline results using Trimble SSE GPS receivers and Trimble SST antennas with high and low antenna heights had vertical errors as large as 17 mm when tropospheric parameters were estimated. The horizontal components were not affected. The results of the antenna height tests are summarized in Table 1.

Table 1: Vertical solutions using high (1.5 m) and low (less than 0.5 m) antenna heights

Antenna heights	No tropospheric estimation (rms in mm)	With tropospheric estimation (rms in mm)
low-low	0.9	7.4
low-high	1.3	5.6
high-high	1.4	4.1

We found that multipath at the low antenna can be easily mismodeled as tropospheric delay. The multipath phase error generated by a low antenna can correlate to tropospheric delay for large intervals of elevation. Specifically, the L1 phase error for a low antenna is long period (more than 1 hour) and often correlates to tropospheric delay, particularly at low elevation angles (15 to 30 degrees) where multipath and tropospheric delays are strong. This can lead to vertical errors of several cm in daily solutions. Based on a simple multipath model and experimental results at

1. We have shown, for example, that even with identical antennas, the use of low antenna mounts can seriously degrade vertical accuracy when tropospheric parameters are estimated. Nevertheless, it should be possible to map and correct for local multipath effects and any phase center pattern distortions resulting from the site antenna mount. This could be accomplished using a zero (or very low) multipath antenna with a well known antenna and mount phase center pattern. Variations in solutions between the zero and site antennas could be stacked for a number of days. Variations that persist in sidereal time could be used to correct for combined multipath and phase pattern effects. However, changes in local environment caused by snow, rain, plant growth, or modification of man-made structures could degrade the accuracy of this correction.

Table Mountain, we conclude that: (1) GPS antennas should not be placed near the ground because the scattering from the ground causes low frequency multipath that can be mis modeled as tropospheric delay resulting in vertical errors as large as several cm, (2) measurements using GPS antennas mounted on tripods at 1.5 m height are generally more accurate because they are subject to high frequency multipath (high frequency multipath is not easily confused with tropospheric delay). Details of the UNAVCO high-low antenna tests are described in http://www.unavco.ucar.edu/docs/science/1995_ant_tests/tblmntn.

It is important to note that for pillar monuments there is the possibility of an additional effect—scattering from the horizontal surface of the pillar immediately below the antenna (Elosegui, and others, 1995). In this case the horizontal top of the monument is the main scatterer and the separation between the antenna and the top of the pillar is important, independent of the height of the monument above the ground. The scattering effect may be enhanced by the presence of a metal plate at the top of the pillar.

Snow and Tropospheric Estimation Effects

Multipath effects have been demonstrated to affect vertical accuracy in the high-low antenna setups described above. In addition, changes in multipath conditions, such as snow at the site, can affect vertical baseline solutions when tropospheric delays are estimated. Such an effect was found using two Trimble SSE antennas on a 55 m baseline with 1 m 0.5 m antenna heights (Chris Alber, doctoral thesis in preparation). Vertical results for one day with snow cover and one without are given in Figure 5.

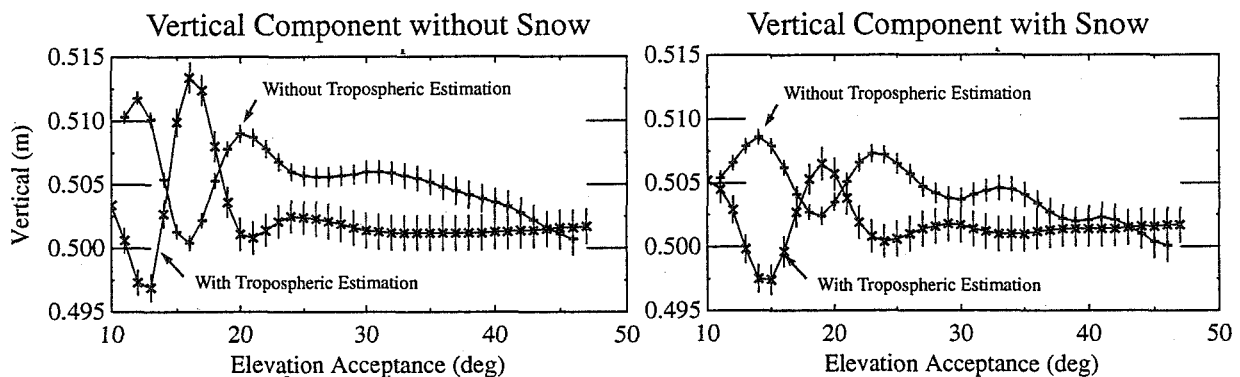


Figure 5: GIPSY processed vertical solutions are shown as a function of minimum satellite elevation acceptance for a day without snow and a day with snow, with and without tropospheric estimation. Each point represent a 24-hour solution using data from all satellites above the minimum elevation mask. Error bars show the formal solution error.

Each point represents the vertical baseline component solution from GIPSY processing using 24 hours of data and all satellites above the minimum elevation mask. The vertical baseline components for no-snow and snow are shown with and without stochastic tropospheric estimation. The results show a sensitivity at the 1 to 2 cm level to minimum elevation acceptance which is caused by multipath effects and is responsible for the errors and variability in vertical solutions from

high-low antenna setups. Of note in this test, however, is the reversal in the sign of the effect when there is snow cover, indicating a large phase change in observed multipath. This effect is enhanced by the low height of one of the antennas. Similar effects were observed with 1-3 meter high monuments in the Swedish permanent network at least part of which was attributed to buildup of ice and snow on one side of the protective cover over the antenna (Elosegui, and others, 1995).

Improved GPS Geodetic Antennas

For the highest accuracy applications such as vertical deformation studies or atmospheric sensing, multipath effects can be a limiting error source. Multipath effects can to some extent be minimized by careful site selection and installation, but can also be reduced by using an antenna with higher multipath suppression, and through software algorithms such as multipath stacking and prediction. One approach to improved antenna design is the addition of a 1 meter choke ring to the JPL/AOA choke ring antenna. This approach is attractive since it could be used to retrofit choke ring antennas currently installed in the IGS global network. Details of this design are described in http://www.unavco.ucar.edu/docs/science/geo_antenna. Improvements in multipath reduction using a 1 meter ground plane with the AOA choke ring have also been demonstrated (Mader and Schenewerk, 1994).

Effects of Antenna Protective Covers

The anechoic chamber tests showed differences between the AOA choke ring and the Ashtech choke ring with protective cover. Subsequent field tests have confirmed that antenna covers significantly influence the vertical solutions. For example, using an Ashtech compressed styrofoam conical cover on only one end of a short baseline causes a 10 mm vertical error in the baseline vector when the tropospheric delay parameter is estimated. Preliminary results of an 1/8 inch thick acrylic dome cover shows a smaller, 2 mm vertical offset. UNAVCO is conducting further tests with a 1/4 inch acrylic cover used with AOA choke ring antennas at many IGS sites.

Summary

Antenna mixing as well as site and antenna height dependent multipath effects may effect GPS accuracy at the level of a few mm to 10 cm (Table 2). Progress is being made by measuring and correcting for mixed antenna effects (using field and chamber data), by moving toward *standard* antennas (JPL-designed choke rings with Dorne-Margolin antenna elements are now available from AOA and Ashtech and will soon be available from Trimble), and by avoiding tropospheric estimation errors associated with low antennas.

Using antenna phase pattern and offset corrections derived from anechoic chamber tests, the accuracy for mixed Trimble SSI (patch antenna with removable ground-plane) and Ashtech and AOA choke ring antennas, with tropospheric estimation, is 12 mm or less in the vertical. Mixing results for other antennas are as high as 5 cm in the vertical. Additional work is needed to reduce antenna mixing errors down to the 1-mm level, to evaluate mixing of similar antennas made by different manufacturers (including different preamplifier designs), and to calibrate monument and cover effects.

References

- Elosegui, P., J.L. Davis, R.T.K. Jaldehag, J.M. Johansson, A.E. Niell and I.I. Shapiro, Geodesy using the Global Positioning System: The effects of signal scattering on estimates of site position, JGR preprint, 1995.
- Mader, G.L. and J.R. MacKay, Calibration of GPS Antenna, draft publication, 1995.
- Mader, G.L. and M. S. Schenewerk, Groundplane Effects on Multipath and Phase Center Location and Calibration of GPS Antennas, Trans. Amer. Geophys. Un., 75, November, 1994, p. 171.
- Rothacher, M. S. Schaer, L. Mervart, and G. Beutler, Determination of Antenna Phase Center Variations Using GPS Data, Paper presented at the 1995 IGS Workshop, Potsdam, Germany, May 15-17, 1995.
- Schupler, B.R., and T.A. Clark, How different antennas affect the GPS Observable, GPS World, p. 32-36, Nov-Dec, 1991.
- Schupler, B.R., R.L. Allshouse, T.A. Clark, 1994, Signal Characteristics of GPS User Antennas, Navigation, 41(3), 277-295, 1994.
- Schupler, B.R., T.A. Clark, and R.L. Allshouse, Characterizations of GPS User Antennas: Reanalysis and New Results, preprint, 1995.

Table 2: SUMMARY OF ANTENNA AND ANTENNA MOUNTING ISSUES

Antenna Phase Center Variations

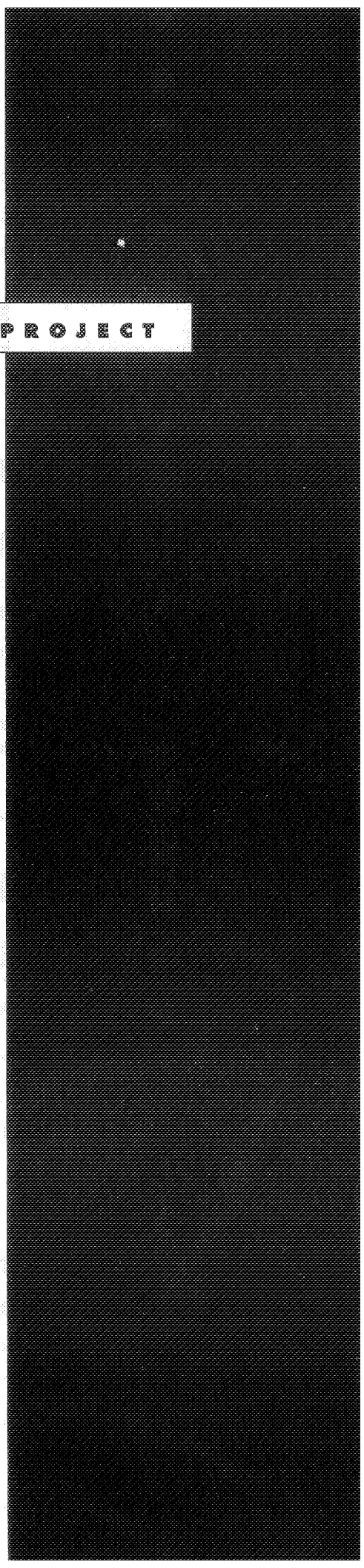
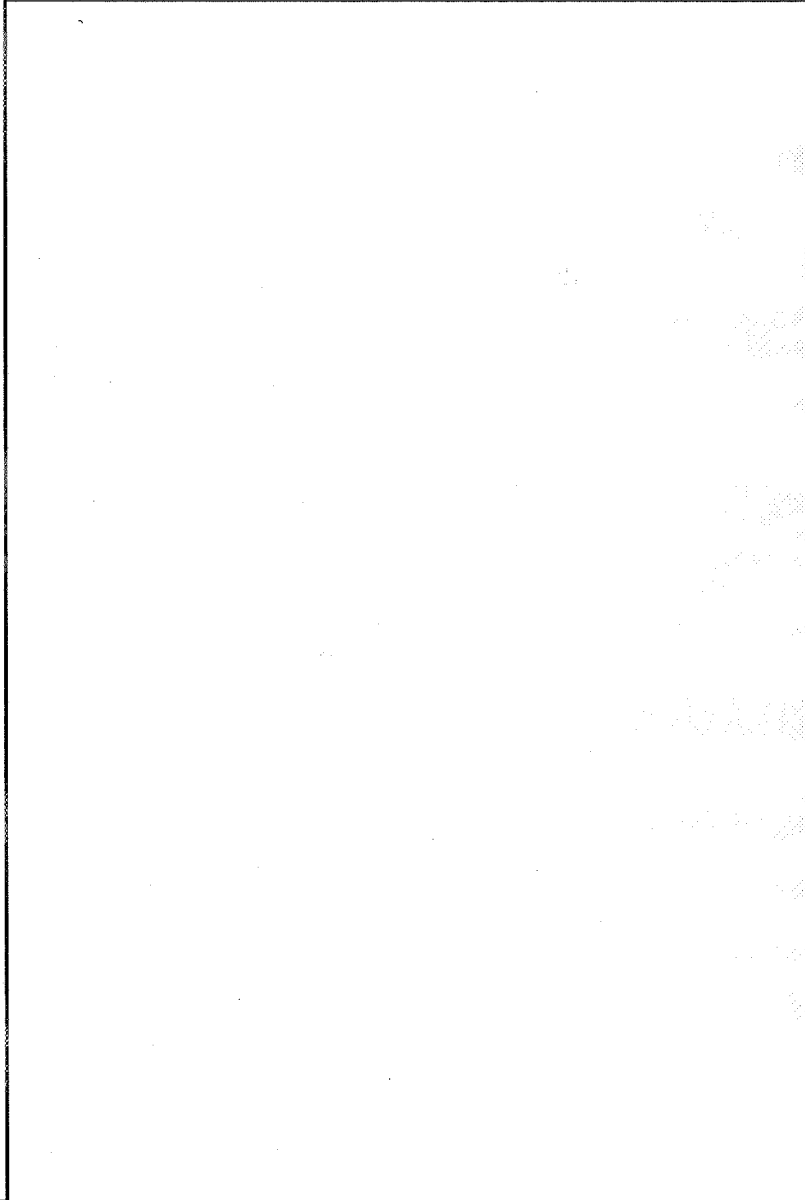
PROBLEM	STATIC POSITION ERROR LEVEL	POSSIBLE SOLUTION
Mixed Antenna Types	up to 8 mm horizontal up to 90 mm vertical	< 3 mm horizontal chamber/ insitu <10 mm to 30 mm anechoic chamber corrections <10 mm insitu GPS calibra- tion (Mader and others)
Like Antenna types with long baseline separation ("see" same satellite at dif- ferent elevation)	up to 0.015 ppm scale factor (Rothacher and others)	Insitu GPS calibration, bet- ter anechoic chamber cor- rections

Multipath and Scattering Effects

PROBLEM	ERROR LEVEL	POSSIBLE SOLUTIONS
Low antenna setup (<0.5 m)	up to 20 mm vertical	setup antenna <1.5 m or flush with the ground, use lower multipath antenna
Snow at site	up to 20 mm vertical	install higher or use lower multipath antenna; keep antenna clear of snow and ice
Protective Covers	2 mm to 15 mm vertical	eliminate cover or use thinner, more microwave transparent cover (best to date is 1/8" acrylic give 2 mm vertical error)
Pillar Signal Scattering	up to 10 mm vertical	microwave absorber under antenna; reduce cross-section of pillar; reduce metal plate under antenna; make pillar more microwave transparent (e.g. carbon fiber)

IGS

SINEX AND PILOT PROJECT



Page intentionally left blank

Compact RINEX Format and Tools

(beta-test version)

Yuki Hatanaka,
Geographical Survey Institute,
Kitasato-1, Tsukuba, Ibaraki, 305 Japan
e-mail: hata@geos.gsi-mc.go.jp

Abstract

A data format and software tools are developed for compression of RINEX II observation files based on two basic ideas: (1) eliminate the redundant information by recording only the variation between adjacent epochs for the epoch date time, event flag, satellite list, LLI, and signal strength, and (2) decreasing the digits of the phase, pseudorange, Doppler and receiver clock data by taking 3rd order differences of those data between adjacent epochs. The size of the files can be reduced 1/8 of the original RINEX files by combining with standard file compression commands.

Introduction

Accompanied with the recent rapid increase of GPS permanent sites in the world, the amount of the data has become huge. We can find the data of nearly 100 stations in the archive at the IGS data centers which exceed 50 Mb/day. This situation causes the long duration time and expensive cost of data transmission by using telephone line or satellite communication or Internet.

An effective GPS file compression format and software tools are developed. Since the RINEX format (Gurtner et al., 1989, 1990) is currently used widely to exchange the GPS data, the compression format is designed to keep complete compatibility with RINEX II observation file format (with a few trivial exception, see the section of Incompleteness). The format is ASCII type, so it can be compressed more by using standard file compression tools on UNIX or DOS. It can be used as an useful tool to reduce data traffic on internet or telephone line and to save the storage space.

Principles

Two basic ideas are used to reduce the size of RINEX file: (1) To eliminate redundant information by recording only the variation of the information. (2) To decrease the digits of the numerical data by taking triple difference of data arc.

(1) elimination of redundancy

Looking into RINEX II observation file format, we notice that some of the information is redundant. For example, the date of epochs, number of satellites, Loss of Lock Indicator (LLI), and signal strength are almost invariant from epoch to epoch. We can reduce the

redundant information if we record only the variation of those information. Comparing the characters of those data between adjacent epochs, the unchanged character is replaced with blank. If some character changes to blank, '&' is recorded.

(2) Reduction of digit of numerical data by taking 3rd order difference of the time series
 Fig.1 shows how the magnitude of the data is reduced by taking multiple order differences. The time series of the data such as phase and pseudorange have strong correlation between epochs. We can reduce the digit of the data by using this property. By taking differences between adjacent epochs, the digit of the data can be reduced and correlation becomes lower. Similar algorithm is used for the compression of seismogram data (Takano, 1990). By repeating the difference operation to the several times, we can reduce the digit more. Table I shows the average number of digit of the differenced data for each data type. (Signs and decimal points are not counted in this table). Empirically, the average number of digit is minimized when we take 3rd order difference which is close to random noise. The algorithm of processing is shown in Appendix I. This algorithm is applied for the data arcs of receiver clock offset and those of each data type of each satellites. This algorithm can be used in real time, since it doesn't need the data of future epoch to make the differences of current epoch. Therefore it's possible to implement this algorithm in the receiver firmware.

Table I The average number of digits of the differenced data
 (Ashtech Z-12, sampling interval : 30s)

order of difference	L1	L2	C1	P1	P2	D1	D2
0	10.7	10.6	11.0	11.0	11.0	6.7	6.6
1	8.0	7.9	7.5	7.5	7.5	4.5	4.4
2	5.9	5.9	5.1	5.1	5.1	2.8	2.7
3	4.3	4.2	3.6	3.6	3.6	2.9	2.8
4	4.3	4.2	3.7	3.6	3.6	3.2	3.1

Description of Compact RINEX format

In the RINEX format, 3 digits are used for fractional part phase, pseudorange and Doppler data (and 9 digit for receiver clock offset). In the Compact RINEX format, those data are multiplied by 1000 (receiver clock offset by 1000000000) to eliminate decimal points. The numerical data should be dealt as integer values to avoid round error in the calculation.

The Compact RINEX format consists of following lines.

- (1) The 1st and 2nd lines shows the Compact RINEX format version and name of software.
- (2) The header lines in the original RINEX file are follows without any modification.
 For every epoch:
- (3) (A32,nA3) : The line of EPOCH/SAT or EVENT FLAG (date, time, satellites, etc.), n is number of satellites and can be more than 12

tskb2010.95o, PRN25, L1 phase

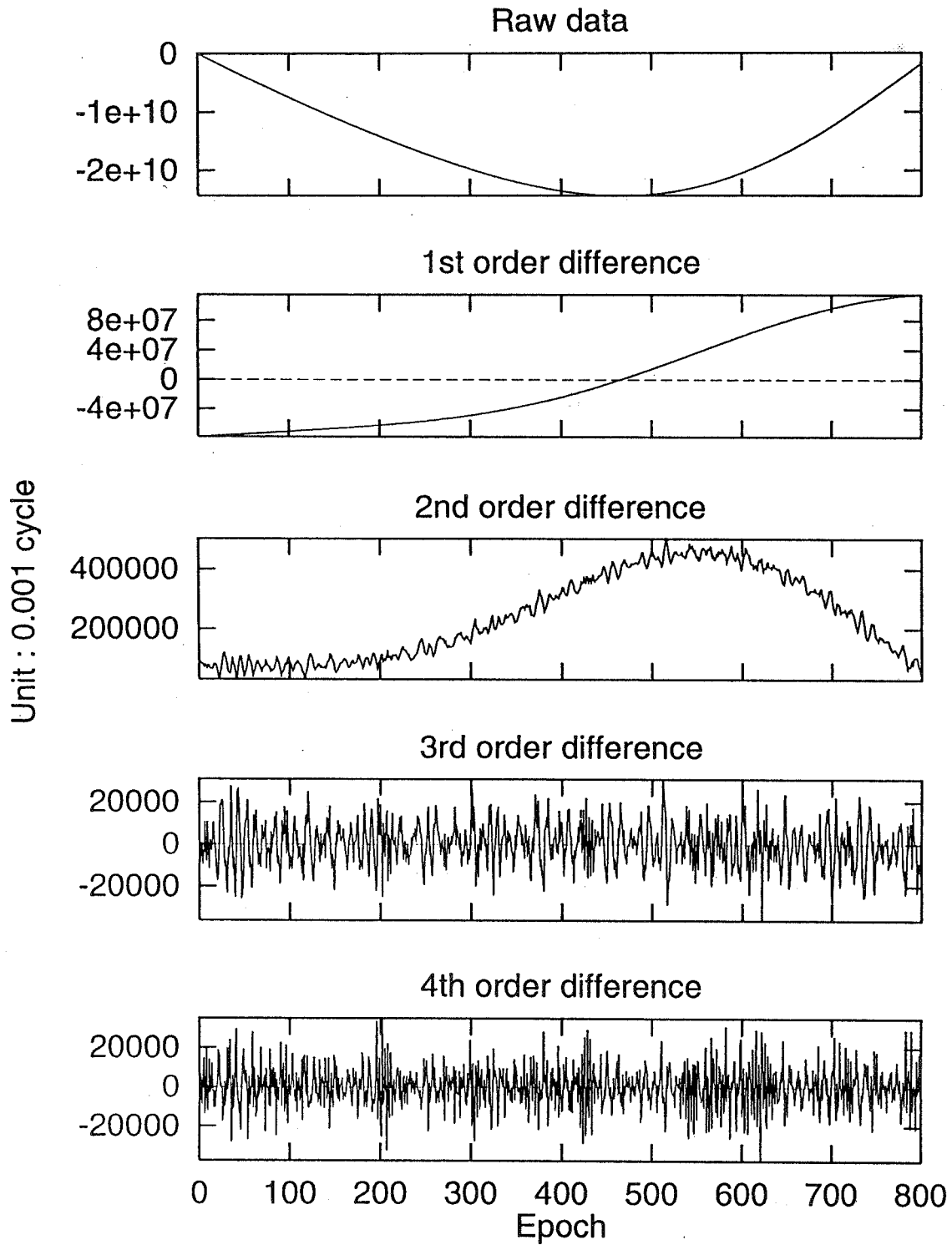


Fig.1 Raw and differenced data for L1 phase of PRN25 in tskb2010.95o.

- (4) (Iv) : differenced data of the receiver clock offset. 'v' means that the length of the integer format is variable and is 0 when the data field is blank in the original RINEX file. When a data arc is initialized, (Iv) is replaced with (I1,"&",Iv) in which 'I1' is for the order of differences for the arc.

For every satellite:

- (5) (n(Iv,x),n(A1,A1)) : differenced observations for all n data types (Iv) followed by change in LLI and signal strength (A1,A1) for all data types. When a data arc is initialized, (Iv,x) is replaced with (I1,"&",Iv,x) in which 'I1' is for the order of differences for the arc.

Lines (5) is repeated for every satellite, and lines (3)-(5) is repeated for every epoch. Only the characters changed from the corresponding field of previous epoch are recorded for (3) and LLI and signal strength in (5). If a character changed to a space, '&' is placed to record this 'disappearance'. Because of this procedure, most of characters are disappeared from those lines. Finally, the spaces at the end of each line of (3)-(5) have to be truncated.

The format allows the arbitral order of the differences (<10) for generality.

When the event flag (>1) is set, the event information lines (such as change of wave length factor) are followed by adding '#' at the first column.

- (6) ("#",A) : event information lines inserted.

The definition of the data arc is important for the differential operation. A data arc of receiver clock offset or each data type/satellite is initialized

- (a) at the first appearance of the corresponding data in the file (mandatory),
- (b) after the epoch of which the original data field is blank (mandatory),
- (c) when event flag (>1) is set (mandatory), and
- (d) at arbitrary epoch (optional).

The feature (d) makes the format more robust, but should not be abused since the compression performance will be worse. The feature (d) will work when the size of differenced data become big by a large cycle slip or reset of clock.

An example of Compact RINEX file and it's original RINEX II file are shown in Appendix II and III, respectively.

Usage of the reducing/recovering software

A source code written in C language (ANSI) for reducing/recovering the RINEX file are developed.

- rnx2crx.c : convert RINEX to Compact RINEX
- crx2rnx.c : recover RINEX file from Compact RINEX file

To see the usage of the command, type

RNX2CRX -h

(The executable file name RNX2CRX is assumed.)

Each software can be used as a command or filter.
[example 1]

```
RNX2CRX rinex.file
```

will create Compact RINEX file with the file name rinex.file_cr.

[example 2]

```
cat rinex.file | RNX2CRX
```

outputs the Compact RINEX data to standard output.

Numerical value of the data is dealt as integer in these software to avoid round error so that the recovered values are completely the same as the original one.

Compression Rate of the Format and Speed Performance of the Tools

By combining the reduction of RINEX file and use of UNIX compress command, the size of the file can be reduced to about 1/8 of the original RINEX file. This size is even much smaller than binary format provided by each receiver manufacture. The Table shows an example by using data of TurboRogue receiver.

Table II comparison of performance (in the case of being applied to tskb3000.95o)

	SIZE (Mb)	RATE (%)
① CONAN BINARY	0.387	20.9
② RINEX	1.848	100.0
③ ② + compress	0.597	32.3
④ Compact RINEX	0.546	29.5
⑤ ④ + compress	0.215	11.6

We can see that the Compact RINEX format realizes smaller file size than UNIX 'compress' command even without using binary coding. Moreover, the size of the compressed Compact RINEX is about 53 % of CONAN binary file (but without navigation message).

The processing time for above file is about 4 seconds by HP9000/735, 22 seconds by Sun SS2, and 10 seconds by Sun SS10. Those are just approximate values since the processing speed may depend on the machine type, OS, compiler, compiler option, etc.

Fig. 2 shows the performance of the software when being applied to all data of IGS archive on Jan 1, 1996 (89 station). The total size of the compressed Compact RINEX files is about 40 % of the current archive to which only the UNIX compress command is applied.

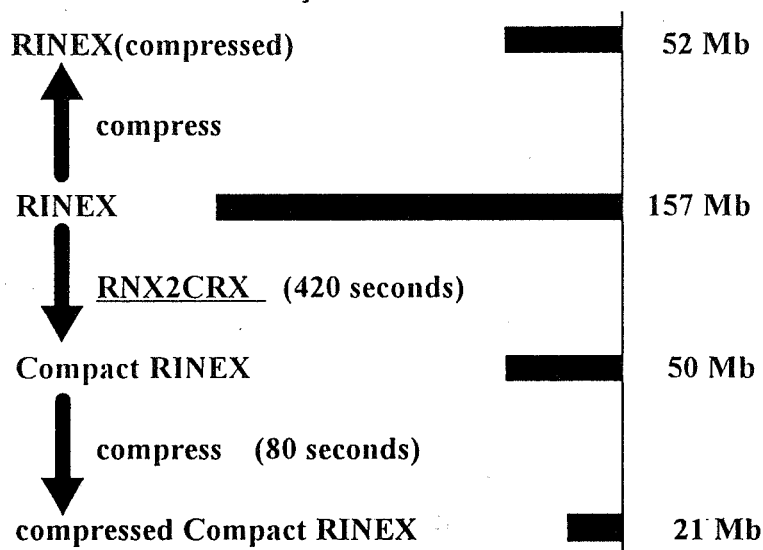


Fig. 2 Performance of the data compression tools when being applied to whole IGS data on Jan 1, 1996 (89 stations). The processing times are for the case of HP9000/735.

Incompleteness

The following information in the original RINEX files will be lost by transforming into Compact RINEX format.:

- (1) meaningless space at the end of each line
- (2) distinguish between numerical format: for example "-0.123" and "-.123".

Although the recovered RINEX file can be different from original one for them, the changes don't affect the numerical values at all.

Availability

The source code of current version of the software and sample data are available from <ftp://terras.gsi-mc.go.jp/pub/software/RNXCMP>

References

- Gurtner, W., G.Mader, D.MacArthur (1989), A Common Exchange Format for GPS Data, GPS Bulletin, Vol.2, No.3, 1-11.
- Gurtner, W., G.Mader (1990), Receiver Independent Exchange Format Version 2, GPS Bulletin, Vol.3, No.3, 1-8.
- Takano, K. (1990), Data Compression Method for Seismic Waves, Program and Abstracts, The Seismological Society of Japan, 1990 No.1, C32-04 (in Japanese).

Appendix I Algorithm for taking the n-th order differences

Let's consider an arc of the GPS data containing a RINEX II file (for example, the P1 pseudorange data of the satellite PRN01).

$$Y0[i], i=1,2,3,\dots,n$$

The order of the range data is more than tens of thousands of km in most cases, but the size of the differences between adjacent epochs is much smaller:

$$Y1[i] = Y0[i] - Y0[i-1], \quad i=2,3,4,\dots,n$$

The digits can be reduced more if we take difference one more time:

$$\begin{aligned} Y2[i] &= Y1[i] - Y1[i-1], \quad i=3,4,5,\dots,n, \\ Y3[i] &= Y2[i] - Y2[i-1], \quad i=4,5,6,\dots,n. \end{aligned}$$

Empirically, the minimum digits can be achieved when we take 3rd-order-difference for GPS data. We can define the new sequence of the differenced data as follows:

$$\begin{aligned} &Y0[1], Y1[2], Y2[3], \\ &Y3[i], i=4,5,6, \dots, n. \end{aligned}$$

The resulting data sequence preserve whole information in the original time series so that we can recover the original data arc $Y0[i]$ from them by following calculation:

$$\begin{aligned} Y2[i] &= Y2[i-1] + Y3[i], \quad i = 4,5,6, \dots, n, \\ Y1[i] &= Y1[i-1] + Y2[i], \quad i = 3,4,5, \dots, n, \\ Y0[i] &= Y0[i-1] + Y1[i], \quad i = 2,3,4, \dots, n. \end{aligned}$$

In general, the order of difference to take can be arbitrary, so the algorithm to take m-th order differences are as follows;

$$Y_j[i] = Y_{j-1}[i] - Y_{j-1}[i-1], \quad i=j+1, \dots, n; j=1, \dots, m.$$

We can save the following data sequence which preserve whole information in the original time series.

$$\begin{aligned} &Y_{j-1}[j], j=1, \dots, m, \\ &Y_m[i], i=m+1, \dots, n. \end{aligned}$$

The original data arc $Y0[i]$ is recovered from them by following algorithm;

$$Y_{j-1}[i] = Y_j[i] + Y_{j-1}[i-1], \quad i=j+1, \dots, n; j=m, \dots, 1.$$

Appendix 2 An example of Compact RINEX file

128

```

REDUCED RINEX VER. 0.3beta
PGM TO REDUCE RNX2CRX Ver.c.1.4beta
2 OBSERVATION DATA G (GPS) RINEX VERSION / TYPE
RGRINEXO V2.4.2 VM EMR 22-NOV-95 21:00 PGM / RUN BY / DATE
BIT 2 OF LLI (+4) FLAGS DATA COLLECTED UNDER "AS" CONDITION COMMENT
.000000000000 HARDWARE CALIBRATION (S) COMMENT
.000000218620 CLOCK OFFSET (S) COMMENT
STATION INFORMATION UPDATED 1995 10 7 COMMENT
ANTENNA: DELTA H (HEIGHT) BELOW REFERS TO THE BOTTOM OF COMMENT
ANTENNA - ADD .110 M FOR L1 AND .128 M FOR L2 PHASE CENT COMMENT
algo CACS-ACP 883160 ALGONQUIN PARK, ONTARIO, CANADA COMMENT
40104M002 MARKER NAME
AUTO-DOWNLOAD NATURAL RESOURCES CA MARKER NUMBER
226 ROGUE SNR-8000 TURBO 3.2.32.1 OBSERVER / AGENCY
173 DORNE MARGOLIN T ANT # / TYPE
918129.6000 -4346071.2000 4561977.8000 APPROX POSITION XYZ
.1000 .0000 .0000 ANTENNA: DELTA H/E/N
1 1 WAVELENGTH FACT L1/2
5 C1 L1 L2 P2 P1 # / TYPES OF OBSERV
30 INTERVAL
1995 11 22 0 0 .000000 TIME OF FIRST OBS
95 11 22 0 0 .0000000 0 6 25 18 14 28 29 22 END OF HEADER

3&23483304611 3&-6922742757 3&-5394331641 3&23483302945 7454
3&21877048460 3&-14051925969 3&-10949548024 3&21877047035 9454
3&24215557627 3&-2595282746 3&-2022292768 3&24215557145 6444
3&-12445464816 3&-9697760203 3&22375464751 3&22375466230 7 8
3&20706081053 3&-21439520675 3&-16706111050 3&20706078869 9464
3&20455520061 3&-20561689014 3&-16022079901 3&20455518464 9464
30

16809664 88341417 68837416 16810379
-12769309 -67104297 -52289052 -12769483
18281939 96071151 74860629 18280910 3
-88677557 -69099356 -16874458 -16874808 9
-1676041 -8807682 -6863128 -1676137
8639385 45399387 35376147 8639385
1 &&

30378 153253 119451 29116
88777 469294 365683 88661
21953 115916 90288 25103
337318 262869 63891 64069
110915 583410 454608 111269
74594 393548 306664 74789
30 29 14 8

-2208 -9585 -7483 -2082
-2618 -17907 -13956 -1568
4241 20994 16352 3502
305 2543 2040 -5570 4
2700 2050 612 873
-1057 -7836 -6109 -1276
2 && 7 29 18 31 22

-1621 -4314 -3433 961
-703 -3011 -2343 -100
-3063 -12857 -10014 -4335
-540 -8018 -6261 3147 3
2789 2169 1165 197
3&24544245672 3&-601 3&-129 3&24544248105 16534
497 3725 2898 240
30 18 5 29

-310 -6510 -5071 -296
-4138 -12393 -9592 -1599
-988 -4386 -3415 -1117
-6019 -22017 -17197 -4838
    
```

```

2892 2302 -444 599
-22541669 -118452695 -92300728 -22543843 & 4
-992 -5637 -4384 -696
3 &&

-3597 -17040 -13286 -3637
2730 7068 5483 -5469
-2922 -16283 -12687 -3235
-1326 -18138 -14113 -7859
2795 2182 1306 523
1311 6104
-1124 -5587 -4360 -875
30

3553 21557 16800 3592
3164 12022 9396 7115 6
-5881 -31603 -24634 -5814
-1525 1399 1112 3413
2614 2057 423 456
2685 9455
881 3489 2720 475
4 &&

3826 18701 14573 5194
1510 -1201 -954 2672
-3615 -17138 -13342 -3251
1018 -3153 -2458 3317
2679 2034 247 907
-924 -5243
543 2926 2281 843
30

560 4248 3323 -815
-3190 906 694 -2738
3570 15668 12201 3476
1306 13907 10819 -3916
2897 2256 770 91
-2032 7193
-1652 -6049 -4713 -2303
5 &&

4046 18101 14094 4900
3764 17402 13573 -1470
1571 12992 10122 1343
5595 22322 17448 8248
2867 2261 454 813
5807 13903
159 -2463 -1918 809
30

1982 9993 7782 410
-425 -860 -689 6227
3749 16838 13125 3933
-525 7133 5481 384
2798 2170 450 268
-2536 -11633 3&-645879073 3&24386514671 434
-1582 -6495 -5061 -1550
6 &&

-949 -856 -666 708
2447 3206 2532 291
3021 16081 12526 2653
-1196 -6095 -4743 -1504
2479 1917 536 860
-443 6683 -92201717 -22516369
53 -329 -261 -181
    
```

Appendix 3 The original RINEX file for the Compact RINEX file shown in Appendix 2

```

2 OBSERVATION DATA G (GPS) RINEX VERSION / TYPE
RGRINEXO V2.4.2 VM EMR 22-NOV-95 21:00 PGM / RUN BY / DATE
BIT 2 OF LLI (+4) FLAGS DATA COLLECTED UNDER "AS" CONDITION COMMENT
.000000000000 HARDWARE CALIBRATION (S) COMMENT
.000000218620 CLOCK OFFSET (S) COMMENT
STATION INFORMATION UPDATED 1995 10 7 COMMENT
ANTENNA: DELTA H (HEIGHT) BELOW REFERS TO THE BOTTOM OF COMMENT
ANTENNA - ADD .110 M FOR L1 AND .128 M FOR L2 PHASE CENT COMMENT
also CACS-ACP 883160 ALGONQUIN PARK, ONTARIO, CANADA MARKER NAME
40104M002 MARKER NUMBER
AUTO-DOWNLOAD NATURAL RESOURCES CA OBSERVER / AGENCY
226 ROGUE SNR-8000 TURBO 3.2.32.1 REC # / TYPE / VERS
173 DORNE MARGOLIN T ANT # / TYPE
APPROX POSITION XYZ
918129.6000 -4346071.2000 4561977.8000 ANTENNA: DELTA H/E/N
.1000 .0000 .0000 WAVELENGTH FACT L1/2
1 1 # / TYPES OF OBSERV
5 C1 L1 L2 P2 P1 INTERVAL
30 TIME OF FIRST OBS
1995 11 22 0 0 .000000 END OF HEADER

95 11 22 0 0 .000000 0 6 25 18 14 28 29 22
23483304.611 -6922742.757 7 -5394331.64145 23483302.9454
21877048.460 -14051925.969 9 -10949548.02445 21877047.0354
24215557.627 -2595282.746 6 -2022292.76844 24215557.1454
-12445464.816 7 -9697760.203 8 22375464.751 22375466.230
20706081.053 -21439520.675 9 -16706111.05046 20706078.8694
20455520.061 -20561689.014 9 -16022079.90146 20455518.4644
95 11 22 0 0 30.0000000 0 6 25 18 14 28 29 22
23500114.275 -6834401.340 7 -5325494.22545 23500113.3244
21864279.151 -14119030.266 9 -11001837.07645 21864277.5524
24233839.566 -2499211.595 6 -1947432.13943 24233838.0554
-12534142.373 7 -9766859.559 9 22358590.293 22358591.422
20704405.012 -21448328.357 9 -16712974.17846 20704402.7324
20464159.446 -20516289.627 9 -15986703.75446 20464157.8494
95 11 22 0 1 .0000000 0 .6 25 18 14 28 29 22
23516954.317 -6745906.670 7 -5256537.35845 23516952.8194
21851598.619 -14185665.269 9 -11053760.44545 21851596.7304
24252143.458 -2403024.528 6 -1872481.22243 24252144.0684
-12622482.612 7 -9835696.046 9 22341779.726 22341780.683
20702839.886 -21456552.629 9 -16719382.69846 20702837.8644
20472873.425 -20470496.692 9 -15951020.94346 20472872.0234
95 11 22 0 1 30.0000000 0 6 25 18 29 14 28 22
23533822.529 -6657268.332 7 -5187468.52345 23533819.3484
21839004.246 -14251848.885 9 -11105332.08745 21839003.0014
20701389.916 -21464172.497 9 -16725320.25846 20701387.7674
24270469.608 -2306719.002 6 -1797437.97744 24270469.6144
-12710482.833 7 -9904267.614 9 22325033.662 22325034.886
20481660.941 -20424318.045 9 -15915037.57746 20481659.7104
95 11 22 0 2 .0000000 0 7 25 29 18 14 28 31 22
23550717.290 -6568490.640 7 -5118291.15345 23550713.8724
20700054.399 -21471190.972 9 -16730789.20146 20700052.3414
21826492.969 -14317593.971 9 -11156562.01645 21826492.0304
24288817.476 -2210303.035 6 -1722308.66543 24288817.8404
-12798140.247 7 -9972572.094 9 22308353.266 22308354.228
24544245.672 -.60116 -.12953 24544248.1054
20490522.491 -20377749.961 9 -15878750.75846 20490521.1504
95 11 22 0 2 30.0000000 0 7 18 25 29 14 28 31 22
21814064.478 -14382907.037 9 -11207455.30345 21814063.5214
23567634.462 -6479585.987 7 -5049014.84045 23567634.7924
20698832.347 -21477612.440 9 -16735792.94246 20698830.4694
24307181.043 -2113798.644 6 -1647110.48343 24307183.9084
-12885451.962 7 -10040607.184 9 22291738.094 22291739.308
24521704.003 -118453.296 6 -92300.85743 24521704.2624
20499457.083 -20330798.077 9 -15842164.87046 20499455.6474
95 11 22 0 3 .0000000 0 7 18 25 29 14 28 31 22
21801715.176 -14447805.123 9 -11258025.23445 21801713.8374
23584576.775 -6390547.305 7 -4979634.10145 23584576.6394
20697720.838 -21483453.184 9 -16740344.16846 20697718.9164
24325558.983 -2017223.967 6 -1571857.54443 24325559.9594

```

```

-12972415.183 7 -10108370.702 9 22275189.452 22275190.649
24499163.645 -236899.897 6
20508463.593 -20283467.980 9 -15805284.27346 20508462.3264
95 11 22 0 3 30.0000000 0 7 18 25 29 14 28 31 22
21789448.616 -14512266.672 9 -11308255.00945 21789446.5704
23601547.393 -6301362.572 6 -4910139.54045 23601546.5284
20696713.991 -21488744.807 9 -16744467.51346 20696711.8684
24343949.771 -1920577.605 6 -1496548.73643 24343949.4064
-13059027.296 7 -10175860.591 9 22258707.763 22258708.707
24476627.283 -355330.919 6
20517542.902 -20235756.181 9 -15768106.24746 20517541.6624
95 11 22 0 4 .0000000 0 7 18 25 29 14 28 31 22
21777268.624 -14576272.983 9 -11358130.05545 21777266.9144
23618547.826 -6212032.989 6 -4840532.11145 23618547.1314
20695808.191 -21493504.447 9 -16748176.31946 20695806.0744
24362354.425 -1823862.711 6 -1421186.51743 24362355.5664
-13145285.622 7 -10243074.817 9 22242293.274 22242294.389
24454093.993 -473751.635 6
20526695.553 -20187659.754 9 -15730628.51146 20526694.4984
95 11 22 0 4 30.0000000 0 7 18 25 29 14 28 31 22
21765175.760 -14639819.808 9 -11407647.04945 21765174.0544
23635574.884 -6122557.650 6 -4770811.12045 23635575.7104
20695007.008 -21497716.436 9 -16751458.38546 20695005.0104
24380774.251 -1727065.378 6 -1345760.06843 24380774.5234
-13231187.264 7 -10310011.124 9 22225946.755 22225947.786
24431561.743 -592154.842 6
20535919.894 -20139184.748 9 -15692855.77846 20535918.5314
95 11 22 0 5 .0000000 0 7 18 25 29 14 28 31 22
21753174.070 -14702889.046 9 -11456791.89745 21753172.8904
23652632.331 -6032919.153 6 -4700962.99445 23652630.7954
20694312.013 -21501367.782 9 -16754033.58946 20694310.0194
24399214.844 -1630163.284 6 -1270251.94143 24399214.5254
-13316729.355 7 -10376667.251 9 22209668.660 22209669.711
24409036.340 -710526.637 6
20545216.084 -20090333.626 9 -15654789.96646 20545214.5704
95 11 22 0 5 30.0000000 0 7 18 25 29 14 28 31 22
21741265.536 -14765470.704 9 -11505556.81745 21741263.8324
23669719.742 -5943118.358 6 -4630988.42245 23669718.6134
20693726.955 -21504441.647 9 -16756698.80646 20693725.0344
24417675.679 -1533149.296 6 -1194656.65543 24417675.9564
-13401909.097 7 -10443041.028 9 22193459.439 22193460.432
24386515.248 -828878.653 6 -645879.07343 24386514.6714
20554582.541 -20041112.883 9 -15616436.13646 20554581.0654
95 11 22 0 6 .0000000 0 7 18 25 29 14 28 31 22
21729449.209 -14827565.638 9 -11553942.47545 21729447.5884
23686839.564 -5853152.059 6 -4560884.87245 23686839.4554
20693254.855 -21506921.950 9 -16758631.51046 20693252.7084
24436155.560 -1436029.509 6 -1118978.95343 24436157.3124
-13486724.011 7 -10509130.538 9 22177319.628 22177320.809
24363998.024 -947204.207 6 -738080.79043 24363998.3024
20564019.318 -19991522.848 9 -15577794.54946 20564017.8354

```


Page intentionally left blank

POLYHEDRON ASSEMBLY AT NEWCASTLE METHOD AND INITIAL RESULTS

Philip Davies
*Department of Surveying,
University of Newcastle-upon-Tyne.*

ABSTRACT

A Global Network Associate Analysis Centre of the IGS was established at the University of Newcastle in 1995 as part of the IGS Pilot Project for Densification of the ITRF. With this project now eight months old, this paper describes in detail the analysis method used at Newcastle to create a weekly G-Sinex solution, the Global component of the integrated IGS Polyhedron. A method of attaching Regional networks to the Global component is also proposed. Some statistics summarising the combined network are presented, and the coordinate repeatability in a recent eleven-week series is assessed and compared to that of the individual Analysis Centre networks. It is found that the median station coordinate standard deviation in the series of free combined networks is 3.6mm in height and under 3.2mm horizontally, exceeding any AC network on this statistic. This relies on imposing the IGS requirement for a Global station: that it is estimated by at least three Analysis Centres.

INTRODUCTION

In the Pilot Project for the construction of the densified IGS Polyhedron by distributed processing, the Global Network Associate Analysis Centres (GNAACs, previously known as a Type Two AACs) have the weekly task of assembling the Polyhedron from its component coordinate solutions (Blewitt et al [1993b], Blewitt et al [1995]). This is undertaken in two stages:

- The Analysis Centre weekly solutions (from now on called A-networks) are obtained from A-Sinex files, compared and combined to form the GNAAC Global component (from now on called the G-network) which is made available as a weekly G-Sinex file.
- Weekly Regional solutions (R-networks) are attached to the Global component (without further adjustment of the G-network). The resulting set of consistent Polyhedron components (the P-network) will be made available in P-Sinex files.

The second item relies on the IGS weekly orbit combination (Beutler et al [1993], Goad [1993], Kouba [1995]). The stations which go into the combined G-network should be those used by the ACs for rigorous orbit and earth orientation estimation, which hence define the primary frame of the Polyhedron and lead to the IGS Orbit. This sparse station set should be deployed as uniformly as possible over the globe (as discussed by Zumberge et al [1995]).

Each A-Sinex currently includes 30-70 stations, with about 20 being estimated by all ACs, and about 60 positioned by at least three ACs. The estimation redundancy of the A-network stations defines the reliability of the G-network (i.e. the ability of a GNAAC to detect outliers and discrepancies in A-networks). Figure 1 below shows station redundancies in the A-networks of a typical week. The IGS definition of a Global station requires that it be positioned by at least 3 ACs, so the two dozen

stations in the first two columns of the chart do not qualify, only appearing in one or two A-networks each week.

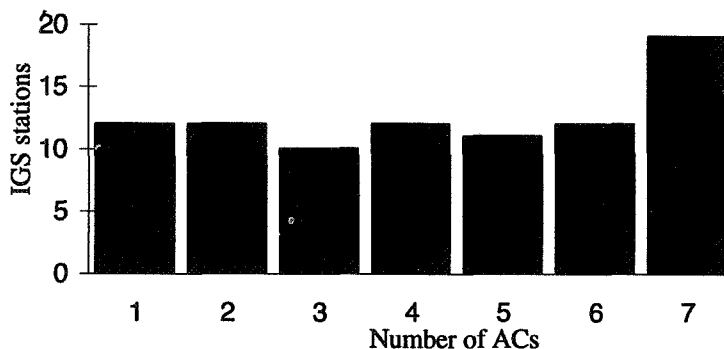


Figure 1 - A-network stations grouped by number of ACs estimating each.

In this paper I focus on the first GNAAC task, G-network assembly. The methodology employed in this analysis is given in section 2, and some results of this are summarised in section 3, where a short time-series of G-networks is presented. Section 4 briefly discusses the second GNAAC task, suggesting a procedure for the attachment of Regional networks.

2 G-NETWORK ANALYSIS

2.1 Parameter matching to a Sinex catalogue

Each Analysis Centre delivers a weekly A-Sinex file. The first step is to extract the set of A-networks from A-Sinex files with a common parameter numbering. Because Sinex is a complex format, this is a rather involved task. Each GPS site has a unique four-character identifier; at each site there may be multiple monuments which within a particular Sinex file are identified by letters A, B, etc. For monuments listed in the ITRF, the unique DOMES code is given. For each monument, multiple station estimates may be given in a Sinex file - this occurs when the monument is estimated at distinct epochs, for instance, or when more than one antenna is operating at the monument. For each station, one or more records are given in each of a set of station attribute tables, describing the antennae, receivers and local tie vectors used during the period of observation. Each of these records includes an epoch range. Sinex format is detailed by Kouba [1996].

A catalogue Sinex file is maintained, giving the same information types for all the stations which might occur in the incoming A-Sinex files. In a series of automatic matching stages, each A-Sinex station is assigned the parameter numbers of a catalogue station. Any discrepancies between the station information in the A-Sinex and that in the catalogue are recorded, and non-unique matches are reported on. If unknown or ambiguous stations are found, the catalogue is updated. By setting the epoch ranges, etc., of the catalogue stations, and flags governing the matching criteria, the analyst can process Sinex files in various analysis contexts.

The result of this for each A-network is:

- an estimate parameter vector y (of coordinate triplets) with a full covariance matrix Σ_y ,
- an a priori parameter vector z with covariance matrix Σ_z ,
- parameter reference lists for both vectors to the catalogue Sinex.

2.2 Constraint removal and datum control

Global GPS analysis as carried out by IGS Analysis Centres observes all the datum elements of a geocentric coordinate frame except network orientation (Blewitt et al [1993a]). Some *a priori* constraint is necessary, at least to establish this orientation and hence write a particular coordinate solution of the normal equations. In Sinex, constraints are represented as an *a priori* coordinate vector and covariance matrix. Minimal (orthogonal to observations) constraints of multiple stations therefore cannot be represented, because the constraint equations must span the coordinate space for a corresponding covariance matrix to exist. This means that the estimated A-networks are always distorted by non-minimal constraints, though perhaps at a negligible level.

We should however be able to recover the normal equations matrix N of an A-network by

$$N = \Sigma_y^{-1} - \underset{z-y}{A} \Sigma_z^{-1} \underset{z-y}{A'} \quad (1)$$

where $\underset{z-y}{A}$ is the left-multiplying binary incidence matrix from the parameter list of vector z to that of vector y (in this case the former is a subset of the latter). [Note: A binary incidence matrix (Searle [1971]) re-orders a parameter vector or matrix inserting zeroes where a parameter in the output list does not occur in the input list: $\underset{z-y}{A} = \underset{y-z}{A'}$. This notation and meaning of $\underset{z-y}{A}$ are used for convenience throughout.]

For a Global GPS free-network, the singular N should have a rank deficiency of three, corresponding to the three orientation unknowns of the coordinate datum, and we require a suitable inversion of N to compute the ‘free’ (undistorted) coordinates. To complicate the situation, A-networks have various *unstated* constraints, which make the true N unknown, and in some cases cause the apparent N to be quite regular. This is not considered a problem because ACs are responsible for ensuring that unstated constraints are minimal or cause only negligible distortion of estimable quantities.

To invert N I use the ‘loose non-minimal constraints’ approach, removing a chosen fraction α of the stated constraints so as to increase the a priori standard deviations of the constrained coordinates to a level where only negligible network distortion is caused. For some A-networks, the stated constraints are insignificant and $\alpha = 0$, whereas for others with significant stated constraints the unstated constraints allow $\alpha = 1$. Also, to improve the numerical stability of some A-networks I add a normal equation component due to three pseudo-observations of net orientation (about the X, Y, and Z axes) with chosen loose standard deviations. These new constraints are orthogonal to the A-network estimable quantities, and loose enough not to distort the combined network. Let the loosely-constrained parameters be x with covariance matrix Σ_x , then

$$\Sigma_x = (\Sigma_y^{-1} - \alpha \underset{z-y}{A} \Sigma_z^{-1} \underset{z-y}{A'} + C' \Sigma_w^{-1} C)^{-1} \quad (2)$$

$$x = \underset{z-y}{A} z + \Sigma_x \Sigma_y^{-1} (y - \underset{z-y}{A} z) \quad (3)$$

where C is the linearised mapping matrix of the three orientation pseudo-observations to the coordinate triplets of y (see e.g. Blaha[1982]), and Σ_w is the 3x3 diagonal covariance matrix of these pseudo-observations, the diagonal elements being σ_{RX}^2 , σ_{RY}^2 and σ_{RZ}^2 . Note that if all A-network constraints were stated, $\alpha = 1$ with finite σ_{RX}^2 , σ_{RY}^2 and σ_{RZ}^2 would correspond to an

'inner constraints' generalised inversion of the normals. The constraints on all the 'loose' A-networks are chosen so estimable quantities differ negligibly from the truly 'free' network case.

2.3 Combination of loose A-networks

The combination of the loose A-networks is a 'sparse matrix' application, in that the overall covariance matrix of the observations (the A-network coordinates) is a block diagonal - no correlation is modelled between the A-networks, making the combination feasible. A normal equations 'block' is formed for each A-network, which in a separate software module are added and solved. The 'observations' and 'parameters' are the same quantities so the first-order design matrices of this Least Squares operation are of the binary incidence type - for this reason the process can also be regarded as a weighted ANOVA.

Firstly, a combination parameter list is formed automatically from the catalogue parameter lists of each A-network, allowing exclusion of A-network parameters flagged as outliers in a previous iteration (see section 2.4 below) or excluded due to discrepancies with the catalogue, and the exclusion of parameters unique to single blocks if required. Let the combined parameters be \mathbf{p} with covariance matrix Σ_p , and the excluded parameters for normal equation block i be \mathbf{u}_i (total n blocks). The subscript notation for the binary incidence matrices \mathbf{A} is used as before:

$$\mathbf{P}_i = \mathbf{A}_{x_i-p} \Sigma_{x_i}^{-1} \mathbf{A}'_{x_i-u_i} (\mathbf{A}_{x_i-u_i} \Sigma_{x_i}^{-1} \mathbf{A}'_{x_i-u_i})^{-1} \mathbf{A}_{x_i-u_i} \Sigma_{x_i}^{-1} \quad (4)$$

$$\mathbf{N}_i = \mathbf{A}_{x_i-p} \Sigma_{x_i}^{-1} \mathbf{A}'_{x_i-p} - \mathbf{P}_i \mathbf{A}'_{x_i-p} \quad (5)$$

$$\mathbf{d}_i = \mathbf{A}_{x_i-p} \Sigma_{x_i}^{-1} \mathbf{x}_i - \mathbf{P}_i \mathbf{x}_i \quad (6)$$

$$\Sigma_p = \left(\sum_{i=1}^n \sigma_i^{-2} \mathbf{N}_i \right)^{-1} \quad (7)$$

$$\mathbf{p} = \Sigma_p \sum_{i=1}^n \sigma_i^{-2} \mathbf{d}_i \quad (8)$$

where σ_i^2 is a variance component (scaling factor) applied to each block (see 2.4 below). The values of $\Sigma_{x_i}^{-1}$ are carried over from eqn. 2, and the bracketed inversion in eqn. 4 is relatively small. Also, note that the \mathbf{A} matrices are notational only - fast reparameterisation routines are used in the software. In fact, the inversion of the normal equations of common parameters (eqn. 7) is the only major computation here. This can be rapidly carried out by Cholesky decomposition ($\mathbf{N} = \mathbf{L}\mathbf{L}'$, \mathbf{L} triangular) - I also use the Singular Value decomposition ($\mathbf{N} = \mathbf{U}\mathbf{D}\mathbf{V}'$, \mathbf{D} diagonal, \mathbf{U} and \mathbf{V} orthogonal) which provides the matrix eigenvalues indicating the regularity of the inversion.

2.4 Residual Analysis

The direct LS coordinate residuals for observation block i given by $\mathbf{v}_i = \mathbf{A}_{p-v_i} \mathbf{p} - \mathbf{A}_{x_i-v_i} \mathbf{x}_i$ (where the parameter list of \mathbf{v}_i is the intersection of those of \mathbf{p} and \mathbf{x}_i) are of little interest, because they are biased by the datum differences of the A-networks. A-network orientation is arbitrary, and the geocentric origin is observed inaccurately (compared to the precision of inter-station baselines). Therefore it is appropriate to remove a seven-parameter similarity transformation between each A-network and the combined G-network, giving post-fit residuals which are independent of the A-network datum. A question arises over appropriate weight matrices for this estimation when the

networks have full covariance matrices. The dispersion of pre-fit residuals (the ‘observations’ of the estimation) is described by the biased covariance matrix

$$\Sigma_{v_i} = \mathbf{A} \Sigma_{x_i} \mathbf{A}' - \mathbf{A} \Sigma_p \mathbf{A}' \quad (9)$$

This matrix is dependent on the A-network loose constraints, which I control by the parameters of eqn. 2. I take the reciprocals of the diagonal elements of eqn. 9 to form a diagonal weight matrix, then iteratively compute the similarity parameters s_i and post-fit residuals o_i . This weighting method and alternatives are still being tested. Blewitt et al [1992] have in a related context explicitly projected the covariance matrix orthogonal to the space defined by the linearised mapping matrix of the 7-parameter transformation, hence obtaining an estimable basis. This is equivalent to fixing all 7 similarity transformation parameters to the estimate coordinates.

The full Σ_{v_i} is used to compute the covariance matrix of o_i , which is required for outlier detection and other statistics. If the linearised mapping matrix of the transformation at convergence of the estimation is \mathbf{B}_i then

$$\Sigma_{o_i} = \Sigma_{v_i} - \mathbf{B}_i (\mathbf{B}' \Sigma_{v_i}^{-1} \mathbf{B})^{-1} \mathbf{B}' \quad (10)$$

The post-fit residuals of each A-network are used for two important residual analyses: variance component estimation (VCE) and outlier detection. These two tasks are mutually dependent, since each relies on the correct fulfilment of the other. A circular problem is ameliorated by assuming that the variance component applied to each Analysis Centre has continuity between weekly epochs, whereas outlying observations do not. A careful balance is nonetheless required between these two objectives in the testing of residuals, which to some extent must involve *ad hoc* modelling choices.

The variance component estimation method I use is a slow-converging variant of Helmert’s iterative method (Grafarend et al [1979], Sahin et al [1992]) in the Helmert blocking setting. In this method one discards the off-diagonal elements of the Helmert matrix (Ziqiang [1989]), making the component for each block dependent on the partitioned residuals for that block only. At convergence, this is equivalent to the full Helmert method and to iterated MINQE and Maximum Likelihood derivations. The scale factor update ρ_i^2 for each block i is given by

$$\mathbf{W}_i = \sigma_i^{-2} \mathbf{A} \mathbf{N}_i \mathbf{A}' \quad (11)$$

$$\rho_i^2 = \frac{\mathbf{o}_i' \mathbf{W}_i \mathbf{o}_i}{m - \text{tr}(\mathbf{W}_i \mathbf{A} \Sigma_p \mathbf{A}')} \quad (12)$$

where \mathbf{W}_i is the weight matrix of the i th reduced observation block and m is the number of estimated parameters. The ‘slow convergence’ of this expression has not caused problems, even when the initial σ_i ’s are far from the final values. Because these factors are highly sensitive to outliers, the A-network scale factors are in practice held fixed from week to week so iterating the G-network formulae (eqns. 4-8) to convergence of eqn. 12 is not a regular requirement - executing eqn. 12 once is sufficient to indicate weekly deviations in variance components.

Outlier detection is carried out using the full-matrix form of Baarda’s w test (Cross [1994]) on the coordinate triplet of each station observation in turn. Before computing this, each A-network block

is scaled by the overall unit variance (chi square per degree of freedom) of the G-network estimation. The Baarda statistic for the j th station of block i is:

$$w_{ij} = \frac{\mathbf{a}'_j \mathbf{W}_i \mathbf{o}_i}{\mathbf{a}'_j \mathbf{W}_i \Sigma_{o_i} \mathbf{W}_i \mathbf{a}_j} \quad (13)$$

where \mathbf{a}_j is a binary incidence vector, the elements of which are unity that correspond to the three parameters of the station j under test, otherwise zero.

In the absence of outliers and if variance scaling is correct, the w_{ij} should be normally distributed with zero mean and unit standard deviation. We can assess the normality of the w_{ij} using skewness and kurtosis values or the Kolmogorov-Smirnoff goodness-of-fit test. For the series presented in the next section, I remove observations whose w_{ij} lie in the outermost 1% of the normal distribution (i.e. 99% confidence level) to improve the 'robustness' of the estimation. Due to the multiple outlier 'masking' effect and the uncertainty in variance scaling increasing the possibility of type I and type II errors, this procedure is by no means perfect. Observations flagged as outliers are excluded from an iteration of eqns (4-8) and the residual analysis steps are repeated.

The Weighted Root-Mean-Square (WRMS) summary statistic is calculated for each A-network with respect to the G-network, and also between each pair of A-networks, and between each A-network and ITRF coordinates. The WRMS values are included as a triangular table in the GNAAC analysis report (see Table 2 below). Because it takes account of parameter weighting, this can be a more useful and stable statistic than a simple RMS when a range of station variances are present in a network.

2.5 GNAAC Products

After residual analysis on the loose solution I constrain the G-network to the conventional Core network of 13 stations in ITRF94. It is this constrained solution and its constraints which are written to the G-Sinex file (with station information provided by the Catalogue Sinex) and delivered to an IGS Global Data Centre (CDDIS). The loose solution can be regained from the G-Sinex by removing constraints (eqns. 2, 3).

A GNAAC analysis report is also produced each week, deposited at CDDIS and distributed to the IGSREPORT email list. This gives information on A-Sinex discrepancies and residual summaries comparing the A-networks, combined G-network and ITRF Core.

3 - A G-NETWORK SERIES

The procedure is now illustrated with some statistics from an eleven-week series of G-networks (GPS Weeks 0840-0850, 11th February - 27th April 1996). Sections 3.3-3.5 provide a simple indication of G-network performance.

The G-networks used here differ from those submitted weekly to CDDIS in that only stations positioned by at least three ACs were included. This is the IGS stated requirement for Global stations (IGS Terms of Reference) so it was applied in this study. The weekly G-network I submit in

the Pilot Program currently includes all the A-network stations, regardless of which column of Figure 1 they belong to. In the GPS weeks used here, 55-60 stations each week met the 3-AC requirement. The six Analysis Centres producing weekly A-networks were included - COD, EMR, ESA, GFZ, JPL and SIO. I do not include the daily Sinex from NGS.

A constant variance component was used for each Analysis Centre to obtain this series. To initialise these components the iterative VCE formula (eqn. 12) was applied to the loosely-constrained A-networks to generate a variance scale factor for each AC in each of the weeks analysed, after removal of the most extreme outliers. The constant variance component for each AC was set to the average of the Centre's components over the series. These factors are listed in Table 1.

COD	EMR	ESA	GFZ	JPL	SIO
47	19	27	42	17	2.4

Table 1 - Variance components applied to ACs

3.1 Residual Analysis

The presence of outliers tends to make the values in Table 1 too large. The A-networks are affected differently by this because some ACs regularly have far-outliers in their A-networks while others do not. The numbers of station observations removed each week using the Baarda statistic at the 99% confidence level (eqn. 13) are given in Figure 2 (unit variance scaling was applied before the outlier test.) The G-network solutions were iterated with outliers removed. Because Table 1 was unchanged in the iteration, the unit variance after the outlier removal tends to be below unity, as shown in Figure 3.

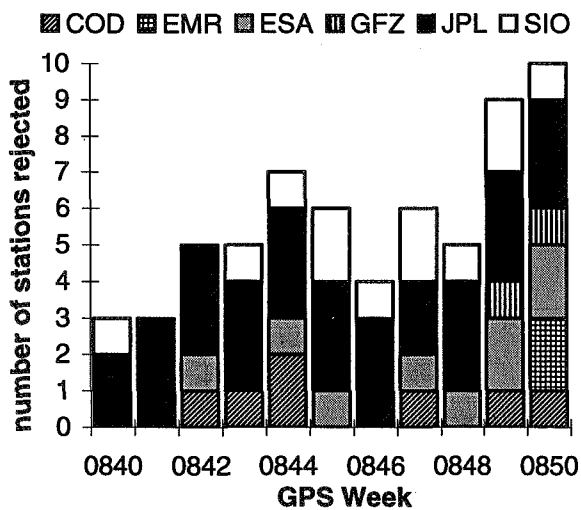


Fig 2 - Outliers at 99% confidence level

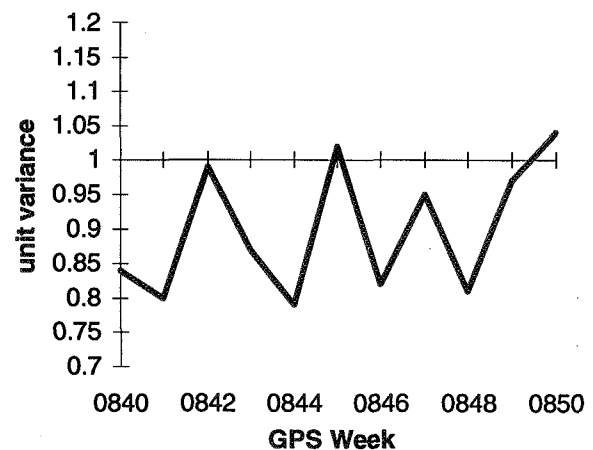


Fig 3 - Unit variance series after outlier rejection

We can examine the deviation in individual AC variance components for each week by computing eqn. 12 after overall unit variance scaling (although eqn. 12 is an iterative expression, the components are already close enough to their correct values to make a single evaluation useful). This results in figure 4.

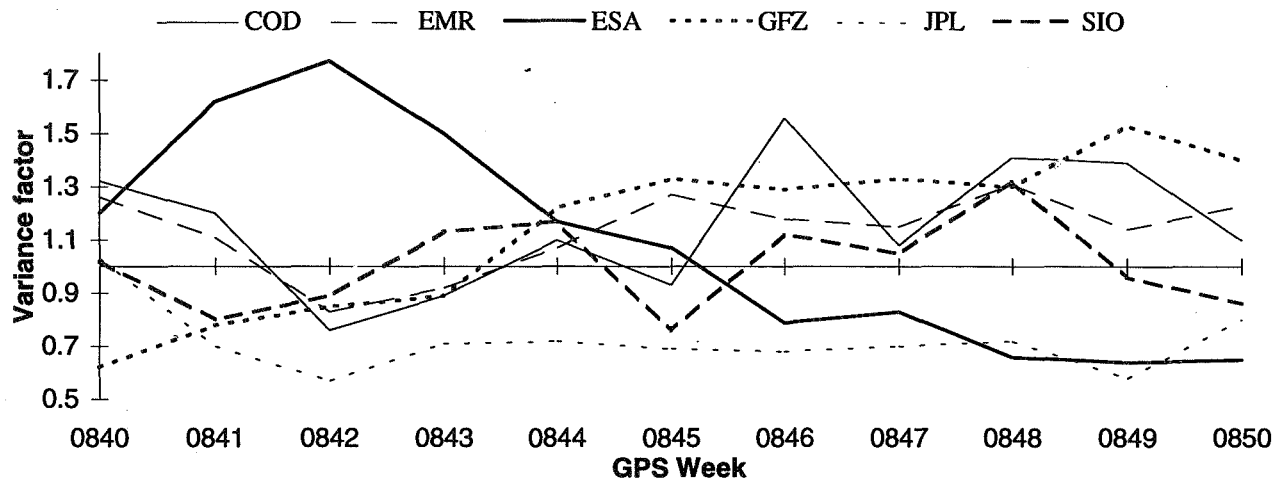


Fig 4 - Weekly variance factor deviations for each AC

Note how the ACs with several outliers removed each week (notably JPL) have variance factor deviations consistently below unity - this is because the initial variance components were influenced by these outliers. It would be wrong to apply these factors in each week, because of their outlier-masking effect. Rather, the long trend in Figure 4 is examined and variance components adjusted over a period of time. Using this approach, the variance components are a function of the outlier detection test used and the confidence level chosen for outlier removal.

3.2 WRMS of postfit residuals

The weighted root-mean-square of post-fit residuals after weighted similarity transformation was calculated between A-network pairs (Table 2), and between A-networks and the G-network (Figure 5).

EMR	ESA	GFZ	JPL	SIO	G	
8.2	11.3	11.0	8.8	10.3	3.5	COD
	14.9	9.9	6.9	7.9	5.9	EMR
		14.5	13.3	11.5	10.9	ESA
			9.7	9.9	10.5	GFZ
				14.9	5.5	JPL
					3.6	SIO

Table 2 - Week 0848 WRMS (mm) of postfit residuals after weighted similarity transformations between each pair of A-networks, and the G-network (code G)

Examination of the residuals and their standard deviations for individual stations in the pairwise comparisons of Table 2 is helpful because they are independent of the combination - they can for instance be used in ad hoc methods for locating outliers. However, to assess G-network consistency we need to examine the variation in the series of independent estimates.

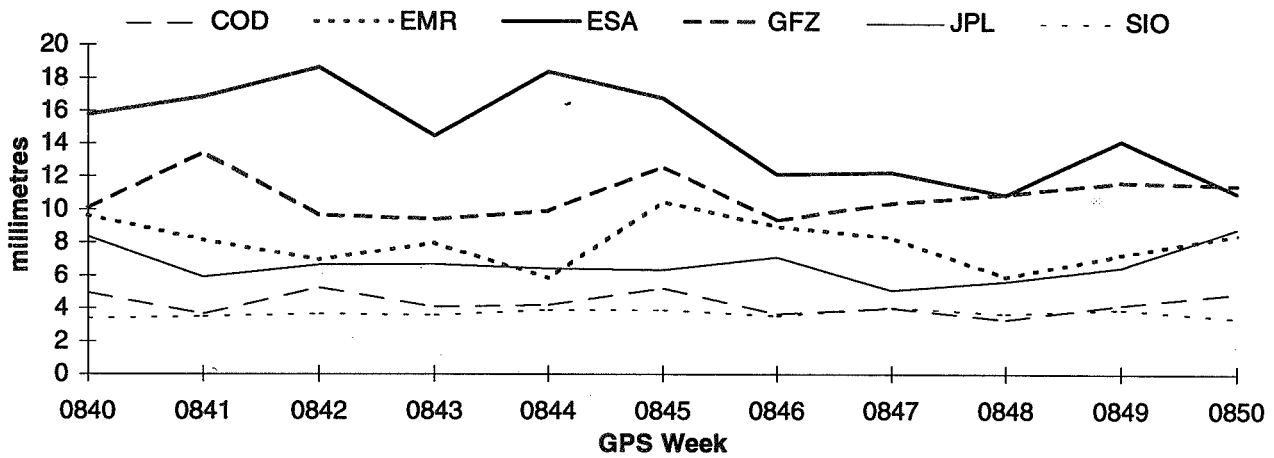


Fig 5 - WRMS of post-fit residuals between each A-network and the G-network in each week.

3.3 Coordinate variation in the G-network series

To look at the coordinate variation in this series of free G-networks I imposed the conditions of no net rotation, translation or scale on a ten-station subset with respect to a G-network in the middle of the series (week 0845). The ten stations selected are estimated by all or almost all Analysis Centres in each week of the series, have a worldwide distribution and are among the best-performing stations. I estimated the unweighted 7-parameter similarity transformations for these ten stations between each G-network in turn and the reference week network, and applied these transformations to obtain the aligned G-networks. The transformation parameters are omitted here - see Table 4 below (ITRF comparison) for an indication of G-network datum variability.

I then took the difference in coordinates for each station between each G-network and the reference network, and obtained this difference in Up, North and East components. For each station, this gives a random-looking scatter of residual components. The variation in each of these residual series can be summarised by its standard deviation, which is independent of the network used as the reference for the alignment step. The standard deviation in (U,N,E) components was calculated for each station. The three sets of SDs are shown in the histograms of figure 6.

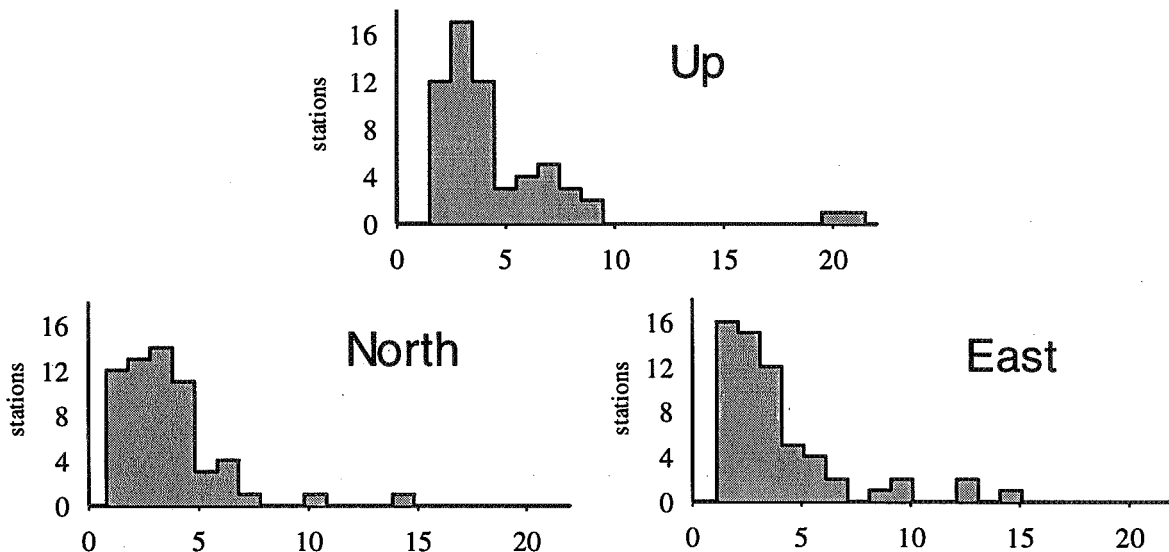


Figure 6 - histograms showing distributions of standard deviations of station coordinate variation (mm)

The standard deviations in height tend to be slightly larger than in horizontal components, also the East component tends to have less variability than the North (global GPS estimates vector lengths parallel to the pole less well than those perpendicular to it). Here one can clearly see the 'bad stations' with coordinate variability well beyond the main group - these are also a feature of A-network series (see table 3 below). There is also a clear secondary modal group of stations, with the main group of stations centred around 2-4mm standard deviation and the secondary group around 5-8mm.

3.4 Repeatability comparison with A-networks

I repeated the alignment procedure for the loose A-networks from each Analysis Centre using the same set of ten stations, and calculated the standard deviation of the component differences for each station in the same way. To present the results in a compact form, I show the quartiles of the set of station standard deviations in Up, North and East components for each Analysis Centre and the G-network (Table 3).

NET		MIN	25%	50%	75%	MAX
COD	U	0.91	2.92	4.74	7.24	24.59
AC	N	1.30	2.41	4.00	5.74	13.91
	E	1.62	2.71	3.74	6.82	24.44
EMR	U	3.44	4.89	6.14	8.05	21.97
AC	N	1.93	3.88	5.59	7.29	12.07
	E	0.90	3.89	5.78	8.23	19.29
ESA	U	3.89	7.33	12.46	22.91	138.66
AC	N	1.71	6.00	9.98	15.25	39.52
	E	2.97	6.82	10.25	18.01	73.23
GFZ	U	3.79	5.55	7.22	10.52	37.48
AC	N	1.74	3.44	5.23	7.21	17.78
	E	1.54	3.78	6.52	10.20	23.65
JPL	U	1.41	3.25	4.40	5.75	90.49
AC	N	1.02	2.58	3.51	5.02	23.78
	E	1.35	2.89	3.80	5.43	141.51
SIO	U	2.58	3.81	4.95	7.23	27.67
AC	N	1.12	2.01	3.88	4.57	15.29
	E	1.71	2.49	4.21	6.46	16.05
G - NET	U	1.48	2.51	3.61	5.49	21.07
	N	0.82	1.94	3.17	4.37	14.59
	E	1.10	1.91	3.04	4.15	14.31

Table 3 - Quartiles of distributions of standard deviations (in mm) of station coordinate variations in series of aligned free-networks, A-nets compared to combined G-net.

Table 3 shows that the values of the 25, 50 (median) and 75 percentiles of the distributions of standard deviations are lower for the G-network than for any of the A-networks - this is true in Up, East and North components. The MAX and MIN columns give the extreme standard deviations in each case (note that the U, N and E components do not necessarily refer to the same station) - in both the G-network is comparable to the highest-repeatability A-networks.

Most A-networks include a few stations with a large dispersion in repeated coordinate estimates, as can be seen by the great difference between the 75 percentile and the maximum in most rows of

Table 3. The ESA and JPL networks especially feature greatly varying station estimates. It should be remembered that not all the A-Sinex data went into the G-networks - only those stations estimated by at least three ACs. The results in Table 3 are only possible given this level of data redundancy, which allows the G-network to function as an effective 'data screen'.

3.5 Comparison with ITRF Core

A 13-station subset of ITRF IGS stations is designated the 'IGS Core network' and is conventionally used for network constraint by IGS agencies. Data from one of the Core stations was unavailable during the period, so only twelve stations were included in this comparison. A weighted similarity transformation between each week's G-network and ITRF94 at the mid-week epoch was estimated - below are shown the transformation parameters and the postfit residual SD and WRMS series. The scale and rotation parameters have been multiplied by the earth radius to give all parameters in millimetres. The arbitrary metre level differences in orientation are quite acceptable.

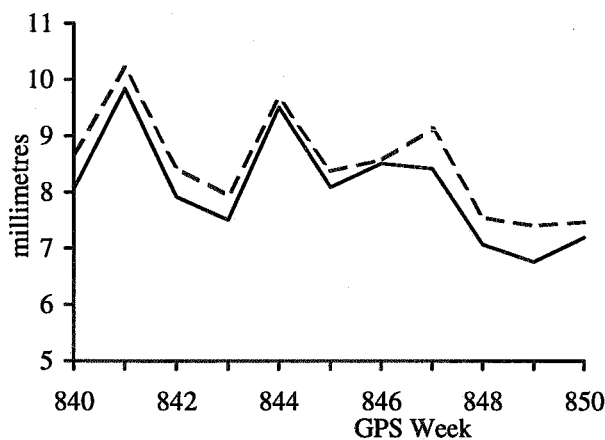


Figure 7 - Standard deviation (dashed line) and WRMS (solid line) of post-fit residuals between G-network and ITRF94 for Core stations.

Wk	t_x	t_y	t_z	r_s	$r r_x$	$r r_y$	$r r_z$
0840	-6	-17	-3	7	1147	-60	-1897
0841	-21	1	-8	8	518	921	-1113
0842	-11	-15	12	11	3416	-698	-2458
0843	-15	-12	14	9	182	-79	-150
0844	-12	-12	25	11	1352	-367	-865
0845	-24	-25	16	9	581	-193	-384
0846	-24	-23	41	10	324	-121	-240
0847	-23	-27	51	8	-432	70	156
0848	-13	-24	37	10	-231	11	86
0849	-17	-29	33	6	83	9	-263
0850	-10	-25	41	12	29	-56	-83

Table 4 - estimated frame parameter differences (mm) between weekly G-network and ITRF94 for Core stations, where r is the earth radius

4 ATTACHMENT OF R-NETWORKS

It is hoped that Regional Network Associate Analysis Centres will begin to submit Regional network solutions (R-Sinex) in the second half of 1996, which GNAACs will integrate with their G-Network to assemble a Polyhedron solution. R-Sinex files will state constraints and station information in the same way as A-Sinex files, so I anticipate applying the procedures described in sections 2.1 and 2.2 in much the same way. Each R-Network will include three or more Global 'Anchor stations' disposed so as to form good fiducial control for the regional network. The attachment of the R-network to the G-network should be such that the Anchor coordinates coincide with the G-network, with the parameters and covariance matrix of the R-network adjusted appropriately. The G-network should not be affected by this step.

One way to accomplish this involves borrowing (not for the first time) from terrestrial geodetic adjustment theory. The principle is that of estimating the local (unshared) parameters of a component network in a multiple-block estimation. In this case the common parameters are the Anchor station coordinates, with however the R-network estimates of these being excluded from the

G-network estimation. Assuming a very loosely constrained Regional solution has been obtained as described in section 2.1, giving 'free' coordinates \mathbf{r} (including Anchor stations) with covariance matrix Σ_r , the Polyhedron coordinates \mathbf{n} of the non-Anchor stations and their covariance matrix can be obtained by: (Cross [1994] p.122)

$$\mathbf{P} = \mathbf{A} \Sigma_r^{-1} \mathbf{A}' \quad (14)$$

$$\mathbf{Q} = \mathbf{A} \Sigma_r^{-1} \mathbf{A} \quad (15)$$

$$\mathbf{n} = \mathbf{P}^{-1} (\mathbf{A} \Sigma_r^{-1} \mathbf{r} - \mathbf{Q}\mathbf{p}) \quad (16)$$

$$\Sigma_n = \mathbf{P}^{-1} + \mathbf{P}^{-1} \mathbf{Q} \Sigma_p \mathbf{Q}' \mathbf{P}^{-1} \quad (17)$$

Since Σ_r^{-1} is known from the constraint removal step, and \mathbf{P} is small (there are only a few Anchor stations), this is a rapid calculation. Eqn. 17 assumes that \mathbf{r} and \mathbf{p} are uncorrelated, the same assumption that was previously made for the A-network combination. The result is equivalent to a simultaneous LS computation in which the Regional estimates of the Anchor stations have been ascribed zero weight.

5 CONCLUSION

The G-network is a high-reliability primary frame for Polyhedron assembly, with the same advantages for GPS networks as a rigorously-estimated highly redundant primary control network had in the days of terrestrial surveying. The repeatability results presented here are evidence of this, and are likely to continue to improve for some time to come. The IGS redundancy requirement of a Global station (at least three independent weekly estimates) is considered basic to a sound Global solution. An interesting extension to this paper would be a quantitative reliability assessment to establish this, e.g. by computing marginally detectable errors with different levels of A-network station set overlap.

REFERENCES

- G Beutler, J Kouba, T Springer [1993]** *Combining the orbits of the IGS Processing Centres*, in Proceedings of the IGS Analysis Centre Workshop, Ottawa, Canada: 12th-14th Oct, 1993, pp20-56
- G Blaha [1982]** *A Note on Adjustment of Free Networks*, Bulletin Geodesique Vol 56 pp281-299
- G Blewitt, M B Heflin, F H Webb, U J Lindqvister, R J Malla [1992]** *Global Coordinates with Centimetre Accuracy in the ITRF using GPS*, Geophysical Research Letters, Vol 19 No 9 pp853-856
- G Blewitt, M B Heflin, Y Vigue, J F Zumberge, D Jefferson, F H Webb [1993a]**, *The Earth Viewed as a Deforming Polyhedron: Method and Results*, in Proceedings of the IGS Workshop, Berne, Switzerland: 25th-26th March, pp218-225
- G Blewitt, Y Bock, G Gendt [1993b]** *Regional Clusters and Distributed Processing*, in Proceedings of the IGS Analysis Centre Workshop, Ottawa, Canada: 12th-14th Oct, 1993, pp62-91
- G Blewitt, Y Bock, J Kouba [1995]** *Constructing the IGS Polyhedron by Distributed Processing*, in Zumberge and Lui [1995] pp21-37
- P A Cross [1994]** *Advanced Least Squares Applied to Position-Fixing*, University of East London Department of Surveying Working Paper 6, 2nd edition.
- C C Goad [1993]** *IGS Orbit Comparisons*, in Proceedings of the IGS Workshop, Berne, Switzerland: 25th-26th March, pp218-225

- E W Grafarend, B Schaffrin [1979]** *Variance-Covariance-Component Estimation of Helmert Type*, Surveying and Mapping, Vol XXXIX No 3 pp225-234
- J Kouba [1995]** *Analysis Coordinator Report*, in IGS Annual Report 1994, IGS Central Bureau, pp29-64
- J Kouba [1996]** *Sinex (version 1.00) Definition*, (in draft), available from IGS Central Bureau Information System
- M Sahin, P A Cross, P C Sellers [1992]** *Variance component Estimation applied to SLR*, Bulletin Geodesique Vol 66 pp284-295
- S R Searle [1971]** *Linear Models*, New York: John Wiley
- O Ziqiang [1989]** *Estimation of Variance and Covariance Components*, Bulletin Geodesique Vol 63 pp139-148
- J F Zumberge, R E Neilan, I I Mueller [1995]** *Densification of the IGS Global Network*, in Zumberge and Liu [1995]
- J F Zumberge, R Liu (editors) [1995]** *Densification of the IERS Terrestrial Reference Frame through Regional GPS Networks*, IGS Workshop Proceedings, Pasadena, USA: 30th Nov - 2nd Dec 1994

Page intentionally left blank

IGS

ATMOSPHERIC TRENDS

Page intentionally left blank

IGS TROPOSPHERIC ESTIMATIONS

-SUMMARY-

Gerd Gendt

Since the monitoring of the atmosphere using the IGS components was first addressed during the 1995 Potsdam Workshop there were a lot of activities on this topic, as examples should be mentioned (i) quality assessment of water vapor determination using ground based GPS measurements (ii) establishment of infrastructure and development of software and technology for GPS contributions to weather forecast. These investigations are of course relevant for climatological studies too.

The aim of this session on ground based GPS meteorology was to give an insight into these activities, to get information from possible customers, to discuss the role of IGS within this topic and to define the next steps.

Eugenia Kalnay from the USA National Centers for Environmental Predictions gave an overview on input data types, data flow and software components used for weather forecast. The quality of weather prediction has been steadily improved during the last decades. This was mainly reached by using more and more data from earth orbiting satellites. Nevertheless, the ocean region lack in data density even today. This gap could partly be filled by GPS/MET, which are especially interesting by its vertical profiles for temperature or water vapor. Ground based derived precipitable water vapor was not tested up to now, but the predictions can benefit from each kind of information given with high quality.

Comparisons of GPS derived vertical integrated water vapor content with water vapor radiometer and radiosonde measurements show a high agreement of about ± 1 mm in precipitable water vapor. This accuracy is sufficient to start using ground based GPS receivers in meteorology. If the global IGS network is equipped with meteorological packages IGS will be capable to contribute to global climate research without great additional effort. By this way, the meteorological community could benefit from cheap (using receivers already installed for other purposes) and continuously derived series.

Comparisons of the zenith path delay series computed by all IGS Analysis Centers (ACs) show a very high consistency corresponding to 1.3 mm precipitable water vapor, but on the other hand these show also systematic differences which have to be investigated. The elimination of systematic errors is especially important for climate research, were we are looking for small signals over long time periods.

Whereas the existing IGS components can contribute to climate studies, many additional efforts have to be made for contributing to weather forecast. With the CORS network a network with real-time transfer of GPS observations and meteorological data was developed and put into operation. This network could provide real-time monitoring of atmospheric water vapor with high quality if good orbit predictions based on super rapid orbits from the IGS ACs will be available.

In different institutions various technologies are under development that could be used for real-time atmospheric monitoring.

The complexity of the atmosphere requires for precise weather forecast a high spatial density of information about the atmospheric parameters. The resulting density of GPS networks will be so high that these networks cannot be analyzed by the IGS. Further on this is not a global problem, and the requirements for a real-time data transfer can only be fulfilled concentrating on each region. That means regional MET-ACs for tropospheric analysis will be installed, which will benefit from the following IGS products:

Data from the global IGS network, which are relevant for this region.

The download interval etc. should be arranged bilateral between the MET-ACs and the sites of interest. It is reasonable to have nearly real-time data transfer only for those data, which will actually be used by MET-ACs.

Predictions based on super rapid IGS orbits.

These predictions could be computed by IGS using the long arc orbits (e.g. 3-day orbits), because these are more stable than the orbits from the last day only.

Although there are no stringent demands for an IGS water vapor product at the moment, IGS should take the initiative and start to offer such a new product. After a pilot phase IGS may recapitulate and decide whether to continue with such a product.

RECOMMENDATIONS

1. The IGS-sites are asked to install MET-packages with the below given characteristics until the end of 1996. The meteorological data (reduced to the GPS-antenna location, RINEX format) should be sent simultaneously with the RINEX observations to the Global Data Centers.
In a pilot phase a time delay of a few days is acceptable for the Met RINEX files.

Installation of MET-packages in the IGS network with the following characteristics:

Pressure	: ≤ 0.5 mbar, very stable ≤ 0.5 mbar throughout 2 years
Temperature	: ≤ 0.5 K
Humidity	: ≤ 10 %
Sampling rate	: ≤ 10 minutes

2. For Climate Research
 - 2.1. Starting from the end of 1996 the Analysis Centers compute series of total zenith path delay (ZPD) with a sampling rate of minimum 2 hours. (Data intervals starting at 00:00 GPS-time).
 - 2.2. An associate IGS processing center combines the individual time series of delay to an IGS Mean series of ZPD and converts the delays to estimates of precipitable water vapor.
By the end of 1996 GFZ will be ready to act as an associate processing center. Other agencies will be invited through a call of participation.
 - 2.3. Formats for exchange and distribution of results should be defined. For the exchange between the ACs and the associate processing center the SINEX format and for distribution of results the RINEX format should be used. Necessary extensions or modification of both formats must be discussed.
-

3. For Weather Forecast
The contribution of IGS to the weather forecast will be restricted on the orbit computation, rapid orbits with 23-hour delay and predicted orbits.

If data of the IGS network are needed the analysis centers engaged in weather forecast should make bilateral agreements for nearly real-time data transfer with tracking sites of interest.

Page intentionally left blank

COMPARISON OF IGS TROPOSPHERE ESTIMATIONS

Gerd Gendt

GeoForschungsZentrum Potsdam, Aufgabenbereich 1,
Telegrafenberg A17, D-14473 Potsdam, Germany

INTRODUCTION

Water vapor is a crucial parameter in atmospheric modeling. It has a very inhomogeneous distribution and a high variability. Continuous and well-distributed measurements of water vapor are therefore of fundamental interest both for short range weather predictions and climatology.

The GPS is a cost-effective technology to provide dense, globally distributed and nearly continuously measured water vapor. Even if we get only the (vertical or lateral) integrated values, this is important information.

There are two approaches in the application of the GPS to meteorology with following characteristics:

Ground-based GPS meteorology:

- Networks of ground-based GPS receivers are used to estimate the vertically integrated water vapor (IWV).
- The great advantage is the nearly continuous measurement of IWV. The spatial distribution depends on the density of the network. (For dense networks lateral gradients of IWV can be deduced)
- Over the oceans good coverage can never be reached.

Space-based GPS meteorology:

- GPS receivers on board a Low Earth Orbiter (LEO) satellite observe very short (~ 1 minute) atmospheric occultations (~500 per day) which provide a vertical refractivity profile (laterally integrated over ~150 - 200 km) .
- The water vapor profile can be deduced if the temperature profile is known, and vice versa.
- It is not continuous at a point, but has a good global distribution.
- Problems may occur in monitoring lower troposphere in the vicinity of high mountains.

These two approaches are not competing but complementary to each other. The IGS is based and focused on the analysis of the global network of ground receivers and can therefore be part of the ground-based GPS meteorology.

Typically the refraction parameter is estimated in form of the total zenith path delay (ZPD), presuming the elevation depending mapping function is known, the wet component changes little over short periods of time and simultaneous measurements in different elevations exist. The ZPD is the sum of the hydrostatic and wet components. Knowing

the surface pressure to 0.5 mbar it is possible to remove the hydrostatic zenith delay with an accuracy of a few millimeters or better and to get the zenith wet path delay (ZWD) without introducing any additional error. Furthermore the error in the mapping function for elevations >15 degrees is not a significant part of the error budget for the ZWD. The parameter of interest for the meteorologist is not the ZWD but the vertically integrated water vapor in terms of precipitable water vapor (PWV). With the knowledge of the surface temperature only, this transformation from ZWD to PWV may be done with an accuracy of 2%. From a variety of experiments the PWV accuracy can be estimated to about 1 mm.

Table 1. Error budget for PVW Estimation (units: mm)

Error Source	PWV	ZPD	Comment	
<i>Estimation error</i>				
orbit	0.2	1.3	10 cm error, 1000 km baseline	a
coordinates	0.5	3.0	1 cm height error	a
multipath	0.3	2.0		a
<i>RSS</i>	0.6			
<i>Conversion error</i>				
Barometric press.	0.2	1.2	0.5 mbar, normal wind	b
Con. ZWD-PWV	0.4	-	2% error (for 20 mm PWV)	b
Physical constants	0.25	1.5		b
<i>RSS</i>	0.5			

a Rocken et al., 1995

b Runge, et al., 1995

The 7 IGS Analysis Centers (AC) routinely analyze more than 50 global distributed IGS tracking stations. To produce the IGS products - precise orbits, earth rotation parameters and station coordinates - the tropospheric refraction has to be modeled and a zenith path delay (ZPD) correction must be adjusted. Up to now the ZPD itself is not a product and therefore the routine analysis is not optimized to get best estimates for it. Nevertheless, the accuracy of its determination is high and converted to precipitable water vapor content its a valuable information for meteorology.

To look into the stability of ZPD determination, comparisons of CODE and GFZ tropospheric estimates were presented already at the last IGS Workshop (Data from 3 weeks in northern winter 1994/95). The general consistency was about ± 10 mm for the stddev and ± 6 mm for the bias. The result was encouraging and stimulated to think about a new IGS product, the IGS mean of PWV, provided that the IGS tracking sites are equipped with automated meteorological packages. In preparation of such a new product the IGS Governing Board recommended to accomplish a more comprehensive comparison

including all ACs and choosing 3 weeks during northern summer (August 1995), to have for the majority of sites not so dry air as in northern winter.

DATA, SOFTWARE

The main features for tropospheric parameter estimation in the software package of all ACs are given in Table 2. There are very different approaches. It should be pointed to those differences, which could be responsible for differences in the tropospheric parameter estimation. A great influence may have the elevation cutoff angle, which varies from 15 to 20 degrees. Whereas all other ACs solve for ZPD independent from interval to interval, EMR and JPL introduce constraints within their Kalman procedure. For poor observed sites and time intervals the constrained solution is naturally smoother, compared to the unconstrained case.

During routine analysis most ACs estimate ZPD parameters in intervals of 4 to 6 hours, so that for this comparison the test weeks had to be reprocessed to get a sampling rate of 2 hours, which was agreed on. For the comparison the GPS weeks 812 to 814 (July 30 to August 21, 1995; DoY 211 to 231; MJD 49928 to 49948) were chosen. The sites used vary from AC to AC, their number can be seen in Table 3. Only those sites analyzed by at least 3 ACs were compared, which reduces its number to about 40.

There were some problems in the calibration of ESA and NGS series, which couldn't be identified and removed. For the NGS estimates this may probably be explained by the fact that NGS is the only AC applying elevation dependent antenna phase corrections. Because of these large biases some results are therefore presented without these two centers.

Table 2. Characteristics of the software packages

	CODE	EMR	ESA	GFZ	JPL	NGS	SIO
Method	doub.diff.	undiff.	doub.diff.	undiff.	undiff.	doub.diff.	doub.diff.
MetData	Hei.-dep. nominal P,T,H	Global constant	Global constant	Hei.-dep. nominal P		Lat.-Hei- DoY Model	Global constant
Tro. Model	Saastam.		Saastam.		Saastam.		
Mapping F.	1/cos(z)	Lanyi	Willmann	1/cos(z)	Lanyi	Niell	Davis
Elev. cutoff	20	15	20	20	15	15	20
Sampl. Rate (Data; min)	2	7.5	6	6	5	0.5	2
Sampl. Rate Tro. Estim.	120	7.5	120	120	5	120	60
Constraints	No	Yes	No	No	Yes	No	No

Table 3. Number of sites and time interval for tropospheric parameter estimation

	No. STA	Tropospheric Estimation (minutes)	Weeks analyzed		
			812	813	814
CODE	58	120.	+	+	+
EMR	28	7.5	+	+	+
ESA	48	120.	-	+	+
GFZ	47	120.	+	+	+
JPL	35	5.	+	+	+
NGS	41	120.	-	+	+
SIO	15	60.	+	+	+

COMBINATION OF MEAN ZPD SERIES

The files used by the individual ACs for storing their tropospheric estimates are different in format and philosophy. To handle all comparisons and the combinations a SINEX-like format for tropospheric series was defined and applied throughout this investigation.

The individual series have of course biases between each other. If a straightforward mean would be computed then gaps in one of the biased input series would produce a jump in the mean series. This is why the following 2-step procedure is used to derive the mean series for a defined interval, e.g. 1 day or 1 week:

- A mean ZPD-file is computed by combining the estimates of all ACs. This file is named IGS-Trop-File.
- No weights are used in the combination.
- The 2-step procedure has the following main steps and works site by site:

A1 Computation of a preliminary IGS-Trop-File.

Mean trop values are computed for those epochs, where **all** ACs have ZPD estimates (to get no jump in the mean by missing ACs).

A2 Computation of the bias between the preliminary IGS-Trop-File and each AC.

B1 Computation of IGS-Trop-File.

Mean ZPD values are computed, where the AC estimates are corrected by the bias from step A2. This way all epochs can be used and a gap in the series of one AC will not result in a gap for the IGS-Trop-File. Outliers are eliminated. The number of contributing ACs is coded for each ZPD value. A series of a single AC is copied into the IGS-Trop-File too.

- B2 Computation of stddev and bias between the IGS-Trop-File and each AC. Only epochs are used where at least 3 ACs have contributed. Outliers are eliminated (with $2.5 \times \text{stddev}$)

RESULTS

First of all differences in pairs were computed to get an insight into the consistency between the individual ACs. This was done using daily and weekly biases for each site, Tab. 4. The stddev for the ZPD-differences is about ± 9 mm. The weekly bias has no significant systematic shift and its stddev over all sites is about ± 5 mm. The consistency between CODE and GFZ is the same as it was obtained in the comparison with data from northern winter 1994/95 (Gendt and Beutler, 1995). From this one may conclude that the accuracy will not depend on the absolute water vapor content. The best agreement is between EMR and JPL, which may be due to the constrained estimation and 15 degree elevation cutoff angle in both series.

There is a high stability in the daily repeatability of the bias for a site, but also a significant site-dependent shift from AC to AC. This high repeatability explains that the improvement in the stddev of ZPD differences is only marginally (~ 1 mm) if daily instead of weekly biases are used. Therefore, to have no jump at the day boundaries by missing sites for a single AC for a single day, weekly biases were computed for the determination of the IGS mean series. In Fig. 1 the daily repeatability of the bias between JPL and other ACs are shown for selected sites. The repeatability is in most cases better than ± 2 mm. The reason for the systematic effects, which reaches values of 1 cm, is not fully explained. Some effects may come from different a priori models, meteorological values and station heights, e.g. 1 cm height change gives 3 mm bias in ZPD. Even having the same coordinates, e.g. for fiducial sites, cutoff angles and software, like EMR and JPL, biases of some 5 mm can be seen. To eliminate all possible sources of biases the coordinates (and so the heights) of as many sites as possible should be agreed on. The higher resulting consistency makes only sense if these coordinates have a high accuracy and will therefor not give systematic errors. For climate research a high long stability is of crucial importance and this implies that significant station height changes should be avoided, at least documented for possible PWV corrections.

Statistics of the ZPD differences between the individual ACs and the IGS mean can be seen from Figs. 2. The stddev and bias are about ± 6 mm and ± 4 mm, respectively, which gives an rms of $\pm 7-8$ mm and corresponds to ± 1.3 mm PWV.

In Figs. 3 some tropospheric series are shown. No bias corrections are performed. It can be seen that the accuracy in the estimations does not depend on the amount of fluctuations in the total ZPD. Even such high fluctuations of ~ 200 mm within hours as for ALGO are reflected in all ACs series with an accuracy comparable to ± 1 mm PWV.

SUMMARY

These comparisons demonstrate the high consistency in the tropospheric estimations between the IGS Analysis Centers, although there are systematic effects which have to be investigated.

The IGS is ready to produce time series of vertical integrated water vapor, provided the meteorological surface parameters are measured within the IGS network. Many of the sites have already meteorological packages installed for other collocated techniques, like VLBI, PRARE, DORIS, SLR. The last step to use these measurements on a regular basis and to install additional meteorological packages should be pushed forward within the IGS, hopefully still in 1996.

Acknowledgement. This comparison was only possible by the support of all IGS Analysis Centers. Thanks to all of them for reprocessing the test weeks 812 to 814 and making available their tropospheric estimates with the agreed upon sampling rate.

REFERENCES

- Gendt, G., G Beutler, 1995, Consistency in the tropospheric estimations using the IGS network, in *Proceedings of the IGS Workshop 'Special Topics and New Directions'*, Potsdam, May 1995, editors G Gendt and G Dick, 1996, pp. 115-127
- Rocken, Ch, F S Solheim, R H Ware, M Exner, D Martin, M Rothacher: Application of IGS data to GPS sensing of the atmosphere for weather and climate research, in *Proceedings of the IGS Workshop 'Special Topics and New Directions'*, Potsdam, May 1995, editors G Gendt and G Dick, 1996, pp. 93-103
- Runge, Th., M Bevis, Y Bar-Sever, S Keihm: Accuracy evaluations of ground-based GPS estimates of precipitable water vapor. *Paper AGU Fall Meeting*, Dec. 12, 1995, San Francisco.

Table 4a. Consistency of ZPD estimates between the Analysis Centers for week 813.
(units: mm)

	No.Sta	Weekly bias		Daily bias	
		Bias (mean of sta)	sdev.	sdev.	Bias (daily repeat.)
CODE-EMR	24	-0.2±6.6	8.9	8.0	±3.9
CODE-GFZ	45	-0.3±3.7	10.6	9.8	±3.7
CODE-JPL	35	-1.1±4.9	8.6	7.8	±3.8
EMR-GFZ	24	-0.9±7.0	8.2	7.6	±3.4
EMR-JPL	21	-1.9±3.6	6.8	6.4	±2.6
GFZ-JPL	31	-0.9±4.9	9.5	9.0	±3.2

Table 4b. Continued, but only for fiducial sites (units: mm)

	No.Sta	Weekly bias		Daily bias	
		Bias (mean of sta)	sdev.	sdev.	Bias (daily repeat.)
CODE-EMR	12	-0.1±4.0	8.2	7.6	±2.8
CODE-GFZ	12	0.4±1.7	9.7	9.4	±2.5
CODE-JPL	12	-0.9±2.3	8.0	7.5	±2.6
EMR-GFZ	12	0.3±4.2	7.8	7.4	±2.1
EMR-JPL	12	-1.0±3.0	6.1	5.8	±1.9
GFZ-JPL	12	1.3±2.3	9.1	8.9	±1.5

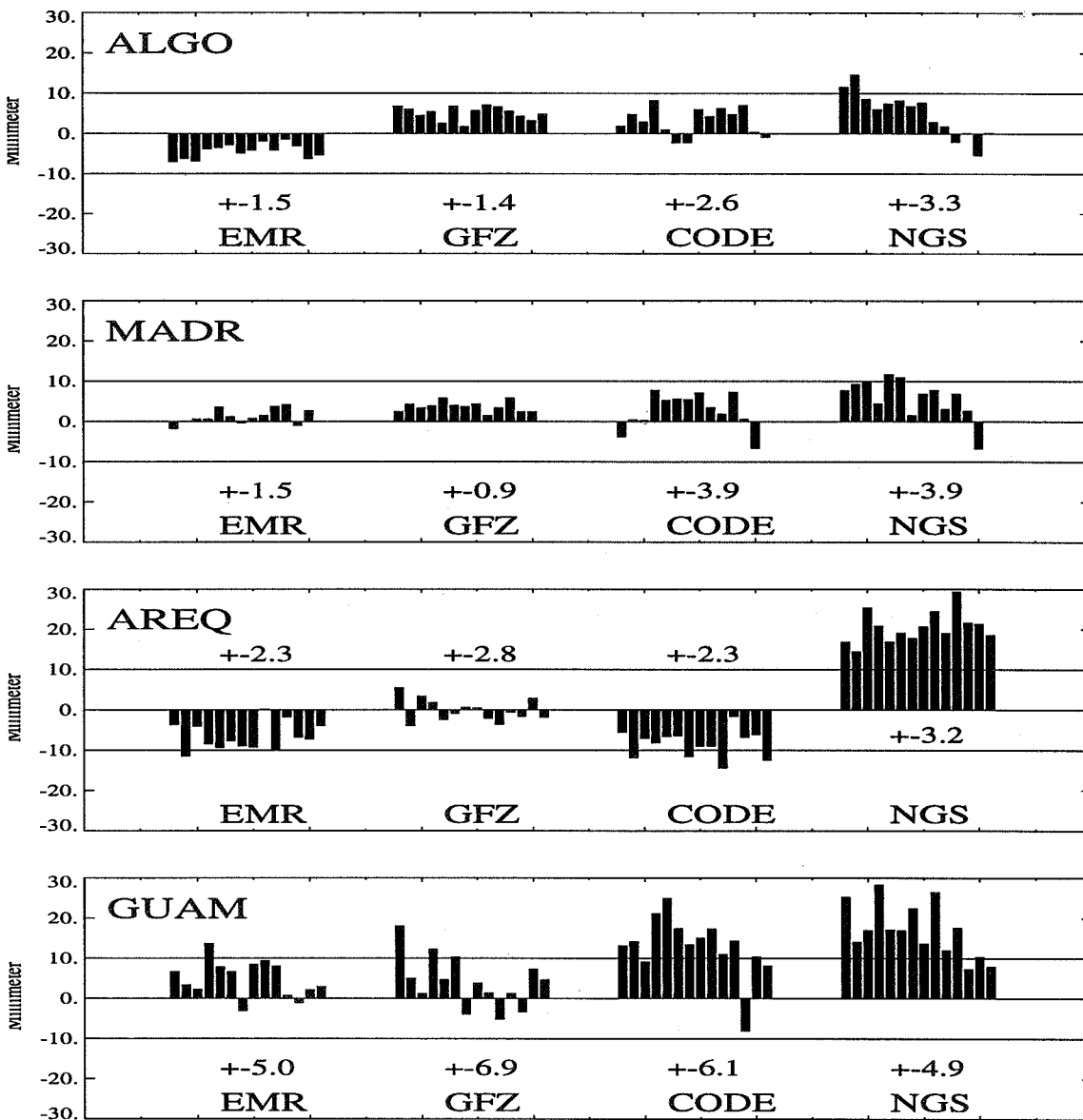


Fig. 1. ZPD biases between JPL and the other IGS Analysis Centers for selected stations with their repeatabily in mm

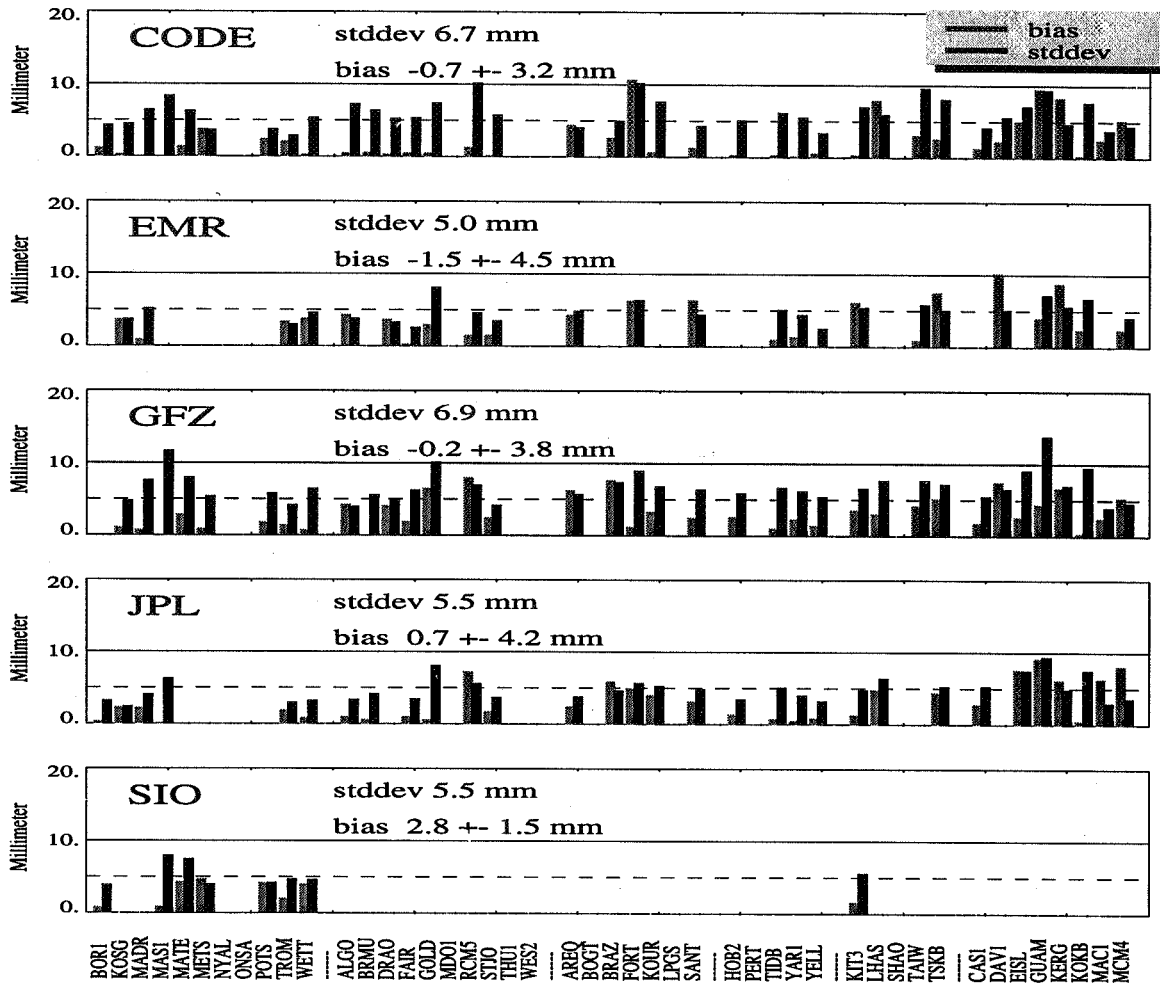


Fig. 2a. Stddev and bias of ZPD differences between the ACs and the IGS Mean, Week 812

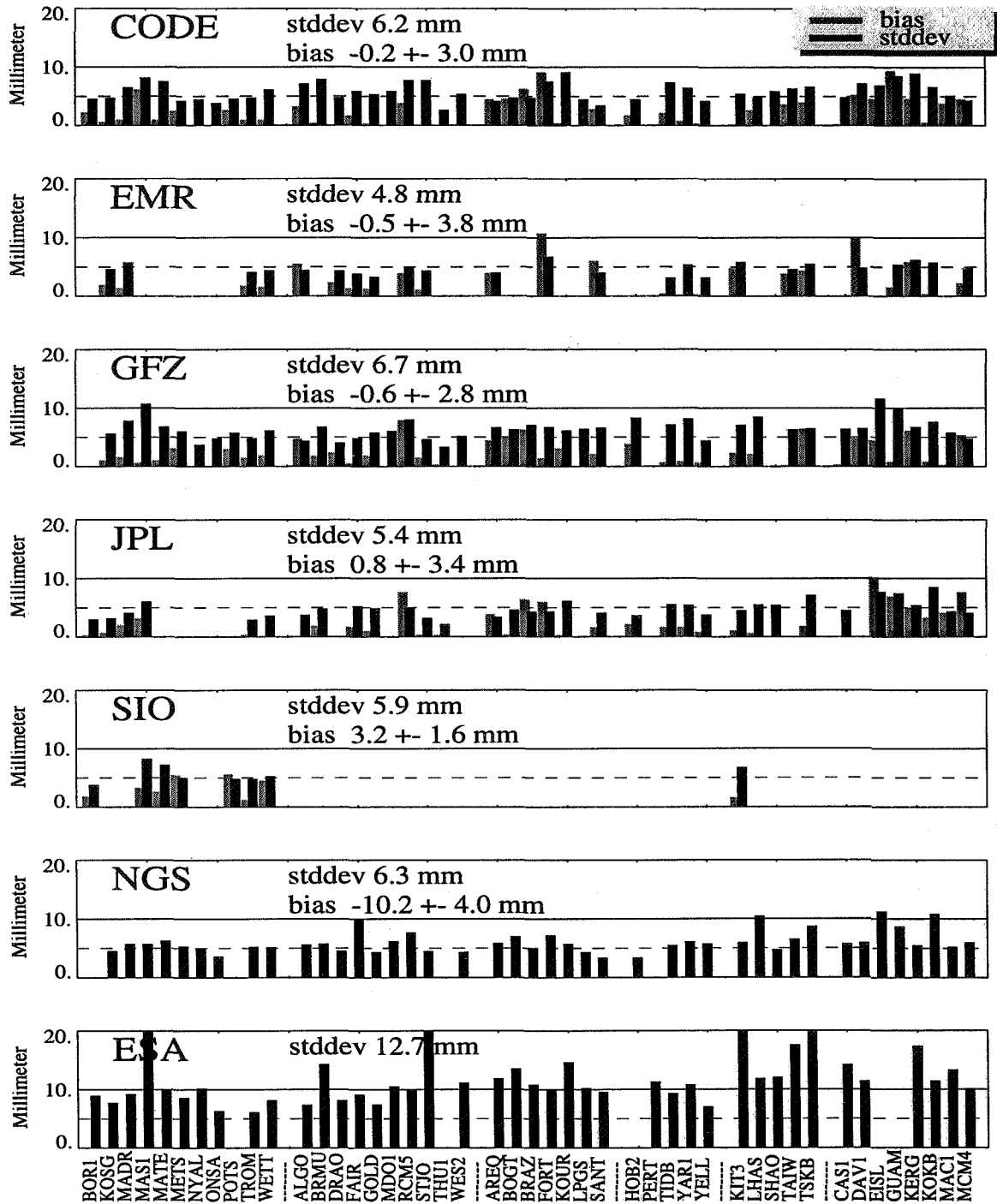


Fig. 2b. Stddev and bias of ZPD differences between the ACs and the IGS Mean, Week 813

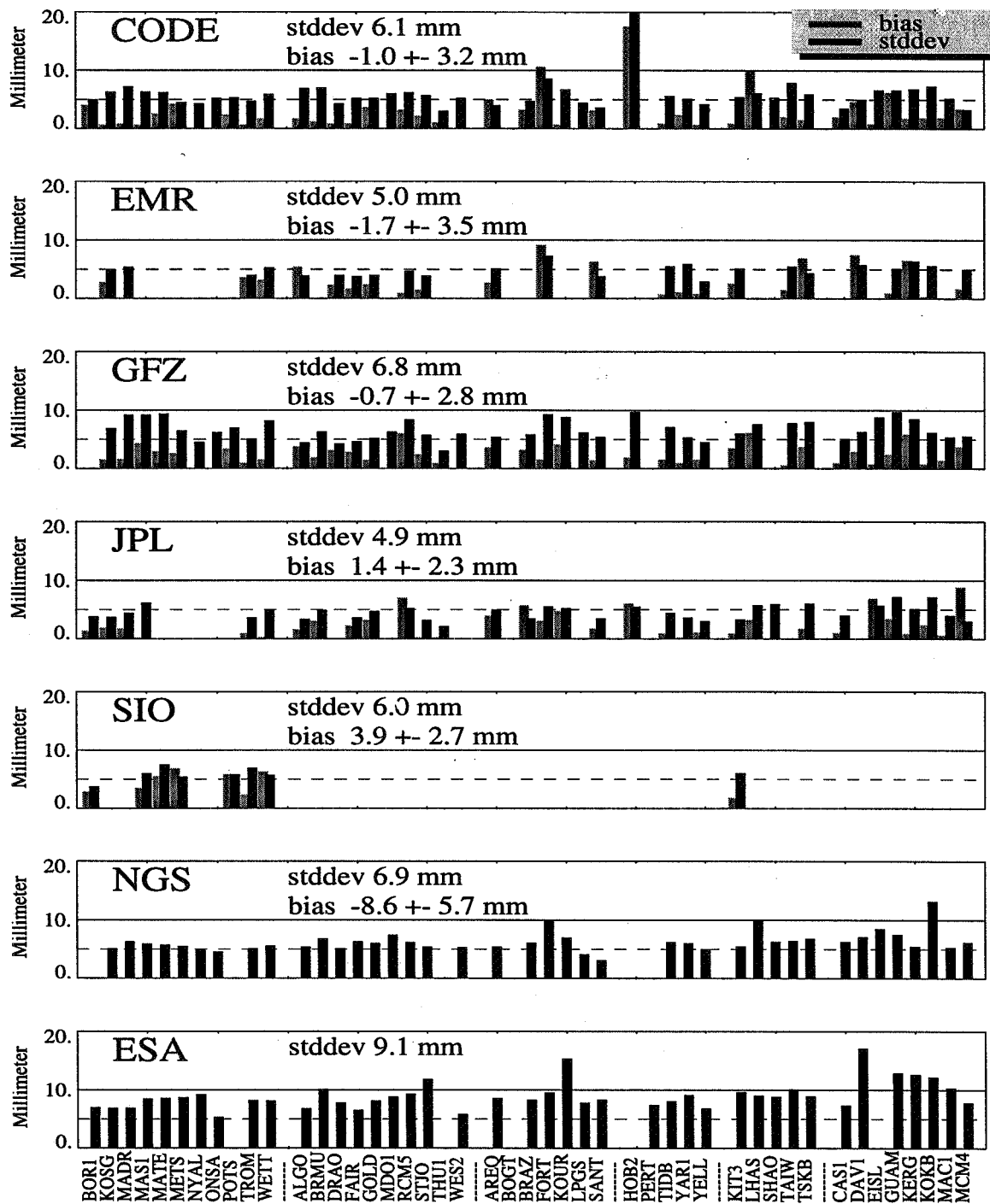


Fig. 2c. Stddev and bias of ZPD differences between the ACs and the IGS Mean, Week 814

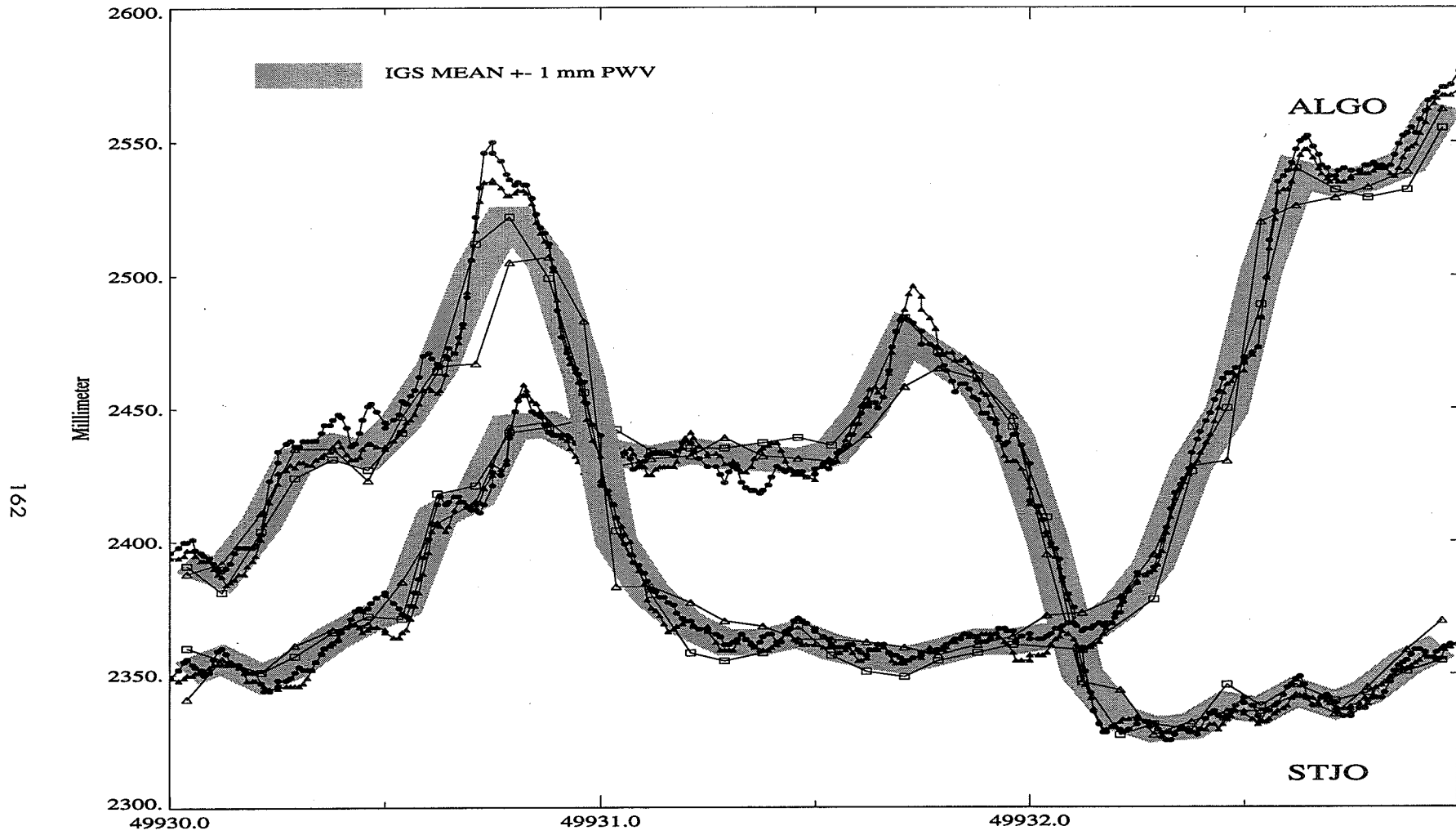


Fig. 3a. Total zenith path delay series of all ACs for ALGO and STJO with given IGS-Mean for selected 3-day interval

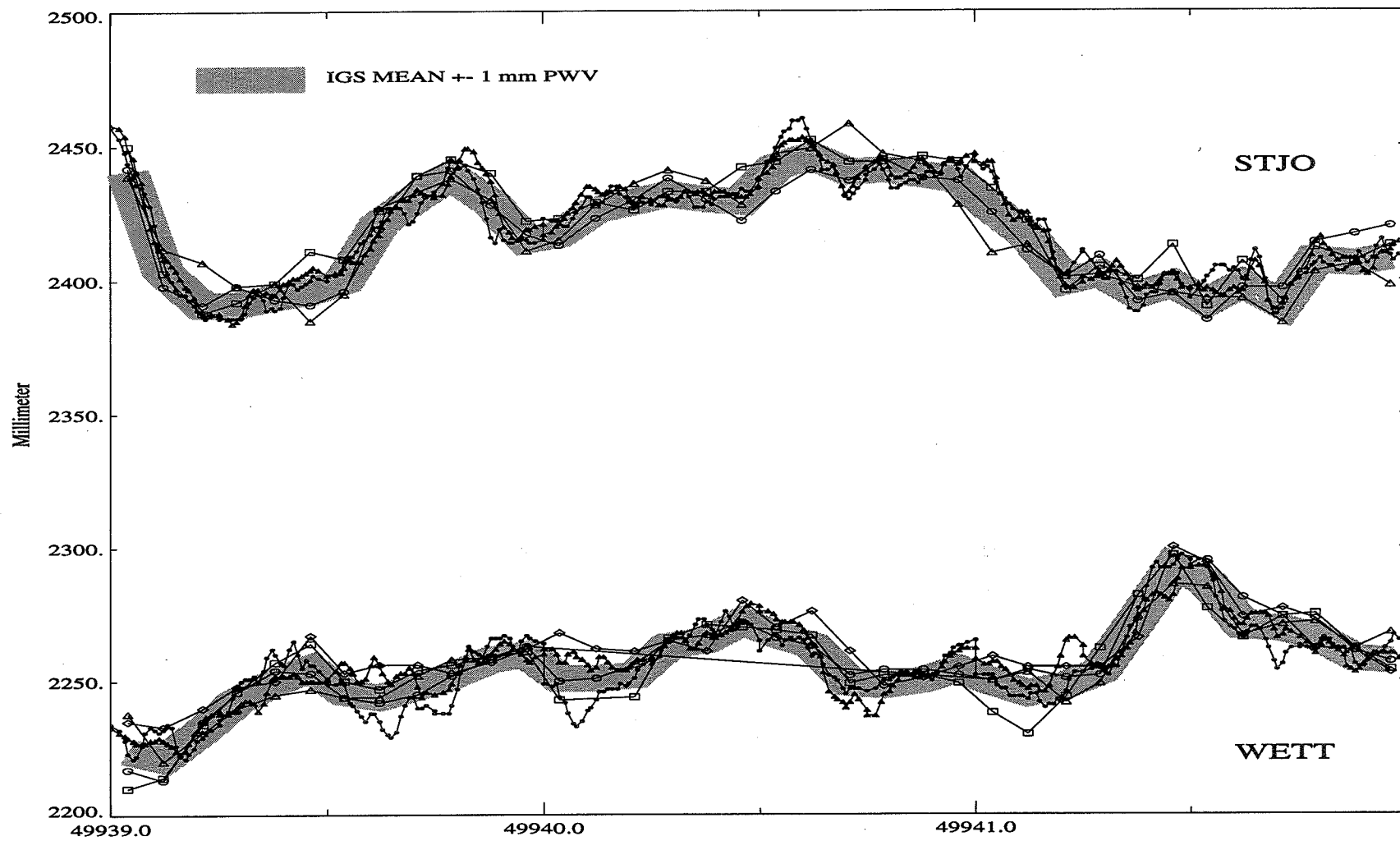


Fig. 3b. Total zenith path delay series of all ACs for STJO and WETT with given IGS-Mean for selected 3-day interval

Page intentionally left blank

Strategies for Near Real Time Estimation of Precipitable Water Vapor

Yoaz E. Bar-Sever
Jet Propulsion Laboratory, California Institute of Technology
Pasadena, CA 91109

INTRODUCTION

Traditionally used for high precision geodesy, the GPS system has recently emerged as an equally powerful tool in atmospheric studies, in particular, climatology and meteorology. There are several products of GPS-based systems that are of interest to climatologists and meteorologists. One of the most useful is the GPS-based estimate of the amount of Precipitable Water Vapor (PWV) in the troposphere. Water vapor is an important variable in the study of climate changes and atmospheric convection (Yuan et al., 1993), and is of crucial importance for severe weather forecasting and operational numerical weather prediction (Kuo et al., 1993).

A ground-based GPS system does not produce estimates of PWV directly. PWV is inferred from a direct estimate of the Total Zenith Delay (TZD), with the help of some ancillary information. The TZD quantifies the atmospheric delay for a GPS signal coming from the zenith direction. It is mapped to the elevation angle of a particular satellite-receiver link by means of an appropriate mapping function, assuming horizontal symmetry. The TZD can be separated into two components, Zenith Dry Delay (ZDD) and Zenith Wet Delay (ZWD). The ZDD is caused by the propagation delay and ray bending due to the dry gases in the troposphere. It can be accurately inferred by using precise measurements of atmospheric pressure at ground level, and removed from the total delay. The remaining ZWD is nearly proportional to the quantity of PWV integrated along the zenith direction. The total PWV can be extracted from the ZWD to an accuracy of a few percent given measurements of the temperature at ground level. (Bevis et al., 1994, Rocken et al., 1993, Yuan et al., 1993). In the absence of pressure or temperature measurements on site, they can be approximated by means of an appropriate climate model. Verification of accuracy of GPS-based estimates of PWV is typically done by comparison with estimates based on the more established techniques of radiosondes and Water Vapor Radiometers (WVR). Several recent comparisons demonstrated that GPS can provide millimeter-level accuracy in measuring PWV (Businger et al., 1996, Elgered et al., 1995, Rocken et al., 1995, Chiswell and Businger, 1995). The current level of accuracy of GPS-based estimates of TZD is believed to be better than 1 cm. The extracted PWV is believed to be 1 - 2 mm accurate.

It is well known that water vapor has significant small-scale variations in time and space (Lilly and Perkey, 1976). The high temporal and spatial resolution of GPS-based estimates of PWV makes the GPS technology unique in its ability to augment the sparse measurements from the radiosondes network. For example, the JPL routine processing of GPS data from the IGS network produces estimates of TZD every five minutes. The only other existing technology for PWV retrieval with high temporal resolution is based on Water Vapor Radiometers (WVR), but their global distribution is extremely sparse due to their high cost. This fact highlights a crucial advantage in exploiting the vast network of GPS ground receivers, namely, its very low cost.

Another unique advantage of GPS-based PWV estimates is the potential availability of data from ground receivers in Near Real Time (NRT), allowing for timely assimilation of the estimates into numerical weather prediction schemes. However, producing PWV estimates from NRT processing of GPS data poses a challenge. Usually, high accuracy estimates are available after processing data from a relatively large global network of receivers. In NRT, only data from a small number of stations is expected and their distribution is unlikely to be global, at least in the near future.

In this paper we discuss various aspects of the process by which ZWD is estimated from GPS data and describe a very simple estimation strategy for NRT applications.

EVALUATING GPS-BASED ESTIMATES OF ZWD

In order to analyze various estimation strategies for ZWD from GPS data we set up an experiment by which we compared GPS-based estimates of PWV with those obtained from a collocated water vapor radiometer. The GPS data used in this experiment was obtained from an 8 channel, dual frequency, TurboRogue GPS receiver that is in continuous operation at a site located at the Jet Propulsion Laboratory. Simultaneous surface pressure and temperature measurements were obtained from a Paroscientific Model 6016B pressure sensor with a stated accuracy of 0.01% of the nominal atmospheric pressure at the comparison site. Surface temperatures were obtained from a temperature sensor contained within the pressure sensor. The water vapor radiometer used in this comparison was a 3 channel design developed at JPL (Keihm, 1991). During the period of the intercomparison, the WVR operated continuously in a fixed scanning pattern. Measurements of the sky brightness temperature were made at a number of elevation angles to allow necessary gain corrections to be made to the WVR signal. PWV estimates used in this comparison were obtained from the WVR measurements made at zenith.

The GPS-based estimates of PWV were obtained by processing the data with the GIPSY/OASIS II software system using the technique of precise-point-positioning (Zumberge et al., 1995). The GPS orbits used in the precise-point-positioning technique were those produced routinely at JPL for the International GPS Service (IGS). The measurement interval is five minutes. Pseudorange measurements are carrier-smoothed and carrier phase measurements are simply decimated to the five minutes mark. The troposphere is modeled as a random walk with a sigma of approximately 1 cm/ $\sqrt{\text{hour}}$. Estimates of ZWD are produced every five minutes.

The experiment spanned the months of August and October, 1995. We will describe results from 18 days during August. WVR measurements from the rest of the month were excluded due to the existence of clouds. WVR measurements were available again for most of October but the result of the comparisons is similar.

When considering the results below, it must be remembered that there are inherent limitations to the accuracy of both WVR and GPS-based estimates of PWV. A simple analysis of major error sources (Runge, 1995) has estimated that the uncertainty in GPS-based estimates of PWV is approximately 1.1 mm for PWV values in the range of 20 mm. Similarly, due to uncertainties in instrument calibrations and retrieval algorithms, the accuracy of WVR measurements of PWV is currently limited to 1 to 1.6 mm.

EFFECTS OF ELEVATION ANGLE CUTOFF

In this experiment we tested the effect of the GPS receiver elevation angle cutoff on the quality of the ZWD estimates. The results are summarized in Figure 1. We found that the standard cutoff of 15 degrees gave rise to a significant bias between the GPS-based estimates of ZWD and PWV and the WVR-based estimates. This bias was reduced dramatically when the elevation angle cutoff was reduced to 7 degrees. An illustration of the different estimates during the first three days in August is presented in Figure 2. Similar behavior was observed with the October data.

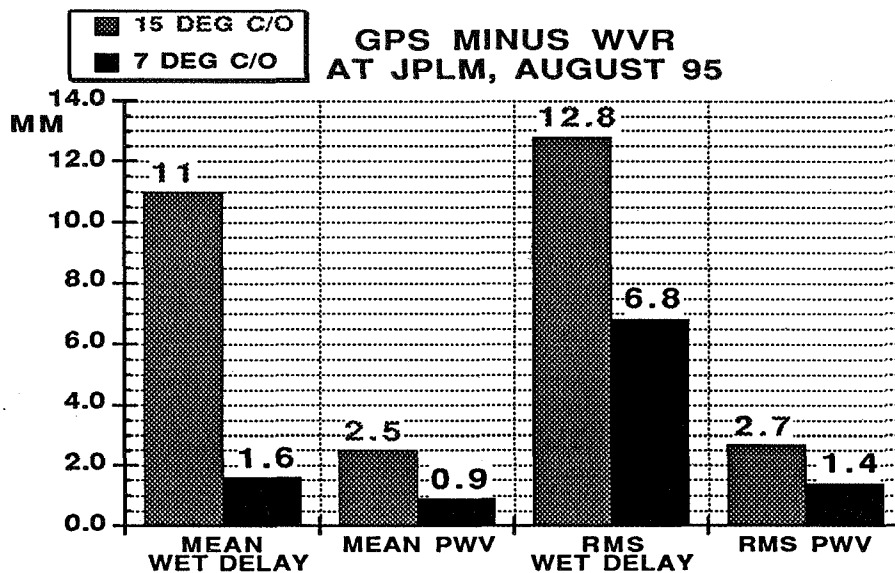


Fig 1. Effects of elevation angle cutoff on difference between GPS-based estimates of ZWD and WVR estimates. Statistics were based on 18 days in August 1995.

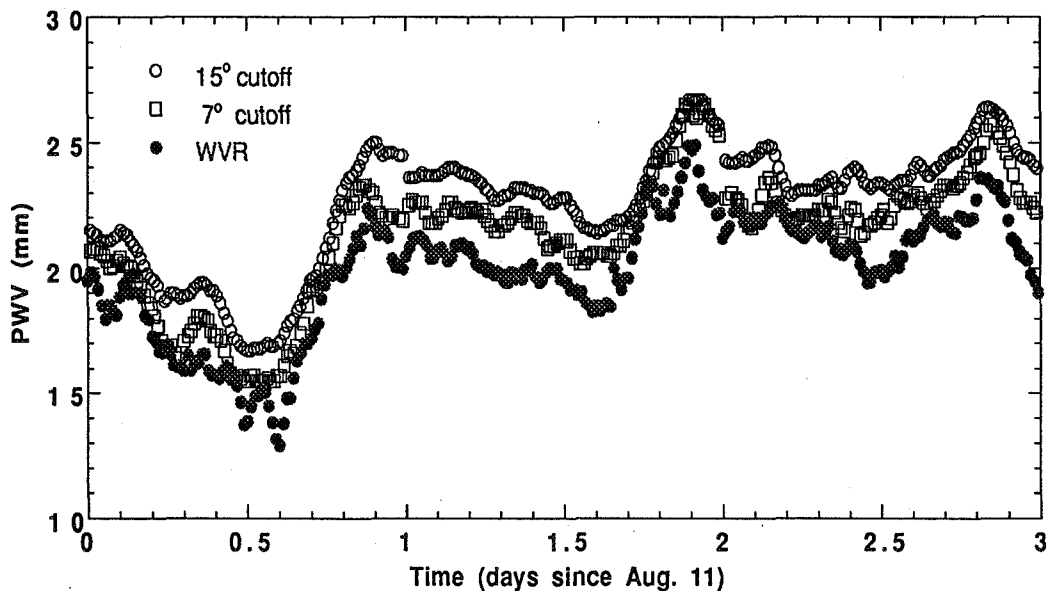


Fig 2. Comparing PWV estimates from WVR and from GPS with two elevation angle cutoffs for three days in August, 1995, at the JPLM site.

Accompanying the bias in ZWD between GPS estimates with different elevation angle cutoffs was a bias in the estimated geodetic height of the station. This bias can be observed in Figure 3, depicting the daily geodetic height estimate over the whole month of August with the two elevation angle cutoff values. The mean bias is 2.5 cm.

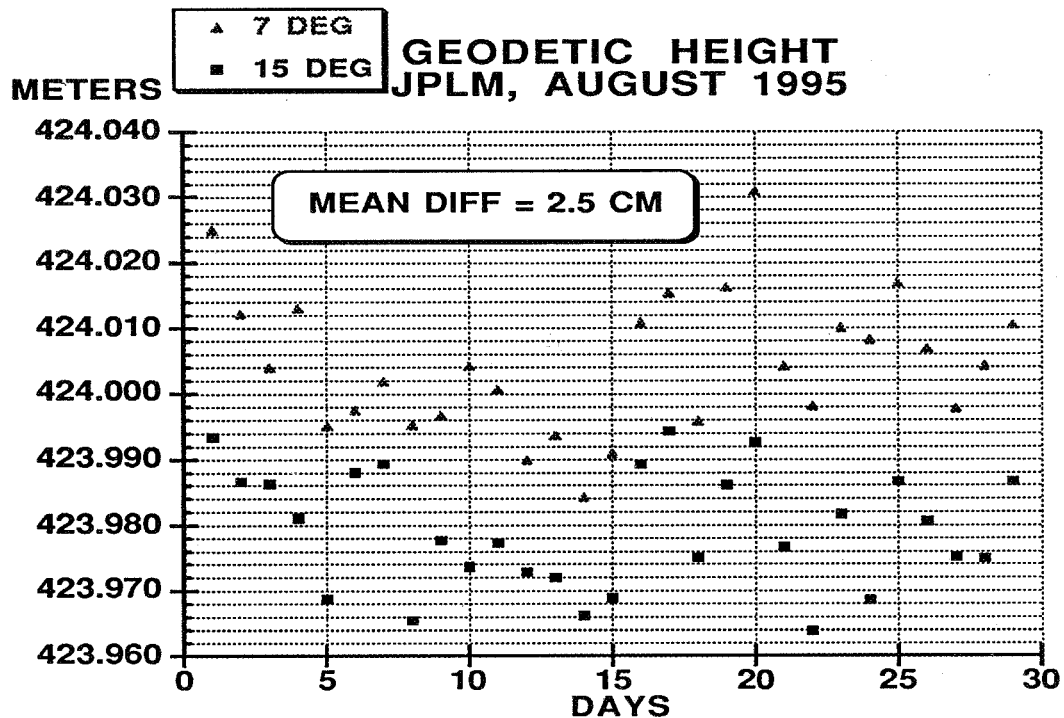


Fig. 3. Estimated geodetic height of JPLM with two elevation angle cutoff values.

Although WVR estimates were not available there, we compared GPS-based estimates of ZWD with the two elevation angle cutoffs for several other sites during January, 1996. We found that the size of the bias between the estimates varies from site to site and it can often be insignificant (less than 5 mm) for many. The largest bias was found at Fortaleza, Brazil (FORT) which is a relatively wet site. (See Figure 4.)

We hypothesize that the improvement in ZWD estimates at lower elevation angle cutoff, as observed at JPLM during August and October, 1995, is due to the reduction in the correlation between ZWD and station height. More experimentation is required in order to establish that this phenomenon is not site/receiver dependent.

In general, lowering the elevation angle cutoff did not have a detrimental effect on station position repeatabilities over a month. It suggests that carrier phase multipath may not be very damaging at 7 degrees elevation.

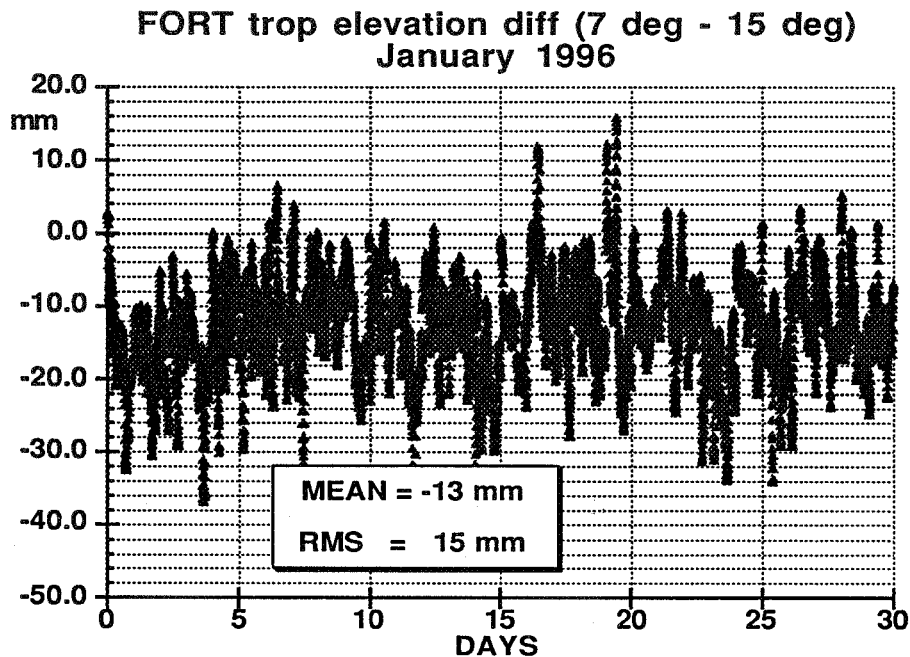


Fig. 4. Difference in ZWD estimates obtained with elevation angle cutoff values of 15 degrees and 7 degrees.

EFFECTS OF GPS YAW ATTITUDE MISMATCHING

GPS satellites display a rather complicated yaw attitude behavior during crossing of the Earth shadow (Bar-Sever et al., 1996, Bar-Sever, 1996). Mismatching this behavior is especially harmful in precise-point-positioning. In this experiment we estimated ZWD at various sites twice: Once with the new yaw attitude model (Bar-Sever, 1996) and once with the old yaw attitude model (the basic ROCK model) that is still in use in many geodetic software systems.

Assuming now that the TZD estimates obtained with the new yaw model are “truth”, and subtracting these estimates from estimates obtained with the ROCK yaw model, there are many cases where the differences significantly exceed 1 cm. Figure 5 depicts examples for FORT and BRMU. TZD values for BRMU (after subtracting the mean), estimated without the yaw model, are also presented in Figure 1 in order to demonstrate that the peaks in the error figure are indeed associated with anomalous features in the estimated value. All the peaks in Figure 1 correspond to epochs of observing an eclipsing satellite during its yaw maneuver. These errors may be unacceptably large for some applications. Errors in TZD are equivalent to errors in ZWD.

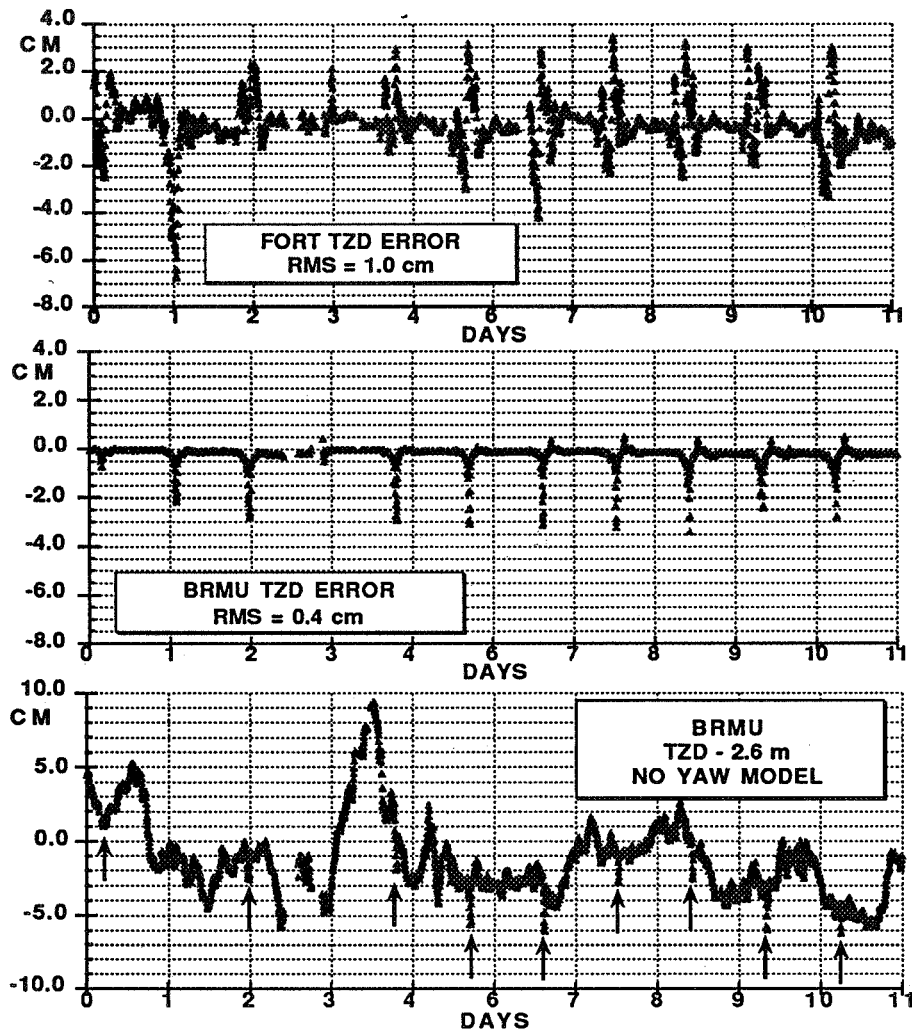


Fig. 5. Effects of omitting the GPS yaw model on estimates of total troposphere zenith delay (TZD) for FORT and BRMU. Estimates of TZD with the full yaw model (with estimated yaw rates) are considered truth. Top: TZD errors for FORT. Middle: TZD errors for BRMU. Bottom: estimated TZD for BRMU after a mean of 2.6 m was taken out and when GPS yaw model was not used. The arrows indicate the anomalous features of the estimates that correspond to the peaks in the error middle figure.

EXTRACTING A SIGNAL FROM THE POST-FIT RESIDUALS

It is a common notion that some tropospheric signal is still present in the carrier phase post-fit residuals. In order to test this notion and its utility for ZWD retrieval, post-fit residuals from receiver-transmitter links with elevation angles greater than 60 degrees were added to the estimated ZWD. If more than one link exists at an epoch, the residuals from all the links were averaged. Crude editing was used to exclude residuals larger than 8 mm. The "corrected" ZWD estimates were then compared to the WVR estimates. This experiment was carried out for the 15 degrees elevation cutoff case (that had a large bias wrt the WVR estimates) and for the 7 degrees elevation cutoff case. The results are summarized in Figure 6. Epochs for which no corrections were available were removed from the statistics.

When residual corrections were applied, the biases with respect to the WVR estimates decreased in both cases, more so for the 15 degrees elevation cutoff case. But in both cases the RMS increased. For the 15 degrees elevation cutoff case the bias decreased for each individual day out of the 18 days in August. In the 7 degrees elevation cutoff case the bias decreased on most individual days. These results support the notion that there is tropospheric signal in the carrier phase post-fit residuals but they also demonstrate that there is a considerable level of noise there. The noise level in the correction may be reduced perhaps, with a more sophisticated editing scheme, but there is no doubt that there is not enough signal in the post-fit residuals to offset the large bias in the estimates. Low elevation angle residuals, though, could be more useful in correcting line-of-sight wet delay because they are expected to contain larger tropospheric signal, in proportion to the larger air mass the signal traverses.

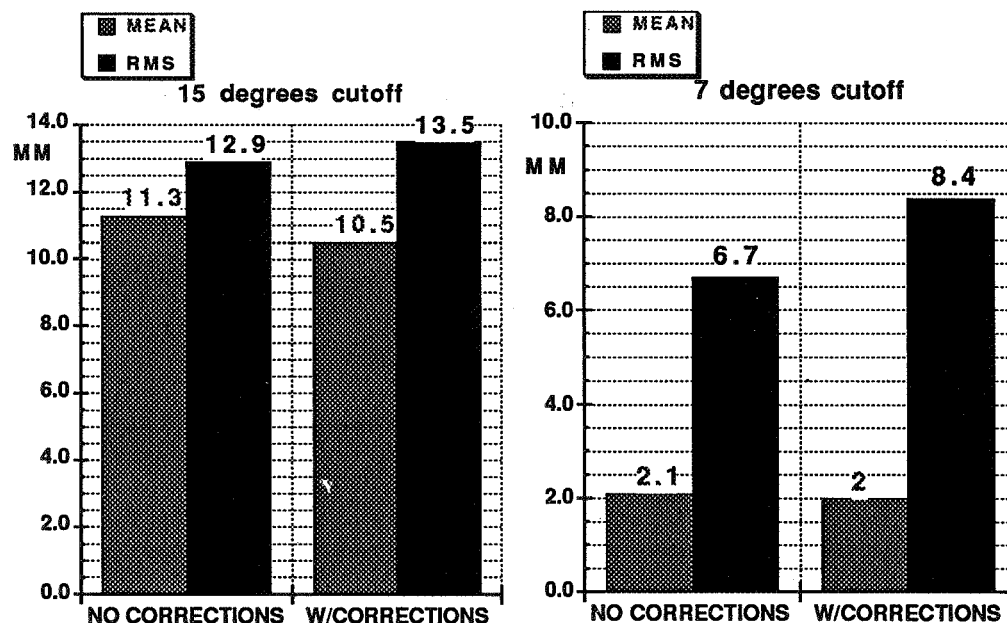


Fig 6. Effects of adding "zenith" residuals to ZWD estimates on the difference between the GPS-based estimates and the WVR estimates.

NEAR REAL TIME ESTIMATION STRATEGIES

To serve as useful input to numerical weather prediction models, the GPS-based estimates of PWV would need to be available within several hours after the data have been collected. In contrast, GPS-based PWV estimates described in the previous sections were produced using precise GPS orbits and clock obtained by processing data from a global network of ~30 GPS receivers and are available 2-4 days after data has been collected. Therefore, it is currently not possible to use precise GPS orbits and clocks as the basis for a system to provide NRT PWV estimates. For this reason, we have investigated the use of "predicted" GPS orbits as an alternative. It should be clear that the results cannot be as accurate as those obtained with precise orbits and clocks. The minimal level of accuracy demanded from the NRT PWV is application-dependent and has not been established yet. In this study, rather arbitrarily, we set the accuracy goal at 2 mm RMS for PWV (approximately 12 mm RMS for ZWD).

The predicted GPS orbits used in this study were obtained by fitting an orbit to four consecutive days of precise daily solutions, adjusting for 6 epoch state parameters and eight additional empirical parameters. The solution was then extrapolated forward using the satellite's dynamics. Orbit error increased quadratically, in this scheme, up to a level of two meters RMS after two days.

Because of Selective Availability (SA) satellite clocks cannot be extrapolated. Hence the need to estimate them (or difference them out). This requires the simultaneous processing of at least two ground stations. We have found that, under certain circumstances, no more than two stations are needed. This forms the simplest scheme for NRT retrieval of ZWD.

When one clock is held as a reference it is possible to solve for the other station clock as well as the ZWD for both stations, and all observed GPS clocks, with a technique equivalent to double differencing. This technique imposes some constraints on the selection of the second station. One of the stations is considered the target of the ZWD estimate. The other is brought in to provide clock resolution. Its ZWD may, or may not, be desired. The two stations should not be too far apart. If they are, they will fail to form enough double differences. They should also not be too close. If they are, the normal equations will tend to be singular and troposphere at the two stations will be strongly correlated. We have found that separation of 200 km - 1000 km usually works well (Figure 7).

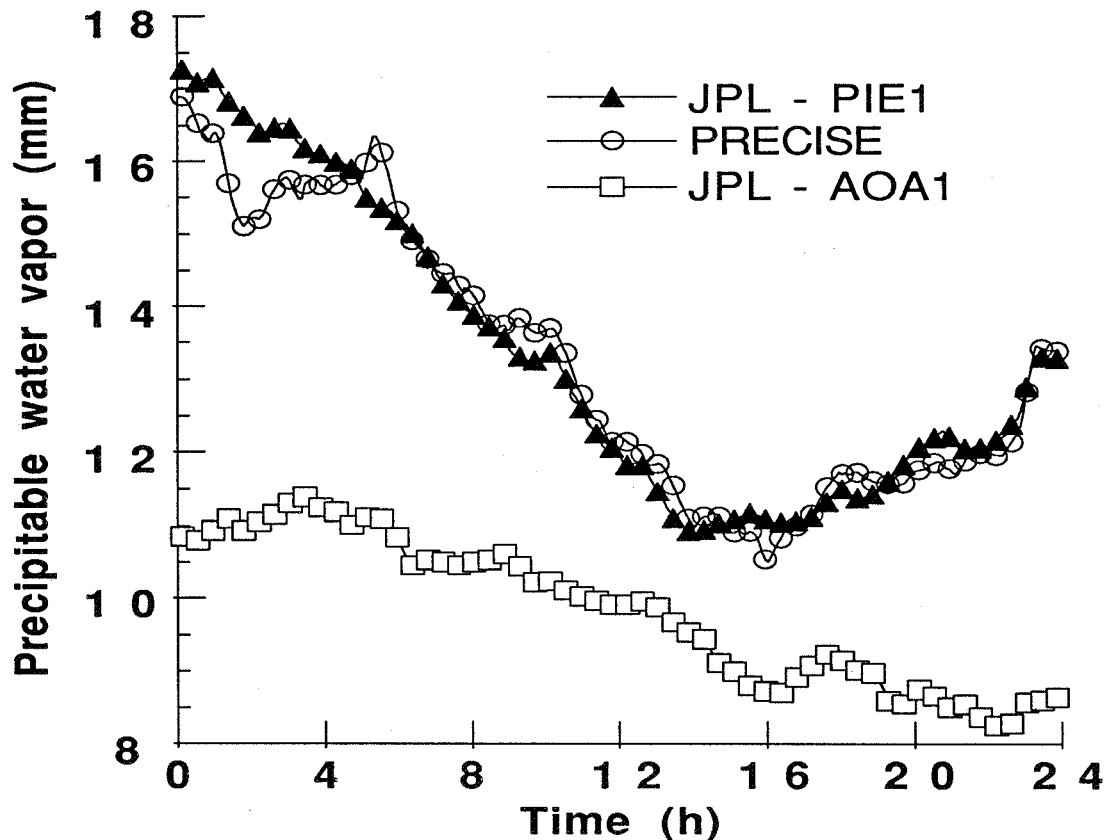


Fig 7. The effect of site separation on the accuracy of GPS-based PWV estimates. The JPL-PIE1 distance is ~1000 km while the JPL-AOA1 distance is ~60 km. The "precise" results are those obtained using post-processed GPS orbits and clocks rather than predicted orbits.

The degradation in the quality of the predicted orbit causes, in turn, a degradation in the quality of the ZWD estimated (Figure 8). It is desired, therefore, that the prediction period be minimized. If orbit errors are potentially too large, a third station can be brought in. The three-station differential solution has enough data strength to adjust the GPS orbit. Moderate baselines between all three stations should be maintained for best results. (Figure 9.)

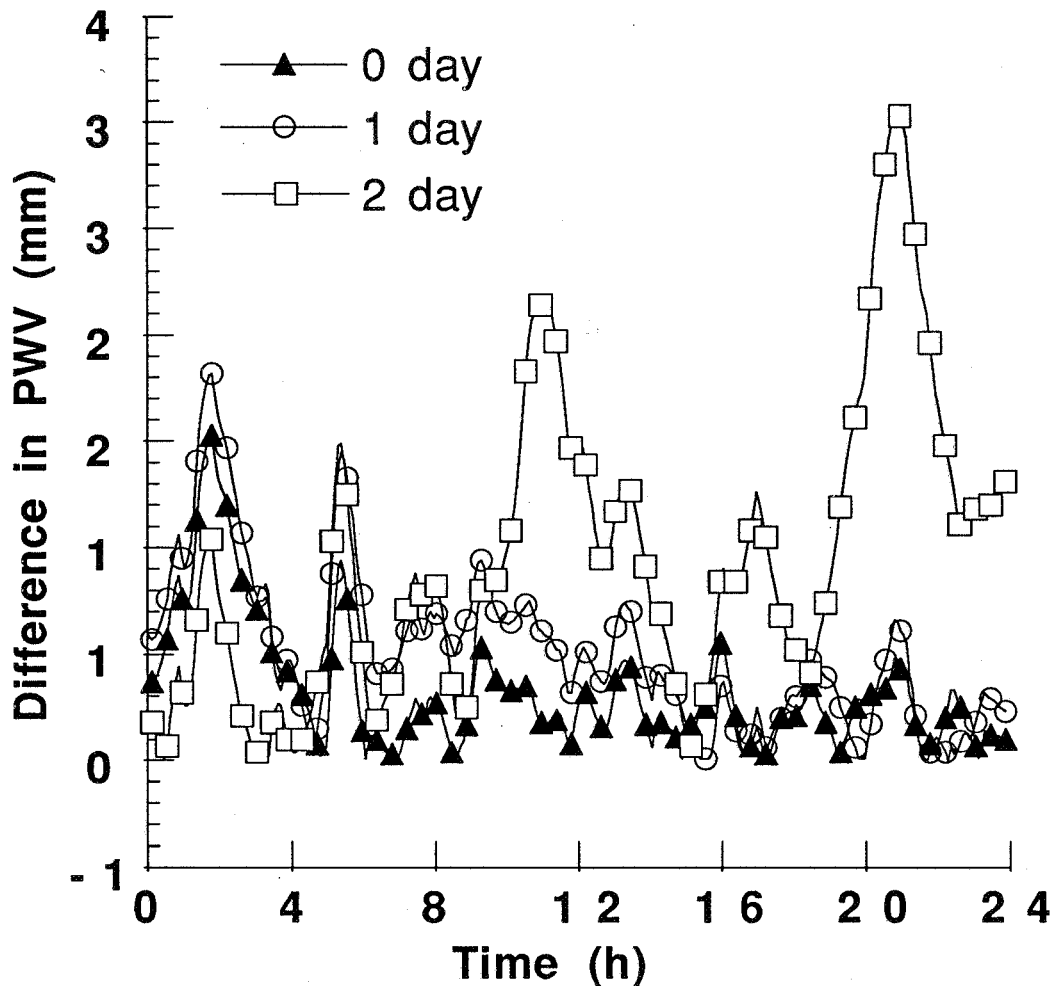


Fig 8. The effect of GPS orbit prediction period on the accuracy of the PWV estimates. The "0 day" graph corresponds to estimates obtained with precise GPS orbits and clocks and no prediction. The "1 day" graph corresponds to estimates obtained using GPS orbits predicted 24 hours. The "2 day" graph corresponds to estimates obtained using GPS orbits predicted 48 hours.

In NRT applications data will arrive at the processing center in small batches. If the batch length is too short there will not be enough data to resolve the ZWD properly, given the temporal correlation of the troposphere delay model. In our test, a minimum of three hours was required to resolve the ZED reasonably well (Figure 10). Processing short batches is possible with proper initialization of the covariance matrix with the covariance of the previous batch.

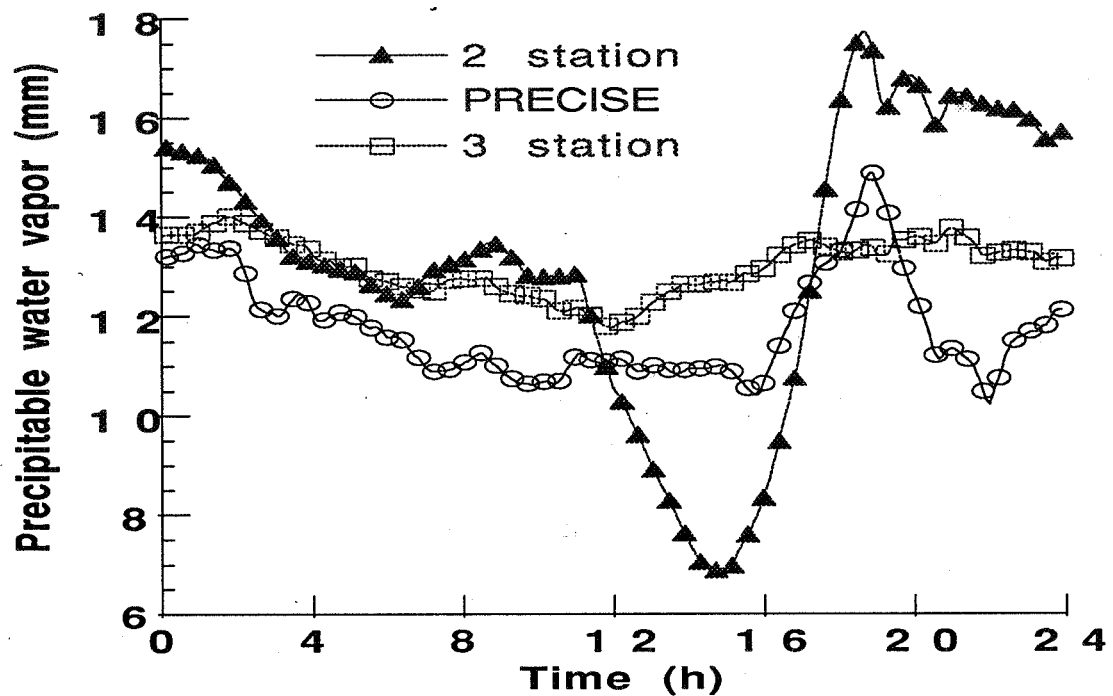


Fig 9. The effect of adding data from a third GPS receiver and adjusting the GPS orbits when estimating PWV values. The two station case used JPL and Pietown, and the three station case added data from LEX1.

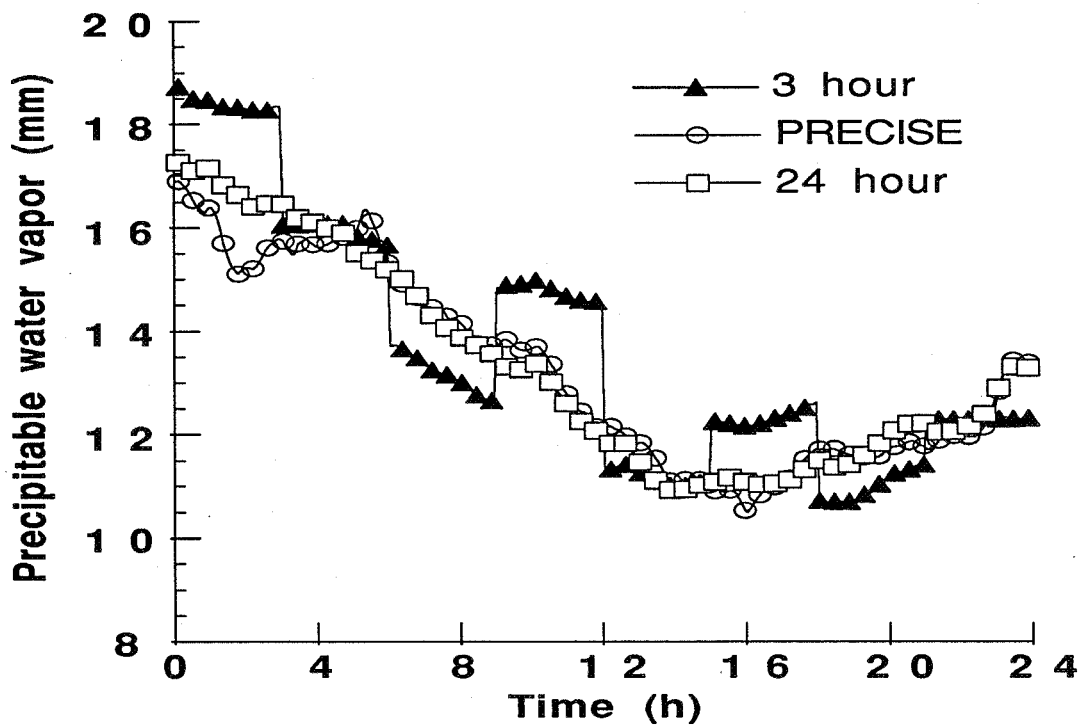


Fig 10. The effect of decreasing the span of the data on the accuracy of GPS-based estimates of PWV. These results were obtained from data recorded at the JPL and Pietown sites.

ACKNOWLEDGMENT

The work described in this paper was carried out in part by the Jet Propulsion Laboratory, California Institute of Technology, under contract with the National Aeronautics and Space Administration.

REFERENCES

Bar-Sever, Y.E., Anselmi, J.A., Bertiger, W.I. and Davis, E.S., Fixing the GPS Bad Attitude: Modeling GPS Satellite Yaw During Eclipse Seasons. *Navigation*, Spring 1996.

Bar-Sever, Y.E., A New Yaw Attitude Model for GPS Satellites. To appear in *J. of Geodesy*, 1996.

Bevis, M., S. Businger, T.A. Herring, C. Rocken, R.A. Anthes and R.H. Ware, 1992, GPS Meteorology: Remote Sensing of Atmospheric Water Vapor using the Global Positioning System, *J. Geophys. Res.*, 97, 15787-15801.

Bevis, M., Businger, S., Chiswell, S., Herring, T.A., Anthes, R.A., Rocken, C. and Ware, R.H., GPS Meteorology: Mapping Zenith Wet Delays onto Precipitable Water, *Journal of Applied Meteorology*, Vol. 33, No. 3, March 1994.

Businger, S., Chiswell, S.R., Bevis, M., Duan, J., Anthes, A., Rocken, C., Ware, R.H., Exner, M., VanHove, T., Solheim, F.S., The Promise of GPS in Atmospheric Monitoring, *Bull. Am. Met. Soc.*, Vol. 77, No. 1, January, 1996.

Chiswell, S.R., Businger, S., Improved Severe Weather Forecasts Using GPS, IUGG XXI General Assembly, Boulder, CO, July, 1995.

Davis, J.L., T.A. Herring, I.I. Shapiro, A.E.E. Rogers, and G. Elgered, 1985, Geodesy by radio interferometry: Effects of atmospheric modeling errors on estimates of baseline length, *Radio Science*, 20, 1593-1607.

Elgered, G., Johansson, J.M., Lindgren, B., Using the Swedish GPS Network to Monitor the Atmospheric Water Vapor Content, IUGG XXI General Assembly, Boulder, CO, July 1995.

Keihm, S.J., 1991, Water vapor radiometer intercomparison experiment, Platteville, Colorado, March 1-14, 1991, Final Report for Battelle Pacific Northwest Laboratories on behalf of the Department of Energy, Jet Propulsion Laboratory, Internal Document, Doc. No. D-8898, Pasadena, CA.

Kuo, Y.H., Guo, Y.R. and Westwater, E.R., Assimilation of Precipitable Water Vapor into a Mesoscale Numerical Model, *Monthly Weather Review*, Vol. 121, No. 4, April 1993.

Lilly, D.K., and Perkey, D.J., Sensitivity of Mesoscale Predictions to Mesoscale Initial Data, Sixth Conference on Weather Forecast and Analysis of the Amer. Meteor. Soc., Albany, NY, 1976.

MacMillan, D.S., Atmospheric gradients from Very Long Baseline Interferometry Observations, *Geophys. Res. Lett.*, Vol. 22, No. 9, May 1995, pp 1041-1044.

Rocken, C., Ware, R., VanHove, T., Solheim, F., Alber, C., Johnson, J., Bevis, M. And Businger, S., Sensing Atmospheric Water Vapor With the Global Positioning System, *Geophys. Res. Lett.*, Vol. 20, No. 23, 1993, pp 2631-2634.

Runge, T.F., P.M. Kroger, Y.E. Bar-Sever and M. Bevis, 1995, Accuracy Evaluation of Ground-based GPS Estimates of Precipitable Water Vapor, *EOS Transactions*, American Geophysical Union, 1995 Fall Meeting, Vol. 76, F146.

Yuan, L., Anthes, R.A., Ware, R.H., Rocken, C., Bonner, W., Bevis, M. and Businger, S., Sensing Climate Change Using the Global Positioning System, *J. Geophys. Res.* Vol. 98, No. 14, pp 14925-14937, 1993.

Zumberge, J.F., Heflin, M.B., Jefferson, D.C., Watkins, M.M. and Webb, F.H., IGS Analysis Center 1994 Annual Report, JPL Publication 95-18, Jet Propulsion Laboratory, Pasadena, CA, September 1, 1995.

Ionosphere Maps - A New Product of IGS ?

- Summary -

J. Feltens

EDS at Orbit Attitude Division, ESA, European Space Operations Centre,
Robert-Bosch-Str. 5, D-64293 Darmstadt, Germany

The IGS workshop in Silver Spring was the first IGS workshop where a sub-session was dedicated to the ionosphere. The sub-session's aim was to find out how ionosphere products could enter into the IGS service palette. In preparation for this IGS workshop an intercomparison of ionosphere products computed at the different Analysis Centers was organized to provide material for the discussion.

A position paper was prepared by J. Feltens, and it was agreed between the different Analysis Centers to concentrate in each of their presentations on a special aspect that is relevant to the development of a common IGS product. Accordingly, the topics of the distinct presentations were widely spread:

- The presentation of CODE concerned the long-term analysis of routinely produced ionosphere maps and experiences made.
- The presentation of UNB provided an analysis of the effect of shell height on high precision ionosphere modeling.
- The presentation of JPL dealt with global ionosphere mapping using GPS.
- A second presentation of JPL pointed out the relevance of GPS/MET data for ionosphere modeling, namely for ionospheric profiling.
- The presentation of DLR showed comparison results of GPS-derived TEC maps with independent ionospheric probing techniques.
- The final presentation, that of ESOC, condensed the first results that came out of the intercomparison and pointed out related aspects of software developments at ESOC.

During the discussion that followed the presentations, four points crystallized out as the most important for next steps to progress. These points are listed in the following sections:

1 Completion of the 5 weeks intercomparison

The intercomparison is not yet complete in two aspects:

- 1) Until now only a general comparison was made to verify overall agreement between the ionosphere products that were computed at the different Analysis Centers. However, a detailed look has still to be made to find out reasons for systematic trends in disagreement and for high levels of disagreement and abnormal behaviour that appeared sometimes. Explanations must be found for those phenomena. Based on the knowledge earned from this closer analysis, repetitions of processing under changed conditions may become necessary, at least for representative parts of the 5 considered weeks.

- 2) Some Analysis Centers did not deliver their results for all 5 weeks yet; they should complete their products.

Finally it was agreed that the intercomparison should be completed within the next few months.

2 Agreement on common standards

The intercomparison showed, that a lot of different assumptions are made in the ionosphere processing at the different Analysis Centers. To achieve a unique IGS product, general standards must be agreed upon among the different Analysis Centers. Relevant topics that were identified in this direction are:

- An official ionosphere product format (IONEX) must be defined.
- A common reference frame (probably solar-magnetic) should be agreed upon.
- A reliable thin-shell elevation angle mapping function should be investigated for, since this could be a significant source of error (e.g. for the discrepancies detected in the satellite/receiver differential delay values between the Analysis Centers - as first intercomparison results show).
- A common ionospheric shell height should be agreed upon which would possibly take into account the temporal and spatial variation of the ionospheric shell height.
- A common elevation cutoff angle might be agreed upon.
- It must be found out in which form ionosphere products shall be provided to the IGS user community, e.g. VTEC values in the form of maps or in the form of model coefficients (VTEC maps in a geographic grid were favoured - model coefficients would necessitate providing also the reference frame). Does it make sense to distribute also differential delay values to IGS users (the majority opinion was not to distribute them)?
- Of the many mathematical models that are currently used only a few should be favoured for presenting global, regional and local VTEC.
- Grid distances must be agreed upon. Grid sizes must be selected so that no interpolation will be necessary to compare different VTEC maps (e.g. 3 degree grid size for global models and 1 degree grid size for regional and local models).
- Time delays in providing products and update times must be agreed upon (near-real time processing will be an important aspect).
- Some accuracy measures must be defined to give information about the VTEC map reliability. It is very essential that the GPS-derived VTEC maps are also verified regularly with respect to independent ionosphere probing techniques over a wide spread geographical area.
- Criteria, e.g. on weighting, must be defined on how to combine the VTEC maps of the different Analysis Centers to produce one official IGS VTEC map that will be provided to the IGS users.

The most efficient way to come to common standards is to delegate certain topics of the above list to dedicated working groups which will work out a proposal for the topic entrusted to them. Each proposal will be presented to the other groups for agreement. E.g. representatives of two Analysis Cent-

ers will have the task to work out a concept of the IONEX format, while members of other Analysis Centers will establish a proposal for a common reference frame. Then the proposals will be exchanged to achieve overall agreement. Once agreement is obtained, corresponding software should be exchanged between the Analysis Centers. This method will have two benefits: 1) Not everybody must take care of everything - which saves working time. 2) By the exchange of software it is ensured that everybody uses the same standards, e.g. for the coordinate transformation to transform into and out of the solar-magnetic reference frame, or to produce identically formatted IONEX files.

3 Continuation of e-mail discussion of results & coordination of future work

Considering the above two Sections 1 & 2, the e-mail discussion should be continued in two corresponding directions:

- 1) The analysis and interpretation of the intercomparison results shall encircle weak points in current ionosphere modeling and remove them.
- 2) Regarding the aspects stated under the above Section 2, and considering the experience that comes out of the intercomparison, common standards and requirements for each product must be defined.

Responsibilities for the Analysis Centers should be defined, depending on their experiences and interests. A timetable should be worked out for the different tasks to perform.

4 Preparation of a pilot phase in which ionosphere products are processed under pre-operational conditions

When tasks stated in the above Sections 2 & 3 are completed, a pilot phase shall be prepared in which ionosphere products are computed at the different Analysis Centers and combined into a common IGS product under quasi-operational conditions. This will also necessitate the establishment of related software. Once this works, the next step after this pilot phase will then be the routine processing and the official distribution of ionosphere products, i.e. making the ionosphere information really a new IGS product.

Additional remark

Additional input for the discussion in form of an e-mail message was provided by DLR, since no one from that Analysis Center could attend the IGS workshop. And there is one important remark in this message that was not covered in the above four sections:

- The designation "ionosphere models" in relation to the GPS-derived VTEC maps may create confusion, since they are not "models" like IRI or Bent, etc. "TEC mapping" or "ionospheric TEC information" are better expressions.

Page intentionally left blank

DAILY GLOBAL IONOSPHERE MAPS BASED ON GPS CARRIER PHASE DATA ROUTINELY PRODUCED BY THE CODE ANALYSIS CENTER

Stefan Schaer, Gerhard Beutler, Markus Rothacher, Timon A. Springer
Astronomical Institute, University of Berne
CH-3012 Bern, Switzerland

ABSTRACT

The Center for Orbit Determination in Europe (CODE) — one of the Analysis Centers of the International GPS Service for Geodynamics (IGS) — produces orbits, Earth orientation parameters, station coordinates, and other parameters of geophysical interest on a daily basis using the *ionosphere-free* linear combination of the doubly differenced GPS carrier phase observations.

Since January 1, 1996, daily global ionosphere maps are routinely estimated as an *additional* product by analyzing the so-called *geometry-free* linear combination, which contains the information on the ionospheric refraction. The Total Electron Content (TEC) is developed into a series of spherical harmonics adopting a single-layer model in a sun-fixed reference frame. For each day a set of TEC coefficients is determined which approximates the average distribution of the vertical TEC on a global scale.

After re-processing all IGS data of the year 1995, a long-time series of TEC parameters is at our disposal indicating that reasonable *absolute* TEC determination is possible even when applying an *interferometric* processing technique. The global ionosphere maps produced are already used in the CODE processing scheme to improve the resolution of the initial carrier phase ambiguities. Spaceborne applications (e.g. altimetry) may benefit from these rapidly available TEC maps. For ionosphere physicists these maps are an alternative source of information about the *deterministic* and *stochastic* behaviour of the ionosphere, that may be correlated with solar and geomagnetic indices and compared to theoretical models.

CODE TEC MAPPING TECHNIQUE

Let us briefly review the TEC modeling features as developed by (Wild, 1994) and those currently used by the CODE Analysis Center for the global (and regional) applications. GPS-derived ionosphere maps are based on the so-called *single-layer* or *thin-shell* model with a simple mapping function. It is assumed that all free electrons are concentrated in a shell of infinitesimal thickness. The height of this idealized layer is usually set to the height of the maximum electron density expected. Furthermore the electron density E —

the surface density of the layer — is assumed to be a function of geocentric latitude β and sun-fixed longitude s .

The *local* ionosphere models presented by (Wild, 1994) were described with a two-dimensional Taylor series expansion. Such local TEC models have proved their usefulness on many occasions. Nevertheless, this TEC representation is *not* well-suited for *global* models because of limitations in the (β, s) -space. Therefore we decided to develop the global TEC into spherical functions. We write the surface density $E(\beta, s)$ representing the TEC distribution on a global scale as

$$E(\beta, s) = \sum_{n=0}^{n_{\max}} \sum_{m=0}^n \tilde{P}_{nm}(\sin \beta) \cdot (a_{nm} \cos ms + b_{nm} \sin ms) \quad \text{with } t \in [t_i, t_{i+1}] \quad (1)$$

where

- n_{\max} is the maximum degree of the spherical harmonic expansion,
- β is the geocentric latitude of the intersection point of the line receiver-satellite with the ionospheric layer,
- $s = t + \lambda - \pi$ is the *mean* sun-fixed longitude of the ionospheric pierce point, which corresponds to the local mean solar time neglecting an additive constant π (or 12 hours),
- t is the Universal Time UT (in radians),
- λ is the geographic longitude of the ionospheric pierce point,
- $[t_i, t_{i+1}]$ is the specified period of validity (of model number i),
- $\tilde{P}_{nm} = \Lambda(n, m) \cdot P_{nm}$ are the *normalized* associated Legendre functions of degree n and order m based on the normalization function $\Lambda(n, m)$ and the unnormalized Legendre functions P_{nm} , and
- a_{nm}, b_{nm} are the *unknown* TEC coefficients of the spherical functions, i.e. the global ionosphere model parameters to be estimated.

Another essential modification of our TEC measurement technique has to be emphasized. The CODE Analysis Center of the IGS produces precise orbits and Earth orientation parameters on a daily basis by analyzing the *ionosphere-free* linear combination of doubly differenced phase observations. As a result of this, *cycle-slip-free* portions of L1 and L2 phase observations are readily available for every day. Consequently the *zero-difference* observable was replaced by the *double-difference* phase observable due to operational considerations. We are fully aware of the fact that by using *double-* instead of *zero-differences* we lose parts of the ionospheric signal, but we have the advantage of *clean* observations. Moreover, we are *not* affected by the degradation of the code measurements under the regime of Anti-Spoofing (AS). This advantage may be “lost” when the next generation of precise code receivers will become available. To get more information about the “new” TEC mapping technique we refer to (Schaer et al., 1995).

IMPLEMENTATION INTO THE CODE PROCESSING SCHEME

The computation of Global Ionosphere Model (GIM) parameters has been completely integrated into the Bernese GPS Software (Rothacher et al., 1996a). The scripts to automate the GIM production were prepared at the end of 1995.

Since January 1, 1996, the GIM estimation procedure is running in an operational mode. Several GIM products are derived every day (Rothacher et al., 1996b):

- (i) Ambiguity-free one-day GIMs are estimated right prior to the ambiguity resolution step. These GIMs are subsequently used to improve the resolution of the initial carrier phase ambiguities on baselines up to 2000 kilometers.
- (ii) Improved GIMs (ambiguity-fixed, with single-layer heights estimated) are derived after ambiguity resolution.

At present, the GIM files containing the TEC coefficients for one day are available with a delay of 4 days.

The main characteristics of the daily GIMs produced by the CODE Analysis Center may be summarized as follows: The *geometry-free* linear combination of double-difference carrier phase observations is processed performing a least-squares adjustment of the observations of the complete IGS network to extract the global TEC information. One observation epoch per 3 minutes is processed using an elevation cut-off angle of at present 20 degrees. Note that — even under AS — *no* restrictions concerning receiver types or satellites have to be made in our approach. The global TEC distribution is represented over 24 hours by spherical harmonics up to degree 8 in a geographical reference frame which is rotating with the *mean* Sun. We adopt a spherical ionospheric shell in a height of 400 kilometers above the Earth's mean surface.

Let us mention that we estimate furthermore *regional* ionosphere maps for Europe based on about 30 European IGS stations in a fully automatic mode since December 1995. These ionosphere maps are used in the processing scheme of the European cluster to support the Quasi-Ionosphere-Free (QIF) ambiguity resolution strategy, too. A description of the QIF strategy is given in (Mervart and Schaer, 1994) and (Mervart, 1995). The European TEC maps are *not* discussed in this article.

Re-Processing of the Year 1995

Supported by the Bernese Processing Engine (BPE), six parallel CPUs, and a powerful data archive system, the re-processing of the entire IGS data set of the year 1995 — GIM products only — could be performed without major problems within eight days.

LONG-TIME SERIES OF DAILY GLOBAL IONOSPHERE MAPS

At present (March 1996), the CODE Analysis Center is processing the data of about 75 globally distributed stations of the world-wide GPS tracking network of the IGS. Figure 1 shows the stations used by CODE.

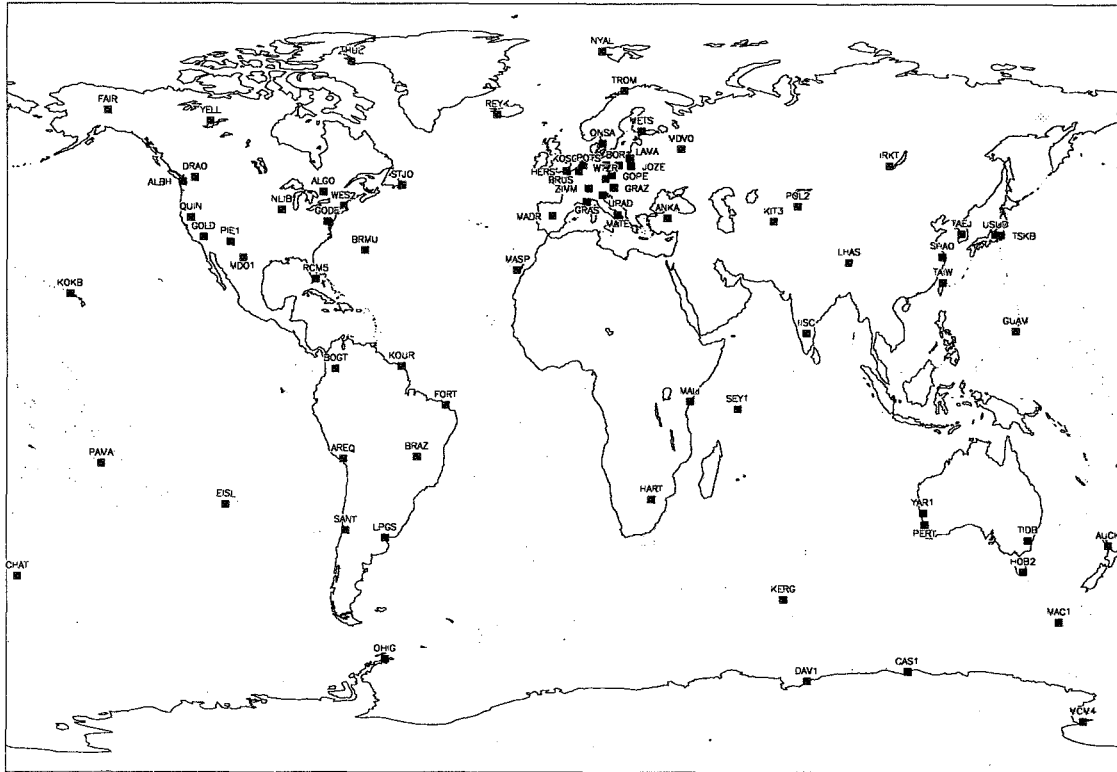


Figure 1. IGS stations used by CODE in 1996.

After re-processing all IGS data of the year 1995 and gathering already generated 1996 GIMs, we may interpret a long-time series of daily global ionosphere maps covering a time span of 427 days, from day 001, 1995 to day 062, 1996 (GPS weeks 782 to 842). This GIM series is represented by thousands of parameters, hence we have to limit the following discussion to few *special* TEC parameters, only.

Important TEC Parameters Describing the Deterministic Part

We already showed in (Schaer et al., 1995) that the zero-degree TEC coefficient a_{00} may be interpreted as the *mean* TEC E_0 per square meter which can be easily converted to the *total* number of ionospheric electrons in the shell. For that reason the quantity E_0 is an excellent parameter to roughly describe the deterministic part of the ionosphere. Figure 2 brings the evolution of the global TEC into focus showing the mean TEC E_0 and, in addition, the *maximum* TEC which has also been extracted from the CODE GIMs. The TEC values are given in so-called TEC Units (TECU), where 1 TECU corresponds to 10^{16} free electrons per square meter. Remember that our one-day GIMs approximate an average TEC distribution over 24 hours, hence our maximum TEC values have to be interpreted accordingly. The three non-AS periods within the time period considered are indicated by dashed lines.

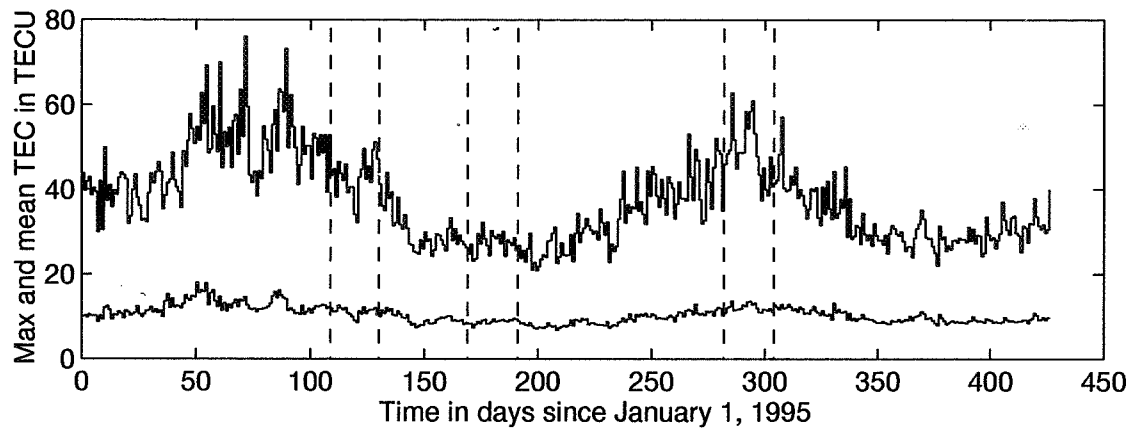


Figure 2. Maximum and mean TEC extracted from the CODE GIMs roughly describing the *deterministic* part of the ionosphere.

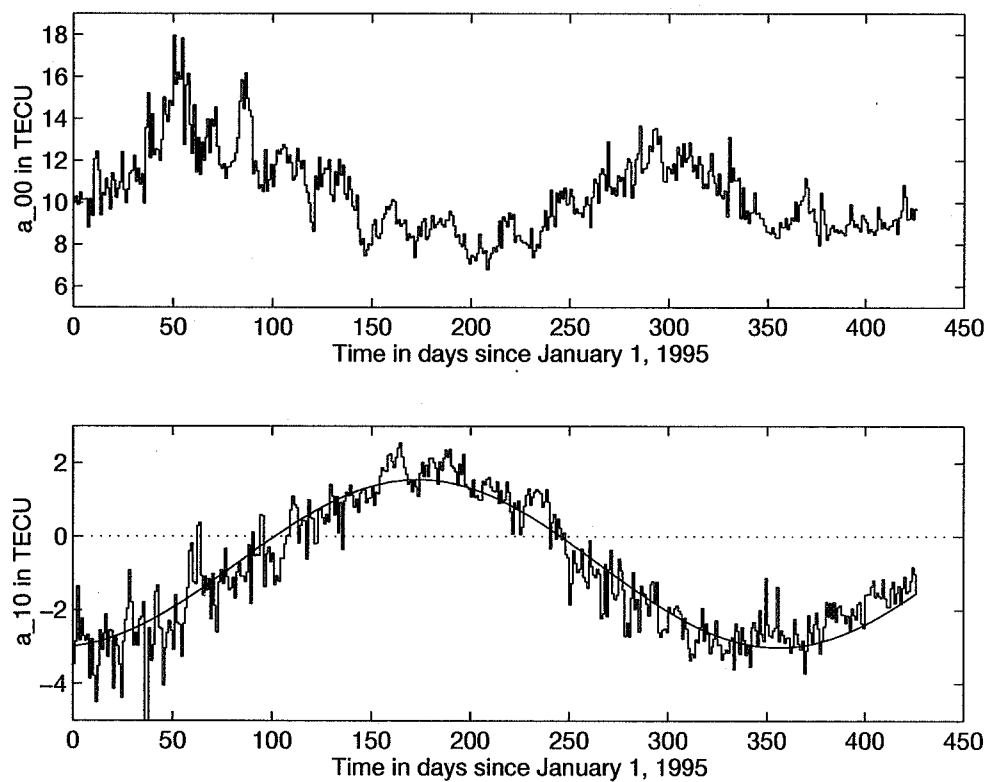


Figure 3. (a) zero-degree TEC coefficient a_{00} (*mean* TEC E_0) and (b) the first-degree coefficient a_{10} which mainly describes the zonal variation.

Figure 3 shows two special TEC parameters of the GIM representation (1) namely the coefficients a_{00} and a_{10} . The zero-degree coefficient a_{00} which corresponds to the mean

TEC E_0 already shown in Figure 2 is plotted in a larger scale here. The variations of the mean TEC even under low-activity conditions is quite impressive. Minima and maxima correspond to 6.8 and 18.0 TECU respectively, or, expressed in number of free electrons, to $3.9 \cdot 10^{31}$ and $1.03 \cdot 10^{32}$ free electrons. The first-degree coefficient a_{10} which describes the latitudinal variation of the global TEC distribution is shown in Figure 3b. The annual variation caused by the inclination of the equatorial plane with respect the ecliptic plane may be seen easily.

A newer example of a CODE GIM (with 64 contributing stations) given in the solar-geographical coordinate system is shown in Figure 4, where the latitude range covered is indicated by two dashed lines. Each individual GIM is parameterized with 81 TEC coefficients.

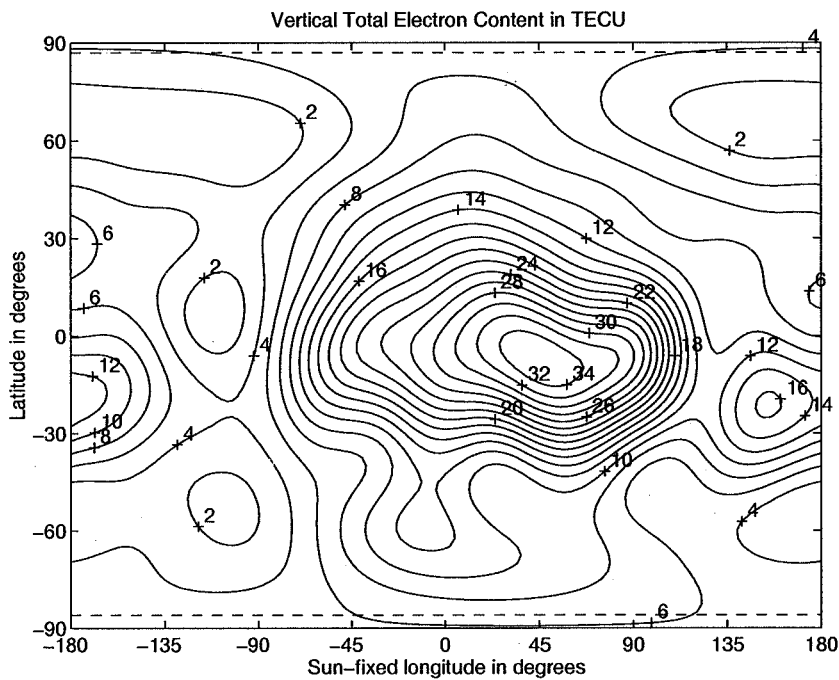


Figure 4. Global Ionosphere Map (GIM) for day 073, 1996.

Derivation of Mean Ionosphere Maps

Let us extract *mean* ionosphere maps — e.g. monthly maps from our daily results. Such maps may be easily derived by averaging the TEC coefficients a_{nm} and b_{nm} over certain time periods. An example is given in Figure 5. Mean GIMs primarily contain average TEC information as visualized in Figure 6 which shows an equatorial cross-section of the mean TEC structure of Figure 5 and in addition the temporal derivative of $E(0, t)$. Here we may recognize for instance that (a) between the end of evening twilight and the beginning of morning twilight the zenith TEC is statistically decreasing with more or less a constant

rate or that (b) the maximum TEC is reached at about 2 hours after midday on average, confirming a well known phenomenon.

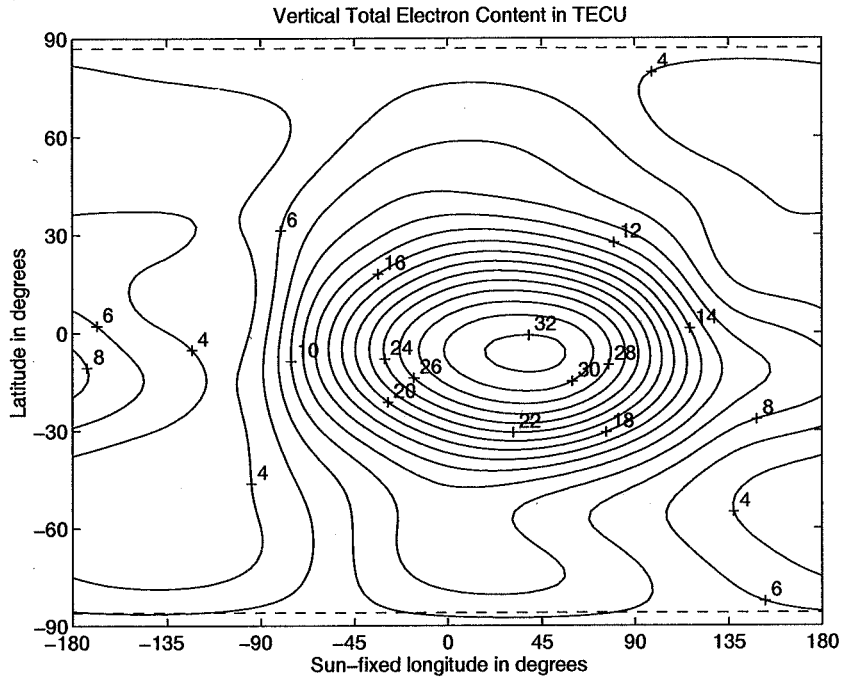


Figure 5. Mean global ionosphere map averaged over all 427 days (61 weeks).

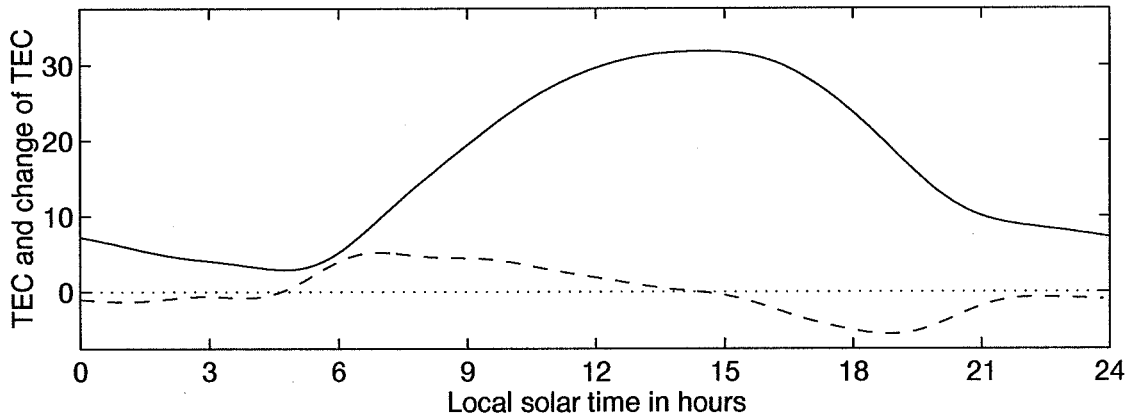


Figure 6. TEC (in TECU) and change of TEC (in TECU/hours) for an average equatorial TEC profile.

Monitoring of the Stochastic Part

At present only one parameter describing the “agitation” of the ionosphere is at our disposal, namely the a posteriori RMS error of unit weight of the least-squares adjustment, which mainly reflects the ionosphere-induced noise of the geometry-free phase observable caused by ionospheric disturbances. The resulting RMS values converted from meters to units of TECU are shown in Figure 7. Notice that we cannot detect any jumps in the evolution of this quantity at the boundaries of the three non-AS periods indicated by dashed lines. This fact again confirms that the quality of CODE GIMs is *not* affected by Anti-Spoofing.

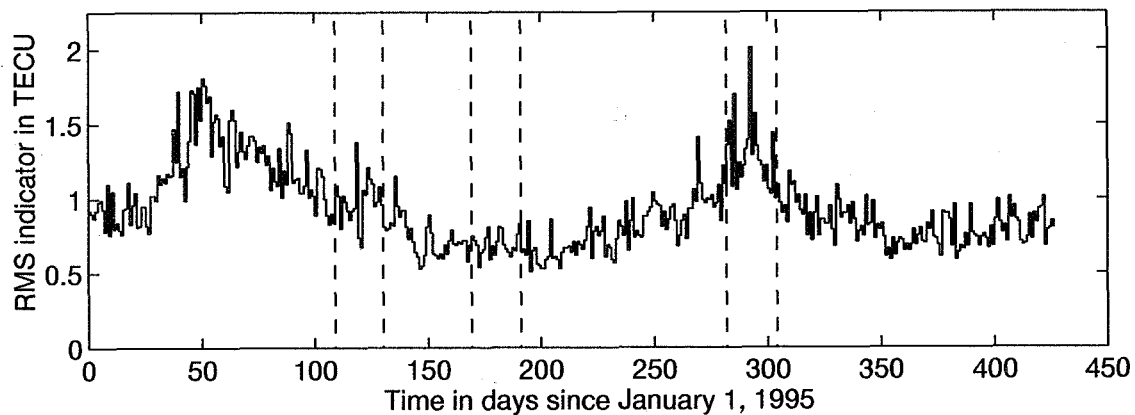


Figure 7. RMS indicator, characterizing the *stochastic* part of the ionosphere on a global scale.

Estimation of Global Shell Heights

We mentioned already that we also derive global ionosphere models where in addition to the TEC coefficients the shell height of the ionosphere is set up as an unknown parameter. In this case the parameter estimation problem is no longer a linear one, which means that we have to improve the GIMs iteratively starting from an initial adjustment. Our daily estimates of the shell height are shown in Figure 8. The dotted line indicates the a priori value used and the solid line shows a linear approximation which lies significantly above the 400-kilometer level generally adopted. We recognize a small linear trend, but this should be interpreted with care because it is based on a trivial shell height model and a mapping function which has to be refined. General considerations concerning the shell height may be found in (Komjathy and Langley, 1996).

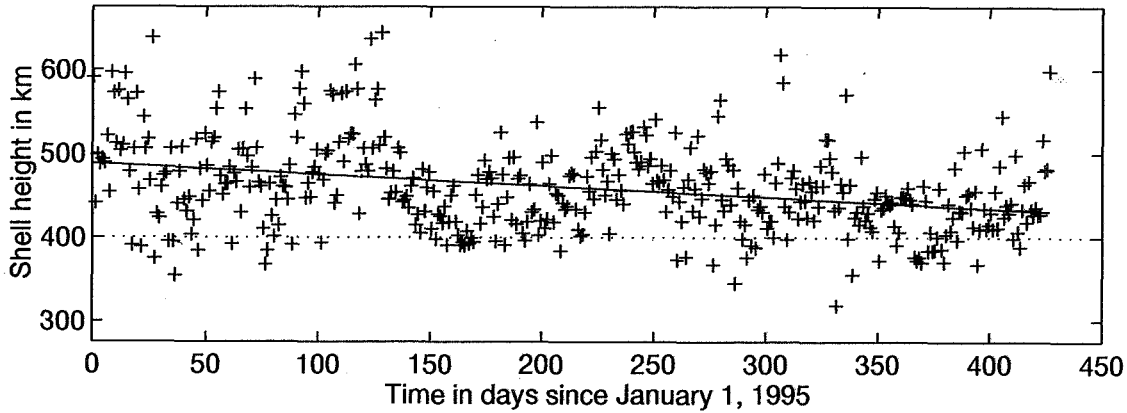


Figure 8. Daily estimates of a common shell height.

Correlation With Solar and Geomagnetic Indices

We may now correlate our TEC coefficient series with solar and geomagnetic indices like *Sunspot number*, *solar radio flux number*, *Kp index*, *Ap index*, etc. This has not been done in detail yet, but we may summarize that

- (i) the dominant double peak within the time span analyzed (see Figures 2 and 9a) is recognizable in solar and geomagnetic parameter series as well (see Figures 9b to 9e),
- (ii) the times of increasing or decreasing *mean* TEC are highly correlated with the times where the solar activity level changes (see Figures 9b and 9c),
- (iii) when performing a spectral analysis the evolution of the mean TEC shows a prominent period of 25 to 30 days which comes from the differential rotation of the Sun, and
- (iv) our RMS indicator (see Figure 7) representing the *stochastic* behaviour of the ionosphere seems to be well correlated with the *Ap* index which characterizes the activity of the geomagnetic field.

Finally the GPS-derived mean TEC E_0 and four solar and geomagnetic parameters obtained from the National Geophysical Data Center, Boulder, Colorado, USA are compared in Figure 9.

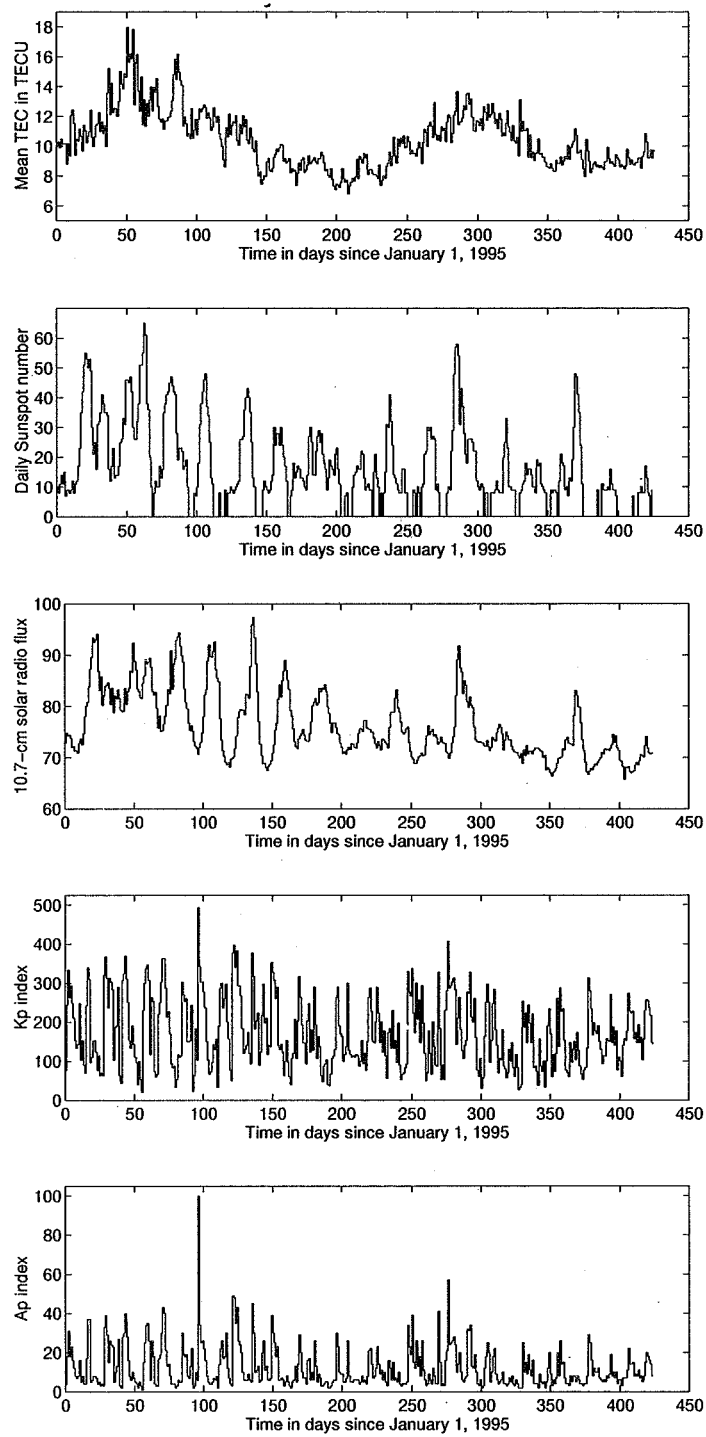


Figure 9. (a) Mean TEC derived by CODE, (b) daily Sunspot number, (c) Ottawa 10.7-cm solar radio flux (in solar flux units), (d) Kp index, and (e) Ap index.

CONCLUSIONS AND OUTLOOK

The global IGS core network of permanently tracking dual-frequency GPS receivers provides a unique opportunity to *continuously* monitor the Vertical Total Electron Content on a global scale. A first long time series of TEC parameters indicates that *absolute* TEC determination is possible even when applying *interferometric* processing techniques. The CODE Analysis Center of the IGS shows that the production of Global Ionosphere Maps (GIMs) in an *automatic* mode is possible — even under Anti-Spoofing (AS) conditions. *No* restrictions concerning receiver types or satellites have to be observed in this approach. If we support the global QIF ambiguity resolution using our one-day GIMs, the number of *resolved* ambiguity parameters is significantly higher. Since January 1, 1996 85 % instead of 75 % of the ambiguity parameters are resolved.

GIM files containing the global TEC information in an internal data format are available via the anonymous FTP server of the CODE processing center starting with January 1, 1995. *Regional* ionosphere maps for Europe routinely generated since December 1995 are available on special request. If there is an interest in *rapid* GIMs, we might consider to establish such a service as part of our *rapid* orbit service. These GIMs (with less contributing stations) could be made available with a delay of about 12 hours, only.

At present one may *not* speak of a high degree of consistency of ionosphere maps produced by several groups analyzing GPS data, therefore TEC comparisons within the IGS and other interested organizations are necessary. Spaceborne applications like e.g. altimetry experiments might be used to validate GPS-derived ionosphere maps, too. Another essential aspect for the future development is an interface between the IGS and the ionosphere research community. We foresee that with high probability the IGS will be heavily involved in the ionosphere research area.

Monitoring the spacial and temporal variability of the *stochastic* part of the ionosphere by analyzing the *time-derivative* of phase observations using similar methods as for the global TEC determination will be our focus in the near future.

REFERENCES

- Beutler, G., I. Bauersima, W. Gurtner, M. Rothacher, T. Schildknecht, 1988, *Atmospheric Refraction and Other Important Biases in GPS Carrier Phase Observations*, Monograph 12, School of Surveying, University of New South Wales, Australia.
- Beutler, G., I. Bauersima, S. Botton, W. Gurtner, M. Rothacher, T. Schildknecht, 1989, Accuracy and biases in the geodetic application of the Global Positioning System, *Manuscripta Geodaetica*, Vol. 14, No. 1, pp. 28–35.
- Beutler, G., I.I. Mueller, R. Neilan, 1994, The International GPS Service for Geodynamics (IGS): Development and Start of Official Service on 1 January 1994, *Bulletin Géodésique*, Vol. 68, No. 1, pp. 43–51.
- Georgiadiou, Y. and A. Kleusberg, 1988, On the effect of ionospheric delay on geodetic relative GPS positioning, *Manuscripta Geodaetica*, Vol. 13, pp. 1–8.

- Komjathy, A. and R. B. Langley, 1996, *The Effect of Shell Height on High Precision Ionospheric Modelling Using GPS*, Paper presented at the IGS AC Workshop, Silver Spring, MD, USA, March 19–21, 1996.
- Lanyi, G. E. and T. Roth, 1988, A comparison of mapped and measured total ionospheric electron content using global positioning system and beacon satellite observations, *Radio Science*, Vol. 23, No. 4, pp. 483–492.
- Mannucci, A. J., B. D. Wilson, D.-N. Yuan, 1994, Monitoring Ionospheric Total Electron Content Using the GPS Global Network and TOPEX/POSEIDON Altimeter Data, *Proceedings of the Beacon Satellite Symposium*, Aberystwyth, Wales, July 1994.
- Mervart, L., G. Beutler, M. Rothacher, U. Wild, 1993, Ambiguity Resolution Strategies Using the Results of the International GPS Geodynamics Service (IGS), *Bulletin Géodésique*, Vol. 68, No. 1, pp. 29–38.
- Mervart, L. and S. Schaer, 1994, *Quasi-Ionosphere-Free (QIF) Ambiguity Resolution Strategy*, Internal report, Astronomical Institute, University of Berne, Switzerland.
- Mervart, L., 1995, Ambiguity Resolution Techniques in Geodetic and Geodynamic Applications of the Global Positioning System, *Geodätisch-geophysikalische Arbeiten in der Schweiz*, Band 53.
- Rothacher, M., G. Beutler, E. Brockmann, W. Gurtner, L. Mervart, S. Schaer, T. A. Springer, 1996, *The Bernese GPS Software Version 4.0: Documentation*, Astronomical Institute, University of Berne, Switzerland (in preparation).
- Rothacher, M., G. Beutler, E. Brockmann, L. Mervart, S. Schaer, T. A. Springer, U. Wild, A. Wiget, C. Boucher, H. Seeger, 1996, *Annual Report 1995 of the CODE Analysis Center of the IGS* (in preparation).
- Schaer, S., 1994, *Stochastische Ionosphärenmodellierung beim Rapid Static Positioning mit GPS*, Diplomarbeit, Astronomisches Institut, Universität Bern.
- Schaer, S., G. Beutler, L. Mervart, M. Rothacher, U. Wild, 1995, Global and Regional Ionosphere Models Using the GPS Double Difference Phase Observable, *Proceedings of the 1995 IGS Workshop*, Potsdam, Germany, May 15–17, 1995, pp. 77–92.
- Wild, U., 1993, Ionosphere and Ambiguity Resolution, *Proceedings of the 1993 IGS Workshop*, March 25–26, 1993, Berne, Switzerland, pp. 361–369.
- Wild, U., 1994, Ionosphere and Satellite Systems: Permanent GPS Tracking Data for Modelling and Monitoring, *Geodätisch-geophysikalische Arbeiten in der Schweiz*, Band 48.
- Wilson, B. D. and A. J. Mannucci, 1993, *Instrumental Biases in Ionospheric measurements Derived from GPS Data*, Paper presented at ION GPS 93, Salt Lake City, September 22–24, 1993.

The Effect of Shell Height on High Precision Ionospheric Modelling Using GPS

A. Komjathy and R.B. Langley

Both at: Geodetic Research Laboratory, Department of Geodesy and Geomatics Engineering
University of New Brunswick, P.O. Box 4400, Fredericton, N.B. E3B 5A3 Canada
Phone: 1-506-453-4698, Fax: 1-506-453-4943, email: w43y@unb.ca, lang@unb.ca

ABSTRACT

The dispersive nature of the ionosphere makes it possible to measure its total electron content (TEC) using dual-frequency Navstar Global Positioning System (GPS) observations collected by permanent networks of GPS receivers. One such network is that of the International GPS Service for Geodynamics (IGS). UNB has participated in an ionospheric experiment along with other ionospheric research groups under the auspices of the IGS and European Space Agency's European Space Operations Centre (ESA/ESOC). A 5 week long period of dual-frequency GPS measurements collected by IGS stations was designated as a test data set for the different research groups to analyse and produce TEC values and satellite-receiver differential delays. One of the primary goals of the experiment was to analyse the effect of geomagnetic disturbances on the ionospheric products. We have used dual-frequency GPS pseudorange and carrier phase observations from six European stations in the IGS network to derive regional TEC values and satellite-receiver differential delays.

In an earlier study we concluded that after processing data from 6 European stations collected over a 7 day period (the first 7 days of the ionospheric experiment organized by ESA/ESOC), we were able to follow highly varying ionospheric conditions associated with geomagnetic disturbances. We investigated the effect of using different elevation cutoff angles and ionospheric shell heights on the TEC estimates and satellite-receiver differential delays. These results pertaining to GPS week 823 have been presented earlier [Komjathy and Langley, 1996]. In our current research, we used 21 days' worth of data in a continuation of the study mentioned earlier with a more rigorous approach for ionospheric shell height determination which has been derived from the International Reference Ionosphere 1990 (IRI90) [Bilitza, 1990]. We looked at the effect of using ionospheric shell heights fixed at a commonly used altitude (400 km) on the TEC and differential delay estimates. We found differences in the differential delays between the two approaches of up to the 0.3 ns (≈ 1 total electron content unit – TECU) level and differences in the TEC estimates up to the 1 TECU (≈ 0.16 m delay on L1) level. We also compared our differential delay estimates with those obtained by other research groups participating in the experiment. We found agreement in the differential delays between three analysis centers at the 1 ns level.

INTRODUCTION

The electromagnetic signals from the GPS satellites must travel through the earth's ionosphere on their way to GPS receivers on or near the earth's surface. Whereas these effects may be considered a nuisance by most GPS users, they will provide the ionospheric community with an opportunity to use GPS as a tool to better understand the plasma surrounding the earth. Dual-frequency GPS observations can be used to eliminate almost all of the ionosphere's effect. To correct data from a single-frequency GPS receiver for the ionospheric effect, it is possible to use empirical models. We are conducting an on-going study to assess the accuracy and efficacy of such models.

We decided to include the new IRI90 model [Bilitza, 1990] in our ionospheric research after Newby [1992] investigated the International Reference Ionosphere 1986 (IRI86) model's performance. Earlier we used Faraday rotation data as "ground-truth" with which we compared the vertical ionospheric range error

corrections predicted by the Broadcast model of the GPS navigation message [Klobuchar, 1986] and the IRI90 model. For low solar activity, mid-latitude conditions we concluded that based on the comparison between the Broadcast and IRI90 models, both for day-time and night-time periods, the IRI90 model appeared to be more accurate than the Broadcast model [Komjathy et al., 1995a ; 1995b]. Since data from the GOES geostationary satellites that would provide the Faraday rotation measurements for use as “ground-truth” is no longer readily available, we have decided to use dual-frequency pseudorange and carrier phase GPS measurements to infer ionospheric TEC.

Early studies used single station observations to estimate the line-of-sight pseudo-TEC which is the sum of the satellite-receiver differential delays and the actual line-of-sight TEC (e.g., Lanyi and Roth [1988], Coco et al. [1991]). Recently the ionospheric community started applying multi-site fitting techniques to produce global and/or regional ionospheric maps with more accurate TEC and differential delay estimates. These ionospheric maps and differential delays are becoming freely accessible on the Internet. As an ionospheric observable, most research groups use a “phase-levelling” technique in which the integer ambiguity afflicted differences of the L1 and L2 (L1-L2) carrier phase measurements are adjusted by a constant value determined for each phase-connected arc of data using precise pseudorange measurements. This technique is widely used to estimate ionospheric model parameters as well as satellite-receiver differential delays (see, e.g., Gao et al. [1994], Sardon et al. [1994], Wilson and Mannucci [1994], and Runge et al. [1995]). It is also feasible to use double-differenced L1-L2 carrier-phase observations to estimate global or regional ionospheric models [Schaer et al. 1995]. The advantage of this latter technique is that by using the double-differenced ionospheric observable, one does not have to estimate the satellite-receiver differential delays as they are differenced away – although some of the resolution of the ionospheric signal is eliminated during the process. A technique used by Bishop et al. [1995] infers TEC and satellite-receiver differential delays by requiring maximum agreement between ionospheric measurements when the observed paths of two satellites cross.

ESTIMATION STRATEGY

The estimation strategy we used is described in Komjathy and Langley [1996] in detail. In this section, we will briefly summarize the basic principles of our technique to help explain the recent improvements we made to the algorithm. We model the ionospheric measurements from a GPS receiver with the commonly used single-layer ionospheric model using the observation equation:

$$I_r^s(t_k) = M(e_r^s) \cdot [a_{0,r}(t_k) + a_{1,r}(t_k) \cdot d\lambda_r^s + a_{2,r}(t_k) \cdot d\phi_r^s] + b_r + b^s$$

where

$I_r^s(t_k)$ is the L1-L2 phase measurement at epoch t_k made by receiver r observing satellite s ,

$M(e_r^s)$ is the thin-shell elevation angle mapping function projecting the line-of-sight measurement to the vertical with e_r^s being the elevation angle of satellite s viewed by receiver r at the subionospheric point – the intersection of the ray path of a signal propagating from the satellite to the receiver with a thin spherical shell (see, e.g., Schaer et al. [1995]),

$a_{0,r}, a_{1,r}, a_{2,r}$ are the parameters for spatial linear approximation of TEC to be estimated per station assuming a first-order Gauss-Markov stochastic process [Gail et al. 1993],

$d\lambda_r^s = \lambda_r^s - \lambda_0$ is the difference between a subionospheric point and the mean longitude of the sun,

$d\phi_r^s = \phi_r^s - \phi_r$ is the difference between the geomagnetic latitude of the subionospheric point and the geomagnetic latitude of the station, and

b_r, b^s refer to the receiver and satellite differential delay respectively.

The three parameters $a_{0,r}, a_{1,r}, a_{2,r}$ in the above equation are estimated for each station using a Kalman filter approach. The prediction and update equations for the state estimation are described by e.g.,

Schwarz [1987], Coster et al. [1992] and van der Wal [1995]. Due to the highly varying ionospheric conditions during the observation window processed, we allowed the model to follow a relatively high 1 TECU per 2 minutes change in the total electron content which resulted in the process noise variance rate of change being $0.008 \text{ TECU}^2 / \text{second}$ characterizing the uncertainties of the dynamic ionospheric model. For the variance of the measurement noise, we used 1 TECU^2 – the assumed uniform uncertainty in the observations.

We estimated the combined satellite-receiver differential delays for station Madrid. In a network solution, additional differential delay parameters for the rest of the stations have to be estimated based on the fact that the other receivers have different differential delays. Therefore, for each station other than station Madrid, an additional differential delay parameter was estimated which is the difference between the receiver differential delay between a station in the network and station Madrid. This technique is described by e.g., Sardon et al. [1994].

We chose a solar-geomagnetic reference frame based on sun-fixed longitude and geomagnetic latitude since the main reason for the ionosphere's existence is the interaction of ionizing radiation (principally from solar ultraviolet and x-ray emissions) with the earth's atmosphere and magnetic field [Langley, 1996]. Furthermore, the ionosphere varies much more slowly in sun-fixed reference frame than in an earth-fixed one. The use of such a reference frame results in more accurate ionospheric delay estimates when using Kalman-filter updating [Mannucci et al., 1995].

A parameter that affects the TEC estimation is the assumed height of the ionospheric shell which plays a role in computing the coordinates of the subionospheric points. It is also an input parameter of the $M(e^{\circ})$ mapping function (see equation). At this stage we use a simple $1/\cos(90^{\circ} - e^{\circ})$ mapping function. Later on, we plan on looking at other mapping functions that would reduce mapping function errors for low elevation angle satellites. The single-layer ionospheric model assumes that the vertical TEC can be approximated by a thin spherical shell which is located at a specified height above the earth's surface. This altitude is often assumed to correspond to the maximum electron density of the ionosphere. Furthermore, it is usually assumed that the ionospheric shell height has no temporal or geographical variation and therefore it is set to a constant value regardless of the time or location of interest. In Komjathy and Langley [1996], we looked at the effect of different fixed ionospheric shell heights of 300, 350, and 400 km and also included variable heights computed by the IRI90 model using F2 layer peak heights. We found that at the 2 TECU level, the ionospheric estimates using these specified heights agree depending on geographic location and time of the day. We also found that using different elevation cutoff angles (15° , 20° , and 25°) had an impact on TEC estimates at the 2 TECU level. These results should be considered only valid for the low solar activity conditions under which the estimates were made.

After the promising results of using the IRI90 model for ionospheric shell height determination, we decided to carry on with this investigation. In our current study, we use the IRI90 model to compute even more accurate ionospheric shell heights by integrating the predicted electron densities through the six subregions of the IRI90 profile. Ionospheric shell height predictions were obtained upon reaching 50 percent of the predicted total electron content during the numerical integration procedure using a step size of 1 km. We computed the predicted total electron content up to an altitude of 1000 km (see Figure 1), consequently, plasmaspheric electron content has not been considered at this stage but its effect should be less than about 50 percent of the night-time total electron content near sunspot minimum [Davies, 1990]. The omission of the plasmaspheric electron content has an effect primarily on the night-time TEC predictions at the 2 TECU level. We believe that this method provides an even more rigorous approach compared to what has been described in Komjathy and Langley [1996]. Note in Figure 1 that the predicted ionospheric shell height is always slightly above the height of the F2 layer peak electron density since the topside region of the ionosphere contains more electrons than the bottomside. The predicted ionospheric shell heights are used as input into our software for estimating TEC maps as well as satellite-receiver differential delays.

THE DATA SET

Along with several other research groups, we participated in an experiment to assess the capabilities of GPS data to provide TEC values. Organized under the auspices of the International GPS Service for Geodynamics (IGS) and the Orbit Attitude Division of the European Space Agency's European Space Operations Centre (ESA/ESOC), the experiment involves the processing and analysis of a 5 week long data set of dual-frequency GPS data from the stations of the IGS network (GPS weeks 823 through 827). We have analysed the GPS data sets from 6 of the European IGS stations. The stations are Madrid, Grasse, Matera, Brussels, Wettzell, and Onsala and are identified on the map in Figure 2. The differences in geomagnetic latitudes of stations Madrid, Grasse, and Matera are less than 5 degrees, and 3.3 degrees in the case of stations Brussels and Wettzell. Therefore, we can identify three distinct latitude regions in our test network (1. Madrid, Grasse, Matera; 2. Brussels, Wettzell; 3. Onsala). All 6 stations use Allen Osborne Associates TurboRogue receivers.

We processed 21 days' worth of data from the 6 stations spanning the time period 15 October to 4 November 1995 (GPS weeks 823, 824, and 825) during which a geomagnetic disturbance occurred [NGDC, 1995]. The planetary equivalent amplitude of magnetic activity a_p suggests that the magnetic disturbance started on 18 October 1995 (day of year 291) and lasted for about 6 days until 23 October 1995 (day 296). The peak ($a_p = 111$) occurred on 19 October 1995. The magnetic disturbance on day 292 affected the diurnal variation of the total electron content. The effect of this disturbance on our TEC estimates has been discussed previously in Komjathy and Langley [1996]. In that study we found that on day 292, at stations Madrid, Grasse and Matera, the diurnal peak of TEC values increased considerably compared to diurnal peaks for the previous days. On the other hand, for stations Brussels, Wettzell and Onsala, the GPS-derived TEC estimates show diurnal peaks with smaller size than the ones on the previous days. Also, even though the magnetic disturbance started during European night-time, it only caused a TEC increase (stations Madrid, Grasse, Matera) and decrease (Brussels, Wettzell) on the following day around noon (day 292). The fact that we detected at some stations a TEC increase and at others a TEC decrease may suggest that the magnetic disturbance was moving equatorward which is a well known feature of such disturbances [Davies, 1990].

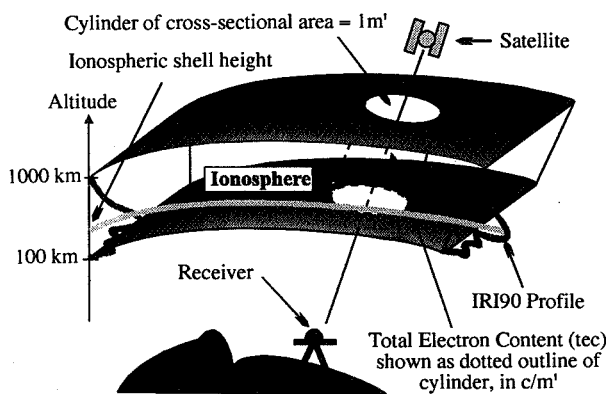


Figure 1. Illustration of ionospheric shell height determination.

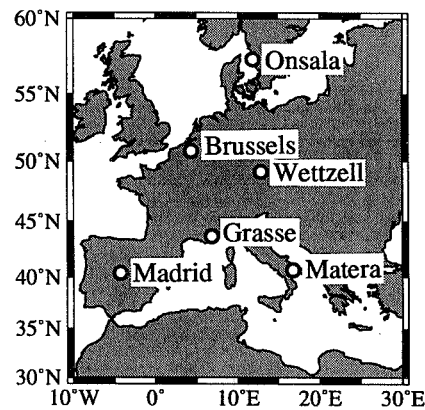


Figure 2. Locations of IGS stations used for data analysis.

RESULTS AND DISCUSSION

We used the PhasEdit version 2.0 automatic data editing program to detect bad points and cycle slips, repair cycle slips and adjust phase ambiguities using the undifferenced data. The program takes advantage of the high precision dual-frequency pseudorange measurements to adjust L1 and L2 phases by an integer number of cycles to agree with the pseudorange measurements [Freymueller, 1995]. Subsequently, a modified version of the University of New Brunswick's Differential POSitioning Program (DIPOP) package was used to estimate ionospheric parameters and satellite-receiver differential delays using a Kalman filter algorithm.

For our investigation, we used the IRI90-derived ionospheric shell height predictions as input into our DIPOP-based processor. As a first step, we computed the IRI90 predicted total electron content by integrating the predicted electron densities along the IRI90 profile. A simplified version of the profile can be seen in Figure 3 (for an explanation of the symbols, see Hakegard [1995] or Bilitza [1990]). Secondly, we used these TEC predictions to integrate the electron densities along the profile again. This time, the goal was to determine the height at which 50 percent of the total electron content was reached. We did this for all six stations we used for data processing for the 21 days under investigation. As an example, we have plotted the predicted ionospheric shell heights for day 288 in Figure 4. We can clearly see a diurnal variation of the IRI90-derived ionospheric shell height. The shell height seems to peak at night-time values of about 400 km and goes down to day-time values typically at the 300 km level. Diurnal curves were plotted for all 6 stations for day 288. There are noticeable differences from station to station even under the current low solar activity conditions. The spatial variation of the ionospheric shell height in our regional network for GPS weeks 823 to 825 was between 10 and 30 km depending on the time of the day.

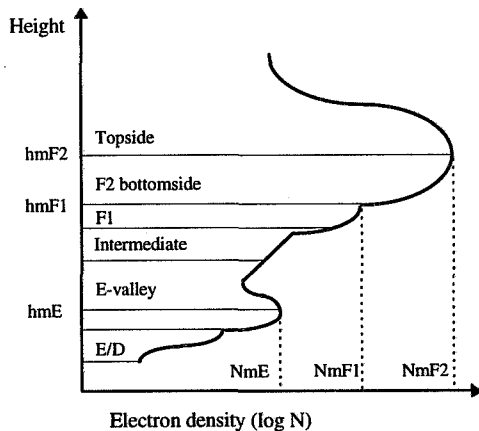


Figure 3. IRI90 profile (after Hakegard, [1995]).

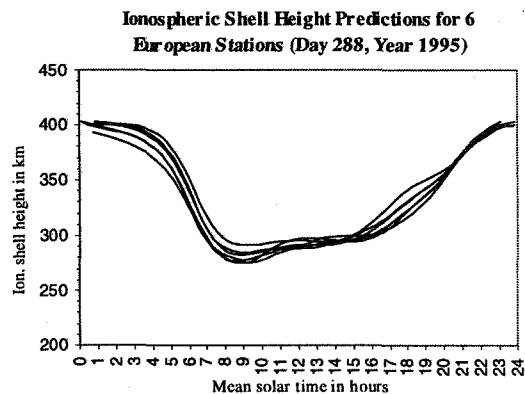


Figure 4. The diurnal variation of the ionospheric shell height.

For a better understanding of the magnitude range of varying ionospheric shell height, we computed the predicted ionospheric shell heights for high (year 1990), medium (year 1992) and low (year 1995) solar activity conditions. In Figure 5, we plotted the diurnal curves for the two stations that are furthest apart in our network: stations Madrid and Onsala. Each diurnal curve represents the conditions for the 15th day of one month of the year displaying not only the diurnal variation but also the seasonal variation of the ionospheric shell height. Note that the x axis is a category time axis on which 12 diurnal curves have been plotted one after the other each representing a "typical day" of a month. The "typical day" was arbitrarily chosen to be the 15th day of the month for illustration purposes. A small discontinuity is visible between some of the curves at 24 hours reflecting month-to-month variations. During high solar activity

conditions, the peak to peak variation of the diurnal curve is between 400 and 600 km, depending on season and geographic location of the station. During medium solar activity conditions, the variation is between 300 and 500 km. For low solar activity conditions this variation is between 300 and 400 km. As solar activity decreases, the dependency on geographic location, at least for our two European stations, becomes less significant. For high solar activity conditions, station Onsala (furthest north in the network) had the highest ionospheric shell heights. Also, during winter months the separation between shell heights predicted for stations Onsala and Madrid seems to be larger than for the rest of the year. For high solar activity conditions, the average ionospheric shell height is around 466 km; for medium solar activity conditions, 385 km; for low solar activity conditions, 335 km. It seems that the diurnal, seasonal, solar-cycle and spatial variations of the ionospheric shell heights are associated with the temporal and spatial variation of the F2 layer peak electron density.

Ionospheric Shell Height Predictions for Stations Madrid and Onsala

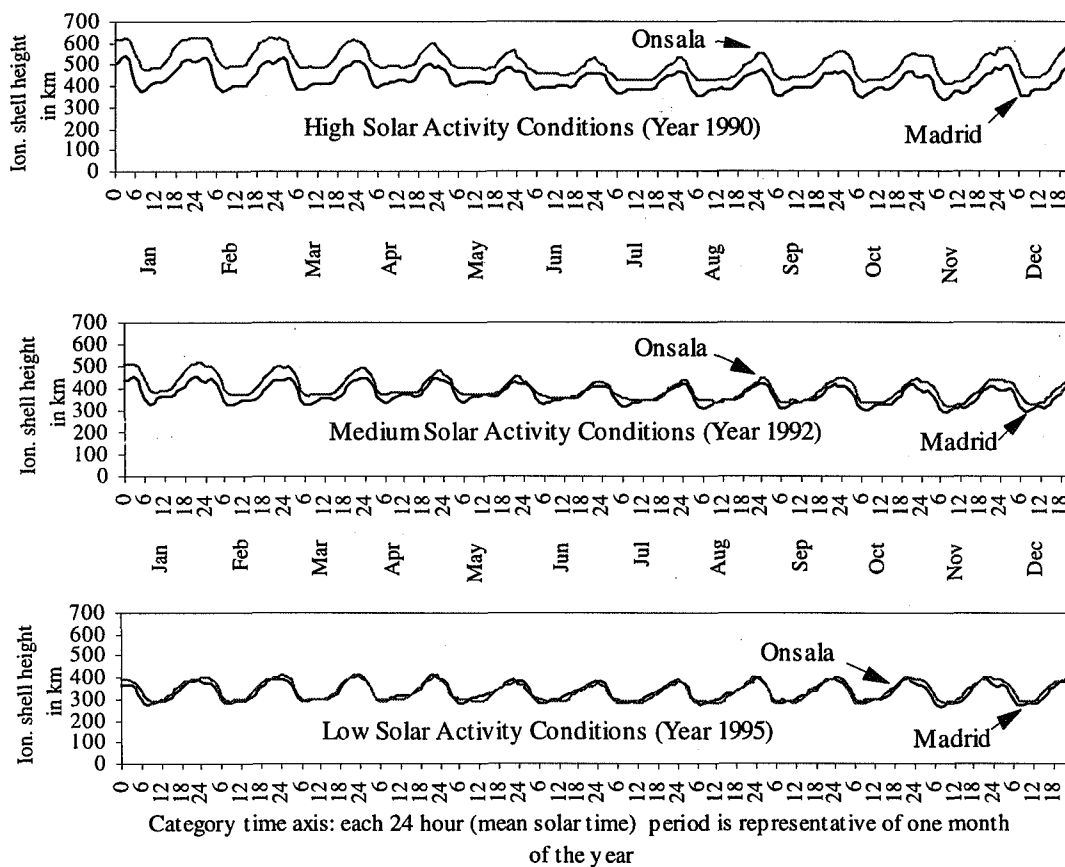


Figure 5. Ionospheric shell height predictions using the IRI90 model.

Using varying ionospheric shell heights as input into our model produces TEC and satellite-receiver differential delay estimates that are somewhat different from those obtained using a fixed ionospheric shell height. To determine the magnitude of the differences, we produced a set of TEC and differential delay estimates using both a commonly adopted fixed ionospheric shell height (400 km) and varying ionospheric shell heights predicted by the IRI90 model as described earlier. The entire 21 days' worth of data was used for this investigation. We differenced the means (over 21 days) of the differential delay estimates for each satellite and station using the varying IRI90-predicted and 400 km ionospheric shell heights. The differences in differential delays can be seen in Figure 6. The differences are less than 0.3 ns with a mean of 0.14 ns and mean standard deviation of 0.13 ns. In Figure 6, the error bars represent the mean standard deviation of the UNB differential delay estimates. We also produced hourly TEC maps at a

1 degree by 1 degree grid spacing for the region displayed in Figure 2. We produced the TEC maps by evaluating at each grid node our expression for the spatial linear approximation of TEC described by the three parameters estimated for each IGS station. For evaluating the model at each grid node, we used the three estimated parameters from the nearest IGS station. In the future, we will modify this approach with an appropriate multi-station weighting scheme. We used both the varying and 400 km ionospheric shell heights to compute different sets of ionospheric maps. We differenced the corresponding TEC values at each grid node that were computed for each hour of the 21 days under investigation. The differences are plotted in Figure 7. The histogram is based on 640,584 ((31 by 41 grid) times (24 hours) times (21 days)) TEC estimates. 53 percent of the differences fall into a bin that can be characterized with a lower boundary of -0.5 TECU and upper boundary of 0 TECU. The mean of the differences is -0.34 TECU and its associated standard deviation is 0.58 TECU. Note that the TEC differences were formed by subtracting TEC values using a 400 km shell height from those using the IRI90-derived shell height TEC values.

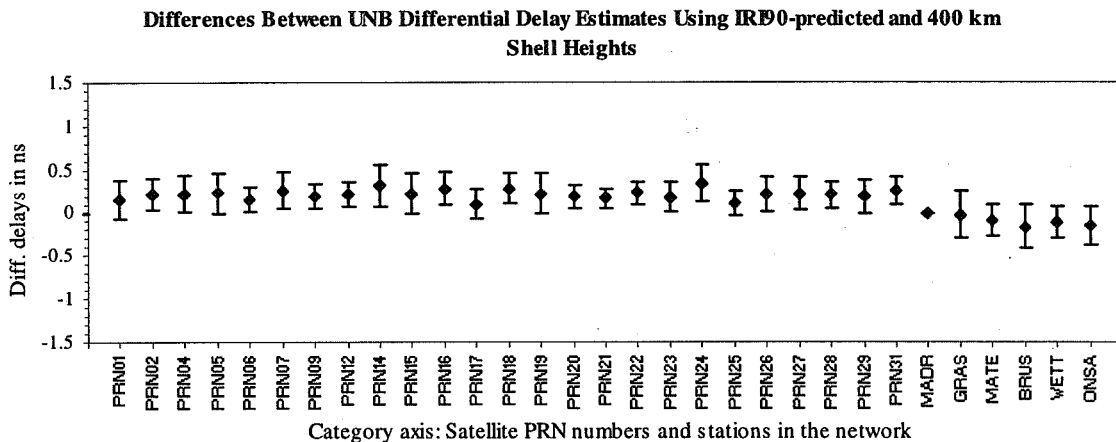


Figure 6. Comparison of satellite-receiver differential delay estimates between using IRI90-derived and 400 km ionospheric shell heights.

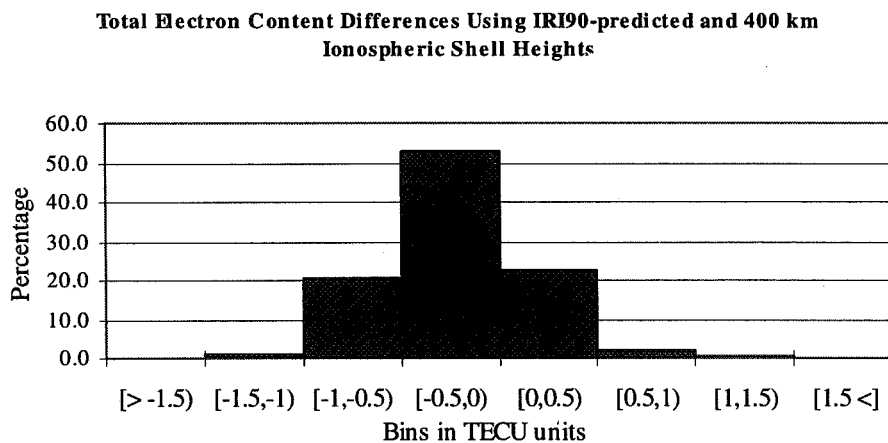


Figure 7. Comparison of TEC estimates between using IRI90-derived and 400 km ionospheric shell heights.

We conclude from this investigation that taking the temporal and spatial variation of the ionospheric shell height into account has an effect on the TEC estimates of up to 1 TECU, and 0.3 ns in the case of the differential delay estimates. These values will likely only hold for mid-latitude conditions at low solar activity levels. As we have seen earlier in Figure 5, during higher solar activity times, we can expect these differences to increase. The 1 TECU level differences are fairly small and may be within the error bars of the TEC estimates. Therefore, we decided not to compare our TEC estimates (maps) with those obtained

by other research groups to try to determine the effects of using different values for the ionospheric shell height. Furthermore, the differences between ionospheric modelling methods used by different groups would make it difficult to draw conclusions on the specific effect of their selected ionospheric shell heights.

Instead, we computed the means and the standard deviations of our daily differential delays for all 21 days. We also obtained a set of differential delay estimates computed by two of the other participating members of the ionospheric experiment, namely, the Deutsche Forschungsanstalt für Luft und Raumfahrt (DLR) Fernerkundungsstation, Neustrelitz, Germany and the European Space Agency’s European Space Operation Centre (ESA/ESOC), Darmstadt, Germany. After computing the means and standard deviations of the differential delays obtained from DLR and ESOC for all 21 days, we computed the differences of the corresponding means. The differences among the 3 analysis centers’ results are displayed in Figure 8.

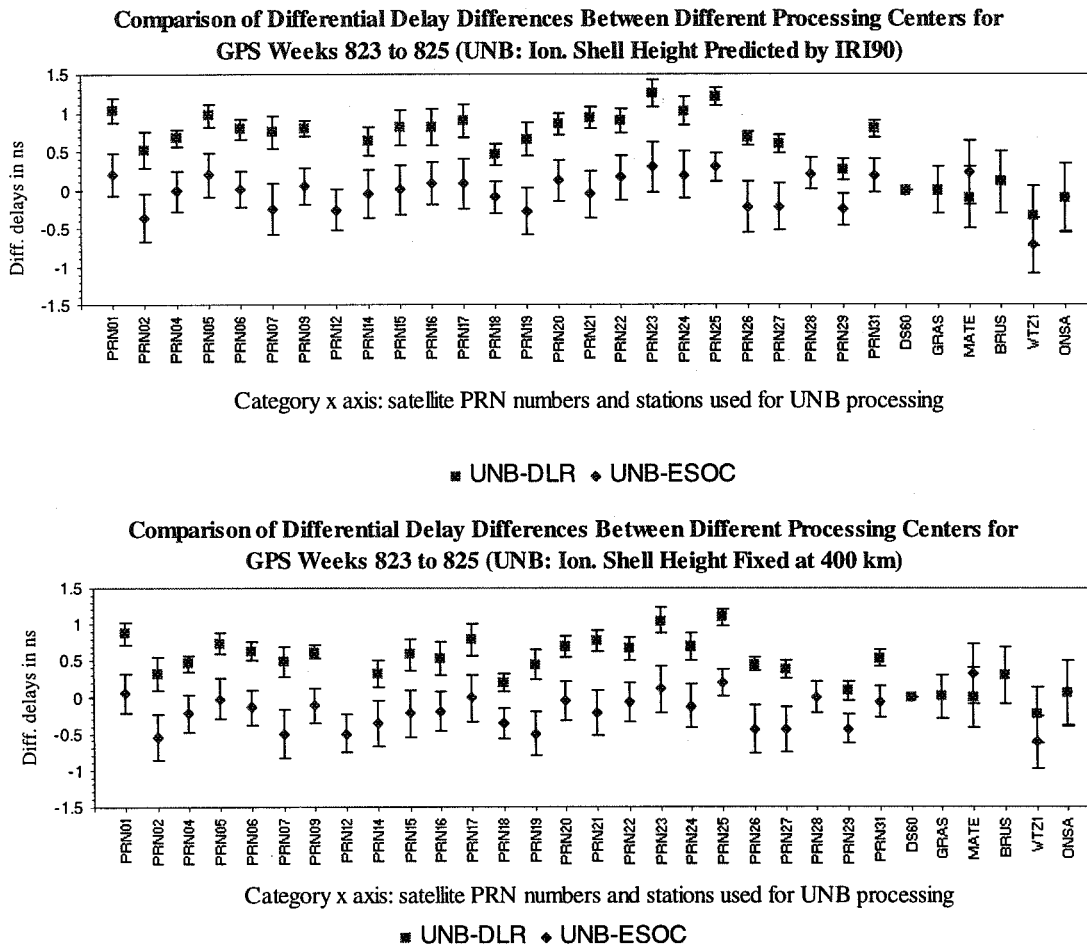


Figure 8. Comparison of differential delay differences between processing centers.

The differences were formed as UNB minus DLR and UNB minus ESOC using both our IRI90-derived shell height results (upper panel) and our results using the 400 km shell height (lower panel). Note in Figure 8 that satellites PRN12 and PRN28 are not used by DLR and stations Grasse and Brussels are not processed by ESOC. The associated standard deviations of the differential delays about the means of the two other processing centers were also plotted. The standard deviations of the means of the UNB differential delays were plotted earlier in Figure 6 and have not been considered in computing the error bars in Figure 8. The differences of the differential delay estimates are at the 1 ns level for both shell height models (upper and lower panel). It is interesting to see that there is a clear bias between the DLR

and ESOC satellite differential delays. A part of the bias can be explained by the fact that the ESOC algorithm uses 350 km for the ionospheric shell height whereas the DRL algorithm uses 400 km. As our investigation indicated in Figure 6, a 0.14 ns level bias can be expected between the differential delay differences using the IRI90-derived differential delays and the ones obtained using 400 km. However, a 1 ns level difference indicates that there are effects coming from other differences in the algorithms used by the processing centers. The fact that the UNB-ESOC differences do not seem to show a consistent bias might be explained by the fact that the mean of the IRI90-predicted diurnal variation of the ionospheric shell height is around 335 km under low solar activity conditions which is close to the 350 km height used by ESOC.

One of the potential error sources that may contribute significantly to the UNB error budget is the mapping function error. Since we use a simple secant mapping function at this stage, this could introduce unwanted errors at low elevation angles (say between 20 and 30 degrees). Throughout our processing, we used a 20 degree elevation cutoff angle. The very ability to do ionospheric modelling is based on the possibility of separating estimates of TEC from differential delays by using the elevation angle dependence of the TEC variation. Should this separation suffer from mapping function errors, a bias could be introduced into both the TEC and differential delay estimates.

It seems that using pre-defined values for ionospheric shell height has a scaling effect on the differential delay estimates. The results presented in Komjathy and Langley [1996] were also indicative of this. The lower the ionospheric shell height is set (arbitrarily or otherwise) from the "true" value, the higher the estimated differential delays will be. Furthermore, this effect seems to have an opposite sign in the case of the TEC estimates: The lower the ionospheric shell height is set from the "true" value, the lower TEC estimates can be expected. Using pre-defined fixed values for ionospheric shell height may lead to errors both in the satellite-receiver differential delays and the TEC estimates. This conclusion seems to be supported by the maximum 0.3 ns error in differential delay differences we found which corresponds to about 1 TECU. This also corresponds to the maximum TEC differences that were found to be at the 1 TECU level (see Figure 7). Using 400 km as a fixed ionospheric shell height during low solar activity conditions overestimates the day-time TEC by up to 1 TECU assuming that the IRI90-derived ionospheric shell height predictions are free of error. In the case of the satellite-receiver differential delays, using a fixed 400 km ionospheric shell height underestimates the differential delays by up to 0.3 ns under the same assumption. We believe these numbers would be even higher for higher solar activity conditions. An approximate value for the error we can expect by inappropriately setting the ionospheric shell height is about 0.5 TECU for every 50 km error in the height. This number corresponds to about 0.14 ns in the case of the differential delays. Also, these numbers could be different when modelling the ionosphere by fitting polynomials to the diurnal variation of TEC over a certain period of time. This procedure inherently averages over different ionospheric shell heights. This can also be a feasible explanation for our not detecting differences between the UNB and ESOC differential delay estimates.

CONCLUSIONS

The concept of accounting for the temporal and spatial variation of the ionospheric shell height using the IRI90 model has been described. We showed that on a small regional network of IGS stations, the predicted ionospheric shell height can vary with geographic location, time of day, season, and solar activity. After comparing our results with those obtained earlier using a fixed ionospheric shell height, we found differences in the differential delays of up to 0.3 ns. A similar study was conducted for the TEC estimates and we found that the estimates can be different by as much as 1 TECU when the temporal and spatial variation of the ionospheric shell height is not considered. We believe that these differences can be even larger during high solar activity conditions.

Furthermore, taking into account the temporal and spatial variation of the ionospheric shell height provides a more rigorous approach when estimating ionospheric model parameters along with satellite-receiver differential delays. By inappropriately setting the ionospheric shell height, we can expect a

possible 0.5 TECU level error for every 50 km error in the shell height. For the differential delays, the equivalent error level is about 0.14 ns.

ACKNOWLEDGEMENTS

We greatly appreciate the assistance of Dieter Bilitza in providing us with an update of the IRI90 model. Funding from the University of New Brunswick and the Natural Sciences and Engineering Research Council of Canada is gratefully acknowledged. Without their help this research could not have been completed.

REFERENCES

- Bilitza, D. (ed.) (1990). *International Reference Ionosphere 1990*. National Space Science Center/World Data Center A for Rockets and Satellites, Lanham, MD. Report Number NSSDC/WDC-A-R&S 90-22.
- Bishop, G.J., A.J. Mazzella, and E.A. Holland (1995). "Application of Score Techniques to Improve Ionospheric Observations". ION GPS-95, Proceedings of the 8th International Technical Meeting of the Satellite Division of The Institute of Navigation, Palm Springs, CA, 12-15 September, The Institute of Navigation, Alexandria, VA, pp. 1209-1218.
- Coco, D.S., C.E. Coker, S.R. Dahlke, and J.R. Clync (1991). "Variability of GPS Satellite Differential Group Delay Biases." IEEE Transactions on Aerospace Systems, Vol. 27, No. 6, pp. 931-938.
- Coster, A.J., E.M. Gaposchkin, and L.E. Thornton (1992). "Real-time Ionospheric Monitoring System Using GPS." Navigation: Journal of the Institute of Navigation. Vol. 39, No. 2, pp. 191-204.
- Davies, K. (1990). *Ionospheric Radio*. Peter Peregrinus Ltd., London, United Kingdom.
- Freymueller, J. (1995). Personal communication. Department of Geophysics, Stanford University, Stanford, CA, January.
- Gail, W.B., B. Prag, D.S. Coco, and C. Coker (1993). "A Statistical Characterization of Local Mid-latitude Total Electron Content." Journal of Geophysical Research, Vol. 98, No. A9, pp. 15,717-15,727.
- Gao, Y., P. Heroux, and J. Kouba (1994). "Estimation of GPS Receiver and Satellite L1/L2 Signal Delay Biases Using Data from CACS." KIS94, Proceedings of the International Symposium on Kinematic Systems in Geodesy, Geomatics, and Navigation, Banff, Alberta, 30 August - 2 September, Department of Geomatics Engineering, The University of Calgary, Calgary, Alberta, pp. 109-117.
- Hakegard, O.P. (1995). *A Regional Ionospheric Model for Real-time Predictions of the Total Electron Content in Wide Area Differential Satellite Navigation Systems*. Dr. Eng. Thesis, Norwegian Institute of Technology, Trondheim, Rapport 429506.
- Klobuchar, J.A. (1986). "Design and Characteristics of the GPS Ionospheric Time Delay Algorithm for Single-Frequency Users." *Proceedings of the PLANS-86 Conference*, Las Vegas, NV, 4-7 November, pp. 280-286.
- Komjathy, A., R.B. Langley, and F. Vejražka (1995a). "A Comparison of Predicted and Measured Ionospheric Range Error Corrections." *EOS Transactions of the American Geophysical Union*, Vol. 76, No. 17, Spring Meeting Supplement, S87.
- Komjathy, A., R.B. Langley, and F. Vejražka (1995b). "Assessment of Two Methods to Provide Ionospheric Range Error Corrections for Single-frequency GPS Users." Presented at IUGG XXI General Assembly, Boulder, CO, 2-14 July 1995.
- Komjathy, A. and R.B. Langley (1996). "An Assessment of Predicted and Measured Ionospheric Total Electron Content Using a Regional GPS Network." Presented at the ION National Technical Meeting, Santa Monica, CA, 22-24 January 1996.
- Langley, R.B. (1996). "Propagation of the GPS Signals." in *GPS for Geodesy*, International School, Delft, The Netherlands, 26 March - 1 April, 1995. Springer-Verlag, New York.
- Lanyi, G.E. and T. Roth (1988). "A Comparison of Mapped and Measured Total Ionospheric Electron Content Using Global Positioning System and Beacon Satellite Observations", *Radio Science*, Vol. 23, No. 4, pp. 483-492.

- Mannucci, A., B. Wilson, and D. Yuan (1995). "An Improved Ionospheric Correction Method for Wide-Area Augmentation Systems." *ION GPS-95, Proceedings of the 8th International Technical Meeting of the Satellite Division of The Institute of Navigation*, Palm Springs, CA, 12-15 September, The Institute of Navigation, Alexandria, VA, pp. 1199-1208.
- National Geophysical Data Center, NGDC (1995). Geomagnetic Database, ftp://www.ngdc.noaa.gov/STP/GEOMAGNETIC_DATA/INDICES/KP_AP/199.v12, accessed January 1996.
- Newby, S.P. (1992). *An Assessment of Empirical Models for the Prediction of the Transionospheric Propagation Delay of Radio Signals*. M.Sc.E. thesis, Department of Surveying Engineering Technical Report No. 160, University of New Brunswick, Fredericton, N.B., Canada.
- Runge, T., U. Lindqwister, A. Mannucci, M. Reyes, B. Wilson, and D. Yuan (1995). "Generation of GPS Observables for Global Ionospheric Mapping." *EOS Transactions of the American Geophysical Union*, Vol. 76, No. 17, Spring Meeting Supplement, S87.
- Sardon, E., A. Rius, and N. Zarraoa (1994). "Estimation of the Transmitter and Receiver Differential Biases and the Ionospheric Total Electron Content from Global Positioning System Observations." *Radio Science*, Vol. 29, No. 3, pp. 577-586.
- Schaer, S., G. Beutler, L. Mervart, and M. Rothacher (1995). "Global and Regional Ionosphere Models Using the GPS Double Difference Phase Observable." Presented at the 1995 IGS Workshop, Potsdam, Germany, 15-17 May.
- Schwarz, K.P. (1987). "Kalman Filtering and Optimal Smoothing." *Papers for the CISM Adjustment and Analysis Seminars*, 2nd ed., The Canadian Institute of Surveying and Mapping, Ottawa, Ontario, Canada, pp. 230-264.
- van der Wal, A. D. (1995). *Evaluation of Strategies for Estimating Residual Neutral-atmosphere Propagation Delay in High Precision Global Positioning System Data Analysis*. M.Sc.E thesis, Department of Geodesy and Geomatics Engineering Technical Report No. 177, University of New Brunswick, Fredericton, N.B., Canada.
- Wilson, B. and A. Mannucci (1994). "Extracting Ionospheric Measurements from GPS in the Presence of Anti-spoofing." *ION GPS-94, Proceedings of the 7th International Technical Meeting of the Satellite Division of The Institute of Navigation*, Salt Lake City, UH, 20-23 September, The Institute of Navigation, Alexandria, VA, Vol. 2, pp. 1599-1608.

Page intentionally left blank

Verification of ESOC Ionosphere Modeling and Status of IGS Intercomparison Activity

J. Feltens¹, J.M. Dow², T.J. Martín-Mur², C. García Martínez³, M.A. Bayona-Pérez³

1. EDS at Orbit Attitude Division, ESA, European Space Operations Centre, Robert-Bosch-Str. 5, D-64293 Darmstadt, Germany

2. ESOC

3. GMV at ESOC

Abstract

ESOC is planning to extend the use of IGS data also for ionospheric modeling. It is intended to provide ionospheric VTEC models and receiver/satellite differential delay values as new IGS products - besides orbits, earth orientation parameters and station coordinates. Different mathematical models were worked out to represent the ionosphere as single layer. ESOC-internally a short term analysis of these models indicated reliable performance.

In preparation of the IGS workshop in Silver Spring a comparison of ionosphere VTEC models originating from different Analysis Centers was organized. This comparison offers the opportunity to verify the modeling & implementations of the participating AC's.

ESOC will use the knowledge earned from this comparison, to define its final mathematical modeling and implement it in the Ionosphere Monitoring Facility (IONMON), which is under development at ESOC. Apart from the routine provision of ionospheric products to IGS, it is intended to use the ionosphere models for the support of other ESA-missions, e.g. ERS and ENVISAT.

1 INTRODUCTION

Since June 1992 ESOC participates as an Analysis Center at IGS. ESOC's activities within IGS include the routine provision of rapid and precise GPS orbits, earth orientation parameters, GPS satellite and station clock parameters, and ground station coordinates (SINEX), as well as GPS data tracking and retrieval from own ESOC tracking sites (currently, March 1996, these are: Kiruna, Kourou, Malindi, Maspalomas, Perth and Villafranca) on routine basis.

The transmission of navigation signals on two well defined frequencies is one of the basic characteristics of GPS. On the other hand, ionospheric effects, that are acting on satellite transmitted signals, are frequency-dependent. So, more or less as a by-product, the global dual-frequency GPS data, daily retrieved as part of ESOC's IGS activities, offer the opportunity to perform some kind of ionosphere monitoring to update ionosphere models using actual GPS data, and to provide these updated ionosphere models for other ESA missions to allow them to make ionospheric corrections on their own tracking data. This was the basic idea to concept and to establish an Ionosphere Monitoring Facility (IONMON) at ESOC.

The IONMON is currently under development, and a prototyping version is close to be operational. This prototyping version was used for an intercomparison of ionosphere products between ESOC and other Analysis Centers in preparation of the IGS workshop in Silver Spring in March 1996 (see also next chapter). The results of this comparison were used to verify the performance of mathemat-

ical modeling in ESOC fits to TEC data. Once the final IONMON software is established, it will replace the prototyping version.

2 IONOSPHERE MODELS - A NEW PRODUCT OF IGS ?

The opportunity to exploit dual-frequency GPS data from IGS for ionosphere monitoring was also recognized by other members of the IGS, and following the IGS workshop in Potsdam in May 1995 it was suggested that a comparison of ionospheric products should be organized between the Analysis Centers.

Several of the Analysis Centers participating in the IGS (JPL, EMR, CODE), as well as some external processing centers (DLR Neustrelitz, University of New Brunswick (UNB) - these will in the following text be denoted as Analysis Centers too) have already experience with the evaluation of ionospheric parameters from dual-frequency GPS data and possess dedicated software. Others (ESOC) are currently implementing ionospheric modeling into their software, as was already mentioned in the above chapter.

In order to bring all the varying activities into one common direction of a routine provision of ionospheric information as a new product of the IGS, an intercomparison of ionosphere products originating from the different Analysis Centers was organized in preparation of the IGS workshop in Silver Spring in March 1996. The intent of this intercomparison was to find out:

- How ionosphere modeling is done at the different Analysis Centers, i.e. which mathematical models, which update rate, which geographical extent, etc.
- Which accuracies are currently obtained.

It is the intent of this paper to present the results of ESOC mathematical model verification in special (see above chapter) and to summarize the intercomparison between the different Analysis Centers in general.

3 MATHEMATICAL MODELS USED AT ESOC

Generally the IONMON offers so called single layer models to represent ionospheric VTEC, i.e. TEC observations are modeled as follows:

$$l + \varepsilon = Map \cdot VTEC + k_j + k^i \quad (3.1)$$

where:

l	TEC observable,
ε	observation noise,
Map	mapping function projecting the observed TEC to the vertical,
$VTEC$	single layer model to represent the vertical TEC,

k_j	receiver differential delay,
k^l	satellite differential delay.

The following general assumptions are made:

- Assumed height of ionospheric shell: $h_I = 350 \text{ km}$.
- Mapping function: Either standard (see e.g. Mannucci et al, 1993), or the so called Q-factor mapping function (see Newby, 1992).
- Elevation cutoff is set equal to $el_{min} = 20^\circ$.
- Elevation-dependent weights are applied to favour high-elevation TEC observables and to prejudice low-elevation TEC observables:

$$W = e^{-\alpha(1 - el/90)^\beta} \quad \text{with} \quad el = \text{elevation}, \alpha = \beta = 2$$

- The reference frame used is aligned to the Sun's direction and to the geomagnetic pole. The algorithm of Biel (1990) is applied to transform from the geographic frame into the geomagnetic one.
- Fits of ionosphere models to TEC observation data are done in batch estimation mode.

Initially restricted to the above listed simple modeling, it is planned to extend the IONMON in successive versions for parameter updates in sequential estimation mode as well as to include more sophisticated models to represent the ionosphere's electron content, e.g. profiles and other physically based models, and evaluation of non-GPS and of satellite-to-satellite tracking data.

Depending on geographic extent, ESOC mathematical modeling can be classified into polynomial, spherical harmonic and Gauss-function fits, as described in the following sections.

3.1 *Polynomials for Local VTEC representations*

Polynomials (ref. R5) are fitted to TEC data which were collected at a certain ESA ground site to obtain a local VTEC model around that ground site in form of a higher-order surface. Fits are done in 6-hour time intervals, and the satellite/receiver differential delay values are constrained to 0.5 nanoseconds with respect to the values obtained from the nighttime fit (see Section 3.4). Polynomial development is linear in latitude and quadratic in local time (cubic for the equatorial ESA stations Kourou and Malindi).

3.2 *Spherical Harmonics for Global/Regional VTEC Models*

Degree and order $n, m = 8$ spherical harmonics (ref. R5) are fitted to regionally (e.g. Europe) and globally collected TEC data. The coefficients a_{10} , a_{11} and b_{11} , which define the origin of the coordinate reference, are kept fixed with zero. Fits are done in 12-hour time intervals, and the satellite/receiver differential delay values are constrained to 0.5 nanoseconds with respect to the values obtained from the nighttime fit (see Section 3.4).

3.3 Gauss-Type Exponential Functions for Global VTEC Models

The method to model the global VTEC with Gauss-Type Exponential (GE) functions was worked out at ESOC, and is under testing now. It is out of the scope of this paper to present the GE-function theory, so only the very basic can be shown here: The VTEC of the above Equation (3.1) is represented by a GE-function single layer model as follows:

$$VTEC = \Xi + \mathcal{G} \cdot e^{-a_1x - a_2x^2 - a_3x^3 - \dots - a_{2n}x^{2n}} \cdot e^{-b_1y - b_2y^2 - b_3y^3 - \dots - b_{2m}y^{2m}} \cdot e^{-c_1xy - c_2x^2y - c_3xy^2 - \dots - c_{l-k+2}x^{k-1}y - \dots - c_lxy^{k-1}} \quad (3.2)$$

with

$$k = \text{minimum}(2n, 2m) \quad l = k \cdot (k - 1) / 2$$

where:

VTEC	single layer VTEC, now represented by a GE-function,
x	independent variable; x is a function of local time,
y	independent variable; y is a function of latitude,
Ξ	constant offset,
\mathcal{G}	amplitude,
a_i	x -coefficients,
b_j	y -coefficients,
c_q	mixed terms coefficients.

The constant offset Ξ , the amplitude \mathcal{G} and the coefficients a_i , b_j , c_q are estimated as unknowns. The degree and order of GE-function development must always be an even one - therefore $2n$ and $2m$ in the above Equation (3.2). The number of mixed terms depends on the degree and order of development. If k is the lower one of degree and order, the total number of mixed terms is given by $l = k \cdot (k-1) / 2$. Local time and geomagnetic latitude are re-scaled into the x, y variables to get appropriate arguments for the GE-function. Unlike polynomials and spherical harmonics, GE-functions are not linear in their coefficients, i.e. initial values are required to establish linear observation equations. This problem can be overcome, when the GE-function is logarithmerized. Provided initial values for the constant offset Ξ and for the satellite/receiver differential delays are known, the observation equation (3.1) can be set up in logarithmerized form, and a first iteration is made in logarithmic mode to get initial values for the amplitude \mathcal{G} and the coefficients a_i , b_j , c_q . All successive iterations are then made in normal mode with linearized observation equations.

Ref. R6 presents the detailed description of the GE-function algorithm development from the first idea to the final formulae (i.e. detailed mathematics, partials, scaling of x, y , first iteration in logarithmic mode, etc.).

Global TEC data are fitted to GE-functions in 12-hour intervals. Degree of development, i.e. local time component, is $2n = 10$ and order, i.e. latitude component, is $2m = 6$. Including the constant offset, the amplitude and the mixed terms, a total of 33 GE-function parameters are estimated (plus unknown satellite/receiver differential delays). The satellite/receiver differential delay values are

constrained to 0.5 nanoseconds with respect to the values obtained from the nighttime fit (see Section 3.4).

3.4 Differential Delay Estimation Procedure

For each day, i.e. in 24-hour intervals, satellite/receiver differential delay values are determined in a special fit into which only global nighttime TEC data enter. A degree $n = 4$ and order $m = 2$ spherical harmonic is used to model the nighttime VTEC. The coefficients a_{10} , a_{11} and b_{11} , which define the origin of the coordinate reference, are kept fixed with zero. No a priori constraints are applied to the satellite/receiver differential delay values, no elevation-dependent weights are applied to the TEC observables. The satellite/receiver differential delays obtained from this nighttime fit are then introduced as reference values into all the other fits for that a day and are constrained with 0.5 nanoseconds in these solutions (see the above Sections 3.1 to 3.3).

4 COMPARISONS - RESULTS

Several Analysis Centers contributed ionospheric products for comparison over the GPSweeks 0823 to 0827: COD provided for these five weeks daily global VTEC maps in a $2^{\circ}.5$ grid. DLR and UNB delivered for weeks 0823 to 0825 hourly regional VTEC maps for the european area in 1° grids and daily satellite/receiver differential delay values. ESOC provided for all five weeks global 12-hour VTEC maps in a $2^{\circ}.5$ grid and 1° gridded local VTEC maps around the ESA ground sites Kiruna, Kourou, Madrid (instead of Villafranca), Maspalomas and Perth. ESOC's algorithms were described in the above Chapter 3. The mathematical approaches of COD, DLR and UNB can be found in (Schaer et al., 1995), (Engler et al., 1993), (Engler et al., 1995) and (Komjathy et al., 1996). Further methods of VTEC map computation are described in (Mannucci et al., 1993) and (Gao et al., 1994).

4.1 VTEC Maps

Five weeks of VTEC maps from four Analysis Centers are quite a lot amount of data to be compared and analyzed. To do this task efficiently, a certain scheme had to be worked out on how to make this intercomparison. The global VTEC maps of COD and ESOC were compared in 12-hour intervals. Comparison of - and with the regional VTEC maps of DLR and UNB and the local maps of ESOC was done in 6-hour intervals, i.e only the 0^h , 6^h , 12^h and 18^h maps of DLR and UNB were included into the comparison.

In the case that global $2^{\circ}.5$ grid maps were compared with 1° grid regional and local maps, linear interpolation was used to calculate VTEC values from the global $2^{\circ}.5$ grids in 1° intervals in the case of non-identical points.

Since the VTEC maps originating from the different Analysis Centers were referred to different reference epochs, rotations had to be made before the comparisons.

Concerning the local ESOC VTEC maps, only the results of the comparison with the Madrid maps were included in this paper.

In spite this comparison scheme reduced the number of possible combinations considerably, the remaining amount of VTEC map pairs to be compared was still too large to analyze all these comparisons by the inspection of plots. Additionally some statistics were appreciated. So a small program called "vteccm" was developed which performs a rapid comparison of two given VTEC maps and provides some general information on their agreement. To do this, vteccm calculates the differences between the two VTEC map files at all grid points. As already mentioned above, linear interpolation is used in non-identical grid points. Considering these differences as residuals, a residual VTEC map is obtained from which a mean offset between the two VTEC maps and a sigma with respect to this mean is calculated. In a next level the residual map is subdivided into 4 equally sized sub-parts, and for each part a sigma with respect to the overall mean is calculated. In the 3rd level the residual VTEC map is subdivided in 16 equally sized parts and the sigmas are computed, and so on. vteccm finally outputs:

- . The minimum and the maximum residual obtained.
- . The mean offset.
- . The overall sigma at the 1st level.
- . 4 sigmas at the 2nd level.
- . 16 sigmas at the 3rd level.
- and so on.

The sigmas at the different levels are arranged in matrix form where their positions in the matrix correspond to the locations of their sub-parts in the residual VTEC map. So from analyzing the sigmas at the different levels one can directly see in which parts of the compared area the differences between the two VTEC maps are the largest. As an example Figure 4.1 presents a vteccm output. In the south-east the residuals are at largest.

AC1: aaa AC2: bbb

the area that was finally compared:

latmax = 70.0 latmin = 30.0

lonmin = -20.0 lonmax = 40.0

vtec1: min = 2.6 max = 11.5 (minimum and maximum value of 1st VTEC map)

vtec2: min = 2.1 max = 16.1 (minimum and maximum value of 2nd VTEC map)

rvtec: min = -4.6 max = 5.2 (minimum and maximum value of the residual VTEC map)

xvtec: min = 2.6 max = 11.5 (minimum and maximum value of the interpolated VTEC map)

*** mean offset -0.26

sigmas at level 1

latitude/longitude range considered at level 1: latmax = 70.0 latmin = 30.0

lonmin = -20.0 lonmax = 40.0

0.145D+01

sigmas at level 2

latitude/longitude range considered at level 2: latmax = 70.0 latmin = 32.5
lonmin = -20.0 lonmax = 37.5

0.117D+01 0.513D+00
0.111D+01 0.180D+01

sigmas at level 3

latitude/longitude range considered at level 3: latmax = 70.0 latmin = 32.5
lonmin = -20.0 lonmax = 37.5

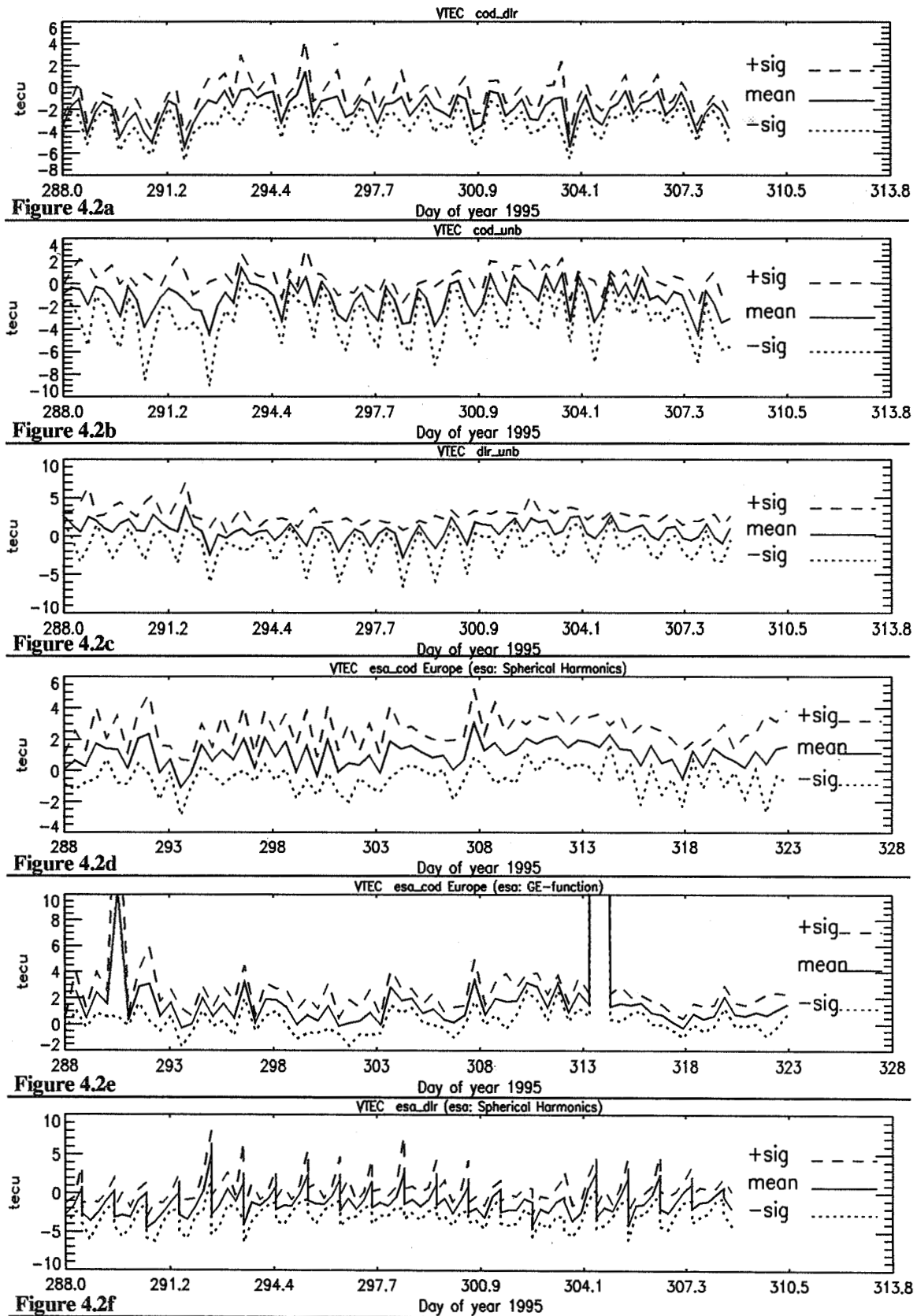
0.106D+01 0.112D+01 0.651D+00 0.148D+00
0.126D+01 0.130D+01 0.554D+00 0.580D+00
0.928D+00 0.810D+00 0.536D+00 0.147D+01
0.185D+01 0.420D+00 0.146D+01 0.298D+01

Figure 4.1: Example Output from the vteccm Program, all numbers are given in [TECU].

vteccm is invoked from a TCL for each VTEC map pair combination of one day, i.e. submission of this TCL once provided the vteccm comparison outputs of all VTEC map pair combinations for that day. The TCL was run for each day of the five weeks, and a quick look on maximum and minimum residuals, mean offset and 1st level sigma gave a fast overview. Only in critical cases - based on the vteccm output - closer consideration was done, i.e in cases of large offsets and/or sigmas. Also a general overview over the day-to-day agreement of certain VTEC map pair combinations was easily obtained.

Figures 4.2 a-k show the comparison results for all considered VTEC map pair combinations, based on the vteccm output. Each plot contains 3 curves: The upper curve shows (mean offset + σ), the middle curve shows (mean offset), and the lower curve shows (mean offset - σ), i.e. at days at which all three curves are close together the agreement between two VTEC maps with respect to the mean offset is good, and in cases of big distances between the curves the agreement is bad.

The following Sub-sections 4.1.1 to 4.1.7 summarize the results obtained for the different comparisons according to the defined scheme, together with some remarks.



Figures 4.2 a-f: Results of VTEC Map Comparison.

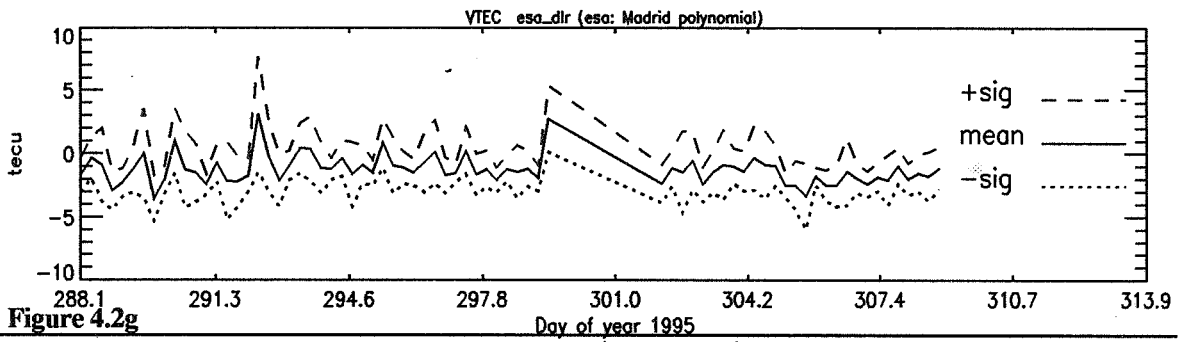


Figure 4.2g

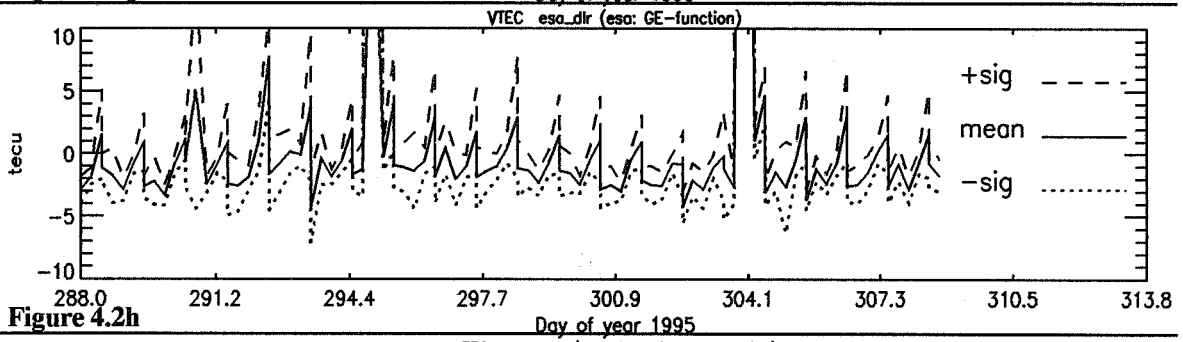


Figure 4.2h

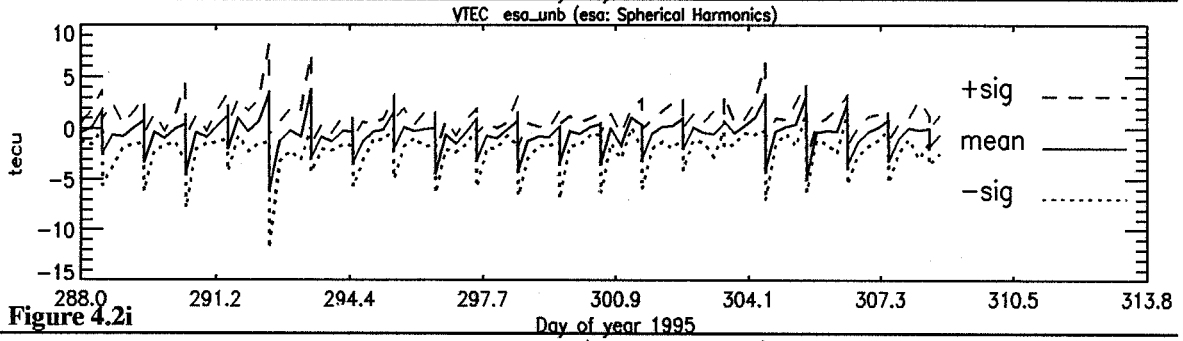


Figure 4.2i

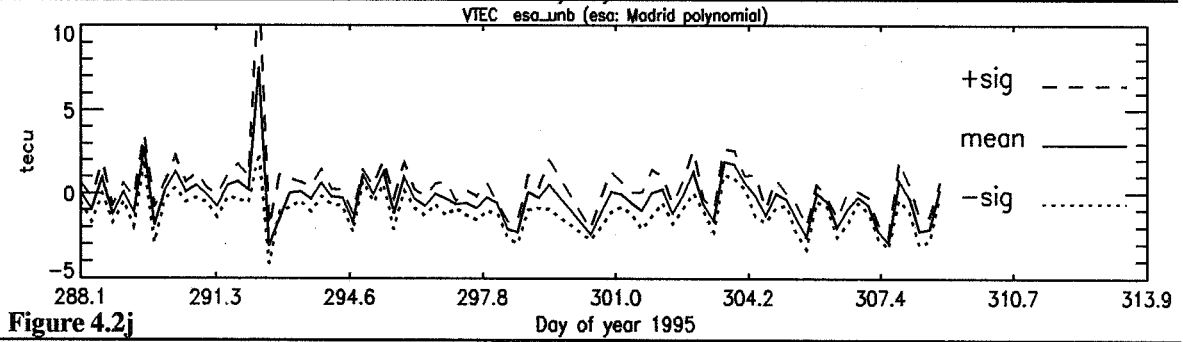


Figure 4.2j

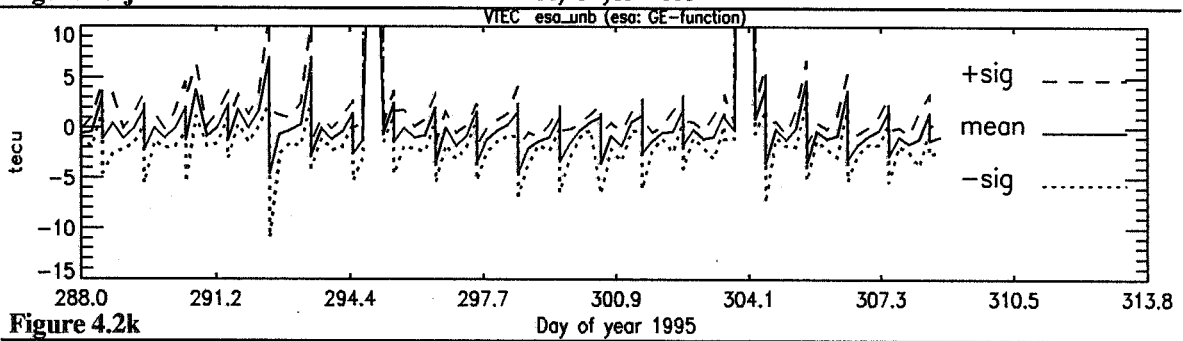


Figure 4.2k

Figures 4.2 g-k: Results of VTEC Map Comparison.

4.1.1 Comparison COD \Leftrightarrow DLR

An offset of 1-5 TECU, in the mean about 2 TECU, can be observed between the COD and the DLR VTEC maps. The offset is always negative. That means that the COD maps are systematically lying below the DLR maps. The sigmas with respect to the daily offsets vary between 1 to 1.5 TECU. A closer look to some days with larger offsets and sigmas showed that generally the agreement seems to be better in the middle of the compared area than at the borders. Figure 4.2a shows the variation of the mean offset and the sigmas over the weeks 0823 - 0825.

4.1.2 Comparison COD \Leftrightarrow UNB

Again an overall negative offset can be recognized, in the mean about -1.5 TECU, i.e. the COD VTEC maps are again lying systematically below the foreign maps - in this case the UNB ones. With respect to the daily mean offsets sigmas of 1-3 TECU can be seen. A closer look to some days with larger offsets and sigmas showed that generally the agreement seems to be best in the center and in the north-east corner of the compared area. Figure 4.2b shows the variation of the mean offset and the sigmas over the weeks 0823 - 0825.

4.1.3 Comparison DLR \Leftrightarrow UNB

No significant systematic offset can be observed between the DLR and the UNB VTEC maps. The daily offsets seem to vary around 1-3 TECU, and the sigmas are in the same order. A closer look to some days with larger offsets and sigmas showed that generally the agreement seems to be worst in the south-east corner of the compared area. Figure 4.2c shows the variation of the mean offset and the sigmas over the weeks 0823 - 0825.

4.1.4 Comparison ESOC \Leftrightarrow COD

Only the global ESOC spherical harmonic and GE-function models were compared with the COD VTEC maps.

Comparison with ESOC spherical harmonics: Comparison was done globally and restricted to the european area. Since especially on the southern hemisphere there are large gaps in station coverage (ESOC uses only Rogue stations in its processing), the spherical harmonics are bad determined in these zones. This leads to abnormal spherical harmonic behaviour in these areas, which can be seen in the VTEC plots in form of high hills and holes of same depth directly near the hills. As the global comparison with COD showed, the mean offsets between ESOC and COD VTEC maps are quite small - but the sigmas are large, up to 10 TEC, and up to 80 TECU in areas where no observation data had entered into the ESOC processing.

So only the comparison results over the region of Europe are presented here. In the european area an overall offset of about 1 TECU can be recognized between ESOC and COD VTEC maps. This offset is always positive, but since COD were now subtracted from the other Analysis Center's maps - in this case ESOC, this means that COD lies again below the foreign model. With respect to this overall offset daily offsets and sigmas seem to vary around 1-2 TECU each. A closer look to some days with larger offsets and sigmas showed that there seems to be a trend that in the north-west corner of the compared area the agreement is worst. Figure 4.2d shows the variation of the mean offset and the sigmas over the weeks 0823 - 0827.

Comparison with GE-functions: Concerning station coverage, the GE-functions are affected similarly as the spherical harmonics, i.e. in areas with good station coverage the GE-functions are good too. Additionally GE-functions seem to be more vulnerable to bad receiver data. The Maspalomas station data, which was known to be problematic at that time, caused for instance every day an abnormal GE-function peak at high northern latitudes. Also the data of Kourou and the Seychelles was problematic. Further tests made as consequence of the comparison results have shown that, after these stations were excluded from GE-function processing, the high-latitude anomaly had disappeared or was at least drastically reduced. Also variations in the degree and order of GE-function development (e.g. $2n = 8, 2m = 4$; $2n = 10, 2m = 4$; $2n = 10, 2m = 8$) caused the anomaly to disappear. Further tests will be necessary to find out an optimal way of GE-function processing.

Because of the problems pointed out above, only the comparison results of the GE-function maps with the COD models over the region of Europe are presented here. As with the spherical harmonics, an overall offset of about 1 TECU can be recognized. Again this overall offset is positive, which means that the COD maps seem to lie below the GE-function models. With respect to this overall offset, daily offset variations of 1-2 TECU can be seen and sigmas around 1 TECU. On day 290 and 313 large outliers are present. These outliers were caused by the above mentioned problematic stations. Apart from these outliers the GE-functions seem to be a little bit closer to the COD models as the ESOC spherical harmonics. A closer look to some days with larger offsets and sigmas seem to indicate that the agreement is a little bit worse in the southern and sometimes in the western part of the compared area. Figure 4.2e shows the variation of the mean offset and the sigmas over the weeks 0823 - 0827.

4.1.5 Comparison ESOC \Leftrightarrow DLR

Comparison with ESOC spherical harmonics: Because the ESOC spherical harmonics are well feeded with observation data in the european area (see above Section 4.1.4), the agreement with the DLR VTEC models is quite good. An overall mean offset of about -1 to -2 TECU seems to be present, which means that the ESOC models lie systematically below the DLR models. Around that overall offset variations and sigmas of about 3 TECU can be seen. Since the 12^h DLR models were compared with the 6^h and the 18^h ESOC spherical harmonic models (both rotated to 12^h), peaks appear every day at 12^h. A closer look to some days with larger offsets and sigmas showed that the worst agreement seems to be at the southern border of the compared area. Figure 4.2f shows the variation of the mean offset and the sigmas over the weeks 0823 - 0825.

Comparison with ESOC local polynomials for Madrid: Also the Madrid local polynomial models seem to show an overall offset of about 1 TECU below the DLR maps and around that overall offset variations and sigmas about 1-3 TECU. Around day 300 there was a data gap. A closer look to some days with larger offsets and sigmas showed that the worst agreement seems to be in the north-west and sometimes in the south-east corner of the compared area. Figure 4.2g shows the variation of the mean offset and the sigmas over the weeks 0823 - 0825.

Comparison with GE-functions: As was pointed out in the above Section 4.1.4, the GE-functions had problems in the high northern latitudes. However, the european area, in which the GE-functions were compared with the DLR VTEC maps, is far enough in the south, so that the agreement was in most cases good. Only on some days, especially on days 295 and 304, the high latitude anomaly propagated so far southward, that it was felt in the comparison. Except from these outliers, mean offsets up to 3 TECU are present without an overall offset. The sigmas around the mean offsets range between 1-3 TECU. Again the 12^h DLR maps were compared with the 6^h and the 18^h ESOC models (both rotated to 12^h). A closer look to some days with larger offsets and sigmas showed the worst

agreement in the north (for the reasons stated above) and sometimes in the south-east. Figure 4.2h shows the variation of the mean offset and the sigmas over the weeks 0823 - 0825.

4.1.6 Comparison ESOC \Leftrightarrow UNB

Comparison with ESOC spherical harmonics: As with the DLR models, the agreement with UNB over the european area is good. An overall offset of -1 TECU seems to be present, i.e. the ESOC maps are lying below the UNB maps. Around that overall offset the daily mean offsets and sigmas seem to vary about 2 TECU. From doy 294 on the variations become smaller but increase again at doy 304. Since the 12^h UNB models were compared with the 6^h and the 18^h ESOC spherical harmonic models (both rotated to 12^h), peaks appear every day at 12^h. A closer look to some days with larger offsets and sigmas showed the worst agreement to be in the north-west and in the south-east corner of the compared area. Figure 4.2i shows the variation of the mean offset and the sigmas over the weeks 0823 - 0825.

Comparison with ESOC local polynomials for Madrid: Madrid local polynomial models and UNB VTEC maps show very close agreement of 0-1 TECU in the daily mean offsets as well as in the sigmas. Only on doy 292 there is a significant outlier; on this day a large geomagnetic field disturbance occurred. A closer look to some days with larger offsets and sigmas showed the worst agreement to be in the north-west and in the south-east corner of the compared area. This north-west/south-east effect was also present in the 9-hour comparison for doy 292, together with a whole sigma level higher as usual. Figure 4.2j shows the variation of the mean offset and the sigmas over the weeks 0823 - 0825.

Comparison with GE-functions: Generally the agreement between GE-functions and UNB VTEC maps is about 1-3 TECU in the mean offsets and sigmas of 1 TECU around these offsets. Because of the problems stated in the above Section 4.1.4, the GE-functions showed sometimes abnormal behaviour in the high northern latitudes. Here this can be seen in form of outliers, especially on doys 295 and 304. Again the 12^h UNB maps were compared with the 6^h and the 18^h ESOC models (both rotated to 12^h). A closer look to some days with larger offsets and sigmas showed, that, apart from casual discrepancies in the north, worst agreement was found in the south-east part of the compared area. Figure 4.2k shows the variation of the mean offset and the sigmas over the weeks 0823 - 0825.

4.1.7 Comparison of ESOC Local with Global Models

As a representative of the five ESA ground sites for which local polynomial models were fitted to at ESOC, only the results for Madrid were presented in the previous sections. To the agreement of the polynomial maps for Kiruna, Kourou, Maspalomas and Perth with the ESOC spherical harmonic and GE-function models some short remarks only:

- Generally good agreement was observed with the Kiruna, Madrid and Perth polynomials: 0-3 TECU mean offsets (1-6 TECU offsets at Perth with the spherical harmonics) and sigmas of 1-3 TECU with respect to these offsets.
- In the case of Kourou and Maspalomas the agreement was significantly worse. Especially from Maspalomas it is well known, that there were considerable receiver problems at the time for which the intercomparison was done. In particular during the week 0826 the Maspalomas data was bad, and in week 0827 Maspalomas provided tracking data only for one and a half day. Quite often unrealistic polynomials were obtained for both stations, Kourou and Maspalomas.
- Generally the GE-functions seem to be closer to the polynomial models than the spherical harmonics.

4.2 Differential Delays

Comparison of differential delays was done between results provided by DLR, UNB and ESOC. The UNB differential delay files contain differential delay values for all satellites and 6 ground stations. DLR provided values for all satellites, except PRN12 and PRN28, and for 16 ground stations. And ESOC determined values for all satellites and 64 ground stations.

The day-to-day variation in the values of all 3 series is in most cases within the 0.5 nanosecond limit. Especially the DLR and ESOC differential delay series seem to indicate a generally higher day-to-day scatter for the stations than for the satellites. Typical examples are Arequipa and Fortaleza. - There are of course also a lot of stations which show the same lower order of scatter as the satellites. The ESOC differential delay files show additionally a clear increase of sigmas of the mean values by a factor 2-3 for GPSweeks 0824 - 0827 with respect to week 0823. This can especially be seen at the satellites.

A comparison between the three series seem to indicate an offset of the DLR series of about 1 nanosecond with respect to the ESOC series, and the UNB series seems to be close to the ESOC results. This was also confirmed by A. Komjathy (private communication). ESOC uses 350 km as ionospheric shell height while DLR and UNB are using 400 km. So ESOC repeated the differential delay estimation for week 0823 also with 400 km shell height. However, no variances of more than 0.2 nanoseconds with respect to the 350 km solution for that week could be observed. A. Komjathy and R.B. Langley (1996) made similar calculations with the same result. Obviously the difference in shell height cannot explain this 1 nanosecond offset. The reason for this offset might come from differences in the algorithms used and/or from the different sets of ground stations used. Additionally DLR rejects the satellites PRN12 and PRN28 in its solution. Figure 4.3 compares the DLR, UNB and ESOC series exemplarily for 2 stations and 4 satellites.

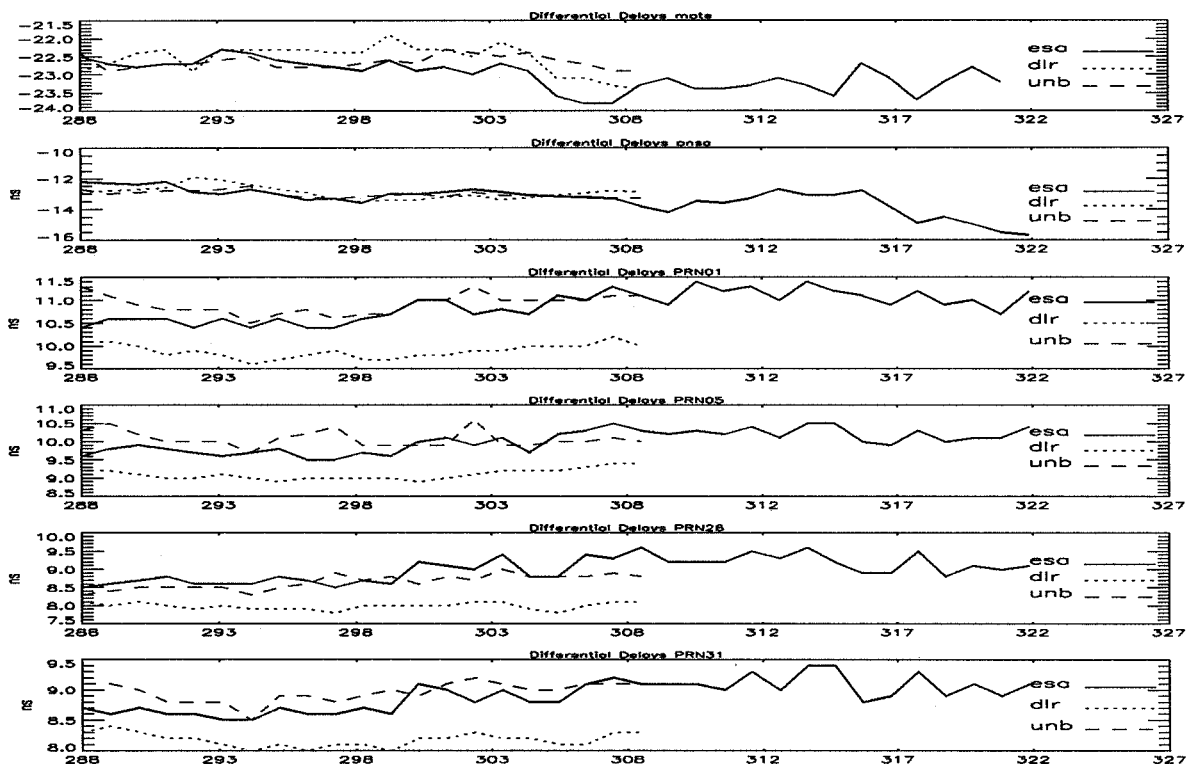


Figure 4.3: Differential Delay Behaviour for a selected Set of Stations and Satellites.

5 CONCLUSIONS

With regard to include ionosphere data into the IGS product list, an intercomparison of ionosphere products provided by different Analysis Centers was organized in preparation of the IGS workshop in Silver Spring in March 1996. Four Analysis Centers contributed to this comparison with own results.

In areas with tracking data of sufficient density the different VTEC models seem to show a general agreement of 5 TECU and better, normally about 3 TECU. For the differential delay values agreement within 1 nanosecond was achieved. In summary the intercomparison results look encouraging to do further steps into the direction of a routine provision of ionosphere maps as new part of IGS.

ESOC used the comparison as opportunity to verify its own mathematical modeling. The following weak points were identified from the analysis of the intercomparison results:

- The ground station net used by ESOC must be densified around the equator and at the southern hemisphere - gaps in station coverage have caused abnormal behaviour of global fits in weakly observed areas.
- Bad receiver data must be identified in a preprocessing step, since it had seriously affected the solutions.
- More testing is necessary to overcome the above mentioned problems and to achieve robust modeling.

Based on the knowledge earned from the intercomparison, the next steps into the direction of IGS must be undertaken now - relevant aspects are pointed out in ref. R4.

Beyond its IGS activities ESOC is also interested to use GPS-derived ionosphere maps to correct ERS-2 and other ESA satellite data.

Acknowledgments

The authors wish to express their acknowledgments to the Analysis Centers for their readiness to contribute to the intercomparison with own results and fruitful discussions. Thanks also to A. Komjathy and R.B. Langley for setting up the GPS-IONO mailing list at the University of New Brunswick which was very helpful for fast exchange of information and discussion.

6 REFERENCES

- R1. Biel, H.A. von (1990): 'The geomagnetic time and position of a terrestrial station.' *Journal of Atmospheric and Terrestrial Physics*, Vol. 52, No. 9, pages 687 - 694, 1990.
- R2. Engler, E., N. Jakowski, A. Jungstand and D. Klähn (1993): 'First experiences in TEC monitoring and modelling at the DLR Remote Sensing Station Neustrelitz.' *Proceedings of the*

GPS/Ionosphere Workshop Modelling the Ionosphere for GPS Applications, DLR/DFD, Fernerkundungsstation Neustrelitz, Germany, September 29-30, 1993, pages 122-125.

- R3. Engler, E., E. Sardón and D. Klähn (1995): 'Real Time Estimation of Ionospheric Delays'. Proceedings of the ION GPS-95, 8th International Technical Meeting of The Satellite Division of The Institute of Navigation, Palm Springs, California, U.S.A., September 12-15, 1995.
- R4. Feltens, J. (1996): 'Ionosphere Models - A New Product of IGS ?', IGS Position Paper, Proceedings of the IGS Analysis Center Workshop, Silver Spring, MD, U.S.A., March 19-21, 1996.
- R5. Feltens, J. (1995a): 'GPS TDAF Ionosphere Monitoring Facility, Mathematical Model Developments'. GTDAF-TN-08 Iss 1/- 11 Sep-95 (ESOC-internal document).
- R6. Feltens, J. (1995b): 'GPS TDAF Ionosphere Monitoring Facility, Examination of the Applicability of Gauss-Type Exponential Functions to Ionospheric Modeling'. GTDAF-TN-09 Iss 1/- 11 Sep-95 (ESOC-internal document).
- R7. Gao, Y., P. Heroux and J. Kouba (1994): 'Estimation of GPS Receiver and Satellite L1/L2 Signal Delay Biases Using Data from CACS'. Proceedings of the International Symposium on Kinematic Systems in Geodesy (KIS94), Geomatics and Navigation, Banff, Canada, August 30 - September 2, 1994, pages 109-117.
- R8. Komjathy, A. and R.B. Langley (1996): 'An Assessment of Predicted and Measured Ionospheric Total Electron Content Using a Regional GPS Network'. Proceedings of the ION GPS-96, 9th International Technical Meeting of The Satellite Division of The Institute of Navigation, Santa Monica, California, U.S.A., January 22-24, 1996.
- R9. Mannucci, A.J., B.D. Wilson and C.D. Edwards (1993): 'A New Method for Monitoring the Earth's Ionospheric Total Electron Content Using the GPS Global Network'. Proceedings of the ION GPS-93, 6th International Technical Meeting of The Satellite Division of The Institute of Navigation, Salt Lake City, Utah, U.S.A., September 22-24, 1993, Vol. II, pages 1323-1332.
- R10. Newby, S.P. (1992): 'An Assessment of Empirical Models for the Prediction of the Transionospheric Propagation Delay of Radio Signals'. University of New Brunswick, Dept. of Surveying and Engineering, Canada, Technical Report No. 160, August 1992.
- R11. Schaer, S., G. Beutler, L. Mervart, M. Rothacher and U. Wild (1995): 'Global and Regional Ionosphere Models Using the GPS Double Difference Phase Observable'. Paper presented at the 1995 IGS Workshop, Potsdam, Germany, May 15-17, 1995.

Page intentionally left blank

Comparison of GPS/IGS-derived TEC data with parameters measured by independent ionospheric probing techniques

N. Jakowski and E. Sardón
DLR e.V., Fernerkundungsstation Neustrelitz,
Kalkhorstweg 53, Germany

Abstract

In order to evaluate TEC-data products derived from numerous GPS/IGS stations, comparisons are made with ionospheric parameters deduced from independent ionospheric measurements. The study includes data obtained from bottomside and topside vertical ionospheric sounding, NNSS radio beacon measurements and incoherent scatter radar probing (EISCAT). The results indicate general physical agreement between the GPS/IGS derived TEC data and the other ionospheric parameters. Furthermore a comparison is made between the GPS-based TEC obtained by different groups using different estimation techniques for the location of the ionosonde station Juliusruh (54.6°N; 13.3°E) during a selected time interval in October, 1995. For the same period, a reference is made to the ionospheric electron content up to 1000 km height deduced from the updated IRI90 model.

1. Introduction

The GPS receiving technique provides a unique possibility to monitor the ionospheric electron content on regional and global scales (Coco, 1991; Wilson et al., 1995, Zarraoa and Sardón, 1996). The derived total electron content (TEC) is an important parameter which, on one hand, characterizes the first order ionospheric propagation error in space-based radio navigation systems and, on the other hand, provides valuable information about the behaviour of the ionosphere/plasmasphere systems.

Since TEC estimations based on dual frequency GPS data require an accurate in-flight-calibration of the differential instrumental delays of the satellites and receivers, the derived TEC data are as accurate as these calibrations have been made. Although different algorithms were developed by different groups to derive the instrumental biases and/or TEC, all these methods utilize simplifying assumptions about the ionospheric behaviour. The accuracy of the corresponding algorithms can be checked by controlling the internal consistency of the derived data products (internal check) and by comparing the data products with equivalent data obtained by independent ionospheric measurements (external check). So independent ionospheric probing techniques such as vertical sounding, incoherent scatter radar, radio beacon measurements provided by satellite systems such as NNSS, PRARE or DORIS or two frequency satellite altimeters can be used to validate the derived TEC data and/or to get a comprehensive insight into ionospheric processes (Jakowski, 1995).

In the following section TEC mapping results obtained in DLR Neustrelitz by using the European IGS network of GPS receivers (e.g. Zumberge et al., 1994) are compared with simultaneously measured ionospheric parameters derived from non-GPS techniques. The used algorithms to derive TEC-maps from GPS measurements are described elsewhere (Sardón et al., 1994, Jakowski and Jungstand, 1994). In particular the analysis includes also comparative studies of TEC mapping made at different centres such as CODE, ESOC, University of New Brunswick and DLR Neustrelitz for October 1995. The GPS-based TEC derived by these groups is also compared with the IRI90 model updated by ionosonde data.

2. Comparison with ionospheric data obtained by independent measurements

2.1 Vertical sounding

Vertical sounding stations provide valuable information about the peak electron density $NmF2$ and the height $hmF2$ of the F2 layer. Combining the peak electron density $NmF2 = 0.0124 \cdot (foF2)^2$ with the derived vertical TEC, the equivalent slab thickness τ of the electron density profile can be derived by applying $\tau = TEC / NmF2$.

The equivalent slab thickness τ is a measure of the width of the electron density profile and ranges in most cases between 200 and 500 km. Due to the enhanced night-time loss of plasma in the bottomside ionosphere, the higher τ values occur generally during night-times. Although $foF2$ and TEC have different physical meanings, the diurnal variation of both parameters should be well correlated.

This is shown in Fig. 1 where hourly $foF2$ data measured by the vertical sounding station Juliusruh (54.6° N; 13.3° E) are plotted against the diurnal behaviour of the corresponding vertical TEC data derived from the regional TEC map.

The diurnal variations of both these parameters are closely correlated thus indicating a reliable TEC estimation algorithm in general. The absolute level of TEC can be checked by computing the equivalent slab thickness values τ .

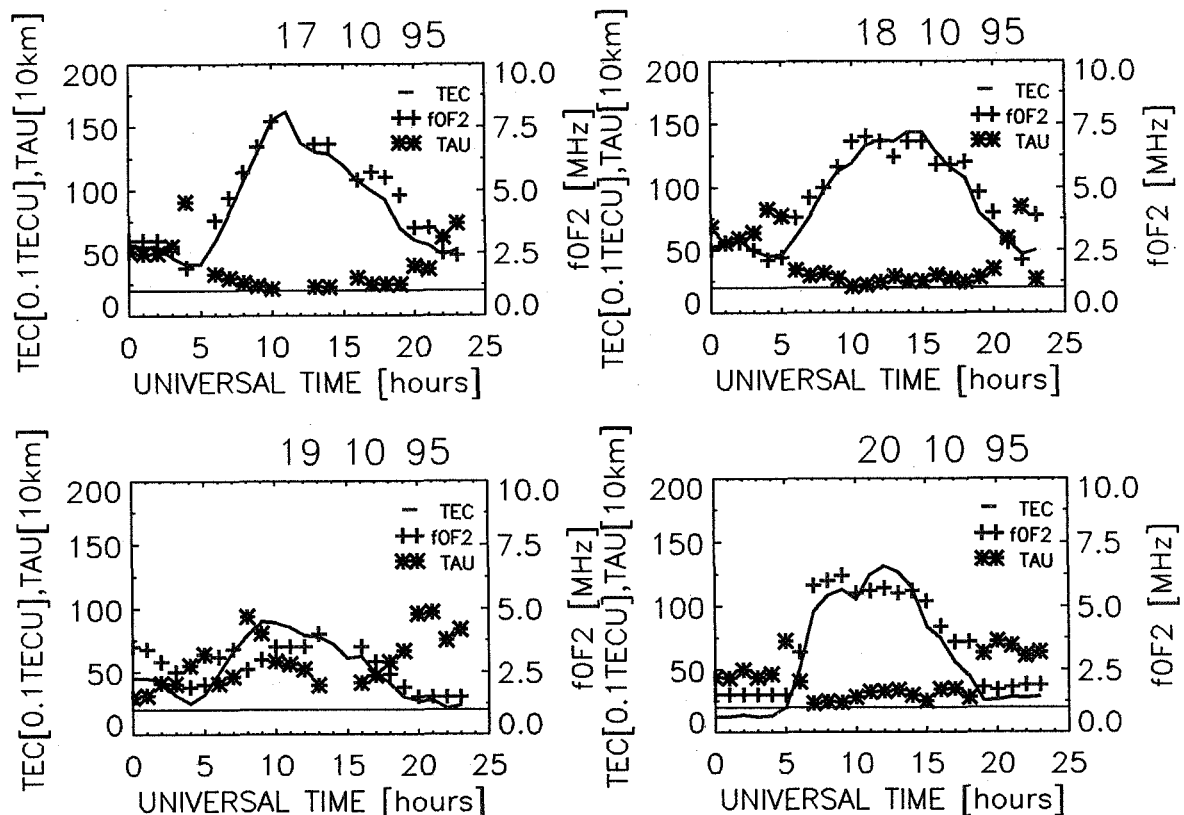


Figure 1

Comparison of GPS derived TEC data with $foF2$ data measured by the ionosonde station Juliusruh for some days in October 1995. The 200 km slab thickness level is marked by a thin line.

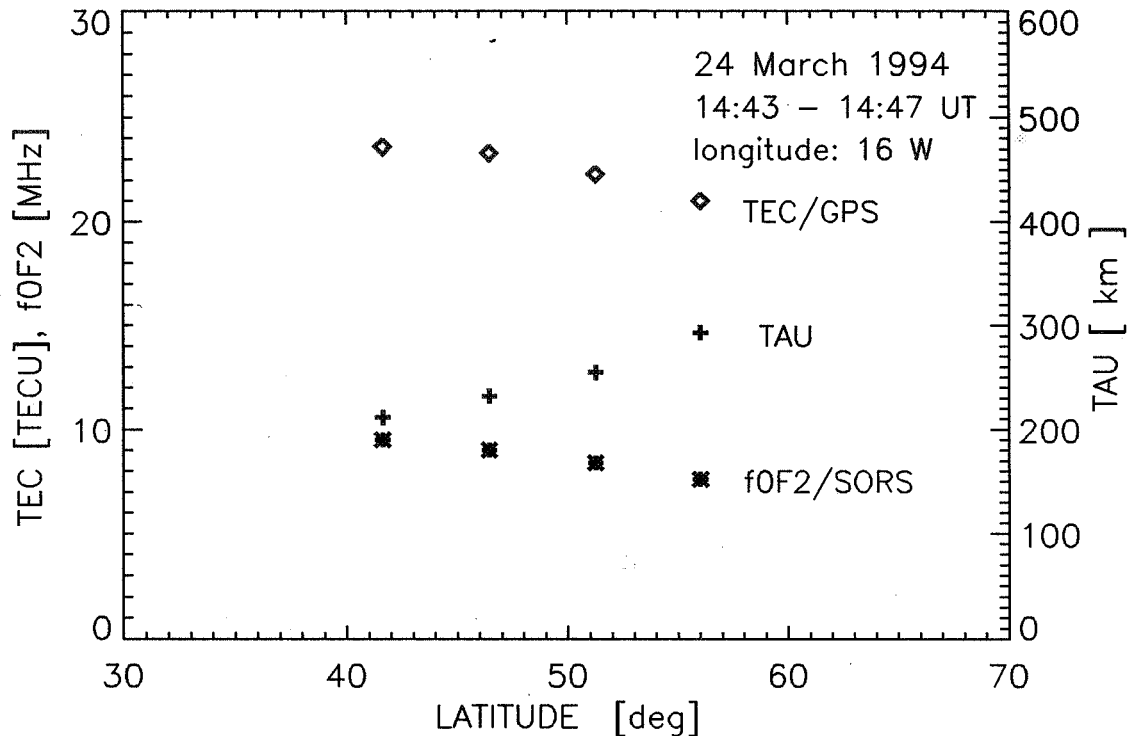


Figure 2

Comparison of GPS derived TEC data with foF2 measured by topside vertical sounding. The F2 layer critical frequency foF2 was measured onboard the Russian CORONAS satellite by the SORS topside sounder during a satellite pass on March 24, 1994 over Europe.

The results indicate an absolute TEC level accuracy in the order of ≤ 3 TECU. Reducing the night-time TEC values by 3 TECU the resulting slab thickness τ is still acceptable. A further lowering of TEC values would provide, however, physically unreasonable low τ values at night.

It should be underlined that especially topside sounder measurements onboard low orbiting satellites can provide valuable information about the peak electron density along the satellite trace. Such an example is given in Fig. 2 where foF2 data measured onboard the Russian CORONAS satellite are compared with the corresponding TEC values of the map along the satellite trace. Again the derived equivalent slab thickness values behave quite "normal" during the satellite pass.

The measured foF2 and hmF2 data can also be used to update ionospheric models such as the International Reference Ionosphere (IRI). A subsequent integration of the vertical electron density profile up to 1000 km height provides the Ionospheric Electron Content IEC or N_I which differs from the total electron content N_T up to GPS heights by the plasmaspheric contribution N_p according to $N_T = N_I + N_p$.

Due to permanent changing geometric relationships between satellite-receiver links, in particular with respect to the geomagnetic field lines, the plasmaspheric contribution will change from satellite to satellite. But nevertheless, an average plasmaspheric electron content in the order of 1...3 TECU should be taken into account over the whole day even under low solar activity conditions (e.g. Soicher, 1976). Fig. 3 illustrates a comparison of TEC data derived from GPS/IGS measurements for the ionosphere over Juliusruh with the diurnal

variation of the IEC derived from IRI90 electron density profiles updated by the ionosonde (IS) data. By the way, it is clearly shown that the non-updated IRI90 model underestimates the observations by more than 50% thus indicating that also well qualified models such as IRI90 fail in describing TEC under geomagnetically disturbed conditions. The correlation between GPS derived TEC data (GPS/IGS) and the IEC data (IS) is quite good. The remaining difference in the order of 1...3 TECU during the night-time could be explained by the plasmaspheric contribution N_p . However, since IRI90 represents only an average behaviour and the internal measuring accuracy of TEC estimations is in the same order as the plasmaspheric content, one should be careful in deriving conclusions about the plasmaspheric content based on such comparisons. A more detailed discussion of this subject is given in section 3.

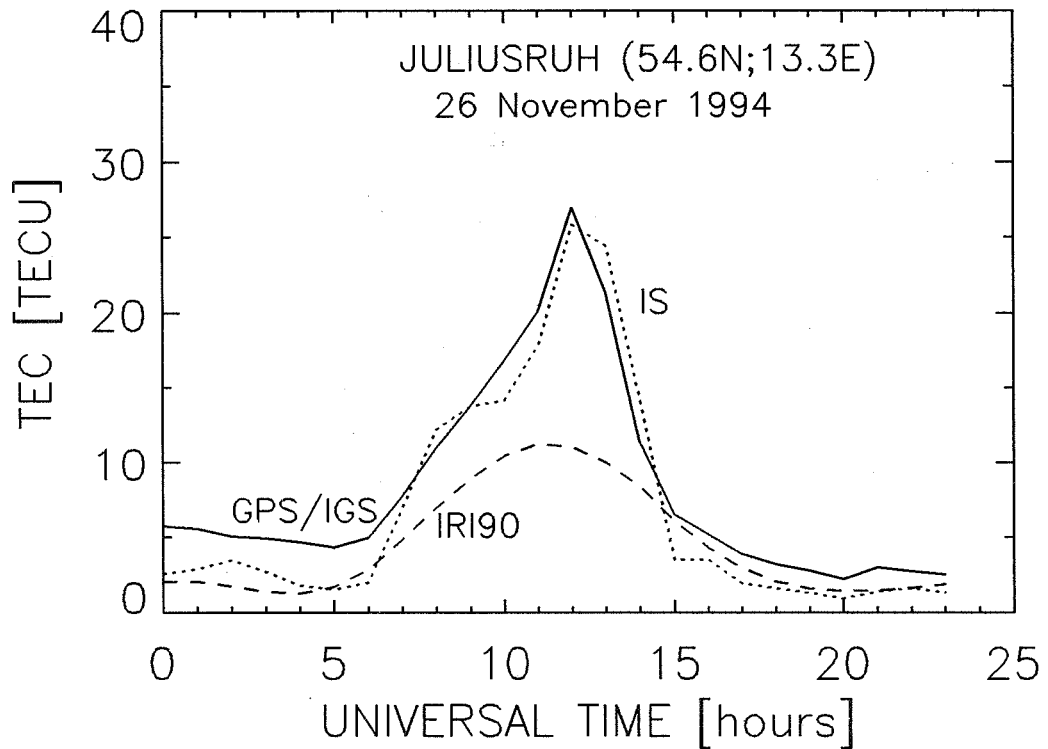


Figure 3
Comparison of GPS derived TEC data (GPS/IGS) with the height integrated electron density profiles computed from the IRI90 model based on CCIR tables (IRI90) and measured vertical sounding data (IS).

2.2 NNSS data

The Navy Navigational Satellite System (NNSS) transmits a pair of coherent carrier frequencies on 150/400 MHz. Such sensitive differential Doppler measurements can provide meridional TEC profiles with a high spatial resolution up to about 10 km. Comparing NNSS with GPS derived TEC data, conclusions about the spatial resolution of the produced TEC maps can be derived. Because the absolute calibration of NNSS data would produce new problems to discuss, we confine our attention only to the relative TEC variations when comparing the corresponding TEC data. As Fig. 4 demonstrates, the occurrence of Travelling Ionospheric Disturbances (TID's) with wavelengths in the order of a few hundred kilometers is well documented in the NNSS data. Due to a number of different reasons such small effects are

commonly not reproduced in the GPS derived TEC data. Considering only the corresponding GPS carrier phase data, TID's should also be observable along the GPS trace, but the interference of the ray path movement through the ionosphere with TID propagation makes their analysis difficult.

It should be underlined that on the other hand large scale phenomena such as the mid-latitude electron density trough are well documented. Although the spatial resolution of NNSS measurements cannot be reached by GPS data, the trough phenomena is well pronounced in the produced maps especially in conjunction with ionospheric storms (e.g. Jakowski, 1995).

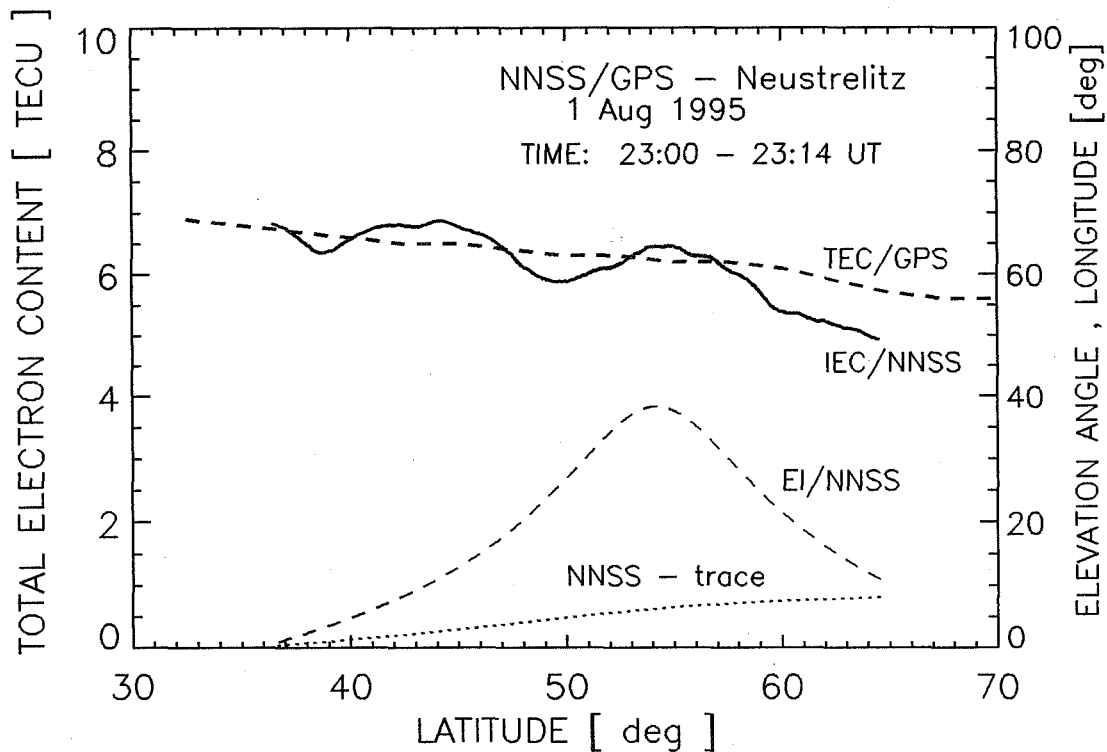


Figure 4
Illustration of a TID observed by NNSS differential Doppler measurements on August 1, 1995.
The corresponding GPS derived TEC data smooth over the TID variation.

2.3 EISCAT data

Incoherent scatter radar measurements provide a number of different ionospheric parameters for complex studies of the ionosphere. So the Common Programme Three (CP-3) of the European Incoherent SCATter facility (EISCAT) in Tromsø measures the electron density along different lines between 62°N and 78°N during 30 min north-south scans. Due to the overlapping region with our routine TEC map a comparison with height integrated CP-3 electron density profiles in the height range 150-500 km is possible. The results obtained on February 4, 1995 are documented in Fig. 5. The difference between EISCAT and GPS derived electron content data should be related to the topside ionosphere/plasmasphere contribution. Since the plasmaspheric content and its behaviour is not well known, such studies could improve our knowledge about plasmasphere-ionosphere relationships especially in high latitudes.

The GPS/IGS based TEC data are deduced from subsequent TEC maps available every 10 minutes in such a way that the angular distance between EISCAT and GPS measuring points is less than 5 degrees. To have more reliable data, several subsequent EISCAT scans were used during the given time interval resulting in more than one electron content value at the fixed latitude points. It is interesting to note that the difference between EISCAT and GPS/IGS derived electron content data decreases significantly with increasing latitude. This could be due to a reduced contribution of the plasmaspheric content expected at high latitudes. It can be seen that a further reduction of the GPS/IGS derived TEC data by more than 1 TECU would lead to unreasonable low values for the topside and plasmaspheric contribution.

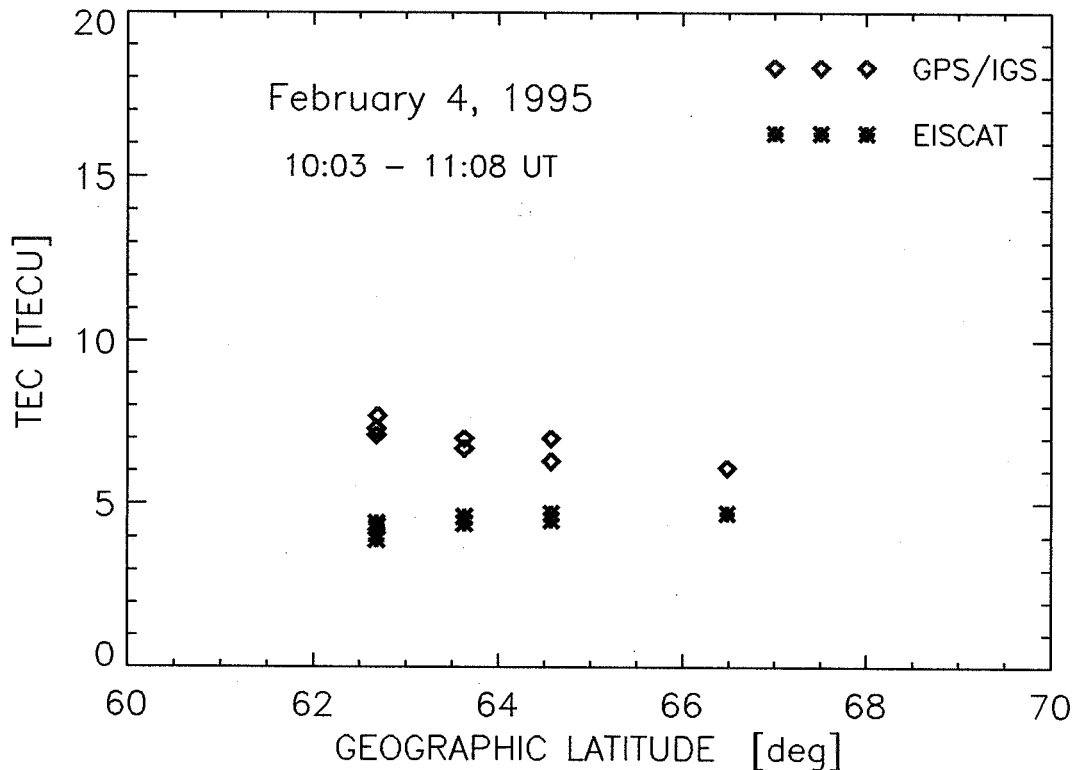


Figure 5
Comparison of electron content data derived from GPS and EISCAT CP-3 measurements on February 4, 1995. The EISCAT IEC data correspond with the integral of the vertical electron density profile in the altitude range of about 150...500 km height.

3. Comparison of vertical TEC data derived by different GPS-based methods and the IRI90 model

In order to compare GPS/IGS TEC data products generated by several groups in a more effective way, a common reference is made to the IEC data derived from height integrated IRI90 electron density profiles up to 1000 km height. To give more realistic results the IRI90 model is updated by hourly ionosonde measurements at Juliusruh as described in section 2.1. Therefore the TEC data products are referred to this location.

As GPS-derived TEC values we use the grid maps estimated by the CODE IGS analysis center (cod), ESOC (esa), the University of New Brunswick (unb) and DLR-Neustrelitz (dlr). The CODE and ESOC groups have computed global TEC maps once per day (at 12 UT) and twice per day (at 6UT and 18UT), respectively, whereas the other two groups provide hourly maps

for the European region. From these maps we have computed the vertical TEC over Juliusruh every hour using the data from the four grid points surrounding the zenith of the ionosonde station as the base for a spatial linear interpolation scheme. To construct hourly TEC values from the daily map of CODE the close longitude-time relationship was used. The ESOC data were processed in the same way, but taking into account a weighted mean of both maps at different hours.

In Fig.6 the different vertical TEC data over Juliusruh are presented for 12 days. For days 19 and 26 of October there were no ionosonde data available, for the other days also some hourly data were rejected. We have also computed the hourly differences between each GPS-based method and the values given by IRI. Fig. 7 presents the average of these differences through the 15th to the 31st of October and Fig.8 shows the corresponding RMS deviations.

As it can be seen in most of the figures, the DLR-TEC values are, in general, larger than the other GPS-based values, but closer to the IRI-values during day-time. The night-time DLR-TEC values are most of the times about 2-3 TECU larger than the rest. On the other hand, the CODE-TEC values are almost always smaller than the rest, both during day and night. For the ESOC-TEC values a discrepancy between consecutive days can be seen, so the last value of the day is about 2 TECU larger than the first one of the next day. From the 15th of October to the 4th of November, the daytime values of DLR and UNB agree very well for 12 days, but for the rest there are maximum differences of 2-4 TECU.

In principle we expect the IRI-IEC values to be smaller than the GPS-derived TEC data, due to the missing plasmaspheric contribution. As already discussed in section 2.1, the difference between corresponding IEC and TEC data is the plasmaspheric content N_p which should be in the order of 1...3 TECU. Due to the higher absolute variability of TEC data at day-time only the night-time data should be considered when discussing the plasmaspheric content.

Fig. 7 indicates a rather stable difference between IEC and TEC-DLR during the night-time. This would agree with the rather stable plasmaspheric electron content. The other stations provide differences which are too low to be interpreted as the plasmaspheric content when taking the IRI90 model as a reference.

4. Summary and Conclusions

The validation of GPS derived TEC maps by independent ionospheric measurements is still an important task to have more knowledge about the absolute and relative accuracy of TEC data products. A variety of ionospheric probing techniques may be used for such comparative studies. In each case additional assumptions have to be made in order to make the different parameters comparable. Since the validation of TEC data by other ionospheric techniques is somewhat complicated, different measuring techniques should be used. The results obtained in this study indicate general physical agreement between the GPS/IGS derived TEC data products at DLR and other ionospheric parameters. Attention should be paid to such comparative studies which provide physically unusual conclusions. This gives the possibility to adjust derived TEC data and/or to get more knowledge about the validity of assumptions or models related to the ionospheric/plasmaspheric behaviour. In the same sense the intercomparison of the results obtained by different mapping techniques is very helpful in examining the different strategies and algorithms to evaluate TEC.

When comparing GPS-based TEC derived by different groups with updated IRI90 model, we find a better consistency in the results of DLR-Neustrelitz. The maximum differences in the GPS-based TEC of the various groups are in the order of 2 .. 4 TECU.

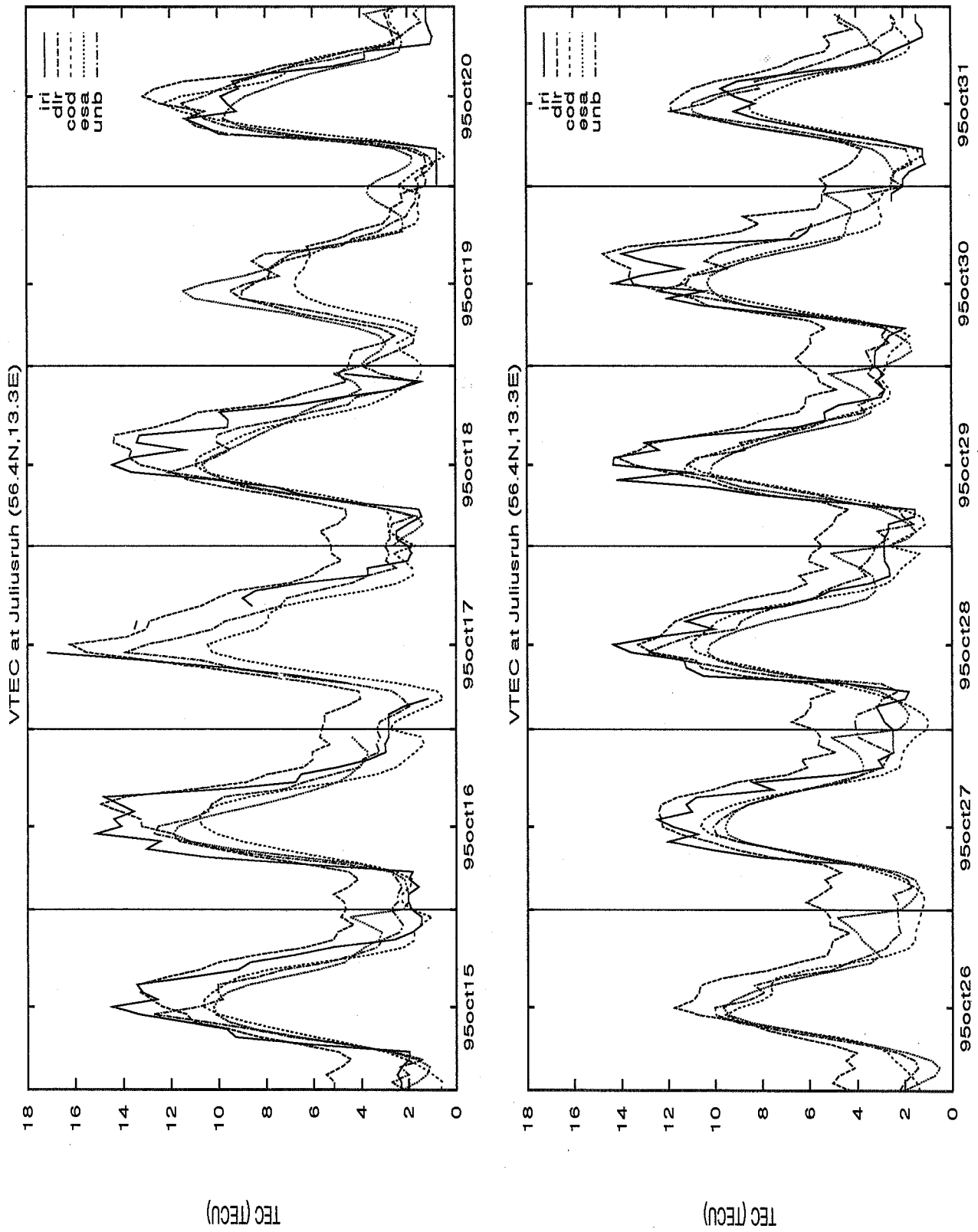


Figure 6
 Vertical TEC computed for Juliusruh using the IRI90 model and the TEC maps provided by several groups using GPS data.

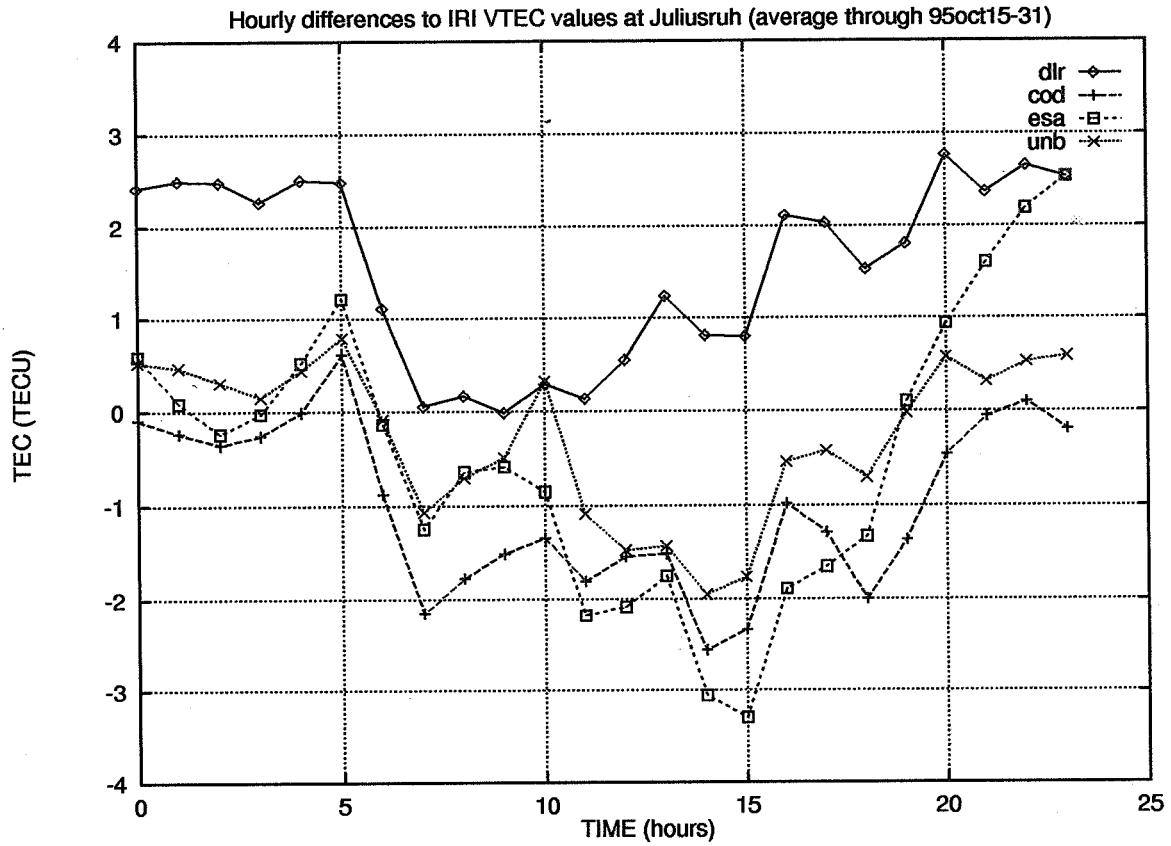


Figure 7
Hourly differences to IRI VTEC value at Juliusruh for the different groups.

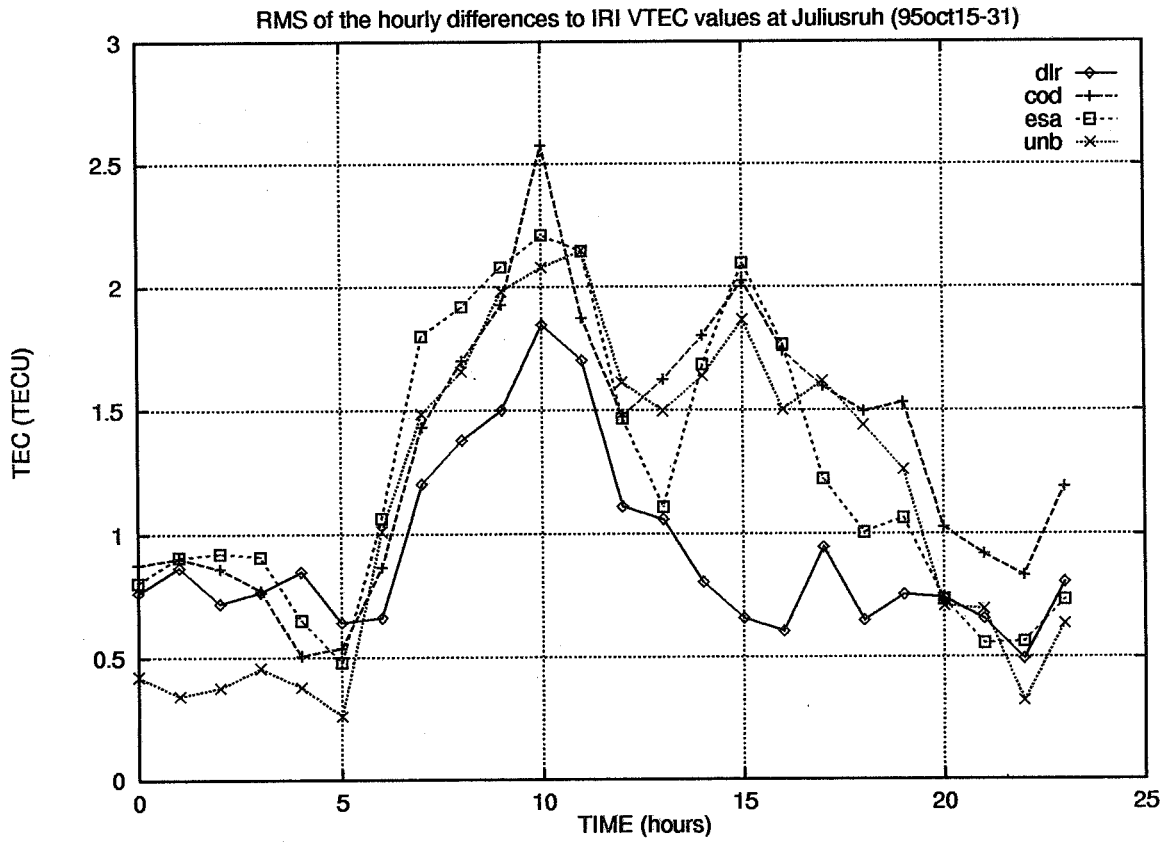


Figure 8
RMS of the hourly differences to IRI VTEC values at Juliusruh for the different groups.

Aknowledgments

The authors express their deep thanks to the colleagues of the IGS community and especially the groups involved in these comparisons who made available high quality GPS data sets and TEC data products, respectively.

We thank also J. Mielich, J. Weiß and I. Prutensky for providing ionosonde data and K. Schlegel for providing EISCAT data.

We are also grateful to D. Adrian for her help in preparing the manuscript.

The research was supported by the German Agency of Space Activities (DARA) under contract 50YI9202.

References

Coco, D., GPS-Satellites of Opportunity for Ionospheric Monitoring, *GPS world*, 47-50, October 1991.

Jakowski N. and A. Jungstand, Modeling the Regional Ionosphere by Using GPS Observations, *Proc. Int., Beacon Sat. Symp.* (Ed.: L. Kersley), University of Wales, Aberystwyth, 11-15 July 1994, pp 366-369.

N. Jakowski, Ionospheric Research and Future Contributions of the IGS Network, paper presented at the IGS-workshop, Potsdam, 15.-17.05.1995.

Sardón. E., A. Rius, and N. Zarraoa, Estimation of the receiver differential biases and the ionospheric total electron content from Global Positioning System observations, *Radio Science*, 29, 577-586, 1994.

Soicher, H., Diurnal, Day-to-Day, and Seasonal Variability of N_F , N_T and N_p at Fort Monmouth, New Jersey, *Proc. Int. Beacon Sat. Symp.* (Ed.: M. Mendillo), Boston 1-4 June, 1976, pp 231-243.

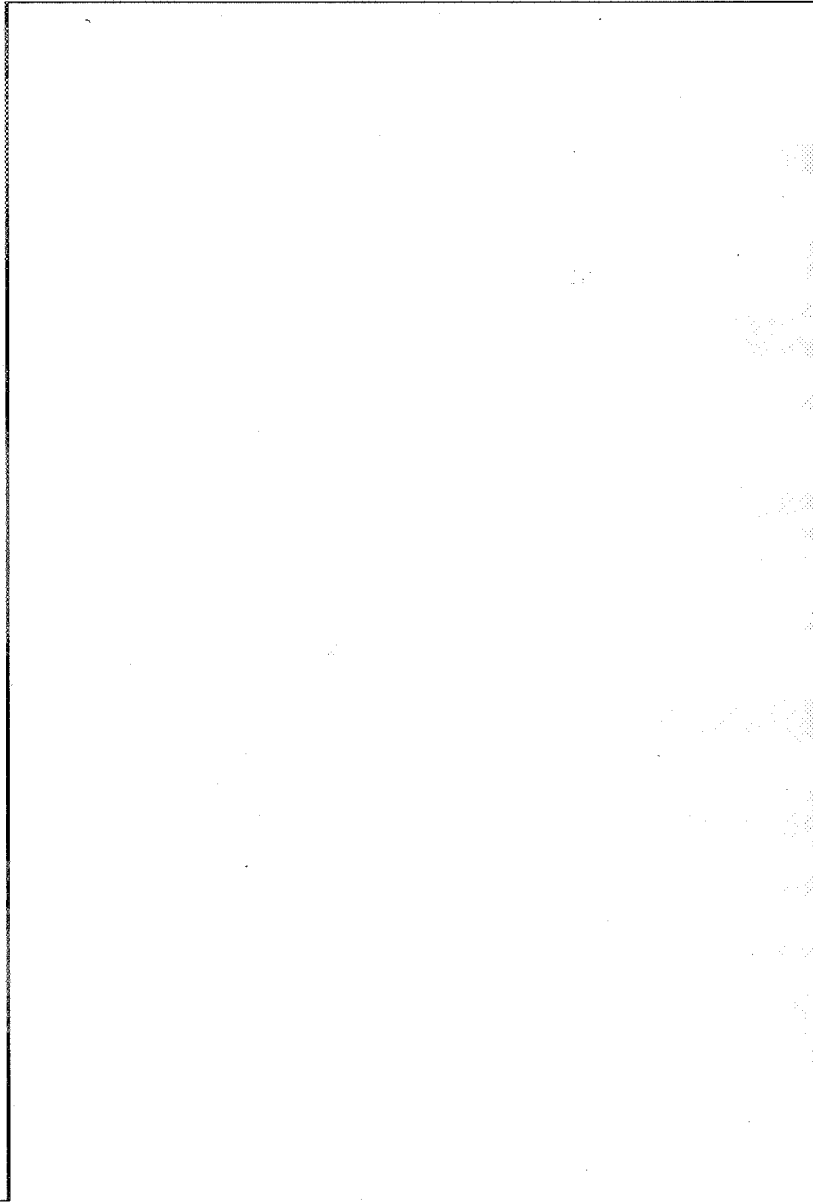
Wilson B.D., A. J. Manucci, and Ch. D. Edwards, Subdaily northern hemisphere ionospheric maps using an extensive network of GPS receivers, *Radio Science* 30, 639-648, 1995.

Zarraoa, N., E. Sardón, Test of GPS for permanent ionospheric TEC monitoring at high latitudes, *Ann. Geophys.* 14, 11-19, 1996.

Zumberge, J., R. Neilan, G. Beutler, and W. Gurtner, The International GPS-Service for Geodynamics-Benefits to Users., *Proc. ION GPS-94*, Salt Lake City, September 20-23, 1994.

IGS

APPENDIX I



Page intentionally left blank

INTRODUCTION

The SINEX acronym was suggested by Blewitt et al. (1994) and the first versions, 0.04, 0.05 and 1.00 evolved from the work and contributions of the SINEX Working Group (WG) chaired by G. Blewitt. The other SINEX WG members consisted of Claude Boucher, Yehuda Bock, Jeff Freymueller, Gerd Gendt, Werner Gurtner, Mike Heflin and Jan Kouba. Also contributions of Z. Altamimi, T. Herring, Phil Davies, Remi Ferland, David Hutchison and other IGS AC colleagues are noted and acknowledged here, in particular all the ACs submitting and using SINEX(0.05) every week since mid 1995, as a part of the IGS ITRF densification pilot project.

SINEX was designed to be modular and general enough to handle GPS as well as other techniques. In particular the information on hardware (receiver, antenna), occupancy and various correspondence between hardware, solution and input files can be preserved, which is essential for any serious analysis and interpretation of GPS results. It preserves input/output compatibility so that output SINEX files can be used (latter on) as input into subsequent computation/solutions. It also provides complete information on apriori information so that it can be removed whenever required, making it unnecessary to submit or distribute multiple (SINEX) solution files, e.g. constrained and unconstrained (free) solution files.

CHANGES FROM VERSION 0.05 TO 1.00

The version 0.05 has undergone some "fine tuning" as the result of the IGS ITRF densification pilot project but it is yet to be proof tested by other techniques. More specifically the following is a summary of the changes and enhancements from the previous version 0.05 to the new version 1.00:

- 1) Backward compatibility with the version 0.05 is assured by the version #, which MUST be coded on the first line.
- 2) Strictly fixed format, all fields are now specified and described in details in the Appendix I. In most cases the format fields are the same as in the version 0.05 with some notable exceptions. For crucial fields such as SOLUTION/ESTIMATE and SOLUTION/MATRIX a generous field length of 21 is specified which should be sufficient for up to 16 significant digits; furthermore the field lengths for receiver and antenna types in the SITE/RECEIVER and SITE/ANTENNA blocks were increased from 16 to 20 chars to make them compatible with RINEX. Also strict adherence to IGS receiver/antenna code names is now required (see the Appendix III for the list of the IGS receiver/antenna standard names).
- 3) The version 1.00 accommodates the CORR matrix type in a different fashion, namely when the CORR matrix type is used in the SOLUTION/MATRIX blocks it is now required that standard deviations (STDs) are coded on the main diagonal, in place of 1.000's. This way the STDs in the CORR matrix could be given to the full precision and they take precedent over any STDs in the SOLUTION/ESTIMATE & SOLUTION/APRIORI blocks which may not be given to a sufficient precision. The other matrix form (e.g. COVA) is still valid and acceptable.

4) A new (mandatory for IGS) block (SOLUTION/STATISTICS) is introduced for needed solution statistics (see the example below)

```
+SOLUTION/STATISTICS
* STATISTICAL PARAMETER _____ VALUE (S) _____
  VARIANCE FACTOR                0.9260149874E-02
  NUMBER OF OBSERVATIONS          811865
  NUMBER OF UNKNOWNNS            22142
  SAMPLING INTERVAL(SECONDS)     120
-SOLUTION/STATISTICS
```

Other possible headings/entries might include e.g.:
 SQUARE SUM RESIDUALS (VTPV)
 NUMBER OF DEGREES OF FREEDOM , etc.

5) Additional standardized parameter code names were introduced to accommodate some specific users, more parameter codes may be introduced as the need arises. For future applications and to ease interpretation, the parameter code fields have been increased from four to six chars in all the relevant (SOLUTION) blocks, with some minor changes in the format fields to accommodate this change. It is suggested that the current (four chars) codes used by IGS (STAX, STAY, STAZ, VELY, VELY, VELZ, LOD, UT, XPO, YPO) are retained for compatibility/continuity reasons and that any new ones take the advantage of the six chars field. E.g. for the orbit parameters the following code names could be suggested:

```
SAT_X PR01  X state of PRN 01
SAT_Y PR01  Y "      "
SAT_Z PR01  Z "      "

SAT_VX PR01  Vx " •    "
.
.
SAT_RP PR01  Rp scale of PRN 01
SAT_GX PR01  Gx "      "
SAT_GZ PR01  Gz "      "
SATYBI PR01  Gy bias   "

TROTOT ALGO  Tropo delay (wet + dry) at ALGO
TRODRY ALGO  Tropo delay (dry)
TROWET ALGO  Tropo delay (wet)
```

etc.

Note: The use of SV rather PR could be considered here, as it is more meaningful, but since the GPS users are accustomed to PRN's (and PRNs are used in sp3) we may not have any other choice. Considering that "P" is used by IERS as the technique code for GPS, it may not be (i.e. "PR") such a bad choice. Other satellite system would then have to be assigned unique code of two chars.

6) The version 1.00 discontinues the practice of using separate OCC_ and SOLN codes in the SITE and SOLUTION blocks, respectively, as it serves no useful purpose. Further more it is suggested to use the SOLN codes for the SITE blocks as well (i.e. SITE/ECCENTRICITY, ./RECEIVER; ./ANTENNA and ./DATA). In most cases for the individual AC SINEXes, the SOLN codes should then be coded with the default characters "-" which could mean that "this

record applies to all estimates" (note SITE+PT+SOLN defines a unique estimate, SITE+PT is equivalent to DOMES (DOMEX) and uniquely identifies a geodetic mark). What is exactly meant should be clear from the examples below:

+SITE/ANTENNA

```
*Code PT SOLN T _Data Start_ _Data End_ _antenna type_ _S/N_
* lines removed
GOLD A ---- P 92:180:00000 95:304:79200 DORNE MARGOLIN R 95
GOLD A ---- P 95:304:79200 00:000:00000 DORNE MARGOLIN T ----
* etc.
* (NOTE: above ANTENNA TYPE FIELD = 20chars)
```

+SITE/ECCENTRICITY

```
*Code PT SOLN T _Data Start_ _Data End_ type _ARP-benchmark (m)
* lines removed
GOLD A ---- P 92:180:00000 95:304:79200 UNE .0000 .0000 .0000
GOLD A ---- P 95:304:79200 00:000:00000 UNE .0025 .0000 .0000
* etc.
* NOTE: Continuity of multiple entry of a site must be adhered, i.e. the
* end epoch of the first ( must be coded) =< the start epoch of the second
* entry.
```

This would allow only one (e.g. SOLN=1) for GOLD in the ESTIMATE blocks. On the other hand if one prefers two SOLNs (e.g. 1 & 2) for GOLD in the ESTIMATE blocks, e.g. before and after an antenna change, then the same (e.g. 1 & 2) SOLN must be used in all GOLD entries in the SITE blocks as well. Conversely when two solutions (SOLN 1, 2) are introduced for some reasons other than instrument/antenna change (e.g. as a result a coseismic change, with the same rec/antenna/eccentricity) then, only one entry in the SITE blocks with the default character codes ("-") in the SOLN field need to be coded or alternatively two identical entries with 1 and 2 in the SOLN field could be used (except, of course, for the start and end epochs which must be continuous and non overlapping). This considerably enhances the SINEX effectiveness.

SINEX SYNTAX

SINEX is an ASCII file with lines of 80chars or less. It consists of a number of blocks which are mutually referenced (related) through station codes/names, epochs and/or index counters. Some blocks consist of descriptive lines (starting in Col.2) and/or fixed format fields with numerous headers and descriptive annotations.

The first line is MANDATORY and must start with "%" in col 1, and contains information about the agency, file identification, solution spans, techniques, type of solution, etc. (for more details see the Appendix I or II). The last line ends with "%ENDSNX".

The SINEX format consists of a number BLOCKS which start with "+" in the first col. followed by a standardized block labels, and each block ends with "-" and the block label. Each block data starts in the column 2 or higher. Blocks can be in any order, provided that they start with (+) and end with (-) block labels. The first header line and most blocks are related through epochs or time stamps in the following format:

YY:DOY:SECOD YY-year; DOY- day of year; SECOD -sec of day;
E.g. the epoch 95:120:86399 denotes April 30, 1995 (23:59:59UT). The epochs 00:00:00000 are allowed in all blocks (except the first header line) and default into the start or end epochs of the first header line which must always be coded. This is particularly useful for some blocks, such as the ones related to hardware, occupancy, which should be centrally archived by IGSCB with 00:00:00000 as the end (current) epochs, and which should be readily usable by ACs for SINEX and other analysis/processing as official (authoritative) IGS information.

COMMENT lines starts with "*" in Col. 1 and can be anywhere within or outside a block, though for the clarity sake, beginning and ends of blocks are preferable. For increased portability, the floating number exponent of "E" should be used rather than "D" or "d" which is not recognized by some compiler/installations. Fields not coded should be filled with "-" characters to allow efficient row and column format readings.

The most important blocks are the SOLUTION blocks. They are in fixed format and have been adopted and used by IERS (ISEF1) submission format as well. (For more information on the format, see the Appendix I). Only two SOLUTION blocks (SOLUTION/ESTIMATE and SOLUTION/MATRIX_ESTIMATE) are MANDATORY and must be coded. They contain complete solutions (apriori + solution vector) and the corresponding standard deviations, and the corresponding matrix. Although various matrix forms are allowed in SINEX (as specified by a matrix type code), triangular correlation matrix (e.g. SOLUTION/MATRIX_ESTIMATE L CORR) is preferred and recommended for IGS since it is easier to visualize. Important but not mandatory (though RECOMMENDED for IGS purposes) are the next two blocks, i.e. the SOLUTION/APRIORI and SOLUTION/MATRIX_APRIORI. The scale of estimated and apriori standard deviations can, in principle, be arbitrary (note even apriori scaling is arbitrary, depending on the observation weighting). However, both estimated and apriori standard deviations (and the corresponding matrices) MUST use the same scaling (i.e. variance) factor. Otherwise the apriori information cannot be rigorously removed to form free solutions (e.g. normal matrices). Scaling between different SINEX solutions is beyond the SINEX format and must be dealt with at the combination/analysis stage.

REFERENCES

Blewitt, G., Y. Bock and J. Kouba: "Constraining the IGS Polyhedron by Distributed Processing", workshop proceedings : Densification of ITRF through Regional GPS Networks, held at JPL, Nov 30-Dec 2, 1994, pp. 21-37.

A P P E N D I X I

S I N E X

V E R S I O N 1 . 0 0

D E T A I L F O R M A T D E S C R I P T I O N

1. INTRODUCTION
2. DATA STRUCTURE
3. HEADER LINE
4. FILE/REFERENCE BLOCK
5. FILE/COMMENT BLOCK
6. INPUT/HISTORY BLOCK
7. INPUT/FILES BLOCK
8. INPUT/ACKNOWLEDGEMENT BLOCK
9. SITE/ID BLOCK
10. SITE/DATA BLOCK
11. SITE/RECEIVER BLOCK
12. SITE/ANTENNA BLOCK
13. SITE/GPS PHASE CENTER BLOCK
14. SITE/ECCENTRICITY BLOCK
15. SOLUTION/EPOCH BLOCK
16. SOLUTION/STATISTICS
17. SOLUTION/ESTIMATE BLOCK
18. SOLUTION/APRIORI BLOCK
19. SOLUTION/MATRIX_ESTIMATE BLOCK
20. SOLUTION/MATRIX_APRIORI BLOCK
21. FOOTER LINE

1. Introduction

This document describes the Software INdependent EXchange (SINEX) format. The need for such a format grew out of the increasing need to exchange station coordinates information. It started in early 1995 by an effort from a number of IGS participants. The format has quickly evolved beyond the original objectives. The information is organized by blocks. The format is designed to be easily extended as need may arise.

2. Data Structure

Each SINEX line has at most 80 ASCII characters. The SINEX file is subdivided in groups of data called blocks. Each block is enclosed by a header and trailer line. Each block has a fixed format. The blocks contain information on the file, its input, the sites and the solution. All elements within a line are defined. A character field without information will have "-"s within its field and a missing numerical element will have a value of 0 within its field. This lets the SINEX file to be accessible "column-wise" as well as "line-wise". Character fields should be left hand justified whenever applicable.

The first character of each line identify the type of information that the line contains. Five characters are reserved. They have the following meaning when they are at the beginning of a line, they identify:

Character	Definition
"%"	Header and trailer line,
"*"	Comment line within the header and trailer line,
"+"	Title at the start of a block
"-"	Title at the end of a block
" "	Data line within a block

No other character is allowed at the beginning of a line.

A SINEX file must start with a Header line and ends with a footer line.

The following blocks are defined:

FILE/REFERENCE
FILE/COMMENT
INPUT/HISTORY
INPUT/FILES
INPUT/ACKNOWLEDGEMENTS
SITE/ID
SITE/DATA
SITE/RECEIVER
SITE/ANTENNA
SITE/GPS_PHASE_CENTER
SITE/ECCENTRICITY
SOLUTION/EPOCH
SOLUTION/STATISTICS
SOLUTION/ESTIMATE
SOLUTION/APRIORI
SOLUTION/MATRIX_ESTIMATE {p} {type}
SOLUTION/MATRIX_APRIORI {p} {type}

Where: {p} L or U
{type} CORR or COVA or INFO or SRIF

These block titles are immediately preceded by a "+" or a "-" as they mark the beginning or the end of a block. The block titles must be in capital letters. After a block has started(+) it must be ended(-) before another

Field	Description	Format
Time	YY:DDD:SSSS. "UTC" YY = last 2 digits of the year, if YY <= 50 implies 21-st century, if YY > 50 implies 20-th century, DDD = 3-digit day in year, SSSS = 5-digit seconds in day.	I2.2, 1H:,I3.3, 1H:,I5.5
Constraint Code	Single digit indicating the constraints: 0-fixed/tight constraints, 1-significant constraints, 2-unconstrained.	A1
Parameter Type	Type of parameter. List of allowed parameters: STAX - station X coordinate, m STAY - station Y coordinate, m STAZ - station Z coordinate, m VELX - station X velocity, m/y VELY - station Y velocity, m/y VELZ - station Z velocity, m/y LOD - length of day, ms UT - delta time UT1-UTC, ms XPO - X polar motion, mas YPO - Y polar motion, mas XPOR - X polar motion rate, ma/d YPOR - Y polar motion rate, ma/d SAT_X - Satellite X coord., m SAT_Y - Satellite Y coord., m SAT_Z - Satellite Z coord., m SAT_VX - Satellite X velocity, m/s SAT_VY - Satellite Y velocity, m/s SAT_VZ - Satellite Z velocity, m/s SAT_RP - Radiation pressure, SAT_GX - GX scale, SAT_GZ - GZ scale, SATYBI - GY bias, m/s ² TROTOT - wet + dry Tropo delay m TRODRY - dry Tropo delay m TROWET - wet Tropo delay m	A6
Site Code	- For stations: Call sign for a site. (It should be consistent with IGS convention). - For satellites: Use "PRXX" where XX is the PRN number.	A4
Point Code	A two character code identifying physical monument within a site. Typically has a code A, but could vary if the site has more than one monument.	A2
Solution ID	Character identifying the solution given for a point at a site. "----" applies to all.	A4
Observation Code.	A single character indicating the technique(s) used to arrive at the solutions obtained in this SINEX file. It should be consistent with the IERS convention. This character code may be: C-Combined techniques used. D-DORIS, L-SLR, M-LLR, P-GPS, R-VLBI.	A1

block can begin. The general structure is as follow:

```

%=SNX..... (Header line)-----|
.....|
+(BLOCK TITLE)-----|
.....|
.....|
-(BLOCK TITLE)-----|
.....|
+(BLOCK TITLE)-----|
.....|
.....|
-(BLOCK TITLE)-----|
.....|
%ENDSNX          (Trailer line)-----|

```

Most fields within a SINEX line are separated by a single space. In the following sections, each SINEX line is defined by its field name, a general description and the (FORTRAN) format.

The comment line (not to be confused with the FILE/COMMENT Block) can be written anywhere within the header and the footer line is defined as:

C O M M E N T D A T A L I N E		
Field	Description	Format
Comment	Any general comment relevant to the SINEX file.	1H*,A79
		80

For example, the use of "*" in the first column can be used to effectively hide information from the software without deleting it from the file.

Some fields are found in several blocks. To keep the description short, they are described in detail here, and will be referred to in the sections with additional information added when necessary. The fields defined below will be referenced to by putting them within square brackets [] when encountered in the following sections.

3. Header Line (Mandatory)

Description

The Header line must be the first line in a SINEX file.

Contents:

HEADER LINE		
Field	Description	Format
First Character	Single character '%' in column #1. No other character than '%' is allowed.	A1
Second Character	Single character '=' in column #2. Indicates 'resultant' solution. No other character than '=' is allowed.	A1
Document Type	Three characters 'SNX' in columns 3 to 5. Indicates that this is a SINEX document.	A3
Format Version	Four digits indicating the version of SINEX format used. '1.00' for this version.	1X,F4.2
File Agency Code	Identify the agency creating the file.	1X,A3
[Time]	Creation time of this SINEX file.	1X,I2.2, 1H:,I3.3, 1H:,I5.5
[Agency Code]	Identify the agency providing the data in the SINEX file	1X,A3
[Time]	Start time of the data used in the SINEX solution Value 00:000:00000 should be avoided.	1X,I2.2, 1H:,I3.3, 1H:,I5.5
[Time]	End time of the data used in the SINEX solution Value 00:000:00000 should be avoided.	1X,I2.2, 1H:,I3.3, 1H:,I5.5
[Observation Code]	Technique(s) used to generate the SINEX solution	1X,A1
Number of Estimates	Number of parameters estimated in this SINEX file. Mandatory field.	1X,I5.5
[Constraint Code]	Single character indicating the constraint in the SINEX solution. Mandatory field.	1X,A1
Solution Contents	Solution types contained in this SINEX file. Each character in this field may be one of the following: X - Station Coordinates, V - Station Velocities, O - Orbits, E - Earth Rotation Parameters T - Troposphere BLANK	5(1X,A1)
		77

Relationship with other blocks:

This line is duplicated as the resultant line of the INPUT/HISTORY Block with the exception of its first character.

4. FILE/REFERENCE Block (Mandatory for IGS)

Description:

This block provides information on the Organization, point of contact, the software and hardware involved in the creation of the file.

Contents:

FILE REFERENCE DATA LINE		
Field	Description	Format
Information Type	<p>Describes the type of information present in the next field. May take on the following values:</p> <ul style="list-style-type: none"> 'DESCRIPTION' - Organization(s) gathering/altering the file contents. 'OUTPUT' - Description of the file contents. 'CONTACT' - Address of the relevant contact. e-mail 'SOFTWARE' - Software used to generate the file. 'HARDWARE' - Computer hardware on which above software was run. 'INPUT' - Brief description of the input used to generate this solution. <p>Any of the above fields may be and in any order.</p>	1X,A18
Information	Relevant information for the type indicated by the previous field.	1X,A60
		80

5. FILE/COMMENT Block (Optional)

Description:

This Block can be used to provide general comments about the SINEX data file.

Contents:

FILE COMMENT DATA LINE		
Field	Description	Format
Comment	Any general comment providing relevant information about the SINEX file.	1X,A79
		80

6. INPUT/HISTORY Block (Recommended)

Description:

This block provides information about the source of the information used to create the current SINEX file.

Contents:

INPUT HISTORY DATA LINE		
Field	Description	Format
File Code	Only one of the following characters is permitted: '+' - This character indicates that the information that follows identify an input solution contributing to this SINEX file. '=' - This character indicates that the information that follows identify the output solution file.	1X,A1
Document Type	Three characters 'SNX' in columns 3 to 5. Indicates that this is a SINEX document.	A3
Format Version	Four digits indicating the version of SINEX format used. '1.00' for this version.	1X,F4.2
[Agency Code]	Identify the agency creating the file.	1X,A3
[Time]	Creation time of this SINEX file.	1X,I2.2, 1H:,I3.3, 1H:,I5.5
[Agency Code]	Identify the agency providing the data in the SINEX file.	1X,A3
[Time]	Start time of the data used in the SINEX solution.	1X,I2.2, 1H:,I3.3, 1H:,I5.5
[Time]	End time of the data used in the SINEX solution.	1X,I2.2, 1H:,I3.3, 1H:,I5.5
[Observation Technique]	Technique(s) used to generate the SINEX solution.	1X,A1
Number of Estimates	Number of parameters estimated in this SINEX file.	1X,I5.5
[Constraint Code]	Single digit indicating the constraint in the SINEX solution.	1X,A1
Solution Contents	Solution types contained in this SINEX file. Each character in this field may be one of the following: X - Station Coordinates, V - Station Velocities, O - Orbits, E - Earth Rotation Parameters T - Troposphere BLANK	6(1X,A1)
		79

Comment:

The final data line "=" describes the current SINEX file and match the Header line with the exception of the first character.

7. INPUT/FILES Block (Optional)

Description:

This block identify the input files and allow for a short comment to be added to describe those files.

Contents:

I N P U T F I L E S D A T A L I N E		
Field	Description	Format
[Agency Code]	Agency creating the solution described in this data line.	1X,A3
[Time]	Time of creation of the input SINEX solution	1X,I2.2, 1H:,I3.3, 1H:,I5.5,
File Name	Name of the file containing the solution described in the current data line.	1X,A29
File Description	General description of the file referred to on this data line.	1X,A32
		80

Comments:

There must be exactly one INPUT/FILES data line for every INPUT/HISTORY data line. The final data line must describe this current SINEX file.

8. INPUT/ACKNOWLEDGEMENTS Block (Optional)

Description:

This block defines the agency codes contributing to the SINEX file.

Contents:

I N P U T A C K N O W L E D G M E N T S D A T A L I N E		
Field	Description	Format
[Agency Code]	Agency(ies) contributing to this SINEX file.	1X,A3
Agency Description	Description of agency code.	1X,A75
		80

9. SITE/ID Block (Mandatory)

Description:

This block provides general information for each site containing estimated parameters.

Contents:

SITE ID DATA LINE		
Field	Description	Format
[Site Code]	Call sign for a site.	1X,A4
[Point Code]	Physical monument used at a site	1X,A2
Unique Monument Identification	Unique alpha-numeric monument identification. For ITRF purposes, it is a nine character DOMES/DOEX number (five/six digits, followed by the single letter 'M' or 'S', followed by four/three digits)	1X,A9
[Observation Code]	Observation technique(s) used.	1X,A1
Station Description	Free-format description of the site, typically the town and/or country.	1X,A22
Approximate Longitude	Approximate longitude of the site in degrees (W/+), minutes and seconds.	1X,I3, 1X,I2, 1X,F4.1
Approximate Latitude	Approximate latitude of the site in degrees (NS/+-), minutes and seconds.	1X,I3, 1X,I2, 1X,F4.1
Approximate Height	Approximate height of the site in meters.	1X,F7.1
		75

10. SITE/DATA Block (Optional)

Description:

This block gives the relationship between the estimated station parameters in the SINEX file and in the input files.

Contents:

S I T E D A T A L I N E		
Field	Description	Format
[Site Code]	Site Code for solved station coordinates.	1X,A4
[Point Code]	Point Code for solved station coordinates.	1X,A2
[Solution ID]	Solution number to which the input in this data line is referred to.	1X,A4
[Site Code]	Site Code from an input SINEX file	1X,A4
[Point Code]	Point code from an input SINEX file.	1X,A2
[Solution ID]	Solution Number for a Site/Point from an input SINEX file.	1X,A4
[Observation Code]	Observation Code for a Site/Point/Solution Number from an input SINEX file.	1X,A1
[Time]	Time of start of data for the input SINEX file.	1X,I2.2, 1H:,I3.3, 1H:,I5.5
[Time]	Time of end of data for the input SINEX file.	1X,I2.2, 1H:,I3.3, 1H:,I5.5
[Agency Code]	Creation Agency Code for the input SINEX file.	1X,A3
[Time]	Creation time for the input SINEX file.	1X,I2.2, 1H:,I3.3, 1H:,I5.5
		71

11. SITE/RECEIVER Block (Mandatory for IGS)

Description:

List the receiver used at each site during the observation period of interest.

Contents:

SITE RECEIVER DATA LINE		
Field	Description	Format
[Site Code]	Site code for which some parameters are estimated.	1X,A4
[Point Code]	Point Code at a site for which some parameters are estimated.	1X,A2
[Solution ID]	Solution Number at a Site/Point code for which some parameters are estimated.	1X,A4
[Observation Code]	Identification of the observation technique used.	1X,A1
[Time]	Time since the receiver has been operating at the Site/Point. Value 00:000:00000 indicates that the receiver has been operating at least since the "File Epoch Start Time".	1X,I2.2, 1H:,I3.3, 1H:,I5.5
[Time]	Time until the receiver is operated at a Site/Point. Value 00:000:00000 indicates that the receiver has been operating at least until the "File Epoch End Time".	1X,I2.2, 1H:,I3.3, 1H:,I5.5
Receiver Type	Receiver Name & model. (See Appendix III for IGS Standard receiver names)	1X,A20
Receiver Serial Number	Serial number of the receiver. Takes on value '-----' if unknown.	1X,A5
Receiver Firmware	Firmware used by this receiver during the epoch specified above. Takes on value '-----' if unknown.	1X,A11
		80

12. SITE/ANTENNA Block (Mandatory for IGS)

Description:

List of antennas used at each site used in the SINEX file.

Contents:

S I T E A N T E N N A D A T A L I N E		
Field	Description	Format
[Site Code]	Site code for which some parameters are estimated.	1X,A4
[Point Code]	Point Code at a site for which some parameters are estimated.	1X,A2
[Solution ID]	Solution Number at a Site/Point code for which some parameters are estimated.	1X,A4
[Observation Code]	Identification of the observation technique used.	1X,A1
[Time]	Time since the antenna has been installed at the Site/Point. Value 00:000:00000 indicates that the antenna has been installed at least since the "File Epoch Start Time".	1X,I2.2, 1H:,I3.3, 1H:,I5.5
[Time]	Time until the antenna is installed at a Site/Point. Value 00:000:00000 indicates that the antenna has been installed at least until the "File Epoch End Time".	1X,I2.2, 1H:,I3.3, 1H:,I5.5
Antenna Type	Antenna name & model. (See Appendix III for IGS Standard antenna names)	1X,A20
Antenna Serial Number	Serial number of the antenna. Takes on value '-----' if unknown.	1X,A5
		68

13. SITE/GPS_PHASE_CENTER Block (Mandatory for IGS)

Description:

List of GPS phase centers offset for all antennas described in the Site Antenna block. The offset is given from the Antenna Reference Point (ARP) to the L1 and L2 phase centers respectively. For IGS purposes see the IGS Central Bureau Information System for ARPs and antenna phase center offsets:

directory: igscb/station/general ; files: antenna.gra and rcv_ant.tab

Contents:

GPS PHASE CENTER DATA LINE		
Field	Description	Format
Antenna Type	Antenna name & model. (See Appendix III for IGS Standard antenna names)	1X,A20
Antenna Serial Number	Serial number of the antenna. Takes on value '-----' if unknown.	1X,A5
L1 Phase Center Up Offset	Up(+) offset from the ARP to the L1 phase center in meters.	1X,F6.4
L1 Phase Center North Offset	North(+) offset from the ARP to the L1 phase center in meters.	1X,F6.4
L1 Phase Center East Offset	East(+) offset from the ARP to the L1 phase center in meters.	1X,F6.4
L2 Phase Center Up Offset	Up(+) offset from the ARP to the L2 phase center in meters.	1X,F6.4
L2 Phase Center North Offset	North(+) offset from the ARP to the L2 phase center in meters.	1X,F6.4
L2 Phase Center East Offset	East(+) offset from the ARP to the L2 phase center in meters.	1X,F6.4
Antenna Calibration model	Name of the antenna model used in the correction of the observations for phase center variations.	1X,A10
		80

14. SITE/ECCENTRICITY Block (Mandatory for IGS)

Description:

List of antenna eccentricities from the Marker to the Antenna Reference Point (ARP). For IGS purposes see the IGS Central Bureau Information System for antenna eccentricities:

directory: igscb/station/tie; files: localtie.tab and localtie.chg

Contents:

SITE ECCENTRICITY DATA LINE		
Field	Description	Format
[Site Code]	Site code for which some parameters are estimated.	1X,A4
[Point Code]	Point Code at a site for which some parameters are estimated.	1X,A2
[Solution ID]	Solution ID at a Site/Point code for which some parameters are estimated.	1X,A4
[Observation Code]	Identification of the observation technique used.	1X,A1
[Time]	Time since the antenna has been installed at the Site/Point. Value 00:000:00000 indicates that the antenna has been installed at least since the "File Epoch Start Time".	1X,I2.2, 1H:,I3.3, 1H:,I5.5
[Time]	Time until the antenna is installed at a Site/Point. Value 00:000:00000 indicates that the antenna has been installed at least until the "File Epoch End Time".	1X,I2.2, 1H:,I3.3, 1H:,I5.5
Eccentricity Reference System	Reference system used to describe vector distance from monument benchmark to the antenna reference point: 'UNE' - Local reference system Up, North, East. 'XYZ' - Cartesian Reference System X, Y, Z. All units are in meters.	1X,A3
Up / X Eccentricity	Up / X offset from the marker to the Antenna reference point (ARP).	1X,F8.4
North / Y Eccentricity	North/Y offset from the marker to the Antenna reference point (ARP).	1X,F8.4
East / Z Eccentricity	East/Z offset from the marker to the Antenna reference point (ARP).	1X,F8.4
		72

15. SOLUTION/EPOCH Block (Mandatory).

Description:

List of solution epoch for each Site Code/Point Code/Solution Number/Observation Code (SPNO) combination.

Contents:

SOLUTION EPOCHS DATA LINE		
Field	Description	Format
[Site Code]	Site code for which some parameters are estimated.	1X,A4
[Point Code]	Point Code at a site for which some parameters are estimated.	1X,A2
[Solution ID]	Solution Number at a Site/Point code for which some parameters are estimated.	1X,A4
[Observation Code]	Identification of the observation technique used.	1X,A1
[Time]	Start time for which the solution identified (SPNO) has observations	1X,I2.2, 1H:,I3.3, 1H:,I5.5
[Time]	End time for which the solution identified (SPNO) has observations	1X,I2.2, 1H:,I3.3, 1H:,I5.5
[Time]	Mean time of the observations for which the solution (SPNO) is derived.	1X,I2.2, 1H:,I3.3, 1H:,I5.5
		54

16. SOLUTION/STATISTICS Block (Optional)

Description:

List of solution epoch for each Site Code/Point Code/Solution Number/Observation Code (SPNO) combination.

Contents:

SOLUTION STATISTICS LINE		
Field	Description	Format
Information Type	<p>Describes the type of information present in the next field. May take on the following values:</p> <p>'NUMBER OF OBSERVATIONS' # of observations used in the adjustment.</p> <p>'NUMBER OF UNKNOWNNS' # of unknowns solved in the adjustment.</p> <p>'SAMPLING INTERVAL (SECONDS)' Interval in seconds between successive observations.</p> <p>'SQUARE SUM OF RESIDUALS (VTPV)' Sum of squares of residuals. (V'PV); V-resid. vector; P- weight matrix</p> <p>'PHASE MEASUREMENTS SIGMA' Sigma used for the phase measurements.</p> <p>'CODE MEASUREMENTS SIGMA' Sigma used for the code (pseudo-range) measurements.</p> <p>'NUMBER OF DEGREES OF FREEDOM' # of observations minus the # of unknowns (df)</p> <p>'VARIANCE FACTOR' Sum of squares of residuals divided by the degrees of freedom (V'PV/df). Equivalent to Chi-squared/df.</p> <p>Any of the above fields may be present and in any order.</p>	1X,A30
Information	Relevant information for the type indicated by the previous field.	1X,F22.15
		54

17. SOLUTION/ESTIMATE Block (Mandatory)

Description:

Estimated parameters.

Contents:

SOLUTION ESTIMATE DATA LINE		
Field	Description	Format
Estimated Parameters Index	Index of estimated parameters. values from 1 to the number of parameters.	1X,I5
[Parameter Type]	Identification of the type of parameter.	1X,A6
[Site Code]	Site code for which some parameters are estimated.	1X,A4
[Point Code]	Point Code at a site for which some parameters are estimated.	1X,A2
[Solution ID]	Solution ID at a Site/Point code for which some parameters are estimated.	1X,A4
[Time]	Epoch at which the estimated parameter is valid.	1X,I2.2, 1H:,I3.3, 1H:,I5.5
Parameter Units	Units used for the estimates and sigmas. Typical units are: m (meters), ms (milliseconds), mas (milli-arc-seconds).	1X,A4
[Constraint Code]	Constraint applied to the parameter.	1X,A1
Parameter Estimate	Estimated value of the parameter.	1X,E21.15
Parameter Standard Deviation	Estimated standard deviation for the parameter.	1X,E11.6
		80

18. SOLUTION/APRIORI Block (Recommended/Mandatory)

Description:

Apriori information for estimated parameters. This block is mandatory if significant constraints have been applied to the estimated parameters in SOLUTION/ESTIMATE Block.

Contents:

SOLUTION ESTIMATE DATA LINE		
Field	Description	Format
Apriori Parameters Index	Index of apriori parameters. values from 1 to the number of parameters.	1X,I5
[Parameter Type]	Identification of the type of parameter. Typical id's are:	1X,A6
[Site Code]	Site code with apriori parameter estimate.	1X,A4
[Point Code]	Point Code with apriori parameter estimate.	1X,A2
[Solution ID]	Solution ID at a Site/Point code with apriori parameter estimate.	1X,A4
[Time]	Epoch at which the apriori parameter is valid.	1X,I2.2, 1H:,I3.3, 1H:,I5.5
Parameter Units	Units used for the aprioris and sigmas. Typical units are: m (meters), ms (milliseconds), mas (milli-arc-seconds).	1X,A4
[Constraint Code]	Constraint applied to the parameter.	1X,A1
Parameter Apriori	Apriori value of the parameter.	1X,E21.15
Parameter Standard Deviation	Apriori standard deviation for the parameter.	1X,E11.6
		80

19. SOLUTION/MATRIX_ESTIMATE Block (Mandatory)

Description:

The Estimate Matrix can be stored in an Upper or Lower triangular form. Only the Upper or Lower portion needs to be stored because the matrix is always symmetrical.

The matrix contents can be:

CORR - Correlation Matrix

COVA - Covariance Matrix

INFO - Information Matrix (of Normals)

SRIF - Square Root Information Filter Matrix

The distinction between the form and its contents is given by the title block which must take one of the following form:

SOLUTION/MATRIX_ESTIMATE L CORR

SOLUTION/MATRIX_ESTIMATE U CORR

SOLUTION/MATRIX_ESTIMATE L COVA

SOLUTION/MATRIX_ESTIMATE U COVA

SOLUTION/MATRIX_ESTIMATE L INFO

SOLUTION/MATRIX_ESTIMATE U INFO

SOLUTION/MATRIX_ESTIMATE L SRIF

SOLUTION/MATRIX_ESTIMATE U SRIF

Contents:

SOLUTION MATRIX ESTIMATE DATA LINE		
Field	Description	Format
Matrix Estimate Row Number	Row index for the Matrix Estimate. It must match the parameter index in the SOLUTION/ESTIMATE block for the same parameter.	1X,I5
Matrix Estimate Column Number	Column index for the Matrix Estimate. It must match the parameter index in the SOLUTION/ESTIMATE block for the same parameter.	1X,I5
First Matrix Estimate Element	Matrix element at the location (Row Number , Column Number).	1X,E21.14
Second Matrix Estimate Element	Matrix element at the location (Row Number , Column Number + 1).	1X,E21.14
Third Matrix Estimate Element	Matrix element at the location (Row Number , Column Number + 2).	1X,E21.14
		78

Comment:

The Matrix Estimate Row/Column Number correspond to the Estimated Parameters Index in the SOLUTION/ESTIMATE block. If the CORR matrix is used, standard deviations must be stored in the diagonal elements.

Missing elements in the matrix are assumed to be zero (0); consequently, zero elements may be omitted.

NOTE: The same scale (variance) factor MUST be used for both MATRIX_ESTIMATE and MATRIX_APRIORI, as well as for the standard deviations in the ESTIMATE and APRIORI Blocks.

20. SOLUTION/MATRIX_APRIORI Block (Recommended/Mandatory)

Description:

The Apriori Matrix can be stored in an Upper or Lower triangular form. Only the Upper or Lower portion needs to be stored because the matrix is always symmetrical. Mandatory if any significant constraint have been applied to the SOLUTION/ESTIMATE.

The matrix contents can be:

CORR - Correlation Matrix

COVA - Covariance Matrix

INFO - Information Matrix (of Normals)

SRIF - Square Root Information Filter Martix

The distinction between the form and its contents is given by the title block which must take one of the following form:

SOLUTION/MATRIX_APRIORI L CORR

SOLUTION/MATRIX_APRIORI U CORR

SOLUTION/MATRIX_APRIORI L COVA

SOLUTION/MATRIX_APRIORI U COVA

SOLUTION/MATRIX_APRIORI L INFO

SOLUTION/MATRIX_APRIORI U INFO

SOLUTION/MATRIX_APRIORI L SRIF

SOLUTION/MATRIX_APRIORI U SRIF

Contents:

SOLUTION MATRIX APRIORI DATA LINE		
Field	Description	Format
Matrix Apriori Row Number	Row index for the Matrix Apriori. It must match the parameter index in the SOLUTION/APRIORI block for the same parameter.	1X, I5
Matrix Apriori Column Number	Column index for the Matrix Estimate. It must match the parameter index in the SOLUTION/APRIORI block for the same parameter.	1X, I5
First Matrix Estimate Element	Matrix element at the location (Row Number , Column Number).	1X, E21.16
Second Matrix Estimate Element	Matrix element at the location (Row Number , Column Number + 1).	1X, E21.16
Third Matrix Estimate Element	Matrix element at the location (Row Number , Column Number + 2).	1X, E21.16
		78

Comment:

The Matrix Apriori Row/Column Number correspond to the Apriori Parameters Index in the SOLUTION/APRIORI block. If the apriori constraint matrix is diagonal and no loss of significant digits occurs by using the Parameter Standard Deviation in the SOLUTION/APRIORI block, then, this block becomes redundant. If the CORR matrix is used, Standard deviations must be stored in the diagonal elements. Missing elements in the matrix are assumed to be zero (0); consequently, zero elements may be omitted.

NOTE: The same scale (variance) factor MUST be used for both MATRIX ESTIMATE and MATRIX APRIORI, as well as for the standard deviations in the ESTIMATE and APRIORI Blocks.

21. Footer Line (Mandatory)

Description:

Marks the end of the SINEX file.

Contents:

FOOTER LINE		
Field	Description	Format
End of SINEX	The seven characters %ENDSNX at the beginning of the last line mark the end of the SINEX file. Mandatory line.	A7
		7

APPENDIX II

Annotated (real) SINEX sample
 (EMR07987.SNX annotated by Philip Davis of NCL (Newcastle AAC))

%=SNX 1.00 NRC 95:123:55260 NRC 95:113:00000 95:120:00000 P 00117 1 X E

* This is an annotated SINEX example, based on the first submission from
 * NRC. It has been amended and extended by NCL to illustrate the full
 * SINEX 1.00 format. Long blocks have been truncated.

* The following convention is followed for start and end date:
 * A start date of 00:000:00000 represents "since the beginning"
 * An end date of 00:000:00000 represents "up to now"
 * ***WARNING: NO overlapping epochs allowed, i.e. epochs referring to the
 * *** same site must be continuous *****

* Constraints code S are determined as follows:
 * (Note this is only SUGGESTION, common sense should be used here)
 * ratio = (apriori std. dev.) / (estimated std. dev.)
 *
 * sqrt(2) =< ratio < sqrt(2) code S = 0 (fixed/constrained)
 * 10 =< ratio < 10 code S = 1 (significant constr.)
 * code S = 2 (loose or unconstr.)

* WARNING: This has not yet been standardized by IGS.

* EOP parameter types:

SINEX	Units		
XPO	mas	(milli-arc seconds)	pole x
YPO	mas	(milli-arc seconds)	y
XPOR	ma/s	(milli-arc seconds/s)	pole x rate
YPOR	ma/s	(milli-arc seconds/s)	y rate
UT	ms	(milli-seconds)	UT1-UTC
LOD	ms	(milli-seconds)	Length of day

* They are put at the end of the APRIORI and ESTIMATE blocks such they
 * can be removed easily.

* In floating-point fields, the E symbol should be used for exponent -
 * other symbols (such as D) are not interpreted correctly by some
 * software (e.g. the ANSI C I/O library).

* Fields should not be left blank if data is not applicable or
 * unavailable. These fields should be filled with a data-not-given
 * character '-' is used here. This enables the file to be read either
 * by column positions of fields, or by tokenising lines by whitespace.

* Block order should be kept consistent to aid readability. The format
 * allows any blocks to be omitted, though obviously some are essential for
 * solution submission, and the inclusion of all blocks is encouraged.

* Note the relational problem annotated in SITE/ANTENNA.

```

* The first and last lines begin '%'. Only '%', '*', '+', '-' and ' ' are
* allowed in the first column, meaning 'begin/end SINEX', 'comment',
* 'start block', 'end block' and 'data line' respectively.
*
* Header line explanation:
*
* '='          Solution operator code. '=' means 'resultant' and is the
*              only legal code in a header line. See INPUT/HISTORY
*              notes.
* 'SNX'       This is a SINEX document. Other formats may use similar
*              headers.
* '1.00'      SINEX version number. MUST be coded. It is used for
*              backward compatibility whenever required.
* 'NRC 95:122:67080' The SINEX reference for this file. SINEX files are
*              referred to by the three-character agency code, and a
*              creation time-stamp in yy:ddd:sssss format. Agency codes
*              should have entries in INPUT/ACKNOWLEDGEMENTS.
* 'NRC 95:113:00000
*           95:120:00000' The agency responsible for the data, and the overall
*              data time span. 'COM' means multiple agencies.
* 'P'        Technique code. 'P' (GPS) 'L' (SLR) 'R' (VLBI)
*              'C' (multiple) and 'M' (ILR) are allowed.
* 00117     This solution estimates 117 parameters.
* 1         Constraint code. '2' (unconstrained), '1' (significant
*              constraints), '0' (fixed/tight constraints) are allowed.
* X E      This solution includes coordinates and EOP. 'X', 'E'
*              and 'V' (velocities) 'O' (orbits) are allowed.
*              (Additional codes may be defined here)
*
-----
*           1           2           3           4           5           6           7           8
*234567890123456789012345678901234567890123456789012345678901234567890
*
-----
+FILE/REFERENCE
* This block always contains the following six records
*info type      info
-----
DESCRIPTION    Natural Resources Canada / Geodetic Surveys, altered by NCL
OUTPUT         NRCan 1995 weekly solution.
CONTACT        ferland@gdim.geod.emr.ca
SOFTWARE       combine v0.01
HARDWARE       HP 750
INPUT          NRCan daily solution
-FILE/REFERENCE
*
-----
+FILE/COMMENT
* This is a free-format block for notes and comments. Substantial remarks
* should go in here, not in * lines.
*
NB This is not an original NRC document.
This is an example SINEX document with truncated blocks. Do not process.
-FILE/COMMENT
*
-----
+INPUT/HISTORY
* Each input solution used to create this solution is listed here. A series
* of + lines give inputs to a combination - the = code is used for the
* resultant. The format is identical to the header line. The last line should
* always refer to this solution, i.e. match the header line.

```

```

*O FM VER AGY TIME STAMP DAT DATA START DATA END T PARAM C TYPE
+SNX 0.04 NRC 95:123:52328 NRC 95:113:00000 95:114:00000 P 00081 2 X E
+SNX 0.04 NRC 95:123:52590 NRC 95:114:00000 95:115:00000 P 00082 2 X E
+SNX 0.04 NRC 95:123:52881 NRC 95:115:00000 95:116:00000 P 00082 2 X E
+SNX 0.04 NRC 95:123:53091 NRC 95:116:00000 95:117:00000 P 00076 2 X E
+SNX 0.04 NRC 95:123:53365 NRC 95:117:00000 95:118:00000 P 00073 2 X E
+SNX 0.04 NRC 95:123:53646 NRC 95:118:00000 95:119:00000 P 00079 2 X E
+SNX 0.04 NRC 95:123:53962 NRC 95:119:00000 95:120:00000 P 00082 2 X E
* ITRF93 ssc/ssv for the 13 ITRF stations in the line below
+SNX 0.04 NRC 95:121:59613 NRC 95:116:00000 95:117:00000 P 00078 0 X V
-SNX 1.00 NRC 95:123:55260 NRC 95:113:00000 95:120:00000 P 00117 1 X E
-INPUT/HISTORY

```

*-----
+INPUT/FILES

* Every SINEX file referenced in INPUT/HISTORY should have a filename entered
* here. The last line of this block is always the name of the current file.
* Path names should be given meaningful aliases to keep them short!

```

*AGY TIME STAMP FILE NAME DESCRIPTION
NRC 95:123:52328 1995/w_798/EMR07980.snx NRC Daily solution
NRC 95:123:52590 1995/w_798/EMR07981.snx NRC Daily solution
NRC 95:123:52881 1995/w_798/EMR07982.snx NRC Daily solution
NRC 95:123:53091 1995/w_798/EMR07983.snx NRC Daily solution
NRC 95:123:53365 1995/w_798/EMR07984.snx NRC Daily solution
NRC 95:123:53646 1995/w_798/EMR07985.snx NRC Daily solution
NRC 95:123:53962 1995/w_798/EMR07986.snx NRC Daily solution
NRC 95:121:59613 stacomb_SINEX/950426_apr.snx ITRF93 for 13 stations
NRC 95:123:55260 stacomb_SINEX/EMR07987.snx Week 798 combination

```

-INPUT/FILES

*-----
+INPUT/ACKNOWLEDGMENTS

* Each agency three-character code used in any other block is explained here.

*AGY DESCRIPTION

NRC Natural Resources Canada, Geodetic surveys
NCL Newcastle AAC, University of Newcastle upon Tyne, England.

-INPUT/ACKNOWLEDGMENTS

*-----
+SITE/ID

* Each physical monument is known in SINEX by a four-character site code*
* (standardised) and an alphabetic point code (arbitrary). Each CODE+PT is
* equivalent to an IERS DOMES (or DOME) code. Each monument estimated in the
* solution has an entry in this block. Unknown DOMES (DOME) codes are
* represented as M or S following the IERS convention.

```

*CODE PT DOMES T STATION DESCRIPTION APPROX_LON APPROX_LAT APP_H
ALBH A 40129M003 P Albert Head, Canada 236 30 45.2 48 23 23.3 31.0
ALGO A 40104M002 P Algonquin Park, Canada 281 55 43.1 45 57 20.9 200.0
AREQ A 42202M005 P Arequipa, Peru 288 30 26.0 -16 27 55.9 2488.0
DAV1 A 66010M001 P Davis, Antarctica 77 58 21.5 -68 34 38.4 96.0
DRAO A 40105M002 P Dom. Radio Obs.,Canada 240 22 30.1 49 19 21.5 541.0
FAIR A 40408M001 P Fairbanks, U.S.A. 212 30 2.8 64 58 40.9 319.0
FORT A 41602M001 P Fortaleza, Brazil 321 34 27.8 -3 52 38.9 19.0
GOLD B 40405S031 P Goldstone, U.S.A. 243 6 38.8 35 25 30.6 986.0
GUAM A 50501M002 P Dedego, Guam 144 52 6.2 13 35 21.4 206.0
KIT3 A 12334M001 P Kitab, Uzbekistan 66 53 7.6 39 8 5.2 622.0
KOKB A 40424M004 P Kokee Park,Haw.,U.S.A. 200 20 6.3 22 7 34.6 1167.0
KOSG A 13504M003 P Kootwijk, Netherlands 5 48 34.8 52 10 42.4 96.0

```

*CODE	PT	DOMES	T	STATION DESCRIPTION	APPROX LON	APPROX LAT	APP H
MADR	A	13407S012	P	Madrid, Spain	355 45 1.3	40 25 45.0	829.0
MCM4	A	66001M003	P	McMurdo, Antarctica	166 40 31.2	-77 50 55.2	-1.0
NRC1	A	M	P	NRC, Ottawa, Canada	284 22 30.0	45 27 15.0	82.0
KERG	A	91201M002	P	Kerguelen Is.	70 15 19.9	-49 21 5.3	73.0
RCM5	A	40499S018	P	Richmond, Flor. U.S.A.	279 36 57.9	25 36 49.7	-15.0
SANT	A	41705M003	P	Santiago, Chile	289 19 53.2	-33 9 1.1	723.0
SCHE	A	M	P	Schefferville, Canada	293 0 .0	55 0 .0	200.0
STJO	A	40101M001	P	St-John's, Canada	307 19 20.2	47 35 42.9	152.0
TIDB	A	50103M108	P	Tidbinbilla, Australia	148 58 48.0	-35 23 57.2	665.0
TROM	A	10302M003	P	Tromso, Norway	18 56 18.0	69 39 45.9	132.0
TSKB	A	21730S005	P	Tuskuba, Japan	140 5 15.0	36 6 20.4	67.0
WETT	A	14201M009	P	Wettzell, Germany	12 52 44.1	49 8 39.3	666.0
YAR1	A	50107M004	P	Yaragadee, Australia	115 20 49.2	-29 2 47.7	241.0
YELL	A	40127M003	P	Yellowknife, Canada	245 31 9.5	62 28 51.3	180.0
TAIW	A	23601M001	P	Taipei, Taiwan	121 32 11.6	25 1 16.8	44.0
HART	A	30302M002	P	Hartebeesthoek, S. A.	27 42 28.0	-25 53 13.6	1555.0
CHUR	A	M	P	Churchill, Canada	266 0 .0	59 0 .0	.0
WILL	A	M	P	Williams Lake, Canada	237 49 55.9	52 14 12.9	1097.0

-SITE/ID

*

+SITE/DATA

* This block contains information on the source of each station.
 * Since point and solution codes are
 * arbitrary, the station name (SITE+PT+SOLN codes) may be different in the
 * input solution - both are given here. Stations which are estimated in
 * multiple input files have several lines here.
 * The information here is fictional, to illustrate the format.
 * Each station is defined in SOLUTION/EPOCHS, and each file (AGY+TIME_STAMP_)
 * appears in INPUT/FILES.

*

*SOLUTION INPUT

*SITE	PT	SOLN	T	DATA START	DATA END	AGY	TIME	STAMP
ALBH	A	1	ALBH B	1 P 95:113:00000	95:120:00000	NRC	95:123:52328	
ALBH	A	1	ALBH A	1 P 95:113:00000	95:120:00000	NRC	95:123:52590	
ALGO	A	1	ALGO A	1 P 95:113:00000	95:120:00000	NRC	95:123:52328	

* etc.

-SITE/DATA

*

+SITE/RECEIVER

* Here each station (SITE+PT+SOLN codes) has receiver details attached. If
 * receivers change during the data span for that station, multiple lines are
 * used here. These data spans must fit within the overall station span
 * (given in SOLUTION/EPOCHS) and should cover the entire span for each station
 * and should not overlap.

*

* Note unknown fields are filled with - characters. No field is left blank.

* ***new to version 1.00***

* The default characters ("----" in the SOLN field means that the information

* refers to all SOLN codes falling in between the start and end epochs.

*

*SITE	PT	SOLN	T	DATA START	DATA END	DESCRIPTION	S/N	FIRMWARE
ALBH	A	1	P	95:012:67680	00:000:00000	ROGUE SNR-8000	292	3.0.32.2
ALGO	A	1	P	94:355:00000	00:000:00000	ROGUE SNR-8000	T226	3.0.32.2
AREQ	A	1	P	94:032:00000	00:000:00000	ROGUE SNR-8000	T253	2.8.32.1x
DAV1	A	1	P	94:192:00000	00:000:00000	ROGUE SNR-8100	C119	2.8.1.1
DRAO	A	1	P	95:102:61530	00:000:00000	ROGUE SNR-8000	347	3.0.32.3

*SITE	PT	SOLN	T	DATA START	DATA END	DESCRIPTION	S/N	FIRMWARE
FAIR	A	1	P	94:125:00000	00:000:00000	ROGUE SNR-8	099	7.8
FORT	A	1	P	93:133:00000	00:000:00000	ROGUE SNR-8000	T119	2.8
GOLD	B	1	P	94:034:00000	00:000:00000	ROGUE SNR-8	-----	7.6
GUAM	A	1	P	95:020:00000	00:000:00000	ROGUE SNR-8000	360	3.0
KIT3	A	1	P	94:274:00000	00:000:00000	ROGUE SNR-8000	T191	2.8.32.1x
KERG	A	1	P	94:320:00000	00:000:00000	ROGUE SNR-8C	CR306	7.8
KOKB	A	1	P	94:125:00000	00:000:00000	ROGUE SNR-8	10	7.8
KOSG	A	1	P	94:327:00000	00:000:00000	ROGUE SNR-8	117	7.8
MADR	A	1	P	94:035:00000	00:000:00000	ROGUE SNR-8	-----	7.6
MCM4	A	1	P	95:025:00000	00:000:00000	ROGUE SNR-8000	275	3.0
NRC1	A	1	P	93:001:00000	00:000:00000	ROGUE SNR-8000	-----	-----
RCM5	A	1	P	95:009:00000	00:000:00000	ROGUE SNR-8000	T160	3.0.32.2
SANT	A	1	P	94:131:00000	00:000:00000	ROGUE SNR-8	95	7.8
SCHE	A	1	P	95:103:00240	00:000:00000	ROGUE SNR-8000	164	3.0.32.2
STJO	A	1	P	95:061:54000	00:000:00000	ROGUE SNR-8000	161	3.3.32.2
TIDB	A	1	P	94:041:00000	00:000:00000	ROGUE SNR-8	3	7.6
TROM	A	1	P	92:259:00000	00:000:00000	ROGUE SNR-8	-----	4.0
TSKB	A	1	P	93:349:00000	00:000:00000	ROGUE SNR-8000	102	2.8
WETT	A	1	P	91:203:00000	00:000:00000	ROGUE SNR-800	200	7.3
YAR1	A	1	P	94:138:00000	00:000:00000	ROGUE SNR-8	9	7.8
YELL	A	1	P	94:131:53520	00:000:00000	ROGUE SNR-8000	T302	2.8.32.1
TAIW	A	1	P	93:293:00000	00:000:00000	ROGUE SNR-8000	201	7.0
HART	A	1	P	91:001:00000	00:000:00000	ROGUE SNR-8	114	7.3
CHUR	A	1	P	94:103:72240	00:000:00000	ROGUE SNR-8000	305	3.0.32.1
WILL	A	1	P	93:279:68580	00:000:00000	ROGUE SNR-8000	165	-----

-SITE/RECEIVER

+SITE/ANTENNA

*

* Here each station (SITE+PT+SOLN codes) has antenna details attached. If
 * antennae change during the data span for that station, multiple lines are
 * used here. These data spans must fit within the overall station span
 * (given in SOLUTION/EPOCHS) and should cover the entire span for each station
 * and should not overlap.

*

* Note unknown fields filled with '-' characters. No field is left blank.

*

new to version 1.00

* The default characters ("----" in the SOLN field means that the information

* refers to all SOLN codes falling in between start and end epoch.

*

*SITE	PT	SOLN	T	DATA START	DATA END	DESCRIPTION	S/N
ALBH	A	1	P	95:011:80100	00:000:00000	DORNE MARGOLIN T	368
ALGO	A	1	P	94:047:69300	00:000:00000	DORNE MARGOLIN T	173
AREQ	A	1	P	94:032:00000	00:000:00000	DORNE MARGOLIN T	294
DAV1	A	1	P	94:192:00000	00:000:00000	DORNE MARGOLIN T	277
DRAO	A	1	P	95:102:64260	00:000:00000	DORNE MARGOLIN T	172
FAIR	A	1	P	91:290:00000	00:000:00000	DORNE MARGOLIN R	96
FORT	A	1	P	93:133:00000	00:000:00000	DORNE MARGOLIN T	119
GOLD	B	1	P	92:180:00000	00:000:00000	DORNE MARGOLIN R	95
GUAM	A	1	P	95:020:00000	00:000:00000	DORNE MARGOLIN T	481
KIT3	A	1	P	94:274:00000	00:000:00000	DORNE MARGOLIN T	362
KERG	A	1	P	94:320:00000	00:000:00000	DORNE MARGOLIN T	154
KOKB	A	1	P	91:106:00000	00:000:00000	DORNE MARGOLIN R	10
KOSG	A	1	P	91:001:00000	00:000:00000	DORNE MARGOLIN B	119
MADR	A	1	P	89:349:00000	00:000:00000	DORNE MARGOLIN R	-----
MCM4	A	1	P	95:025:00000	00:000:00000	DORNE MARGOLIN T	363
NRC1	A	1	P	93:001:00000	00:000:00000	DORNE MARGOLIN T	-----

*SITE	PT	SOLN	T	DATA START	DATA END	DESCRIPTION	S/N
RCM5	A	1	P	94:195:00000	00:000:00000	DORNE MARGOLIN T	148
SANT	A	1	P	92:035:00000	00:000:00000	DORNE MARGOLIN R	95
SCHE	A	1	P	94:196:00420	00:000:00000	DORNE MARGOLIN T	386
STJO	A	1	P	95:061:78960	00:000:00000	DORNE MARGOLIN T	171
TIDB	A	1	P	92:033:00000	00:000:00000	DORNE MARGOLIN R	2
TROM	A	1	P	92:259:00000	00:000:00000	DORNE MARGOLIN B	-----
TSKB	A	1	P	94:227:00000	00:000:00000	DORNE MARGOLIN T	105
WETT	A	1	P	91:203:00000	00:000:00000	DORNE MARGOLIN B	113
YAR1	A	1	P	90:337:00000	00:000:00000	DORNE MARGOLIN R	3
YELL	A	1	P	94:075:72000	00:000:00000	DORNE MARGOLIN T	273
TAIW	A	1	P	90:335:00000	00:000:00000	DORNE MARGOLIN B	118
HART	A	1	P	95:026:00000	00:000:00000	DORNE MARGOLIN T	-----
CHUR	A	1	P	94:103:72240	00:000:00000	DORNE MARGOLIN T	387
WILL	A	1	P	93:279:68580	00:000:00000	DORNE MARGOLIN T	-----

-SITE/ANTENNA

*

+SITE/GPS_PHASE_CENTER

*

* Here each antenna (DESCRIPTION + S/N fields) listed in SITE/ANTENNA has phase center details attached.

*

* Note unknown fields filled with - characters. No field is left blank.

*

*

*DESCRIPTION	S/N	UP	NORTH	EAST	UP	NORTH	EAST	AZ	EL
		L1->ARP (m)			L2->ARP (m)				
DORNE MARGOLIN B	-----	.0780	.0000	.0000	.0960	.0000	.0000		None
DORNE MARGOLIN B	113	.0780	.0000	.0000	.0960	.0000	.0000		None
DORNE MARGOLIN B	119	.0780	.0000	.0000	.0960	.0000	.0000		None
DORNE MARGOLIN R	-----	.0780	.0000	.0000	.0960	.0000	.0000		None
DORNE MARGOLIN R	2	.0780	.0000	.0000	.0960	.0000	.0000		None
DORNE MARGOLIN R	3	.0780	.0000	.0000	.0960	.0000	.0000		None
DORNE MARGOLIN R	10	.0780	.0000	.0000	.0960	.0000	.0000		None
DORNE MARGOLIN R	95	.0780	.0000	.0000	.0960	.0000	.0000		None
DORNE MARGOLIN R	96	.0780	.0000	.0000	.0960	.0000	.0000		None
DORNE MARGOLIN T	-----	.1100	.0000	.0000	.1280	.0000	.0000		None
DORNE MARGOLIN T	105	.1100	.0000	.0000	.1280	.0000	.0000		None
DORNE MARGOLIN T	119	.1100	.0000	.0000	.1280	.0000	.0000		None
DORNE MARGOLIN T	148	.1100	.0000	.0000	.1280	.0000	.0000		None
DORNE MARGOLIN T	154	.1100	.0000	.0000	.1280	.0000	.0000		None
DORNE MARGOLIN T	171	.1100	.0000	.0000	.1280	.0000	.0000		None
DORNE MARGOLIN T	172	.1100	.0000	.0000	.1280	.0000	.0000		None

-SITE/GPS_PHASE_CENTER

*

+SITE/ECCENTRICITY

*

* Here each station (SITE+PT+SOLN codes) has eccentricity vectors attached. If these change during the data span for that station, multiple lines are used here. These data spans must fit within the overall station span (given in SOLUTION/EPOCHS), should cover the entire span for each station and must not overlap.

*SITE	PT	SOLN	T	DATA	START	DATA	END	AXE	UP	NORTH	EAST
									ARP-->	BENCHMARK (m)	
ALBH	A	1	P	95:011:80100	00:000:00000	UNE			.1000	.0000	.0000
ALGO	A	1	P	94:139:00000	00:000:00000	UNE			.1000	.0000	.0000
AREQ	A	1	P	94:088:00000	00:000:00000	UNE			.0610	.0000	.0000
DAV1	A	1	P	94:192:00000	00:000:00000	UNE			.0035	.0000	.0000
DRAO	A	1	P	95:102:64260	00:000:00000	UNE			.1000	.0000	.0000
FAIR	A	1	P	91:290:00000	00:000:00000	UNE			.1160	.0000	.0000
FORT	A	1	P	93:133:00000	00:000:00000	UNE			.6430	.0000	.0000
GOLD	B	1	P	92:180:00000	00:000:00000	UNE			.0000	.0000	.0000
GUAM	A	1	P	95:020:00000	00:000:00000	UNE			.0614	.0000	.0000
KIT3	A	1	P	94:274:00000	00:000:00000	UNE			.0460	.0000	.0000
KERG	A	1	P	94:320:00000	00:000:00000	UNE			.4200	.0000	.0000
KOKB	A	1	P	91:106:00000	00:000:00000	UNE			.0930	.0000	.0000
KOSG	A	1	P	94:001:00000	00:000:00000	UNE			.1050	.0000	.0000
MADR	A	1	P	89:349:00000	00:000:00000	UNE			.0000	.0000	.0000
MCM4	A	1	P	95:025:00000	00:000:00000	UNE			.1830	.0000	.0000
NRC1	A	1	P	93:001:00000	00:000:00000	UNE			.0000	.0000	.0000
RCM5	A	1	P	93:284:00000	00:000:00000	UNE			.0000	.0000	.0000
SANT	A	1	P	92:035:00000	00:000:00000	UNE			.0930	.0000	.0000
SCHE	A	1	P	94:196:00420	00:000:00000	UNE			.1000	.0000	.0000
STJO	A	1	P	95:057:48480	00:000:00000	UNE			.1000	.0000	.0000
TIDB	A	1	P	92:033:00000	00:000:00000	UNE			.0920	.0000	.0000
TROM	A	1	P	92:259:00000	00:000:00000	UNE			2.4734	.0000	.0000
TSKB	A	1	P	94:227:00000	00:000:00000	UNE			.0000	.0000	.0000
WETT	A	1	P	91:203:00000	00:000:00000	UNE			.0000	.0000	.0000
YAR1	A	1	P	90:337:00000	00:000:00000	UNE			.0730	.0000	.0000
YELL	A	1	P	94:287:00900	00:000:00000	UNE			.1000	.0000	.0000
TAIW	A	1	P	90:335:00000	00:000:00000	UNE			1.7685	.0000	.0000
HART	A	1	P	91:001:00000	00:000:00000	UNE			9.7540	.0000	.0000
CHUR	A	1	P	94:103:72240	00:000:00000	UNE			.0000	.0000	.0000
WILL	A	1	P	93:279:68580	00:000:00000	UNE			.0010	.0000	.0000

-SITE/ECCENTRICITY

*

+SOLUTION/EPOCHS

*

* This block is the logical starting-point for interpreting the file, since it
 * defines the stations in the solution. A station is particular solution for
 * a monument, referenced by SITE, PT and SOLN codes. Multiple integer solution
 * codes may be used (arbitrarily) to give multiple solutions for a point in the
 * same estimate - at different epochs, for instance.

*

* Each station invoked here should have one or more entries in each of
 * SITE/RECEIVER, SITE/ANTENNA, SITE/DATA and SITE/ECCENTRICITY.

* The monument (SITE+PT) should be defined in SITE/ID.

*

*SITE	PT	SOLN	T	DATA	START	DATA	END	MEAN	EPOCH
ALBH	A	1	P	95:113:00000	95:120:00000	95:116:43200			
ALGO	A	1	P	95:113:00000	95:120:00000	95:116:43200			
AREQ	A	1	P	95:113:00000	95:120:00000	95:116:28800			
CHUR	A	1	P	95:118:00000	95:120:00000	95:119:00000			
DAV1	A	1	P	95:113:00000	95:114:00000	95:113:43200			
DRAO	A	1	P	95:113:00000	95:120:00000	95:116:43200			
FAIR	A	1	P	95:113:00000	95:120:00000	95:116:43200			
FORT	A	1	P	95:113:00000	95:118:00000	95:115:21600			
GOLD	B	1	P	95:113:00000	95:120:00000	95:116:43200			
GUAM	A	1	P	95:113:00000	95:120:00000	95:116:43200			
HART	A	1	P	95:115:00000	95:120:00000	95:117:28800			

*SITE	PT	SOLN	T	DATA START	DATA END	MEAN EPOCH
KERG	A	1	P	95:113:00000	95:120:00000	95:116:43200
KIT3	A	1	P	95:113:00000	95:119:00000	95:116:00000
KOKB	A	1	P	95:113:00000	95:120:00000	95:116:43200
KOSG	A	1	P	95:113:00000	95:120:00000	95:116:43200
MADR	A	1	P	95:113:00000	95:120:00000	95:116:43200
MCM4	A	1	P	95:113:00000	95:120:00000	95:116:14400
NRC1	A	1	P	95:113:00000	95:120:00000	95:116:43200
RCM5	A	1	P	95:113:00000	95:120:00000	95:116:43200
SANT	A	1	P	95:113:00000	95:120:00000	95:116:43200
SCHE	A	1	P	95:113:00000	95:116:00000	95:114:43200
STJO	A	1	P	95:113:00000	95:120:00000	95:116:43200
TAIW	A	1	P	95:114:00000	95:120:00000	95:117:43200
TIDB	A	1	P	95:113:00000	95:120:00000	95:116:43200
TROM	A	1	P	95:113:00000	95:120:00000	95:116:43200
TSKB	A	1	P	95:113:00000	95:120:00000	95:116:43200
WETT	A	1	P	95:113:00000	95:120:00000	95:116:00000
WILL	A	1	P	95:118:00000	95:120:00000	95:119:00000
YAR1	A	1	P	95:113:00000	95:120:00000	95:116:43200
YELL	A	1	P	95:113:00000	95:120:00000	95:116:43200

-SOLUTION/EPOCHS

+SOLUTION/ESTIMATE

*

* The parameter estimates are written here. Parameter types STAX, STAY, STAZ,
 * VELX, VELY, VELZ (coordinate and velocity x, y, z) are followed by a
 * station reference. Erp types LOD, UT, XPO, YPO have no station. The
 * constraint code (0, 1 or 2) is given here for each parameter - the empty
 * fields are filled with a data-not-given character (-)

*

*

*** New to version 1.00 ***

*

TYPE increased to 6 chars, ESTIMATED Value field to 21 chars, STD

*

decreased to 11chars (included here for information only) ***

*

The STDs for consistency must be the same as the corresponding values

*

derived from the MATRIX blocks, which are given to full num. precision.

*INDEX	TYPE	CODE	PT	SOLN	REF	EPOCH	UNIT	S	ESTIMATED VALUE	STD DEV
1	STAX	ALBH	A	1	95:116:43200	m	2	-	.234133292758691E+7	.1845776E-2
2	STAY	ALBH	A	1	95:116:43200	m	2	-	.353904953122971E+7	.1890911E-2
3	STAZ	ALBH	A	1	95:116:43200	m	2	-	.4745791466277621E+7	.2075918E-2
4	STAX	ALGO	A	1	95:116:43200	m	1	-	.9181294929904674E+6	.1768625E-2
5	STAY	ALGO	A	1	95:116:43200	m	1	-	.434607120901217E+7	.1797731E-2
6	STAZ	ALGO	A	1	95:116:43200	m	1	-	.4561977840428489E+7	.1878956E-2
7	STAX	AREQ	A	1	95:116:28800	m	2	-	.1942826687525561E+7	.6477347E-2
8	STAY	AREQ	A	1	95:116:28800	m	2	-	.580407019776578E+7	.8829387E-2
9	STAZ	AREQ	A	1	95:116:28800	m	2	-	.179689395509440E+7	.3872643E-2
10	STAX	CHUR	A	1	95:119:00000	m	2	-	.236438707221352E+6	.2190659E-2
11	STAY	CHUR	A	1	95:119:00000	m	2	-	.330761674613259E+7	.2499980E-2
12	STAZ	CHUR	A	1	95:119:00000	m	2	-	.5430049170384845E+7	.3338507E-2
13	STAX	DAV1	A	1	95:113:43200	m	2	-	.4868545524273632E+6	.5143560E-2
14	STAY	DAV1	A	1	95:113:43200	m	2	-	.2285099364466271E+7	.5465295E-2
15	STAZ	DAV1	A	1	95:113:43200	m	2	-	.591495576584752E+7	.8718856E-2
16	STAX	DRAO	A	1	95:116:43200	m	2	-	.205916467723249E+7	.1818058E-2
17	STAY	DRAO	A	1	95:116:43200	m	2	-	.362110834605865E+7	.1859042E-2
18	STAZ	DRAO	A	1	95:116:43200	m	2	-	.4814432386809346E+7	.2053716E-2
19	STAX	FAIR	A	1	95:116:43200	m	0	-	.228162142409438E+7	.2008781E-2
20	STAY	FAIR	A	1	95:116:43200	m	0	-	.145359574941003E+7	.2100198E-2
21	STAZ	FAIR	A	1	95:116:43200	m	0	-	.5756961936406008E+7	.2509140E-2
22	STAX	FORT	A	1	95:115:21600	m	2	-	.4985386578502384E+7	.1084655E-1

*INDEX	TYPE	CODE	PT	SOLN	REF	EPOCH	UNIT	S	ESTIMATED VALUE	STD DEV
23	STAY	FORT	A	1	95:115:21600	m	2	-.395499854274894E+7	.9229132E-2	
24	STAZ	FORT	A	1	95:115:21600	m	2	-.428426474252779E+6	.2879426E-2	
25	STAX	GOLD	B	1	95:116:43200	m	1	-.235361417310070E+7	.2060113E-2	
26	STAY	GOLD	B	1	95:116:43200	m	1	-.464138536535744E+7	.2135362E-2	
27	STAZ	GOLD	B	1	95:116:43200	m	1	.3676976474604919E+7	.2151652E-2	
28	STAX	GUAM	A	1	95:116:43200	m	2	-.507131279252173E+7	.3359775E-2	
29	STAY	GUAM	A	1	95:116:43200	m	2	.3568363515536474E+7	.3434317E-2	
30	STAZ	GUAM	A	1	95:116:43200	m	2	.1488904271291384E+7	.2465369E-2	
31	STAX	HART	A	1	95:117:28800	m	0	.5084625439996016E+7	.3117434E-2	
32	STAY	HART	A	1	95:117:28800	m	0	.2670366550990838E+7	.2988406E-2	
33	STAZ	HART	A	1	95:117:28800	m	1	-.276849396332954E+7	.2436794E-2	
34	STAX	KERG	A	1	95:116:43200	m	2	.1406337354635808E+7	.3228912E-2	
35	STAY	KERG	A	1	95:116:43200	m	2	.3918161143630010E+7	.3090251E-2	
36	STAZ	KERG	A	1	95:116:43200	m	2	-.481616739541420E+7	.2887894E-2	
37	STAX	KIT3	A	1	95:116:00000	m	2	.1944945408967126E+7	.3880638E-2	
38	STAY	KIT3	A	1	95:116:00000	m	2	.4556652228809900E+7	.4395018E-2	
39	STAZ	KIT3	A	1	95:116:00000	m	2	.4004325952269760E+7	.4075488E-2	
40	STAX	KOKB	A	1	95:116:43200	m	0	-.554383812506372E+7	.2572993E-2	
41	STAY	KOKB	A	1	95:116:43200	m	0	-.205458735000368E+7	.2349073E-2	
42	STAZ	KOKB	A	1	95:116:43200	m	1	.2387809656652860E+7	.2100031E-2	
43	STAX	KOSG	A	1	95:116:43200	m	1	.3899225249570046E+7	.1777152E-2	
44	STAY	KOSG	A	1	95:116:43200	m	1	.3967318114717967E+6	.1725390E-2	
45	STAZ	KOSG	A	1	95:116:43200	m	1	.5015078333904634E+7	.1593831E-2	
46	STAX	MADR	A	1	95:116:43200	m	1	.4849202445485532E+7	.1730374E-2	
47	STAY	MADR	A	1	95:116:43200	m	1	-.360329133978604E+6	.1739288E-2	
48	STAZ	MADR	A	1	95:116:43200	m	1	.4114913089855005E+7	.1417137E-2	
49	STAX	MCM4	A	1	95:116:14400	m	2	-.131170323900895E+7	.2978227E-2	
50	STAY	MCM4	A	1	95:116:14400	m	2	.3108151420651672E+6	.3072598E-2	
51	STAZ	MCM4	A	1	95:116:14400	m	2	-.621325504790322E+7	.4581133E-2	
52	STAX	NRC1	A	1	95:116:43200	m	2	.1112777313114861E+7	.1834574E-2	
53	STAY	NRC1	A	1	95:116:43200	m	2	-.434147580328482E+7	.1899372E-2	
54	STAZ	NRC1	A	1	95:116:43200	m	2	.4522955793195269E+7	.2001532E-2	
55	STAX	RCM5	A	1	95:116:43200	m	2	.9613347339731020E+6	.2721087E-2	
56	STAY	RCM5	A	1	95:116:43200	m	2	-.567407417401052E+7	.4543879E-2	
57	STAZ	RCM5	A	1	95:116:43200	m	2	.2740535190143120E+7	.2918609E-2	
58	STAX	SANT	A	1	95:116:43200	m	0	.1769693284302684E+7	.3096912E-2	
59	STAY	SANT	A	1	95:116:43200	m	0	-.504457411643344E+7	.3047045E-2	
60	STAZ	SANT	A	1	95:116:43200	m	1	-.346832104809249E+7	.2679039E-2	
61	STAX	SCHE	A	1	95:114:43200	m	2	.1450982826872315E+7	.2170755E-2	
62	STAY	SCHE	A	1	95:114:43200	m	2	-.338693424191906E+7	.2378425E-2	
63	STAZ	SCHE	A	1	95:114:43200	m	2	.5189301335610829E+7	.2882939E-2	
64	STAX	STJO	A	1	95:116:43200	m	2	.2612631222496210E+7	.1852240E-2	
65	STAY	STJO	A	1	95:116:43200	m	2	-.342680699958938E+7	.1909100E-2	
66	STAZ	STJO	A	1	95:116:43200	m	2	.4686757814504888E+7	.1941888E-2	
67	STAX	TAIW	A	1	95:117:43200	m	2	-.302478192993486E+7	.3600265E-2	
68	STAY	TAIW	A	1	95:117:43200	m	2	.4928936907613859E+7	.4052780E-2	
69	STAZ	TAIW	A	1	95:117:43200	m	2	.2681234449924764E+7	.2902421E-2	
70	STAX	TIDB	A	1	95:116:43200	m	0	-.446099608394879E+7	.2950717E-2	
71	STAY	TIDB	A	1	95:116:43200	m	0	.2682557122624863E+7	.2958276E-2	
72	STAZ	TIDB	A	1	95:116:43200	m	1	-.367444382121832E+7	.2716867E-2	
73	STAX	TROM	A	1	95:116:43200	m	1	.2102940345331658E+7	.2258738E-2	
74	STAY	TROM	A	1	95:116:43200	m	1	.7215693988724571E+6	.2336037E-2	
75	STAZ	TROM	A	1	95:116:43200	m	0	.5958192085393612E+7	.3604893E-2	
76	STAX	TSKB	A	1	95:116:43200	m	2	-.395719924355657E+7	.2924832E-2	
77	STAY	TSKB	A	1	95:116:43200	m	2	.3310199709624858E+7	.3038009E-2	
78	STAZ	TSKB	A	1	95:116:43200	m	2	.3737711702012423E+7	.2546651E-2	
79	STAX	WETT	A	1	95:116:00000	m	1	.4075578580084480E+7	.1776241E-2	

*INDEX	TYPE	CODE	PT	SOLN	REF EPOCH	UNIT	S	ESTIMATED VALUE	STD DEV
80	STAY	WETT	A	1	95:116:00000	m	1	.9318526769029480E+6	.1731380E-2
81	STAZ	WETT	A	1	95:116:00000	m	0	.4801570021461830E+7	.1457045E-2
82	STAX	WILL	A	1	95:119:00000	m	2	-.208425800223933E+7	.2188081E-2
83	STAY	WILL	A	1	95:119:00000	m	2	-.331387295088804E+7	.2351786E-2
84	STAZ	WILL	A	1	95:119:00000	m	2	.5019853121097040E+7	.2824378E-2
85	STAX	YAR1	A	1	95:116:43200	m	1	-.238902544223632E+7	.2931452E-2
86	STAY	YAR1	A	1	95:116:43200	m	1	.5043316884438646E+7	.2937762E-2
87	STAZ	YAR1	A	1	95:116:43200	m	1	-.307853084113885E+7	.2538746E-2
88	STAX	YELL	A	1	95:116:43200	m	1	-.122445249322380E+7	.2055871E-2
89	STAY	YELL	A	1	95:116:43200	m	1	-.268921606751285E+7	.2061675E-2
90	STAZ	YELL	A	1	95:116:43200	m	1	.5633638286707014E+7	.3035230E-2
91	LOD	----	--	1	95:113:43200	ms	2	.2871055744817214E+1	.1212729E-1
92	LOD	----	--	2	95:114:43200	ms	2	.2959652540110830E+1	.1131045E-1
93	LOD	----	--	3	95:115:43200	ms	2	.2973492029661421E+1	.1201761E-1
94	LOD	----	--	4	95:116:43200	ms	2	.2919511470925497E+1	.1199782E-1
95	LOD	----	--	5	95:117:43200	ms	2	.2799350739071390E+1	.1192584E-1
96	LOD	----	--	6	95:118:43200	ms	2	.2600397770842830E+1	.1188556E-1
97	LOD	----	--	7	95:119:43200	ms	2	.2430330357604413E+1	.1082158E-1
98	UT	----	--	1	95:114:43200	ms	2	.8722024405764063E+2	.1318171E-1
99	UT	----	--	2	95:115:43200	ms	2	.8430515991559695E+2	.1575504E-1
100	UT	----	--	3	95:116:43200	ms	2	.8136510032786199E+2	.1745336E-1
101	UT	----	--	4	95:117:43200	ms	2	.7849507028080811E+2	.1867862E-1
102	UT	----	--	5	95:118:43200	ms	2	.7572503990368940E+2	.1998887E-1
103	UT	----	--	6	95:119:43200	ms	2	.7312024540830212E+2	.2099974E-1
104	XPO	----	--	1	95:113:43200	mas	2	.1029608387361842E+3	.7876117E-1
105	XPO	----	--	2	95:114:43200	mas	2	.1069725602672064E+3	.7569313E-1
106	XPO	----	--	3	95:115:43200	mas	2	.1113899879374726E+3	.7622913E-1
107	XPO	----	--	4	95:116:43200	mas	2	.1154778670578098E+3	.7722355E-1
108	XPO	----	--	5	95:117:43200	mas	2	.1194089883086856E+3	.7541868E-1
109	XPO	----	--	6	95:118:43200	mas	2	.1236303461298091E+3	.7505631E-1
110	XPO	----	--	7	95:119:43200	mas	2	.1275168152328533E+3	.7039234E-1
111	YPO	----	--	1	95:113:43200	mas	2	.5530926512007116E+3	.9289514E-1
112	YPO	----	--	2	95:114:43200	mas	2	.5521110887312243E+3	.8795571E-1
113	YPO	----	--	3	95:115:43200	mas	2	.5512599272862197E+3	.8666021E-1
114	YPO	----	--	4	95:116:43200	mas	2	.5497716474578965E+3	.8859832E-1
115	YPO	----	--	5	95:117:43200	mas	2	.5485830683498143E+3	.8738927E-1
116	YPO	----	--	6	95:118:43200	mas	2	.5470190294873472E+3	.8867092E-1
117	YPO	----	--	7	95:119:43200	mas	2	.5455323053395770E+3	.8377195E-1

-SOLUTION/ESTIMATE

-----*

+SOLUTION/APRIORI

*

* The same format as the previous block, but parameters given, and their order, can be different.

*

* ITRF93(1995.318) coord. constraints for the 13 stations applied (ITRF SSC+

* SSV sigmas used, responsible for correlation in APRIORI matrix)

*

*** New to version 1.00 ***

*

TYPE increased to 6 chars, ESTIMATED Value field to 21 chars, STD

*

decreased to 11chars (included here for information only) ***

*

The STDs for consistency must be the same as the corresponding values

*

derived from the MATRIX blocks.

*

*INDEX	TYPE	CODE	PT	SOLN	REF	EPOCH	UNIT	S	ESTIMATED VALUE	STD DEV
1	STAX	ALGO	A	1	95:116:43200	m	2	.91812950316301E+06	.300264E-02	
2	STAY	ALGO	A	1	95:116:43200	m	2	-.43460712286616E+07	.300413E-02	
3	STAZ	ALGO	A	1	95:116:43200	m	2	.45619778480795E+07	.300413E-02	
4	STAX	FAIR	A	1	95:116:43200	m	2	-.22816214309794E+07	.300148E-02	
5	STAY	FAIR	A	1	95:116:43200	m	2	-.14535957605986E+07	.300264E-02	
6	STAZ	FAIR	A	1	95:116:43200	m	2	.57569619418178E+07	.300264E-02	
7	STAX	GOLD	B	1	95:116:43200	m	2	-.23536141750178E+07	.400111E-02	
8	STAY	GOLD	B	1	95:116:43200	m	2	-.46413853870781E+07	.500089E-02	
9	STAZ	GOLD	B	1	95:116:43200	m	2	.36769764725192E+07	.500089E-02	
10	STAX	HART	A	1	95:116:43200	m	2	.50846254292986E+07	.401782E-02	
11	STAY	HART	A	1	95:116:43200	m	2	.26703665485452E+07	.400793E-02	
12	STAZ	HART	A	1	95:116:43200	m	2	-.27684939831945E+07	.400607E-02	
13	STAX	KOKB	A	1	95:116:43200	m	2	-.55438381300644E+07	.300413E-02	
14	STAY	KOKB	A	1	95:116:43200	m	2	-.20545873456548E+07	.300264E-02	
15	STAZ	KOKB	A	1	95:116:43200	m	2	.23878096512000E+07	.300413E-02	
16	STAX	KOSG	A	1	95:116:43200	m	2	.38992252531315E+07	.502860E-02	
17	STAY	KOSG	A	1	95:116:43200	m	2	.39673180967945E+06	.502534E-02	
18	STAZ	KOSG	A	1	95:116:43200	m	2	.50150783278438E+07	.304205E-02	
19	STAX	MADR	A	1	95:116:43200	m	2	.48492024545575E+07	.300595E-02	
20	STAY	MADR	A	1	95:116:43200	m	2	-.36032914100548E+06	.300264E-02	
21	STAZ	MADR	A	1	95:116:43200	m	2	.41149130953329E+07	.200891E-02	
22	STAX	SANT	A	1	95:116:43200	m	2	.17696932851836E+07	.405435E-02	
23	STAY	SANT	A	1	95:116:43200	m	2	-.50445741389849E+07	.403570E-02	
24	STAZ	SANT	A	1	95:116:43200	m	2	-.34683210399342E+07	.406511E-02	
25	STAX	TIDB	A	1	95:116:43200	m	2	-.44609960811534E+07	.400793E-02	
26	STAY	TIDB	A	1	95:116:43200	m	2	.26825571044644E+07	.400446E-02	
27	STAZ	TIDB	A	1	95:116:43200	m	2	-.36744438230192E+07	.400607E-02	
28	STAX	TROM	A	1	95:116:43200	m	2	.21029403520603E+07	.422320E-02	
29	STAY	TROM	A	1	95:116:43200	m	2	.72156940310411E+06	.413292E-02	
30	STAZ	TROM	A	1	95:116:43200	m	2	.59581920940479E+07	.490313E-02	
31	STAX	WETT	A	1	95:116:43200	m	2	.40755785850603E+07	.300264E-02	
32	STAY	WETT	A	1	95:116:43200	m	2	.93185266801781E+06	.300148E-02	
33	STAZ	WETT	A	1	95:116:43200	m	2	.48015700238753E+07	.200396E-02	
34	STAX	YARI	A	1	95:116:43200	m	2	-.23890254414616E+07	.500803E-02	
35	STAY	YARI	A	1	95:116:43200	m	2	.50433168528356E+07	.501674E-02	
36	STAZ	YARI	A	1	95:116:43200	m	2	-.30785308583027E+07	.401238E-02	
37	STAX	YELL	A	1	95:116:43200	m	2	-.12244524961055E+07	.320725E-02	
38	STAY	YELL	A	1	95:116:43200	m	2	-.26892160698110E+07	.338846E-02	
39	STAZ	YELL	A	1	95:116:43200	m	2	.56336382822123E+07	.484908E-02	
40	VELX	ALGO	A	1	95:116:43200	m/y	2	-.21700000000000E-01	.400000E-03	
41	VELY	ALGO	A	1	95:116:43200	m/y	2	-.21000000000000E-02	.500000E-03	
42	VELZ	ALGO	A	1	95:116:43200	m/y	2	.66000000000000E-02	.500000E-03	
43	VELX	FAIR	A	1	95:116:43200	m/y	2	-.28500000000000E-01	.300000E-03	
44	VELY	FAIR	A	1	95:116:43200	m/y	2	-.19000000000000E-02	.400000E-03	
45	VELZ	FAIR	A	1	95:116:43200	m/y	2	-.10100000000000E-01	.400000E-03	
46	VELX	GOLD	B	1	95:116:43200	m/y	2	-.19100000000000E-01	.300000E-03	
47	VELY	GOLD	B	1	95:116:43200	m/y	2	.61000000000000E-02	.300000E-03	
48	VELZ	GOLD	B	1	95:116:43200	m/y	2	-.47000000000000E-02	.300000E-03	
49	VELX	HART	A	1	95:116:43200	m/y	2	-.54000000000000E-02	.120000E-02	
50	VELY	HART	A	1	95:116:43200	m/y	2	.17600000000000E-01	.800000E-03	
51	VELZ	HART	A	1	95:116:43200	m/y	2	.21600000000000E-01	.700000E-03	
52	VELX	KOKB	A	1	95:116:43200	m/y	2	-.12900000000000E-01	.500000E-03	
53	VELY	KOKB	A	1	95:116:43200	m/y	2	.61400000000000E-01	.400000E-03	
54	VELZ	KOKB	A	1	95:116:43200	m/y	2	.29200000000000E-01	.500000E-03	
55	VELX	KOSG	A	1	95:116:43200	m/y	2	-.21800000000000E-01	.170000E-02	
56	VELY	KOSG	A	1	95:116:43200	m/y	2	.21200000000000E-01	.160000E-02	
57	VELZ	KOSG	A	1	95:116:43200	m/y	2	.12200000000000E-01	.160000E-02	

*INDEX	TYPE	CODE	PT	SOLN	REF	EPOCH	UNIT	S	ESTIMATED VALUE	STD DEV
58	VELX	MADR	A	1	95:116:43200	m/y	2	-	.141000000000000E-01	.600000E-03
59	VELY	MADR	A	1	95:116:43200	m/y	2	-	.222000000000000E-01	.400000E-03
60	VELZ	MADR	A	1	95:116:43200	m/y	2	-	.201000000000000E-01	.600000E-03
61	VELX	SANT	A	1	95:116:43200	m/y	2	-	.228000000000000E-01	.210000E-02
62	VELY	SANT	A	1	95:116:43200	m/y	2	-	.630000000000000E-02	.170000E-02
63	VELZ	SANT	A	1	95:116:43200	m/y	2	-	.256000000000000E-01	.230000E-02
64	VELX	TIDB	A	1	95:116:43200	m/y	2	-	.354000000000000E-01	.800000E-03
65	VELY	TIDB	A	1	95:116:43200	m/y	2	-	.170000000000000E-02	.600000E-03
66	VELZ	TIDB	A	1	95:116:43200	m/y	2	-	.412000000000000E-01	.700000E-03
67	VELX	TROM	A	1	95:116:43200	m/y	2	-	.252000000000000E-01	.430000E-02
68	VELY	TROM	A	1	95:116:43200	m/y	2	-	.162000000000000E-01	.330000E-02
69	VELZ	TROM	A	1	95:116:43200	m/y	2	-	.650000000000000E-02	.900000E-02
70	VELX	WETT	A	1	95:116:43200	m/y	2	-	.252000000000000E-01	.400000E-03
71	VELY	WETT	A	1	95:116:43200	m/y	2	-	.191000000000000E-01	.300000E-03
72	VELZ	WETT	A	1	95:116:43200	m/y	2	-	.123000000000000E-01	.400000E-03
73	VELX	YAR1	A	1	95:116:43200	m/y	2	-	.459000000000000E-01	.900000E-03
74	VELY	YAR1	A	1	95:116:43200	m/y	2	-	.900000000000000E-02	.130000E-02
75	VELZ	YAR1	A	1	95:116:43200	m/y	2	-	.403000000000000E-01	.100000E-02
76	VELX	YELL	A	1	95:116:43200	m/y	2	-	.289000000000000E-01	.360000E-02
77	VELY	YELL	A	1	95:116:43200	m/y	2	-	.600000000000000E-03	.500000E-02
78	VELZ	YELL	A	1	95:116:43200	m/y	2	-	.250000000000000E-02	.870000E-02

-SOLUTION/APRIORI

*

+SOLUTION/MATRIX ESTIMATE L CORR

* Lower triangular correlation matrix elements, referenced by two parameter

* index numbers from SOLUTION/ESTIMATE, are given here.

*

***New to version 1.00 ***

*

The PARA fields increased to 21 chars, For CORR STDs must be given on

*

the main diagonal

*

*PARAL	PARA2	PARA2+0	PARA2+1	PARA2+2
1	1	.184577690512345-02		
2	1	.29425156137028E-01	.18909112191234E-02	
3	1	-.26004023015799E+00	-.28793741628090E+00	.20759188181234E+01
4	1	.54687523972711E+00	-.65452884277258E-01	-.43204669126067E-01
4	4	.17686254341234E-02		
5	1	-.39819911260492E-01	.40433299131131E+00	.11136939059432E+00
5	4	-.50106659384620E-02	.17977311401234E-02	
6	1	-.35321953180784E-01	.14019789950983E+00	.42813765846990E+00
6	4	.49918344878102E-01	-.26545148121353E+00	.18789567101234E-02
7	1	.69393516209264E-01	-.50927698251188E-01	-.18770770478848E-02
7	4	.11249919556344E+00	.36417010197355E-01	-.96512409551535E-02

*.....2290 lines deleted.....

117	1	.39554853137016E-02	-.14701327842692E+00	-.21849261652602E+00
117	4	.61854528268407E-01	-.15582766664907E+00	-.35595192513222E+00
117	7	-.14839162033233E-01	.10088643393429E-01	-.34620521010973E+00
117	10	.24473678103268E-01	-.17719246220580E+00	-.11471841650685E+00
117	13	.13124059834379E-01	.19447280189975E+00	.55372167099218E-01
117	16	.11834483725591E-01	-.15394348548100E+00	-.23577099430936E+00
117	19	-.69920935880248E-02	-.15152016672011E+00	-.15707791358241E-01
117	22	.56262209482092E-02	.44664432377454E-01	-.29206116099859E+00
117	25	.13595733163360E-01	-.36791832813222E-01	-.34302028599229E+00
117	28	.49976730750360E-01	-.52603056350601E-02	.35995661727203E+00
117	31	.58434167118809E-01	.79162912401483E-01	.19036198391000E+00
117	34	.18742319369700E-01	.29877748842137E+00	.27423619442271E+00
117	37	.37293677828651E-01	-.26370207939877E-01	.28314439940865E+00
117	40	-.15793512947600E-01	.16902050747741E-01	-.68991757800683E-01

*PARA1	PARA2	PARA2+0	PARA2+1	PARA2+2
117	43	.13839204459350E-01	-.90319568728349E-01	.87241280008327E-01
117	46	.17373506530565E-02	.75995410738772E-02	-.22097307167853E-01
117	49	-.31558372465614E-02	.33086324692108E+00	-.21155116202680E-01
117	52	.52662048663150E-01	-.96698061270683E-01	-.38697065241955E+00
117	55	.17854027402451E-01	.45413441850211E-01	-.39199818754031E+00
117	58	-.20557084589204E-01	.17772427521895E+00	-.38888132782579E+00
117	61	.51717169153988E-01	-.12774683850231E+00	-.18640329670510E+00
117	64	.60566764029226E-01	-.96756801702711E-01	-.31097880769930E+00
117	67	.15946573701026E-01	-.52959490859687E-01	.43877479729634E+00
117	70	-.56965234511833E-01	.12258278357446E+00	.20637613018780E+00
117	73	.10379256768073E-01	-.13337986646258E+00	.34656771257246E-01
117	76	.45650296192972E-01	-.14097331082148E+00	.31904369696173E+00
117	79	-.15366288987877E-01	-.76872083582857E-01	.14681131961463E+00
117	82	-.71521817107470E-02	-.14261694699670E+00	-.12950060100137E+00
117	85	-.46279787222485E-01	.17675785161574E+00	.43321519299327E+00
117	88	.17270566844414E-02	-.17956461690783E+00	-.95965022007633E-01
117	91	.67279754048700E-02	.17105290276520E-01	.96879240353699E-02
117	94	.46879651728024E-02	.15162522246501E-02	.16405537485657E-01
117	97	-.33487318865767E-01	-.15479070213606E-01	-.17088921255237E-01
117	100	-.10651453627699E-01	-.97673708447794E-02	-.44763578708339E-02
117	103	-.10868132563959E-01	.55392984612278E-01	.38519367197329E-01
117	106	.56288295168491E-01	.61044503649448E-01	.62180451664303E-01
117	109	.48458825773687E-01	.64903577511731E-01	.46603628193206E+00
117	112	.50888540957265E+00	.49512938569870E+00	.49390806153475E+00
117	115	.49291348118876E+00	.51840633003163E+00	.83771951711234E-01

-SOLUTION/MATRIX_ESTIMATE L CORR

*

+SOLUTION/MATRIX_APRIORI L CORR

*

* Same format as SOLUTION/MATRIX_ESTIMATE, but a priori values.

*

* Here NRC has only used the first column, This is valid, but wastes space.

*

New to version 1.00 *

*

The PARA fields increased to 21 chars, For CORR, STDs must be given on

*

the main diagonal

*PARA1	PARA2	PARA2+0	PARA2+1	PARA2+2
1	1	.3002645981234567E-02		
2	2	.3004133331239875E-02		
3	3	.3004133333333333E-02		
4	4	.3001488651234567E-02		
5	5	.3002645982345343E-02		
6	6	.3002645981234567E-02		
7	7	.4001116611234567E-02		
8	8	.5000893333333333E-02		
9	9	.5000893333333333E-02		
10	10	.4017828541234567E-02		
11	11	.4007933581234567E-02		
12	12	.4006075555555556E-02		
13	13	.3004133333333333E-02		
14	14	.3002645981234567E-02		
15	15	.3004133333333333E-02		
16	16	.5028606666666666E-02		
17	17	.5025348391234567E-02		
18	18	.3042059581234567E-02		
19	19	.3005950191234567E-02		
20	20	.3002645981234567E-02		
21	21	.2008914271234567E-02		

*PARA1	PARA2	PARA2+0	PARA2+1	PARA2+2
22	22	.4054352301234567E-02		
23	23	.4035701301234567E-02		
24	24	.4065111141234567E-02		
25	25	.4007933581234567E-02		
26	26	.4004464581234567E-02		
27	27	.400607555555556E-02		
28	28	.4223205911234567E-02		
29	29	.4132920301234567E-02		
30	30	.4903133751234567E-02		
31	31	.3002645981234567E-02		
32	32	.3001488651234567E-02		
33	33	.2003966791234567E-02		
34	34	.5008034271234567E-02		
35	35	.5016748271234567E-02		
36	36	.4012389333333333E-02		
37	37	.3207259781234567E-02		
38	38	.3388466301234567E-02		
39	39	.4849083081234567E-02		

-SOLUTION/MATRIX APRIORI L CORR

*-----

%ENDSNX

APPENDIX III

The standard IGS Receiver/Antenna name list (IGSCB information System:
ftp igsb.jpl.nasa.gov; file: igsb/station/general/rcvr_ant.tab)

ROGUE Receivers	Description
ROGUE SNR-8	2 unit rack-mounted (big Rogue)
ROGUE SNR-800	1 unit rack-mounted (big Rogue)
ROGUE SNR-8A	MiniRogue -- not CONAN compatible
ROGUE SNR-8C	MiniRogue -- CONAN compatible
ROGUE SNR-8000	TurboRogue (field unit)
ROGUE SNR-8100	TurboRogue (rack mount)
ROGUE SNR-12	TurboRogue (12 channel)
ROGUE SNR-12 RM	TurboRogue (12 channel, rack mount)
ROGUE Antennae	Description
DORNE MARGOLIN R	Antenna with chokering for Rogues (JPL design)
DORNE MARGOLIN B	Antenna with chokering for Rogues (AOA design)
DORNE MARGOLIN T	Antenna with chokering for TurboRogues
TRIMBLE Receivers	Description
TRIMBLE 4000S	
TRIMBLE 4000SE	
TRIMBLE 4000SL	
TRIMBLE 4000ST	
TRIMBLE 4000SX	
TRIMBLE 4000SLD	Dual freq. L1 c/a; L2 squaring
TRIMBLE 4000SST	Dual freq. L1 c/a; L2 squaring; L2 p-code optional
TRIMBLE 4000SSE	Dual freq. p-code on L1 and L2; xcr Y-code
TRIMBLE Antennae	Description
4000SE INTERNAL	
4000SL MICRO	(Round)
4000SLD L1/L2	Dual freq. geodetic receiver (SLD series)
4000ST INTERNAL	
4000ST KINEMATIC	Single freq. without a ground plane
4000ST L1 GEODETIC	To use with single freq. geodetic receiver
4000ST L1/L2 GEOD	Dual freq. geodetic receiver (Mod.14532)
4000SX MICRO	(Square)
TR GEOD L1/L2 GP	Geod. L1/L2 compact; grd. plane incl . (Mod.22020)
TR GEOD L1/L2 W/O GP	Geod. L1/L2 compact; grd. plane removed (Mod.22020)
M-PULSE L1/L2 SURVEY	MicroPulse L1/L2 GPS Surveying Antenna 90LL12300
DORNE MARGOLIN TRIM	Antenna with chokering (Trimble design)

MINIMAC Receivers	Description
MINIMAC 2816AT	Rack-mounted (used in CIGNET and NIED)
MINIMAC 2816	Field unit
MINIMAC Antennae	Description
MACROMETER X-DIPOLE	Crossed-dipole antenna with large ground plane
MINIMAC PATCH	Patch antenna
ASHTECH Receivers	Description
ASHTECH xxxxxxxx	xxxxxxx is the receiver type to be found in the receiver-generated S-file, e.g. LM-XII3 or L-XII
ASHTECH Antennae	Description
GEODETIC L1/L2 L	Dual freq. with ground plane (LD-XII & MD-XII)
GEODETIC L1/L2 P	Dual freq. with ground plane (P-12)
GEODETIC III L1/L2	Dual freq. with ground plane
DORNE MARGOLIN ASH	Antenna with choking (Ashtech design)
MARINE/RANGE	Single freq. with a smaller ground plane
A-C L1	Single freq. w/o ground plane for aircraft use
A-C L1/L2	Dual freq. without ground plane for aircraft use
LEICA Receivers	Description
SR299	Geodetic receiver, internal antenna
SR299E	Geodetic receiver, external antenna
LEICA Antenna	Description
INTERNAL	Internal antenna of SR299 receiver
EXTERNAL WITH GP	External antenna of SR299E with groundplane
EXTERNAL WITHOUT GP	External antenna of SR299E, without groundplane

APPENDIX IV

CODING STATION INFORMATION CHANGES IN SINEX V1.00: A SAMPLE

There are THREE valid ways of coding a mid-week station receiver/antenna change in weekly SINEX v1.00. To demonstrate this a recent change at GRAZ (week 0859) to show them below. To quote SINEX v1.00 definition "SITE+PT+SOLN defines a unique estimate, SITE+PT is equivalent to DOMES (DOMEX) and uniquely identifies a geodetic mark".

Case (i): To state two separate estimates at a site, assuming the mark has changed. We call these marks GRAZ A and GRAZ B, and don't re-use the old DOMES code, but code the second estimate with unknown DOMES:

```
+SITE/ID
GRAZ A 11001M002 P GRAZ          15 29 36.5 47 4 1.7 538.3
GRAZ B ----- P GRAZ          15 29 36.5 47 4 1.7 538.3
-SITE/ID
+SITE/RECEIVER
GRAZ A ---- P 96:174:00000 96:176:86369 ROGUE SNR-8C          -----
GRAZ B ---- P 96:177:00000 96:182:86369 ROGUE SNR-8000        -----
-SITE/RECEIVER
+SITE/ANTENNA
GRAZ A ---- P 96:174:00000 96:176:86369 DORNE MARGOLIN B      128
GRAZ B ---- P 96:177:00000 96:182:86369 DORNE MARGOLIN T      457
-SITE/ANTENNA
+SITE/ECCENTRICITY
GRAZ A ---- P 96:174:00000 96:176:86369 UNE 2.0680 0.0000 0.0000
GRAZ B ---- P 96:177:00000 96:182:86369 UNE 1.9640 0.0000 0.0000
-SITE/ECCENTRICITY
+SOLUTION/EPOCHS
GRAZ A 1 P 96:174:00000 96:176:86369 96:175:43185
GRAZ B 1 P 96:177:00000 96:182:86369 96:179:86385
-SOLUTION/EPOCHS
```

It is illegal to give GRAZ B the same DOMES as GRAZ A (see quote above).

Case (ii) To state two separate estimates at a site, reduced to a common mark. These are called GRAZ A 1 and GRAZ A 2, and both use a single SITE/ID line because there's only one mark:

```
+SITE/ID
GRAZ A 11001M002 P GRAZ          15 29 36.5 47 4 1.7 538.3
-SITE/ID
+SITE/RECEIVER
GRAZ A 0001 P 96:174:00000 96:176:86369 ROGUE SNR-8C          -----
GRAZ A 0002 P 96:177:00000 96:182:86369 ROGUE SNR-8000        -----
-SITE/RECEIVER
+SITE/ANTENNA
GRAZ A 0001 P 96:174:00000 96:176:86369 DORNE MARGOLIN B      128
GRAZ A 0002 P 96:177:00000 96:182:86369 DORNE MARGOLIN T      457
```

```

-SITE/ANTENNA
+SITE/ECCENTRICITY
  GRAZ A 0001 P 96:174:00000 96:176:86369 UNE 2.0680 0.0000 0.0000
  GRAZ A 0002 P 96:177:00000 96:182:86369 UNE 1.9640 0.0000 0.0000
-SITE/ECCENTRICITY
+SOLUTION/EPOCHS
  GRAZ A 0001 P 96:174:00000 96:176:86369 96:175:43185
  GRAZ A 0002 P 96:177:00000 96:182:86369 96:179:86385
-SOLUTION/EPOCHS

```

Case (iii) To state a single estimate at a site, where the station information changed during the data span. In this case there should be only one SOLUTION/EPOCHS entry, for GRAZ A 1. As many SITE/... entries may be used as required, in this example we need two in each block.

```

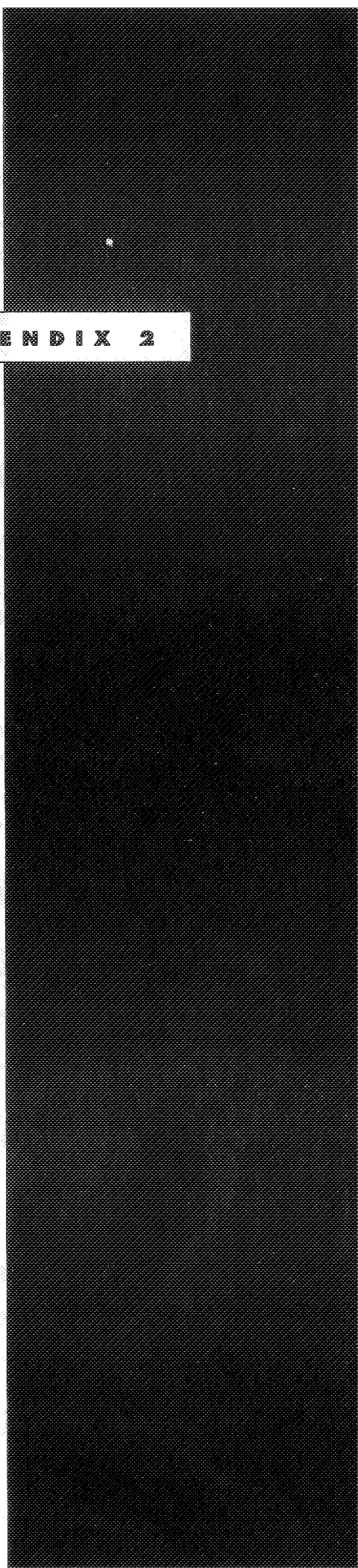
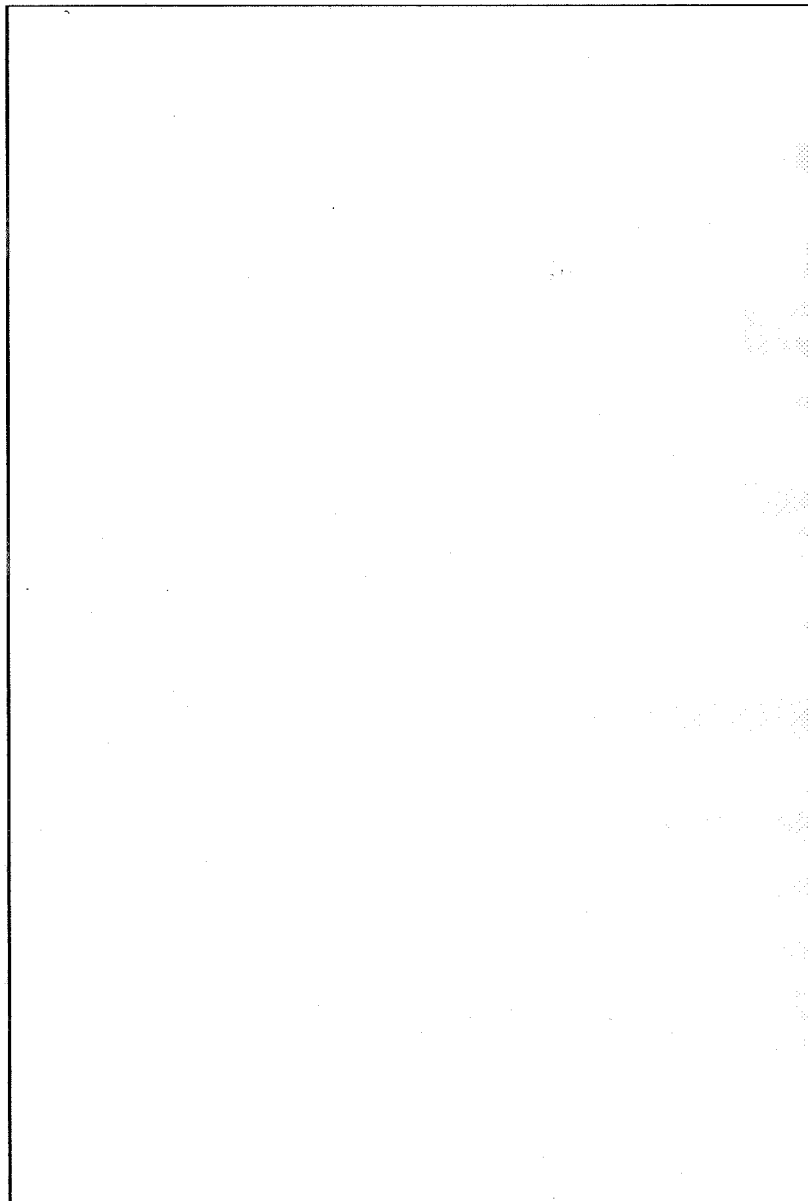
+SITE/ID
  GRAZ A 11001M002 P GRAZ 15 29 36.5 47 4 1.7 538.3
-SITE/ID
+SITE/RECEIVER
  GRAZ A ---- P 96:174:00000 96:176:86369 ROGUE SNR-8C -----
  GRAZ A ---- P 96:177:00000 96:182:86369 ROGUE SNR-8000 -----
-SITE/RECEIVER
+SITE/ANTENNA
  GRAZ A ---- P 96:174:00000 96:176:86369 DORNE MARGOLIN B 128
  GRAZ A ---- P 96:177:00000 96:182:86369 DORNE MARGOLIN T 457
-SITE/ANTENNA
+SITE/ECCENTRICITY
  GRAZ A ---- P 96:174:00000 96:176:86369 UNE 2.0680 0.0000 0.0000
  GRAZ A ---- P 96:177:00000 96:182:86369 UNE 1.9640 0.0000 0.0000
-SITE/ECCENTRICITY
+SOLUTION/EPOCHS
  GRAZ A 1 P 96:174:00000 96:182:86369 96:178:00000
-SOLUTION/EPOCHS

```

Note that in this case no SOLN codes are required in the SITE/... blocks! The records are well ordered by their data start/stop fields. This is a change from the accepted SINEX v0.05 usage.

IGS

APPENDIX 2



Page intentionally left blank

Towards a new IGS Orbit Model

T.A. SPRINGER, G. BEUTLER, M. ROTHACHER

Astronomical Institute
University of Berne
Sidlerstrasse 5
CH-3012 Bern
Switzerland

March 19, 1996

Why a new IGS Orbit Model ?

- The existing model including Rock4/42 Solar Radiation Pressure was developed **before** the availability of highly accurate orbits.
- It therefore cannot take into account subtleties which became apparent through IGS operations.
- The existing model is **not** suited for long arcs.
- The consistency of individual IGS 1-day orbit series and the consistency between these series soon reaches 1–5 cm level rms.

Where are we today?

Within the IGS we are aware of:

- The CODE Extended Orbit Model (Beutler et al, 1993) on which the IGS long-arc analysis is based,
 - developments at MIT (used by SIO) leading to a dramatic improvement of the SIO orbit series,
 - developments at JPL to model satellites during their “eclipse seasons”.
-
- Subsequently we will discuss the experiences made with the CODE Extended Orbit Model.

History of the Extended CODE Orbit Model

- Developed in 1993 (!) at CODE.
- Used since early 1994 for the long arc analysis of the IGS orbit combination.
- Routinely used at CODE to check orbit quality of the routine IGS processing.
- In January 1996 fully integrated into the Bernese software.

The Extended CODE Orbit Model

The radiation pressure model may be written as:

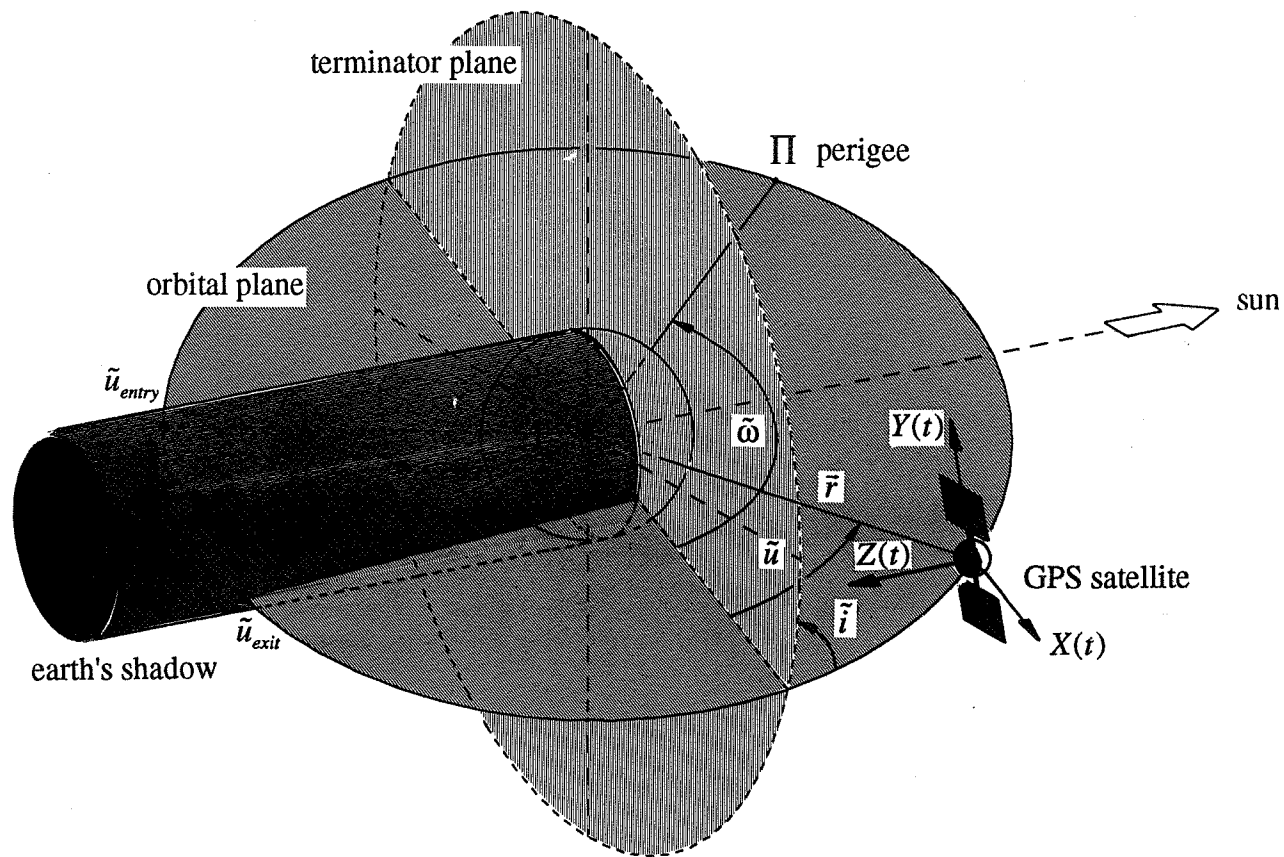
$$a_{rpr} = a_{ROCK} + a_D + a_Y + a_X$$

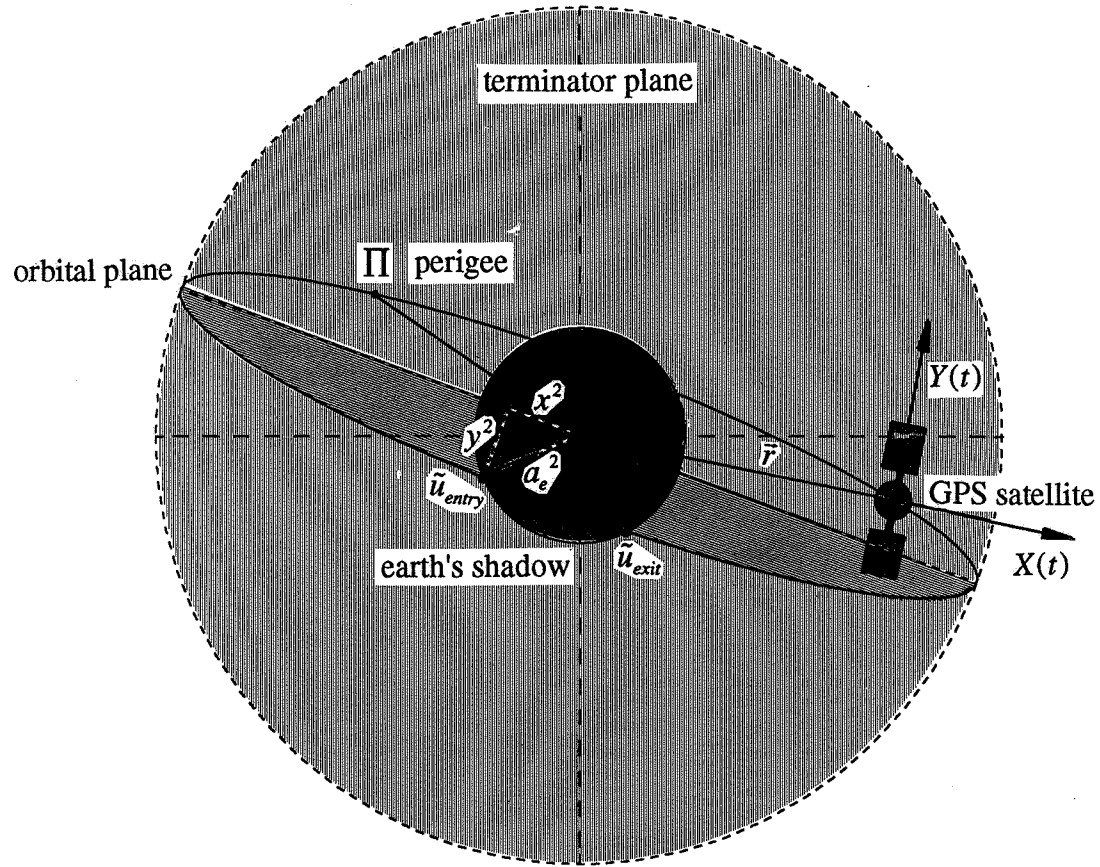
where a_{ROCK} is the acceleration due to the Rock-model, and

$$\begin{aligned} a_D &= [a_{D0} + a_{DC} \cos u + a_{DS} \sin u]e_D = D(u)e_D \\ a_Y &= [a_{Y0} + a_{YC} \cos u + a_{YS} \sin u]e_Y = Y(u)e_Y \\ a_X &= [a_{X0} + a_{XC} \cos u + a_{XS} \sin u]e_X = X(u)e_X \end{aligned}$$

where a_{D0} , a_{DC} , a_{DS} , a_{Y0} , a_{YC} , a_{YS} , a_{X0} , a_{XC} , and a_{XS} are the nine parameters of the Extended Model,

- e_D is the unit vector sun-satellite,
- e_Y is the unit vector along the spacecraft's solar-panel axis,
- $e_X = e_Y \times e_D$,
- u is the argument of latitude at time t .

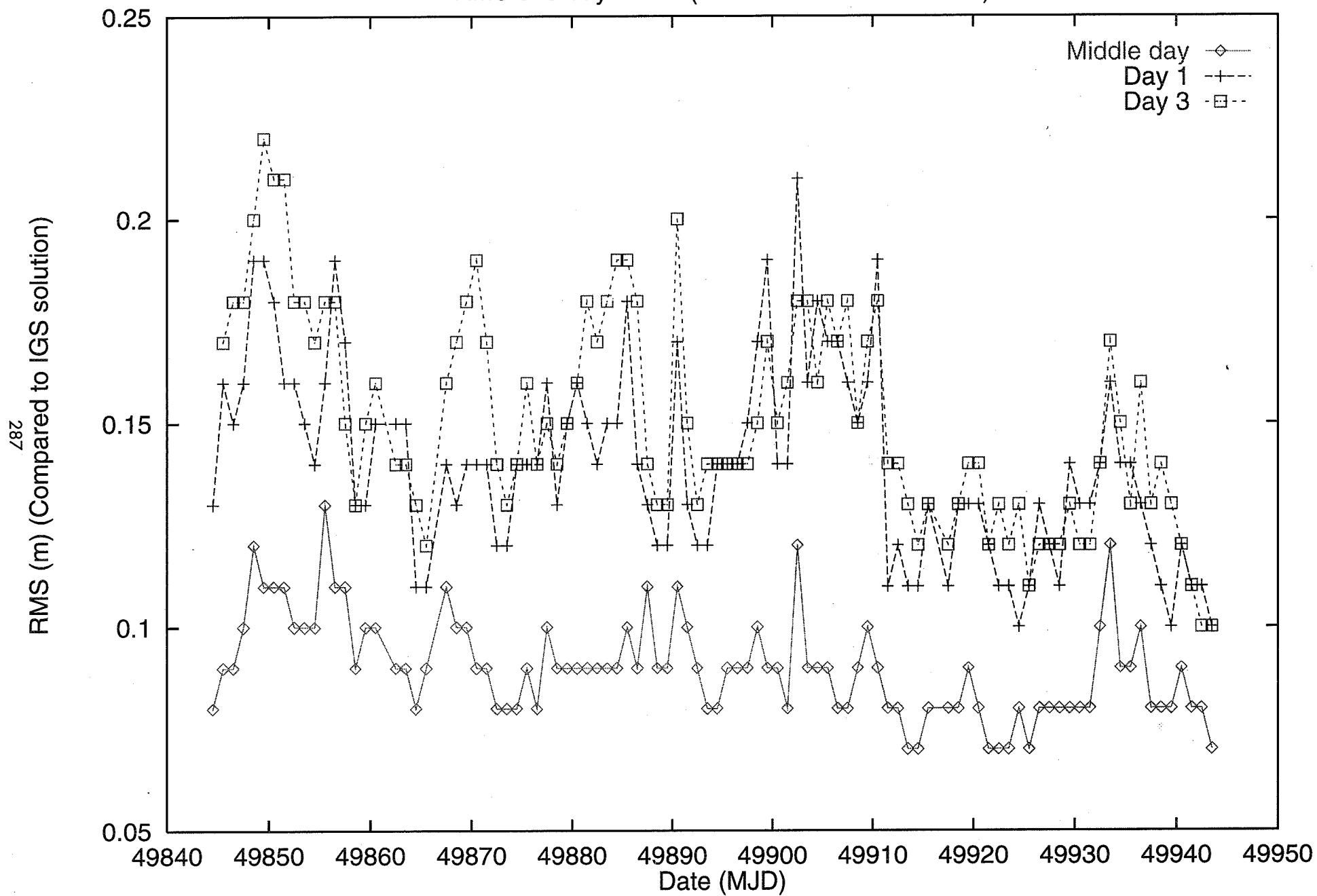




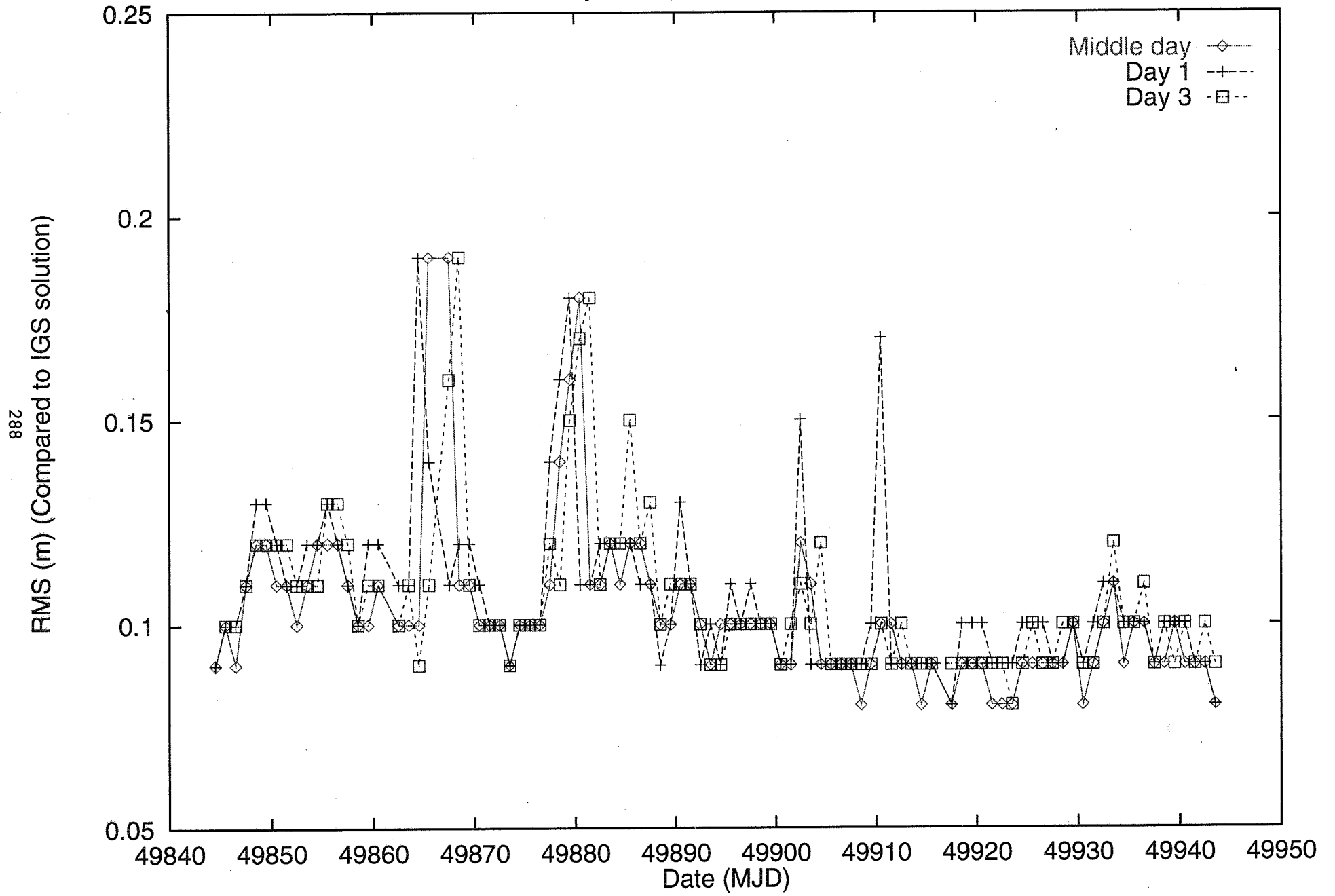
Why the Extended CODE Orbit Model

- Conventional 8 or 9 parameter orbit models are no longer adequate for high precision orbits ($< 10cm$),
- “stochastic” pulses are capable of absorbing orbit model deficiencies but a better “deterministic” model is preferable,
- in more than 2 years of IGS orbit combinations, the model has shown that it is capable of modeling the satellites over 7 days at the few centimeter level,
- all days of an n-day arc have the same quality,
- it removes the so called “y-shift” of the orbit- and coordinate-systems,
- it allows much better orbit predictions.

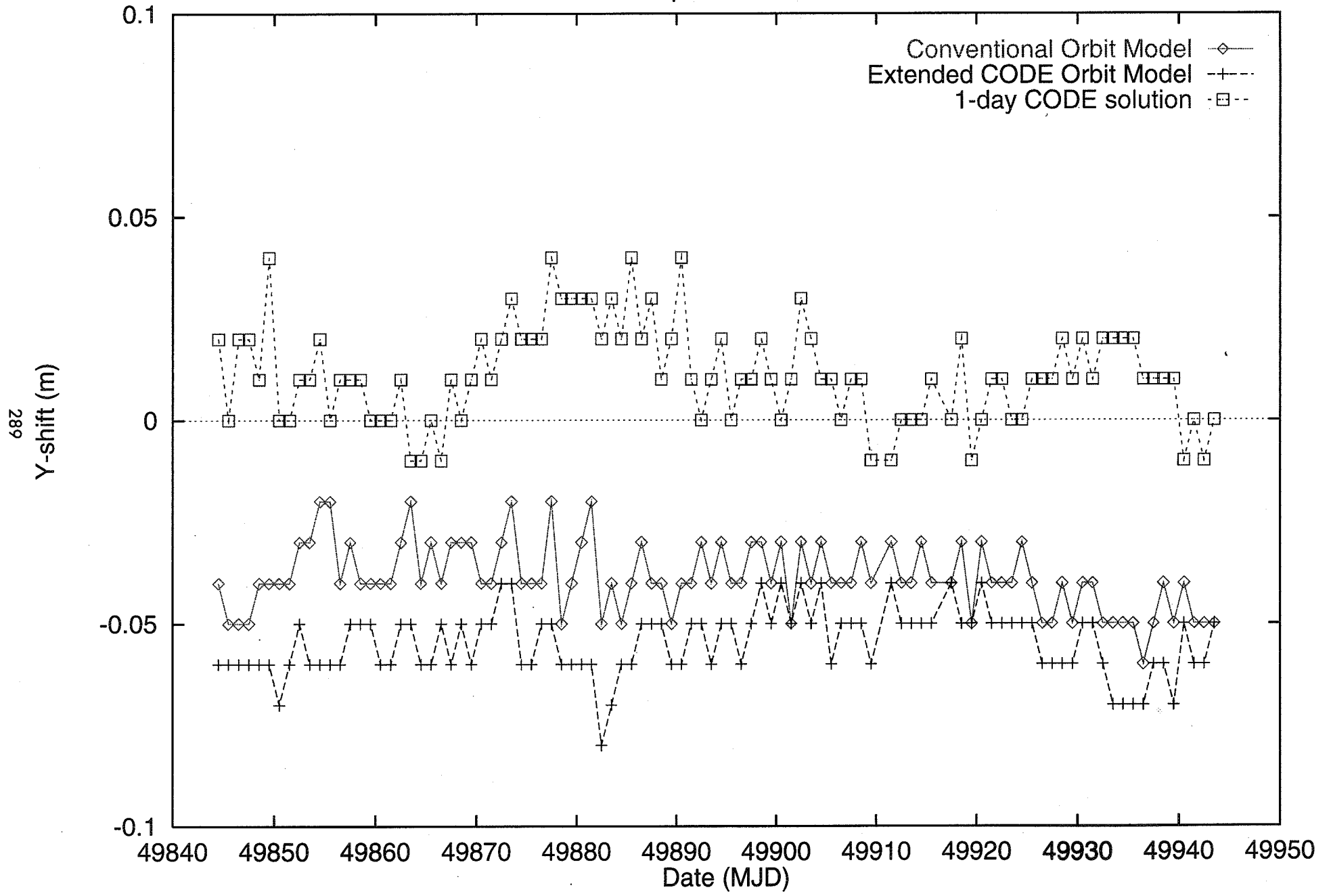
RMS of 3-day Orbits (Conventional Orbit Model)



RMS of 3-day Orbit (Extended CODE Orbit Model)

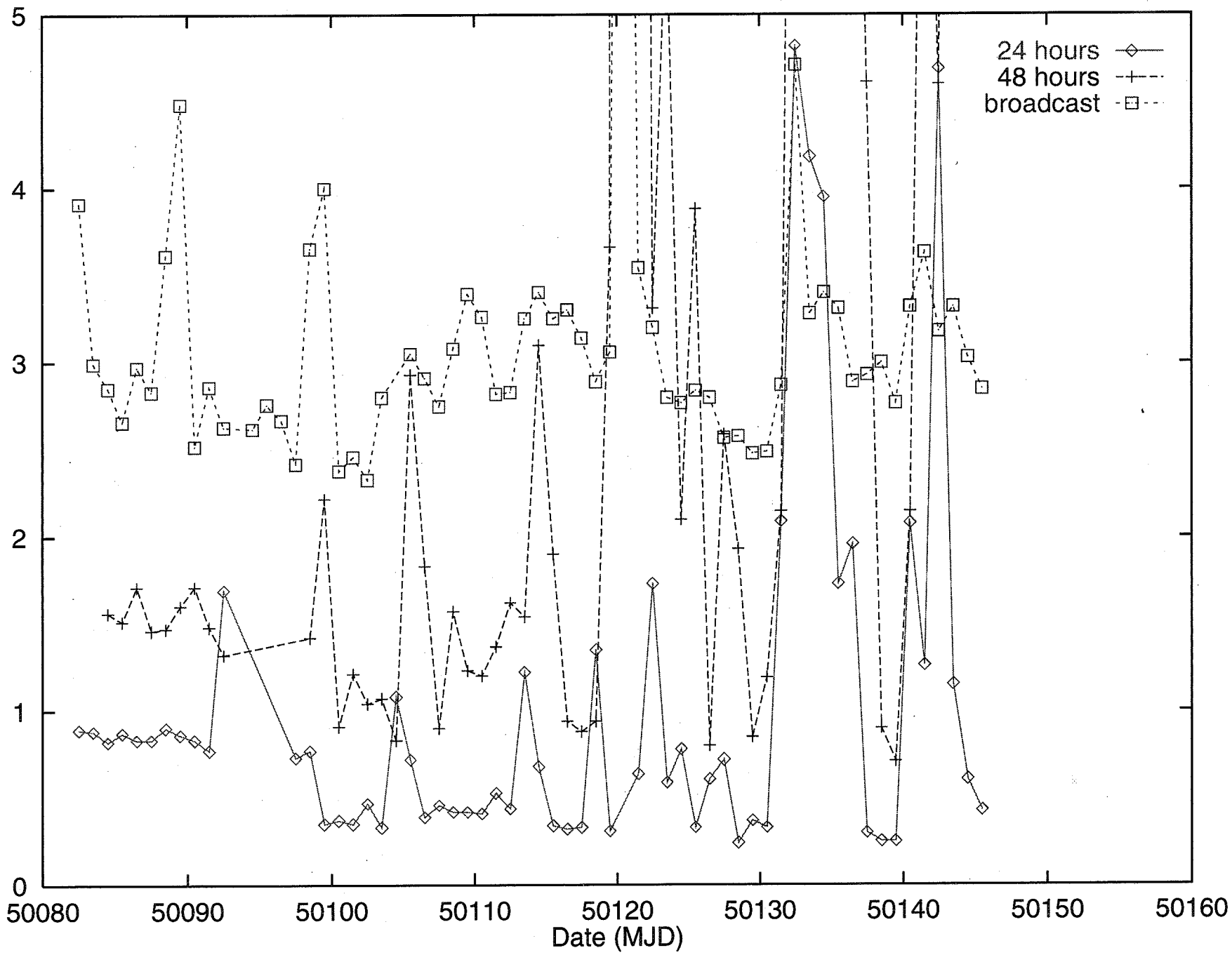


Y-shift of Orbit compared to IGS Combined Orbit



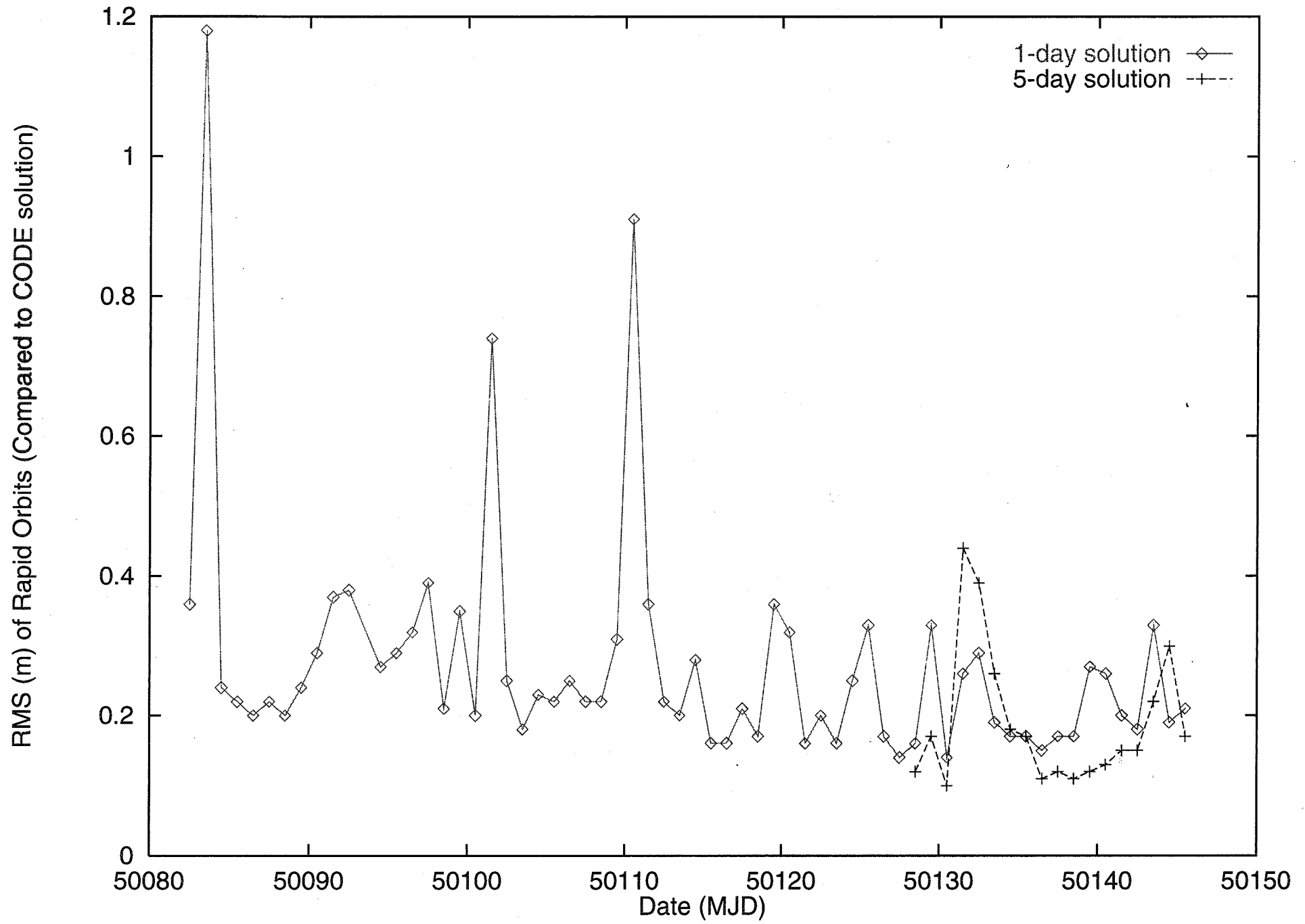
289

RMS (m) of Predicted Orbits (Compared to CODE solution)



Use of the Extended CODE Orbit Model for Rapid Orbits

- Rapid Orbits at CODE are orbits generated around 12 hours UT for the preceding day.
- Possibility to use long(er) arcs because all days show the same quality,
- with longer arcs the (Rapid) Orbit becomes much less sensitive to the number of available stations.
- Currently we use a 5-day arc, where our contribution to the IGS Preliminary Orbit is the last day of this arc.
- Solution is created using normal equation stacking (ADDNEQ). The final 5-day solution takes only 5 min of CPU (on a Alpha 600 5/266).
- Possibility to use two days of our official IGS processing which contain our full network (currently at maximum 76 stations).



Problem areas with Orbit Modeling

- In general each acceleration term (dynamical parameter) will create an out-of-plane (W) component which may implicitly (through a resulting net rotation of all orbital planes) affect the transformation parameters between the inertial and the terrestrial reference frames (ICRF and ITRF):

- Motion of node for satellite k over 1 revolution:

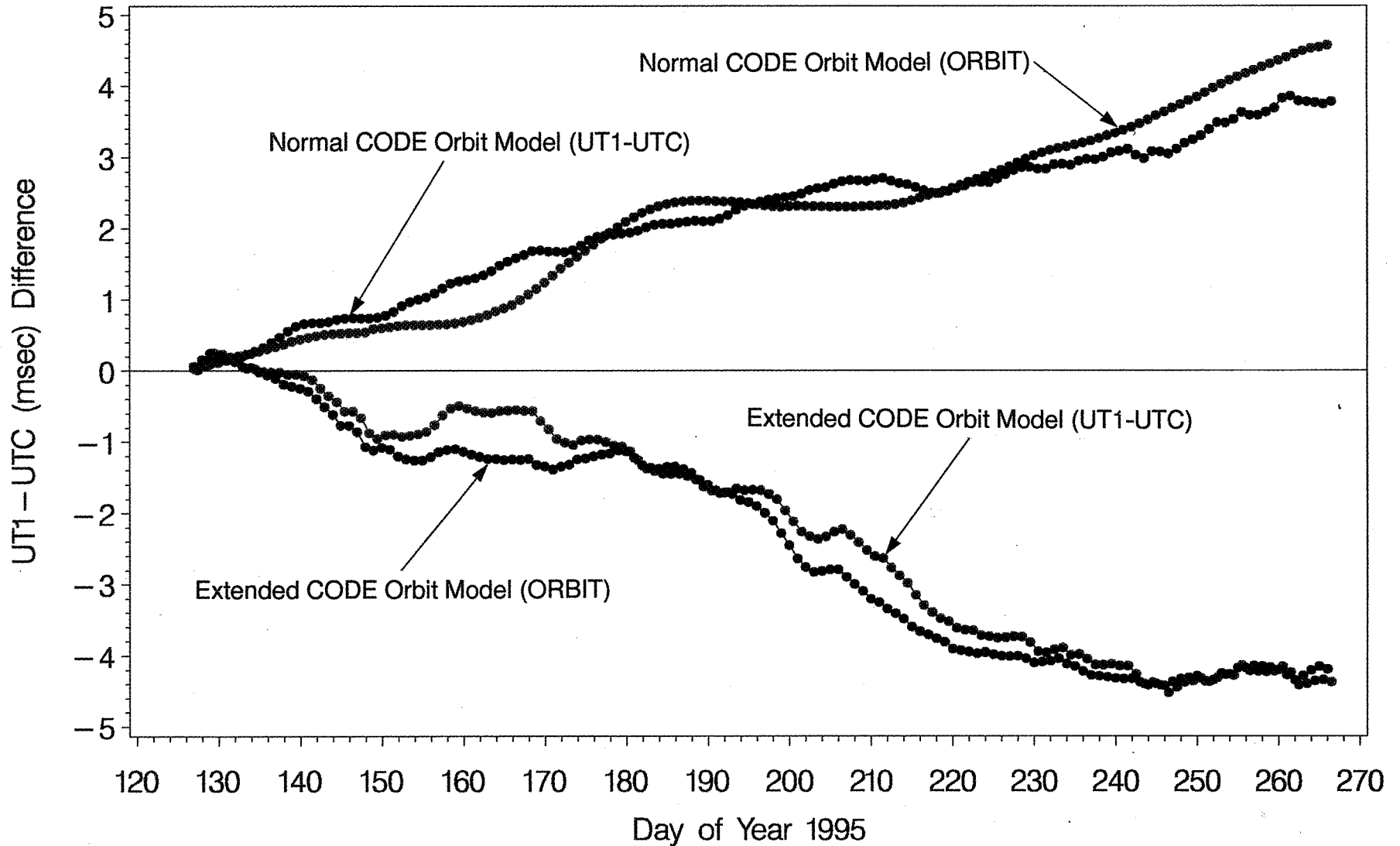
$$\delta\Omega_k(t_0, t) = \frac{1}{n_k \cdot a_k \cdot \sin i_k} \cdot \int_{t_0}^t \sin u_k \cdot W_k(t) \cdot dt'$$

- Mean motion of the entire GPS orbit system:

$$\dot{\Omega}_{mean}(t) = \frac{1}{n_{sat}} \cdot \sum_{k=1}^{n_{sat}} \frac{1}{U_k} \cdot \delta\Omega_k(t - \frac{1}{2}U_k, t + \frac{1}{2}U_k)$$

- Similar equations may be extracted for change of inclination (correlation with nutation!).

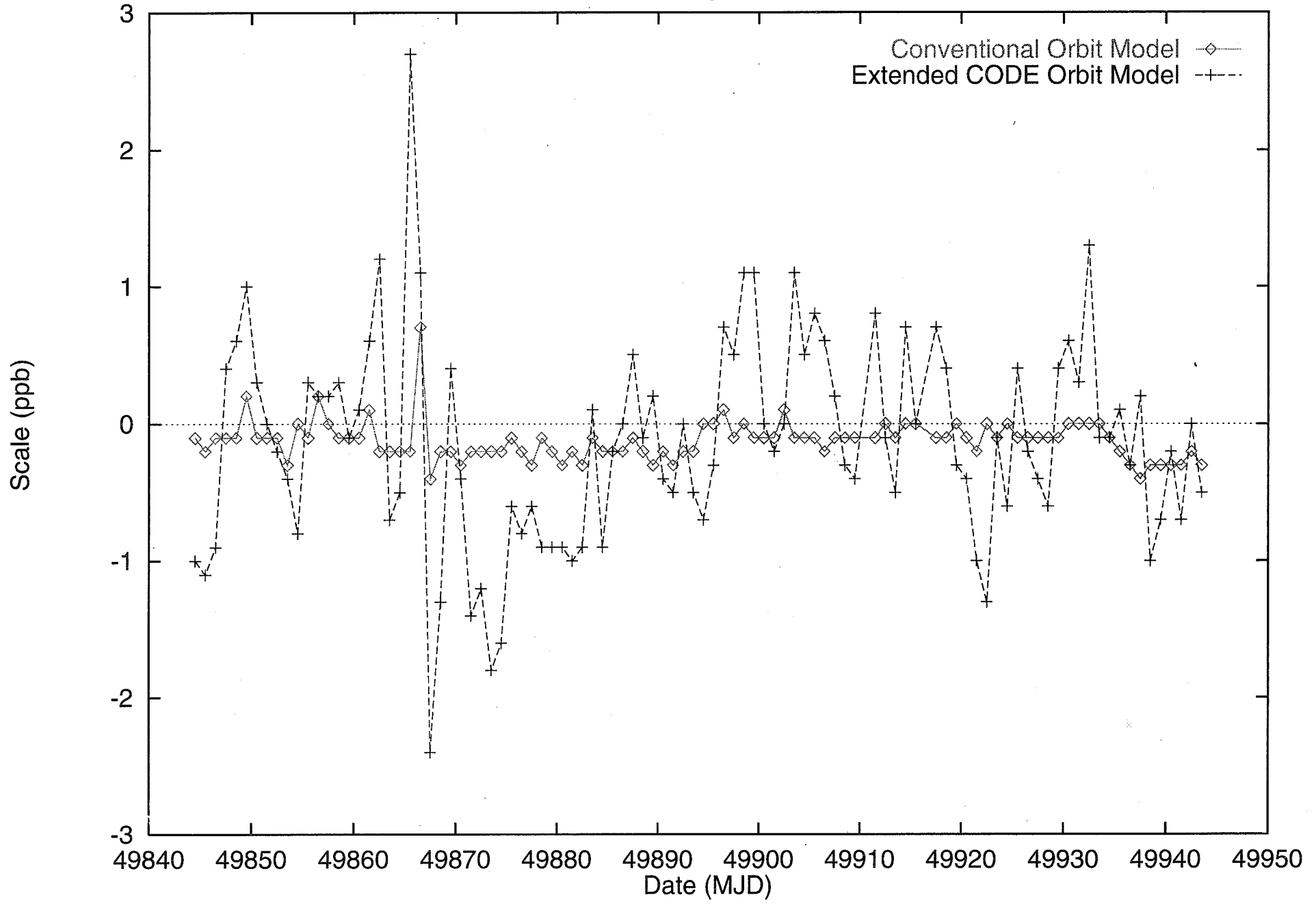
UT1-UTC differences to Bulletin A EOP Series and resulting Orbit Rotation due to RPR-Model



- Normal CODE Orbit Model (UT1-UTC)
- Normal CODE Orbit Model (ORBIT)
- Extended CODE Orbit Model (UT1-UTC)
- Extended CODE Orbit Model (ORBIT)

Difference in Orbit Scale compared to IGS Combined Orbit

Conventional Orbit Model \diamond —
Extended CODE Orbit Model +---



Conclusions concerning Extended CODE Orbit Model

- All individual days of an n-day arc are of the same (high) quality.
- Possibility to create arcs of at least 7 days.
- No “y-shift” problem.
- Rapid orbits within 12 hours at the 10 cm level.
- (Rapid) Orbit predictions for the next 24 hours are at the 30 cm level.
- Correlations with UT1-UTC and nutation series exist, but additional constraints will cope with this problem (to be shown).

Conclusions concerning the IGS Orbit Model

- We believe that a new IGS Orbit Model should be **defined**.
- This model may be general in the sense that it will leave some degree of freedom to each IGS Analysis Center.
- We believe that all experiences gained in the context of GPS high accuracy orbit modeling should be used to develop this **new IGS Standard**.
- We believe that the new model also should become part of the **new IERS standards**.

Page intentionally left blank

MULTI-TECHNIQUE EOP COMBINATION

D. Gambis

Central Bureau of IERS, Paris Observatory, FRANCE

IGS Workshop, Silver Spring, March 19-21 1996

UT1 based on both VLBI and GPS

The approach

- GPS high-frequency variations associated with long-term VLBI variations
- Procedure has to be the most simple as possible for clarity of the process.
- High frequency terms are removed in VLBI series while they are kept for internal GPS "UT1" series.
- The critical point concerns the threshold determination within which the high-frequency information contained in the GPS series is valuable.

Summary

Universal Time solution combined by IERS is mainly based on VLBI inertial techniques.

Although space techniques like SLR or GPS have reached a remarkable precision they do not give access to a highly accurate non-rotating reference frame, which restricts the possibility of determining directly UT1 from the processing of their observations.

Due principally to uncertainties in the even zonal harmonics and in various models (ocean tides), long-term error drifts are introduced in the node motion and consequently in UT1 of which estimation is completely correlated with the node variations.

It is however possible to use the valuable short-term fluctuations given by GPS calibrated with the long-term variations of the solution given by inertial techniques to derive a composite UT1 solution of great interest for its precision and time resolution but also for its economic advantage.

Precision of UT based on VLBI and GPS techniques

VLBI UT1 Precision:

One -hour intensive (daily)	15 μ s
24-hour (7-days)	7 μ s

- high-frequency variations of UT(GPS) for densification:

based on

- one solution (CODE or EMR) : 27 μ s
- a combined solution of 3 GPS solutions : 25 μ s

- Near-real time using GPS for prediction

Operational precision in case of VLBI contribution every 10, 20 or 30 days. UT1(GPS) is used from the last VLBI data.

VLBI sampling	UT1 precision
10 days	200 μ s
20 days	300 μ s
30 days	500 μ s

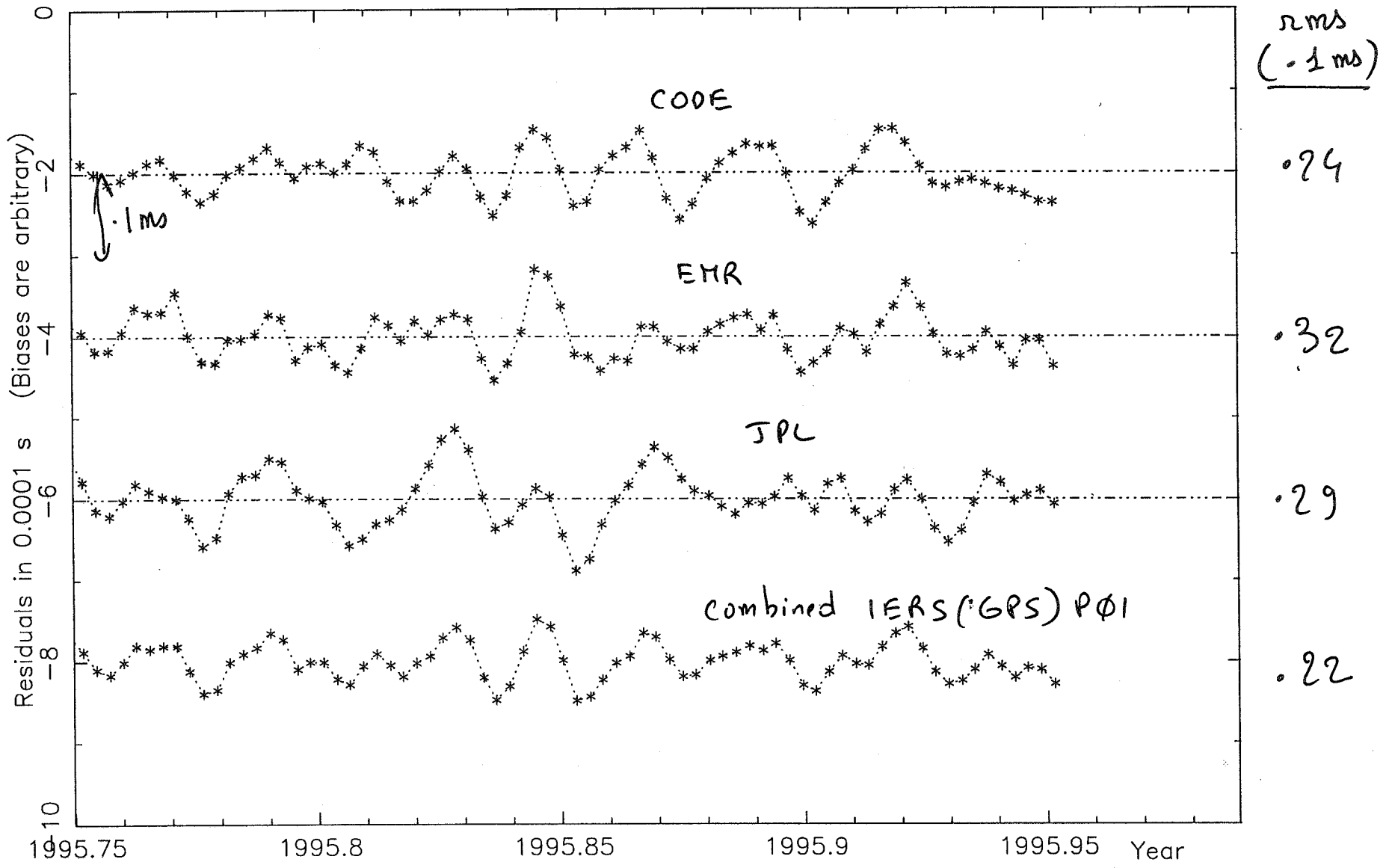
Conclusions

- Long-term GPS "UT1" series not directly usable for Earth Orientation.
- Possibility to use external reference (VLBI, IERS) for long-term calibration.
- Combined UT1 solution routinely computed at IERS/BC
- Precision comparable to other series (NOAA, USNO, CSR).
- Combination of independant UT1(GPS) solutions improves the final solution by elimination of white noise.
- High sampling contribution (1 day).
- Operational precision in case of VLBI contribution every 10, 20 or 30 days. UT1(GPS) is used from the last VLBI data.

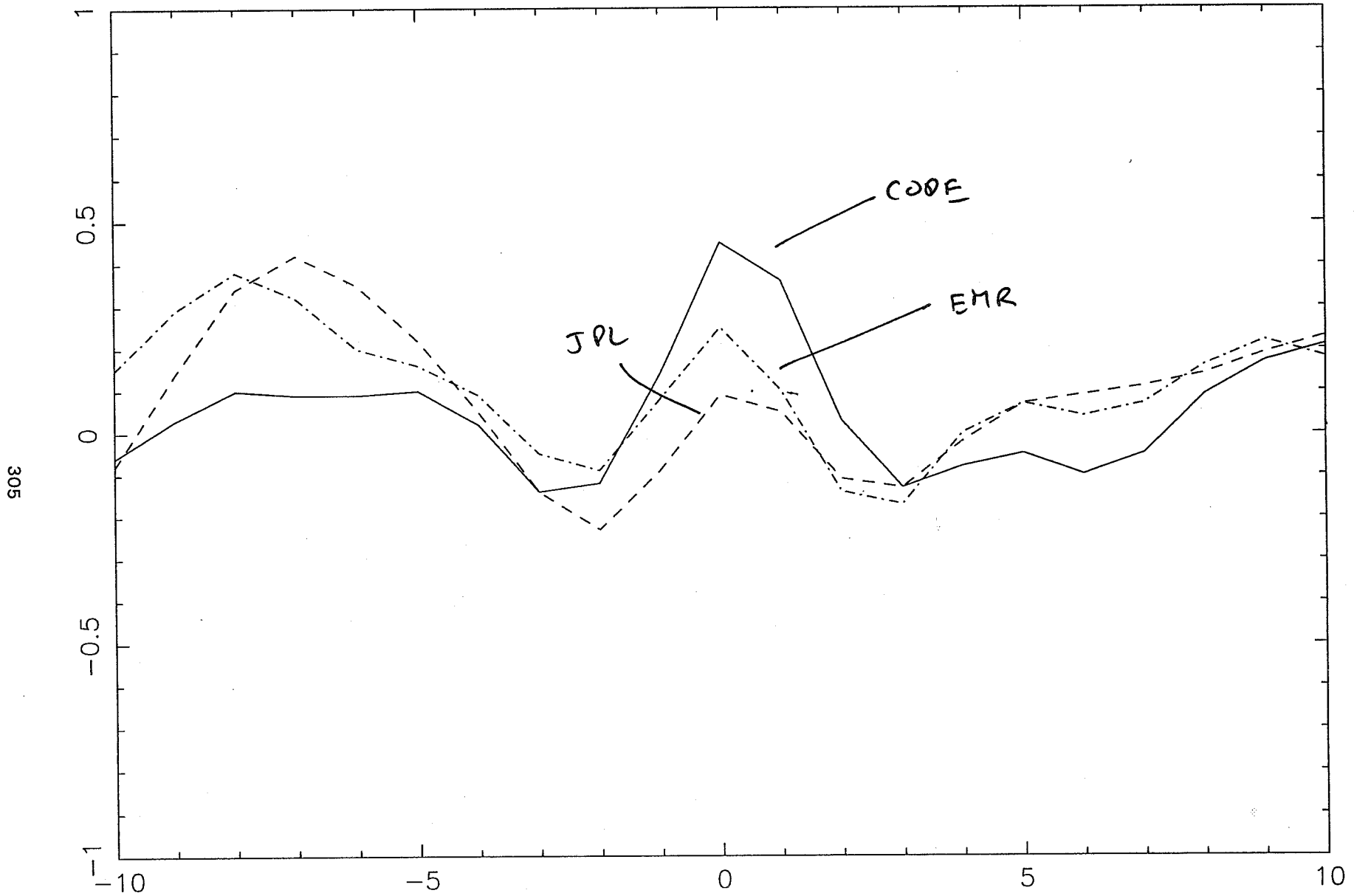
VLBI sampling	UT1 precision
10 days	0.2 ms
20 days	0.3 ms
30 days	0.5 ms

UT1: HIGH-FREQUENCY RESIDUALS, CODE, EMR, JPL, IERS(GPS) - EOP(IERS) C 04

304



CORRELATION BETWEEN HIGH-FREQUENCY VARIATIONS OF CODE, EMR AND JPL



Over 1995.75 → 1996.0

Page intentionally left blank

SPECIAL GPS SOLUTIONS BASED ON ITRF94

Z. Altamimi
Institute Geographique National
France

ITRF94_P1 : Extract of GPS stations from ITRF94 solution at 93.0

ITRF94_P2 : Combination of the 3 GPS solutions used in the ITRF94
Expressed in the ITRF94

ITRF94_P3 : Combination of VLBI, SLR, DORIS and
local ties for GPS stations

Comparison ITRF94_P1/P2 at 93.0

	N	SP cm	SU cm	SX cm	WSP cm	WSU cm	WSX cm
ITRF94_P1	80	.3	.4	.3	.2	.4	.3
ITRF94_P2	80	.2	.7	.5	.1	.3	.2

Comparison ITRF94_P1/P3 at 93.0

	N	SP cm	SU cm	SX cm	WSP cm	WSU cm	WSX cm
ITRF94_P1	46	.4	.4	.4	.3	.4	.3
ITRF94_P3	46	.7	1.6	1.1	.6	.8	.6

Comparison ITRF94_P2/P3 at 93.0

	N	SP cm	SU cm	SX cm	WSP cm	WSU cm	WSX cm
ITRF94_P2	46	.5	1.2	.8	.2	.4	.3
ITRF94_P3	46	1.0	2.0	1.4	.9	1.2	1.0

**Ashtech Radome Tests
on
Dorne-Margolin Choke Ring Antennas**

R. King, A.E. Niell, McClusky, and T. Herring

GPS Systems

2 Ashtech Z-12s - with or without Ashtech radome

1 AOA TurboRogue - no radome

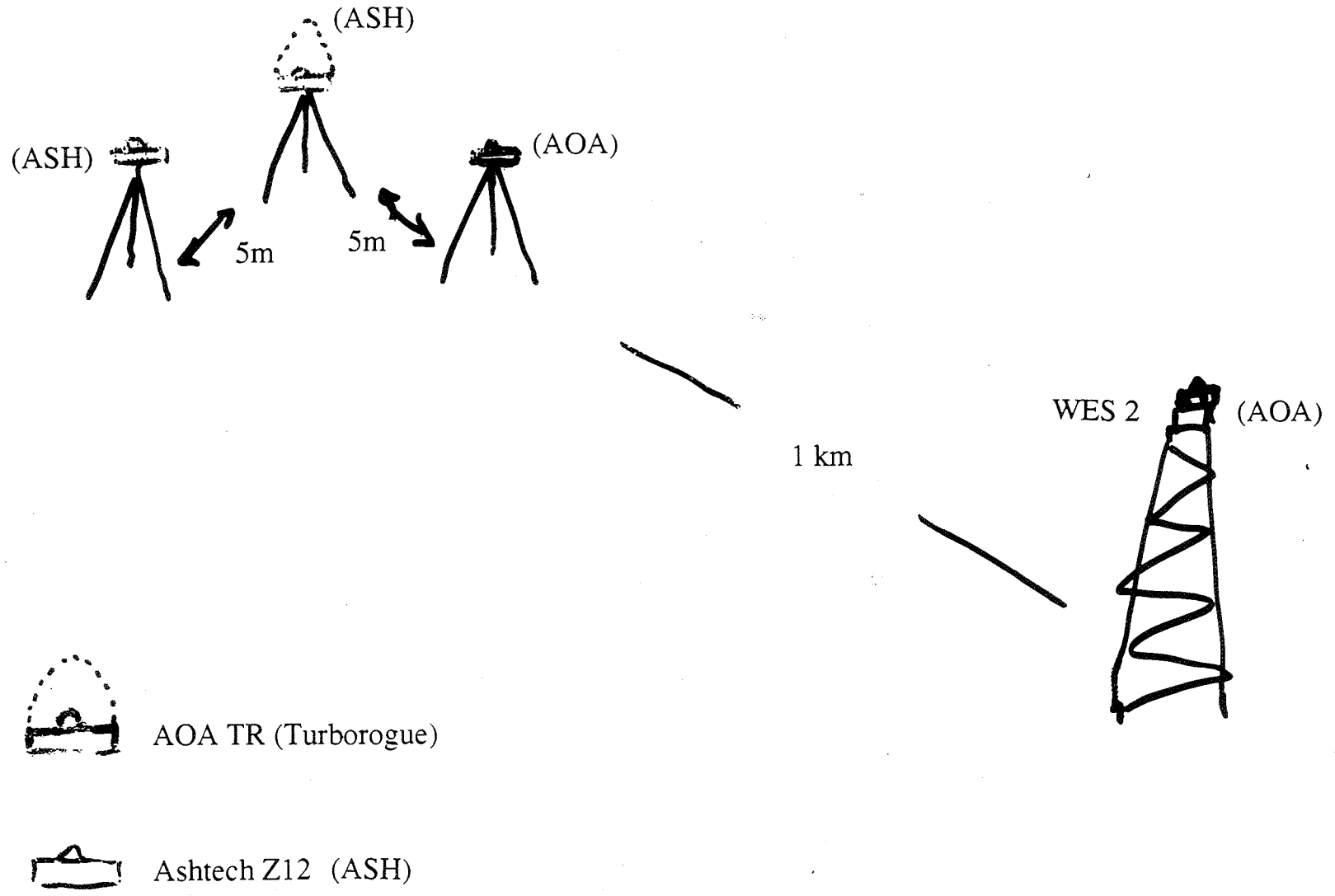
Dorne-Margolin choke ring (DM/CR) antennas

~5 meter separation of antennas

LC observable

Solve for antenna positions and tropospheres relative to WES2

(TurboRogue DM/CR ~1 km away)



Ashtech Radome Tests on Dorne-Margolin Choke Ring Antennas

No-Radome Solutions

- 1) Height difference compared to theodolite leveling
15° and 5° minimum elevation:

AshtechE - AOA 1 mm
AshtechW - AOA 10 mm

Use "standard antenna on
tripod & do absolute
position differences

- 2) Interchange AOA and Ashtech DM/CR antennas on AshtechW

< 2 mm difference in any coordinate

Effect of Radome

Add radome to AshtechE

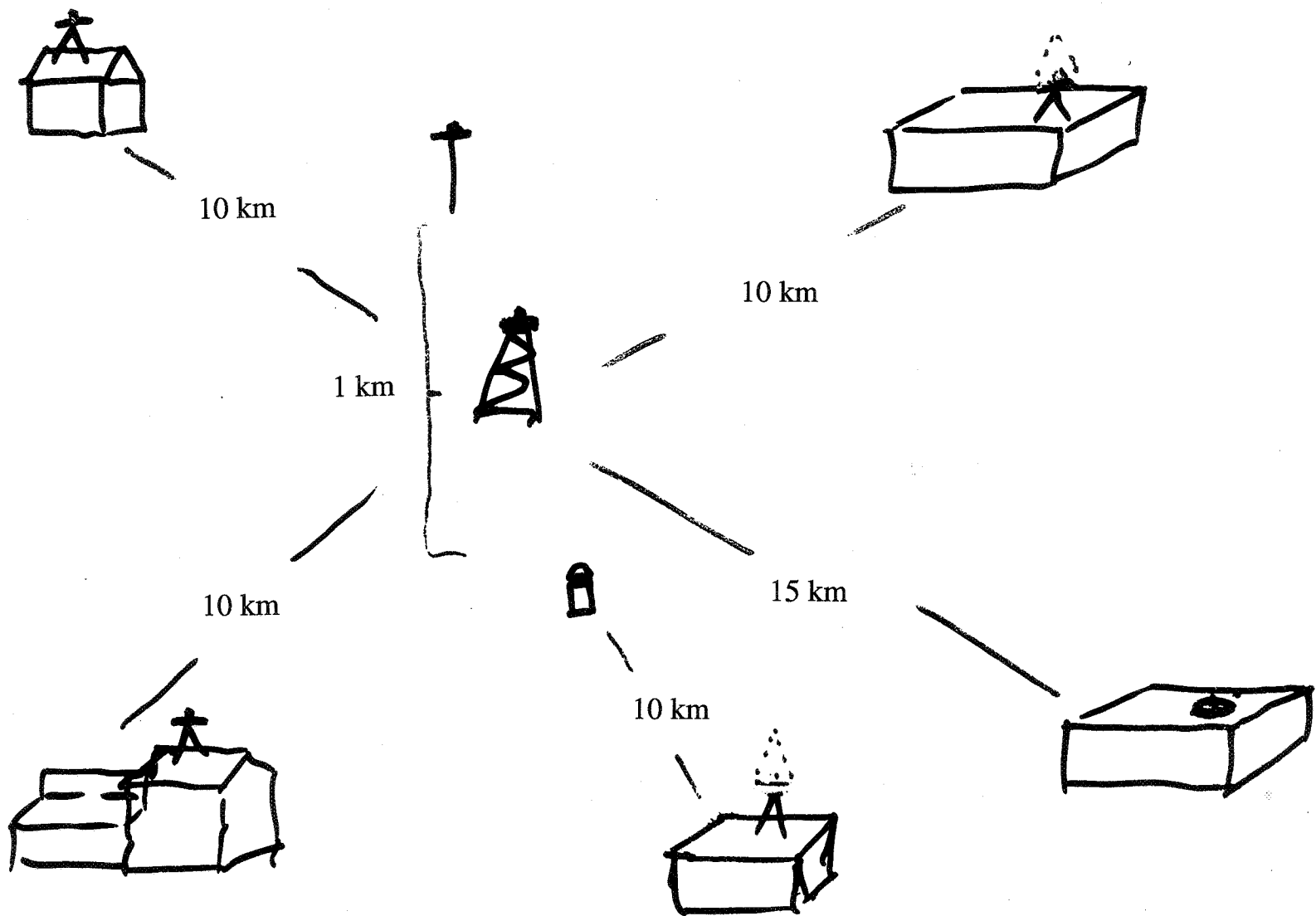
elev_min	Δh
15°	-15 ± 2 mm
5°	-5 ± 2 mm

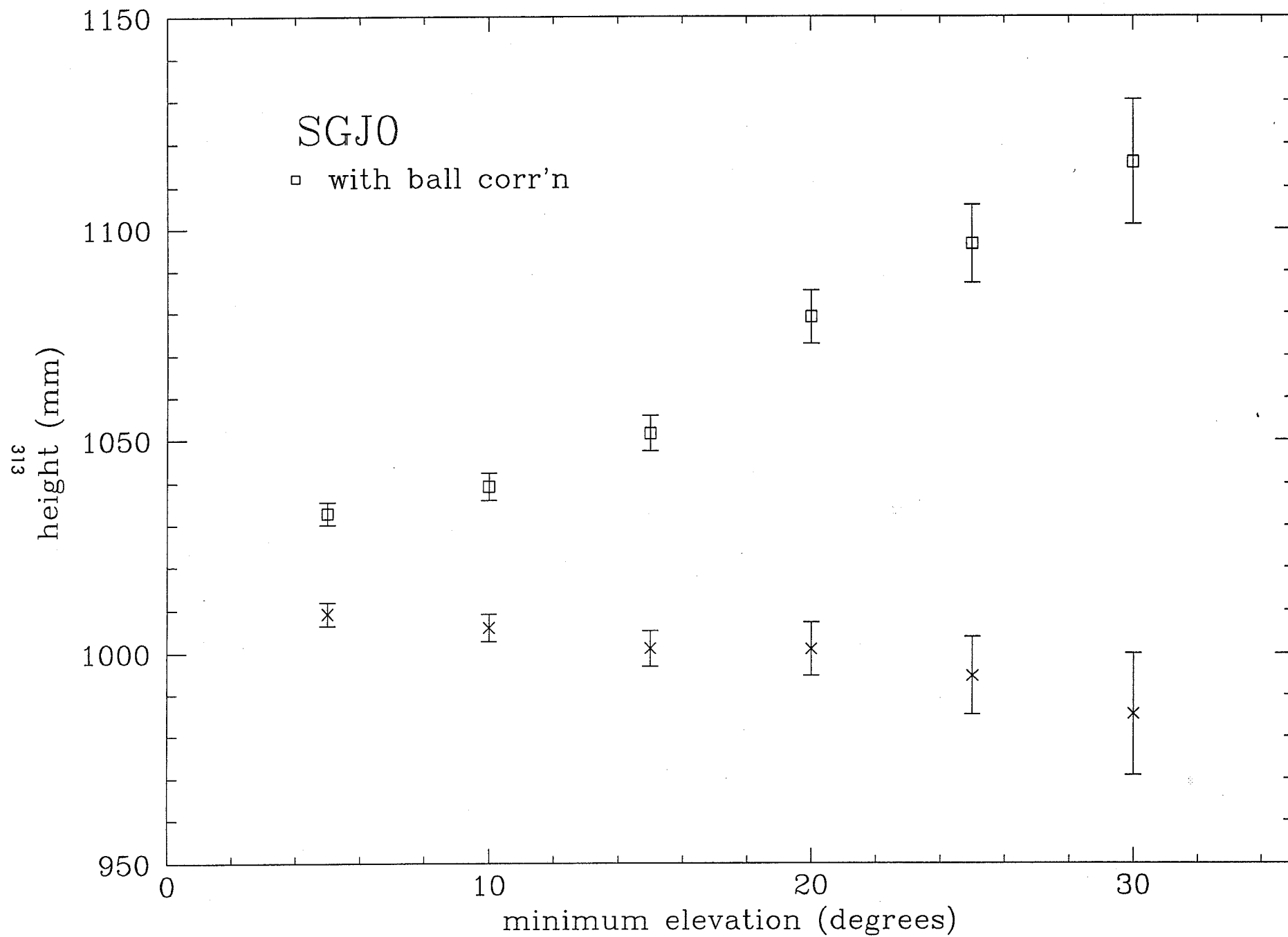
UNAVCO -10 mm

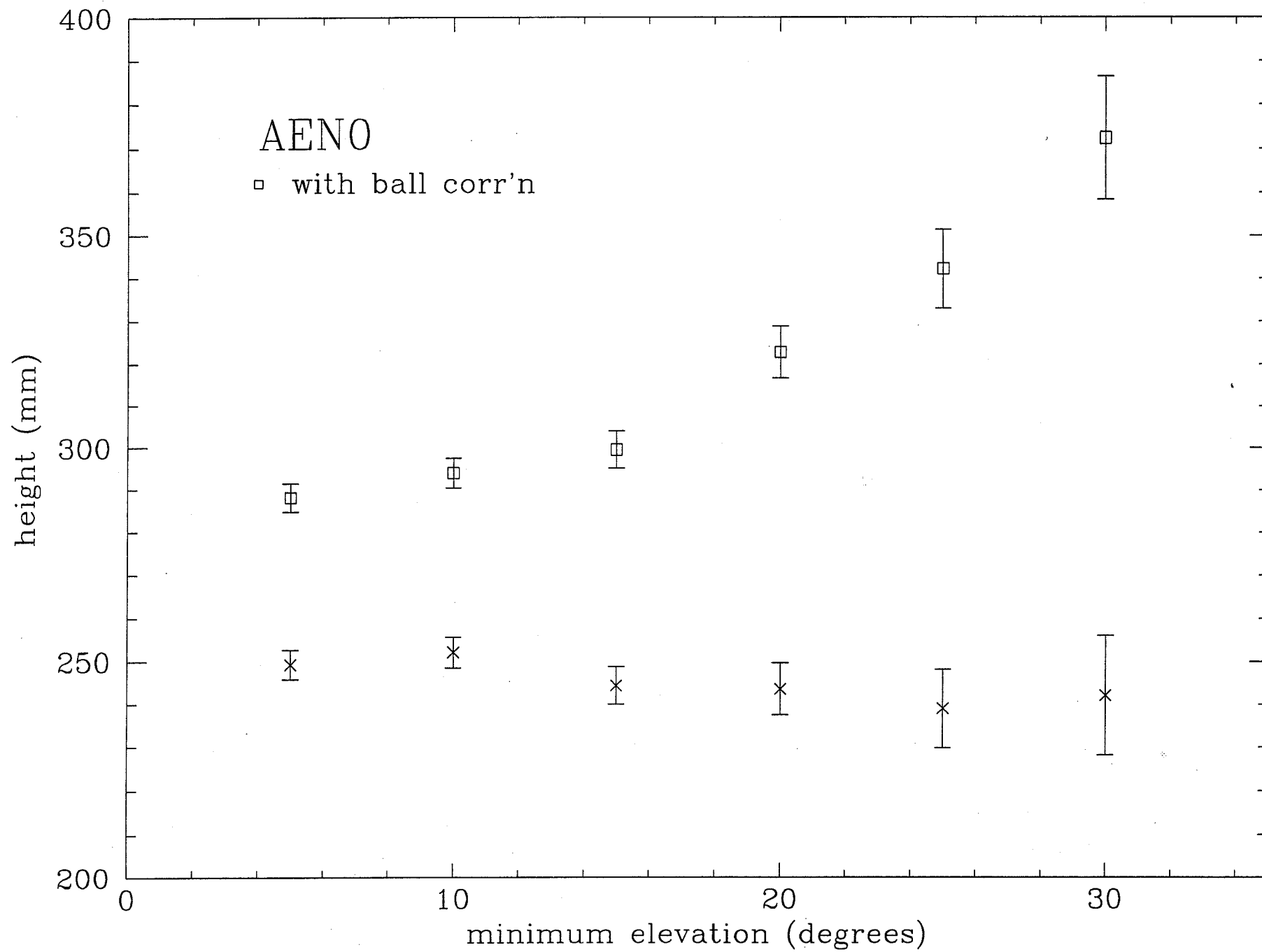
Don't use radomes without testing effect

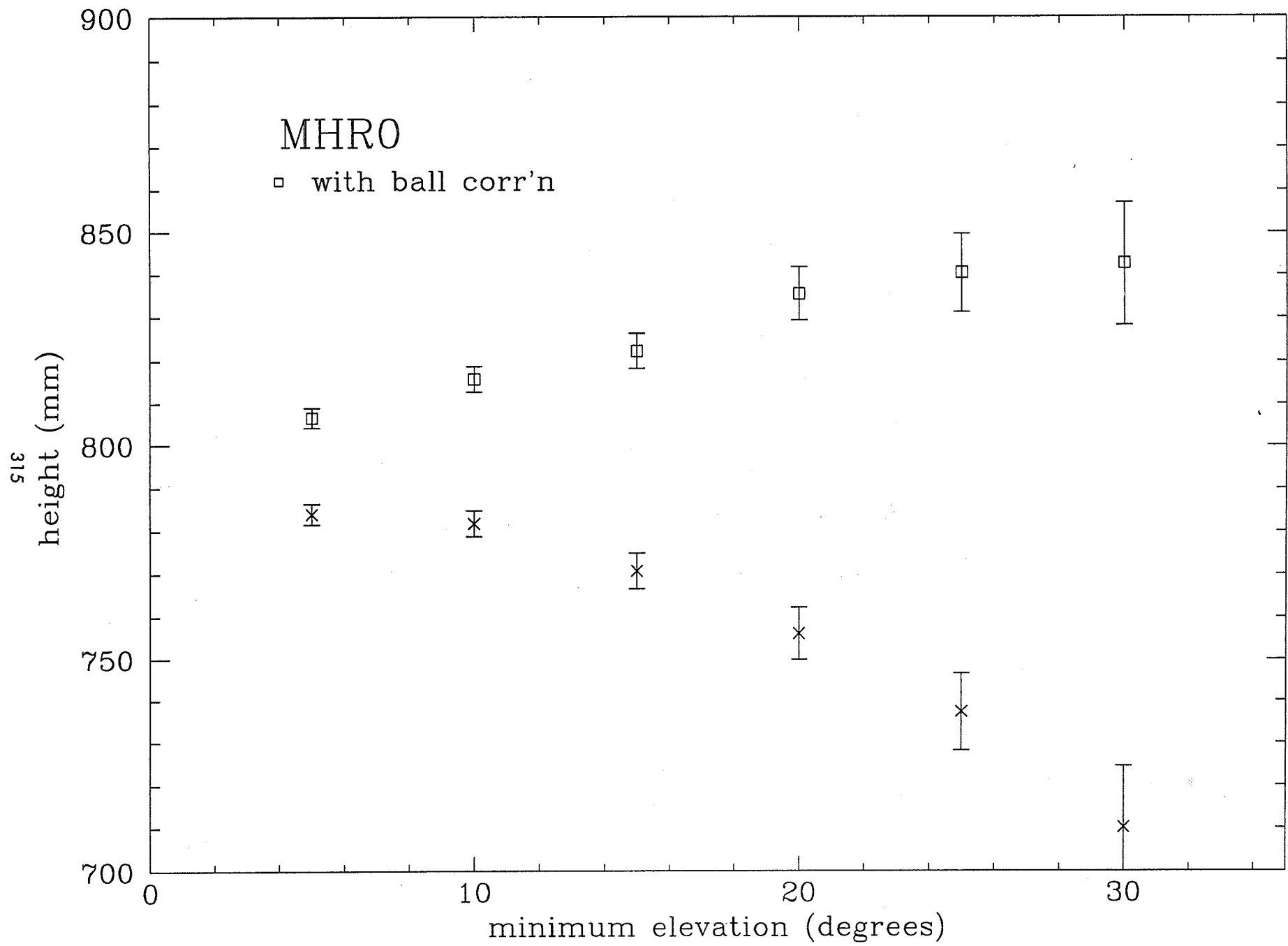
A. E. Niell
NRC Workshop
96/03/11

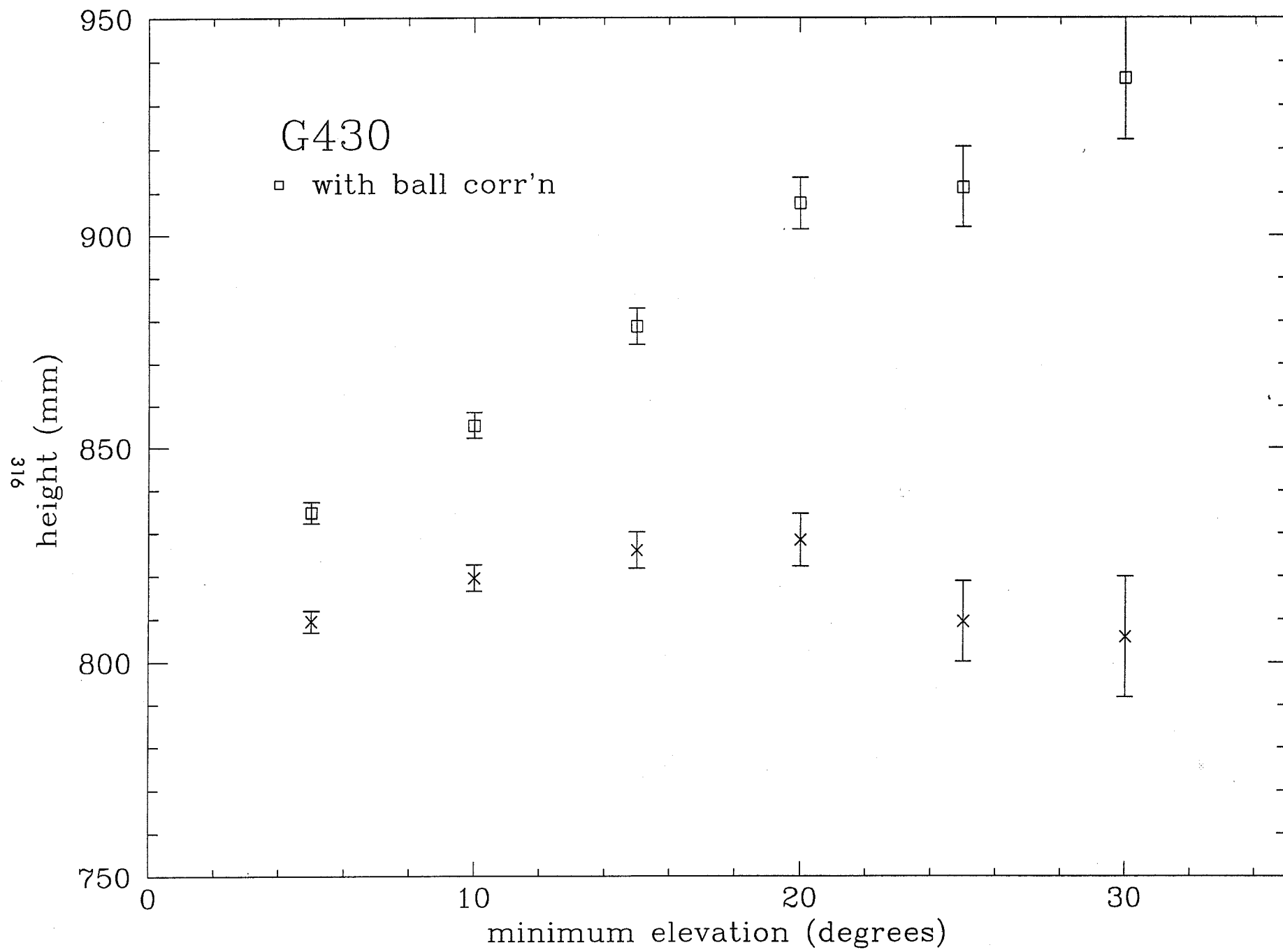
AOA TR (AOA)
Ashtech Z12 (ASH)

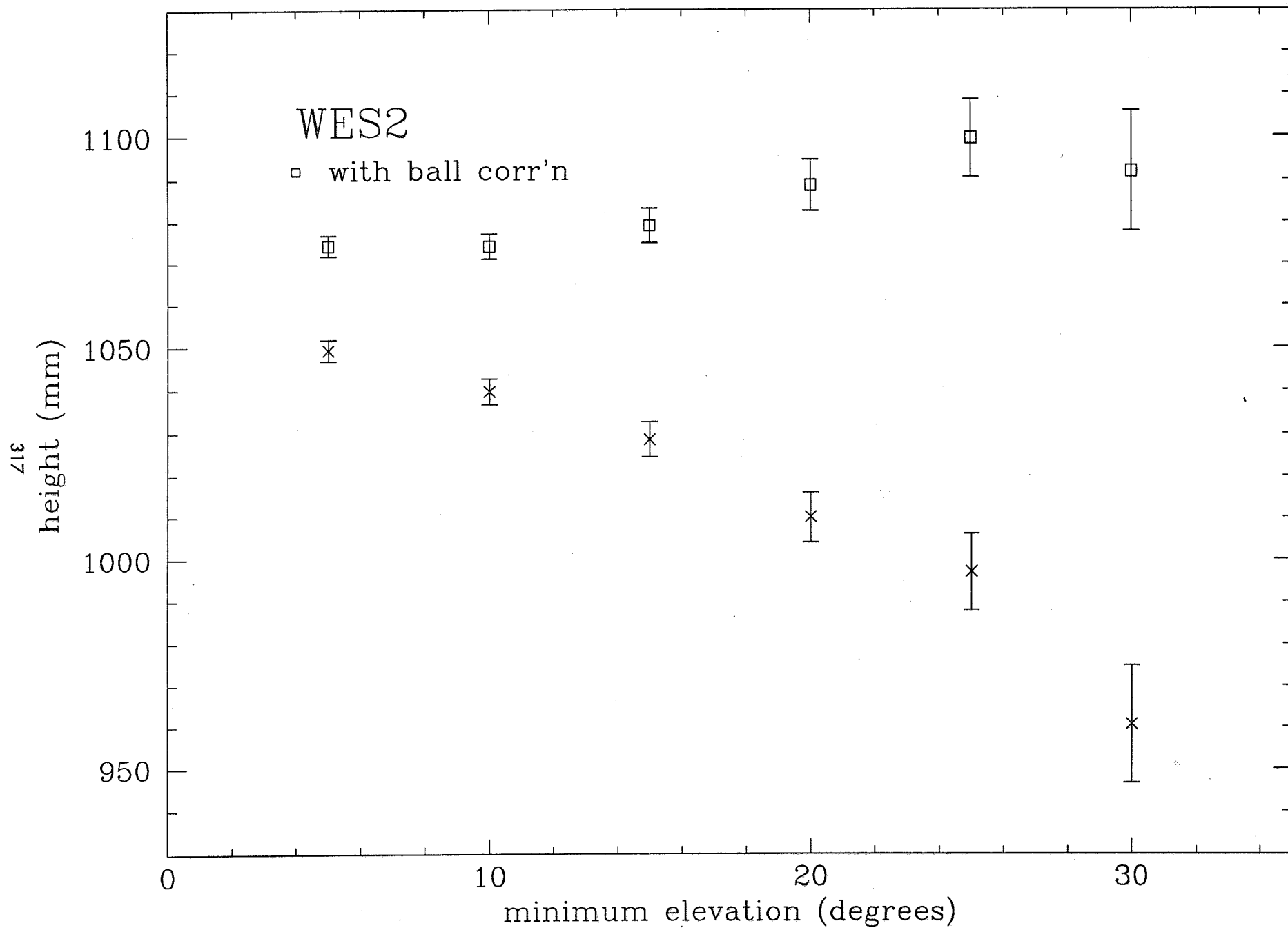


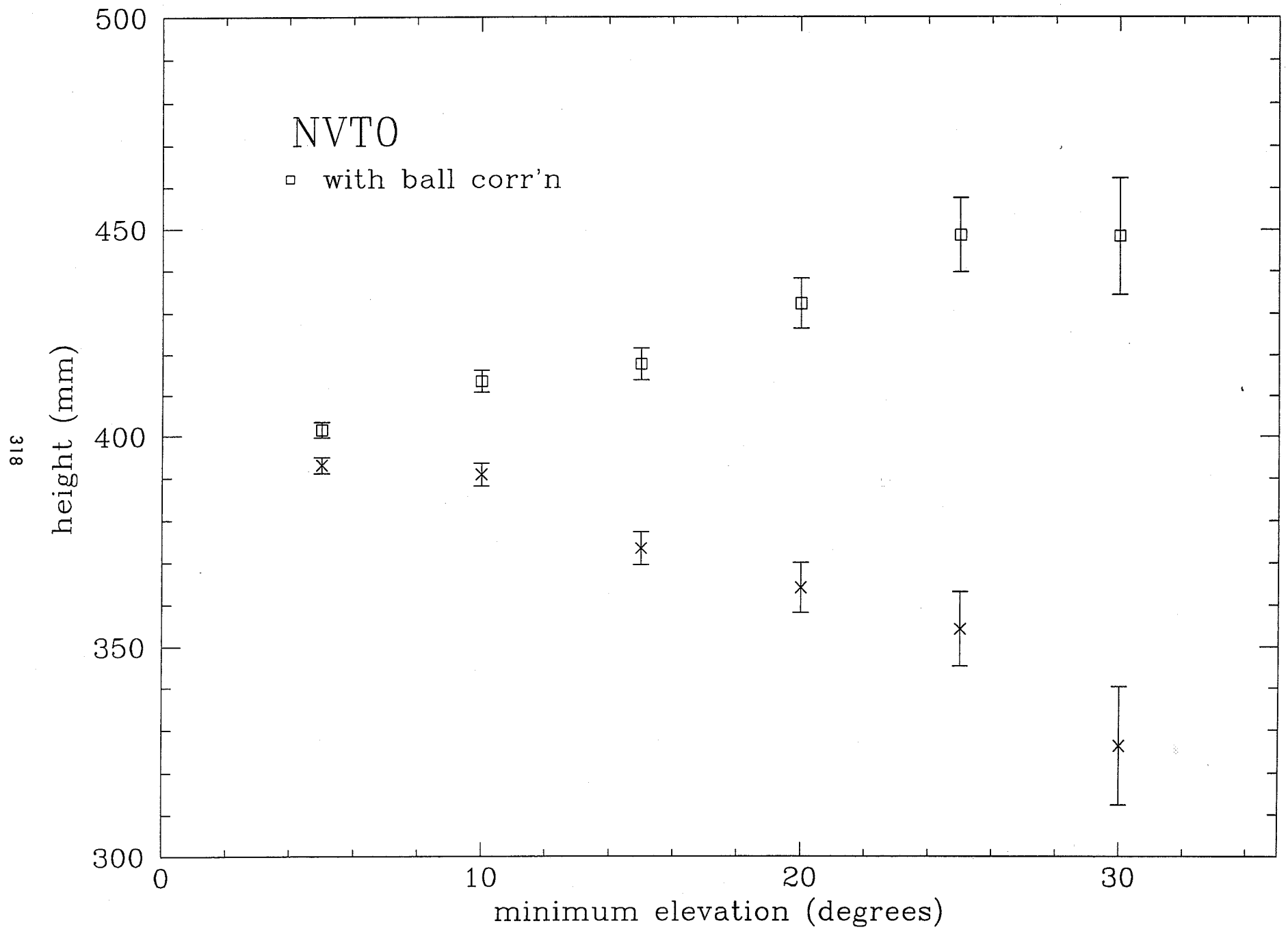


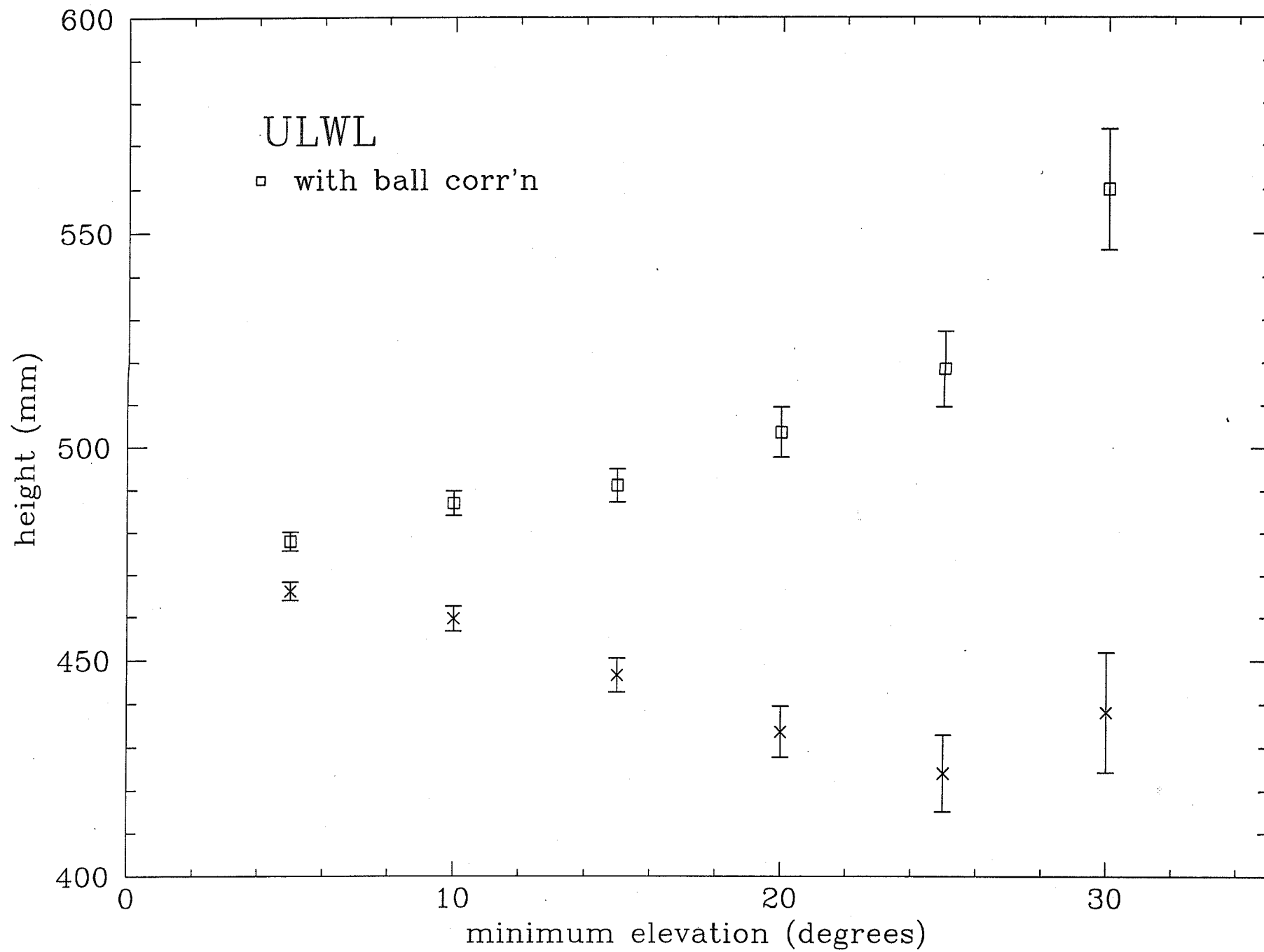












RECOMMENDATIONS

- 1) For choke ring antennas do NOT apply any correction**
- 2) At all sites compare height difference to levelling to 2 near-by (5m) antennas (as function of elevation)**

ANTENNA PHASE CENTER OFFSETS AND VARIATIONS ESTIMATED FROM GPS DATA

M. Rothacher, S. Schär

Astronomical Institute
University of Berne
Switzerland

IGS ANALYSIS CENTER WORKSHOP

in
Silver Springs , USA

March 19-21, 1996

Content:

1. Introduction
2. Calibration Campaigns, Processing Strategy
3. Mean Phase Center Offsets
4. Elevation- and Azimuth-Dependent Variations
5. Conclusions/Recommendations

Introduction

- **Two types of biases:**

- Combination of *different antenna* types
→ main effect in height (up to 10 cm).
Relative calibration possible with GPS data from very short, known baselines.
- On long baselines for the *same antenna* type
→ main effect in baseline length (up to 0.01 ppm).
Absolute calibration only possible with chamber measurements.

- **Impact on the IGS:**

- Densification of the IGS network using different receiver/antenna types.
- Antenna changes at the IGS sites.
- Systematic biases in results when changing the elevation cut-off angle (e.g. for AS data).

Antenna Calibration Campaigns

Thun'94:

- 2 24-hour sessions
- Antennas switched between sessions
- Organized by the *Federal Office of Topography*, Switzerland

Wetzell'95-1:

- 4 24-hour sessions
- Antennas switched and rotated by 180 degrees between sessions
- Organized by the *Institute for Applied Geodesy*, Germany

Antenna (Receiver)	Thun'94	Wett'95	B
ROGUE DORNE MARGOLIN T	1	3	x
ROGUE DORNE MARGOLIN B	---	1	
4000ST L1/L2 GEOD (SN 14532)	2	2	x
TR GEOD L1/L2 (SN 22020, w+w/o GP)	2	2	x
SR299E EXTERNAL (w+w/o GP)	2	---	
SR299 INTERNAL	---	2	
ASHTECH GEOD L1/L2 P (SN 700228)	2	2	

Estimation Strategy

The Bernese GPS Software was modified to:

- Estimate antenna phase center *offsets*.
- Estimate *elevation- and azimuth-dependent* phase center variations.
- Allow for different antenna *orientations*.

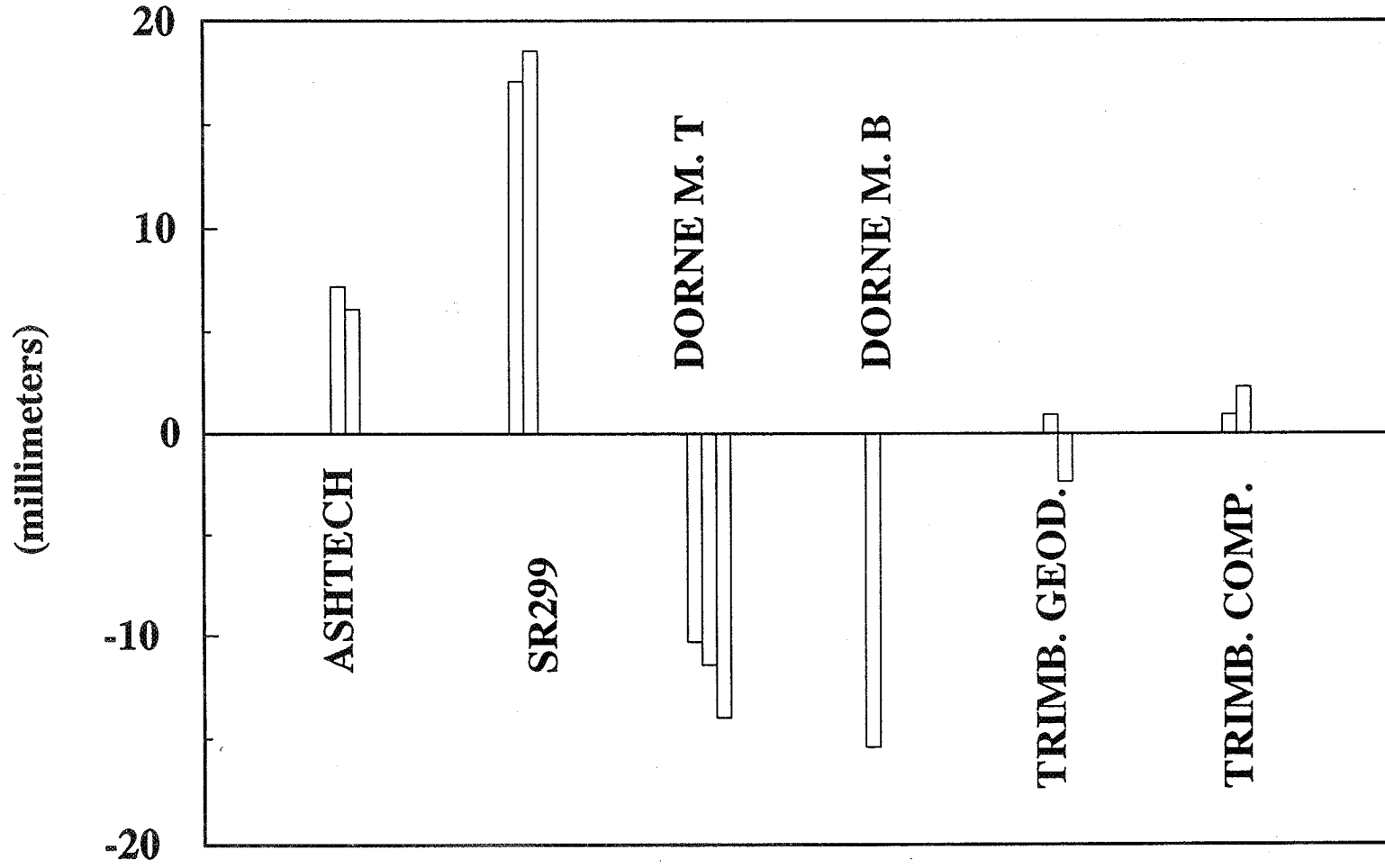
Estimation of Mean Phase Center Offsets:

- Mean phase centers depend on the elevation cut-off angle. We used a cut-off of 20 degrees.
- Wettzell: The horizontal antenna offsets and the horizontal site coordinates could be estimated *simultaneously* (rotation of the antennas).
- Thun: Site coordinates fixed to ground truth.

Elevation- and Azimuth-Dependent Variations:

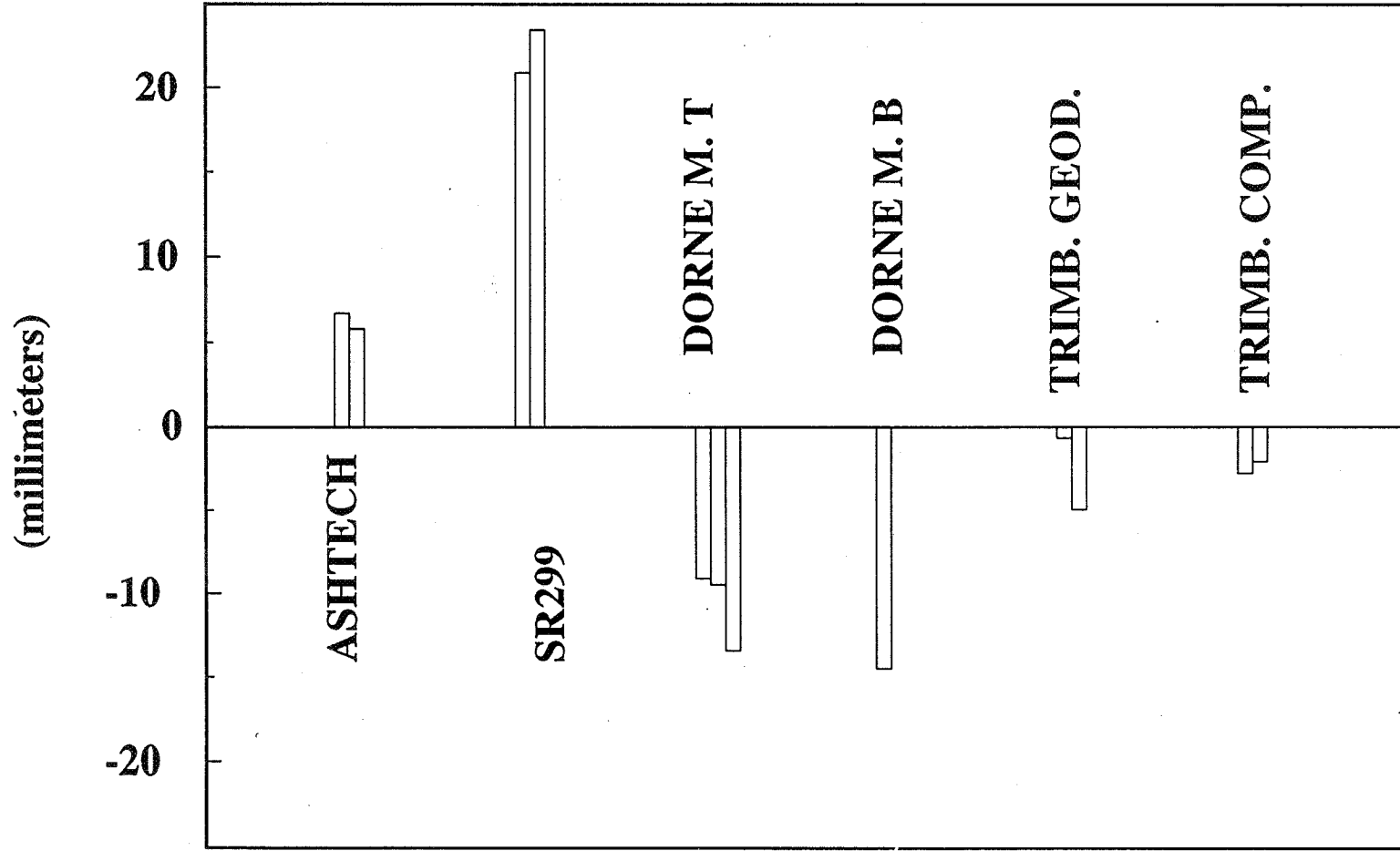
- Model: *Spherical harmonics* or a *grid*.
- Estimation of *elevation-dependent* variations: The station heights have to be known and fixed.
- Estimation of *azimuth-dependent* variations: Due to the rotation of the antennas the azimuth-dependency could be estimated together with the horizontal site coordinates.

Vertical Antenna Offsets Frequency L1



Vertical Antenna Offsets

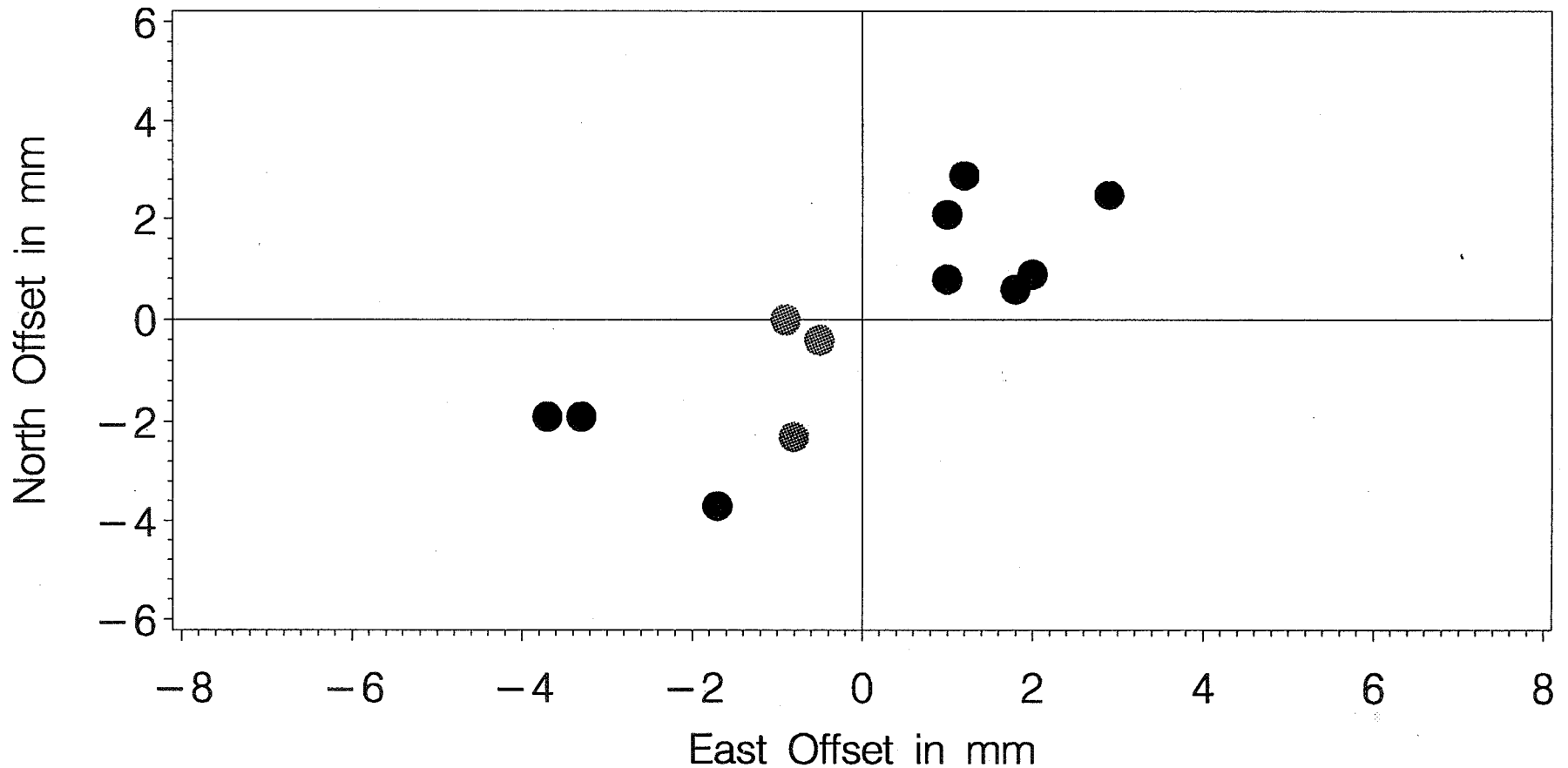
Frequency L2



"MEAN" HORIZONTAL ANTENNA PHASE CENTER OFFSETS

Thun GPS Campaign 1994

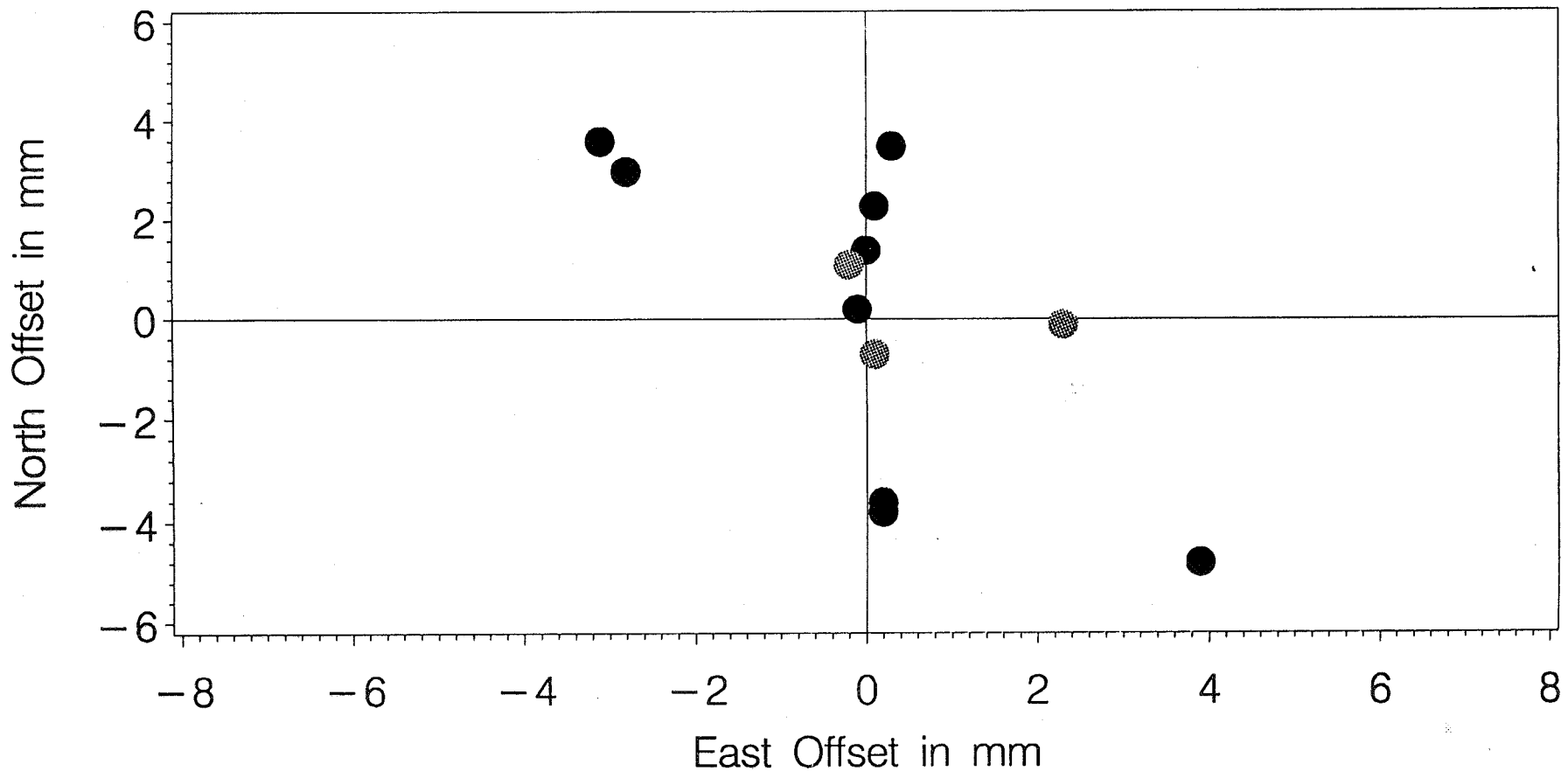
FREQ=1



"MEAN" HORIZONTAL ANTENNA PHASE CENTER OFFSETS

Thun GPS Campaign 1994

FREQ = 2



328

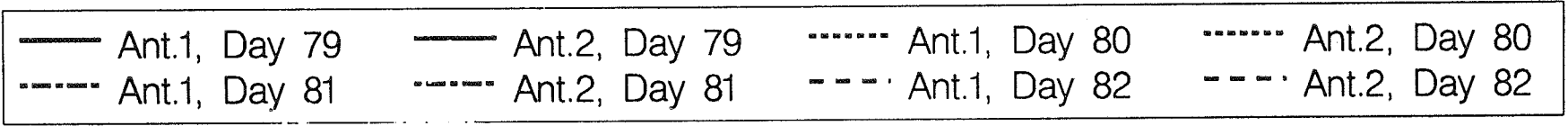
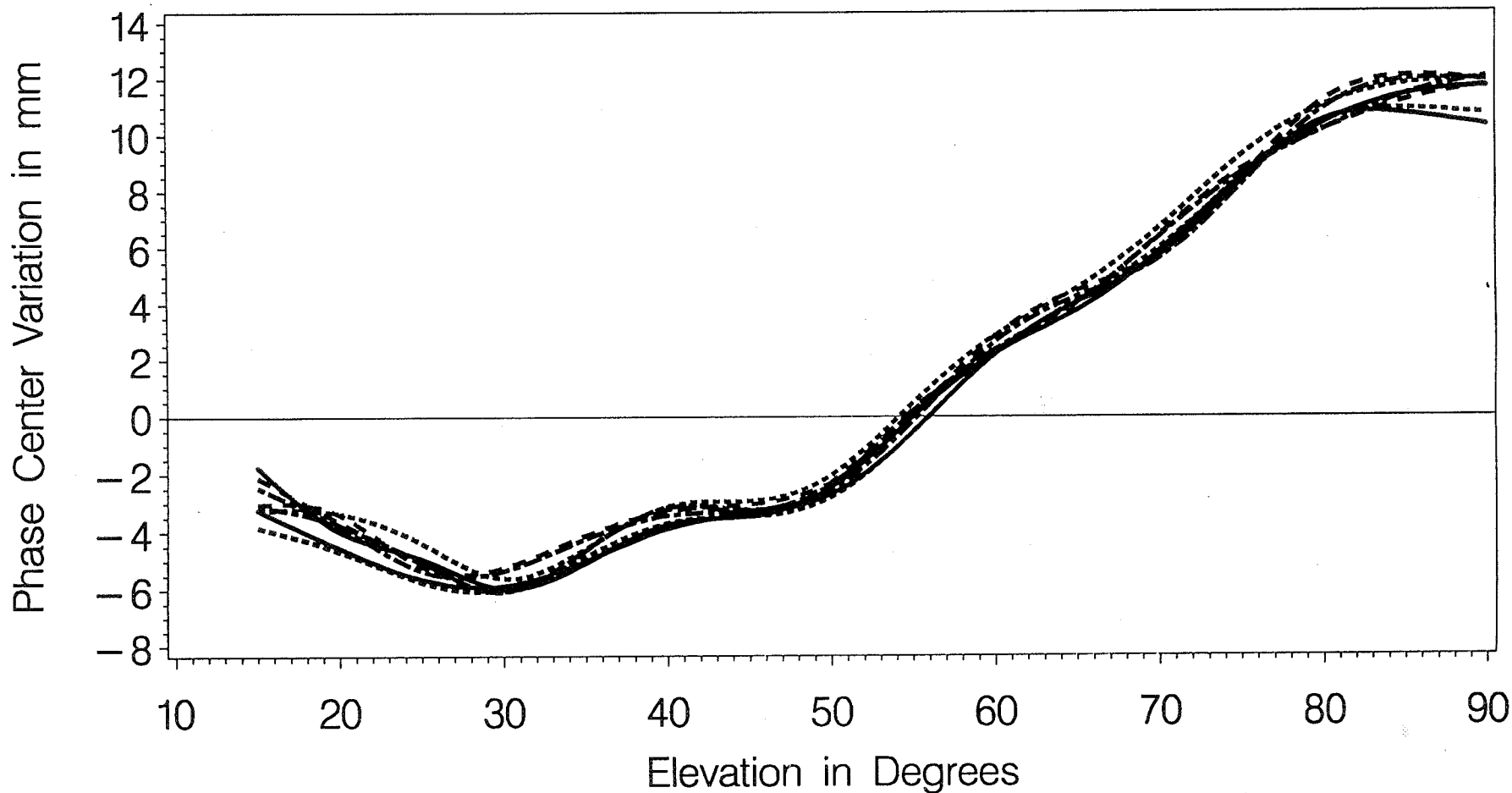
- | | | |
|-----------------|-------------------|-------------------|
| ••• Trim. Geod | ••• Trim. Comp GP | ••• Trim. Comp WO |
| ••• Ashtech | ••• SR299 Ext. GP | ••• SR299 Ext. WO |
| ••• Dorne Mar T | | |

ELEV. - DEP. PCV REPEATABILITY FOR DORNE MARGOLIN T

Reference: Dorne Margolin T; Wettzell Campaign

FREQ=1

329

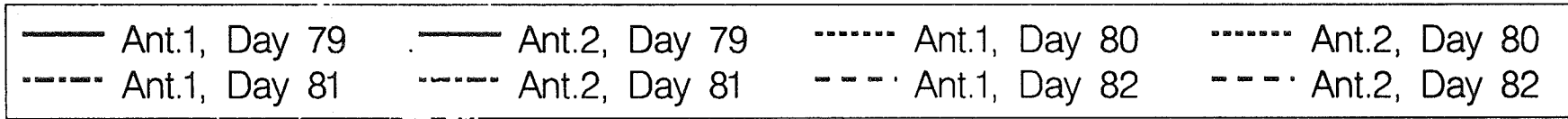
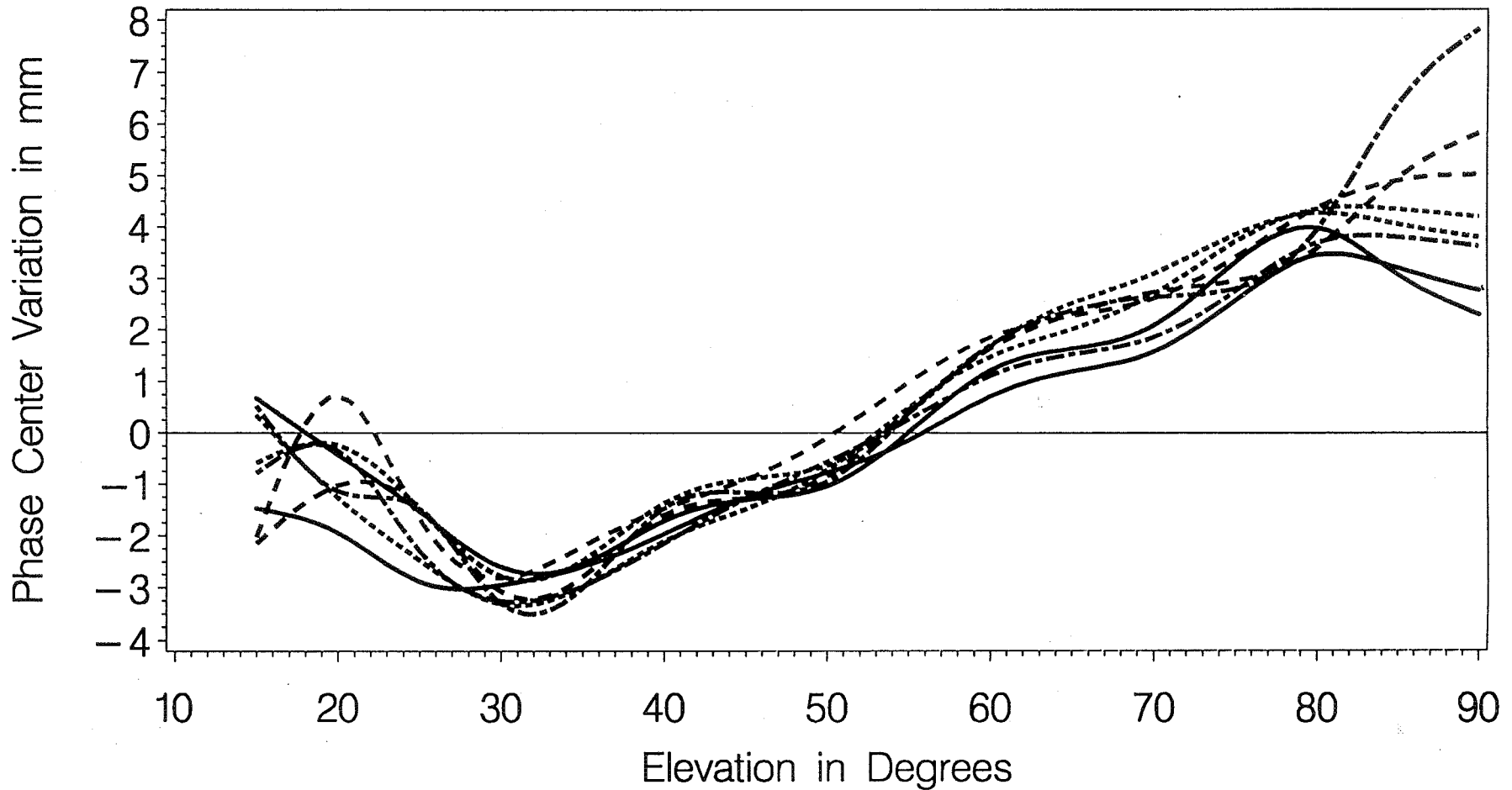


ELEV. - DEP. PCV REPEATABILITY FOR DORNE MARGOLIN T

Reference: Dorne Margolin T; Wettzell Campaign

FREQ=2

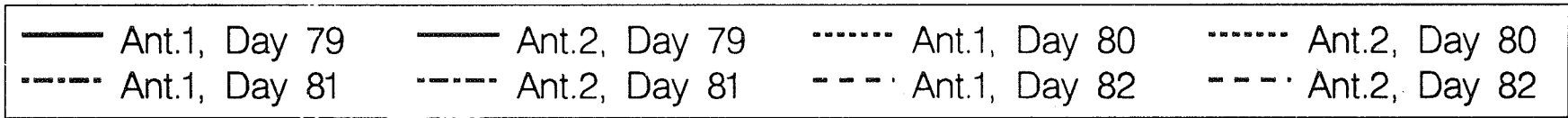
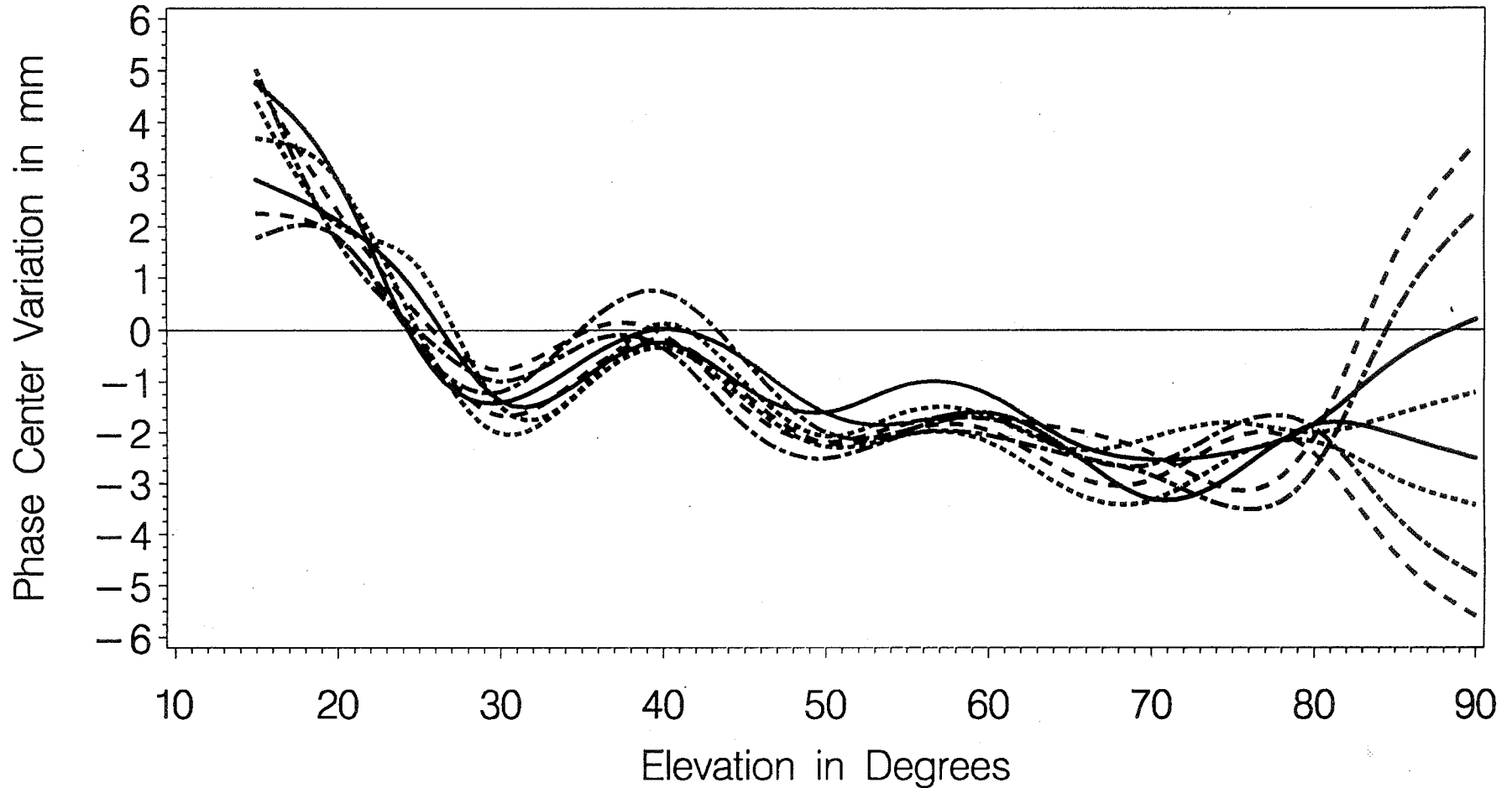
330



ELEV. - DEP. PCV REPEATABILITY FOR SR299 INTERNAL

Reference: Dorne Margolin T; Wettzell Campaign

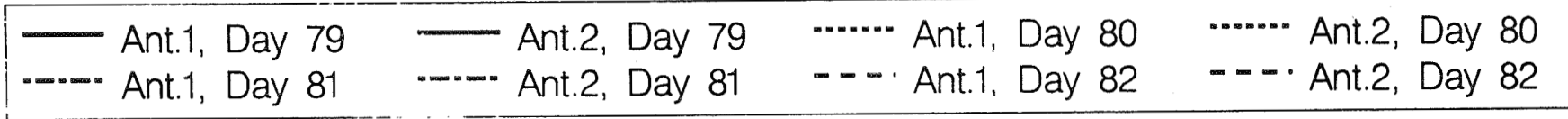
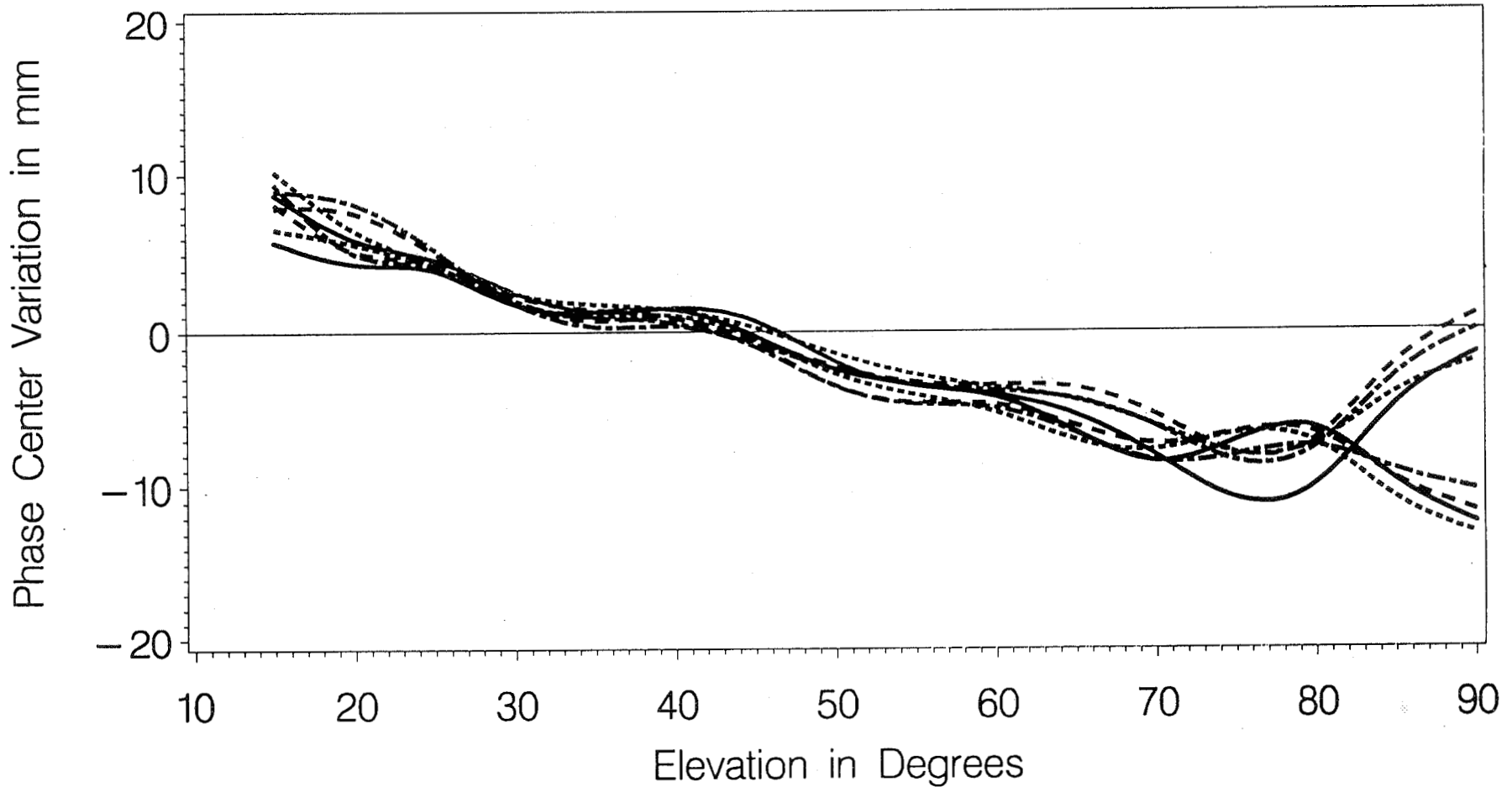
FREQ=1



ELEV. - DEP. PCV REPEATABILITY FOR SR299 INTERNAL

Reference: Dorne Margolin T; Wettzell Campaign

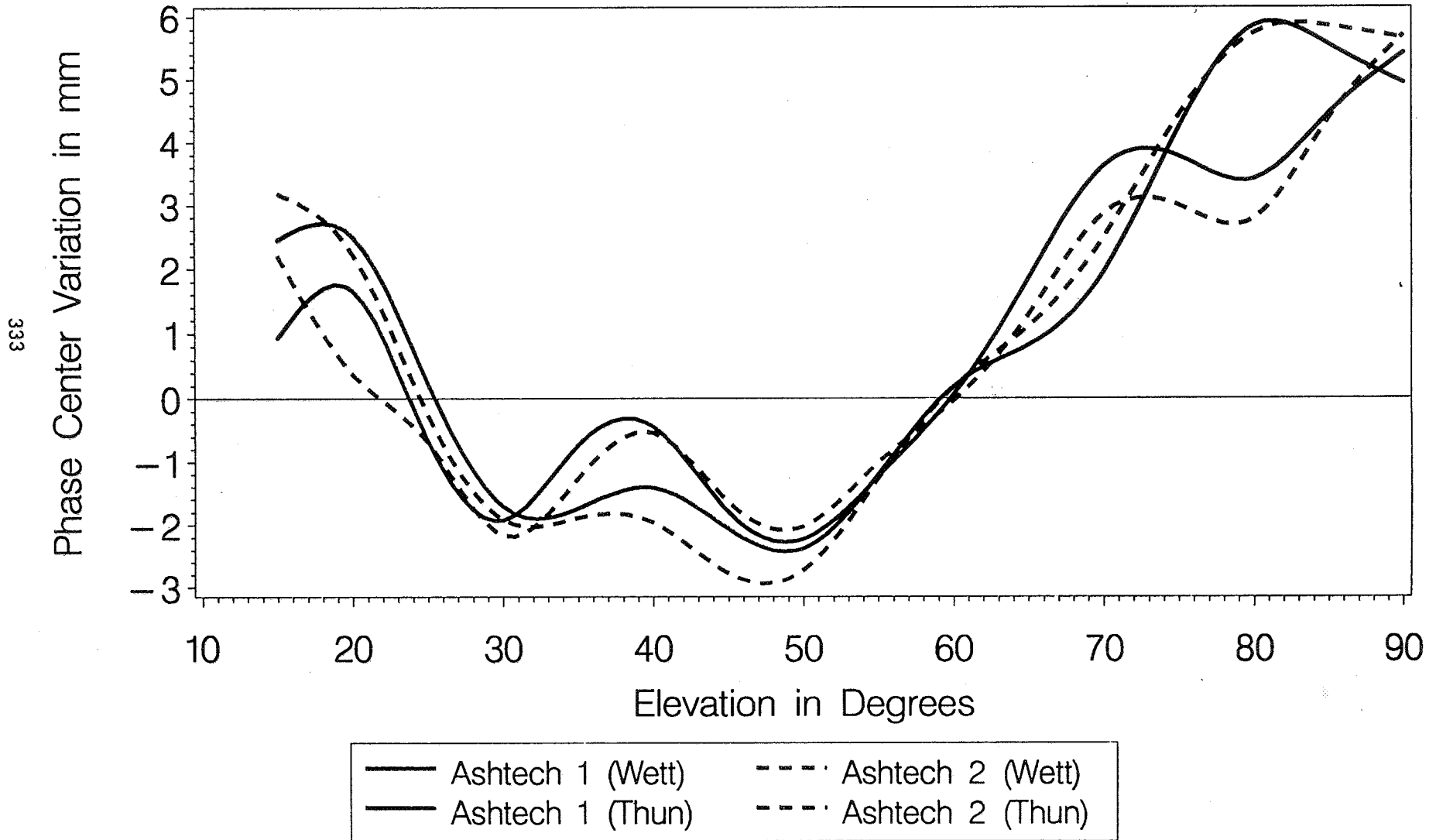
FREQ = 2



ELEV. - DEP. PHASE CENTER VARIATION FOR ASHTECH

Reference Antenna for Estimation: Dorne Margolin T

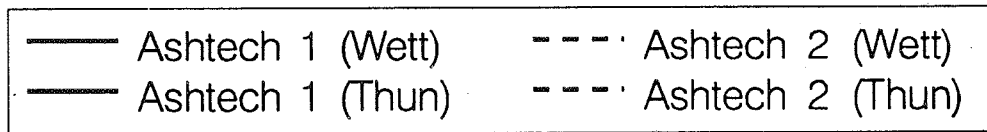
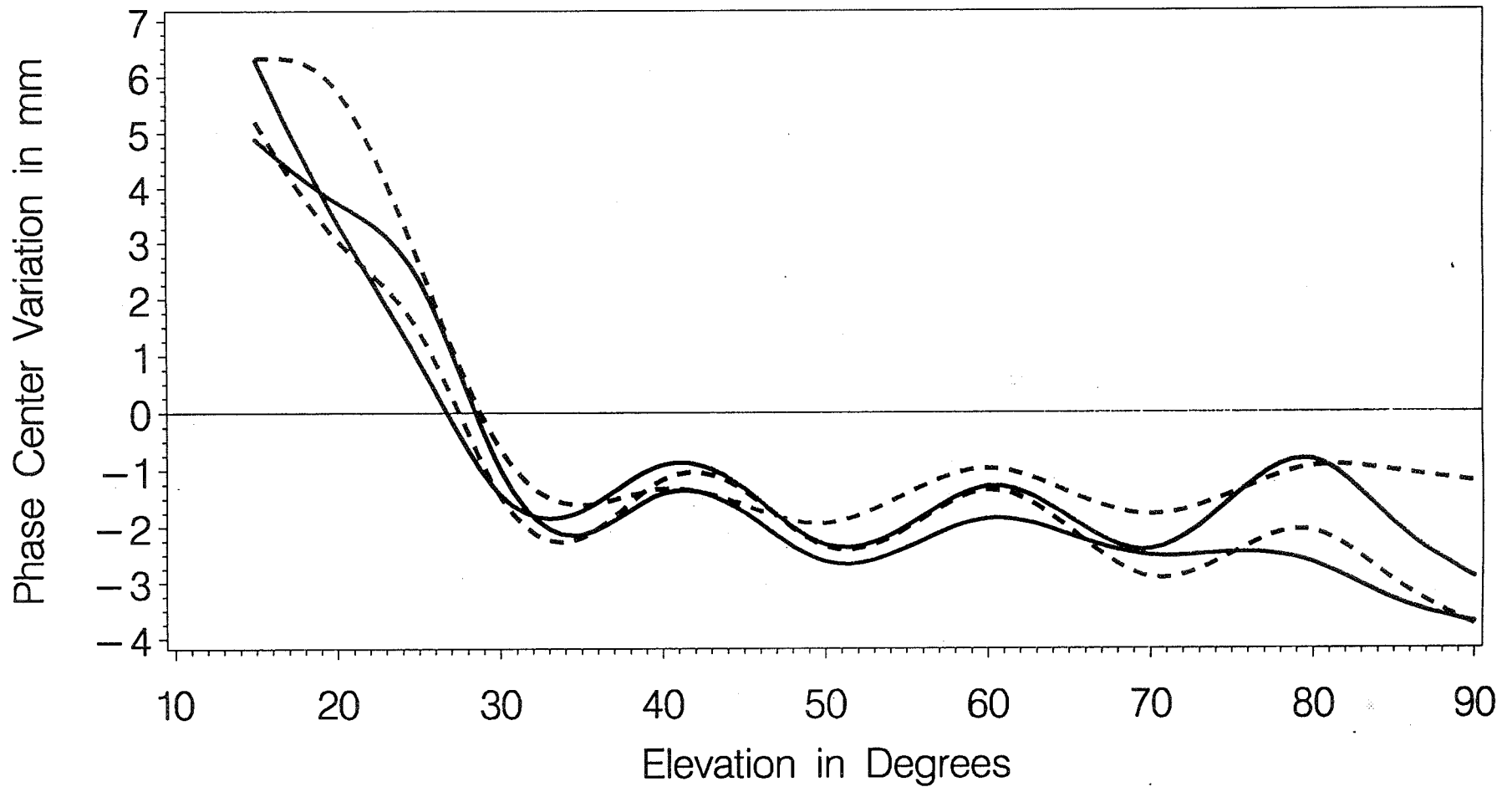
FREQ=1



ELEV. - DEP. PHASE CENTER VARIATION FOR ASHTECH

Reference Antenna for Estimation: Dorne Margolin T

FREQ = 2

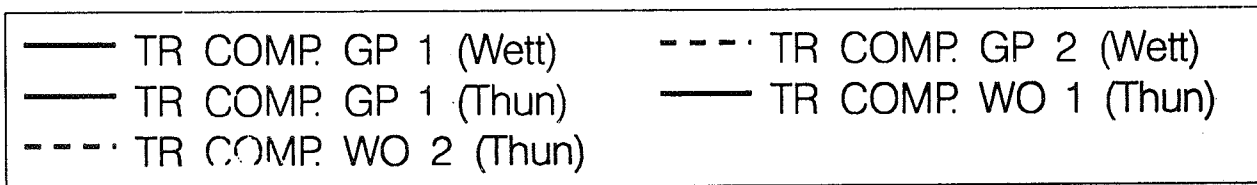
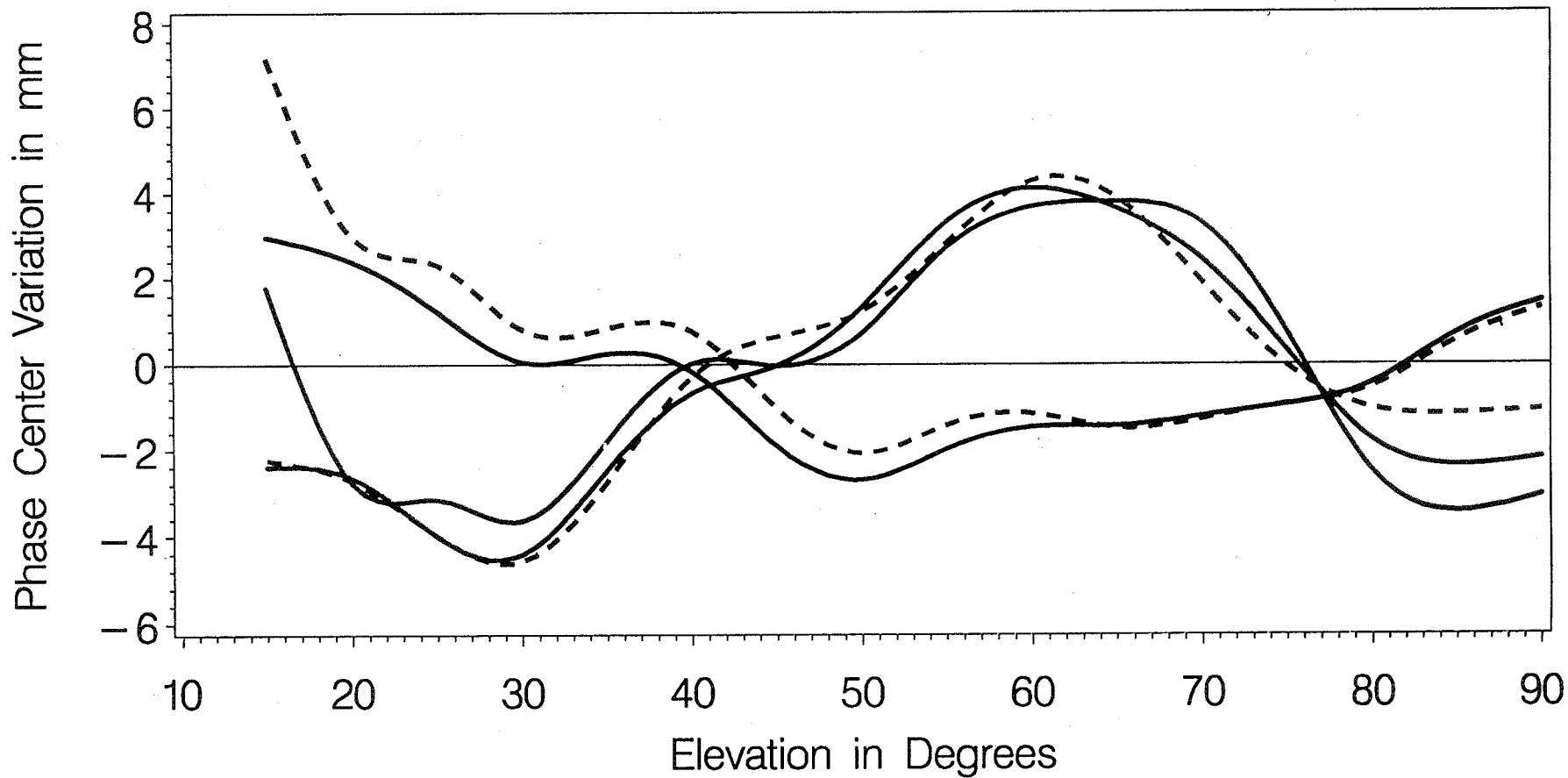


ELEV. - DEP. PHASE CENTER VARIATION FOR TRIMBLE COMPACT

Reference Antenna for Estimation: Dorne Margolin T

FREQ=1

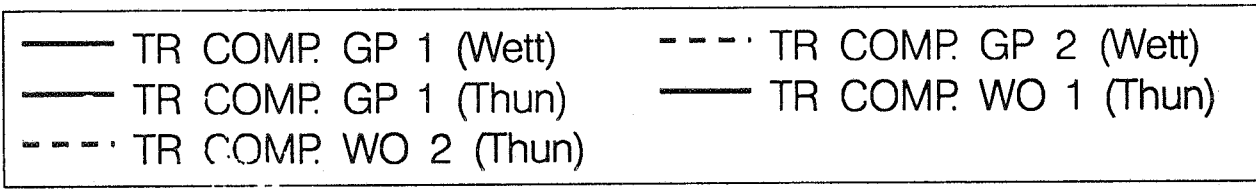
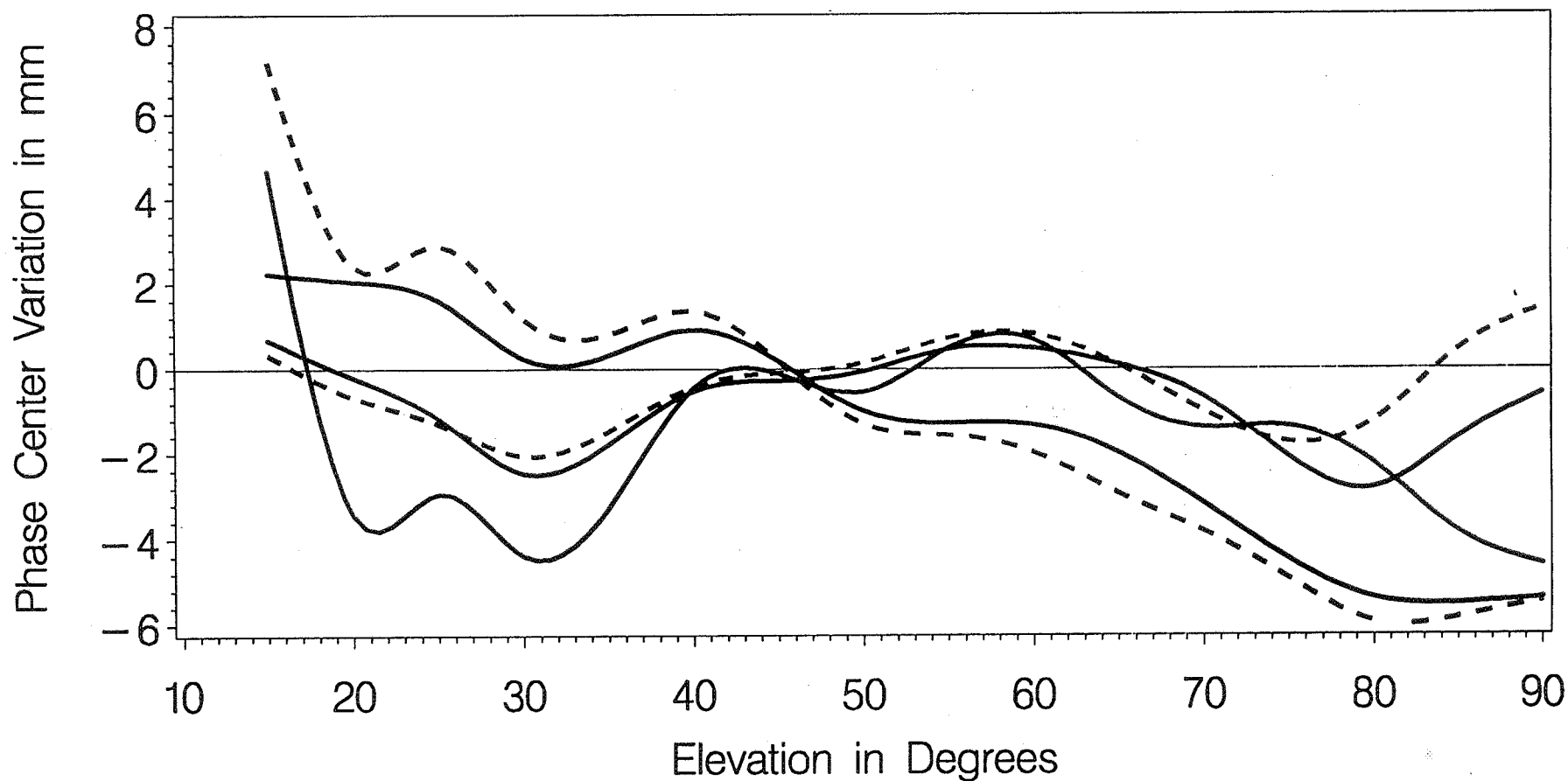
335



ELEV. - DEP. PHASE CENTER VARIATION FOR TRIMBLE COMPACT

Reference Antenna for Estimation: Dorne Margolin T

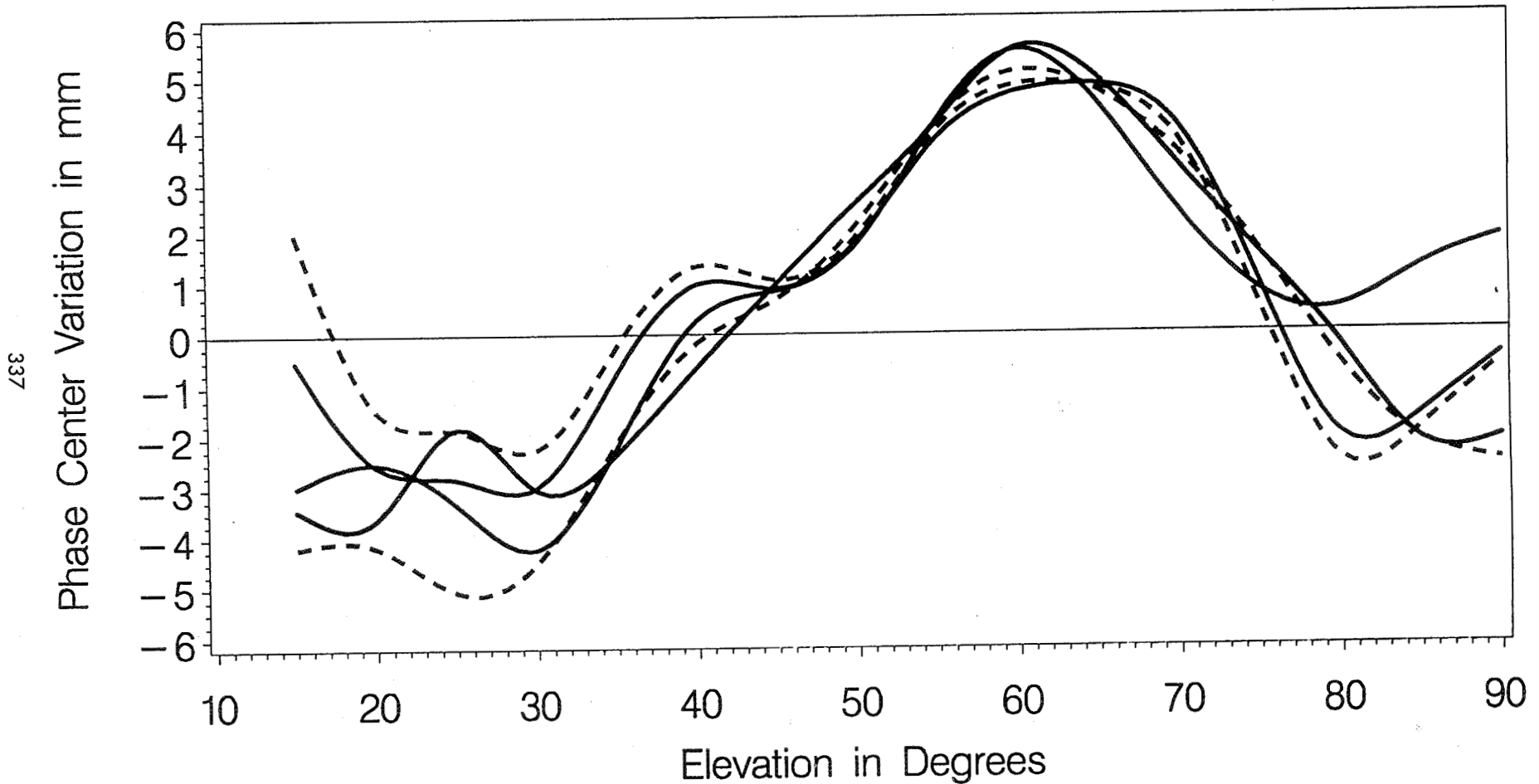
FREQ=2



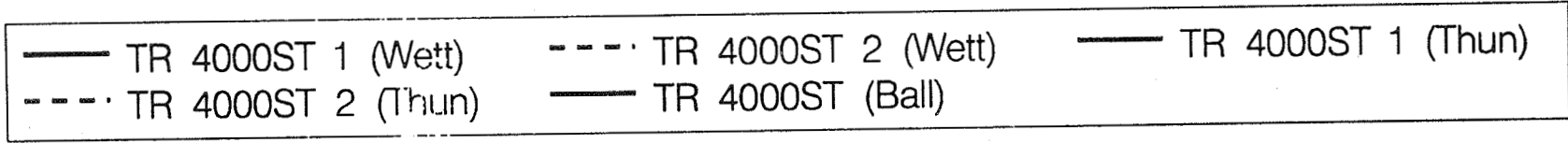
ELEV. - DEP. PCV: COMPARED TO CHAMBER RESULTS

Reference Antenna for Estimation: Dorne Margolin T

FREQ=1



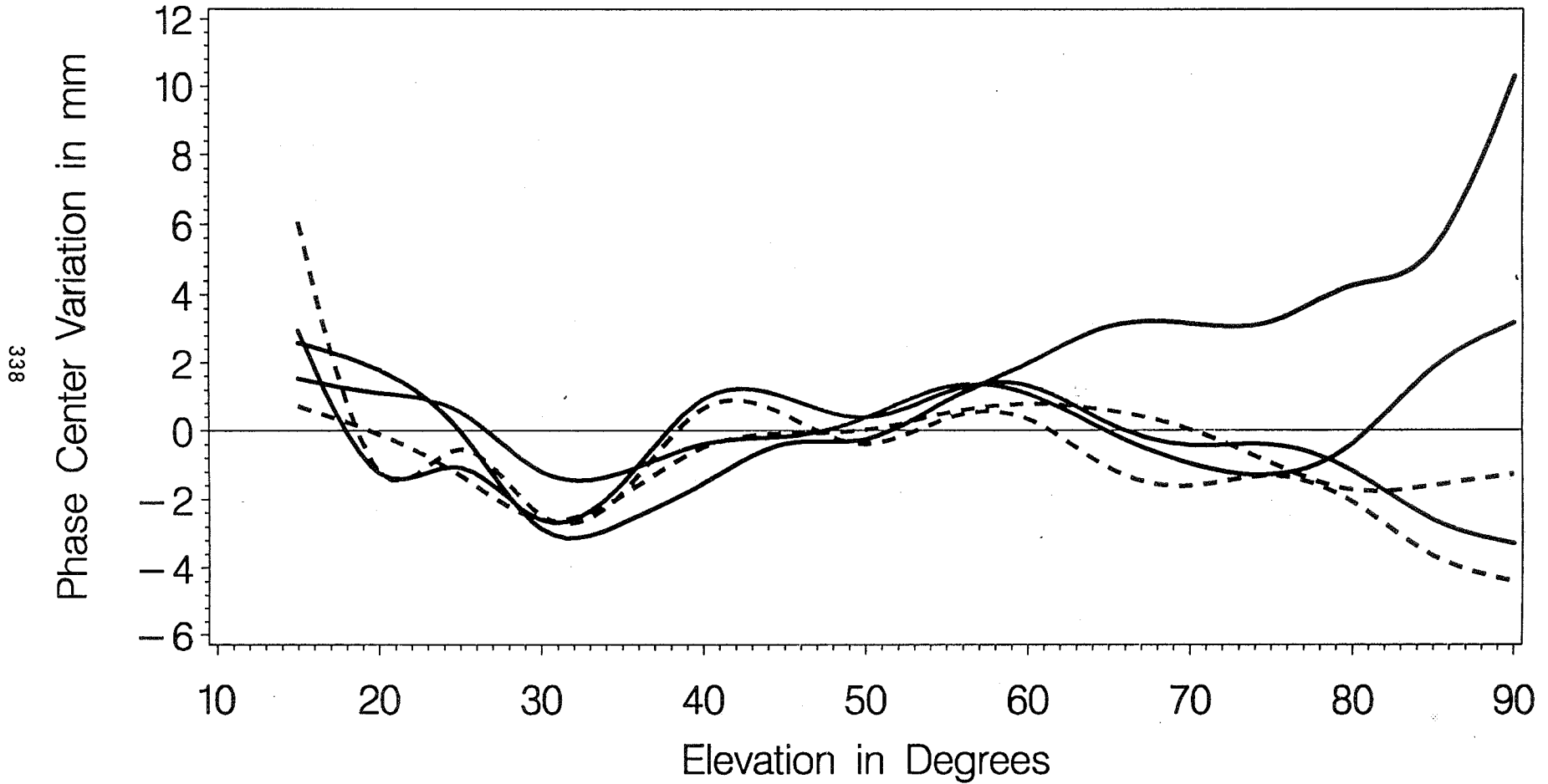
337



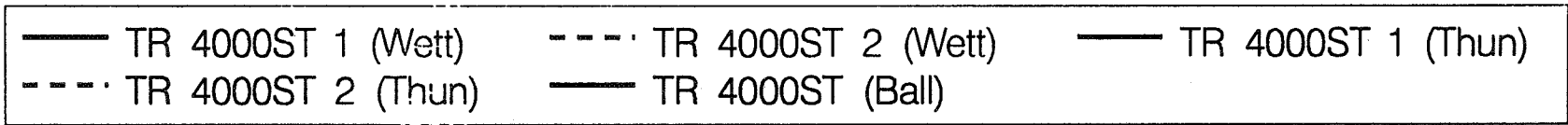
ELEV. - DEP. PCV: COMPARED TO CHAMBER RESULTS

Reference Antenna for Estimation: Dorne Margolin T

FREQ = 2



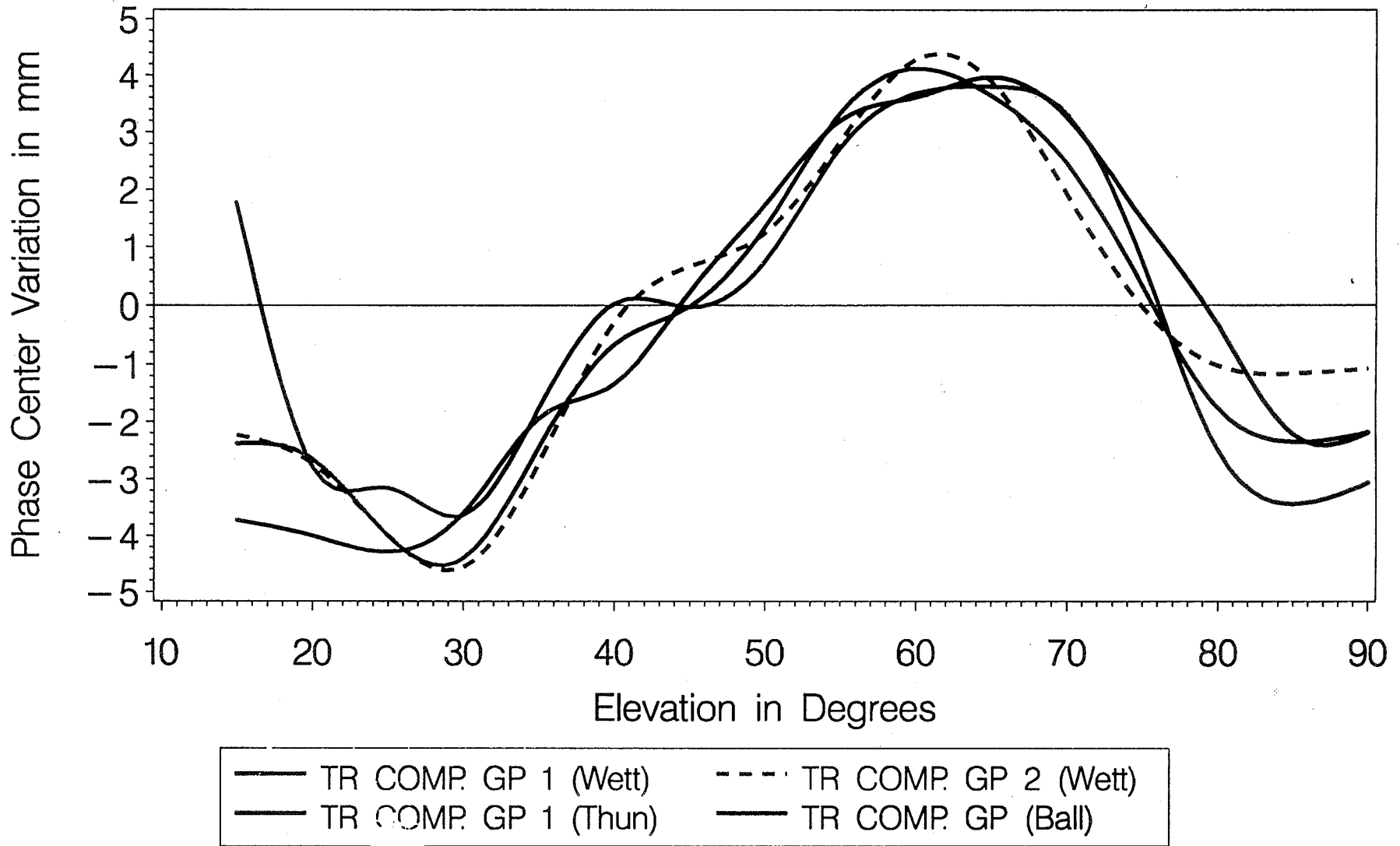
338



ELEV. – DEP. PCV: COMPARISON TO CHAMBER RESULTS

Reference Antenna for Estimation: Dorne Margolin T

FREQ=1

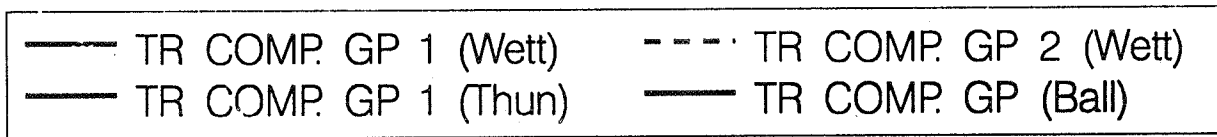
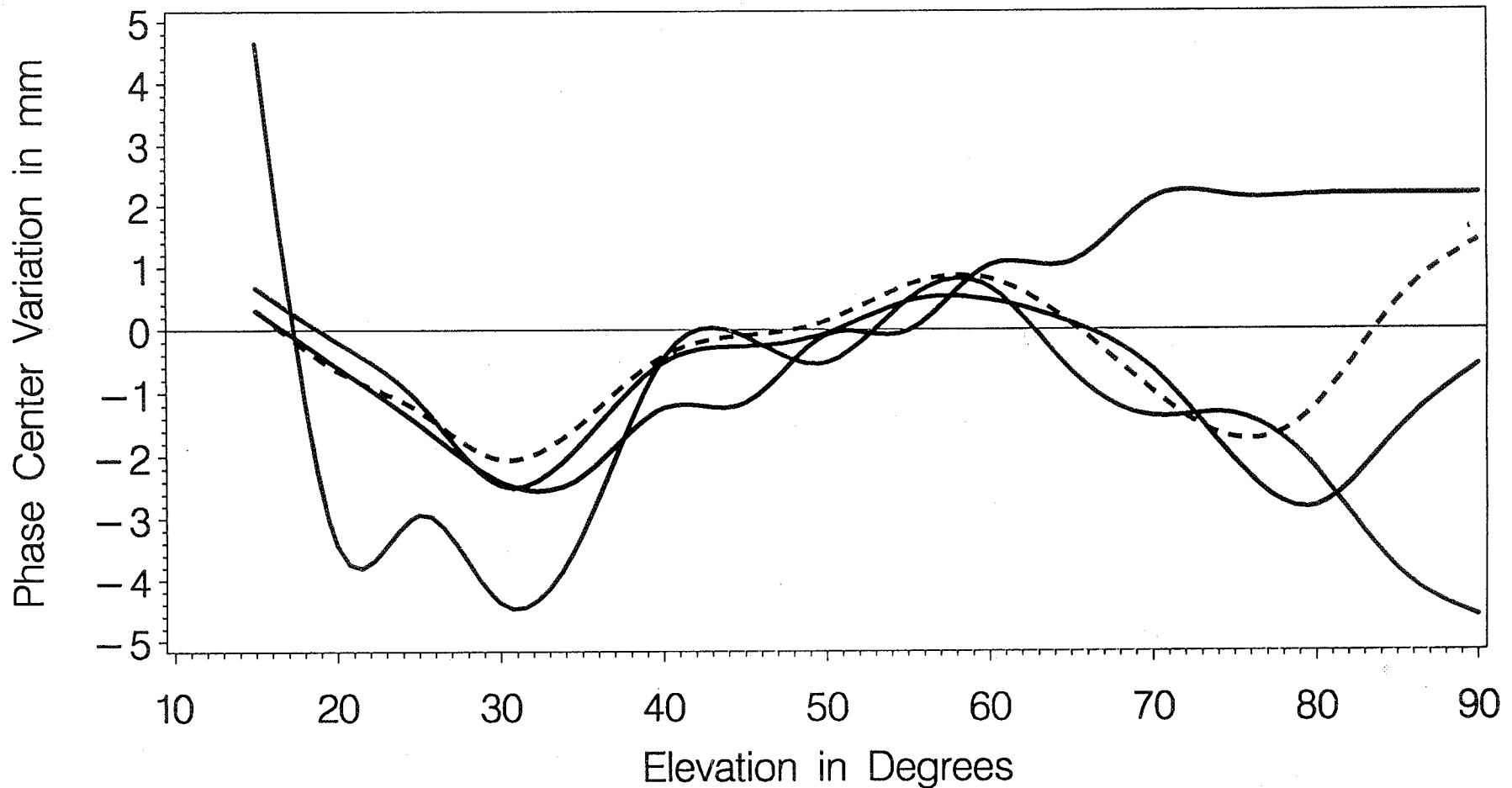


ELEV. - DEP. PCV: COMPARISON TO CHAMBER RESULTS

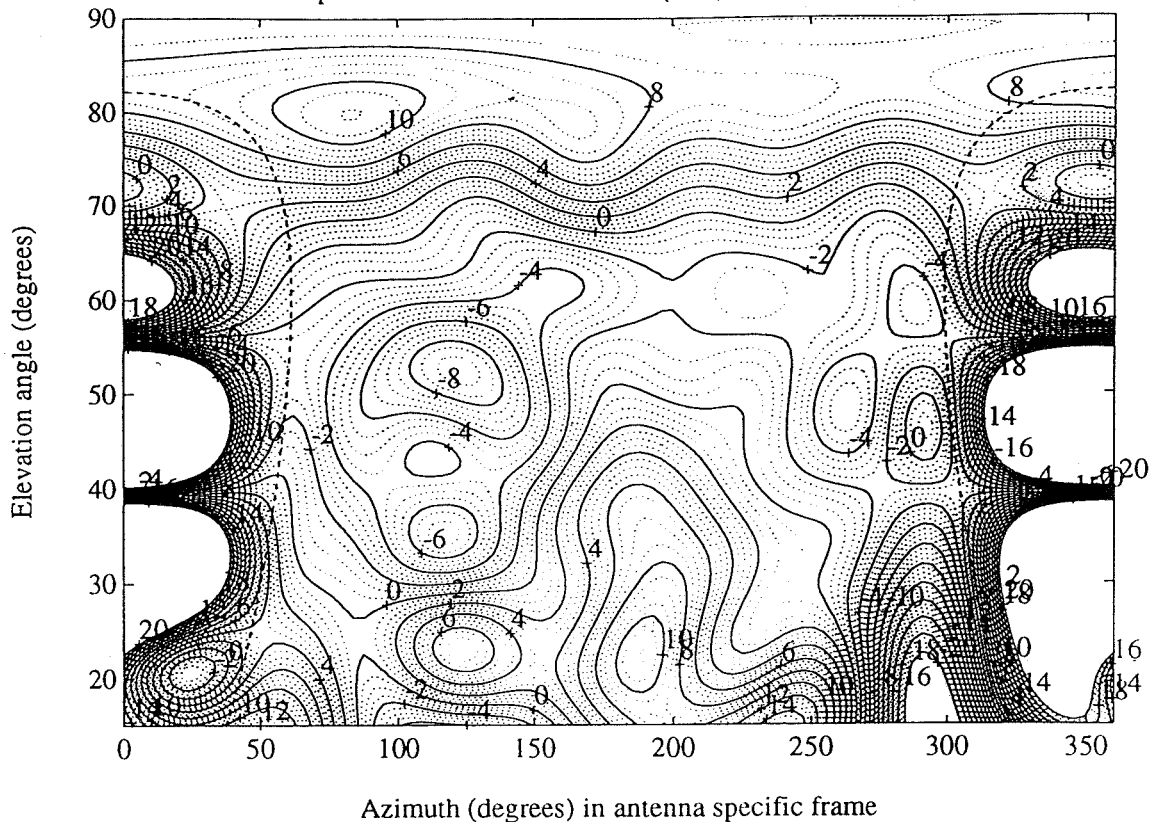
Reference Antenna for Estimation: Dorne Margolin T

FREQ=2

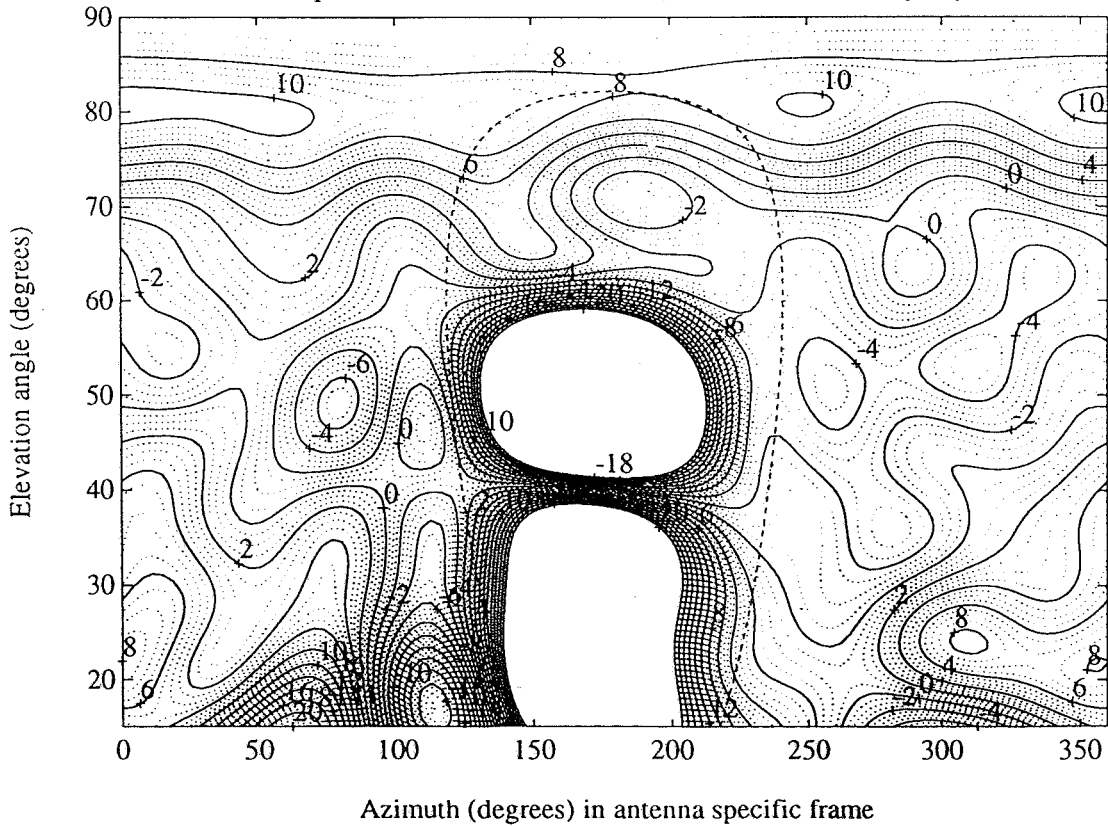
340



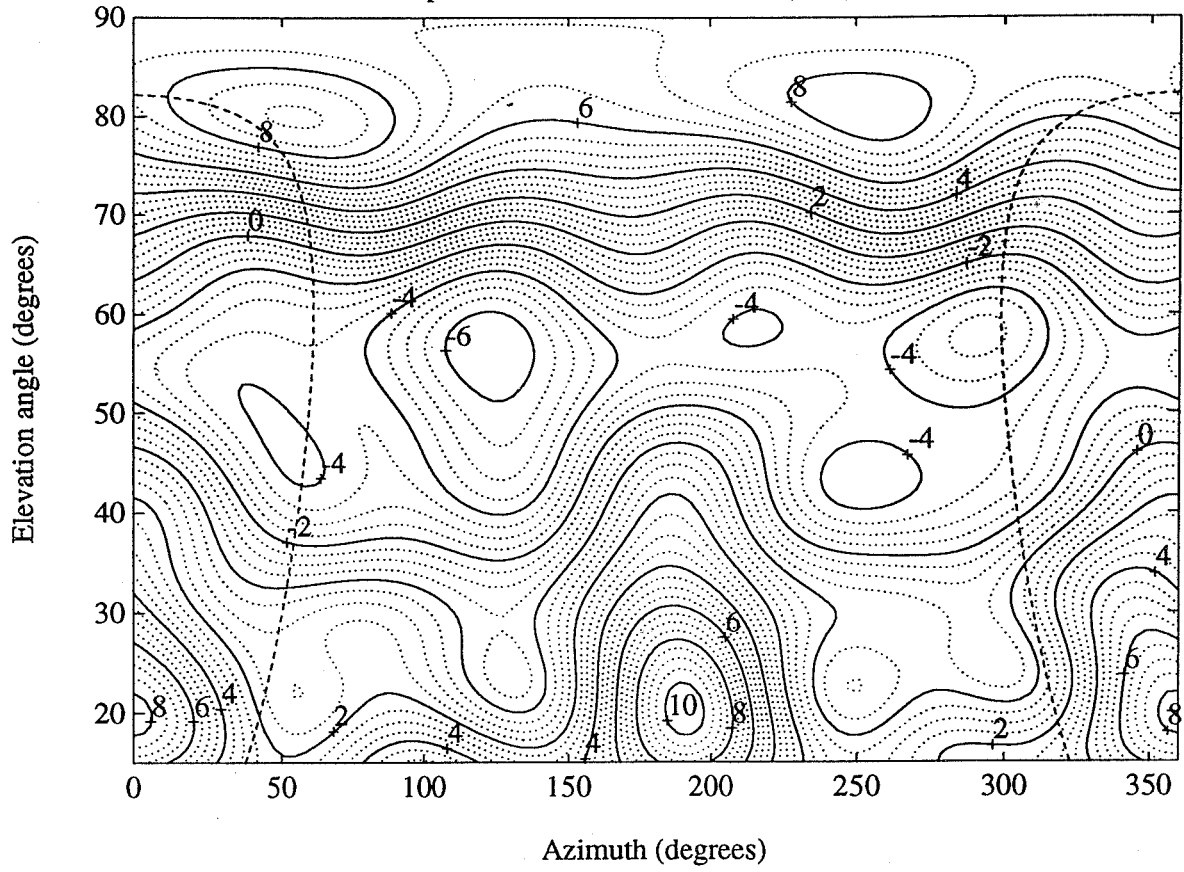
Antenna phase center variations in L1 (mm): Ashtech 1, only day 079



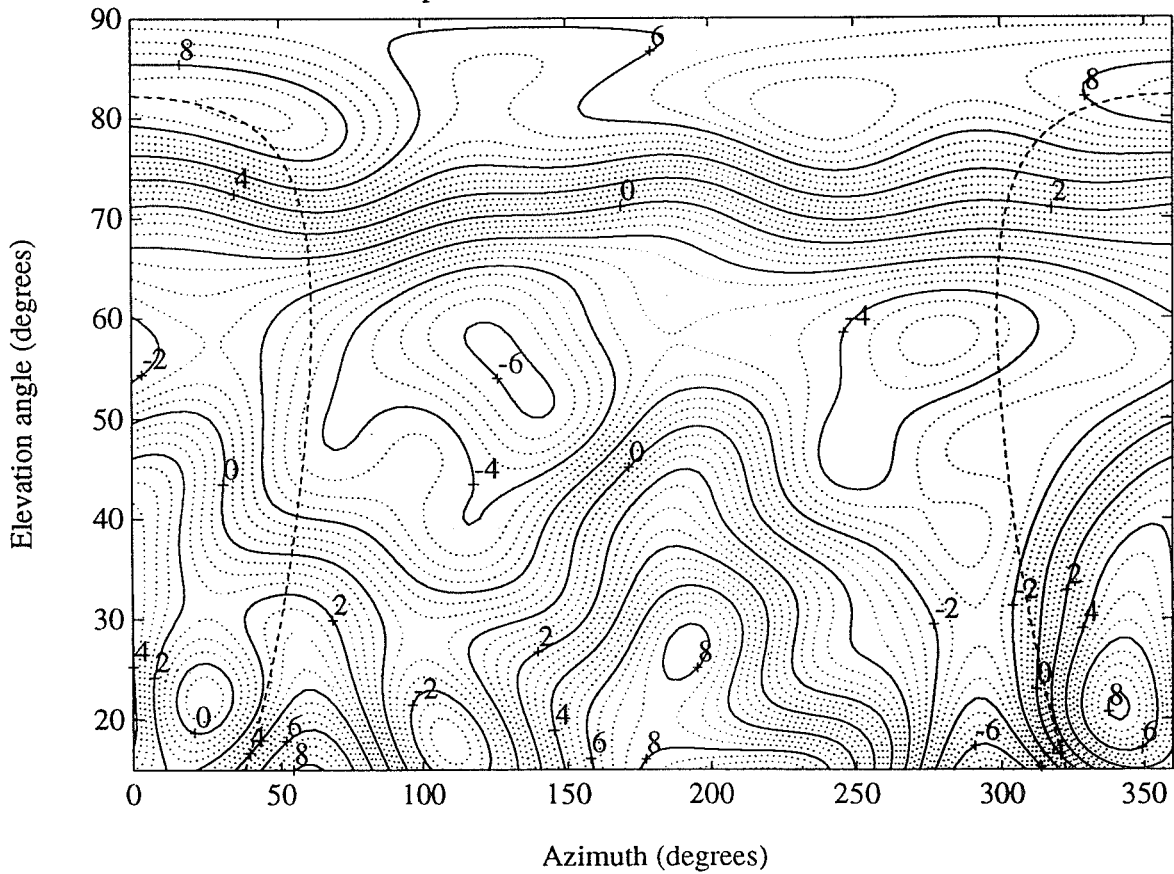
Antenna phase center variations in L1 (mm): Ashtech 1, only day 080



Antenna phase center variations in L1 (mm): Ashtech 2

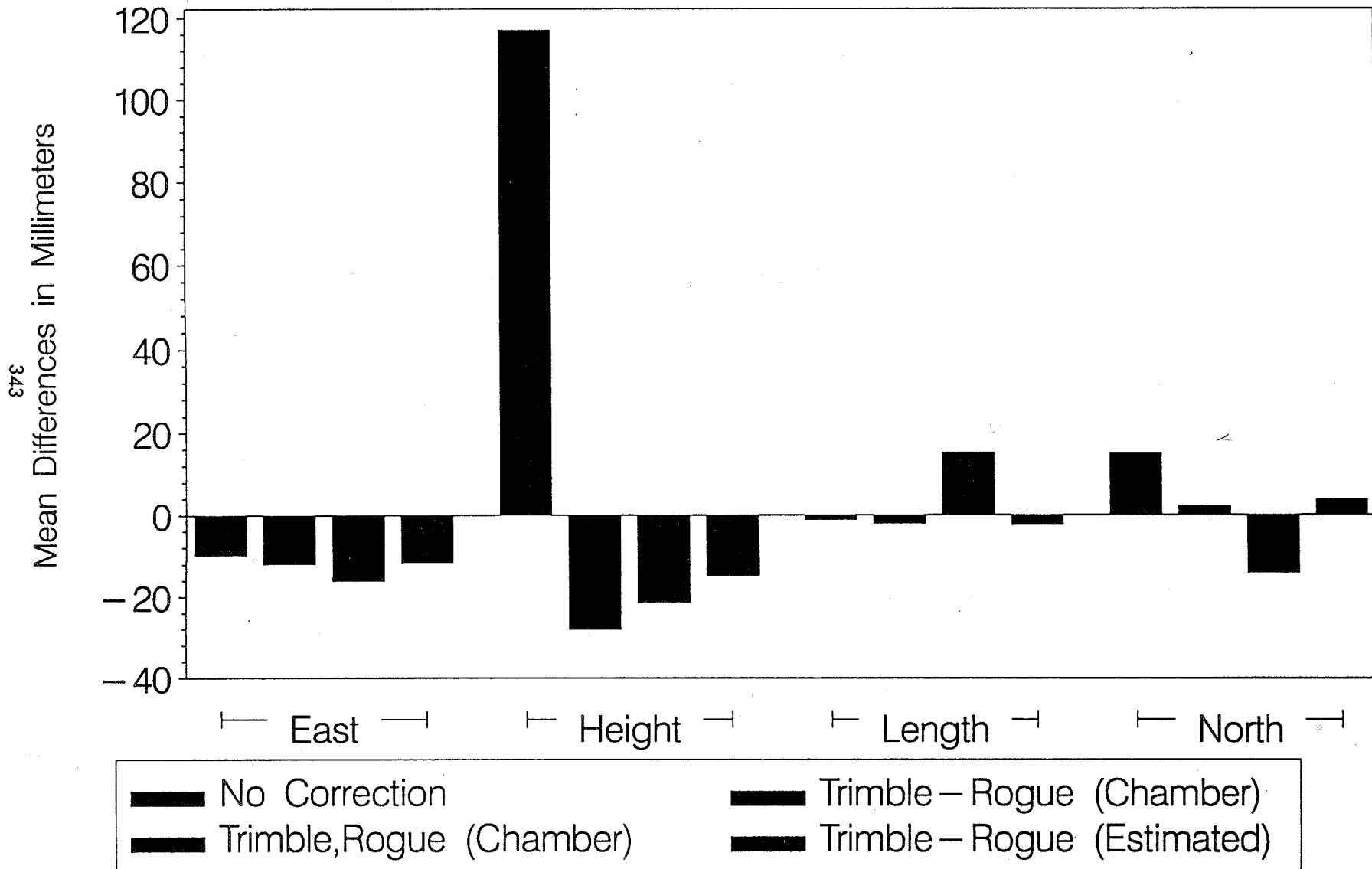


Antenna phase center variations in L1 (mm): Ashtech 1

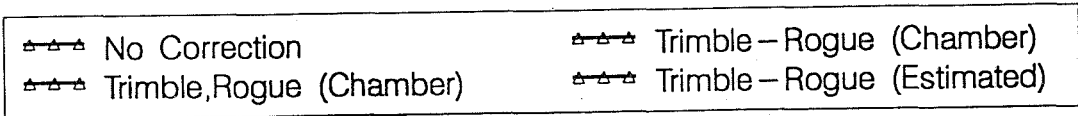
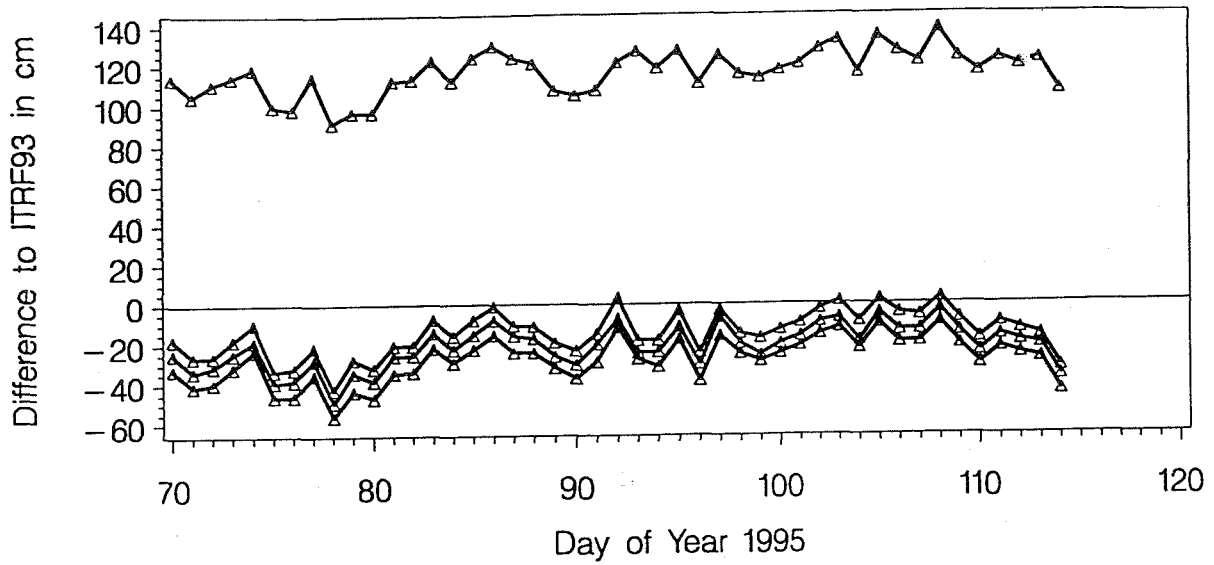


ANTENNA PHASE CENTER VARIATIONS (L3)

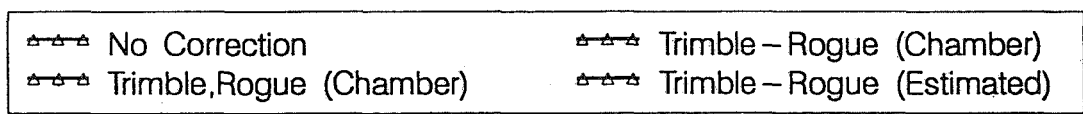
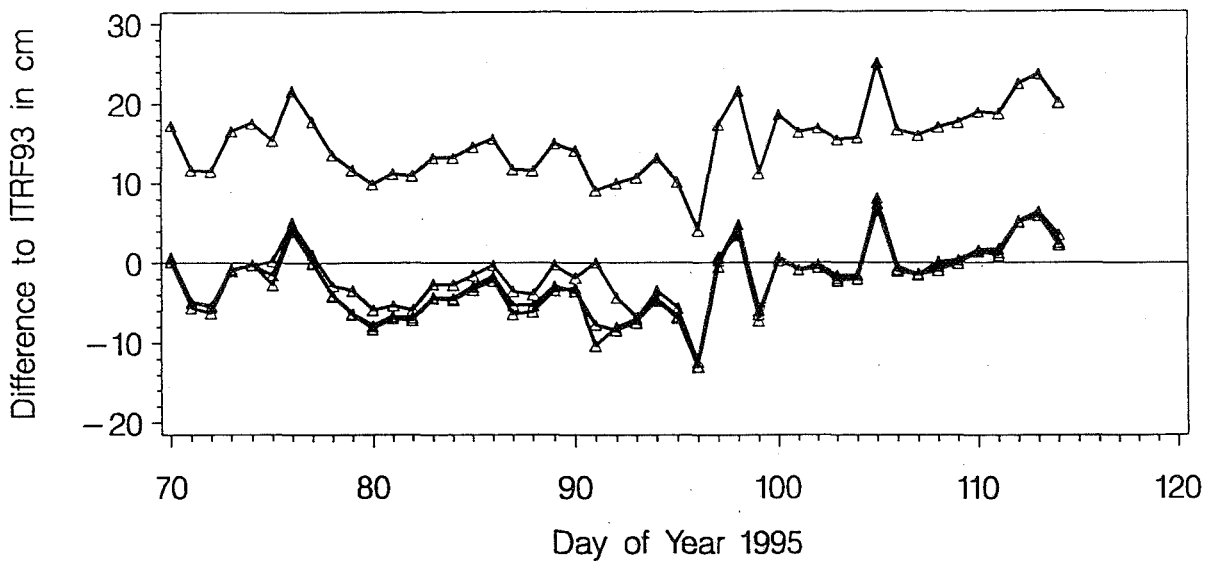
Baseline ONSA – ZIMM (1207 km) compared to ITRF93 (50 Days)



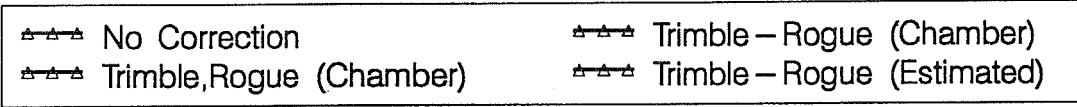
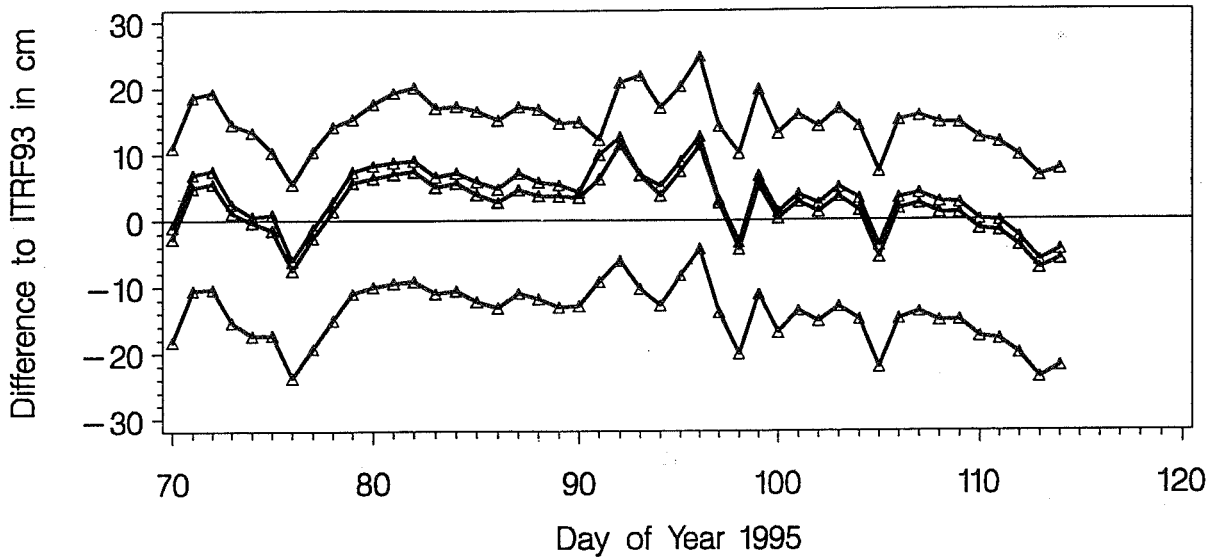
ANTENNA PHASE CENTER VARIATIONS (L3)
 Baseline ONSA-ZIMM (1207 km) compared to ITRF93
 Component = Height



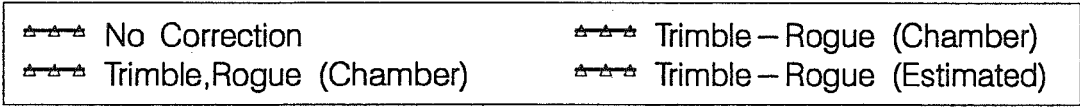
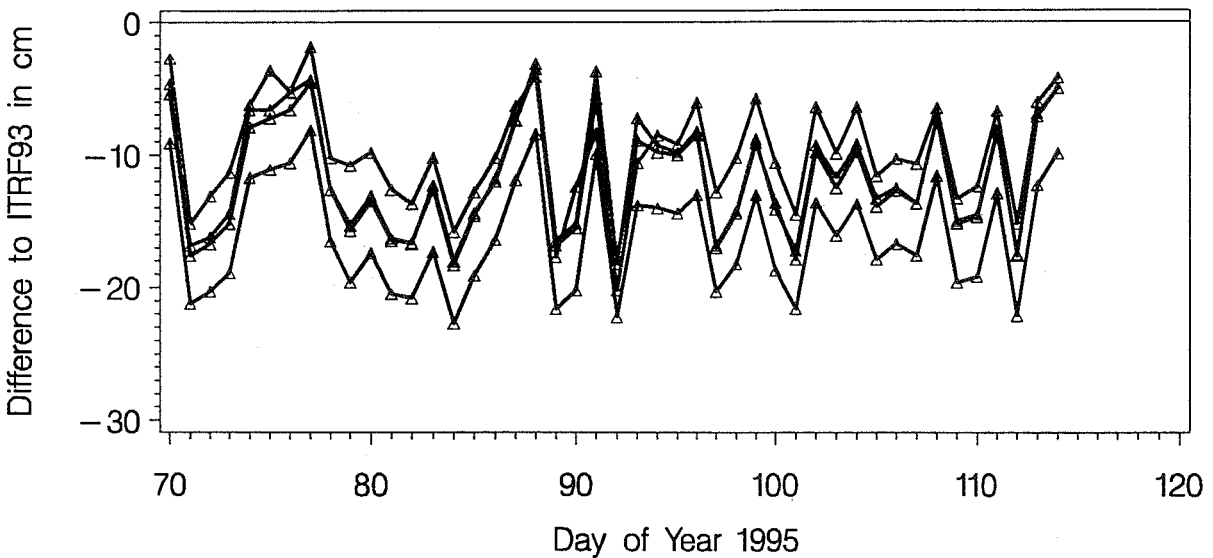
ANTENNA PHASE CENTER VARIATIONS (L3)
 Baseline ONSA-ZIMM (1207 km) compared to ITRF93
 Component = Length



ANTENNA PHASE CENTER VARIATIONS (L3)
 Baseline ONSA–ZIMM (1207 km) compared to ITRF93
 Component = North



ANTENNA PHASE CENTER VARIATIONS (L3)
 Baseline ONSA–ZIMM (1207 km) compared to ITRF93
 Component = East



Conclusions

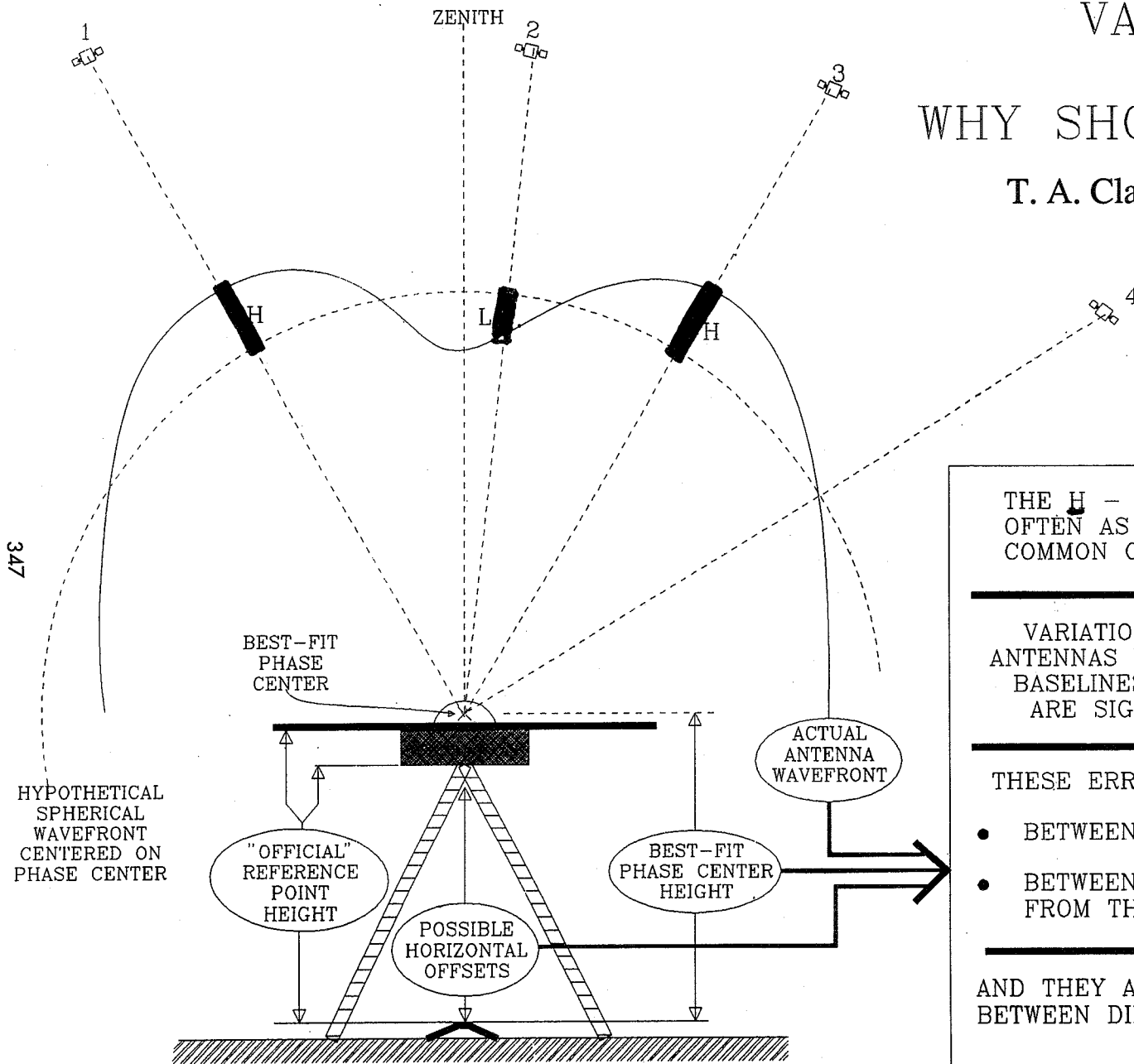
- Using GPS data it is possible to estimate the *relative* antenna phase center *offsets* and *variations* with good agreement between campaigns (different local environments).
- Comparisons with *absolute calibrations* from chamber tests still show some problems.

Recommendations

- A set of *mean antenna offsets* should be put together (for users not having the possibility to introduce elevation-dependent corrections). Cut-off angle: 15 or/and 20 degrees.
- A set of *elevation-dependent* corrections for all geodetic antenna types should be obtained from a combination of GPS and chamber values.
- The *absolute* calibrations have to be obtained from chamber measurements in such a way, that *no scale biases* are produced in global or regional network solutions !
- Steps to reach this goal: (1) Put together all antenna results and information available. (2) Combine them *to a set of correction values* as consistent as possible. (3) Individual groups check these values before they are distributed.

WHAT ARE PHASE-CENTER VARIATIONS AND WHY SHOULD I WORRY?

T. A. Clark and B. R. Schupler



347

THE **H** - **L** - **H** VARIATIONS ARE OFTEN AS MUCH AS ± 2 cm FOR COMMON GEODETIC ANTENNAS.

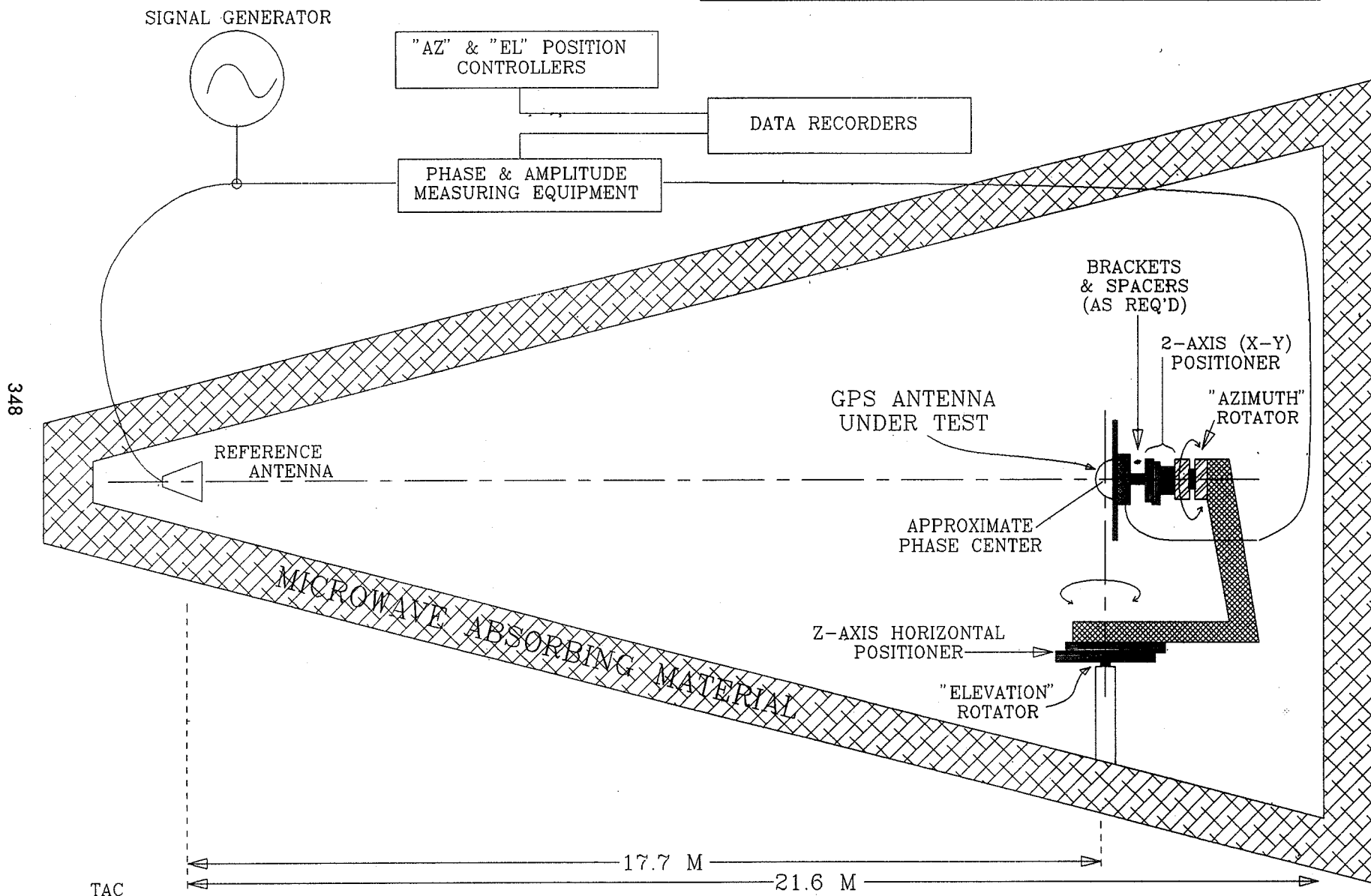
VARIATIONS BETWEEN IDENTICAL ANTENNAS DO NOT CANCEL ON LONG BASELINES SINCE ZENITH ANGLES ARE SIGNIFICANTLY DIFFERENT.

THESE ERRORS MAY BE DIFFERENT:

- BETWEEN L1 and L2
- BETWEEN DIFFERENT ANTENNAS FROM THE SAME MANUFACTURER

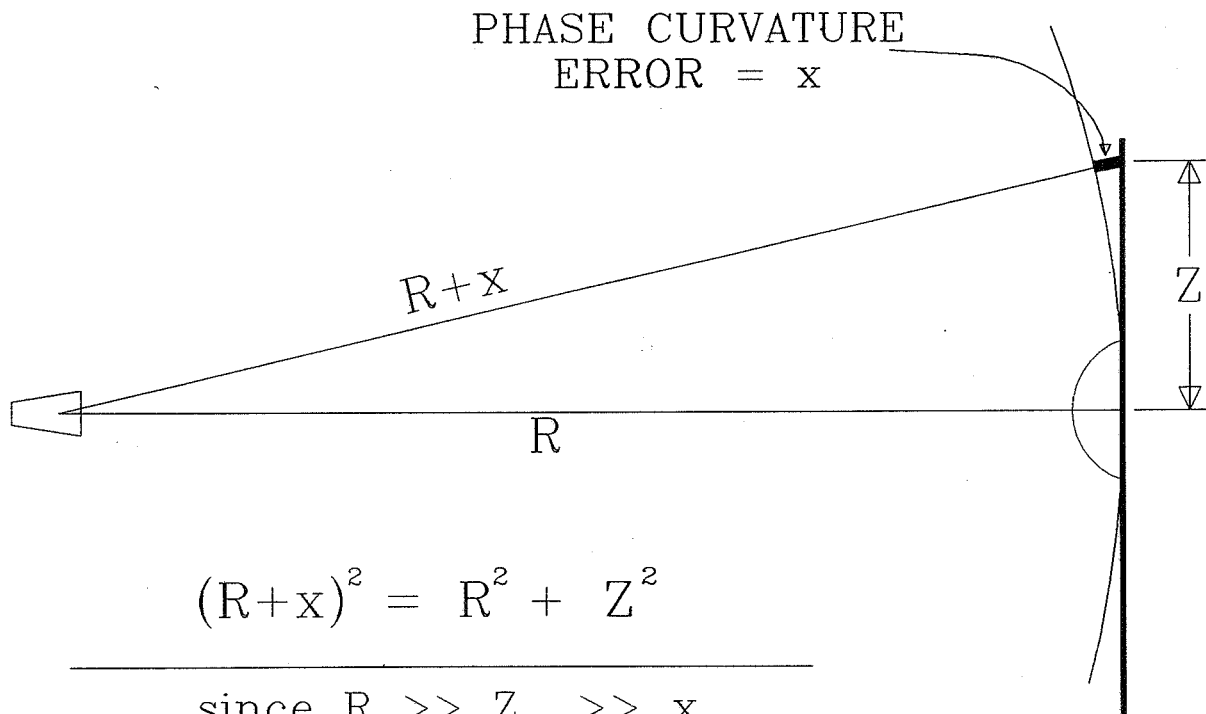
AND THEY ARE DEFINITELY DIFFERENT BETWEEN DIFFERENT MANUFACTURERS!

INDOOR ANECHOIC CHAMBER NASA/GSFC Bldg 19



348

HOW BIG SHOULD AN ANTENNA RANGE BE ?



$$(R+x)^2 = R^2 + Z^2$$

since $R \gg Z \gg x$

$$R^2 + 2Rx + x^2 \sim R^2 + 2Rx$$

$$\therefore 2Rx \sim Z^2$$

For $x < 2\text{mm} \sim \lambda/100$ pk-to-pk,

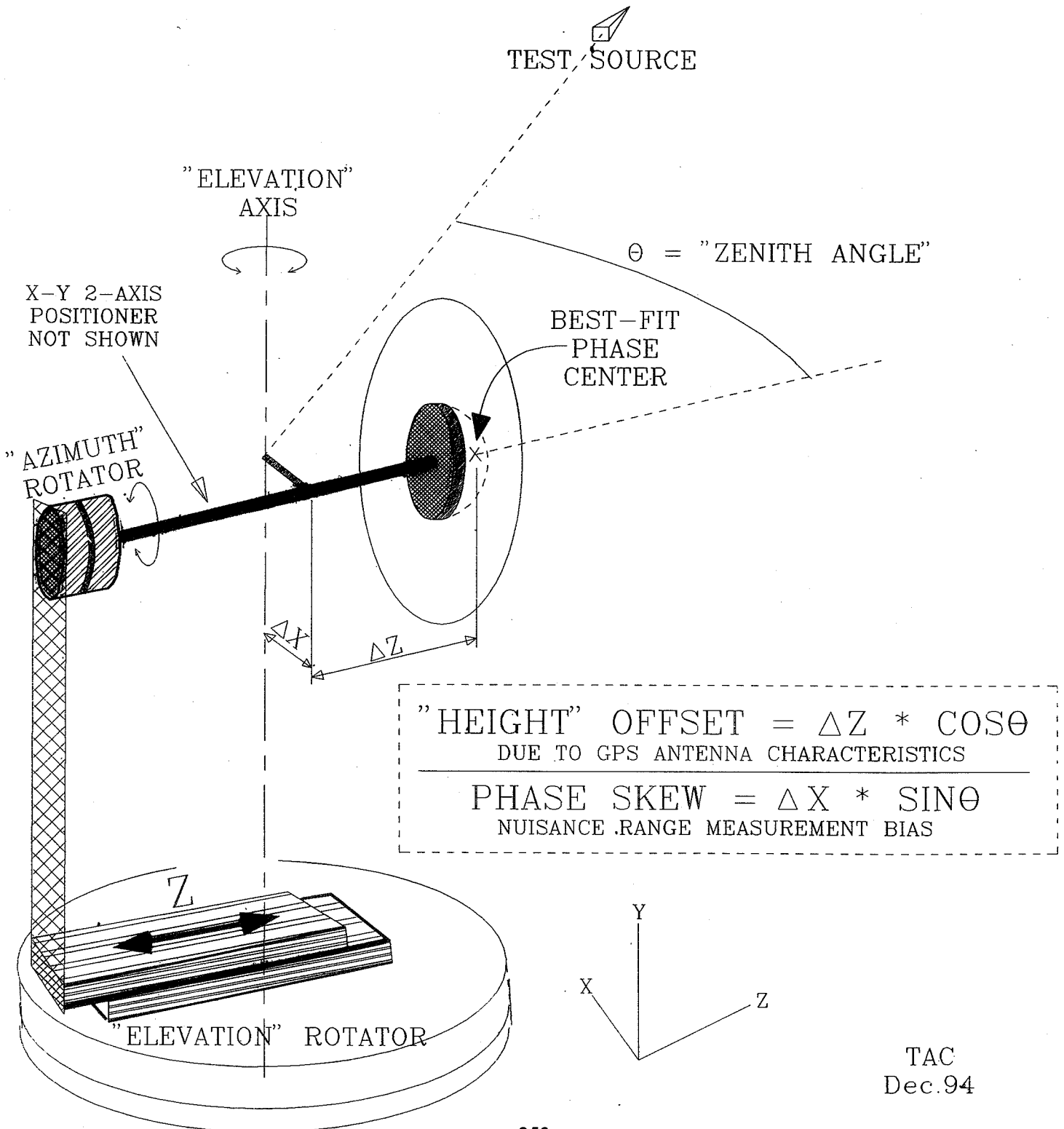
$$R \geq 50 * Z^2 / \lambda$$

For typical GPS antennas, $Z \leq \lambda$

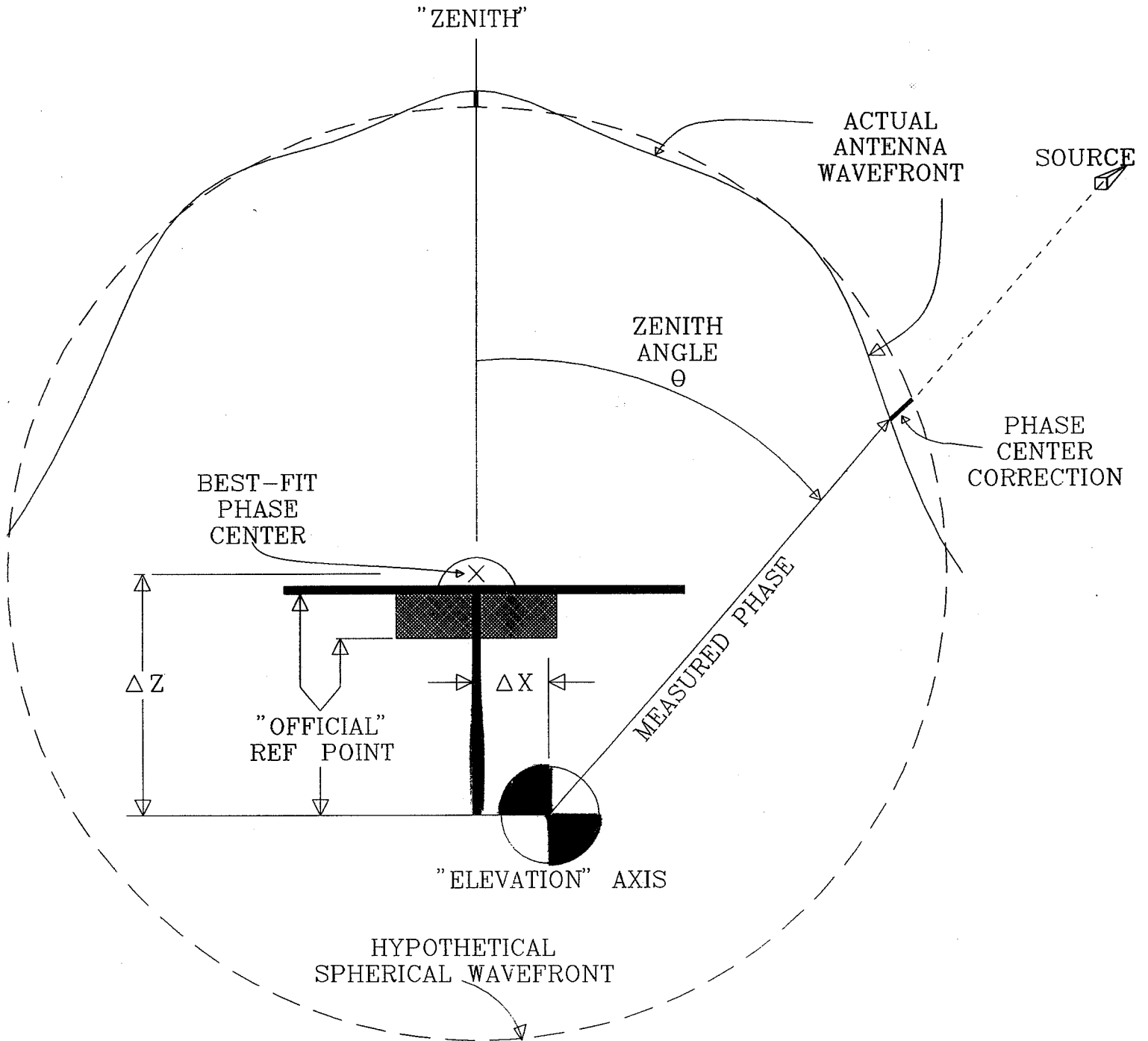
$$\therefore R \geq 50\lambda \sim 12 \text{ Meters}$$

is a reasonable criterion for the size of a GPS antenna range

ANTENNA PATTERN MEASUREMENTS -- POSITIONER GEOMETRY --



MEASURING PHASE CENTER CORRECTIONS



BEST-FIT PHASE CENTER OFFSET =
 MEASURED PHASE
 - $\Delta Z * \cos\theta$
 - $\Delta X * \sin\theta$
 + "OFFICIAL" REFERENCE POINT DEFINITION

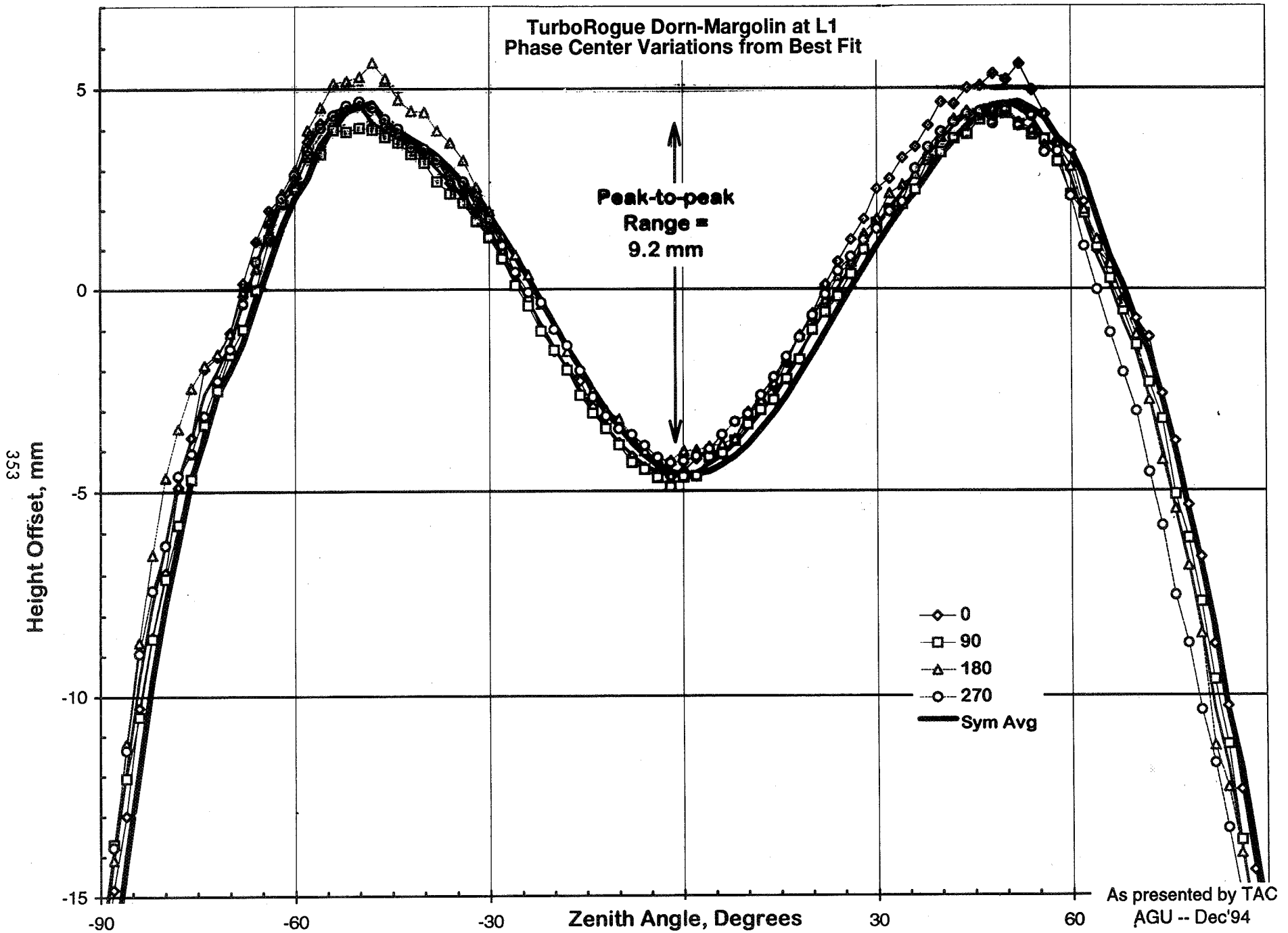
[WHERE $\Delta X \ll \Delta Y \ll$ SOURCE DISTANCE]

THE PHASE CENTER IS NOT A POINT!

IT MOVES WITH ELEVATION.

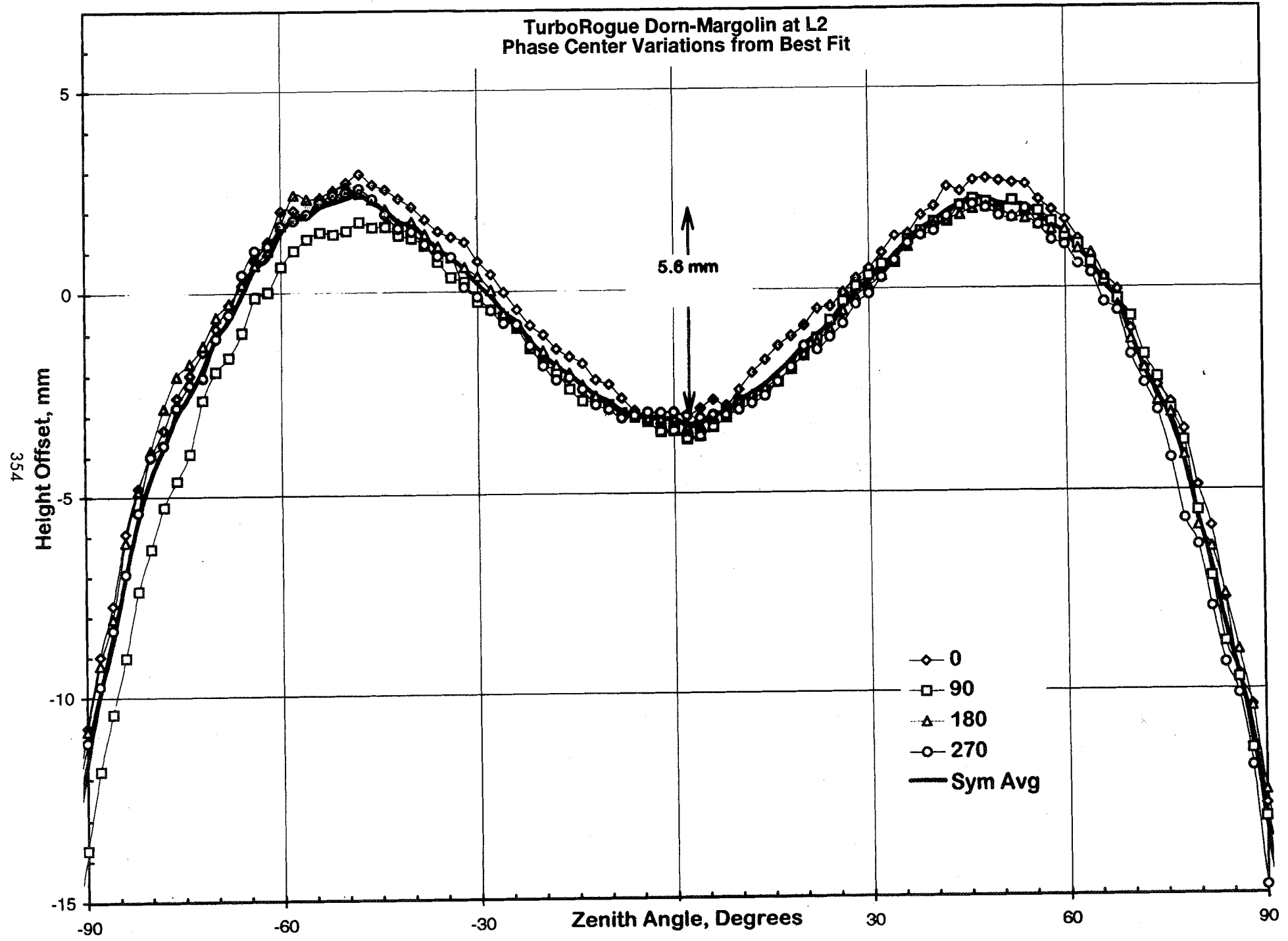
IT MOVES WITH FREQUENCY.

IT MAY NOT BE AZIMUTHALLY SYMETRIC

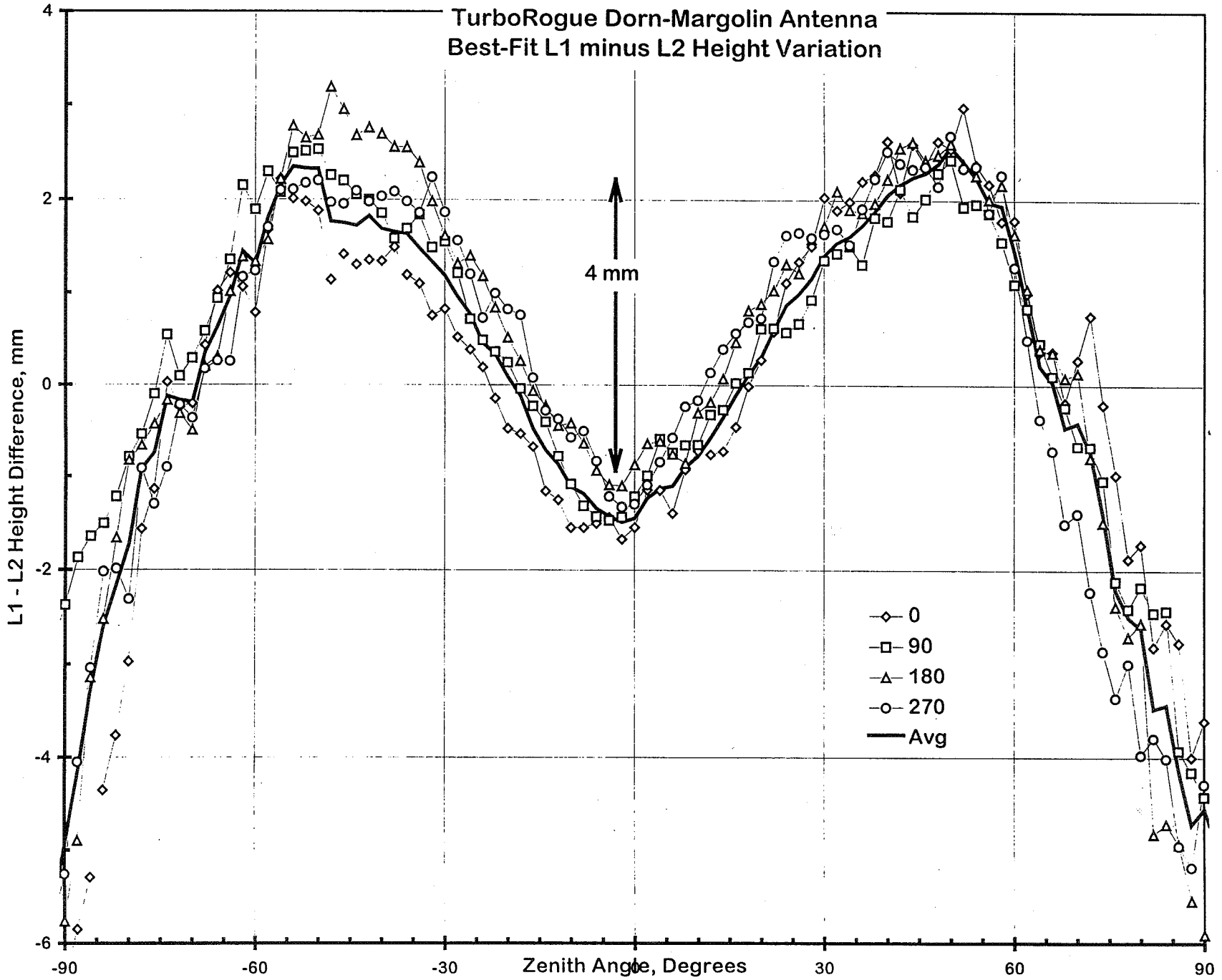


As presented by TAC
AGU -- Dec'94

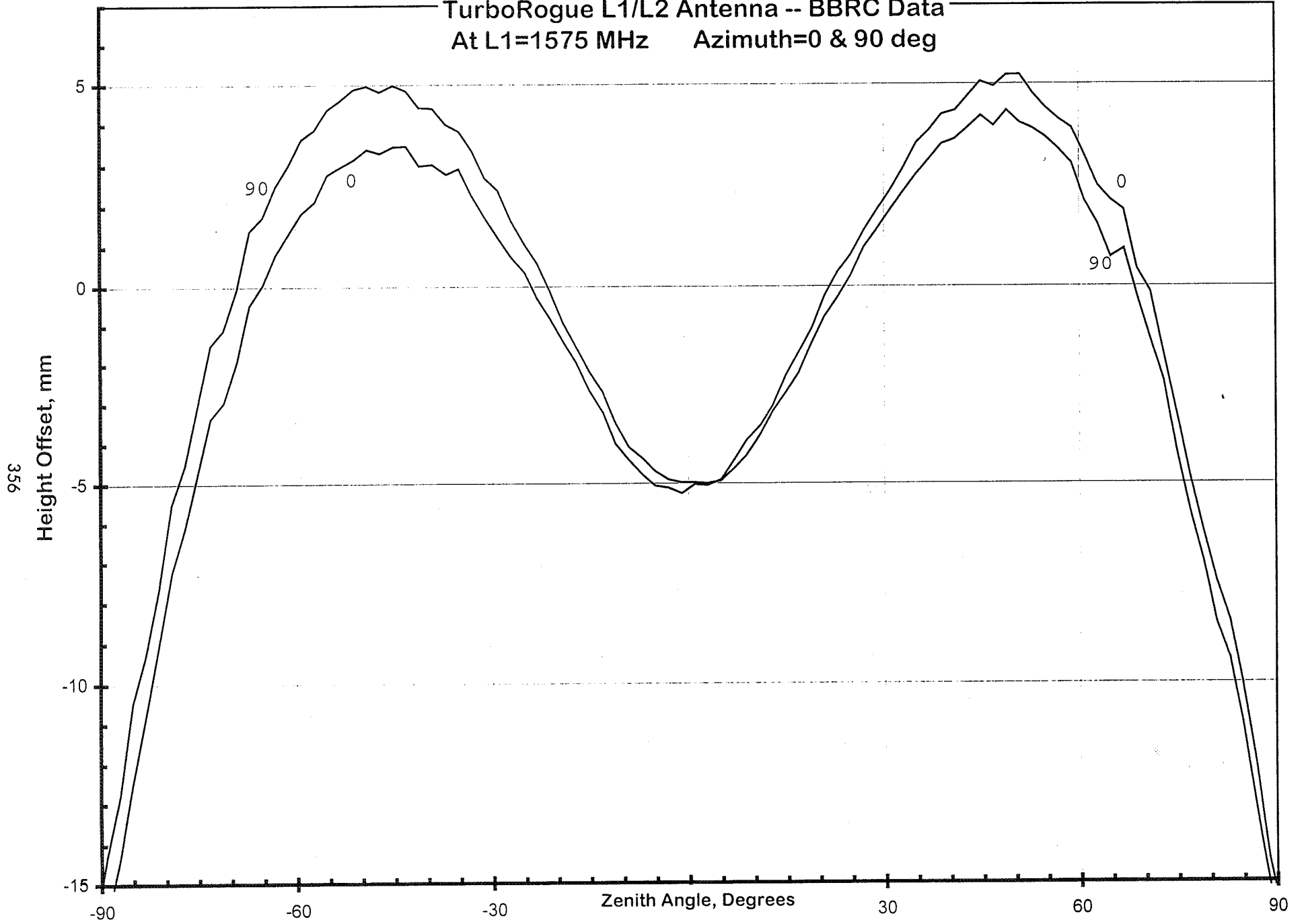
TurboRogue Dorn-Margolin at L2
Phase Center Variations from Best Fit



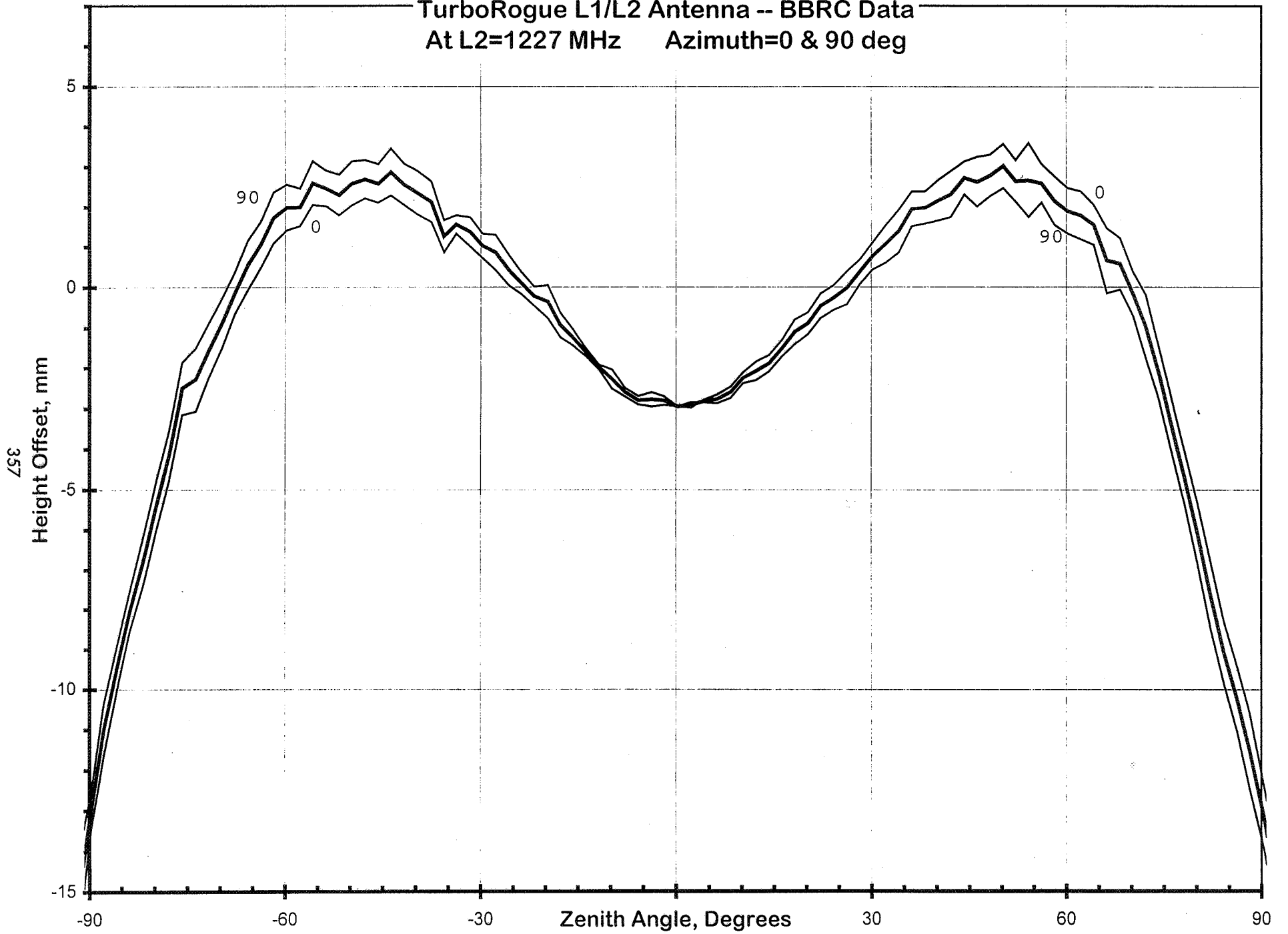
TurboRogue Dorn-Margolin Antenna
Best-Fit L1 minus L2 Height Variation



TurboRogue L1/L2 Antenna -- BBRC Data
At L1=1575 MHz Azimuth=0 & 90 deg



TurboRogue L1/L2 Antenna -- BBRC Data
At L2=1227 MHz Azimuth=0 & 90 deg



NOT YET COMPARED

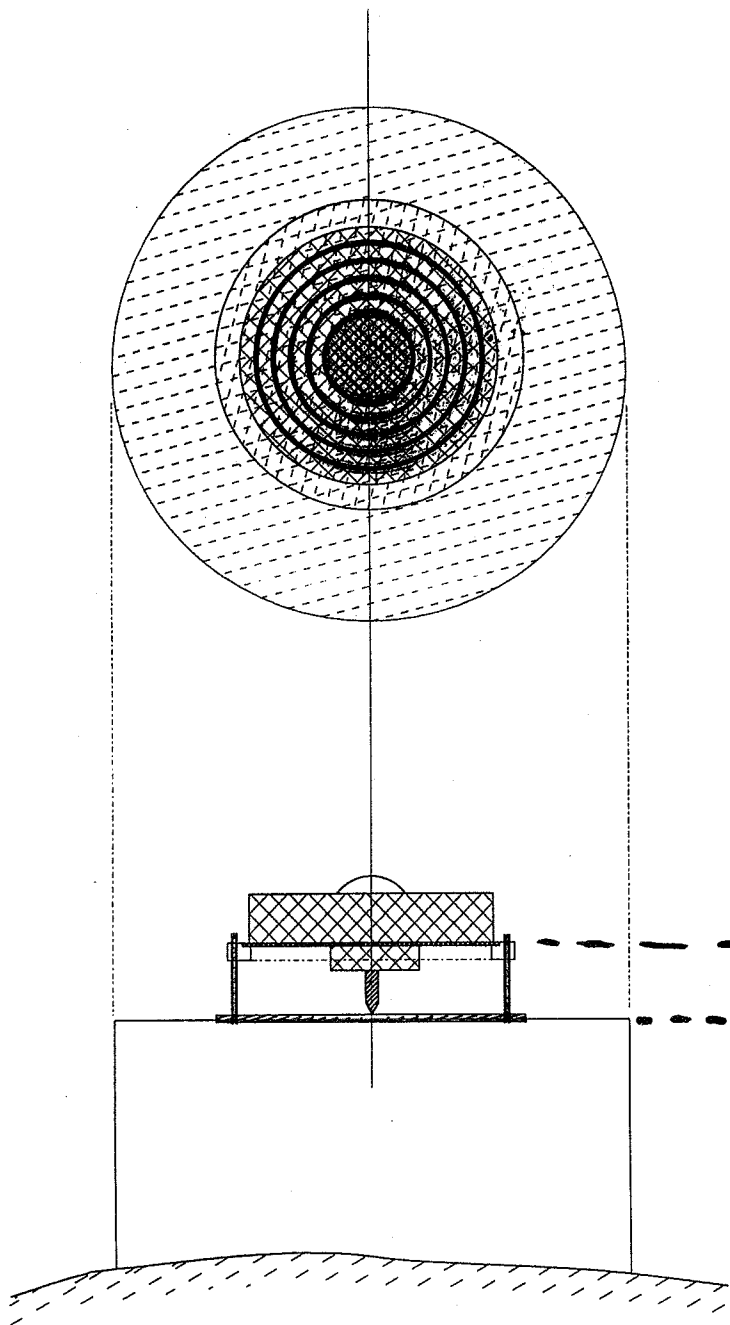
- **OUR RECENT ASHTECH RESULTS COMPARISONS WITH OUR EARLIER DM RESULTS**
- **OUR RESULTS WITH UNAVCO/BALL**
- **RANGE RESULTS VS. "ON THE AIR" RESULTS**

FUTURE WORK

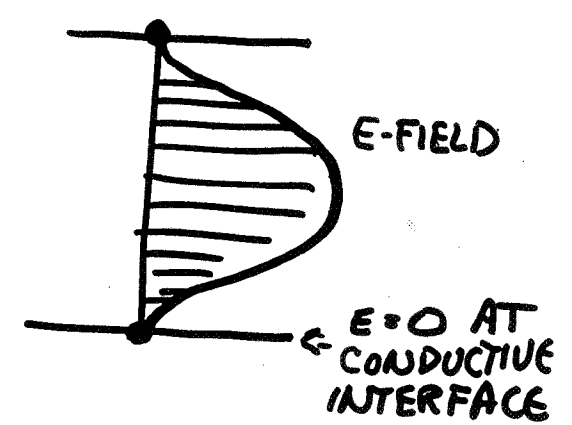
- WE NOW HAVE A D-M ANTENNA TO TRY ON ALL THE RANGES “ZEBRA STRIPE”
 - DO THE RANGES GET THE SAME RESULTS ON THE SAME ANTENNA?
- WORK HARD TO RELATE THE MECHANICAL STRUCTURE TO THE ANTENNA
- TEST THE EFFECT OF VARIOUS RADOMES
- AUTOMATE THE MEASUREMENT & ANALYSIS PROCEDURE
- PRODUCE THE PRODUCT THE USERS REALLY NEED

“MULTIPATH”

- **NEAR FIELD**
 - ANYTHING WITHIN $\sim Z_1$ OF THE ANTENNA PERTURBS THE PHASE & AMPLITUDE PATTERNS
- **A.K.A. SCATTERING**
- **FAR FIELD REFLECTORS MANY 1 AWAY**



10 cm = $\lambda/2$] = RESONANT "CAVITY"

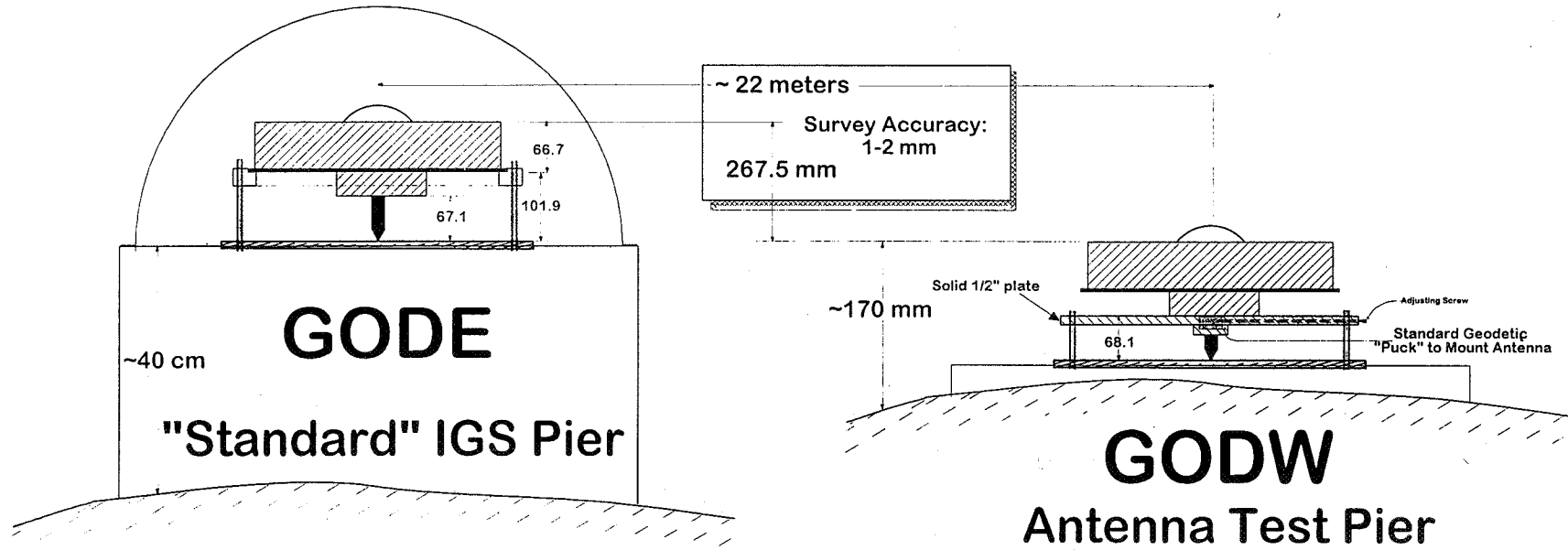


Our Testing Methodology:

- ◇ Try several simple schemes to “kill” the cavity resonance and/or absorb the “scattered” RF energy in the antenna backplane area:
 - Microwave Absorber (like Elosegui *et al*).
 - Add a “skirt” to keep RF out.
 - “Spoil” the cavity resonance.

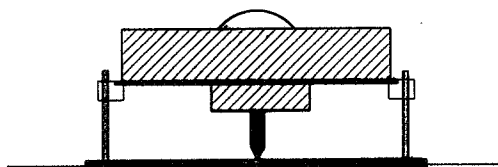
- ◇ Take several days of data with each scheme being tried on the “operational” GODE IGS site antenna. The reference is the GODW antenna ~22 meters away.
 - GODE is a normal IGS operational site, using standard 8-channel TurboRogue.
 - GODW using new 12-channel TurboRogue.
 - GODW using new design “spike mount” (which should minimize the resonance problems).
 - GODE&GODW both use identical Dorn-Margolin choke-ring antennas.
 - GODW setup not changed during the tests.
 - The GODE-GODW baseline has been surveyed to an accuracy ~1-2 mm, so we can compare GPS results with “ground truth”.

- ◇ Process the GODE-GODW data using *GIPSY* and JPL-supplied orbit/clock for each day:
 - Use common atmosphere for GODE&GODW.
 - Vary Elevation Cutoff from 10° to 50°.
 - Compare the results with ground survey “truth”.

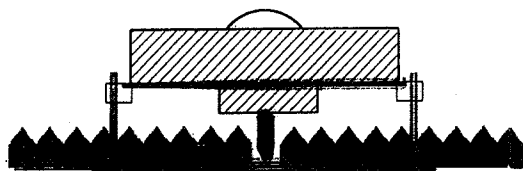


The Calibrated GPS Antenna Range at GGAO

Four different cases we tested on the normal GODE IGS antenna at GGAO*:

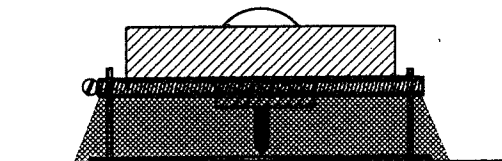


1 The "Standard" IGS Configuration



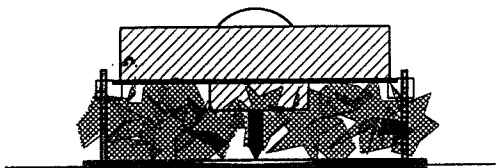
2 **ABSORBER** (similar to Elosegui et al):
Commercial Microwave Absorbing Material
(We also tried barbecue charcoal,
but it did not work too well)

PRICE: ~\$100
Special
Purchase



3 **Aluminum Skirt: Conical Reflecting Skirt**
made of ordinary aluminum window screen,
held on by long hose clamp.

PRICE: ~\$20
@ Local
Hardware
Store



4 **Aluminum Foil wads, filling the region**
behind the antenna.

PRICE: << \$1
@ Local
Supermarket

* GGAO = Goddard Geophysical & Astronomical Observatory
GODE = GODdard East pier, GODW = GODdard West

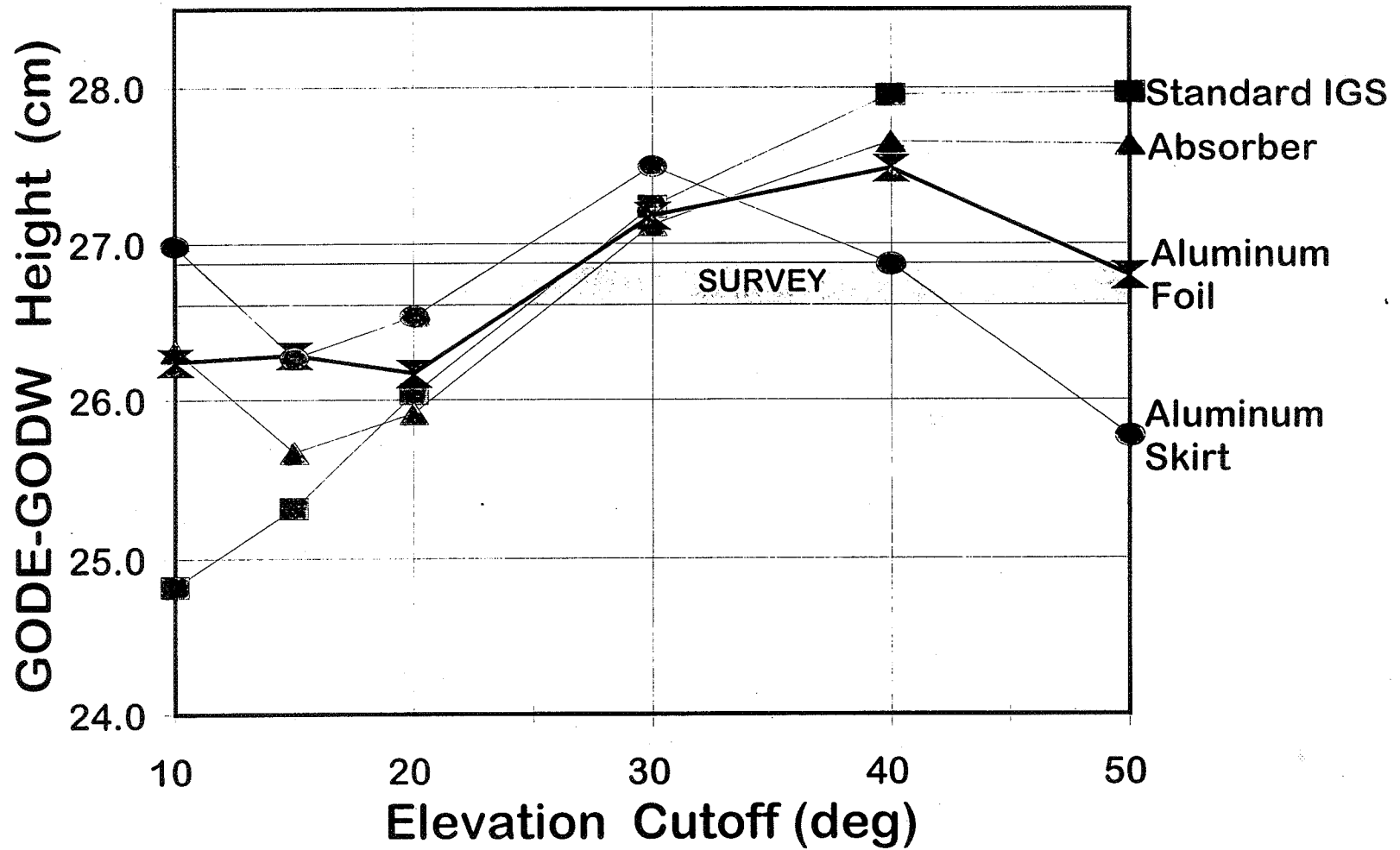
The Results (1):

- ① Our “Standard IGS” results are similar to Elosegui *et al*. They observed 45 mm height variation for elevation cutoffs from 5° to 50°, where we observe 31 mm from 10° to 50°.
- ② As reported by Elosegui *et al*, the addition of microwave ABSORBER in the backplane area reduces the effect. They report a factor ~8 improvement with the absorber they used. We used a different type of absorber and see an improvement ~3. (We also tried using ordinary barbecue charcoal briquettes as an absorber but found the approach ineffective.)
- ③ The two new “fixes” we tried, a conductive SKIRT and filling the backplane area with household aluminum FOIL, worked as well as the microwave absorber.
- ④ The SKIRT shows systematic variations in the GODE-GODW height with elevation cutoffs. This is probably the result of changes in the phase pattern of the choke-ring antenna due to the addition of the skirt. (We did not attempt to measure the phase/amplitude patterns of the antenna with the added skirt).

The Results (2):

- ⑤ The use of Aluminum FOIL in the backplane area appears to be a very effective way to suppress the “Spike” resonance! The peak-to-peak variations in recovered height with the foil were only 16 mm and the mean value agrees with ground survey “truth” to <2 mm.
- ⑥ The FOIL “fix” is particularly attractive since the cost is very low (<\$1.00), and since the material can be obtained at a local super-market *anywhere in the world*.
- ⑦ The ~16 mm systematic elevation angle variation is probably due to residual “ground clutter” multipath on the GODW antenna (only ~1 wavelength above ground). We plan additional tests to verify this hypothesis.
- ⑧ There may be some small systematic biases at levels ~2-3 mm due to dielectric effects in the radome used to protect GODW from the environment. Additional tests are planned to quantify radome-induced biases.

Suppressing the "Spike" Multipath



Page intentionally left blank

MIT T2 Analysis Report

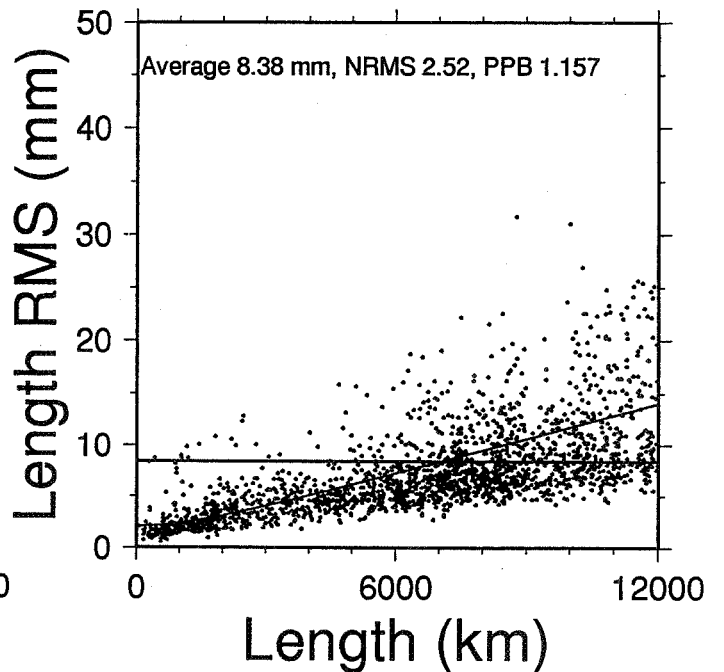
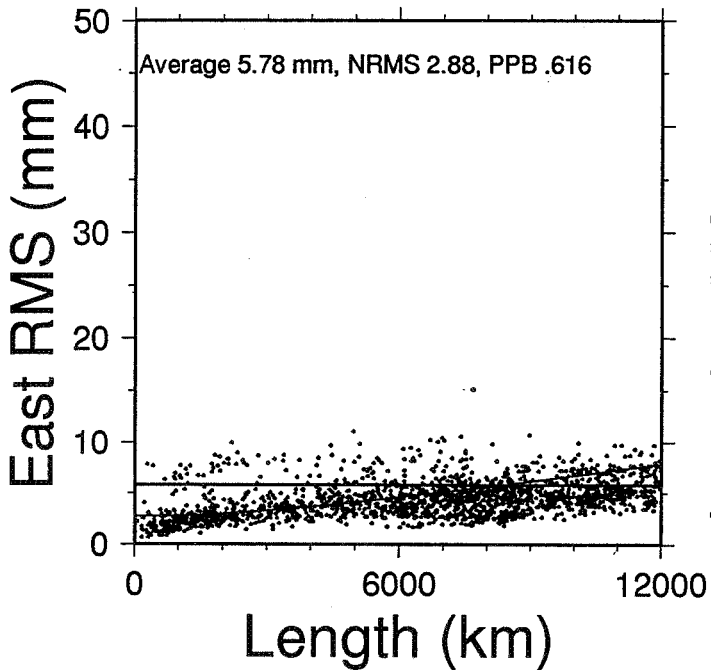
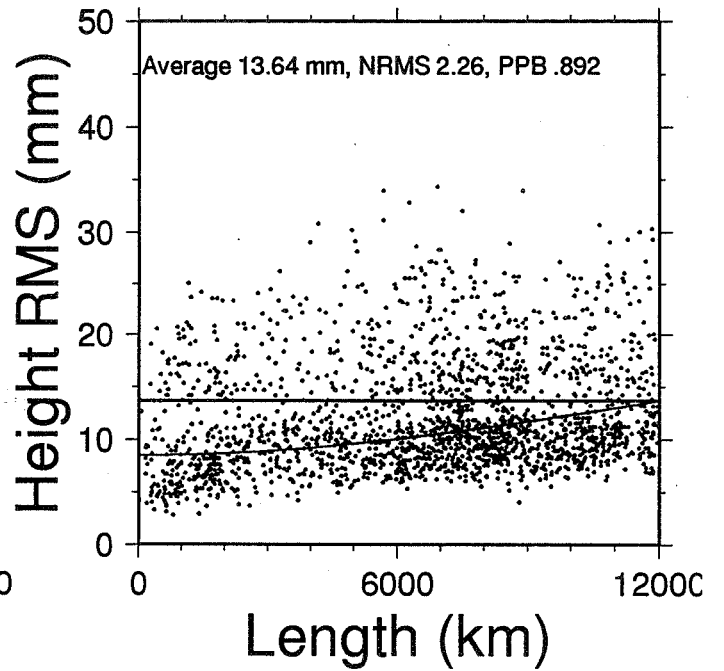
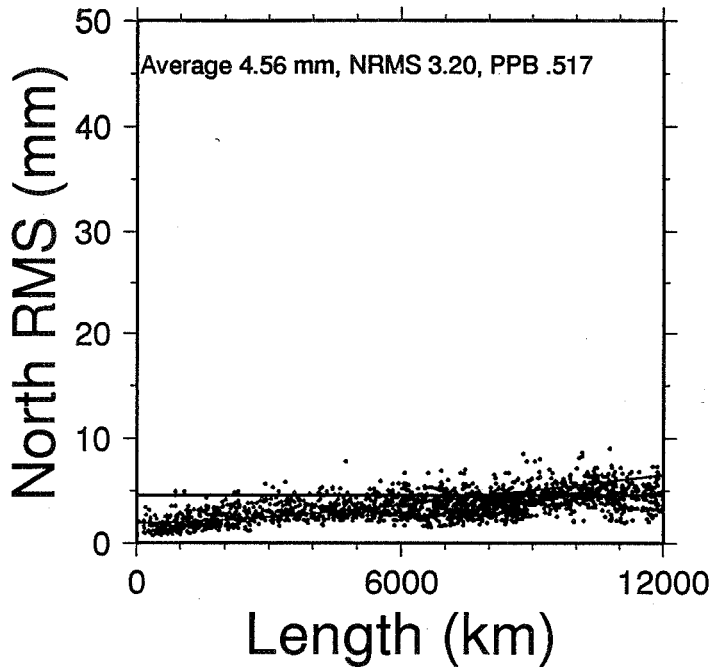
Thomas A Herring

- **Procedures:**
 - Constraints removed for all centers except JPL and ESA
 - Center variances based on χ^2 when "core" constrained
 - Two analyses performed each week:
 - (a) Tight solution with core constrained
 - (b) Loose solution with translation, rotation and scale constraint applied.
 - RMS fits to core and common sites reported for ITRF-93 and Combined solution

- **Differences from other centers**
 - RMS fits are computed with height variance 10 times greater than horizontal
 - Translation constraint is forced through covariance matrix (means not a simple translation).

- **Results**
 - Repeatabilities for longest running centers
 - Weight comparison
 - Specific site position evolution for 6 months of data.

Comb_0819_0842 Combined Analysis



Center weights

Center	Variance	χ^2/f		
		North	East	Height
Comb		10.2	8.3	5.1
COD	12.3	88.5	100.4	35.1
EMR	36.8	65.0	78.7	31.4
GFZ	38.6	55.5	31.2	16.0
JPL	11.8	32.8	15.4	11.0
SIO	1.6	7.8	5.7	4.0

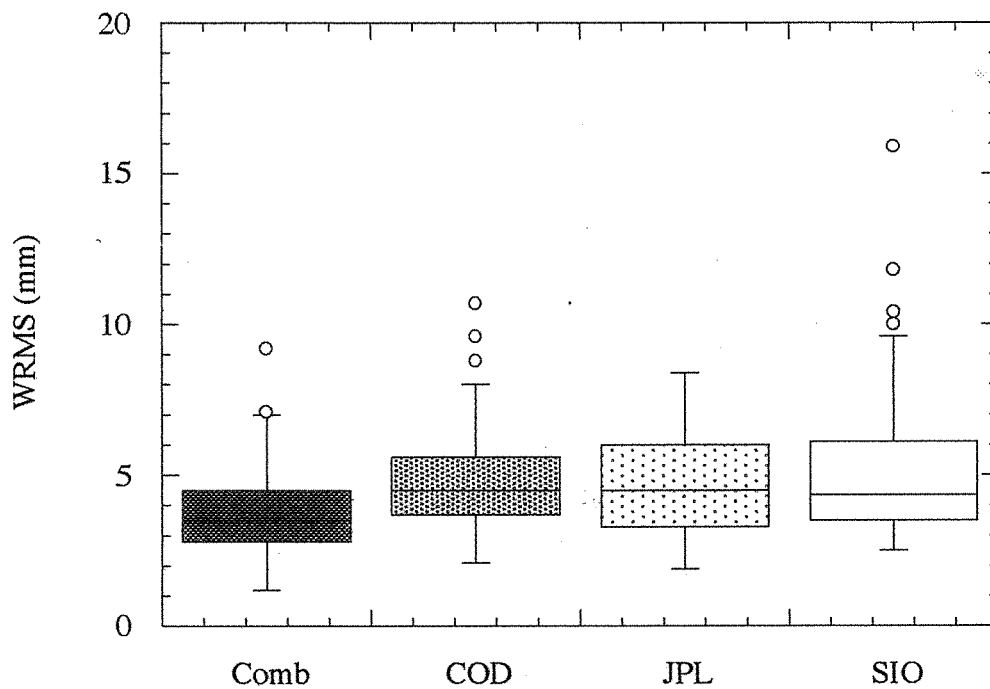
- Reasons for differences:
 - Systematic variations in position common to many analysis centers.
 - Stations not common so direct comparison difficult.
 - COD/JPL and SIO produce very similar quality results and have similar weights in the combination.

- Average repeatability (about mean) for Combined solution:

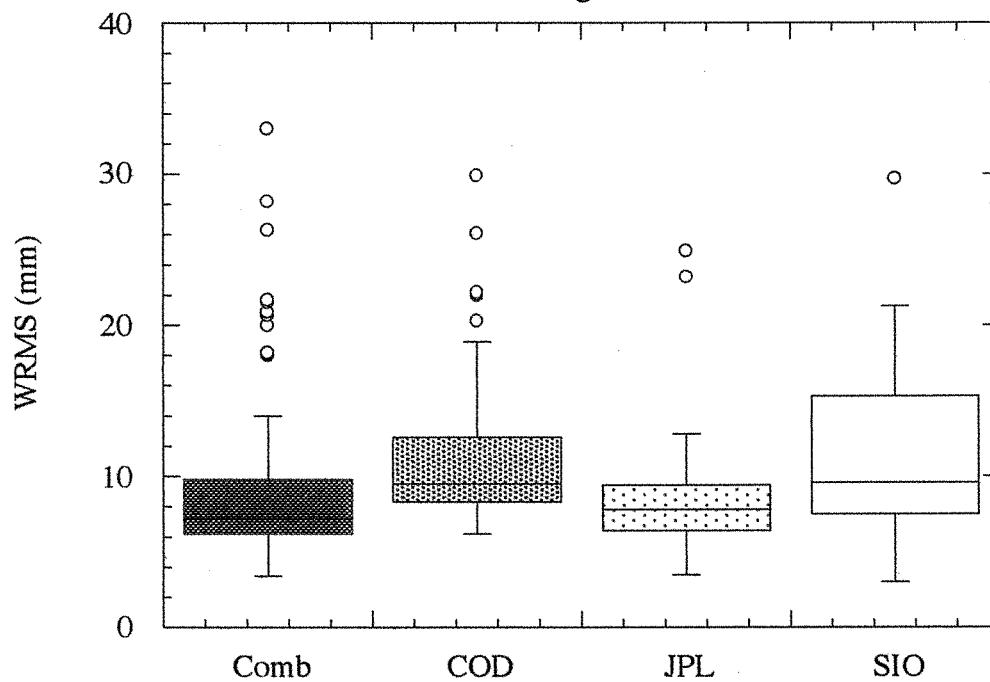
NORTH	4.5 mm
EAST	5.8 mm
HEIGHT	13.6 mm

Clearly some poor performance stations.

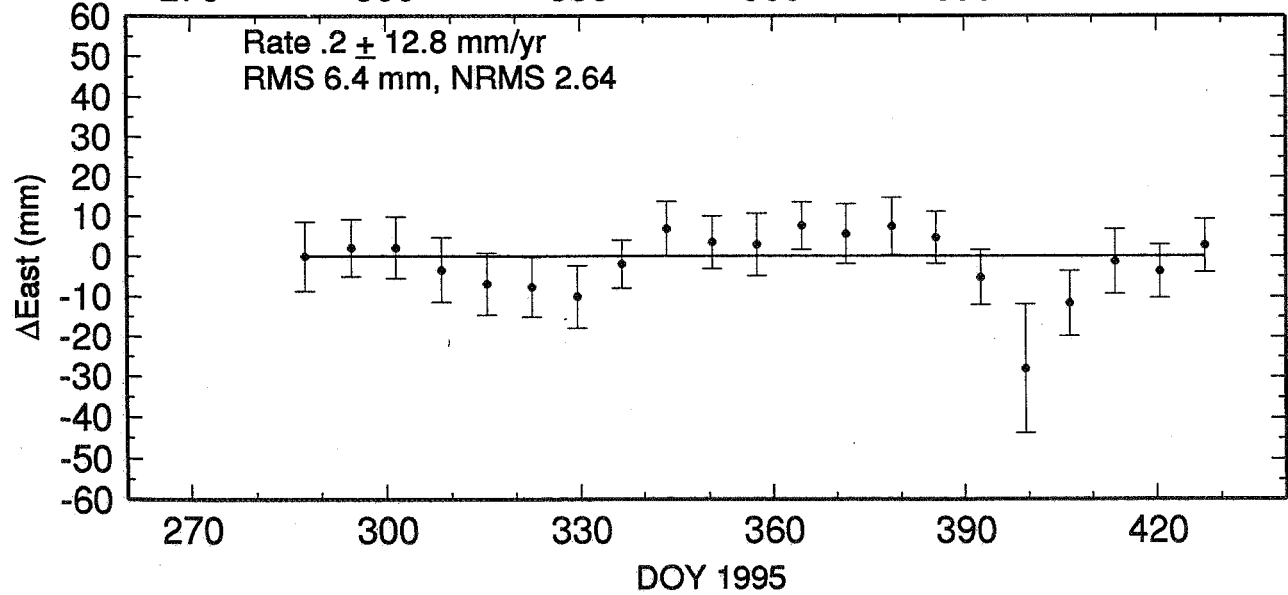
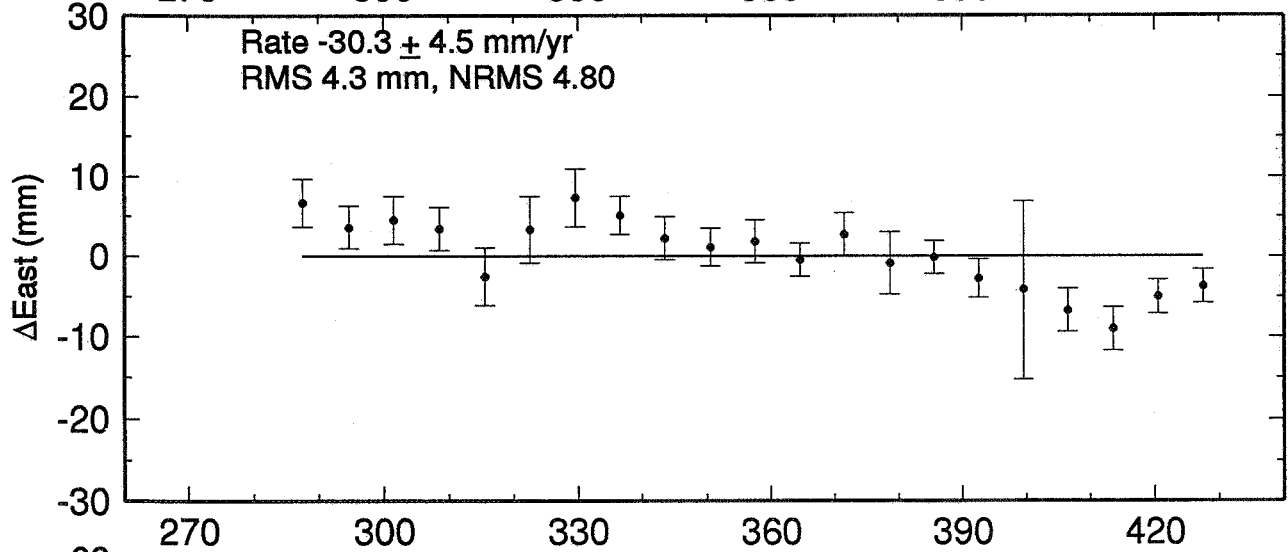
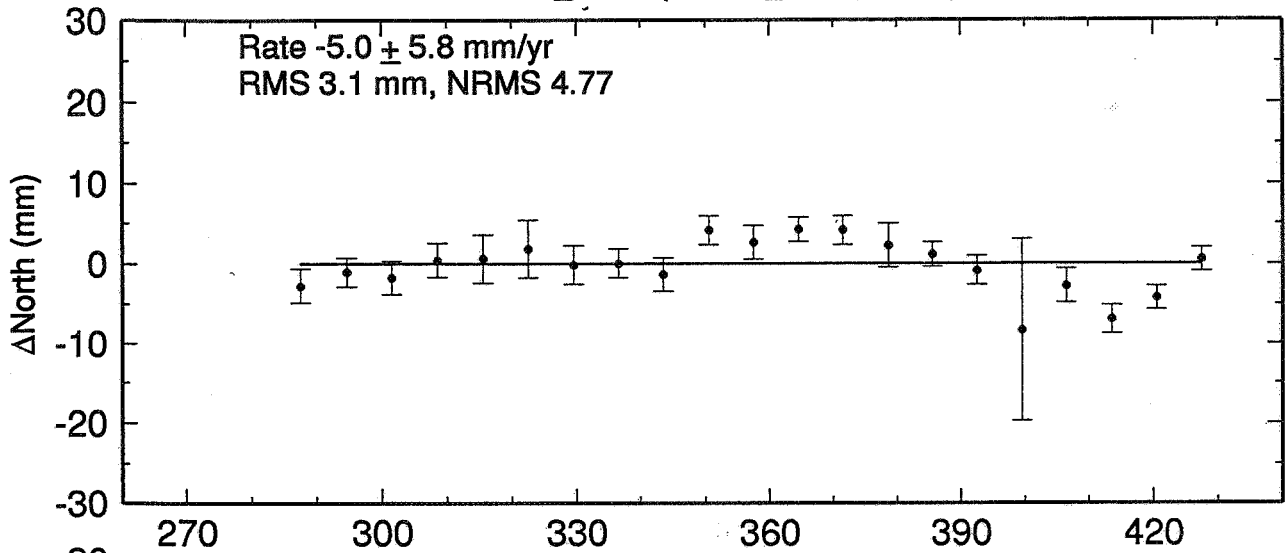
Distribution North RMS scatters



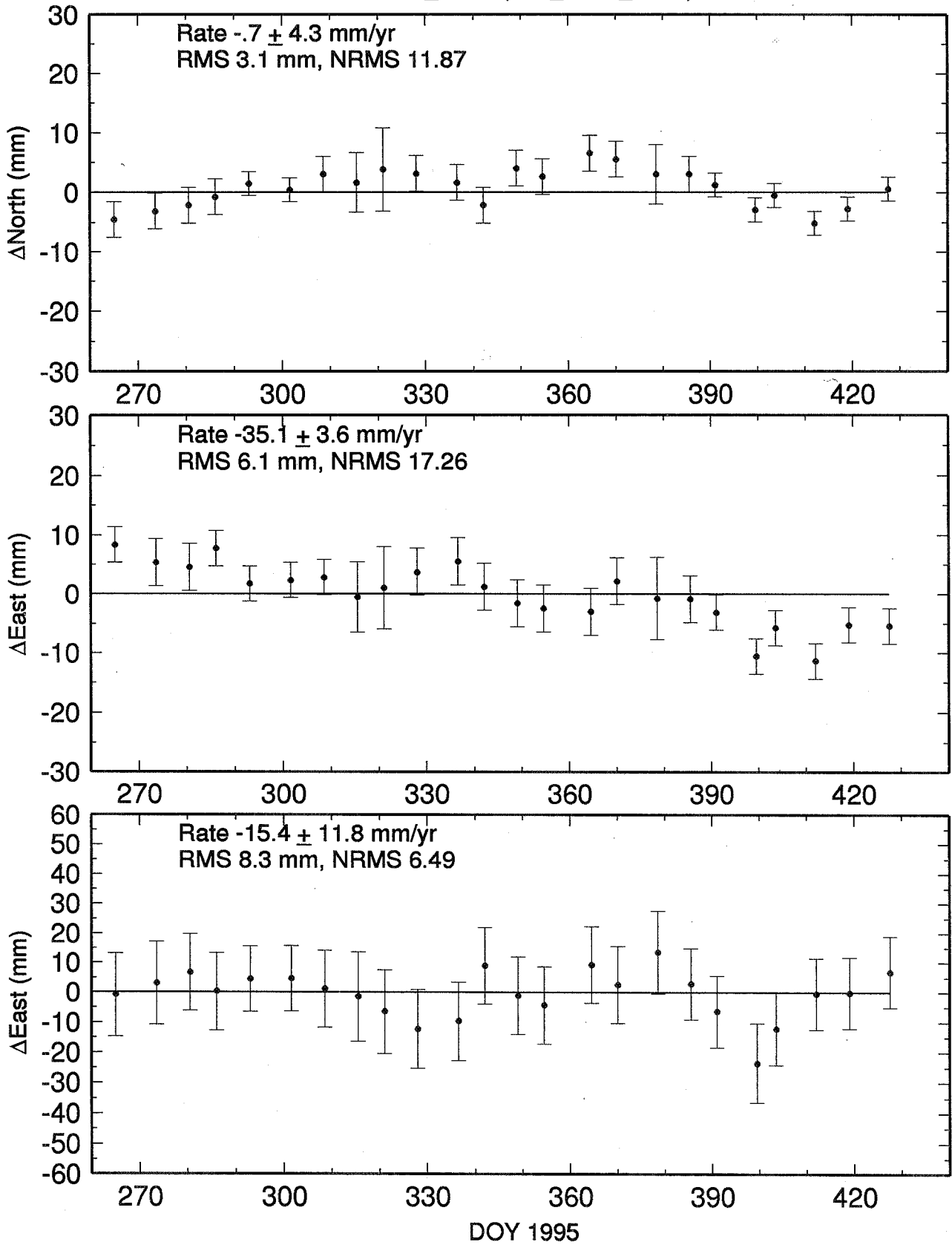
Distribution Height RMS scatters



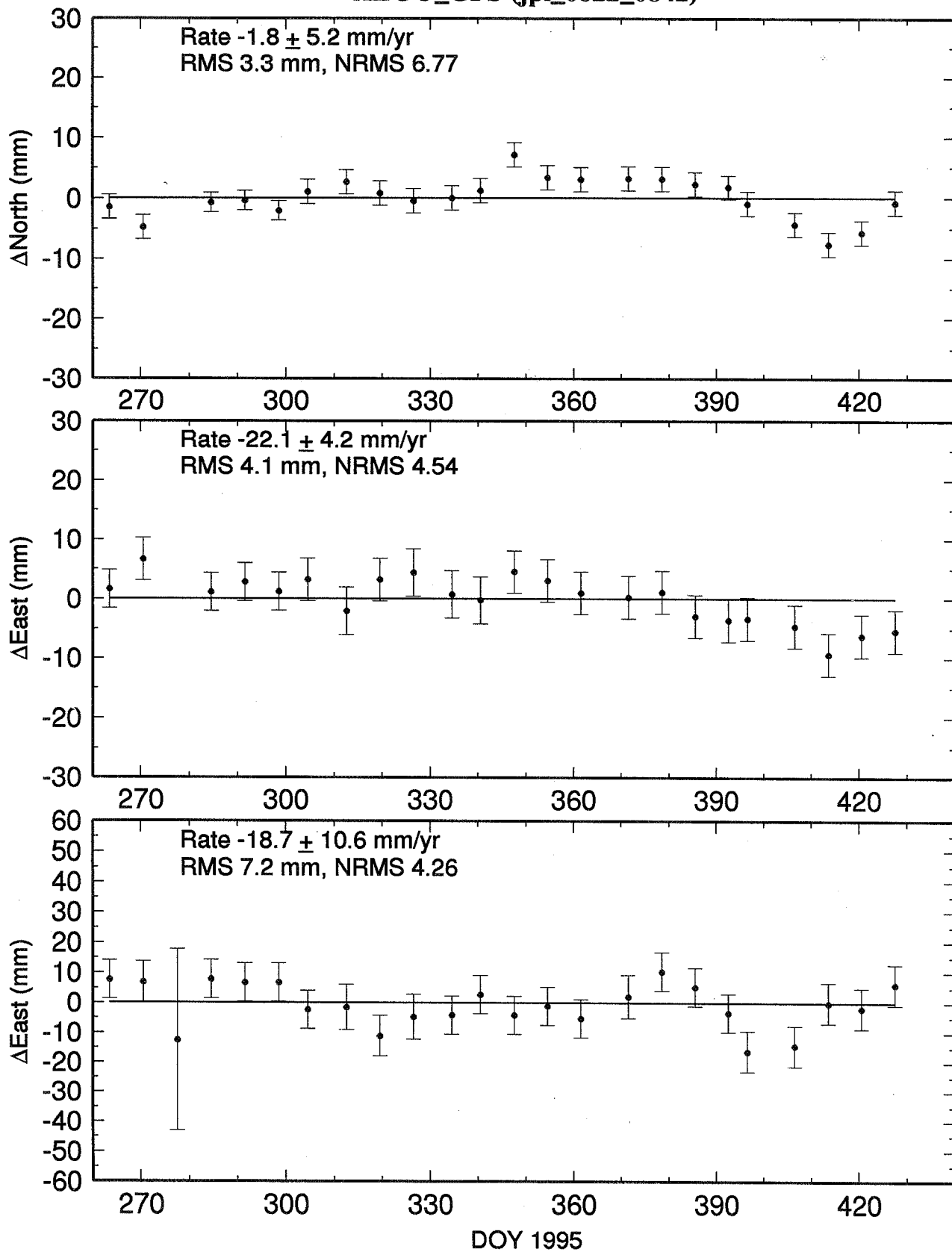
ALGO_GPS (Comb_0819_0842)



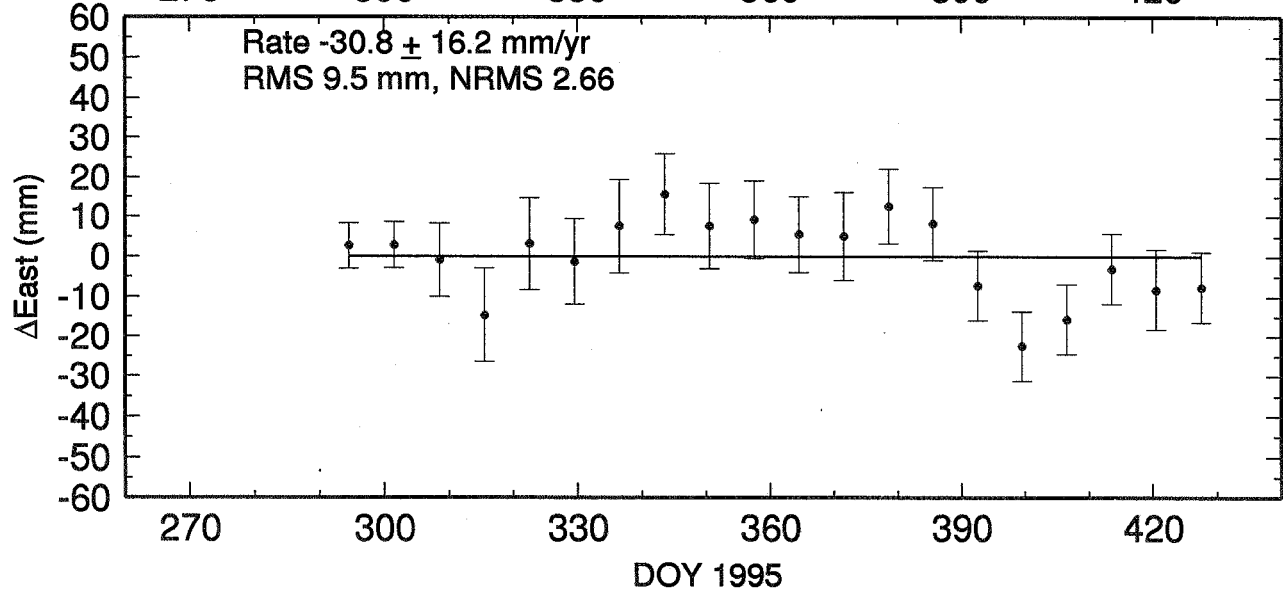
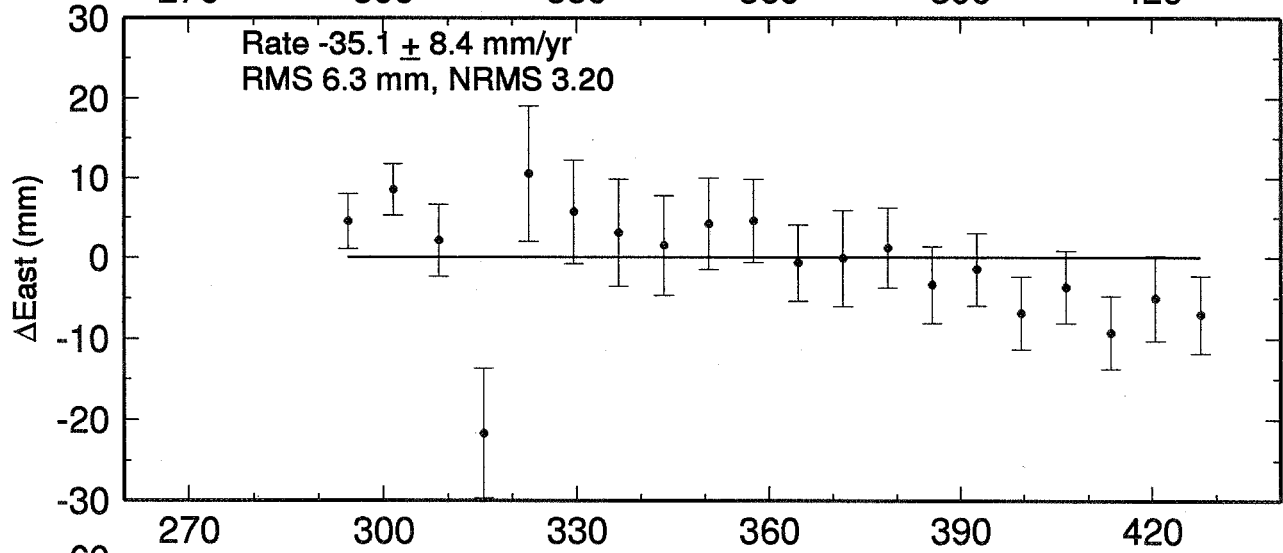
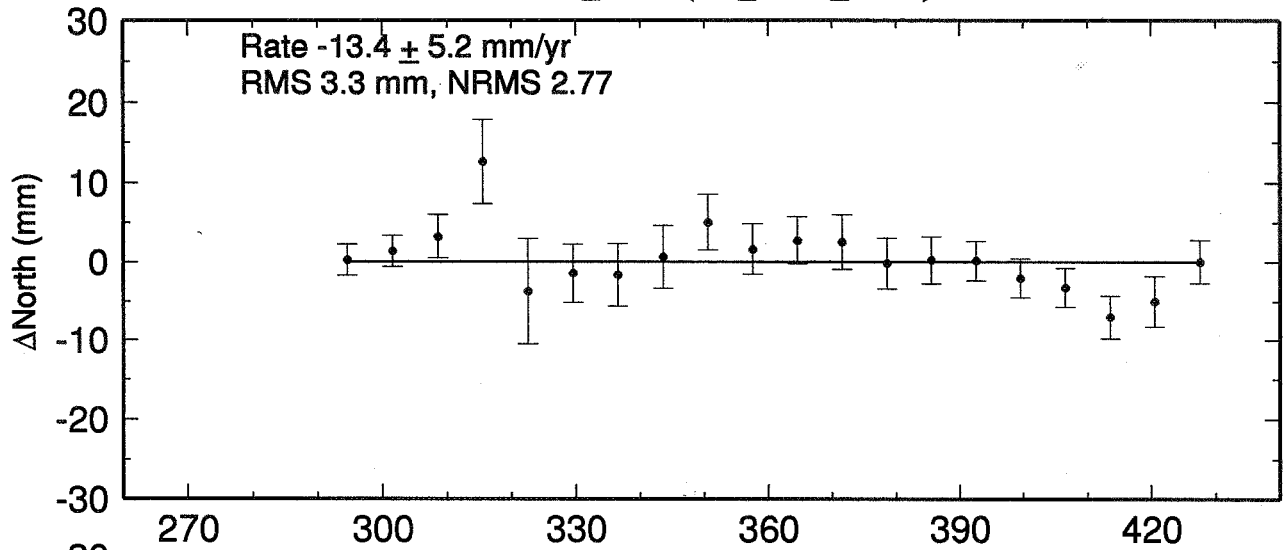
ALGO_GPS (cod_0822_0842)



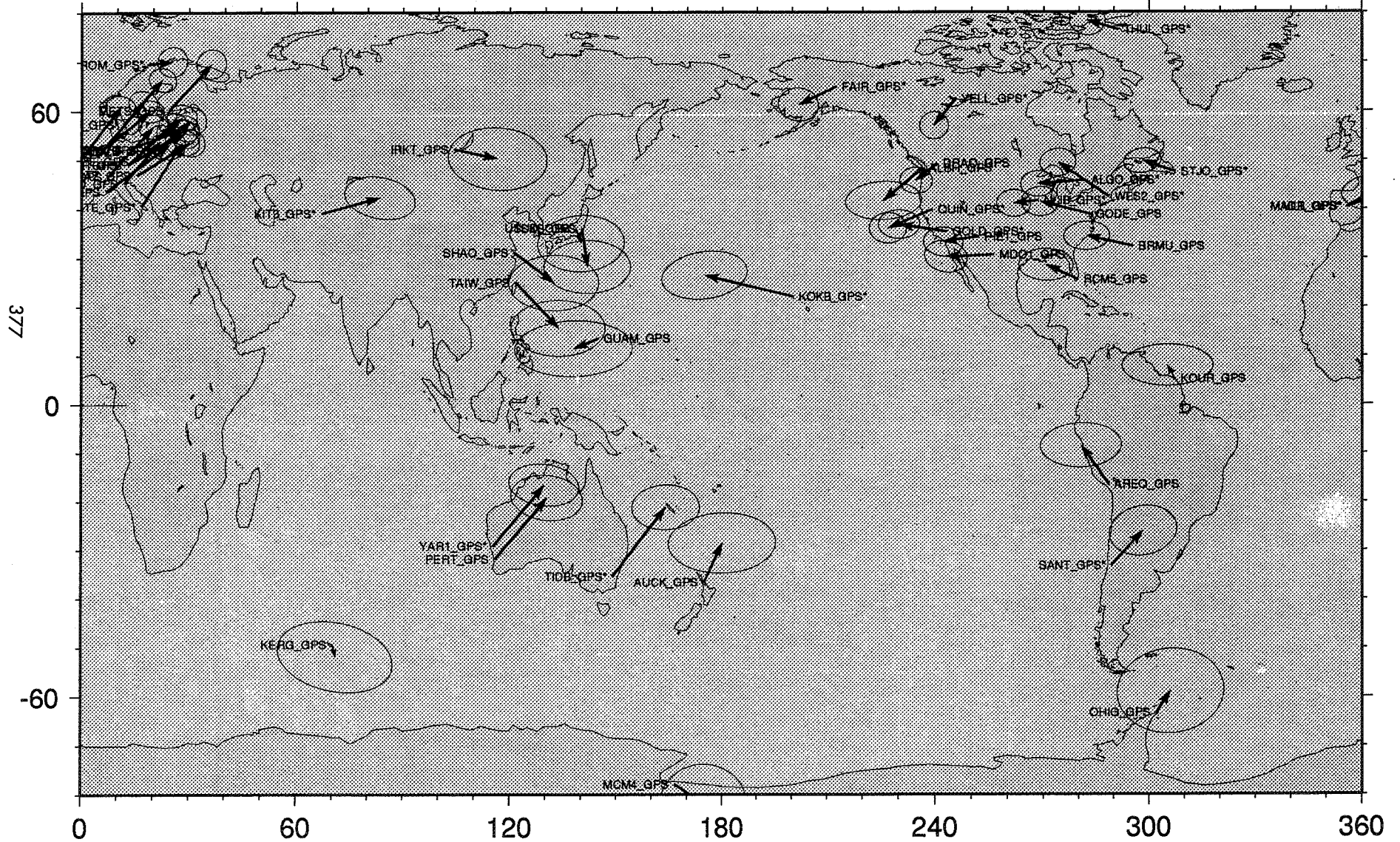
ALGO_GPS (jpl_0822_0842)



ALGO_GPS (sio_0822_0842)



New Global GPS sites (Excluding ITRF93 Sites)



Problems

- Analysis centers not reporting analysis changes
- Missing pieces in the SINEX files
- SINEX entries not the actual values being used in the processing.
- Bad eccentricity entries
- Weighting for centers: Need data decimation and assumed standard deviation of phase data

IONOSPHERIC PROFILING USING GPS/MET DATA

George Hajj and Larry Romans

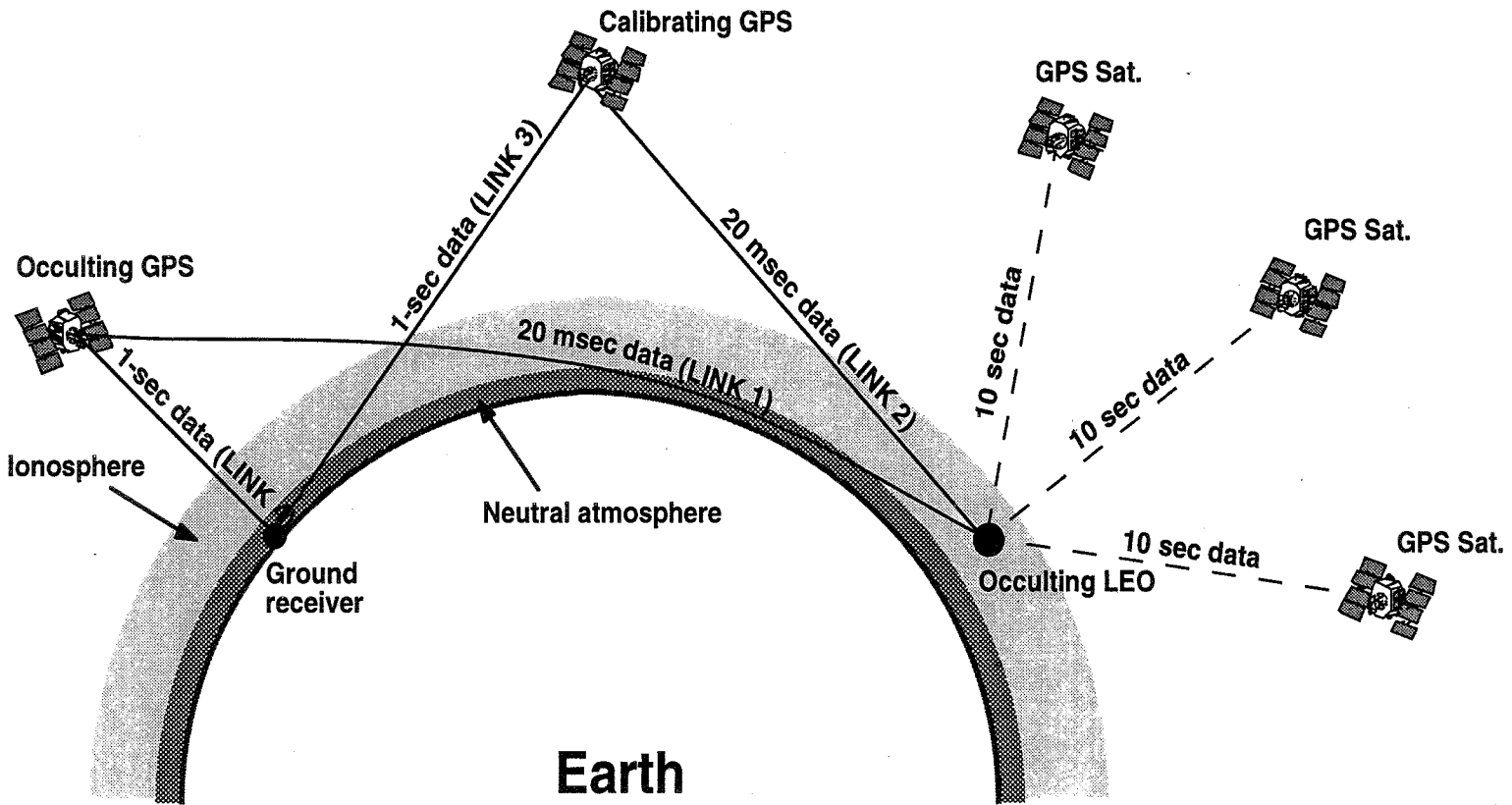
**Jet Propulsion Laboratory
California Institute of Technology**

**IGS Workshop
Silver Spring, 19-21 March, 1996**

SCOPE OF TALK

- Description of GPS occultation technique
- GPS/MET data processing system
- Example of GPS/MET data products
 - Temperature and water vapor profiles (Kursinski et al. *Science*, Vol. 271, pp. 1107-1110, 1996)
 - Ionospheric profiles (Hajj and Romans, *Proc. of the Institute of Navigation 52nd Annual Meeting*, Cambridge, Mass., June 19-21, 1996)
- Preliminary validation of ionospheric profiles

CALIBRATION OF GPS-LEO OCCULTATION SIGNAL



OBTAINING TEMPERATURE AND PRESSURE FROM REFRACTIVITY

$$N = (n-1) \times 10^6 = \text{Hydrostatic } 77.6 \frac{P}{T} + \text{Moist } 3.73 \times 10^5 \frac{P_W}{T^2} - \text{Ionosphere } 40.3 \times 10^6 \frac{n_e}{f^2} \\ + \text{higher order ionospheric terms}$$

- Equation of state

$$P = \frac{\rho RT}{m}$$

- Hydrostatic equilibrium equation

$$\frac{\partial P}{\partial h} = -g\rho$$

n = index of refraction

N = refractivity

P = total pressure

T = temperature

P_W = water vapor partial pressure

n_e = electron density

f = operating frequency

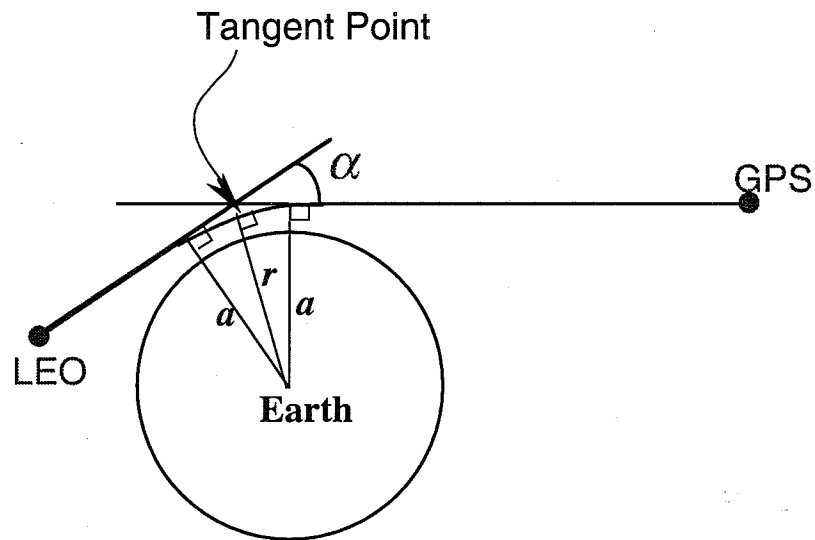
ρ = density

h = height

g = gravitational acceleration

OCCULTATION GEOMETRY AND THE ABEL TRANSFORM

LEO OBSERVING A GPS SATELLITE



383

- Assume spherical symmetry

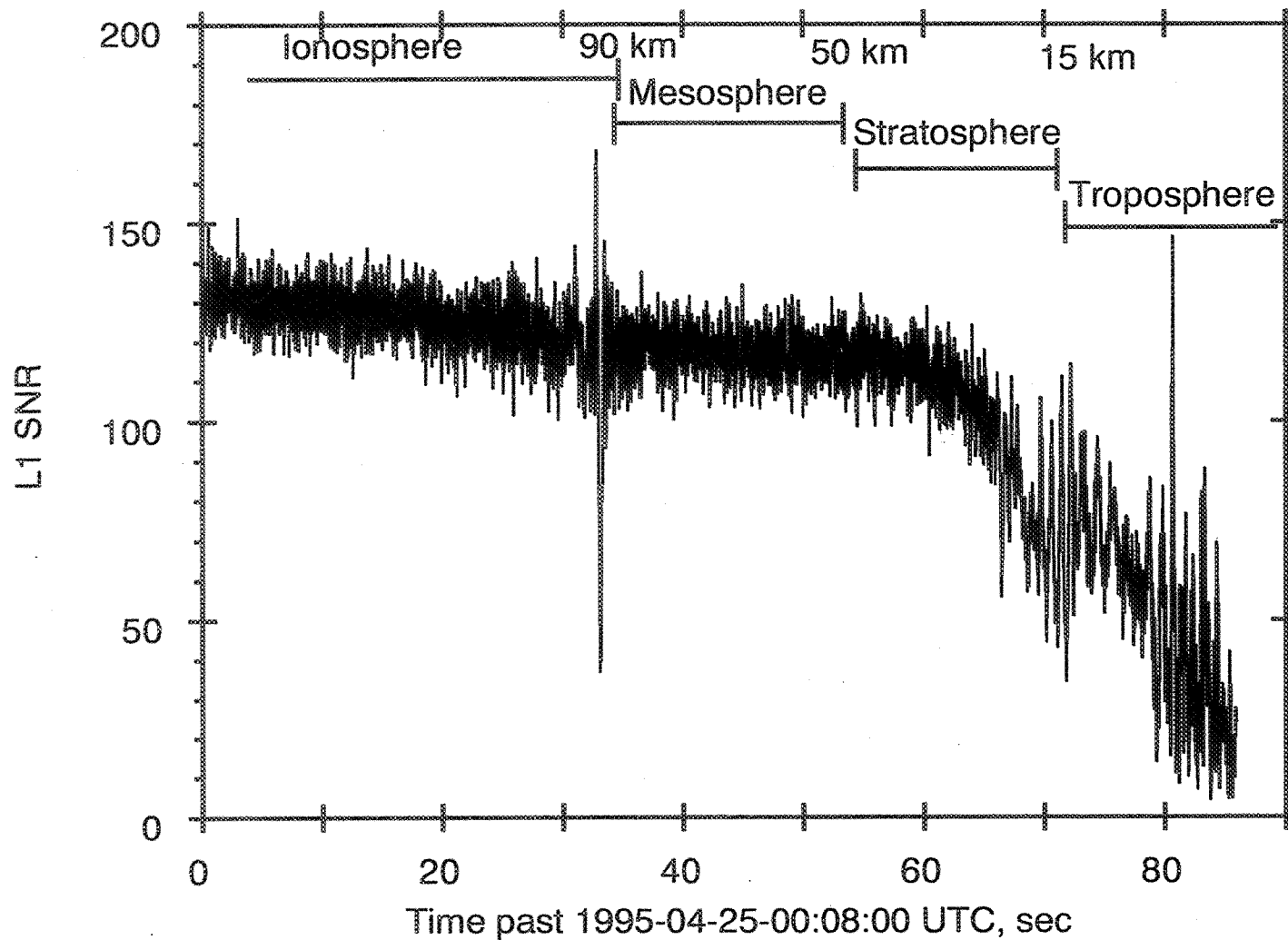
Forward propagation

$$\alpha = -2a \int_{r_0}^{\infty} \frac{d \ln(n) / dr}{\sqrt{r^2 n^2 - a^2}} dr$$

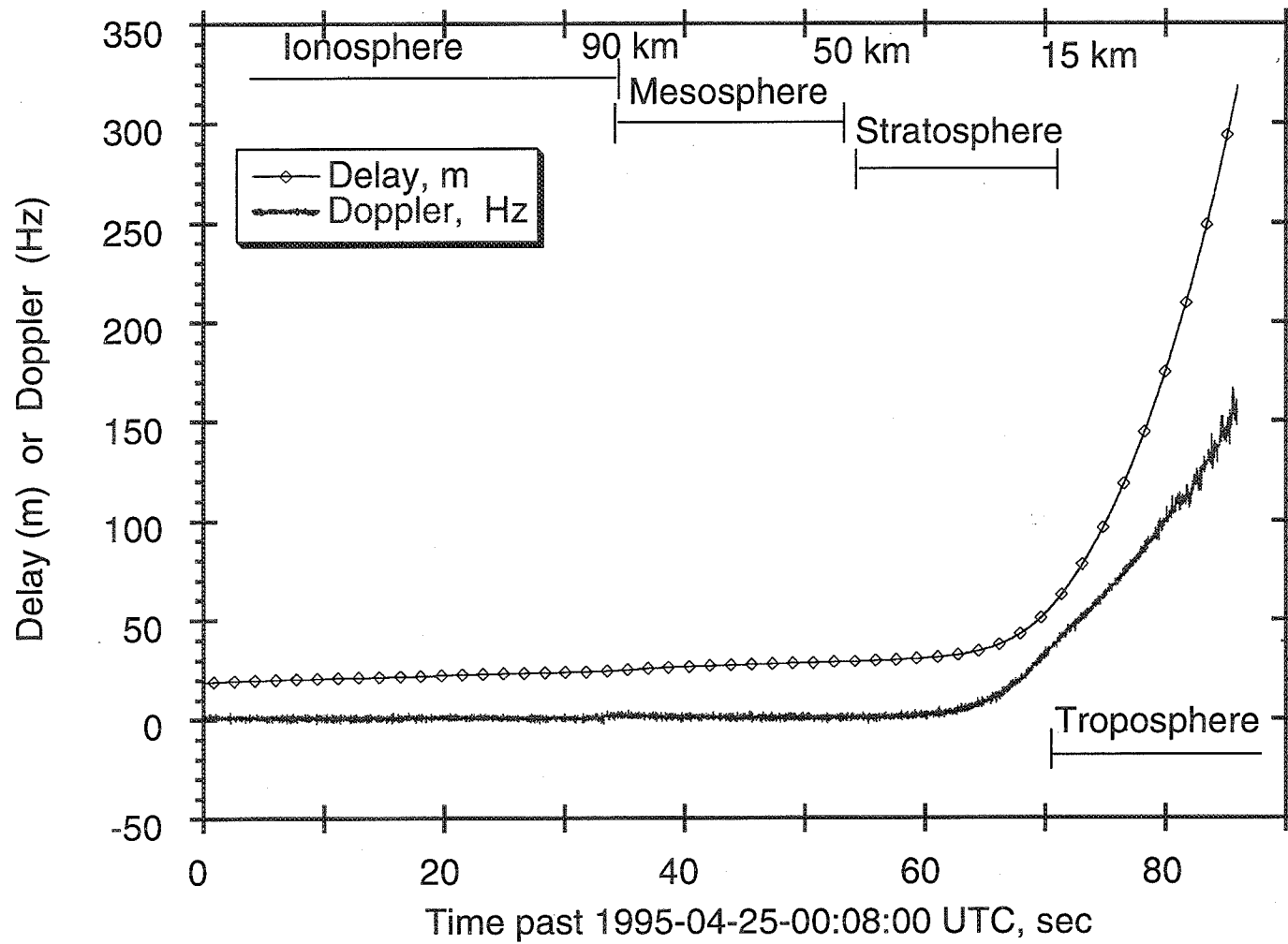
Abel inversion

$$\Rightarrow \ln(n(r)) = \frac{1}{\pi} \int_{nr}^{\infty} \frac{\alpha}{\sqrt{a^2 - r^2 n^2}} da$$

Signal to noise ratio of occulting L1 signal

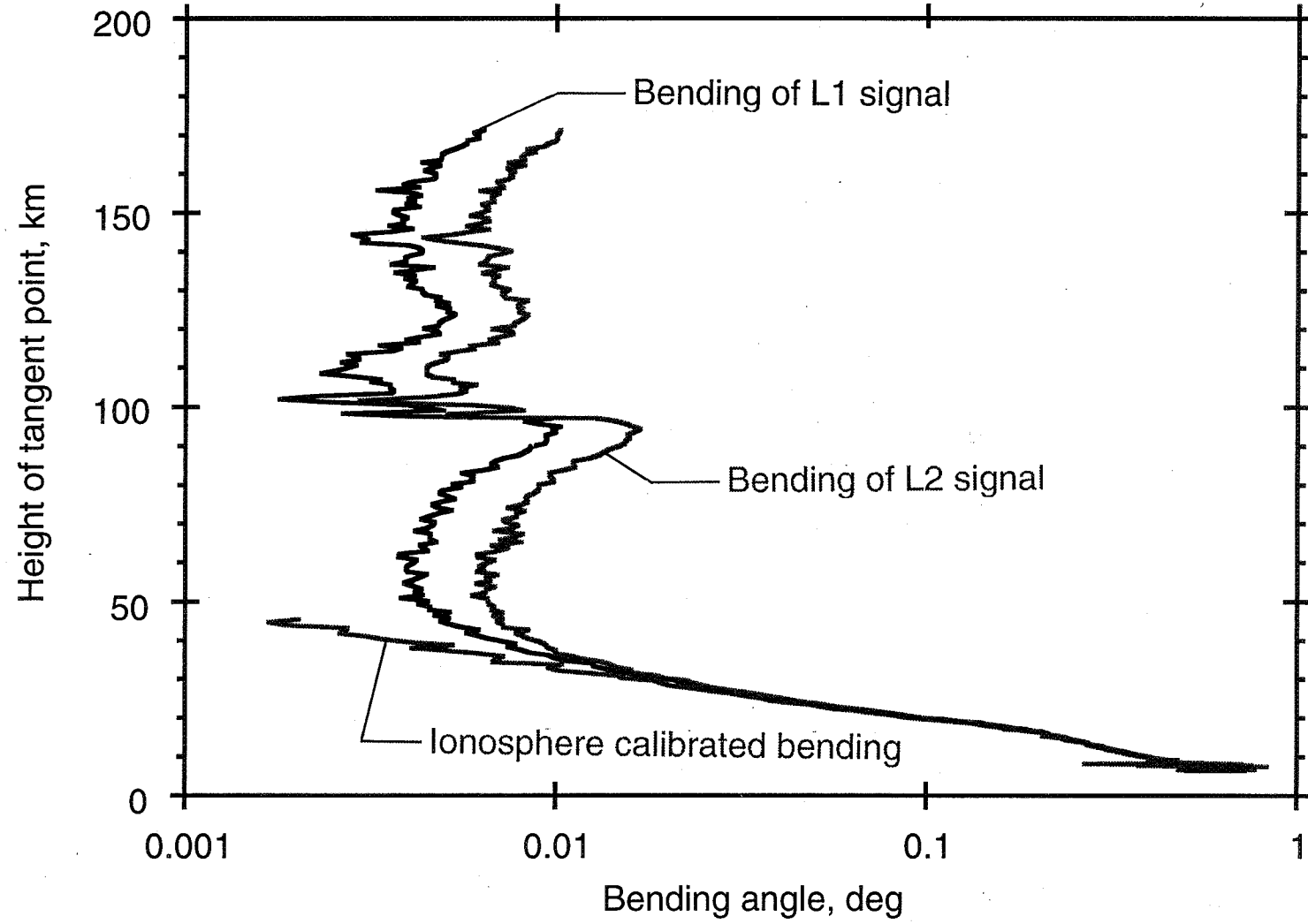


Extra delay and Doppler shift of L1 signal due to atmosphere



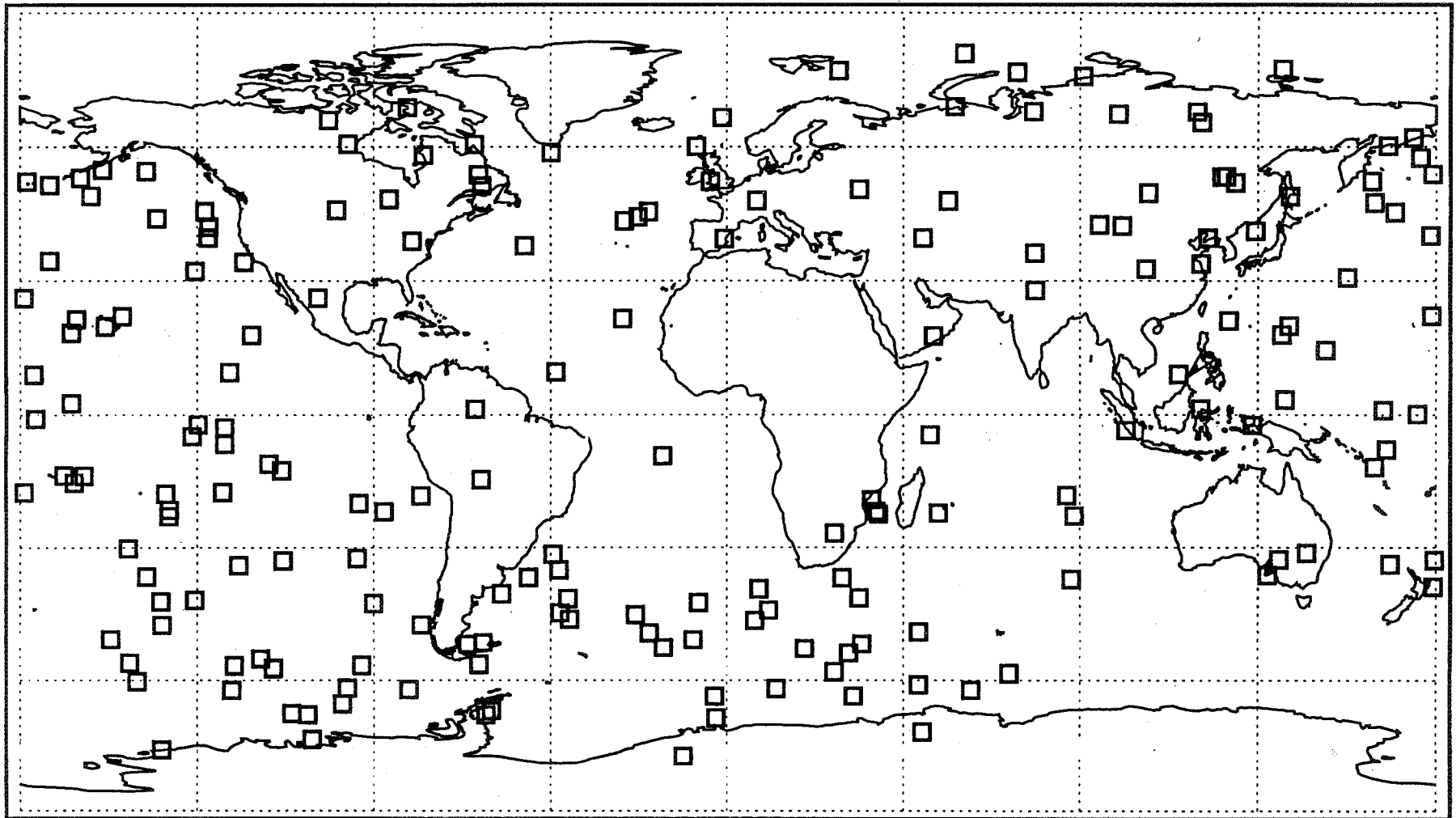
Bending of signal as a function of height from surface

Occultation at -14 N. Lat, 190 E. Lon, 95-4-25, noon local time

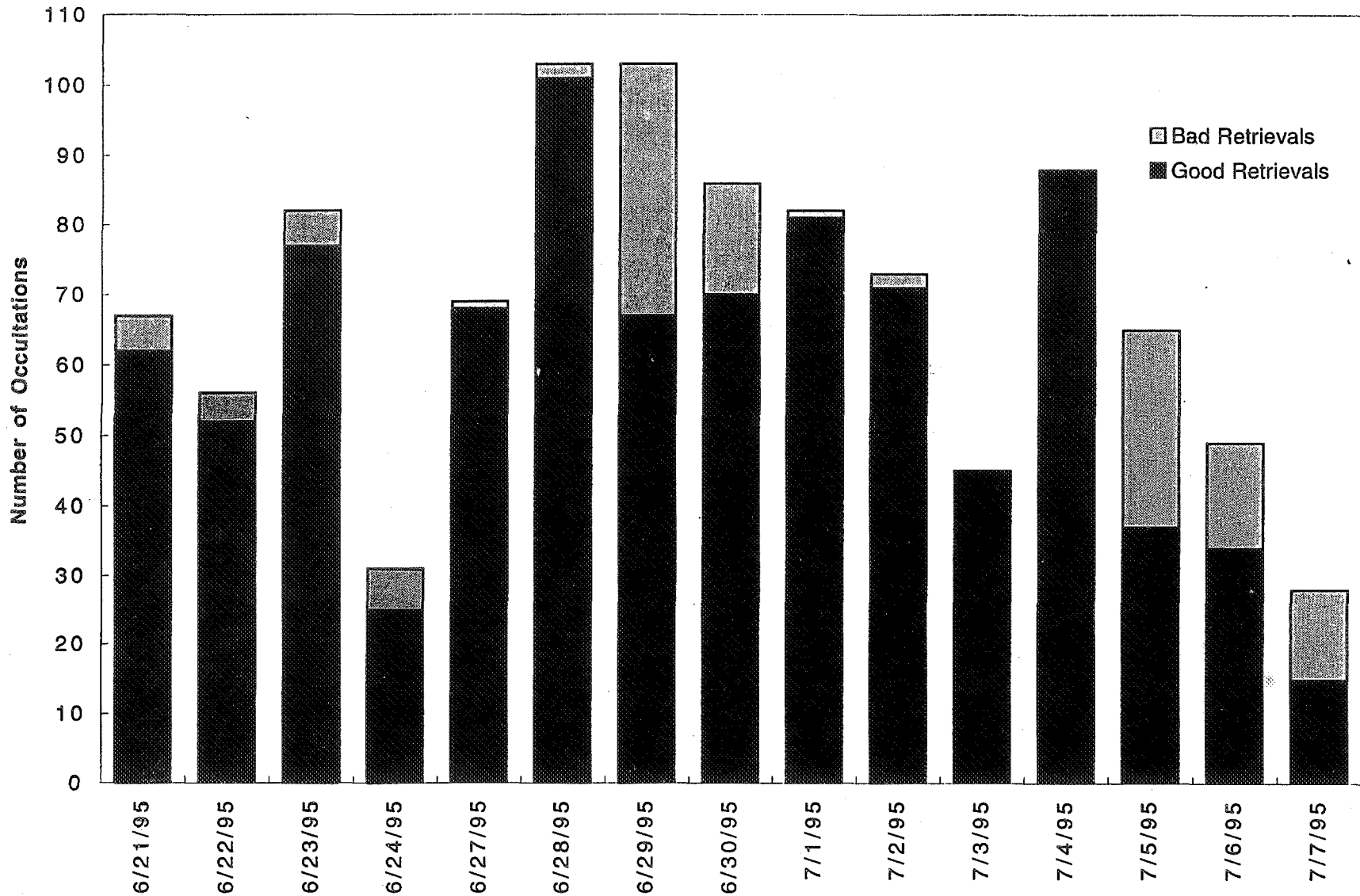


Occultation Locations for

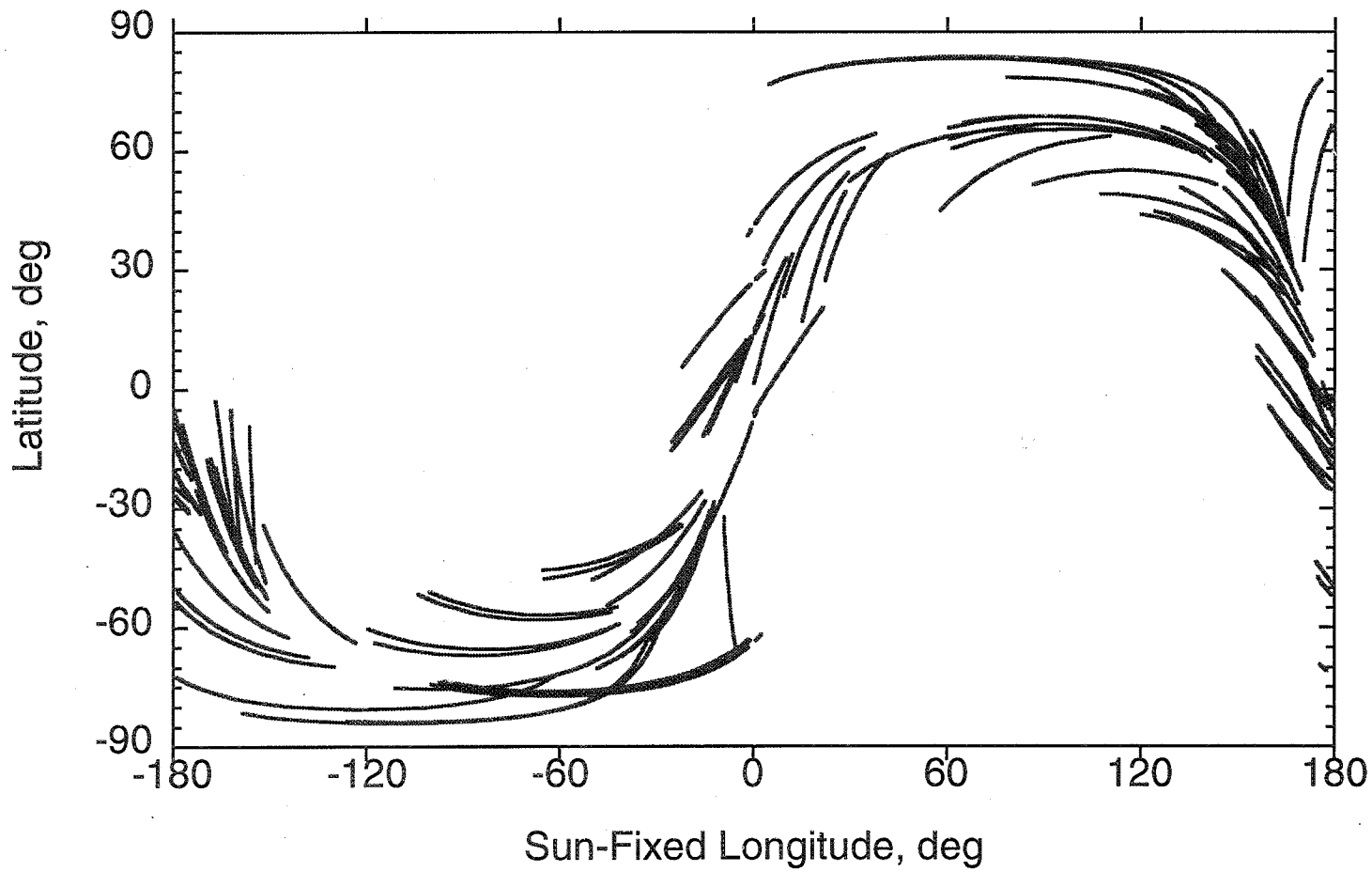
95/04/24, 95/04/25, 95/05/04 and 95/05/05



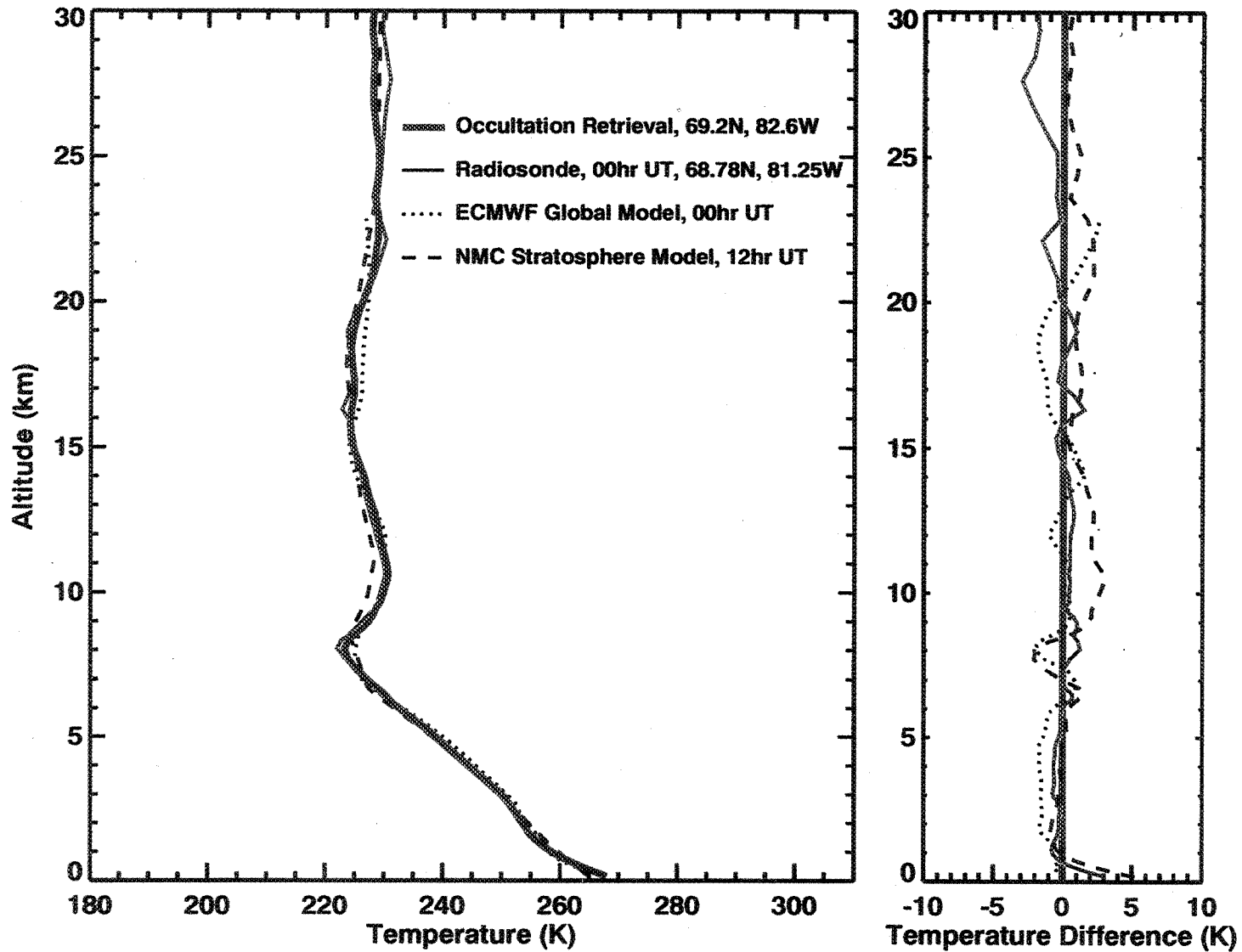
Occultations - June/July 1995



**GPS/MET COVERAGE IN SUN-FIXED COORDINATES IN 24 HOURS,
MAY 4, 1995**

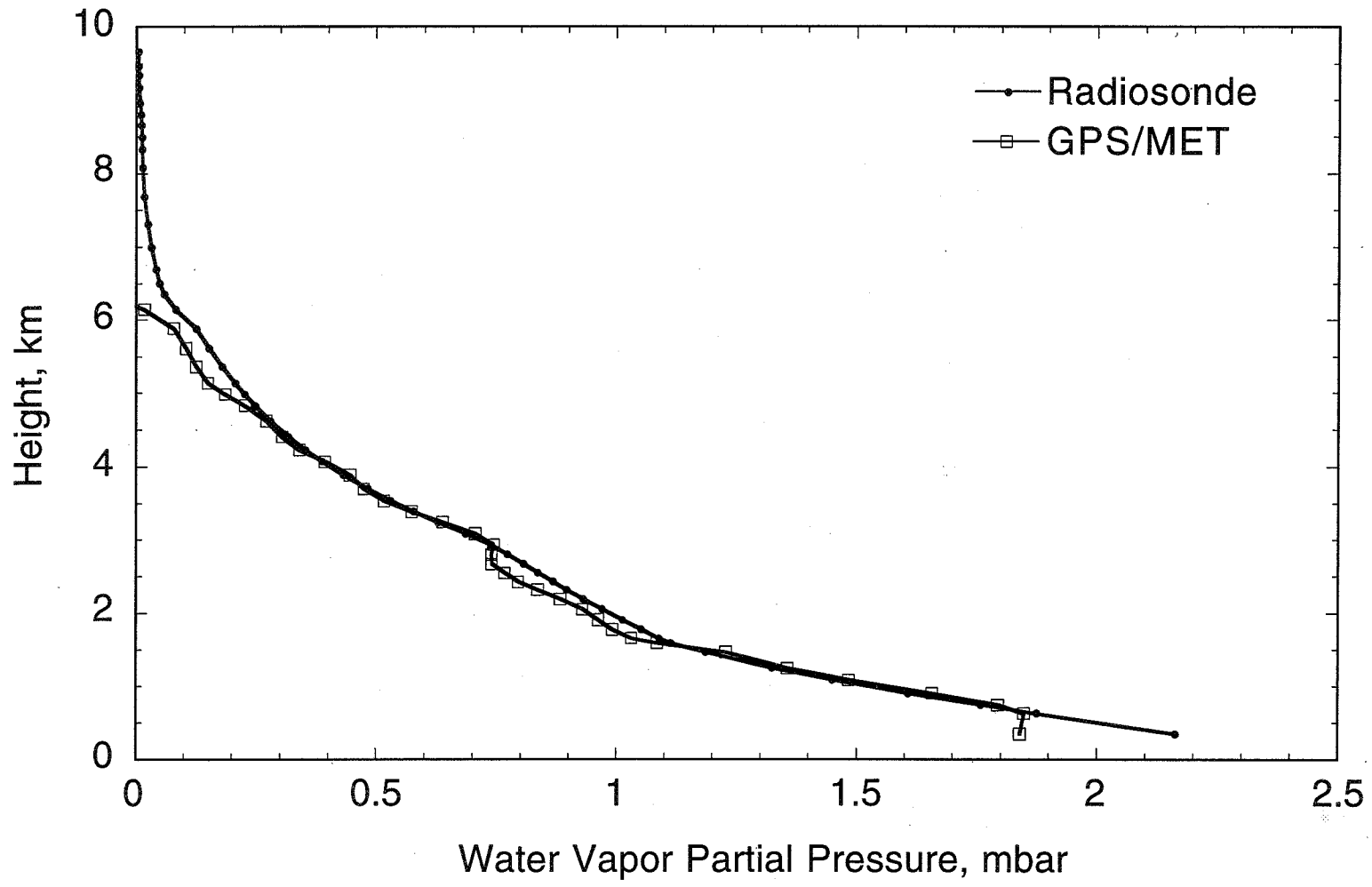


Hall Beach, Northwest Territories, 1995/05/05 at 01:33



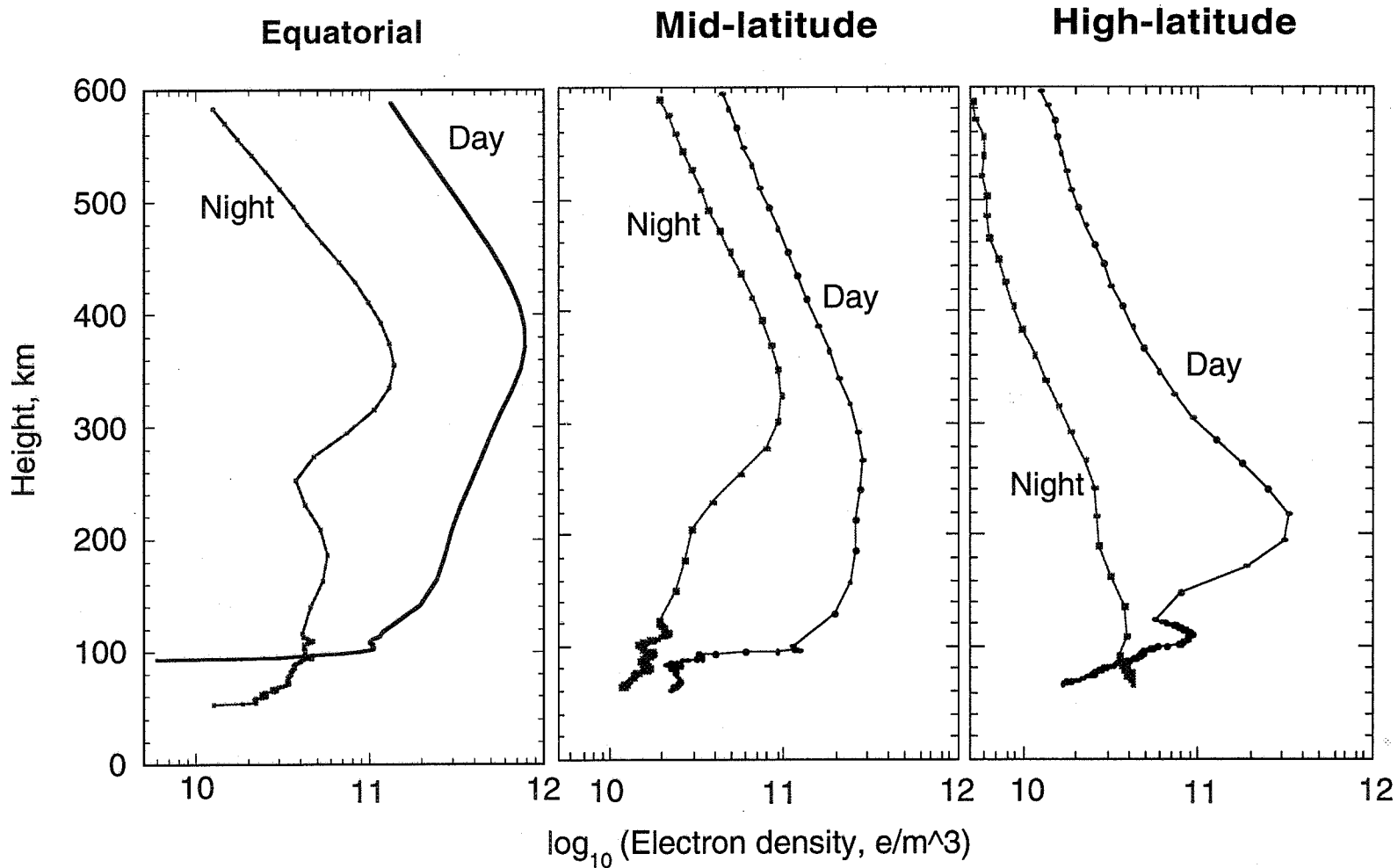
390

WATER VAPOR PARTIAL PRESSURE MEASUREMENTS High Latitude Region

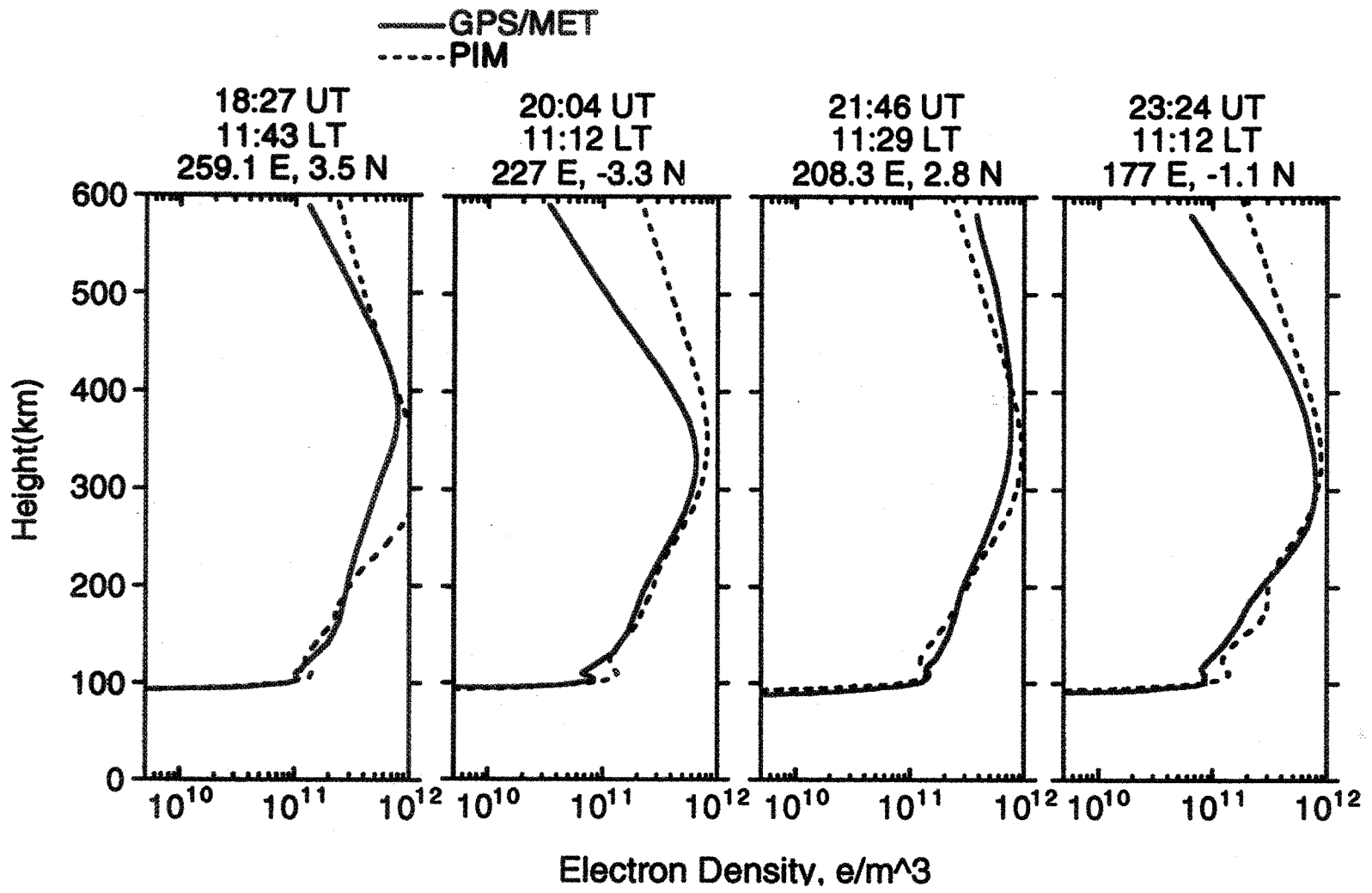


Electron density profiles from GPS/MET for May 4, 1995 (spherical symmetry assumed)

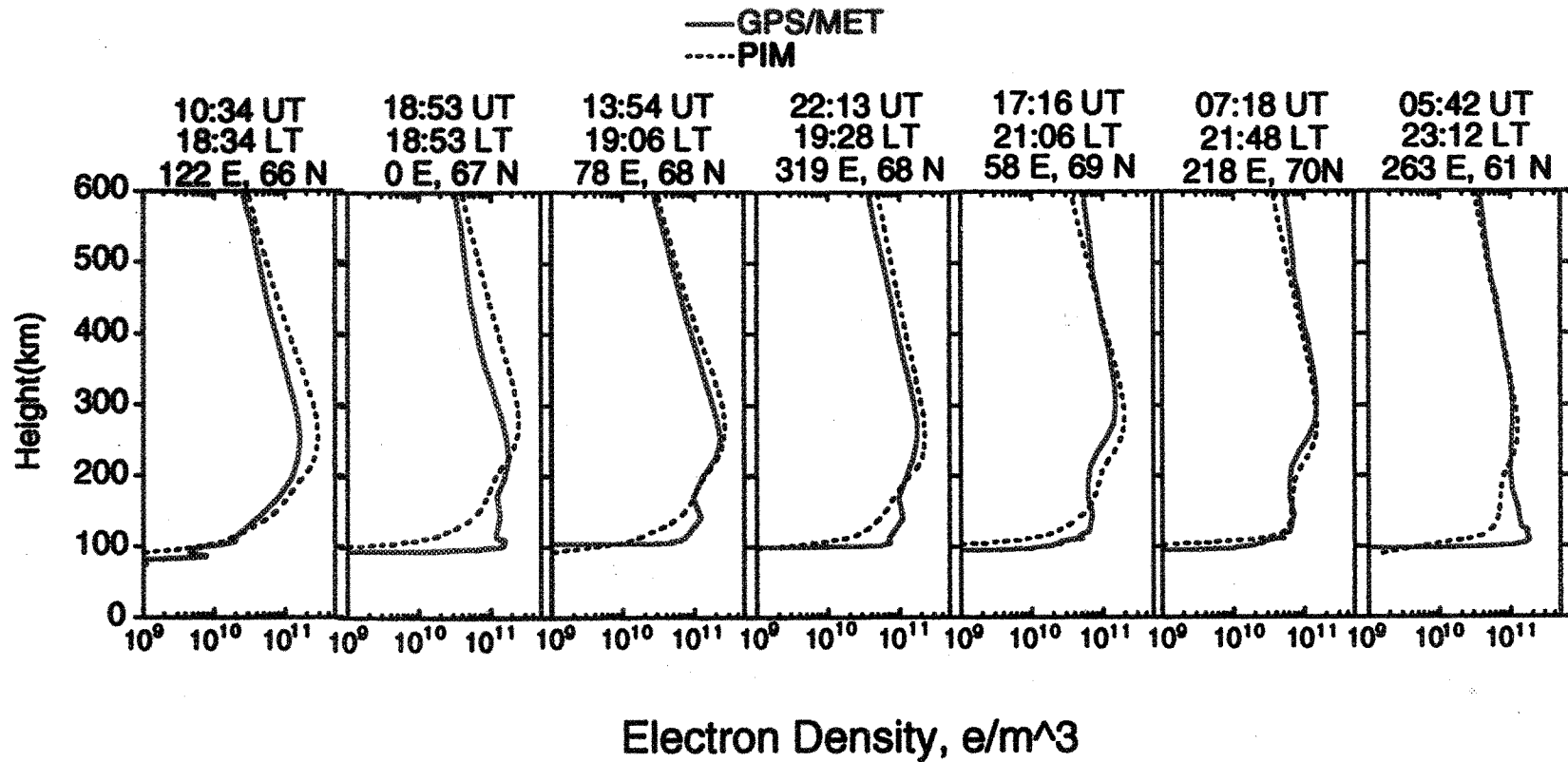
— About noon local time
— About midnight local time



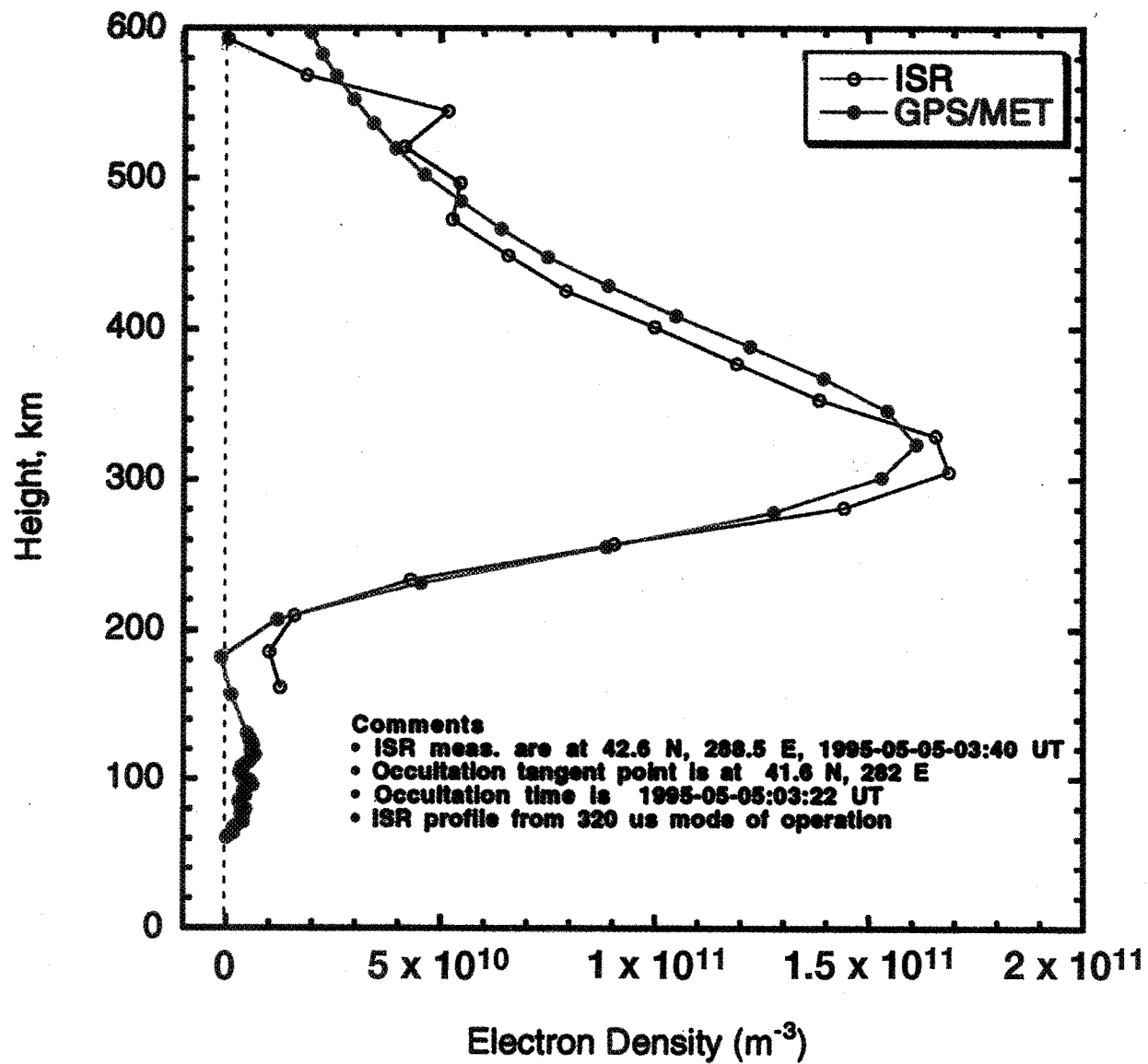
ELECTRON DENSITY PROFILES FROM GPS/MET AND THE PARAMETRIZED IONOSPHERIC MODEL OBTAINED FOR MAY 4, 1995 AT ABOUT THE SAME LATITUDE AND LOCAL TIME



**ELECTRON DENSITY PROFILES FROM GPS/MET AND THE
PARAMETRIZED IONOSPHERIC MODEL
OBTAINED FOR MAY 4, 1995 AT ABOUT THE SAME LATITUDE**



Electron density profiles measured at the Millstone Hill incoherent scatter radar and derived from a nearby GPS/MET occultation



CONCLUSION

- Advantages of GPS radio occultations in the ionosphere
 - provide a simple and relatively inexpensive means of profiling the ionosphere
 - provide electron density profiles with a high vertical resolution (1km)
 - provide a global and continuous coverage
- Disadvantages of GPS radio occultation in the ionosphere
 - The measurement is an integrated measurement over a large distance
 - Spherical symmetry assumption in the ionosphere introduces an error of 0-50% in determining the peak electron density
 - Imposing constraints on horizontal gradient (such as from ground zenith TEC maps) can bring the error to < 20% (Hajj et al., *Int. J. Imaging Sys. and Tech.*, Vol. 5, pp. 174-184, 1994)

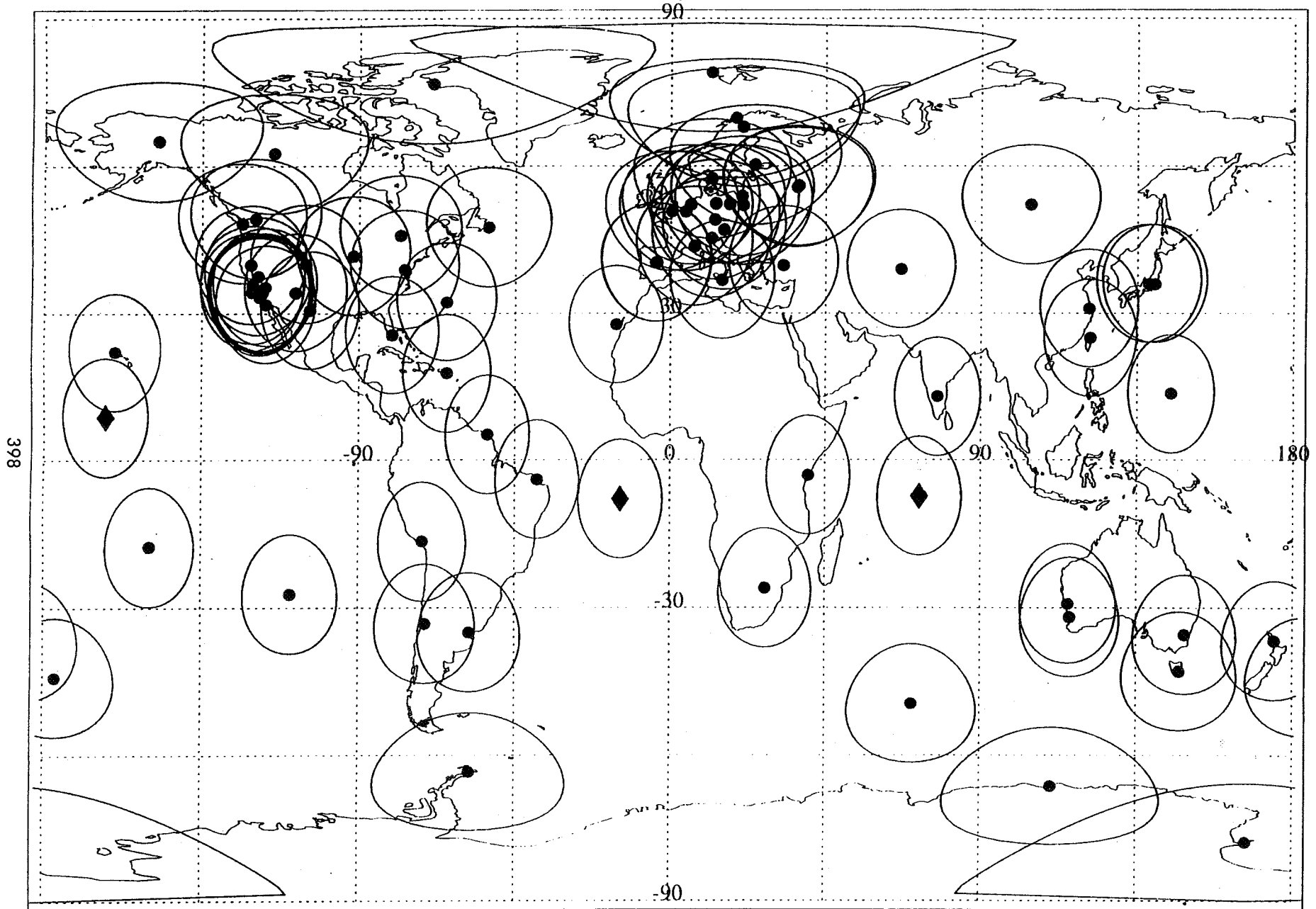
Global Ionospheric Mapping using GPS: Validation and Future Prospects

Brian D. Wilson
Anthony J. Mannucci
Dah-Ning Yuan
Christian Ho
Xiaoqing Pi
Tom Runge
Ulf J. Lindqwister

GPS Networks and Operations Group
Tracking Systems and Applications Section
Jet Propulsion Laboratory, California Institute of Technology

IGS Workshop, Silver Spring, MD
March 21, 1996

GPS Global Network: Coverage at Ionospheric Altitudes
February 1996



10 degree elevation mask. Effective shell height of 400km.

Ionospheric Applications

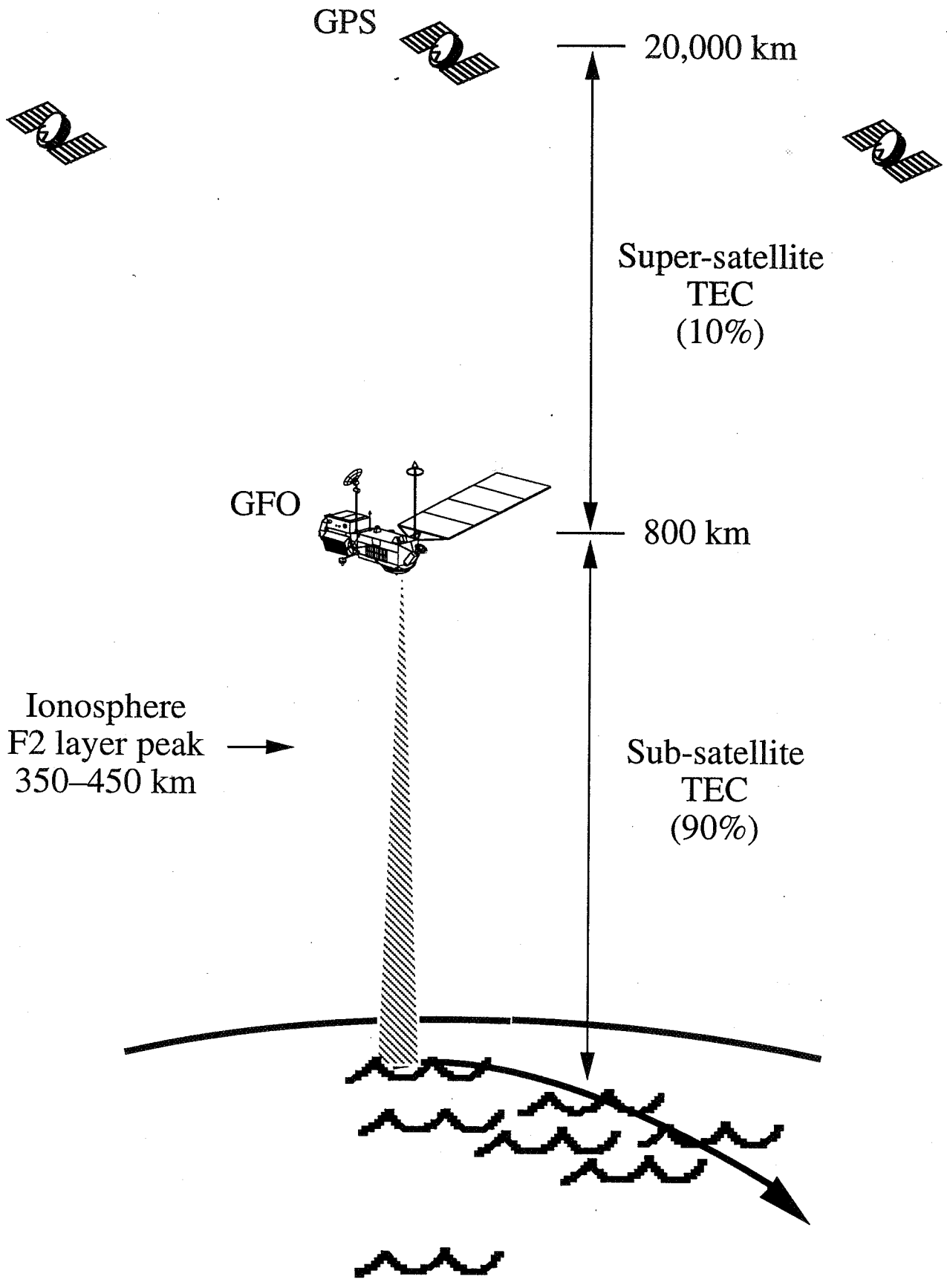
- Single-site GPS-based ionospheric calibrations for S-band tracking applications and local ionospheric studies.
- Global Ionospheric Mapping (GIM) with an accuracy of 5–10 TEC units.
 - Use GPS data from 95+ dual-frequency receiver sites.
 - Snapshot of the ionosphere every half-hour.
 - Optimal combination of model information and iono. measurements (near real-time Kalman filter).
- Ionospheric calibration for remote tracking sites without a GPS receiver.
- Global calibration of single-frequency ocean altimetry missions: ERS-1, ERS-2, and GEOSAT follow-on (GFO).
- Ionospheric correction maps for single-frequency GPS users.
- Real-time Wide Area Differential GPS (WADGPS) over the continental U. S. or the entire globe.
- Near real-time ionospheric storm monitoring/forecasting (space weather).
- Ionospheric studies: GPS signal fading, ionospheric scintillation.

Tropospheric Applications

- Single-site GPS-based tropospheric calibrations for tracking applications and local water vapor studies.
- Troposphere is too variable to interpolate a global map of water vapor, but can compute local measurements of water vapor in near real-time.
- Estimate the wet and dry zenith delays separately using temperature and pressure data from a local meteorology package.
- Convert wet delay to real-time precipitable water vapor (PWV), a primary input to weather prediction models.
- Water vapor content is the most uncertain parameter in weather prediction.

Space-borne GPS Applications

- Occultation data from a dual-frequency GPS receiver on a low-Earth orbiter (LEO).
- Ionosphere: Track the non-geometric changes in phase to compute electron density profiles as a function of altitude.
- Neutral atmosphere: Invert the ray-bending data to compute the index of refraction as a function of altitude. From this, one can compute temperature or water vapor as a function of altitude.
- Proof of concept: GPS/MET mission currently flying.
- Space-borne GPS constellation: autonomous navigation and occultation science in a small micro-satellite.
- Global 3D ionospheric “tomography”.



Types of Global Ionosphere Models

- Mathematical/Physical
first principles calculation of ion densities, temperatures and velocities
SUPIM* (Graham Bailey et al., Univ. of Sheffield, G.B.), Schunk et al., Utah State Univ.
- Climatological
month-by-month fits to data, organized by geographic location, local time, season, solar and geomagnetic activity
Bent* (1967), IRI-90*, PIM* (Parametrized Ionosphere Model)
- Semi-empirical
a database of calculated ionosphere densities, adjusted by data
PRISM* (Parametrized Real-Time Ionosphere Model)
- Data-driven
interpolated measurements of total electron content
GIM* (Global Ionospheric Maps)

Question: What approach works "best"?

*Running at JPL

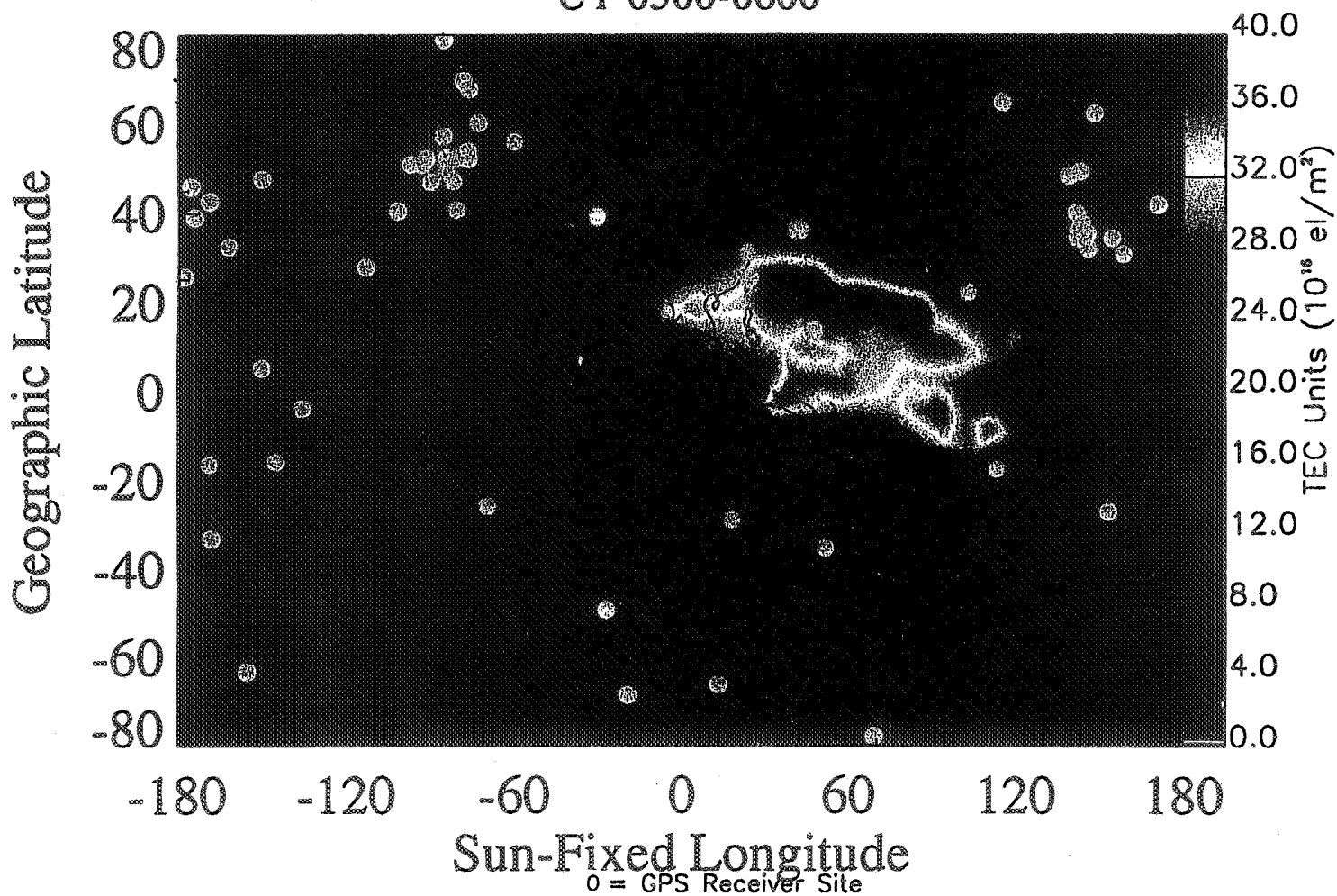
Global Ionospheric Maps (GIM)

- Data-driven maps based on interpolating GPS TEC measurements on global scales.
- Maps are updated every few minutes to hourly
- Self-calibrating: simultaneously solve for inter-frequency biases
- Accuracy: 5–10 TECU globally
- A flexible scheme based on sequential Kalman filtering
- Grid-based approach
- Interpolation algorithm based on cubic splines (spherical geometry)
- Solar-geomagnetic reference frame

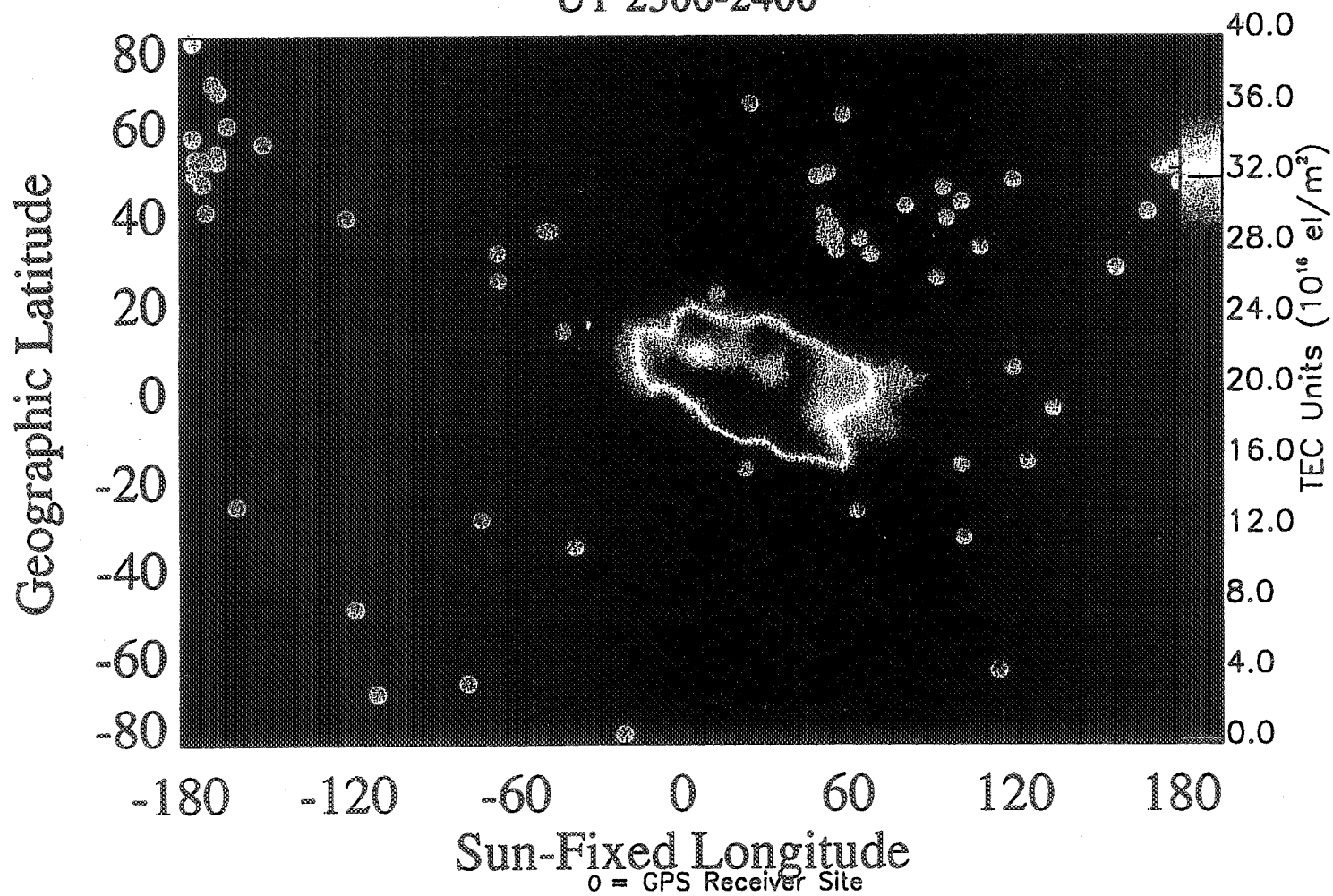
GIM combines data + models with appropriate weighting:

- Climatological models can be used to initialize or aid the maps
- A priori model electron density profiles can be scaled to avoid scaling slant measurements to vertical

Global Ionosphere Map: May 4, 1995
UT 0500-0600



Global Ionosphere Map: May 4, 1995
UT 2300-2400



Validation of Global Ionospheric Maps

TEC model validation:

- Extensive comparisons with vertical TEC data from the TOPEX dual-frequency altimeter.
- TOPEX (altitude 1330 km) is continuously operating and covers the latitude range 68S to 68N.
- TOPEX accuracy is approximately 3 TECU.

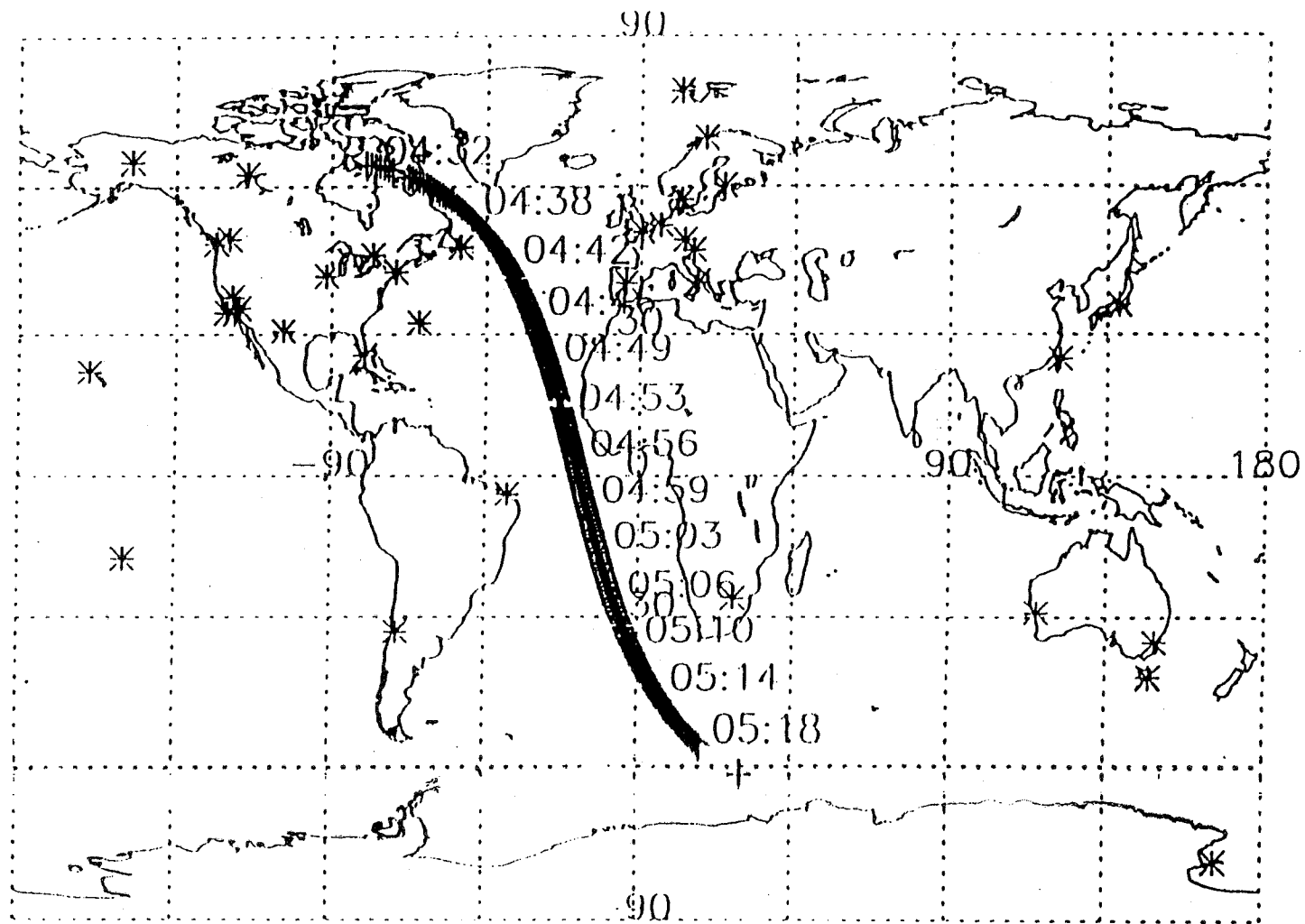
Intra-ionospheric model validation:

- LOS TEC from ALEXIS satellite (Los Alamos) orbiting at 800 km.
- Use GIM and Bent/IRI90 model info. to predict TEC below 800 km.
- Preliminary comparisons show 3–4 TECU agreement.

Comparisons with GPS/MET:

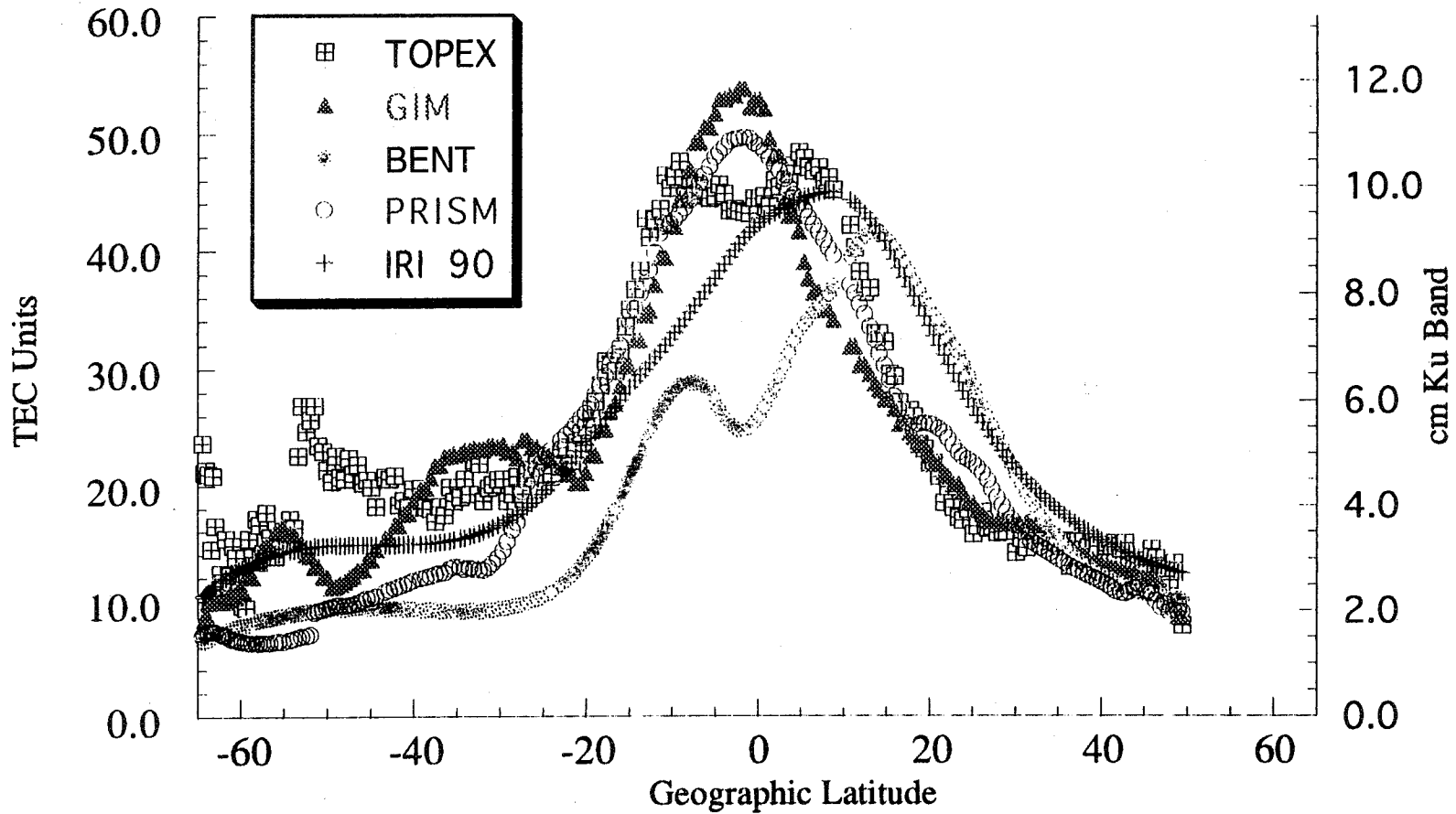
- TEC from GIM vs. integrated GPS/MET profile.
- Preliminary results show agreement to 2.3 TECU (RMS differences).

TOPEX Ground Track
August 17, 1993 — Pass 22
4.55-5.35 UT

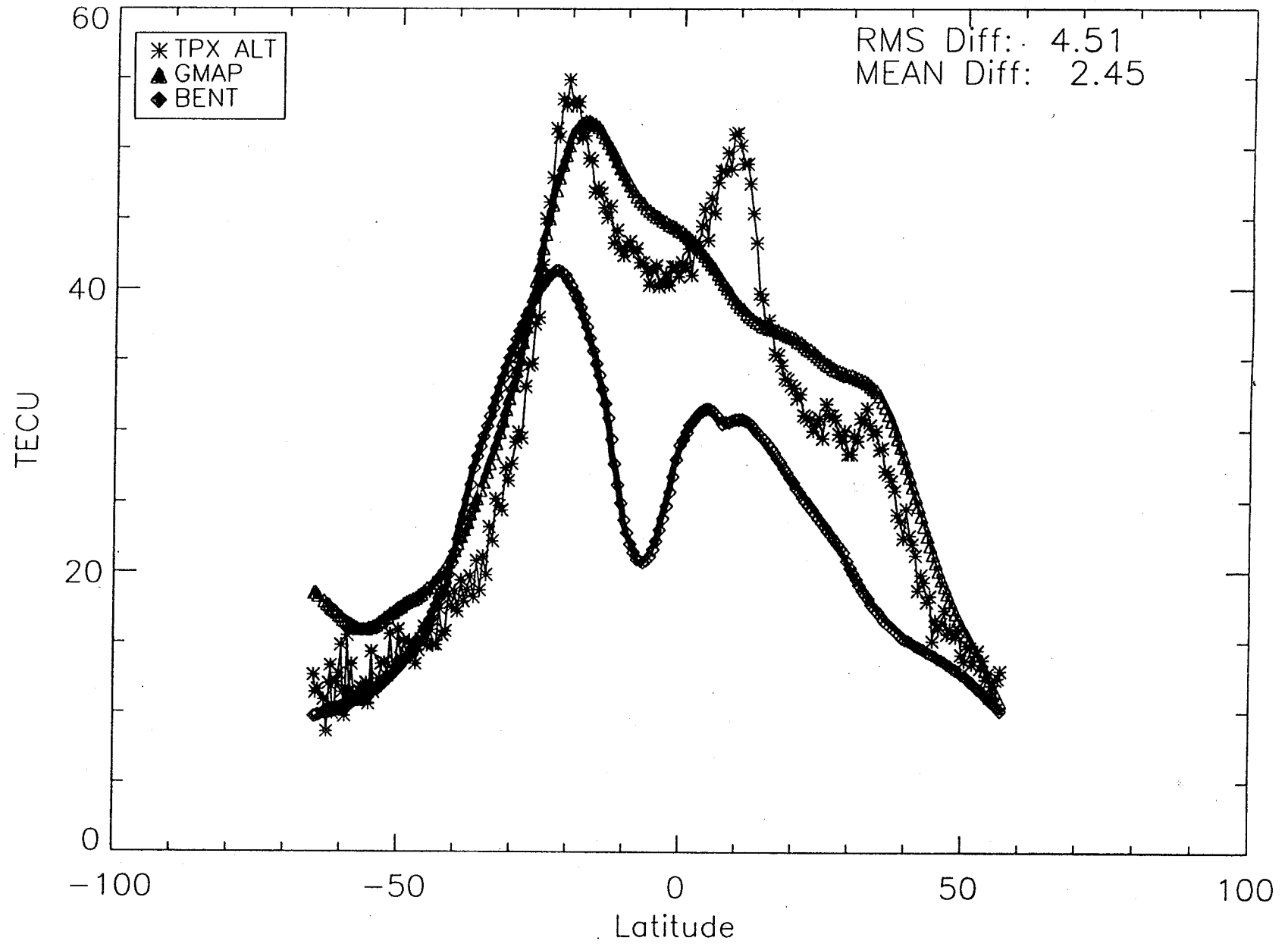


Comparisons with TOPEX TEC, August 17, 1993 Pass Time: 1.70-2.62 UT

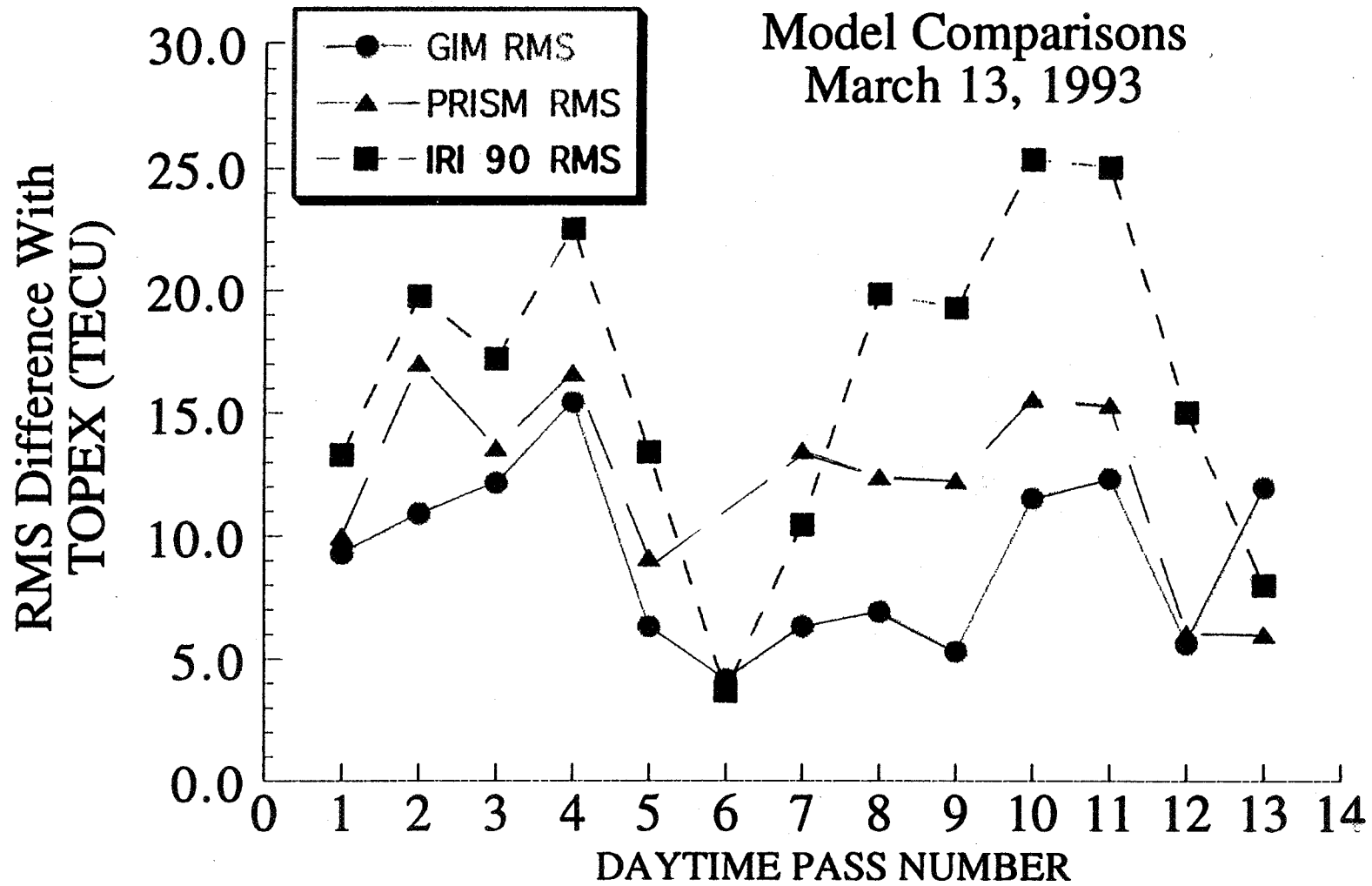
409



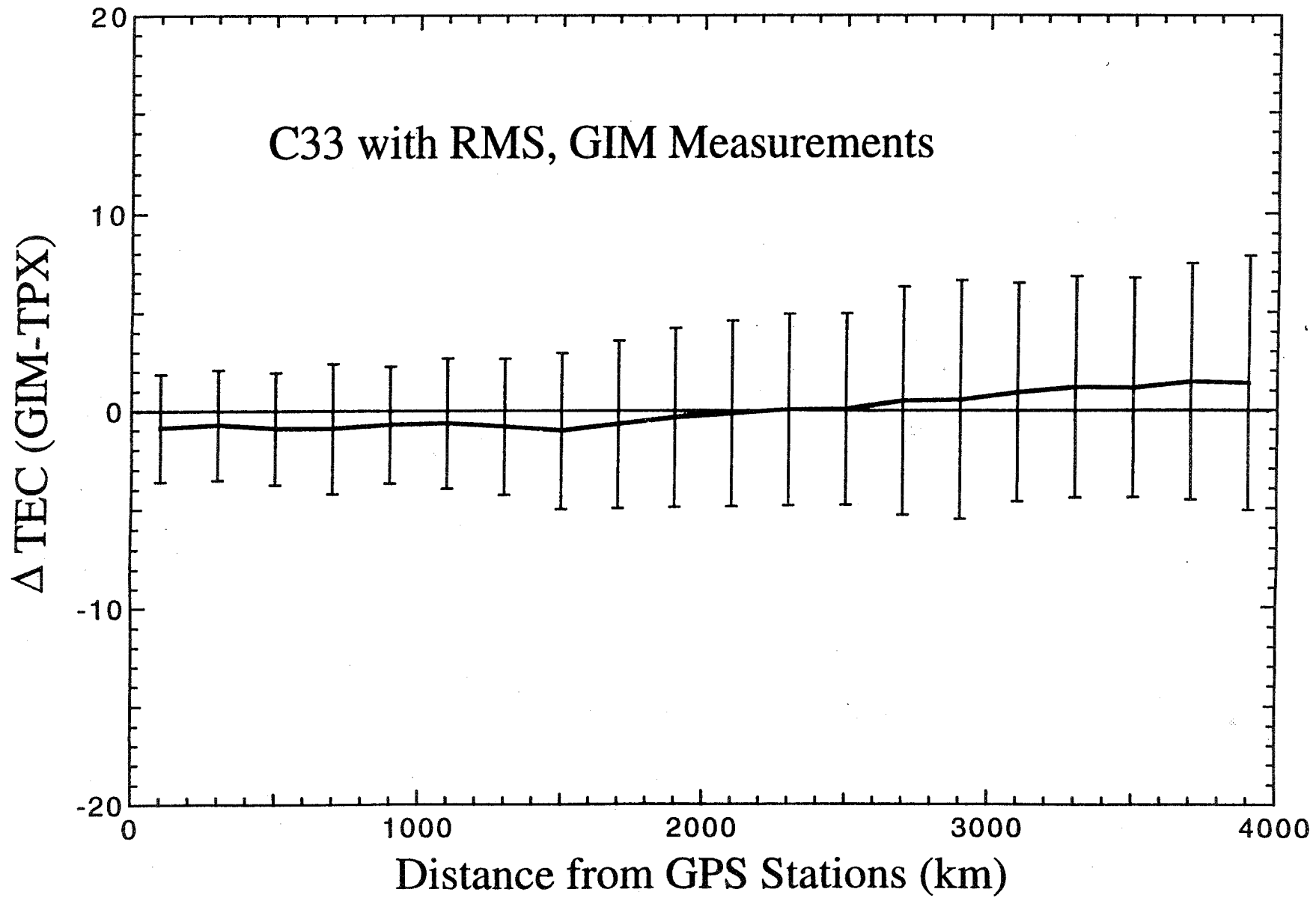
mgb13555.232_bentc2k9C.cmp
Begin: 20.05 End: 20.81 (hours)

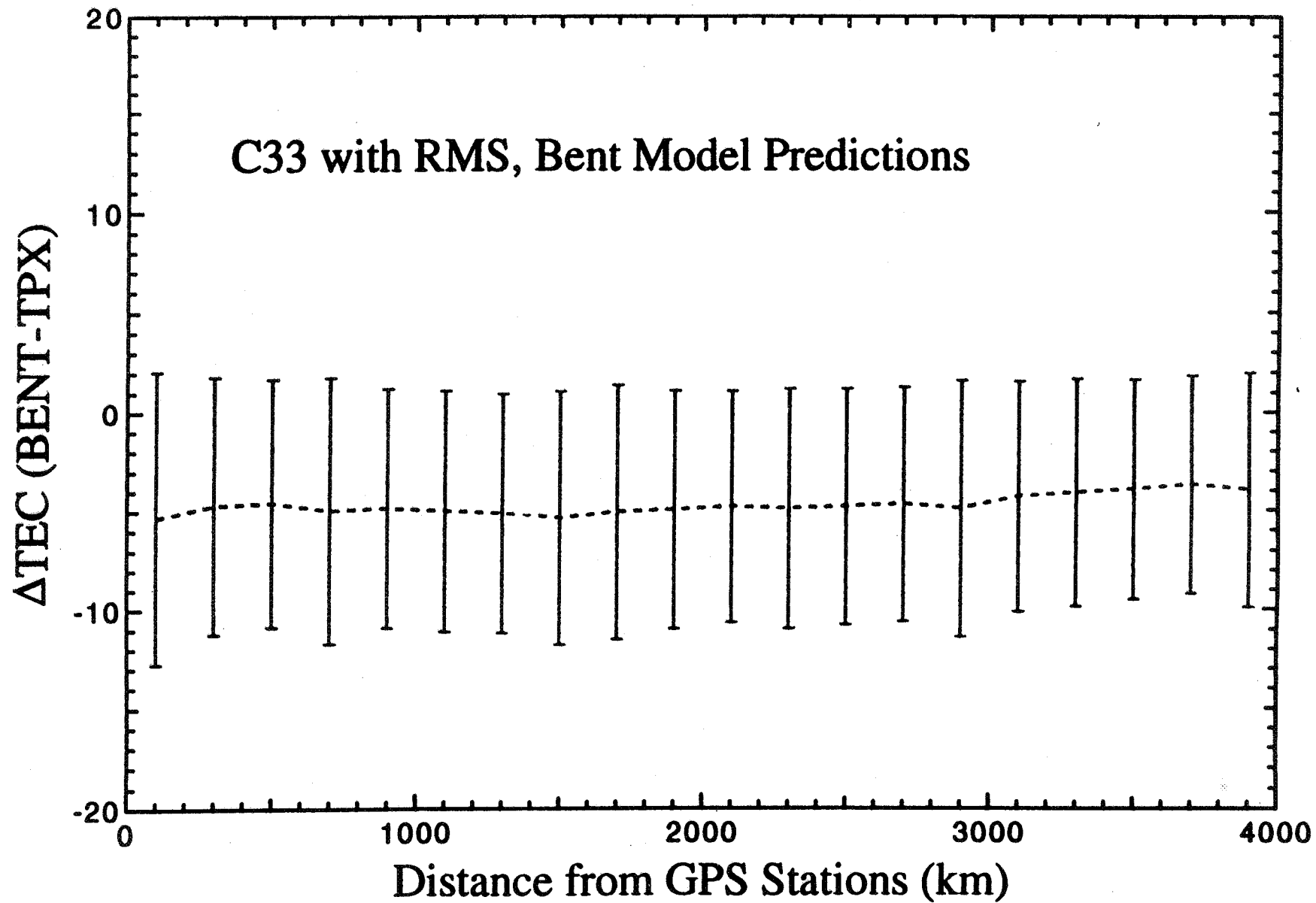


410



C33 with RMS, GIM Measurements



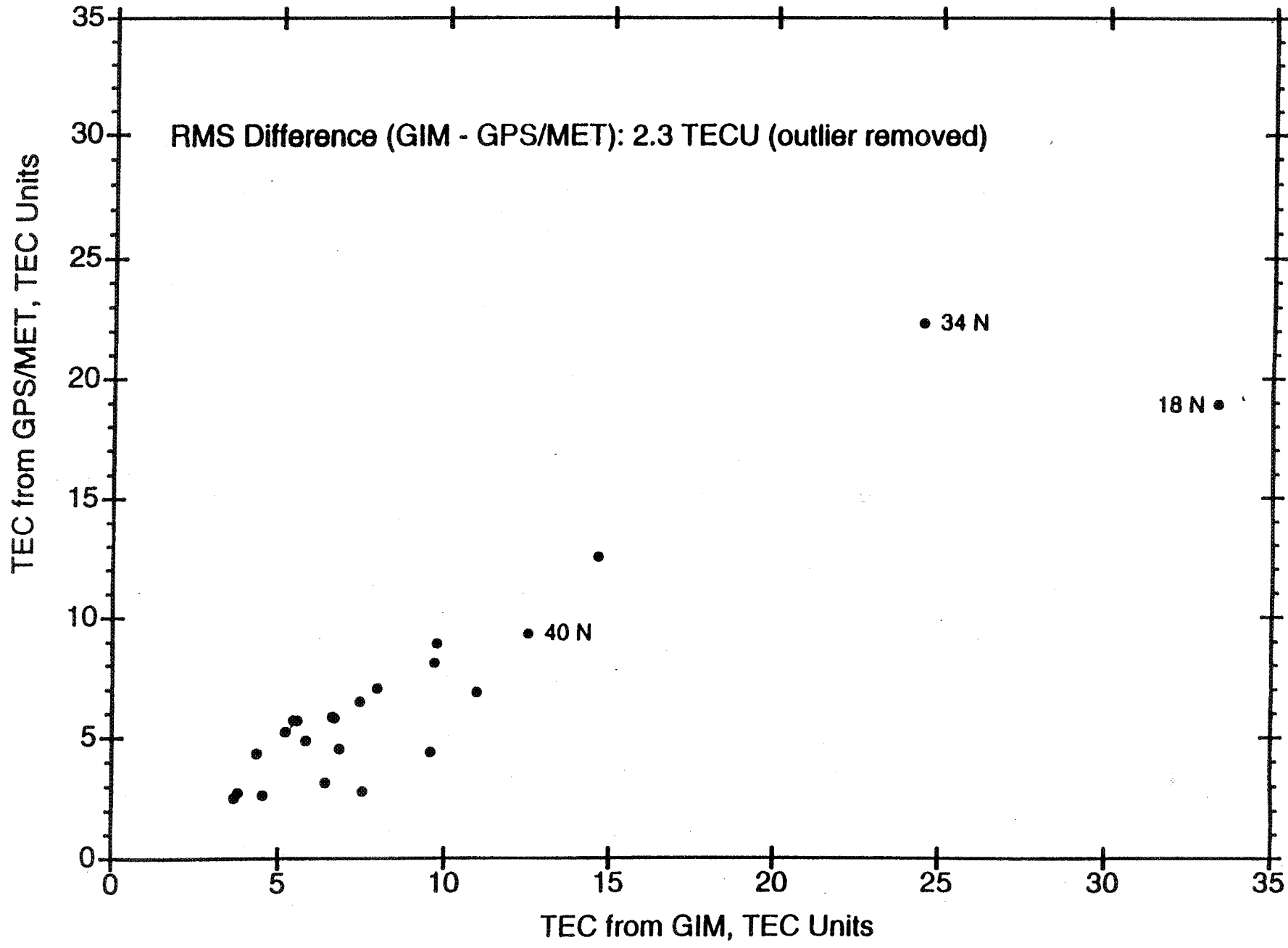


Models vs. TOPEX for NRT TEC Network

Geomagnetic Region	Model	# of Points	RMS Error (TECU)	% increase in Accuracy over Bent
ALL	Bent	5404	8.9	—
ALL	PIM	5404	9.7	-9%
ALL	PRISM	5404	6.9	+22%
ALL	GIM	5404	6.1	+31%
LOW	Bent	2342	11.5	—
LOW	PIM	2342	11.7	-2%
LOW	PRISM	2342	8.0	+30%
LOW	GIM	2342	7.7	+33%
MID	Bent	2089	6.1	—
MID	PIM	2089	8.0	-31%
MID	PRISM	2089	6.0	+2%
MID	GIM	2089	4.5	+26%
HIGH	Bent	973	6.7	—
HIGH	PIM	973	7.5	-12%
HIGH	PRISM	973	5.7	+15%
HIGH	GIM	973	4.8	+28%

- No data input: Bent & PIM.
- Global GPS input: GIM & PRISM.

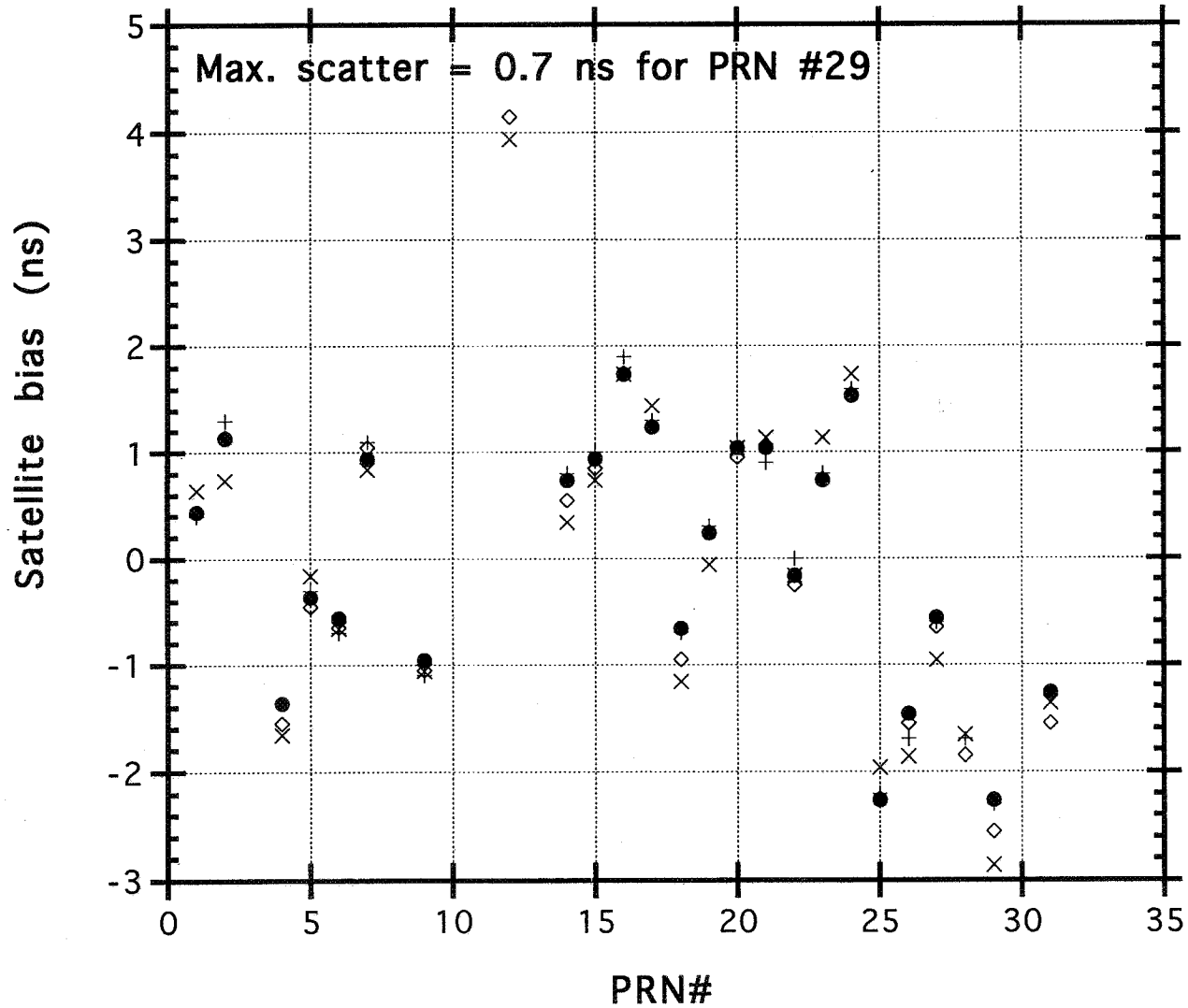
Comparisons between zenith TEC derived from GPS/MET and GIM



Relative sat. bias comparison for GPS week 823

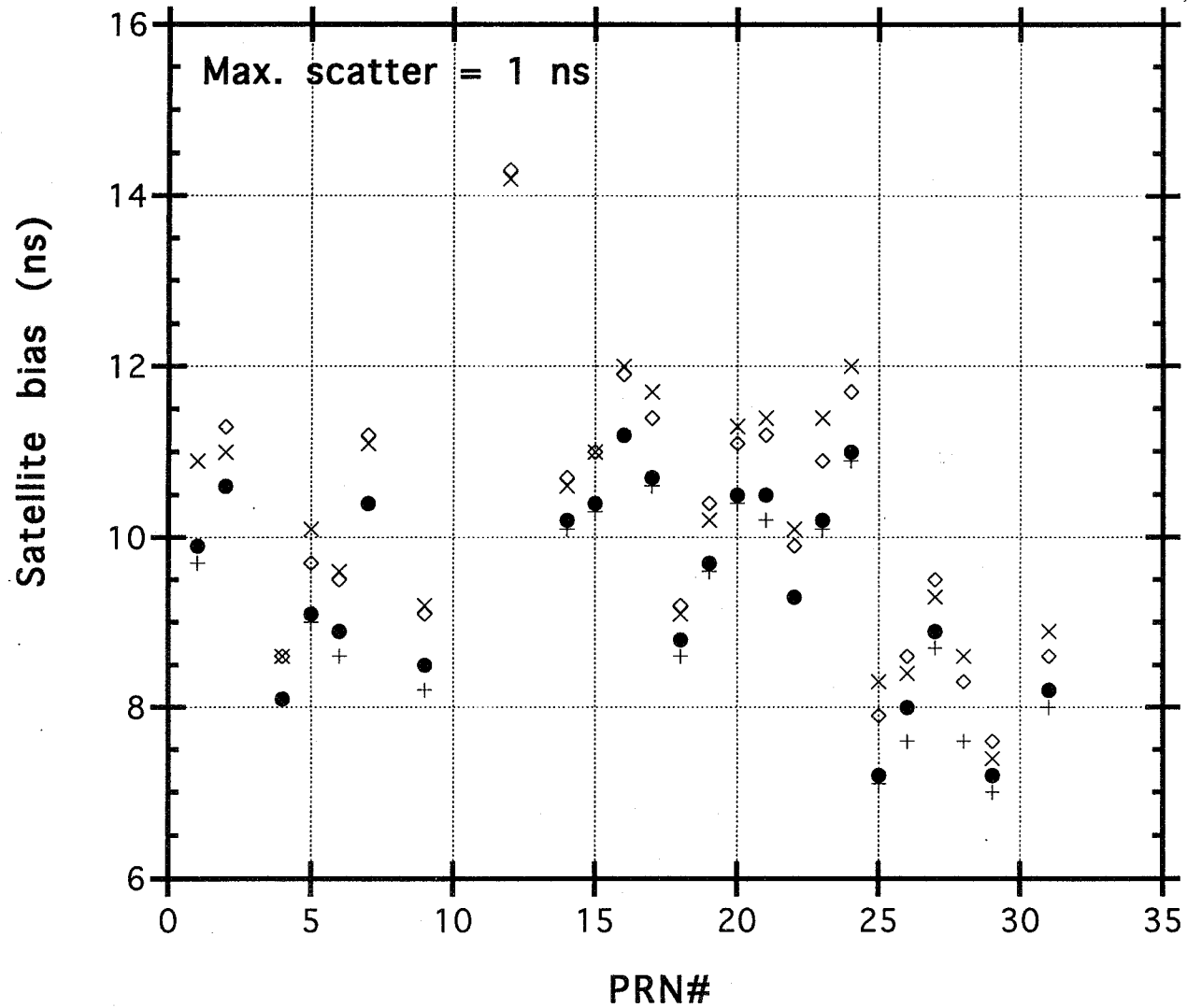
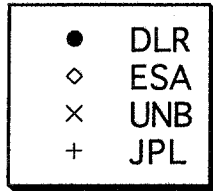
(setting Madrid rcvr bias = 0)

- DLR (minus mean)
- ◇ ESA (minus mean)
- × UNB (minus mean)
- + JPL (minus mean)



Satellite bias comparison for GPS week 823

(setting Madrid rcvr bias = 0)



Future Resources & Directions

- Resources:
 - Ever expanding ground-based GPS network.
 - Constellation of LEOs.
- Real-time GPS applications:
 - Real-time, globally-distributed TEC measurements.
 - Ionospheric storm monitoring/forecasting.
 - Real-time monitoring of GPS signal fading and other negative effects on GPS positioning & navigation.
 - Timely precipitable water vapor measurements => weather prediction.
- Improvements in GIM modeling:
 - Tailor fitting/parametrization strategy for specific applications.
 - Optimize use and adjustment of *a priori* electron density profiles.
 - Incorporate information from not just climatological models but also physical models into the mapping procedure.
- Ultimate goal: Recast a three-dimensional, physical ionosphere model into a form suitable for assimilating real-time ionospheric measurements from ground and space-borne GPS receivers, ionosondes, top-side sounders, DMSP, other satellites, etc.

Contact Information

- Dr. Ulf J. Lindqwister (group supervisor)
MS 238-600
Jet Propulsion Laboratory
4800 Oak Grove Dr.
Pasadena, CA 91109-8099

(818) 354-1734
ujl@quimby.jpl.nasa.gov

- Brian D. Wilson
MS 238-600
(818) 354-2790
bdw@logos.jpl.nasa.gov

- Anthony J. Mannucci
MS 238-600
(818) 354-1699
tonym@lurleen.jpl.nasa.gov

Page intentionally left blank



**The Potential Use of GPS/Met in
Operational Numerical Weather Prediction**

Ronald D. McPherson

March 11, 1996

Eugenia Kalnay

Steve Lord

Environmental Modeling Center



Outline

- Existing data base for operational NWP
 - Sources
 - Coverage
 - Gaps

- Recent advances in data assimilation
 - Direct assimilation of observed parameters
 - Use of ensembles for Adaptive Observing Systems

- Potential role for GPS/Met
 - Good news
 - Bad (?) news
 - Recommendation

Numerical Weather Prediction

The forecast skill has more than doubled since the 1970's:

- Today's 3-day forecasts are better than the 1-2 day forecasts in 1980
- This winter, for the first time, the 5-day forecast had an anomaly correlation with the "truth" (analysis) of 82%!
- Some winter storms are now predicted by the NWS one week in advance



Current Sources of Observations

Radiosonde network

Polar orbiters

Geostationary satellites

Aircraft

Profilers

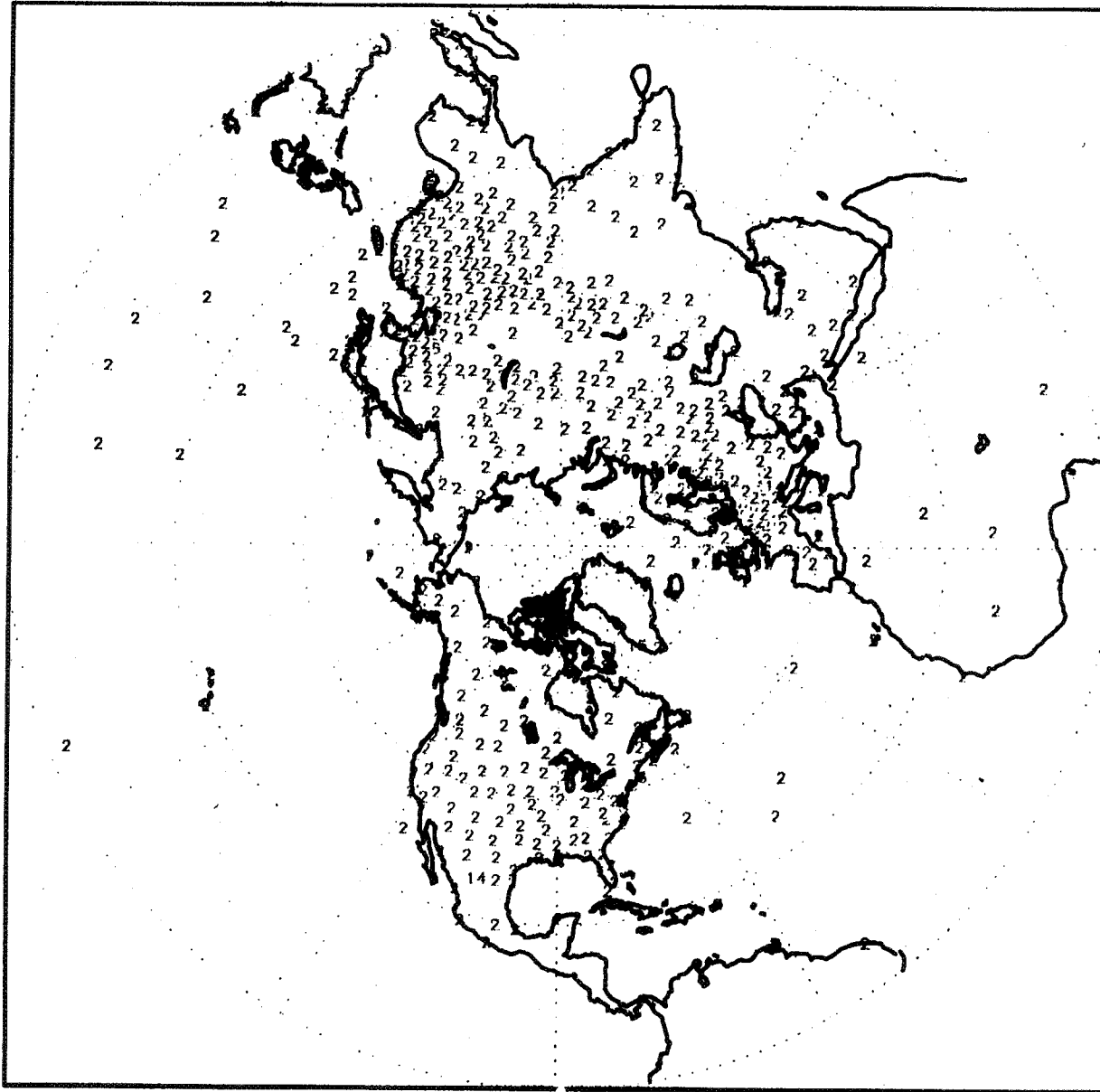
Radars

Surface stations

Ships

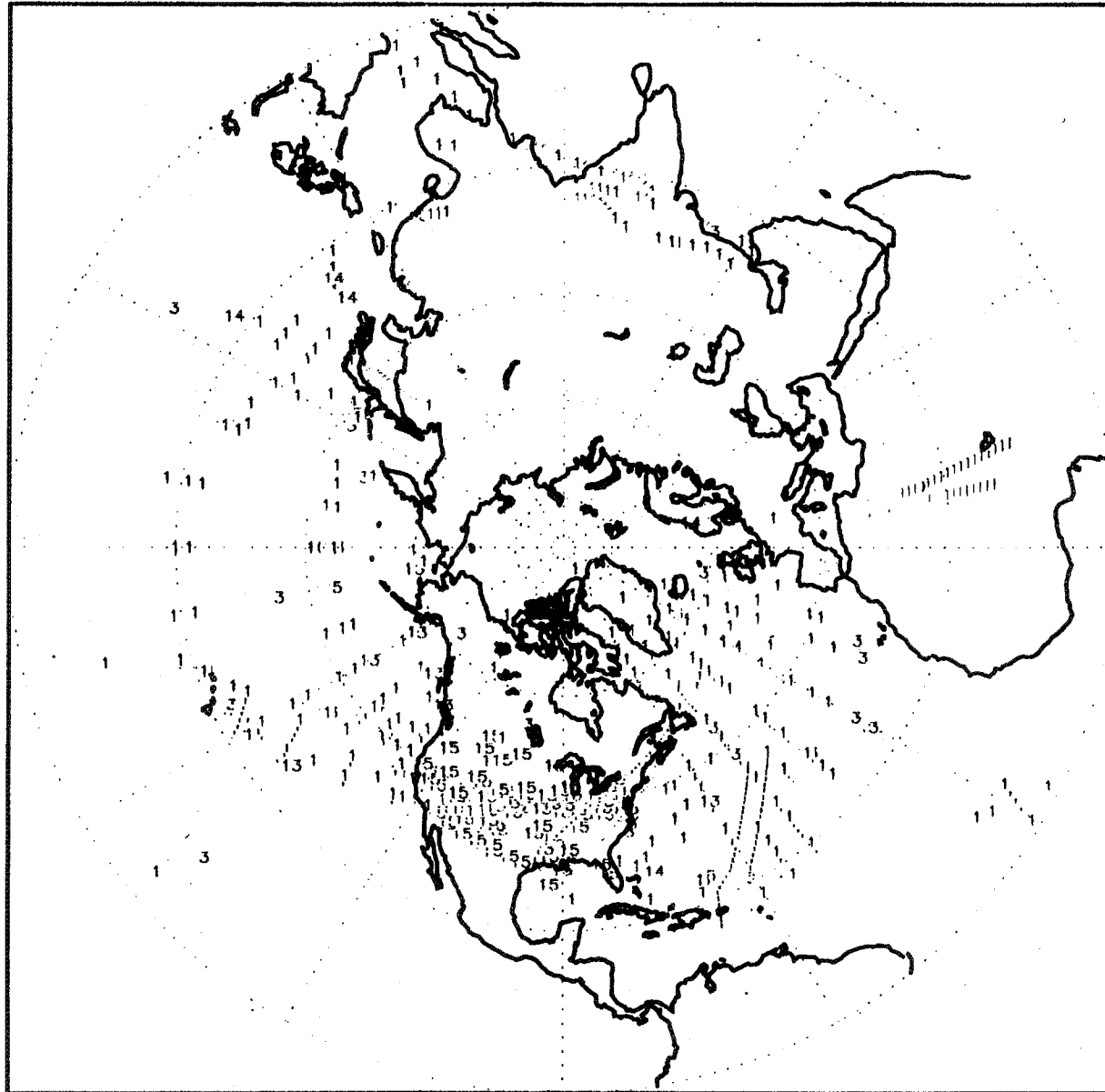
Buoys

upa obs 00Z26FEB1996



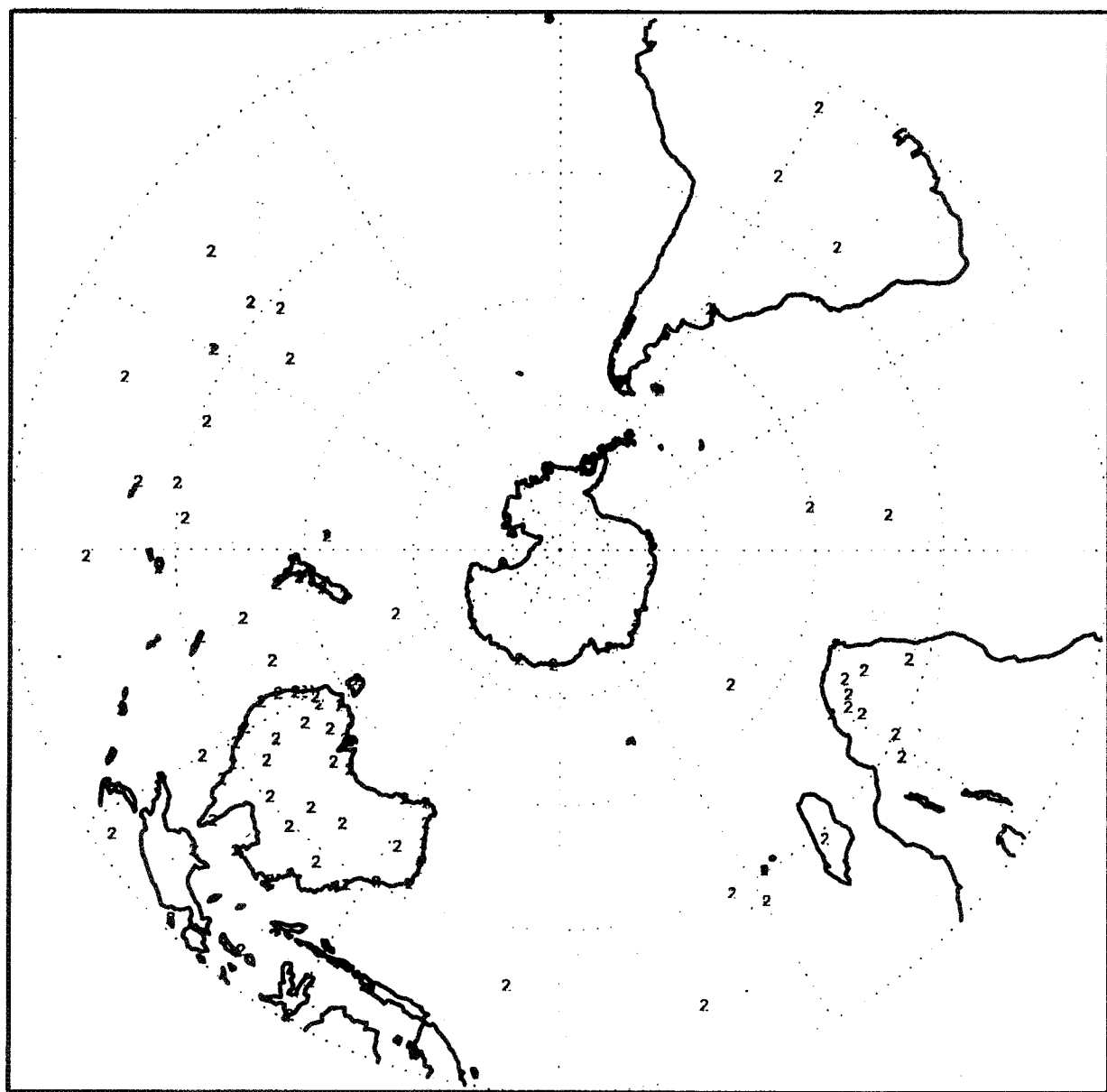
(500-500) NOBS=567 for WIND

acft obs 00Z26FEB1996



(200-350) NOBS=1175 for WIND

upa obs 00Z26FEB1996

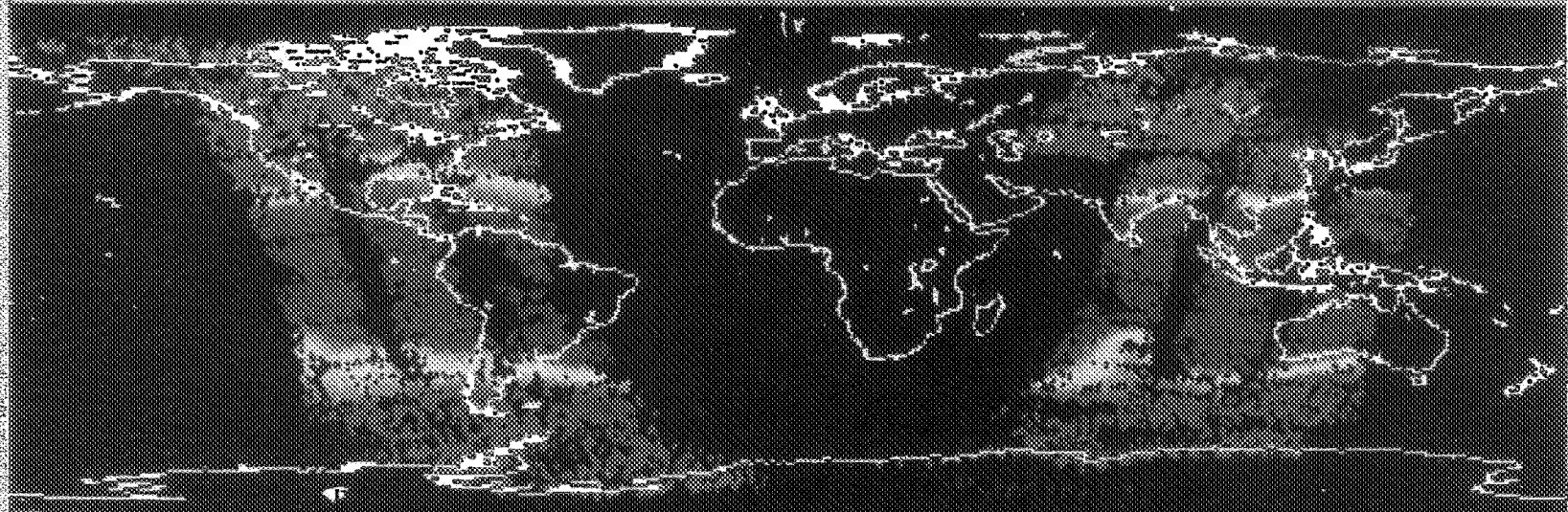


(500-500) NOBS=106 for WIND

427

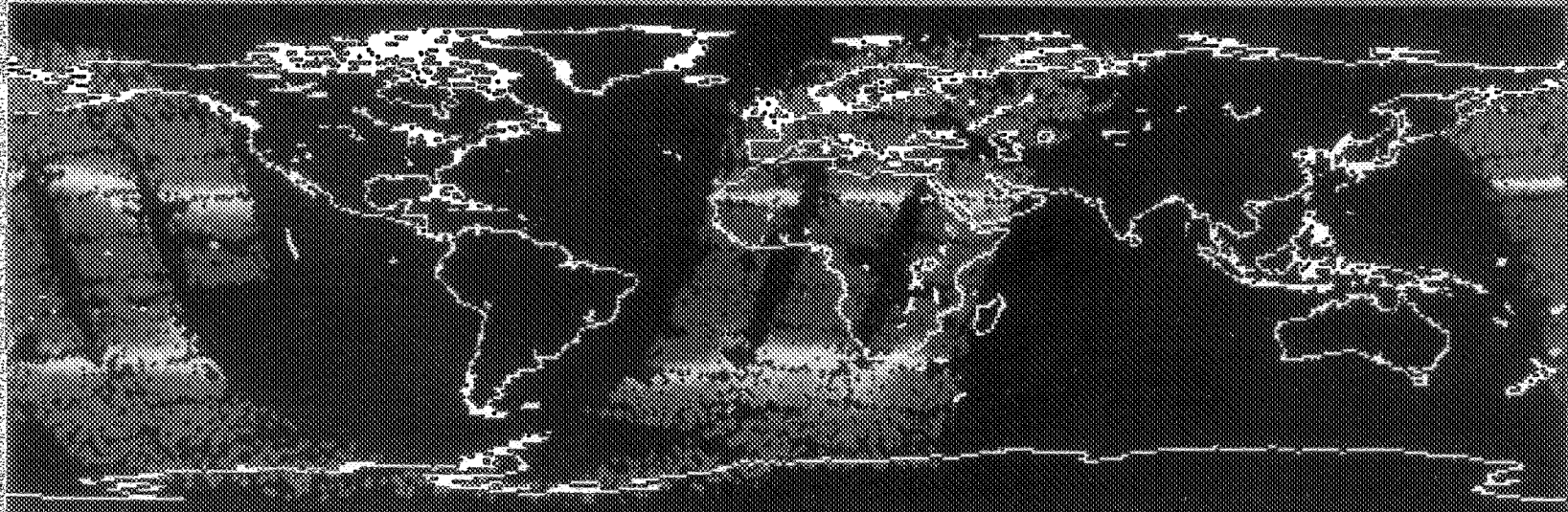
MSU CH. 2 BTEMP
NOAA-12 OPER
02/25/96 2200 - 02/25/96 0300

-90.90 LAT
-180.180 LON
5 HOURS

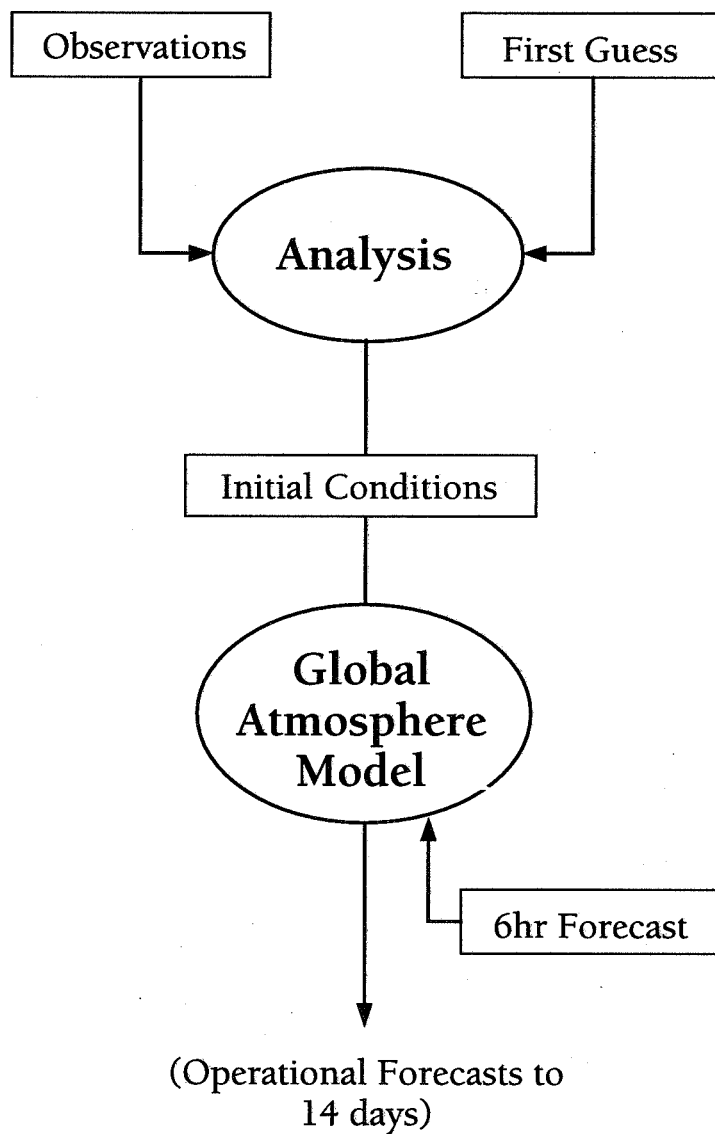


MSU CH. 2 BTEMP
NOAA-14 OPER
02/25/96 2200 - 02/25/96 0300

-90.90 LAT
-180.180 LON
5 HOURS



4-dim Data Assimilation



Analysis x has to be

- very close to observations y

- very close to 6hr forecast X_b


$$\min J = \text{distance}(x, y) + \text{distance}(x, X_b)(x)$$

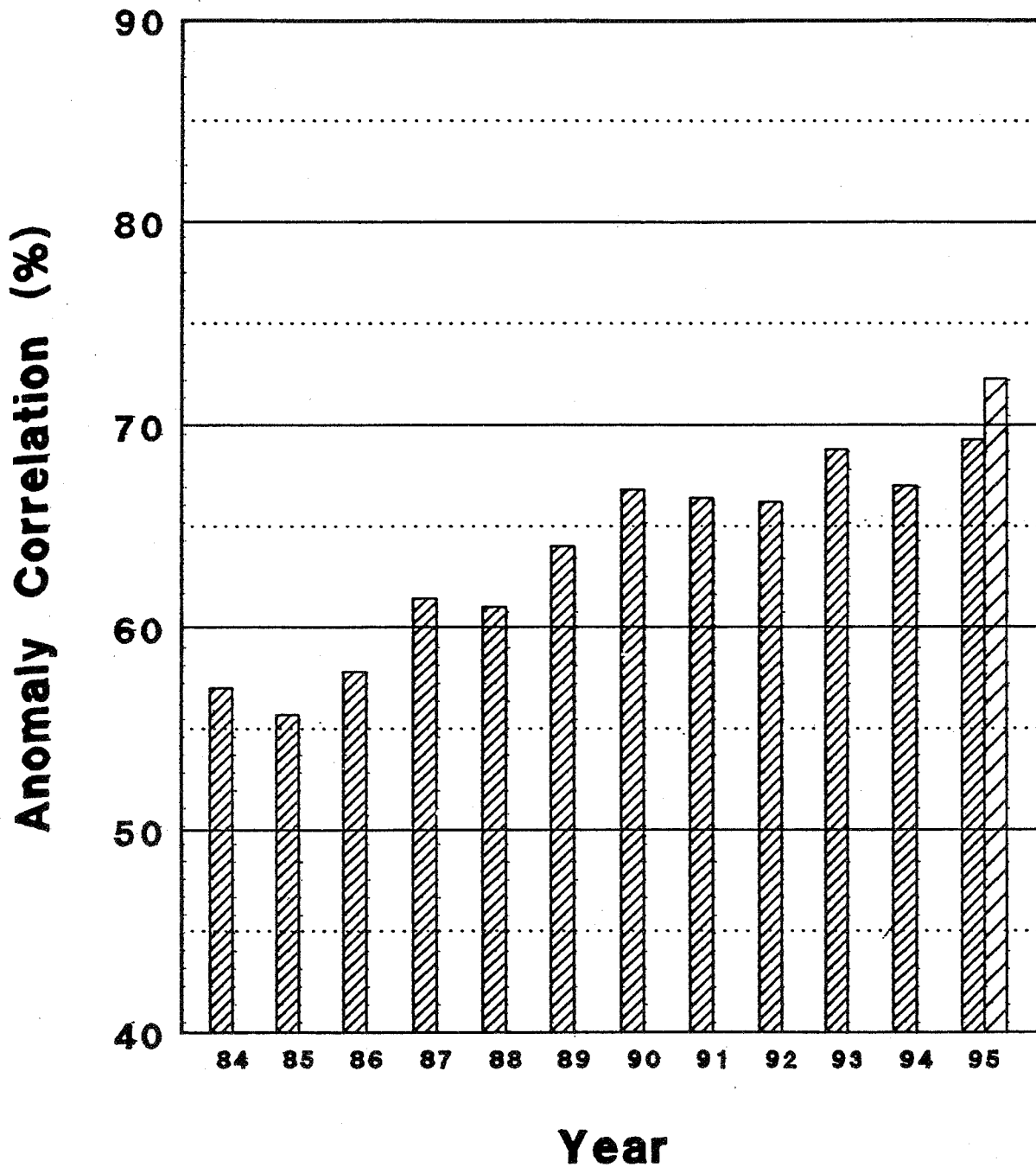
The model variables are temp t ,
winds, moisture q and pressure.

Remote measurements are radiances, refractivities

- We used to convert the sat. obs. of radiances into atm. temperature t and humidity q soundings: satellite retrievals
- We now convert the model t and q into satellite radiances
- The direct assimilation of TOVS radiances has been the largest single improvement in the last decade
- For the first time, satellite data are clearly improving the NH forecasts (17 years after TIROS N)

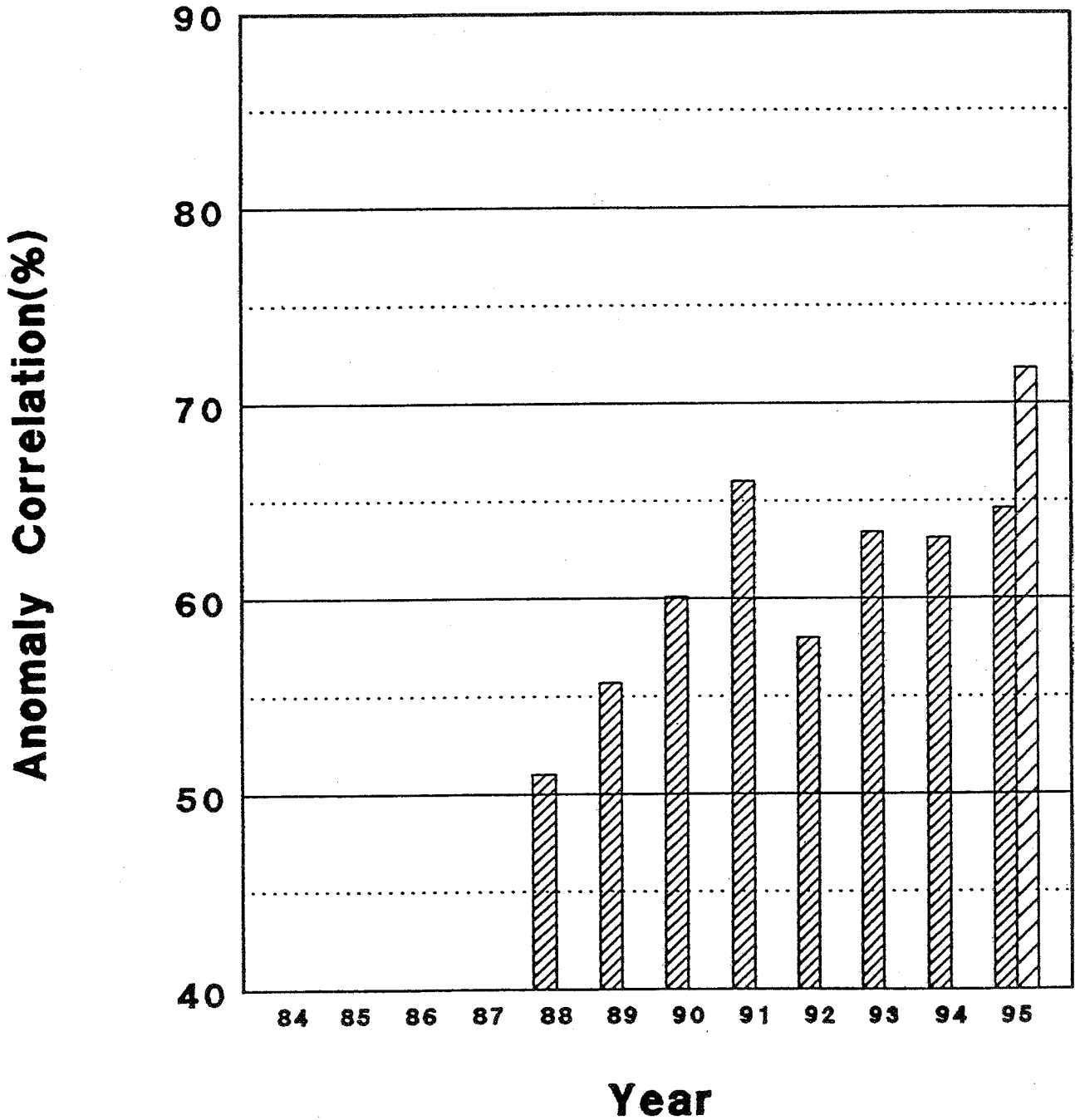
5-Day Forecasts Jun-Aug
500-mb ht, zonal waves 1-20 N Hem

 **OPNL**  **RADIANCES**



5-Day Forecasts Jun-Aug
500-mb ht, zonal waves 1-20 S Hem

 **OPNL**  **RADIANCES**



Analysis theory

The global analysis system produces an analysis through the minimization of an objective function given by

$$J = (\mathbf{x} - \mathbf{x}_b)^T \mathbf{B}^{-1}(\mathbf{x} - \mathbf{x}_b) + (\mathbf{K}(\mathbf{x}) - \mathbf{y})^T \mathbf{O}^{-1}(\mathbf{K}(\mathbf{x}) - \mathbf{y}) + J_c$$

where

\mathbf{x} is the analysis variable,

\mathbf{x}_b is the background field (a 6 hour forecast),

\mathbf{B} is the back ground error covariance matrix,

\mathbf{y} is a vector of all the observations,

\mathbf{O} is the observational error covariance matrix,

\mathbf{K} is the transformation operator from the analysis variable to the form of the observation vector

J_c is a dynamical constraint term

Goal: Adjusts the analysis to fit the information in the data.

The \mathbf{K} operator for the refractivity data represents the transformation of the analysis variables (τ, q, p) to refractivity.

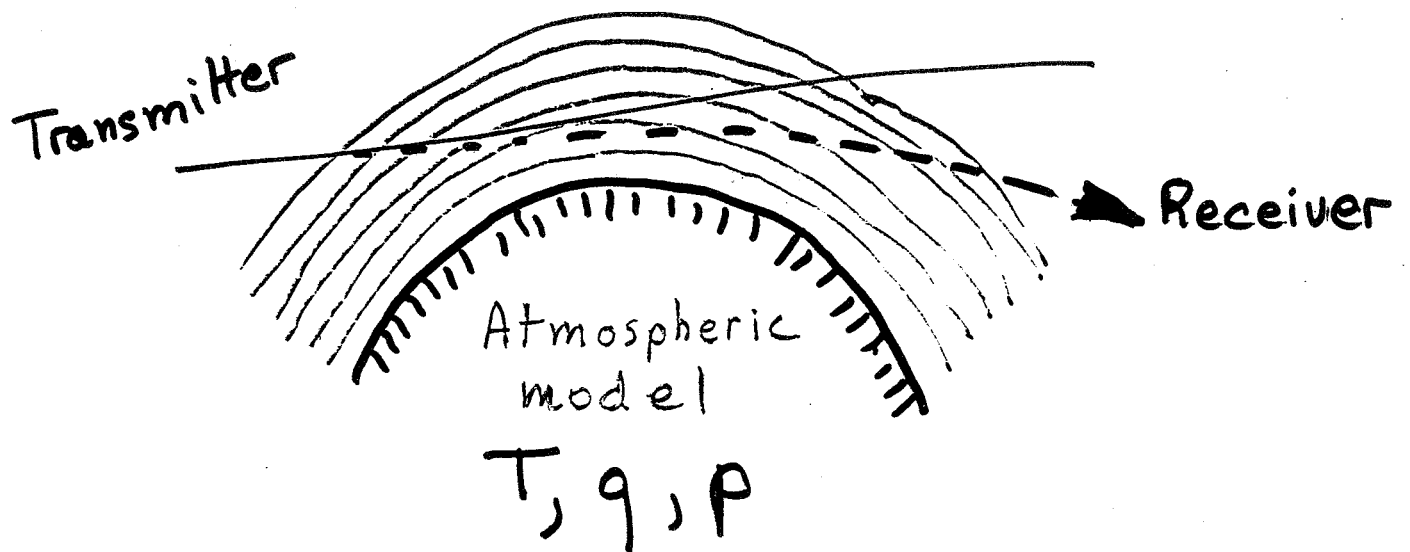
required tools for minimization:

full forward operator

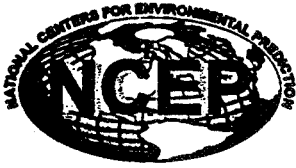
tangent linear model (TGL) of the forward operator

the adjoint of TGL

For refraction angle data, forward ray-tracing its TGL and adjoint are needed

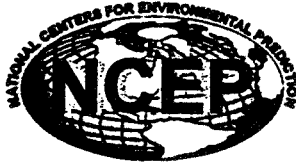


- We need a ray tracing model for GTS-MET
- Also a linear tangent (perturbation) model and its adjoint
- They need to be accurate and if possible efficient



Principal Gaps in the Existing Observing System

- Wind profiles over ocean areas
- Moisture profiles



Potential Role for GPS/Met

- Good News:

In modern data assimilation technology, a framework exists within which GPS/Met data can be used effectively, with a relatively short learning period.

- Bad (?) News:

Any new observing system must compete with existing observing systems, and that field is not uncrowded.

- Recommendation for GPS/Met:

Aim at:

Either fill a known “gap” in the current observing system.

or

Provide cheaper and/or better data than the current system provides.

Message-ID: <9603130956.AA17430@kora.nz.dlr.de>
Date: Wed, 13 Mar 1996 10:56:02 +0100
From: Esther Sardon <sardon@NZ.DLR.DE>
Subject: DLR-Neustrelitz comments over ionospheric IGS products
To: Multiple recipients of list GPS-IONO <GPS-IONO@LISTSERV.UNB.CA>

Dear colleagues,

As I wrote two weeks ago, unfortunately nobody from DLR-Neustrelitz will take part in the next IGS meeting. But we are very interested in the collaboration with the other groups and in the discussion over ionospheric IGS products.

These are our comments to the questions that Feltens proposed at the end of his position paper:

DLR COMMENTS FOR THE DISCUSSION OVER IONOSPHERIC IGS PRODUCTS

0. General comment

To use "ionospheric models" for the possible IGS ionospheric products can create confusion, because we will not make a "model" like IRI, Bent, etc.. but we will provide TEC data, as a set of grid points or as a set of coefficients.

We propose to use the expression "TEC mapping" or "ionospheric TEC information" instead of "ionosphere models".

1. Potential users:

In general, we can distinguish two kinds of potential users for the ionospheric IGS products: single frequency users (GPS and other techniques) and scientists interested in ionospheric studies. But, depending on the time delay allowed by the users, we see the following groups:

- Navigation: real-time ionospheric corrections
- Radio communication: real-time ionospheric conditions
- Surveying: precise ionospheric corrections (within few days)
- Ionospheric physics: high accuracy VTEC/profiles/gradients (within weeks)
- others (radioastronomy, altimetry, etc..)

For these ionospheric products, in the near future, the navigation group can become the biggest group of users, and we should take it into account.

2. Possible products

The main IGS ionospheric product should be TEC values. They can be provided as TEC maps, but also a set of coefficients can be used to describe the ionospheric behaviour. The TEC maps are, in principle, easier to use than a set of coefficients because no knowledge about the used reference frame is needed. We propose to distribute the TEC information through maps.

Depending on the application we can think in users of global, regional and local ionospheric information. These three kind of maps should be provided, specifying in each case the level of accuracy.

In principle, the differential delays are only of interest for the people using GPS to derive TEC values. In the first step, we should not provide this information (maybe only upon request). But further work of internal comparisons to obtain reliable sets of biases must continue.

3. Delay in providing the products

So far, using IGS data, we can only provide ionospheric products obtained in post-processing. That means 1 or 2 days of delay as minimum. This should be enough for some applications, but others (mainly navigation and radio communication) need, at least, near real-time ionospheric information. For post-processed products we propose a maximum delay of one week.

In DLR-Neustrelitz we have developed a system for real-time estimation of TEC, that could be applied to the IGS stations. For that real-time estimation, a data rate higher than 30 seconds is convenient. We propose a campaign for testing the real-time estimation of TEC with IGS data, consisting of two steps:

- a) real-time simulations:
that means to operate a reduced number (5 or 6) of IGS stations with higher data rate (10 seconds) in a certain region (for example, Europe) and to process the data at DLR-Neustrelitz using the real-time algorithms
- b) real-time connections:
that means to implement a real-time connection between such a small sub-net to demonstrate the capabilities.

4. Time intervals of update:

For the methods of TEC estimation using a Kalman filter, it is very easy to change the update rate, and made it as high as the data rate (30 seconds). But in this case we will generate rather large files that will contain "redundant" information in case of quiet ionospheric days. In our comparisons we have used 1 hour update rate, but in this time the ionosphere can change quite a lot, mainly at low latitudes or during quite perturbed days. We propose a maximum update rate of 10 minutes.

Other methods, based on spherical harmonics or batch analysis for example, estimate a set of coefficients describing the ionosphere that are "valid" for a certain period (normally several hours). In this case, to use a high update rate means to repeat the same information several times.

We can provide highly update (10 minutes) REGIONAL and LOCAL TEC information and keep hourly or lower updated TEC information for GLOBAL maps.

5. Which mathematical models:

Possible mathematical representations of the ionosphere are:

- Spherical harmonics: good global representation method.
- Kalman filter: good local representations. Possibly applicable to global grids as well. The model can be auto-improved from the accumulated information over gradients or stochastic variations.
- Batch analysis with low order polynomials: subject to errors due to unaccounted variations of the ionosphere.

Based also on point 4, we propose to use Kalman filter approaches for regional and local TEC maps and spherical harmonics and tessellation into spherical triangles for global TEC maps.

6. Reference frame definition

For comparison and for users application, geographical frames are preferable.

For model development, any other frame may be chosen, but that should be probably irrelevant, except if detailed comparisons (deep to the code) are intended.

7. IGS format

We support the idea of using the IONEX format, similar to RINEX format, to provide VTEC maps in the form of grid data.

8. Next steps

Complete the comparison between different groups and evaluate the internal precision/accuracy of the work. Validation of the TEC products with independent measurements of equivalent parameters should be continued, especially in high and low latitudes.

Define requirements for each product and responsibilities for the analysis centers. Depending on experience and interests, different centers could offer different products. For example, DLR-Neustrelitz is ready to provide regional European TEC maps in the frame of IGS work, and test the extension towards real-time ionospheric products.

Best regards,

Esther Sardon

```
.....  
. Esther Sardon Phone: +49 3981 480130 .  
. DLR Fernerkundungsstation Neustrelitz FAX: +49 3981 480299 .  
. Kalkhorstweg 53 .  
. D-17235 Neustrelitz e-mail: sardon@nz.dlr.de .  
. Germany .  
.....
```

End of Message

===== REST OF RFC822 HEADER =====

```
Received: from esoc.esa.de by VMPROFS.ESOC.ESA.DE (IBM VM SMTP V2R2) with TCP;  
Wed, 13 Mar 96 11:13:31 EWT  
Received: by esoc.esa.de (8.6.12/ESARLY1.8)  
id KAA02853; Wed, 13 Mar 1996 10:14:58 GMT  
Received: from listserv.gmd.de(192.88.97.1) by com28.esoc.esa.de via smap  
(g3.0.3)  
id xmaa02812; Wed, 13 Mar 96 10:14:41 GMT  
Received: from listserv.gmd.de by listserv.gmd.de (LSMTP for OpenVMS v1.0a) wit  
h  
SMTP id <14.6BB1A9FE@listserv.gmd.de>; Wed, 13 Mar 1996 11:12:24 +0100  
Received: from LISTSERV.UNB.CA by LISTSERV.UNB.CA (LISTSERV-TCP/IP release  
1.8b) with spool id 1674137 for GPS-IONO@LISTSERV.UNB.CA; Wed, 13 Mar  
1996 06:04:36 -0400  
Received: (from kora.nz.dlr.de Y129.247.236.1") by unb.ca (8.7.4/960123-14:25)  
id GAA16609 for <GPS-IONO@LISTSERV.UNB.CA>; Wed, 13 Mar 1996 06:04:22  
-0400 (AST)  
Received: from nvwgs3.dlr.de (nvwgs3.nz.dlr.de) by kora.nz.dlr.de (4.1/SMI-4.1)  
id AA17430; Wed, 13 Mar 96 10:56:02 +0100  
Reply-To: GPS for IONOspheric research <GPS-IONO@LISTSERV.UNB.CA>  
Sender: GPS for IONOspheric research <GPS-IONO@LISTSERV.UNB.CA>
```

Page intentionally left blank

**GPS Orbit Determination
Including Various Addjustments**

GODIVA

C. Goad, A. Mueller

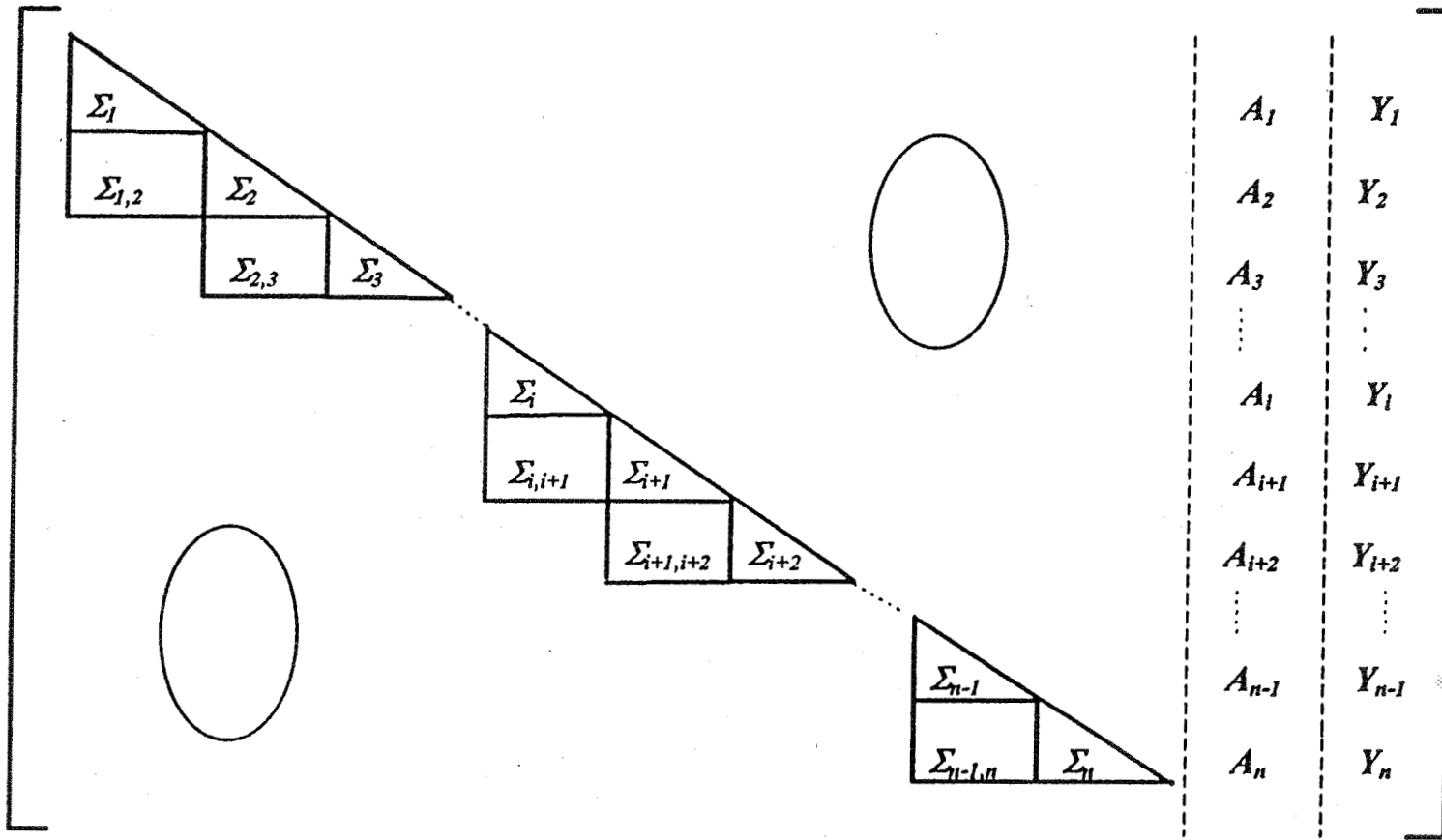
***HARDWARE/SOFTWARE
CONFIGURATION***

***P 90
Windows NT
Microsoft NT Fortran***

An automated procedure for generating an optimum set of linearly independent ion-free triple differences according to C.C. Goad and A. Mueller (1988)

- the Cholesky decomposition of the covariance matrix of the triple differences is performed*
- the linear dependency between the measurements is revealed by displaying a zero diagonal element on the corresponding position in the Cholesky factor*
- allows access to 100% of linearly independent information*
- single precision operation is OK for this task (fast !)*

The decorrelation scheme using Cholesky decomposition of the covariance matrix



Application of Triple Difference

Advantage: - no separate data editing since cycle slips are treated as data outliers and are rejected during the adjustment

- no nuisance parameters (ambiguities), thus the size of the normal matrix is significantly reduced with respect to the normal matrix for undifferenced, single or double differenced observations

Disadvantage: correlation between epochs, thus the covariance matrix is a full or a banded matrix, depending on the differencing scheme (inverting such a matrix is not practical !)

*Application of the Cholesky
decomposition in the observation
decorrelation*

$$(\mathbf{A}^T \Sigma^{-1} \mathbf{A}) \boldsymbol{\xi} = \mathbf{A}^T \Sigma^{-1} \mathbf{Y} \quad \text{and} \quad \Sigma = \mathbf{L} \mathbf{L}^T$$

$$\tilde{\mathbf{A}}^T \tilde{\mathbf{A}} \boldsymbol{\xi} = \tilde{\mathbf{A}}^T \tilde{\mathbf{Y}}$$

$$\tilde{\mathbf{A}} = \mathbf{L}^{-1} \mathbf{A} \quad \text{and} \quad \tilde{\mathbf{Y}} = \mathbf{L}^{-1} \mathbf{Y}$$

$$\mathbf{L} \tilde{\mathbf{A}} = \mathbf{A} \quad \text{and} \quad \mathbf{L} \tilde{\mathbf{Y}} = \mathbf{Y}$$

Schaffrin-Grafarend Theorem

$$E\{\mathbf{Y}\} = \mathbf{A}\xi + \mathbf{B}\eta, \quad D\{\mathbf{Y}\} = \mathbf{P}^{-1}\sigma^2$$

Choose transformation matrix \mathbf{R} such that one gets:

$$E\{\mathbf{R}^T\mathbf{Y}\} = \mathbf{R}^T\mathbf{A}\xi \quad \text{and} \quad D\{\mathbf{R}^T\mathbf{Y}\} = \mathbf{R}^T\mathbf{P}^{-1}\mathbf{R}\sigma^2$$

Solution of ξ is identical in both adjustments!

Double Differences

Equivalent Set of Observations

 Y_1 Y_2 Y_3

.

.

.

 Y_{N-1} Y_N Y_1 $Y_2 - Y_1$ $Y_3 - Y_2$

.

.

.

 $Y_{N-1} - Y_{N-2}$ $Y_N - Y_{N-1}$

TIMING REQUIREMENTS

Automatic Data Downloading (Internet)
1 hour

Data Base Creation and Preprocessing
1.5 hours

Orbit Determination
(35 min/iteration) x 5 iterations = 3 hours

Total Processing Time = 5.5 hours

DYNAMIC MODEL

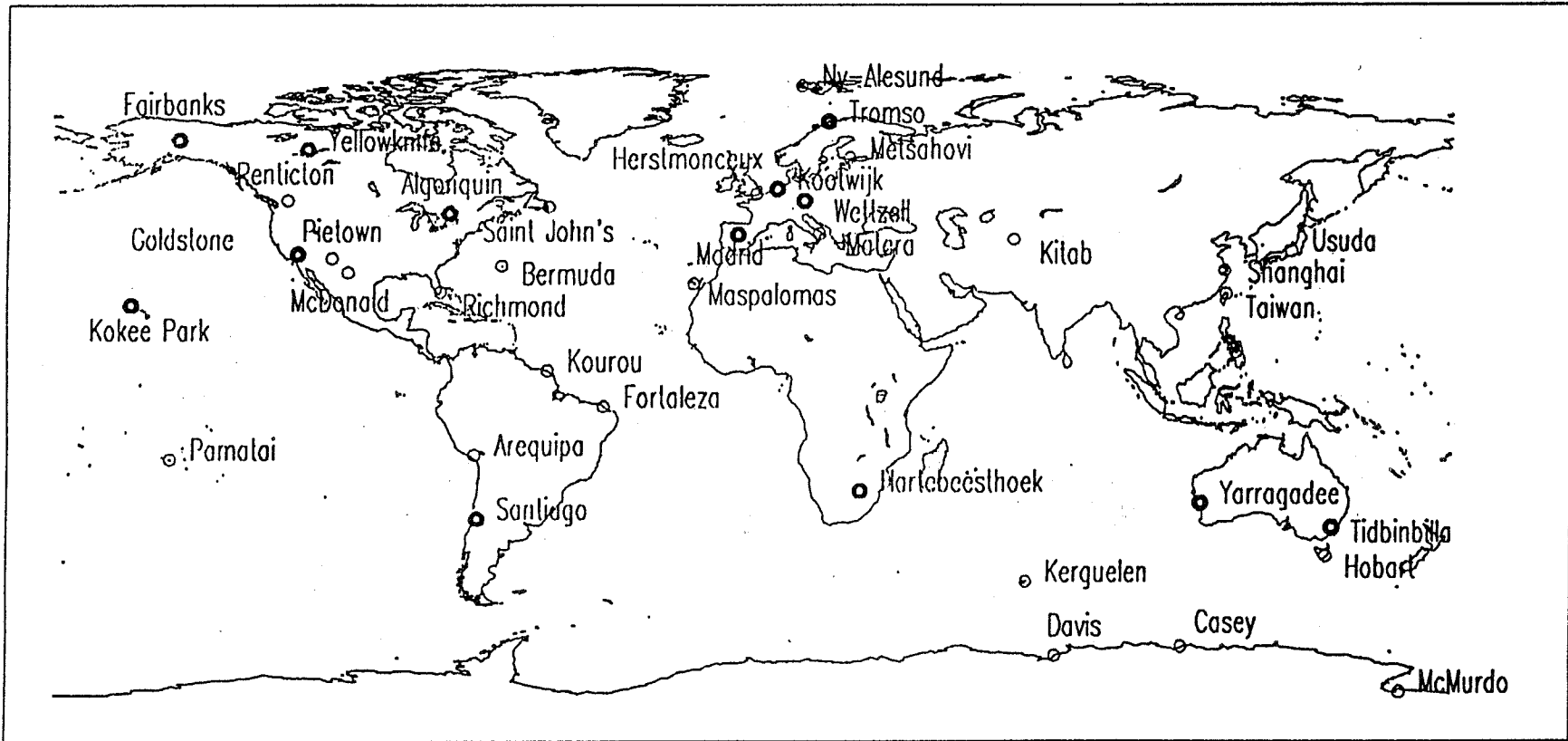
<i>Geopotential</i>	<i>GEM-T3 up to degree and order 8 plus \bar{C}_{21} and \bar{S}_{21} according to IERS standards</i>
	<i>$GM_E = 3.98600436 \times 10^{14} \text{ m}^3/\text{s}^2$.</i>
	<i>$a_e = 6378137 \text{ m}$</i>
<i>Third-body</i>	<i>Sun and Moon regarded as point masses</i>
	<i>Ephemeris: JPL DE-200</i>
	<i>$GM_{sun} = 132712440000.0 \text{ km}^3/\text{s}^2$</i>
	<i>$GM_{moon} = 4902.7991 \text{ km}^3/\text{s}^2$</i>
<i>Solar Radiation Pressure</i>	<i>ROCK4 and ROCK42 models for Block I and II satellites, respectively</i>
	<i>Satellite masses are obtained from table 3 of Fliegel and Gallini (1992) and IGS Electronic Mail (see e.g., Mail #654)</i>
	<i>Y-bias</i>
	<i>Earth shadow model: Umbra and Penumbra</i>
<i>Tidal Forces</i>	<i>Solid earth tides: Wahr model with $k_2 = 0.30$</i>
	<i>Ocean tides: Schwiderski model</i>
<i>Relativistic Correction</i>	<i>IERS Standards</i>
<i>Numerical Integration</i>	<i>Variable-order / variable-stepsizes of the Adam's type</i> <i>Arc length: 32 hours (4+24+4)</i>

MEASUREMENT MODEL

<i>Basic Observable</i>	<p><i>Triple Difference, Ionospheric-Free Linear Combination</i></p> <p><i>Sampling Rate: 15 minutes</i></p> <p><i>Weighting: Uniform, with 1cm standard deviation for the single phase</i></p> <p><i>Elevation Angle Cutoff: 16 degrees</i></p>
<i>Ground Antenna Phase Center</i>	<p><i>Offset - applied</i></p> <p><i>Elevation-dependent phase center correction - not applied</i></p>
<i>Troposphere</i>	<i>Modified Hopfield with mapping function developed by Goad and Goodman</i>
<i>Ionosphere</i>	<i>Not modeled, ion-free combination used</i>
<i>Plate Motion</i>	<i>ITRF93 Station Velocities, fixed</i>
<i>Station Tidal Displacement</i>	<i>Solid Earth Tides, according to IERS Standards</i>
<i>Station Displacement Due to the Dynamic Pole</i>	<i>According to IERS Standards</i>
<i>Satellite Center of Mass Correction</i>	<p><i>Block I: 0.211 m, 0.000 m, 0.854 m</i></p> <p><i>Block II/IIA: 0.279 m, 0.000 m, 1.023 m</i></p>

SOLUTION PARAMETERS

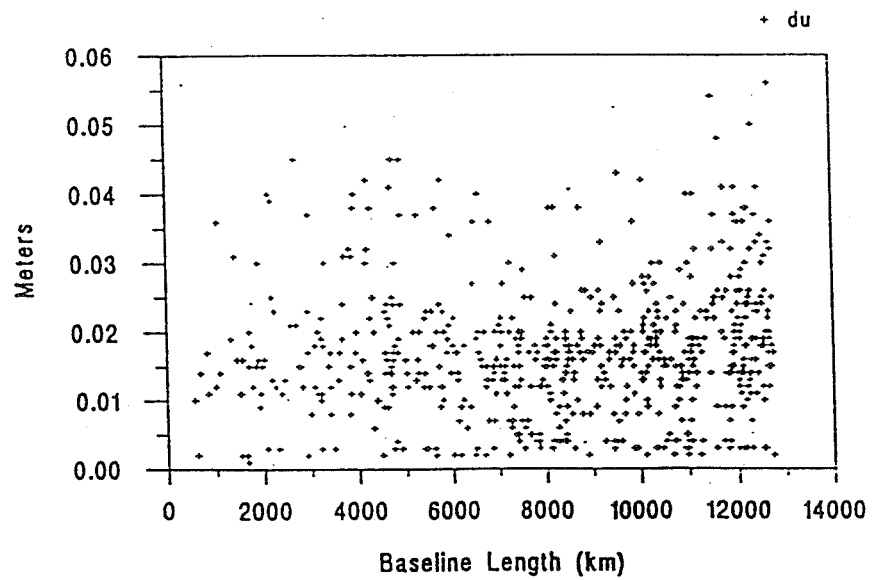
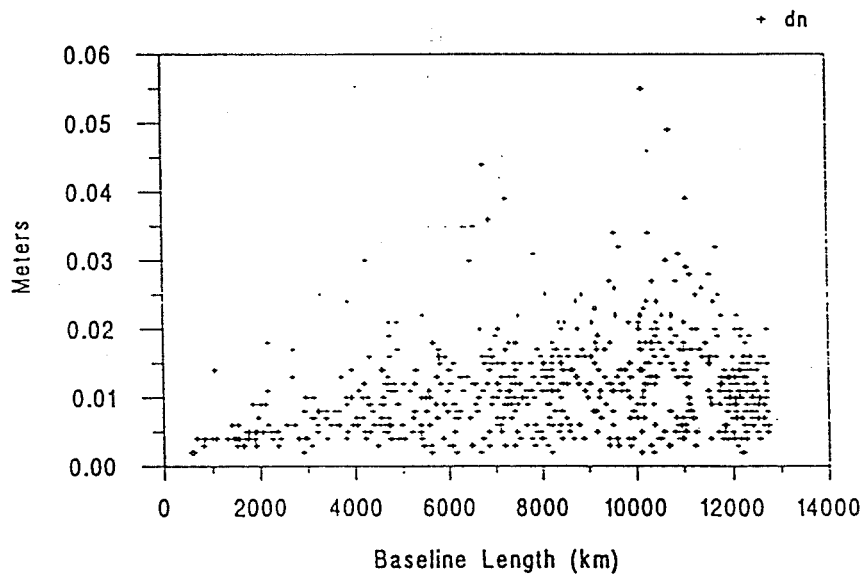
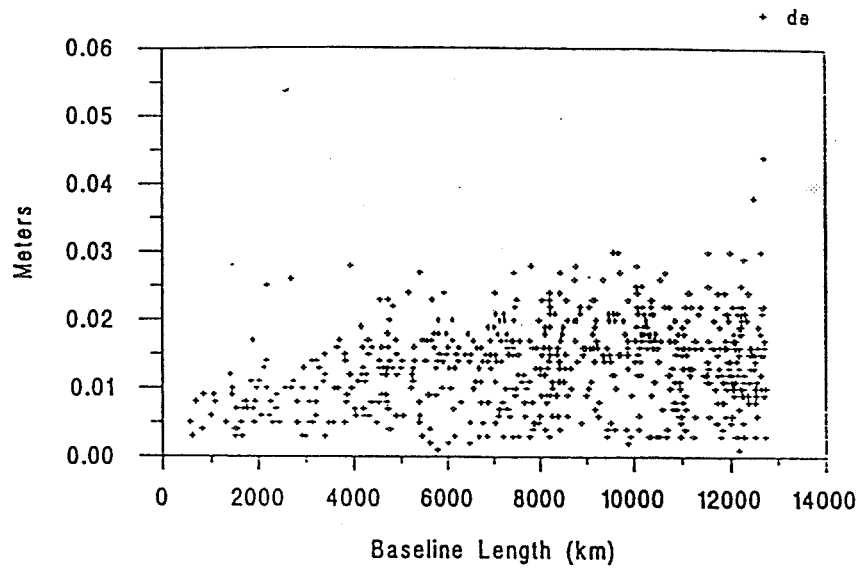
PRODUCT	APRIORI VALUE	APRIORI CONSTRAINT
SATELLITE POSITION	FORMER SOLUTION	1.0 m
SATELLITE VELOCITY	FORMER SOLUTION	10^{-4} m
SOLAR RADIATION PRESSURE S_x, S_z SCALING FACTORS Y-BIAS SCALING FACTOR	FORMER SOLUTION	0.1 0.15
COORDINATES FOR 23 TRACKING STATIONS (13 FIXED IERS STATIONS)	FORMER SOLUTION IGS MAIL 819	50.0 m 3-5 mm
TROPOSPHERIC SCALING FACTORS (AT FOUR - HOUR INTERVAL)	1.0	0.1
EARTH ROTATION PARAMETERS: RATE OF (UT1-TAI) Xpole, Ypole OFFSETS	BULLETIN B	6.5×10^{-3} sec / day 9.7×10^{-2} arcsec / da
TOTAL ARC LENGTH: 32 hours (4+24+4)		



- Fiducial Stations
- Estimated Stations

	EMR	ESA	GFZ	JPL	NGS	SIO	OSU	IGS
COD	18.0	20.3	17.9	15.3	24.8	28.6	18.2	10.75
EMR		22.9	18.7	17.0	25.3	27.0	19.2	12.46
ESA			20.5	22.6	28.8	30.9	22.3	18.21
GFZ				16.7	26.6	28.0	18.9	11.79
JPL					25.0	26.3	18.5	9.75
NGS						29.6	27.0	20.86
SIO							28.2	23.64
OSU								15.36

The Mean RMS of fit in [cm] of orbit comparison among the IGS centers including OSU, for GPS weeks 784-787



Critical Components of our Procedure

- 1. The choice of the procedure for generating an optimum set of linearly independent observations*
- 2. Iterative solution and data editing as a part of the least squares adjustment, repeated every iteration*

Processing Times (hours)
90 MHz PC

	<u>32 Stations</u>	<u>74 Stations</u>
Predict	0.06	0.06
Generate TD's	0.05	1.20
	<u>Per Iteration</u>	
Measurement Reduction	0.05	0.25
Cholesky	0.02	0.60
Forward Substitution	0.10	1.60
Accumulation	0.20	1.80
Solution	<u>0.02</u>	<u>0.15</u>
Total	0.41	4.40

CORS PROJECT

N. Weston

**National Geodetic Survey
National Ocean Service
NOAA
Silver Spring, Maryland**

Project Chief: William Strange
phone: 301-713-3222
Internet: bstrange@ngs.noaa.gov

Deputy Project Chief: Paul R. Spofford
phone: 301-713-3205
Internet: pauls@ngs.noaa.gov

Technical staff: LT(jg) Neil Weston, NOAA
phone: 301-713-3234
Internet: nweston@ngs.noaa.gov

Donald Haw
phone: 301-713-3208
don@ngs.noaa.gov

James Drosdak
phone: 301-713-3219
Internet: jimd@ngs.noaa.gov

CORS OBJECTIVES

- SUPPORT NGS SURVEYING
- BASE STATION ACCESS TO NSRS
- MONITOR MOTIONS
- PROMOTE STANDARDIZATION
- PROVIDE DATA
- SUPPORT POSITIONING AND NON-POSITIONING APPLICATIONS

CORS STANDARDS ACTIVITIES

- CORS STATION STANDARDS
 - TO BE ISSUED JUNE/JULY 1996
 - REQUIRED AND DESIRED ACTIVITIES

- RINEX VERSION 2 STANDARDS
 - OPTIONAL FIELDS REQUIRED FOR INCLUSION
 - IN COLLABORATION WITH USERS AND
HARDWARE VENDORS

- REQUIRED ANTENNA PHASE CENTER MODELS
 - HARDWARE VENDORS/STANDARD NAMES

- METEOROLOGICAL SENSORS
 - NOAA FORECAST SYSTEMS LABORATORY

CORS COMPONENTS

- GPS OBSERVATION STATIONS
- DATA TRANSMISSION
- CENTRAL FACILITY
 - DATA FORMATTING
 - QUALITY CONTROL
 - DATA ARCHIVING
- DATA DISTRIBUTION

MAJOR CONSIDERATIONS

- **SAMPLE RATE**
- **REAL TIME DATA TRANSMISSION**
- **MONUMENT STABILITY**
- **DATA FORMAT**
- **COORDINATE SYSTEM**

CORS STATION TYPES

- TYPE A
 - MULTIPLE RECEIVERS AT STATION
 - 99 PERCENT RELIABILITY
 - VARIABLE SAMPLE RATE (2 TO 30 SECONDS)
 - IMMEDIATE DATA ACCESS VIA PACKET SERVICE (X.25)
 - HOURLY DATA FILES

- TYPE B
 - SINGLE RECEIVER AT STATION
 - 30 SECOND SAMPLE RATE
 - DAILY DATA ACCESS VIA INTERNET/MODEM
 - DAILY DATA FILES

COAST GUARD STATIONS

RECEIVERS:

- TWO (2) ASHTECH Z12 RECEIVERS AT EACH SITE

SAMPLING RATE:

- 5 SECOND PLANNED (1 SECOND POSSIBLE)

TRANSMISSION TO CENTRAL FACILITY:

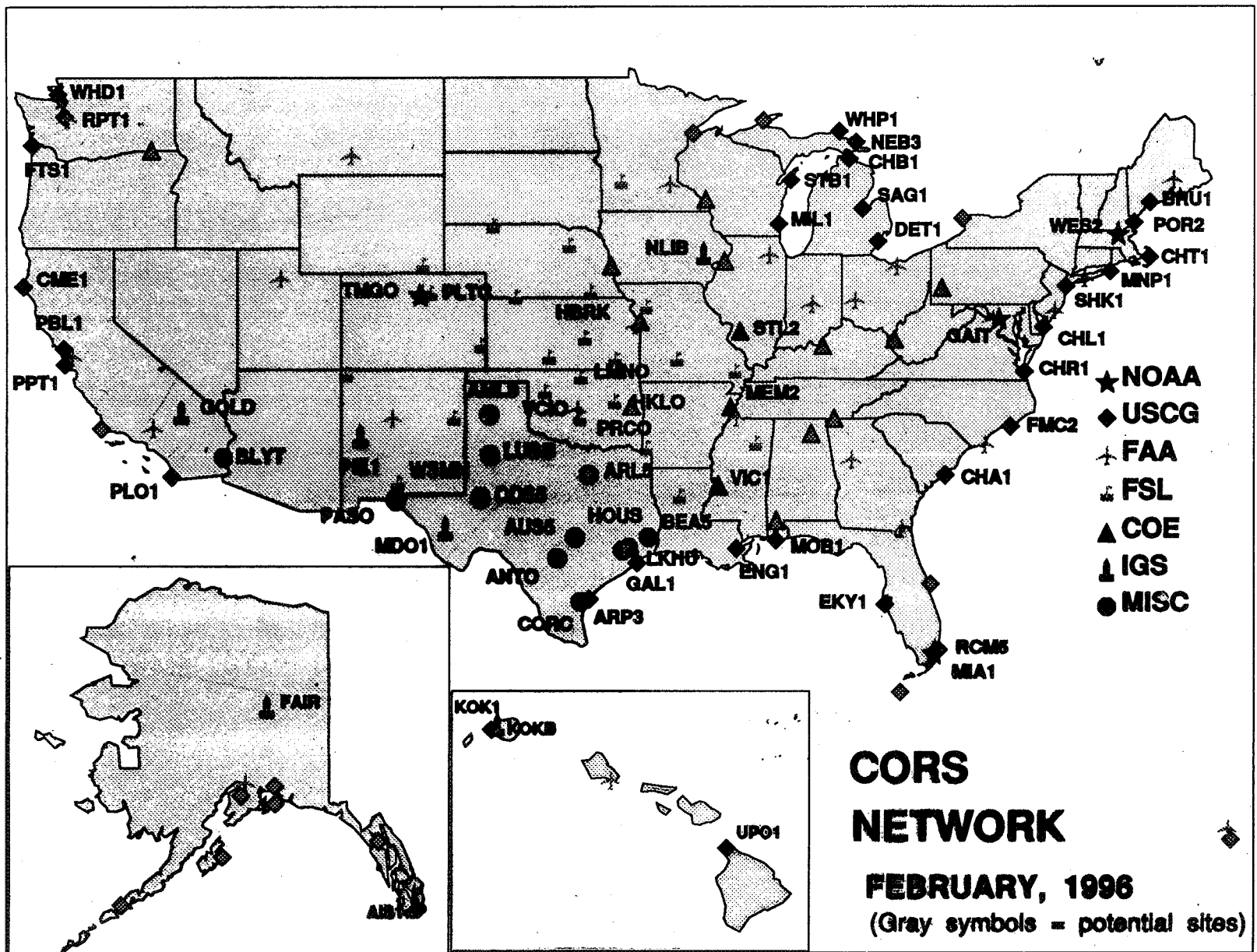
- AT&T FTS2000, X.25 PACKET SERVICE
- DATA TRANSMITTED AFTER EACH SAMPLE - NO ON SITE STORAGE

AMOUNT OF DATA TRANSFERRED:

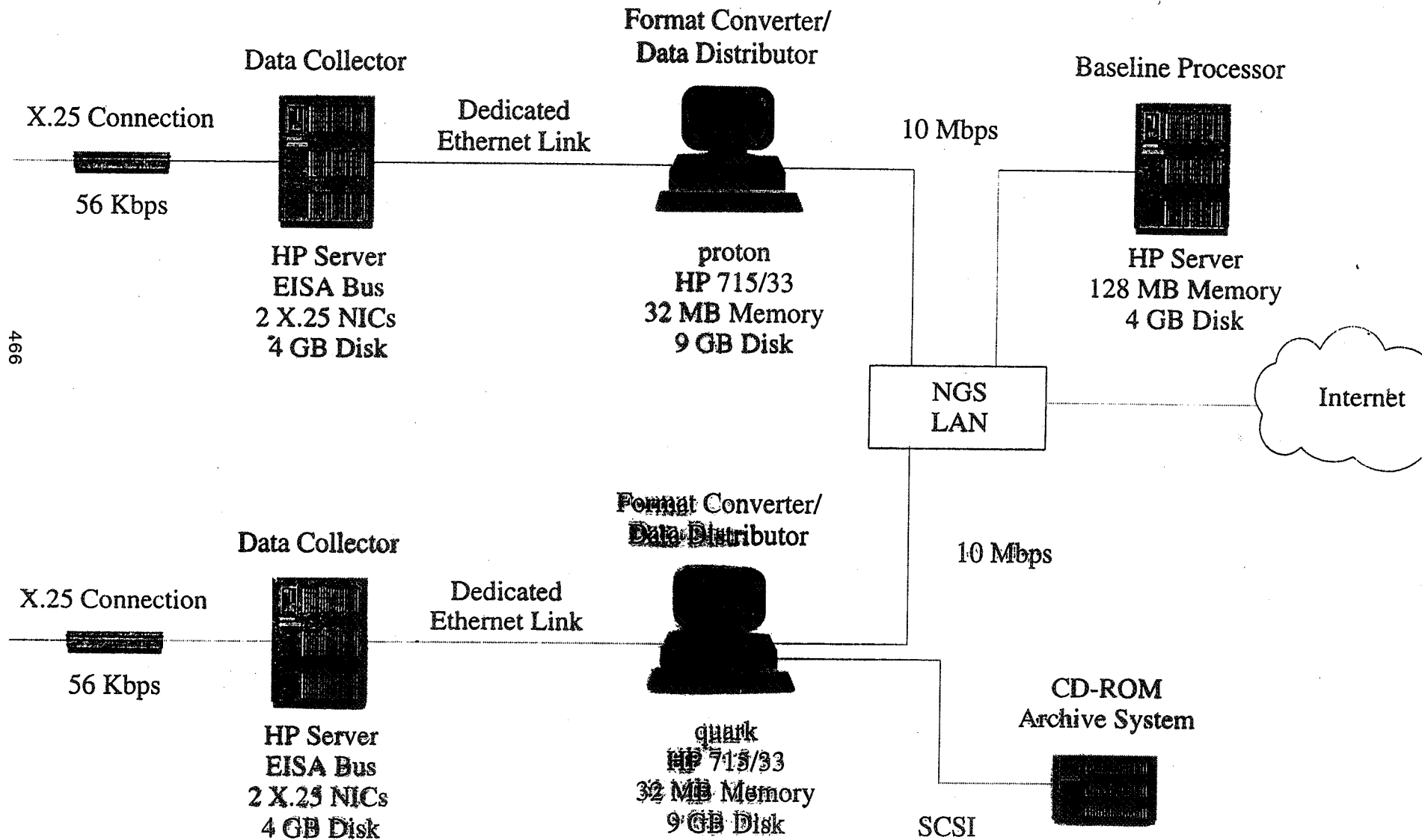
- ~5 Mbytes/DAY/STATION

PARTICIPATING CORS OBSERVING STATIONS

- U.S. COAST GUARD/U.S. ARMY CORPS OF ENGINEERS
- NASA/JPL/IGS
- U.S. GEOLOGICAL SURVEY
- NOAA
- TEXAS DEPARTMENT OF TRANSPORTATION
- FAA



CORS Data Collection and Distribution (Proposed Configuration, Phase 1.1)



ITRF94 VS CORS_ESTIMATES



RMS DISCREPANCY

North	5.6 mm
East	7.0 mm
Up	12.4 mm

METEOROLOGICAL PACKAGES (GSOS)

NATIONAL DATA BUOY CENTER
STENNIS SPACE CENTER

- NDBC developed a small meteorological sensor package (GSOS) that could be installed at the USCGD GPS sites.
- Will interface with the AT&T X.25 packet switching network (via a PAD).
- Transmit data to NGS on command (normally every 5 minutes).
- Merge 5 minute data epochs into an hourly file (RINEX format).

PTB 200 SERIES DIGITAL BAROMETERS

FEATURES

- TOTAL ACCURACY INCLUDING ONE YEAR DRIFT
 - PTB 200A +/- 0.20 mbar
 - PTB 201A +/- .03 mbar
- 600 to 1100 mbar PRESSURE RANGE
- -40[∞] to +60[∞] C OPERATING TEMPERATURE RANGE
- RS 232C OR TTL LEVEL SERIAL INTERFACE

APPLICATIONS

- BAROMETRIC TRANSFER STANDARD
- WEATHER STATIONS
- ENVIRONMENTAL DATA LOGGING
- DATA BUOYS AND SHIPS

HMP 233 HUMIDITY/DEWPOINT TRANSMITTER

FEATURES

- ON-SITE ONE-POINT CALIBRATION CAN BE PERFORMED WITHIN A MATTER OF MINUTES WITHOUT DISTURBING THE UNITS OPERATION

- SELECTION OF OUTPUT PARAMETERS
 - RELATIVE HUMIDITY
 - DEWPOINT
 - TEMPERATURE

- SELECTION OF TEMPERATURE RANGE

- RELATIVE HUMIDITY
 - MEASUREMENT RANGE 0 TO 100%
 - ACCURACY +/- 1%RH
 - RESPONSE TIME 15 SECONDS

- TEMPERATURE
 - MEASUREMENT RANGE -40° TO 80° C
 - ACCURACY +/- 0.2° C

POTENTIAL FUTURE STATIONS

- FEDERAL AVIATION ADMINISTRATION WAAS
- ADDITIONAL USGS/COE INLAND WATERWAYS STATIONS
- FAA LOCAL AREA DGPS SITES
- USCG-TYPE NATIONWIDE EXTENSION
- FEDERAL AGENCY SURVEYING/MAPPING REQUIREMENTS
- STATE AND LOCAL AGENCY COOPERATION
- MEXICAN NATIONAL NETWORK

Page intentionally left blank

NOAA GPS Antenna-Calibration Website

G. L. Mader

<http://www.grdl.noaa.gov/>

GPS/PROJECTS/ANTCAL/

antcal_toc.html

Page intentionally left blank

**Average Median Data Delivery/Retrieval Delay
at CDDIS for 1996 (All Sites)**

C. Noll

Source	Sites	Average Median Delay*
AUSLIG	CAS1	131.50
	DAV1, HOB2, MAC1	493.55
CIGNET	BRMU, FORT, HNPT, KELY, RCM5, SOL1, USNA, WES2	5.58
	WUHN	66.42
ESA	KIRU, KOUR, PERT, VILL	4.38
	MAS1	12.54
	MALI	22.30
GFZ	POTS	8.64
	LPGS	19.92
	KIT3, ZWEN	41.01
GS1	TAIW, TSKB	4.43
IGN	BRUS, GRAZ, HERS, KOSG, METS, NYAL, OHIG, ONSA, TROM, WETT, ZIMM	8.57
	BOR1, GRAS, HART, KERG, MATE, REYK, WTZR	13.79
	JOZE, PAMA	19.72
	IRKT, MDVO	37.66
	ANKR	61.20
JPL	AOA1, CARR, CAT1, CIT1, LBCH, MCM4, OAT2, SPK1, UCLP, WHC1, WH1	6.61
	CASA, CRO1, GOLD, HARV, MADR, MDO1, QUIN, TIDB	9.18
	AREQ, CICE, EISL, FAIR, GODE, JPLM, KOKB, SANT, SEY1, SNI1, USC1, THU1, USUD, WLSN, YAR1	11.41
	AUCK, BOGT, CHAT, GUAM, IISC, NLIB, PIE1, SHAO	25.18
	MOIN	65.57
KOREA	TAEJ	2.75
NRCAN	ALBH, ALGO, DRAO, STJO, YELL	4.03
SIO	MONP, PIN1, PVEP, SIO3, VNDP	8.86
UNAVCO	POL2	38.22

* Figure determined by averaging median time value for the specified sites; each site's time value is a median time over a two month period in 1996. Times are in UTC and represent the time data were available in public disk area.

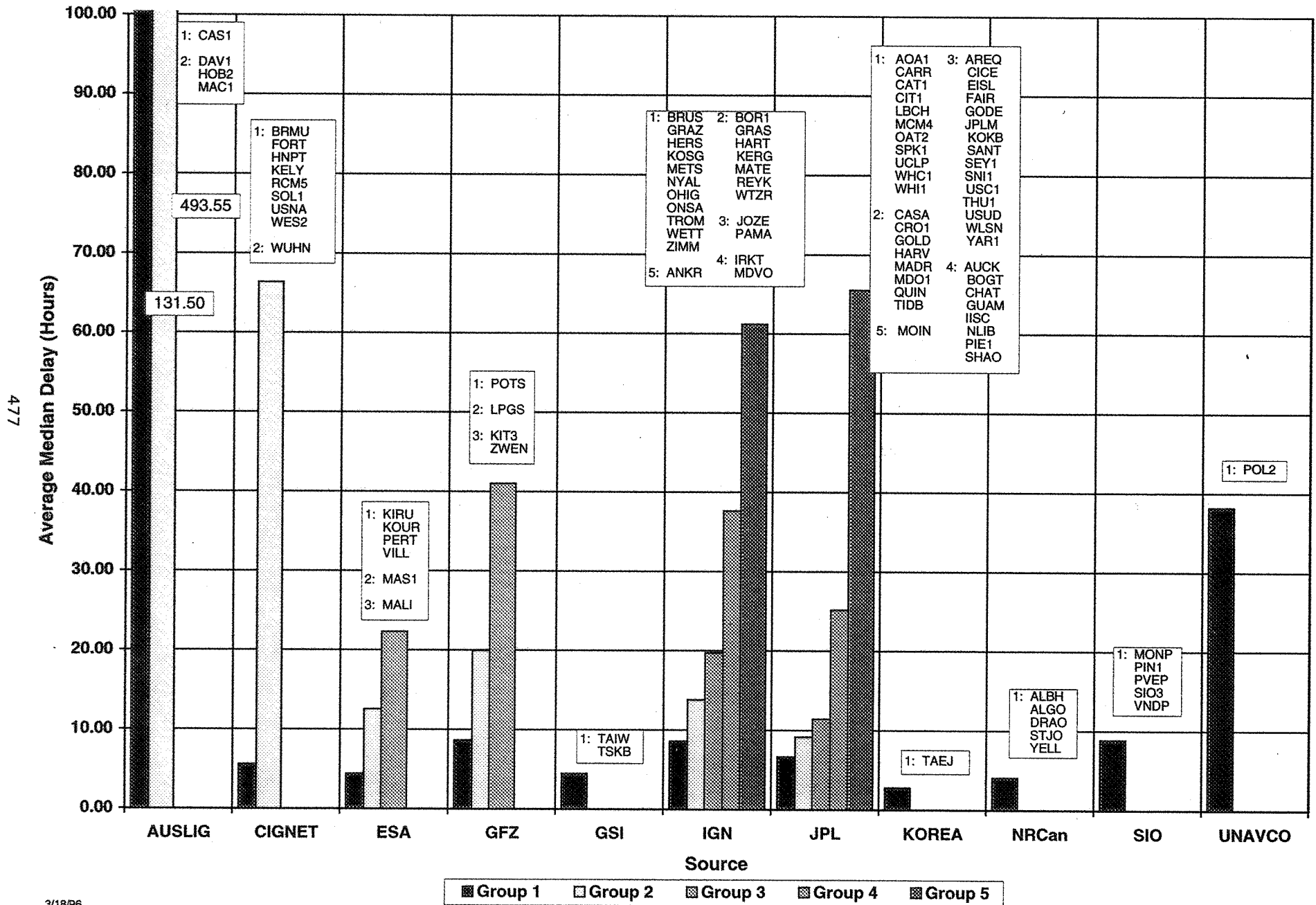
CDDIS Data Processing Schedule

Source	Put/Get	No. Times/Day	Put/Get Times	CDDIS Processing Times
AUSLIG	Get	1	06:30	06:30
CIGNET	Put	1	23:45	00:15, 11:00 (1)
ESA	Put	1	21:00	22:00, 00:30, 07:30
GFZ	Put	4	02:00, 08:00, 14:00, 20:00	03:30, 08:30, 15:30, 20:30
GSI	Put	1	19:30	20:00, 01:30
IGN	Put	4	02:00, 7:30, 14:00, 19:00	03:00, 08:00, 15:00, 20:00
JPL	Get/Put	1	01:30, 03:30, 5:00, 17:00	01:30, 03:30, 05:30, 17:00 (2)
KOREA	Put	1	19:30	21:45, 01:15
NRCan	Put	1	22:45	23:00, 16:00 (1)
SIO	Get	1	04:30	04:30
UNAVCO	Put	1	12:00	13:30

All times are CDDIS times (EST); adding five hours results in UTC time.

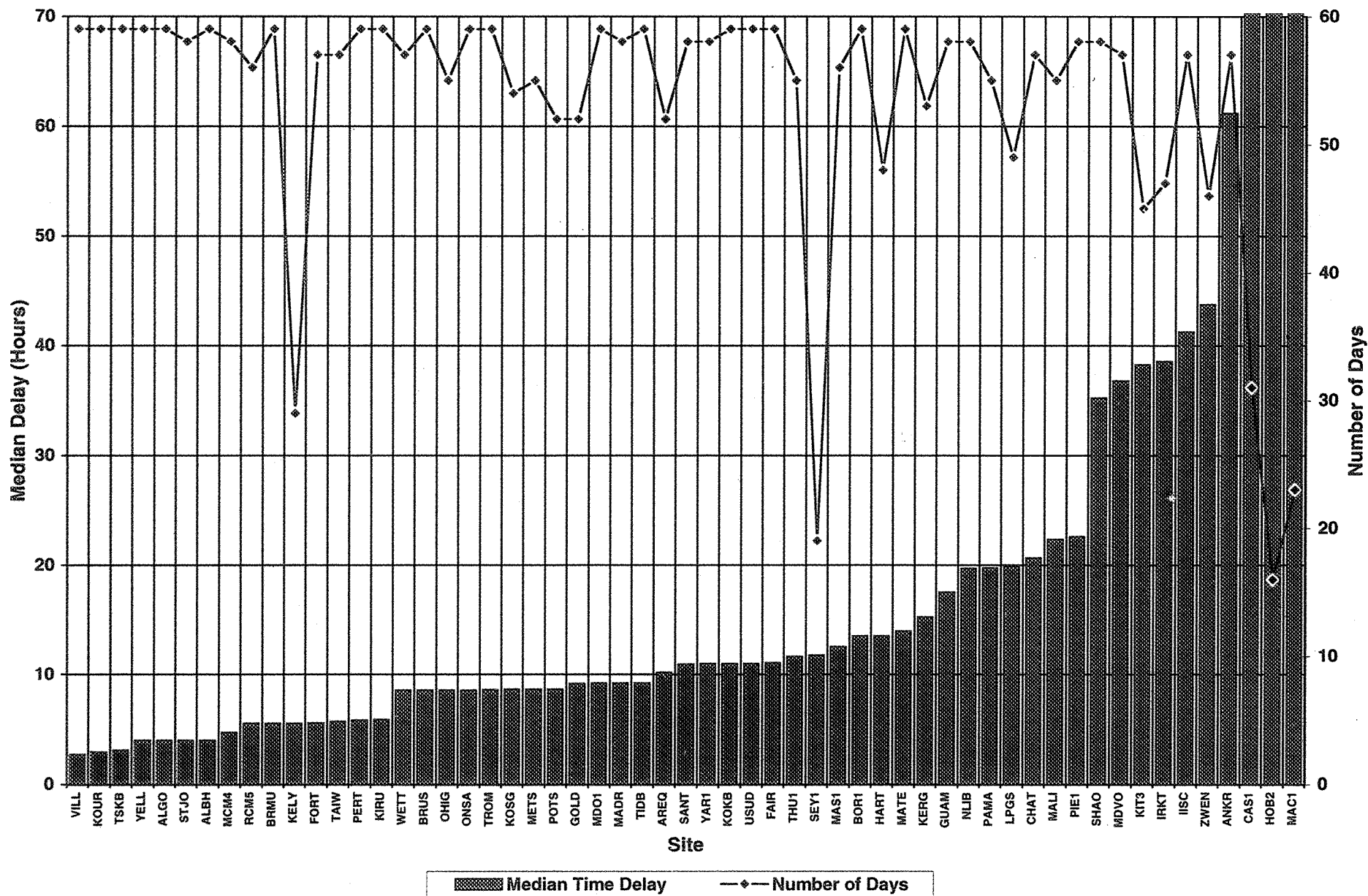
- (1) Processing software is executed a second time in order to archive any late data.
- (2) JPL PUT process to CDDIS executes ~05:00; CDDIS executes GET procedures several times to retrieve data quicker.

Average Median Data Delivery Delay for 1996 (All Sites)



Median Data Delivery Delay for 1996 (Global Sites)

478



CIGNET Data Delivery Statistics (1996)

